ALT INTERNATIONAL CONFERENCE
Advanced Laser Technologies

# ALT'26 | BOOK OF ABSTRACTS

## THE 33rd INTERNATIONAL CONFERENCE ADVANCED LASER TECHNOLOGIES

28 September – 3 October 2026

Samarkand, Uzbekistan

УДК 535.21; 535.23; 535.33; 535.37
ББК 22.343.4; 22.344; 22.345

**Abstracts of the 33rd International Conference on Advanced Laser Technologies – 2026. – 354 c.**

ISBN 978-5-6056411-2-4

The book contains abstracts of ALT'26 conference reports devoted to fundamental and applied aspects of innovative laser technologies: laser-matter interaction, biomedical photonics, laser systems and materials, laser diagnostics and spectroscopy, nonlinear and terahertz photonics, photonics in quantum technologies, advanced optical materials and metamaterials, agricultural and biophysical photonics. The book contains abstracts of plenary, invited, oral and poster presentations. The official language of the conference is English.

ALT Conference Books of Abstracts are available on the website:
https://altconference.org/proceedings

ISBN 978-5-6056411-2-4
9 785605 641124 >

© Prokhorov General Physics Institute
of the Russian Academy of Sciences, 2026
© Samarkand State University named
after Sharof Rashidov
© MESOL LLC, 2026

Подписано в печать 25.09.2026. Тираж 350 экз.

Отпечатано: ООО «АДМИРАЛ ПРИНТ»,
Москва, ул. Барклая, д. 13 стр. 1

ALT INTERNATIONAL CONFERENCE
Advanced Laser Technologies

# 33RD INTERNATIONAL CONFERENCE ON ADVANCED LASER TECHNOLOGIES (ALT'26)

## BOOK OF ABSTRACTS

Samarkand, Uzbekistan,
28 September – 3 October 2026

ALT INTERNATIONAL CONFERENCE
Advanced Laser Technologies

# TABLE OF CONTENTS


| | |
|---|---|
| PLENARY SPEAKERS | 5 |
| BIOMEDICAL PHOTONICS | 15 |
| LASER DIAGNOSTICS AND SPECTROSCOPY | 75 |
| LASER SYSTEMS AND MATERIALS | 123 |
| LASER-MATTER INTERACTION | 189 |
| NANOPHOTONICS | 247 |
| NONLINEAR AND TERAHERTZ PHOTONICS | 290 |
| PHOTONICS IN QUANTUM TECHNOLOGIES | 326 |

ALT INTERNATIONAL CONFERENCE
Advanced Laser Technologies

# PLENARY SPEAKERS

# Perovskite Quantum dots for Adanced Lasing, Nanophotonics and Optoelectronics

**A. Zakhidov**

*NanoTech Institute & Physics Dept, University of Texas at Dallas, Richardson, USA*
*Samarkand Quantum Center, Samarkand State University, Samarkand, Uzbekistan*

*zakhidov@utdallas.edu*

Hybrid halide perovskites attracted enormous attention as a new magic class of quantum materials and a playground for optoelectronics and photonics. Solar Cell PV and light emitting devices, LEDs have been broadly developed. Particularly we suggested new architectures with ions that can be attractive for low-dimensional perovskites: 2-D layered systems and Quantum Dots (QDs). In my talk I will describe progress in research of Perovskite QDs in Samarkand Quantum Center (SQC) and UTD, particularly for advanced lasing systems, nanophotonics and optoelectronics.

The emphasis will be on new architecture of optoelectronic devices. So Luminescent Solar Cells, with perovskite QDs which are now studied in Samarkand Quantum Center (SQC) will be discussed in detail. In such LSC, the QDs embedded in polymeric or glass layer forming a waveguide structure play a main role as photoactive converter. Solar light is absorbed by QDs, prepared in SQC, and re-emitted as bright luminescence, that is waveguided along the PA layer towards the edges, where the narrow PV cells absorb photons from QDs and convert to electric power with high efficiency. This type of LSC does not need charge collecting layers and electrodes, and these advantages will be discussed and some new architecture suggested for lasing in nanoimprinted photonic crystal structures and light emitting perovskite devices.

Blue electroluminescence is highly desired for emerging perovskite light-emitting devices for display applications and optoelectronics in general. However, saturated, efficient, and stable blue emission has been challenging to achieve. We leverage $CsPbBr_{3-x}Cl_x$ mixed-halide perovskites, polyelectrolytes, and a salt additive to demonstrate pure blue emission from single-layer light-emitting electrochemical cells (PeLECs). Substituting Cl into $CsPbBr_3$ produced luminescence from green through blue.

Overall, we demonstrate that low-dimensional perovskite nanophotonic and optoelectronic devices, based on QDs and 2-D layered structures with hybrid ligands show superior performance among blue perovskite LEDs and general LECs. We also demonstrate guest-host single PeLEC with widely tunable emitted color.

We have studied photoluminescence of pero-QD embedded into two types of photonic crystals: synthetic opals and inverted opal films, and demonstrated stable CW lasing at room temperatures.

Now we are working on electro-lasing designs for nanoimprinted photonic structures.

I will summarize my talk with comments on the importance of theoretical physics approaches for new challenges for understanding and designing novel QD based quantum materials with unique properties for qubits, sensors and related quantum devices. Excitonic Polaritons in 2-D perovskites and Quantum Dots with single photon emission are particularly attractive quantum materials that will be among intensive investigation in SQC with collaborators worldwide

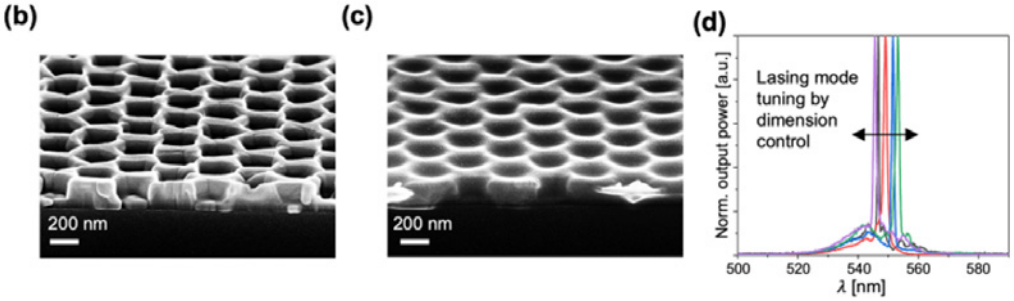


SEM images of the nanoimprinted $MAPbBr_3$ 2D PhC laser (b) before and (c) after PC

# Femtosecond Filament Remote Sensing

W. Liu

*Institute of Modern Optics, Nankai University*

*liuweiewi@nankai.edu.cn*

Recently, the rapidly developing femtosecond laser filament technology provided a new opportunity for the remote sensing. Here we propose a novel filament-based ionizing radiation sensing method, and clarify the interaction mechanism between filaments and ionizing radiation from systematic experiment to microscopic theory. ion mechanism between filaments and ionizing radiation from systematic experiment to microscopic theory. Specifically, it is demonstrated that the energetic electrons produced by α radiation in air can be effectively accelerated within the filament, serving as seed electrons, which will enhance nitrogen fluorescence. The extended nitrogen fluorescence lifetime of ~1 ns is also observed. LThis paper also proposes a remote 3D imaging method for concrete surface defects using acoustic pulses induced by femtosecond laser filamentation. The concrete defect detection system employs the time-of-flight principle to achieve 3D morphology imaging and the experimental results show that the depth detection range of defects ranges from 3 mm to 50 mm and the lateral resolution can be up to 0.3 mm when the concrete sample is 30 m away from the detection system.

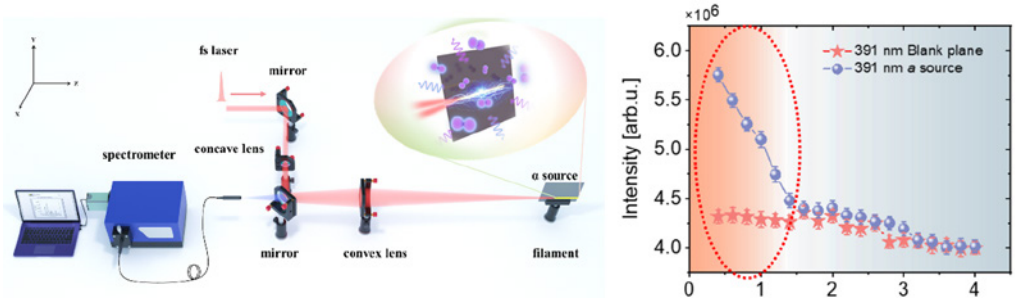


**Fig. 1** Filament based ionizing radiation sensing.

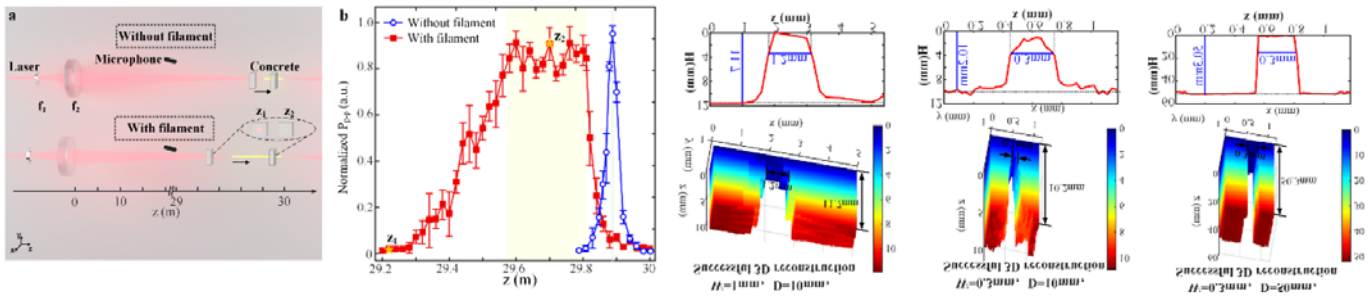


**Fig. 2** Remote 3D imaging results of concrete surface defects based on filament-induced acoustic pulses.

At the end, a highly directional amplified fluorescence confined by a self-waveguide induced by an air filament at a remote distance will be discussed. The structure of the waveguide is similar to conventional optical waveguides and is proven to arise from the amplification of fluorescence inside the filament. The backward detection efficiency could be improved by two orders of magnitude, compared to conventional isotropic fluorescence. This considerable advantage significantly boosts the detection sensitivity and extends the detection ranges in remote sensing applications.

[1] Pengfei Qi, Haiyi Liu, Jiewei Guo, Nan Zhang, Lu Sun, Shishi Tao, Binpeng Shang, Lie Lin and Weiwei Liu, Filament based ionizing radiation sensing. Opto-Electron Adv 8, 250144(2025)..
[2] Jiayun Xue, Lu Sun, Yuezheng Wang, Haiyi Liu, Pengfei Qi, See Leang Chin, Pierre Agostini, Weiwei Liu, Air Waveguiding of Lasing Induced by Long-Distance Filament. Laser & Photonics Reviews (2026): e71025.

# Progress in the development of efficient Quantum Dot based room temperature THz sources

**E.U. Rafailov**

*Optoelectronics and Biomedical Photonics Group, Aston Institute of Photonic Technologies, Aston University, Birmingham, B4 7ET, UK*

*e.rafailov@aston.ac.uk*

Quantum-dot (QD) semiconductor structures, traditionally developed as gain media for advanced laser systems, have recently emerged as promising platforms for compact terahertz (THz) sources. Their unique combination of broadband optical absorption, ultrafast carrier dynamics, and engineered electronic states enables new approaches to efficient THz radiation generation. In this work, we present recent advances in both continuous-wave (CW) and pulsed THz emission from QD-based photoconductive antennas enhanced with optical nanoantennae. The incorporation of nanoantennae within the photoconductive gap significantly enhances optical field localisation and carrier generation efficiency, enabling room-temperature operation within an ultra-compact device footprint. Furthermore, the integration of bandgap-engineered semiconductor materials, quantum-confined structures, and interdigitated electrode architectures broadens the optical pump wavelength range, improves carrier transport, and increases THz generation efficiency. Recent developments demonstrate that QD-based architectures can overcome several limitations of conventional photoconductive THz emitters, offering enhanced performance, low power consumption, and compatibility with photonic integration. These advances position QD-enabled photoconductive antennas as a highly promising platform for next-generation compact THz sources with applications in spectroscopy, imaging, sensing, and future high-speed wireless communication systems.

# Time-resolved fluorescence spectroscopy and imaging: applications and clinical relevance

**V. Shcheslavskiy[1], W. Becker[2]**

*1- Privolzhsky Research Medical University, Minin and Pozharsky Sq. 10/1, 603950 Nizhny Novgorod, Russia*
*2- Becker&Hickl GmbH, Nunsdorfer Ring 7-9, 12277 Berlin, Germany*

*vis@becker-hickl.de*

Time-correlated single photon counting (TCSPC) emerged as a technology in 1961 when Bollinger and Thomas published an article titled "Measurement of Time Dependence of Scintillation Intensity by a Delayed Coincidence Method" [1]. This technology probably had not survived had there not been developments in the field of pulsed lasers, ultrafast and ultrasensitive detectors, and ultrafast electronics. A major advancement in this field occurred in 1991, when fluorescence decay kinetics could be measured using TCSPC not just at a single point, but across multiple dimensions—including spatial coordinates, wavelength, polarization, and other parameters [2]. This breakthrough was key to the use of TCSPC as a fluorescence-lifetime imaging (FLIM) technique in microscopy, life sciences, and, over the past decade, in clinical research [3,4]. Fluorescence lifetime measurements are now possible not only in solutions but also on single molecules, cells, biological tissues, and even whole organs and small animals. While the fluorescence lifetime was once used merely to describe how long a molecule remains in its excited state, it has now become a marker of the molecule's microenvironment, as it is sensitive to temperature, viscosity, refractive index, acidity, and other physico-chemical parameters [5–7]. In this presentation we will introduce the audience to the technical backgrounds of TCSPC and its general features, show what TCSPC based fluorescence and phosphorescence lifetime imaging entails, how these techniques can address challenges in biology and medicine, and, finally, what limitations they still face despite their many strengths.

V. Shcheslavskiy acknowledges the support of RSF grant 24-19-00618.

1. L.M. Bollinger, G.E. Thomas, Measurement of the time dependence of Scintillation Intensity by a Delayed-Coincidence Method, Rev. Sci. Instr. 32, 1044-1050 (1961).
2. W. Becker, H. Stiel, E. Klose, Flexible Instrument for time-correlated single photon counting, Rev. Sci. Instr. 62, 2991-2996 (1991).
3. V.I. Shcheslavskiy, M. V. Shirmanova,| K. S. Yashin, A. C. Rück, M. C. Skala, W. Becker, J. Biophot. 0:e202400450 (2025).
4. R. Datta, T. Heaster, J. Sharick et al, Fluorescence lifetime imaging microscopy: fundamentals and advances in instrumentation, analysis, and applications, J. Biomed. Opt. 25, 071203 (2020).
5. K. Okabe, N. Inada, C. Gota, et al, Intracellular temperature mapping with a fluorescent polymeric thermometer and fluorescence lifetime imaging microscopy, Nat. Commun., 3 ,705 (2012).
6. K. Suhling, J. Siegel, D. Philips, et al, Imaging the environment of green fluorescent protein, Biophys. J., 83, 3589–3595(2002).
7. L. Shimolina, M. Izquierdo, I. López-Duarte, et al., Imaging tumor microscopic viscosity in vivo using molecular rotors, Sci. Rep. 7, 41097 (2017).

# Fundamentals, Throughput Breakthroughs, and Applications of Laser-generated Nanoparticales in Liquides

**A. Ziefuss, S. Barcikowski**

*Technical Chemistry I and Center for Nanointegration Duisburg-Essen (CENIDE) University of Duisburg-Essen, Universitätsstraße 7, 45141 Essen, Germany*

*Stephan.Barcikowski@uni-due.de*

Laser-based nanoparticle (NP) synthesis in liquids provides unique access to surfactant-free nanomaterials with high purity and compositional flexibility. However, NP productivity remains one of the central challenges of the field. Following major advances in laser ablation in liquids (LAL), further increases in production rates have become increasingly difficult due to fundamental limitations such as cavitation bubble shielding and the restricted availability of target material within the laser interaction zone. [1]

Microparticle laser fragmentation in liquids (MP-LFL) offers a fundamentally different approach by replacing a stationary bulk target with suspended MPs that are continuously replenished during processing. Beyond increasing material availability, this concept enables new laser–particle interaction regimes for NP generation. In the ultrashort-pulsed regime, MP-LFL is governed by stress confinement and photomechanical fragmentation mechanisms. However, significant energy losses to e.g. shock waves and cavitation bubbles, limit overall mass conversion.[2]

A fundamentally different picture emerges for nanosecond laser pulses. Owing to the longer pulse duration, thermal diffusion during the laser pulse extends beyond the optical penetration depth and can approach the characteristic MP dimension. Matching thermal penetration depth and particle size enables highly efficient photothermal fragmentation. Using silver MPs as a model system, nanosecond MP-LFL yields sub-10 nm NPs with near-quantitative single-pulse conversion, record mass yields, and gram-per-hour production rates under continuous-flow conditions (Fig. 1a). [3]

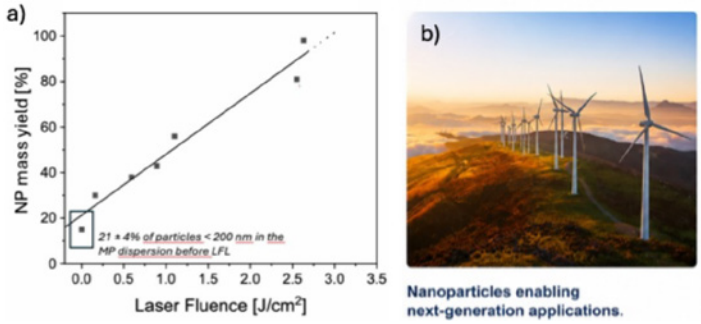


**Fig. 1**: (a) Laser fluence dependence of nanoparticle yield during nanosecond MP-LFL. (b) Application perspective: feedstock engineering with laser-generated nanoparticles for additive manufacturing, from polymer prototyping to permanent magnets

The resulting throughput breakthrough extends the relevance of laser-generated NPs far beyond NP synthesis itself. Many emerging technologies require gram-scale quantities of functional NPs, making productivity a key prerequisite for implementation. The presentation, therefore, concludes with examples from additive manufacturing, where laser-generated NPs are employed as functional feedstock additives to tailor laser energy absorption, microstructure evolution, and material performance. Case studies ranging from polymer powder bed fusion [4] for rapid prototyping to nanoparticle-assisted processing of Nd–Fe–B permanent magnets [5] for energy technologies such as wind turbines illustrate (Fig. 1B) how advances in NP production can translate into new opportunities for laser-based manufacturing.

Together, these results demonstrate how fundamental insights into laser–particle interactions can enable throughput breakthroughs and establish laser-generated nanoparticles as enabling materials for next-generation manufacturing technologies.

[1] F. Waag, R. Streubel, B. Gökce, et al., Appl. Nanosci. 11, 1303, 2021
[2] M. Spellauge, M. Tack, R. Streubel, M. Miertz, K. S. Exner, S. Reichenberger, S. Barcikowski, H. P. Huber, A. R. Ziefuss, Small 19, 2023
[3] A. R. Ziefuss, N. Stratmann, C. Reifenrath, G. Kanu, N. Bernd, S. Disch, S. Barcikowski, Optics Letters. 51, 2026
[4] N. Stratmann, M. Willeke, S. Leupold, M. Schmidt, S. Barcikowski, A. R. Ziefuss, CIRP Procedia, 124, 2024
[5] P. Gabriel, V. Nallathambi, J.Liu, F. Staab, T. D. Oyedeji, Y. Yang, N. Hantke, E. Adabifiroozjaei, O.Recalde-Benitez, L.Molina-Luna, Z. Rao, B. Gault, J. T. Sehrt, F. Scheibel, K. Skokov, B.-X. Xu, K. Durst, O. Gutfleisch, S.Barcikowski, A.R. Ziefuss, Adv Sci, 11(46), 2023

# Selected biomedical applications in fast volumetric imaging using light-sheet microscopy

**P. Loza-Alvaez**

*ICFO - The Institute of Photonic Sciences, Barcelona Institute of Science and Technology, Castelldefels (Barcelona) 08860, Spain*

*Pablo.Loza@icfo.eu*

Light-sheet fluorescence microscopy (LSFM) operates by illuminating the sample with a thin sheet of excitation light, while the emitted fluorescence is captured through a detection objective positioned perpendicular to the illumination plane. This configuration enables highly efficient excitation and signal collection. As a result, the light exposure on the specimen is minimized, leading to reduced photobleaching and consequently lower phototoxicity.

LSFM has emerged as a powerful approach for rapid three-dimensional imaging of biological specimens. In this work, I will describe our efforts to achieve fast volumetric imaging tailored for high-throughput applications, utilizing a fluidic setup.

In the second part, I will introduce a LSFM system designed for high-speed volumetric imaging that employs an electrically tunable lens (ETL). This configuration enables dynamic focusing and is applied to monitor spontaneous calcium ($Ca^{2+}$) activity, as indicated by GCaMP fluorescence signals.

Finally, I will present an approach that integrates wavefront coding (WFC) with machine learning in an LSFM framework, enabling the visualization of the three-dimensional dynamics of sperm flagellar motion.

# Innovative Technologies for Targeted Irradiation of Deep-Seated Tumors

**S.M. Deyev**

*Lebedev Physical Institute of the Russian Academy of Sciences, Moscow, Russia*
*Shemyakin-Ovchinnikov Institute of Bioorganic Chemistry, Russian Academy of Sciences, Moscow, Russia*
*National Research Centre "Kurchatov Institute", Moscow, Russia*

*biomem@mail.ru*

The selectivity of therapeutic agent delivery to target cells is important in order to reduce the overall toxic load on the body. We have proposed a number of approaches based on multifunctional structures that combine highly selective elements for recognizing tumor cells and agents for accurate diagnosis and effective cancer therapy. We demonstrate a synergistic strategy of combination immuno/chemotherapy implying vectoring of oncomarkers sites with compounds having a different mechanism of action.

We introduce the concept of genetically encoded bioluminescence resonance energy transfer (BRET)-activated PDT, which combines an internal light source and a photosensitizer in a singlegenetic construct, which can be delivered to tumors seated at virtually unlimited depth and then triggered their treatment.

We also use riboflavin (vitamin B2, Rf) as a photosensitizer capable to generate reactive oxygen species under UV-blue irradiation and kill cancer cells. In order to translate the riboflavin-mediated PDT to deep-seated tumors, one needs to deliver UV-blue excitation light deep into tissue. In order to extend the treatment depth ~10-fold in biological tissue, we introduced upconversion nanoparticles (UCNPs), that were capable to efficiently convert deeply-penetrating near-infrared light into UV-blue light by resonant energy transfer processes to Rf using the moderate intensity and doses of NIR light acceptable for PDT procedures.

We also will review several approaches to improve the pharmacokinetics, extend blood residence and reduce renal uptake of nanoparticles developed in our team [1–5].

[1] I.V. Zelepukin, O.Y. Griaznova, K.G. Shevchenko, et al. Flash drug release from nanoparticles accumulated in the targeted blood vessels facilitates the tumour treatment. *Nat Commun*., vol.13(1), 6910, (2022).
[2] I.V. Zelepukin, K.G. Shevchenko, S.M. Deyev, Rediscovery of mononuclear phagocyte system blockade for nanoparticle drug delivery. *Nat Commun*., vol. 15, 4366, (2024).
[3] E.I. Shramova, S.P. Chumakov, V.O. Shipunova, et al. Genetically encoded BRET-activated photodynamic therapy for the treatment of deep-seated tumors. *Light Sci Appl*., vol. 11, 38, (2022).
[4] I.B. Belyaev, O.Y. Griaznova, A.V., et al. Beyond the EPR effect: Intravital microscopy analysis of nanoparticle drug delivery to tumors. *Adv Drug Deliv Rev*., vol. 219, 115550, (2025).
[5] H. Lin, Z. Li, I.V. Zelepukin, et al. Effects of nanoparticle physicochemical properties on macrophage polarization. *J Control Release*, vol. 387, 114215 (2025).

# Advanced Technologies of Nuclear Medicine and Radiology

**I. Zavestovskaya**[1,2]

*1- National Research Center "Kurchatov Institute", 1 Kurchatov Square, Moscow, Russia*
*2- Lebedev Physics Institute of the Russian Academy of Sciences, Leninsky pr. 53, Moscow, Russia*

*zavestovskayain@lebedev.ru*

Modern nuclear medicine is a high-tech, interdisciplinary field based on the application of nuclear physics methods in medicine, along with laser, biophotonic, biochemical, and nanotechnologies. The main areas of modern nuclear medicine include radionuclide and radiation diagnostics and therapy, which are based on the effect of ionizing radiation on biological tissue. The goal of treatment is the effective destruction of diseased tissue with minimal impact on healthy organs and tissues. Nuclear medicine as defined by the IAEA - a field of medicine that uses radiation of radionuclides injected into the blood and localized in tumors for diagnosis and treatment. Radiation of radionuclides initiates radiation-induced DNA damage of actively proliferating cancer cells, while γ and positron radiation of radionuclides can be used to accurately determine the distribution of radionuclides throughout the body. Problems: Radionuclides, circulating in the blood, settle in all organs, in tumors – no more than 13 %. In Radiation diagnostics and therapy External sources of radiation (for example, high-energy X-rays, ion rays) is focusing directly on the tumor to cause the death of cancer cells, Problems: With external irradiation, healthy tissues are also irradiated. To reduce normal tissue damage the total dose is divided it into small fractions. The typical schemes consist of fractions of approximately 2 Gy, delivered once a day on week within the period of several weeks.

Recent data which we have in realization of the joint projects with LPI, Tsyb Radiological Center, MEPHI, BINP and ICG SB RAS show that the field of nuclear medicine can be significantly expanded by integrating with nanomedicine, which utilizes different types of nanomaterials including nanoparticles (NPs) as carriers of radionuclides or as radiosensitizers for radiation therapy and/or active agents for imaging (radiopharmaceutical medicines in situ). The synergy of nanotechnology with nuclear medicine opens up a new direction of cancer imaging and therapy - nuclear nanotheranostics.

We propose different types of NPs synthesized by promising laser-based approaches as a NPs for nanotheranostics. One can use these methods to make stable colloidal dispersions of nanoparticles in both organic and aqueous media, which are suitable for a multitude of applications across the important fields of health care. Laser-synthesized NPs have ideal round shape, controllable size with low size dispersion, and are free of any toxic impurities, which promises a better transport in vivo and the absence of side effects. We demonstrate the possibility for fast PEGylization and vectorization of laser-synthesized NPs with darpins and affibodies.

Proton, ion and neutron capture therapy technologies are being researched using the unique accelerator infrastructure of the Kurchatov Institute, LPI, BINP and Tsyb Center. Technologies of targeted proton and neutron capture therapy using promising nanoparticles and systems based on them as therapy sensitizers are considered. The introduction of non-radioactive materials that can be activated from the outside using various external sources of nuclear particles to produce radioactivity in situ is one of the new directions of activation of nanodrugs at the site of a cancerous tumor, which can be considered as in situ production of radiopharmaceuticals. Such binary radiotherapy technologies become especially efficient when one can achieve a high tumor/non-tumor action contrast, which enables to minimize side effects related to the irradiation of healthy issues. The results of the synergistic effect of various types of ionizing radiation, as well as the technology of combined exposure to ionizing radiation and recombinant immunotoxins, either individually or in combination with nanoparticles, are also presented. The results represent the work of a large interdisciplinary team in the development of new effective technologies for hadron therapy, including the development of an innovative platform for nuclear nanomedicine and nanoradiology using a Russian accelerator complex. The implementation of these technologies will ensure the availability of high-tech, effective treatment of socially significant diseases.

Acknowledgements: The study is supported by the Ministry of Science and Higher Education of RF (project No 075-15-2025-453), RSF (project No 24-62-00018).

# CVD diamond for lasers and photonics: growth, properties, treatment, examples of applications

**V. Ralchenko**

*Prokhorov General Physics Institute of Russian Academy of Sciences, Vavilov str. 38, 119991 Moscow, Russia*

*vg_ralchenko@mail.ru*

Recent years are marked with a great progress in synthesis of high-quality diamond, a precious material for lasers, photonics and electronics. Diamond has attracted considerable attention owing to its unique properties, such as a wide bandgap of 5.45 eV, transparency in a wide spectral range from UV to far IR, record high thermal conductivity, low thermal expansion coefficient, high Raman gain, high hole and electron mobility, high breakdown electric field strength, high mechanical strength, high chemical inertness and high radiation hardness. Using these advantages, a variety of applications are already developed, including solar blind UV detectors, powerful Raman lasers, IR optical components, X-ray refractive lenses, fast bolometer, substrates for thermal managements in lasers and LED, and power electronic devices. Also, diamond has a large number of color centers such as NV (nitrogen-vacancy), SiV and GeV, prospective for quantum optical technologies as single photon emitters and sensors.

Here, a technique for growth of diamond single crystals by microwave plasma chemical vapor deposition (CVD) [1] from methane-hydrogen gas mixtures will be presented, particularly paying attention to optical spectroscopy for *in situ* diagnostics of the plasma and the crystal. The data on the crystal quality as assessed with different characterization methods, will be given, and examples of diamond devices and components will be shown. On the other hand, lasers seem to be an ideal tool for treatment of superhard diamond, and now they are routinely used for diamond cutting, patterning, smoothing, formation of conductive graphitic structures on the surface as well in the bulk, particularly to fabricate UV and particle detectors. It is generally accepted that synthetic diamond nowdays is becoming the available material for most demanded photonic applications.

[1] J.C. Arnault, S. Saada, V. Ralchenko, CVD grown single crystal diamond: a review, Physica Status Solidi (RRL)–Rapid Research Letters, 16, 2100354 (2022).

ALT INTERNATIONAL CONFERENCE
Advanced Laser Technologies

# BIOMEDICAL PHOTONICS

# Breakthrough benefits of laser biomedical technologies thanks to tissue optical clearing

**V. Tuchin**

*Institute of Physics and Science Medical Center, Saratov State University, Saratov, Russian Federation*
*Laboratory of Biophotonics, Tomsk State University, Tomsk, Russian Federation*
*Laboratory of Laser Diagnostics of Technical and Living Systems, Institute of Precision Mechanics and Control, FRC "Saratov Scientific Centre of the Russian Academy of Sciences," Saratov, Russian Federation*

*tuchinvv@mail.ru*

This work summarizes the advantages in the development of tissue optical clearing (TOC) technologies using biocompatible immersion optical clearing agents (OCAs) for intravital optical imaging, laser diagnostics, and laser therapy. It will be shown that the TOC method significantly improves and expands the capabilities of advanced multimodal laser spectroscopy/imaging and laser phototherapy technologies. Delivery of the appropriate OCA to living tissue ensures its transparency over a broad spectral range from deep UV to near-IR and further to THz, where the most lasers and laser systems are operating. TOC method increases the imaging depth with enhanced contrast. Furthermore, it provides additional markers for monitoring diabetes mellitus complications and cancer cell detection using robust laser systems for measurements of molecular diffusivity and blood microcirculation.

This paper summarizes cutting-edge developments in tissue optical clearing (TOC) technology using biocompatible immersion optical clearing agents (OCAs) for intravital optical imaging, laser diagnostics, and laser therapy [1-4]. It will be demonstrated that TOC significantly improves and expands the capabilities of multimodal laser spectroscopy/imaging and laser phototherapy technologies. Delivery of appropriate OCAs to living tissue ensures its transparency across a broad spectral range from deep UV to NIR and further to THz, where most lasers and laser systems operate. TOC increases visualization depth with improved contrast. Furthermore, it provides additional markers for monitoring diabetes mellitus complications and detecting cancer cells using robust laser systems for measuring molecular diffusion and blood microcirculation.

This study was supported by the RSF grant no. 24-44-00082.

[1] L. Oliveira, V. Tuchin, The Optical Clearing Method - A New Tool for Clinical Practice and Biomedical Engineering (Springer) (2019).
[2] V. Tuchin, D. Zhu, E. Genina (Eds.), Handbook of Tissue Optical Clearing (CRC Press) (2022).
[3] D. Zhu, V.V. Tuchin, BME Front. **5**, 0058 (2024).
[4] V.V. Tuchin, T. Dai, L.M. Oliveira, Adv. Drug Delivery Rev. **226**, 115699 (2025).

# Molecular Signatures of Early Multicellularity in Yeast: From Single Cells to Multicellular Clusters

**Chia-Liang Cheng, Pooja Manik Badgujar, Chia-Hsuan Tsou, A.V. Karmenyan**

*Department of Physics, National Dong Hwa University, Hualien 97401, Taiwan*

*clcheng@gms.ndhu.edu.tw*

The evolution of multicellularity is one of the most significant transitions in the history of life, yet the biochemical and metabolic changes that happen in its earliest stages are not fully understood [1]. In this study, we explore the emergence of multicellular "Snowflake" yeast in ***Saccharomyces cerevisiae*** through gravitational-settling selection without genetic engineering. This experimentally evolved system offers a manageable model to study how cellular cooperation and spatial organization develop from unicellular ancestors. Using a combined imaging approach that includes confocal microscopy, Raman spectroscopy, and Two-Photon Fluorescence Lifetime Imaging (TP-FLIM), we identify coordinated molecular and metabolic changes linked to cluster formation. Raman mapping shows extensive remodeling of lipids, proteins, and sterol-related components during the shift from single cells to multicellular groups. Notably, biochemical differences appear within clusters, indicating spatial specialization. Complementary TP-FLIM analysis reveals metabolic gradients and different redox states between outer and inner cells, suggesting early metabolic differentiation.

Focusing on snowflake yeast as a model of evolutionary innovation, we are now applying 2P-FLIM and Raman spectroscopy to detect shifts in metabolic state, bioenergetics, and fluorescence lifetimes associated with the spontaneous transition from unicellular to multicellular behavior. A single mutation in yeast that disrupts daughter cell separation leads to clonal clustering and coordinated growth, forming collectives with emergent individuality. This work suggests that carotenoids and redox-sensitive molecules may serve as ancient and conserved mediators in regeneration and multicellularity [2]. Raman band assignments revealed spatially resolved variations in lipid-associated peaks (1445 $cm^{-1}$), protein amide I features (1650 $cm^{-1}$), and sterol-related signatures consistent with ergosterol distribution. Our imaging-driven approach provides a molecular framework to study how life reorganizes itself from repairing tissue to evolving complexity. This study integrates label-free imaging techniques, including 2P-FLIM and Raman spectroscopy, to explore carotenoid-mediated redox signaling across regeneration and the emergence of multicellularity in snowflake yeast and other biosystems. Using non-invasive spectroscopic imaging tools, we track carotenoid-driven redox signaling and metabolic coordination, which may underlie both regenerative capacity and early multicellular identity.

[1] Ratcliff, W., Fankhauser, J., Rogers, D. *et al.* Origins of multicellular evolvability in snowflake yeast. *Nat Commun* **6**, 6102 (2015).
[2] P. M. Badgujar, Y.-C. Lin, Z.-R. Lin, M.-D. Lin, C.-L. Cheng, Raman spectroscopic signals of carotenoid distribution during stages of cell growth of unicellular organisms and plant cells *J Raman Spectrosc* 2023, 54(7), 706.

# Skin optical clearing: an innovative approach to cancer diagnostics

**E.A. Genina[1], I.A. Serebryakova[1], Yu.I. Surkov[1], V. Tuchin[1,4,5]**

*1- Optics and Biophotonics Department, Saratov State University, 83, Astrakhanskaya St., Saratov, 410012 Russia*
*2- Laboratory of Laser Molecular Imaging and Machine Learning,*
*National Research Tomsk State University, 36, Lenin Ave., Tomsk, 634050 Russia*
*3 - Institute of Precision Mechanics and Control, FRC "Saratov Scientific Centre of the RAS",*
*24, Rabochaya St., Saratov, 410028 Russia*

*eagenina@yandex.ru*

The aim of this study was to develop an improved multimodal approach that combines data from optical coherence tomography (OCT) at a wavelength of 930 nm, diffuse reflection spectroscopy (DRS) in the range of 400-900 nm and high-frequency ultrasound (HFUS) at frequencies of 33 and 75 MHz. A multimodal contact gel (MCG) with the properties of an ultrasonic contact gel and an optical clearing agent was developed specifically for use in both optical and ultrasound methods. It was characterized by high biocompatibility, acoustic conductivity, sufficient viscosity and possessing the properties of an optical clearing agent.

The study included volunteers with clinically confirmed benign neoplasms (BN) and basal cell carcinoma (BCC). MCG was tested only on BN. Visualization and measurements of the spectra were performed 15 minutes after topical application of MCG.

Using a comprehensive analysis of geometric, textural, and spectral characteristics of neoplasms, the most informative parameters for each modality were identified. Machine learning models were trained for each modality, and their weighted-voting fusion achieved 96% accuracy for the binary classification (BCC vs BN) (Fig. 1).

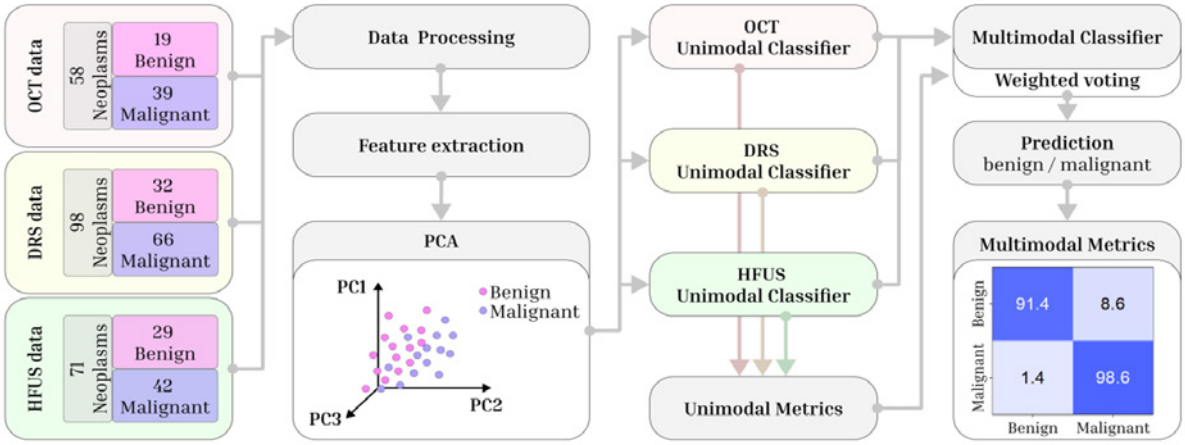


**Fig. 1.** Scheme of the sequence of training stages of a multimodal classifier for the diagnosis of human skin neoplasms.

Skin optical clearing with the use of MCG provided improvement of the quality of noninvasive visualization of skin structures by stabilizing contact, reducing the effect of surface scattering, increasing the contrast of visualization of structural elements, reducing the variability associated with the microrelief of the surface, and increasing the reproducibility of multimodal measurements. The integration of the optical clearing into multimodal screening, which included OCT, DRS, and HFUS improved the diagnostic information and expanded the possibilities for differential diagnosis of BN and potentially malignant neoplasms.

The work was supported by RSF grant 23-14-00287-P.

# Application of radiopaque and magnetic resonance agents for optical clearing of nail bed skin

**A. Lugovtsov[1], P. Moldon[1], D. Umerenkov[1], P. Ermolinskiy[1]**
**M. Maksimov[1], P. Timoshina[2], V. Tuchin[2], A. Priezzhev[1]**

*1- Lomonosov Moscow State University, 1-2 Leninskiye Gory, Moscow, Russia, 119991*
*2- Chernyshevsky Saratov State University, 83 Astrakhanskaya str., Saratov, Russia, 410012*

*anlug@biomedphotonics.ru*

The optical clearing (OC) method is widely used for many biomedical applications and for studying the biological tissues, as well as in modern diagnostics approaches. For example, vital digital capillaroscopy is a method widely used for visualisation of human capillaries *in vivo*, in particular, of nail bed capillaries to identify disorders of the circulatory system at the early stages and to monitor the effectiveness of treatment of different pathologies related with microcirculatory alterations [1]. It is obvious that OC can enhance the accuracy and informativeness of capillaroscopy [2, 3]. The OC technique is based on application of optical clearing agents (OCA) for increasing the depth of light penetration into the biological tissues and, as a result, to improve the visualization of blood capillaries in nail bed skin [4]. When applied to a tissue surface, OCA penetrate inside the tissue and reduce the contribution of multiple light scattering to image formation. The mechanism of their operation is based on a decrease in the relative refractive index of optical inhomogeneities after diffuse penetration into the tissue. There are many substances that can be used as OCAs. For example, glycerol, cedar oil, mineral oil, oleic acid and various combinations of these agents are suitable for these purposes. However, the important issue limiting their use is biocompatibility and safety. Currently, the search for new agents that have been well studied in terms of the safety of their introduction into the body continues. One of the promising agents for OC can be well-studied drugs that are used for increasing the contrast of magnetic resonance and computed tomography images.

The aim of this study was to investigate the potential use of magnetic resonance (MR) and radiopaque contrast (RP) agents to improve visualization of the human nail bed for digital capillaroscopy *in vivo* using the OC method.

The efficacy of OC after application of MR agents (gadovist, magnevist) and RP agents (accupaque, visipaque) as they penetrated into the tissue was assessed by optical coherence tomography by registration of changes in the light extinction coefficient. Each agent was applied onto the nail bed surface of six healthy volunteers on the surface area located in 2 mm from the eponychium. The OCAs penetrate into the bloodstream through the walls of capillaries in the deep layers of biological tissues. Most of OCA are osmotically active and can change the microrheological properties of blood, which determine blood viscosity, that in turn can locally alter the diagnosed blood flow, introducing errors in capillary blood flow measurements using digital capillaroscopy. The effect of OCAs on RBC aggregation and deformability properties was measured *in vitro* by diffuse light scattering method [1].

All tested agents reduced the extinction coefficient of the nail bed skin, confirming their effectiveness for OC. The highest effect of OC was observed at depths of 0–50 μm when using the RP agent visipaque combined with auxiliary substances (dimethyl sulfoxide). For this depth range, a decrease in the extinction coefficient of 30±11% was observed. This effect is presumably associated with tissue dehydration, which increases the depth of light penetration. Thus, MR and RP agents may be effective for OC of nail bed skin and may hold promise for capillary studies using digital capillaroscopy. The necessity to correct the parameters measured using digital capillaroscopy was demonstrated. The study was supported by the Russian Science Foundation (Grant No. 25-15-00172).

[1] A. Lugovtsov, Y. Gurfinkel, P. Ermolinskiy, A. Maslyanitsina, L. Dyachuk, A. Priezzhev, Optical assessment of alterations of microrheologic and microcirculation parameters in cardiovascular diseases, Biomedical Optics Express. vol. 10, pp. 3974-3986, (2019).
[2] P.A. Moldon, et al., Influence of optical clearing agents on the scattering properties of human nail bed and blood microrheological properties: in vivo and in vitro study, Journal of Biophotonics, pp. e202300524, (2024).
[3] A. Timoshina, Y. Surkov, A. Lugovtsov, A. Priezzhev, V. Tuchin, Transmission laser speckle contrast imaging combined with optical clearing using magnetic resonance contrast agents, Lasers in Surgery and Medicine, vol. 57(7), lsm.70051, (2025).
[4] E. Genina, A. Bashkatov, Y. Sinichkin, I. Yanina, V. Tuchin, Optical clearing of biological tissues: Prospects of application in medical diagnostics and phototherapy. Journal of Biomedical Science and Engineering, vol. 1, pp. 22-58, (2015).

# From a label-free photonic signature to molecular identity: MALDI-TOF assignment of the chromophore of evolved multicellularity in snowflake yeast

**P.M. Badgujar, A.A. Patil, A. Karmenyan, Chia-Hsuan, Wen-Ping Peng, Chia-Liang Cheng**

*IR-Laboratory, Department of Physics, National Dong Hwa University, Hualien 974301, Taiwan, ROC*

*clcheng@gms.ndhu.edu.tw*

The transition from solitary cells to cooperative multicellular collectives is one of evolutionary biology's most fundamental and least molecularly resolved events. The "snowflake yeast" model, in which *Saccharomyces cerevisiae* forms heritable clonal clusters under repeated gravitational settling or centrifugation, provides experimentally tractable access to this transition in real time. However, the accompanying molecular changes have remained difficult to interrogate in living cells without staining or fixation. We address this with a two-modality label-free photonic platform combining confocal Raman microspectroscopy (532 nm excitation, position-resolved across single clusters) and two-photon fluorescence-lifetime imaging microscopy (2P-FLIM) with phasor analysis (740 nm), co-registered with Calcofluor White and confocal reflectance for cellular reference. Ancestor cells (AN-D0), single-cell controls, and evolved branched clusters at G3–G15 (n = 5 lineages per regime) were profiled side by side. Three independent observations converge. (i) A new Raman band at 1577–1580 $cm^{-1}$ emerges in evolved multicellular lineages and localises specifically to mother daughter junctions; the resonance-Raman carotenoid markers at 1525 and 1156 $cm^{-1}$ coexist as a polyene background. (ii) 2P-FLIM resolves a ~2.8 ns lifetime component at the same junctions, distinct from the NAD(P)H/FAD baseline of single cells and consistent with a flavin, free-base porphyrin, or open-chain bilin chromophore. (iii) The two photonic readouts agree in space and across evolutionary time. MALDI-TOF chromophore identification by exact mass is in progress to discriminate the three candidates. Co-registered Raman and 2P-FLIM thus read out a major evolutionary transition entirely label-free, opening a non-perturbing photonic route to biomarkers of cooperative multicellularity in living cells.

# Interrogation of the urethral tissues by multimodal optical and acoustic approaches

**E. Kiseleva[1], O. Streltsova[1], A. Sovetsky[2], S. Zubova[1], M. Novgorodskaya[1,3], A. Kuyarov[1], A. Potapov[1], V. Vlasov[1], Y. Korzhimanova[1], A. Matveyev[2], L. Matveyev[2], V. Zaitsev[2], E. Gubarkova[1], G. Gelikonov[2], N. Gladkova[1]**

*1- Privolzhsky Research Medical University, 603005, 10/1, Minin and Pozharsky Square, Nizhny Novgorod, Russia;*
*2- A.V. Gaponov-Grekhov Institute of Applied Physics of the Russian Academy of Sciences, 603155, 46, Ulyanova str., Nizhny Novgorod, Russia;*
*3- Lobachevsky State University of Nizhny Novgorod, 603022, 23, Gagarin Avenue, Nizhny Novgorod, Russia.*

*kiseleva84@gmail.com*

It is believed that the criterion for primary urethral pain syndrome (PUPS) is the absence of any structural changes in the urethra. However, using visual assessment of cross-polarization optical coherence tomography (CP OCT) images we previously demonstrated that in PUPS, both inflammation and fibrosis can be observed in the urethral tissues, although other clinical methods did not detect these changes [1].

The aim of this study was to investigate structural changes of urethra and its blood flow in patients with PUPS using multiparametric analysis of CP OCT images and transvaginal ultrasound (TVUS) with Doppler and elastography functions.

Materials and methods. A total of 69 women were examined using TVUS: 45 with PUPS and 24 with norm. The Philips EPIQ5 system was used equipped with a highly sensitive transvaginal sensor with frequency of 6.5 and 7 MHz. The OCT study included 35 patients: 25 with PUPS and 10 with norm. Time-domain "OCT-1300U" device (Biomedtech LLC, Russia) using an endoscopic probe (outer diameter 2.7 mm), which was placed in contact with the surface of the examined tissue of the urethra was used. Multiparametric analysis of CP OCT images based on calculation of the attenuation coefficient and speckle contrast. The main examined parameters were: epithelial thickness, thickness of the upper part of the lamina propria (UpLP), maximum value of depolarization ratio (Max DR), and blood vessel density (VD).

Results. It is shown that in PUPS, calculated parameters are changed relative to normal values. An increase in the thickness of the epithelium and the upper part of the LP is observed; the Max DR value increases by 11.3 times compared to norm, which indicates fibrosis and proliferation of connective tissue; moreover, in PUPS the VD values reduced by 2.6 times. In patients with PUPS the urethra retained the shape of a straight tube in only 60% of cases, with a lumen expansion of up to 6.6±0.8 mm. In the 40% of cases the urethra was either funnel-shaped or flask-shaped. The average urethral wall thickness in patients with PUPS was 3.3±1.2 mm, exceeding the normal value of 2.7±0.4 mm ($p=0.111$). In patients with PUPS, Doppler-US revealed a statistically significant increase in periurethral blood vessel RI compared to the normal value: 0.83±0.06 versus 0.68±0.04 ($p<0.0001$). Ultrasound elastography revealed stiffening of the urethral wall tissue in patients with PUPS.

Conclusion. Using multiparametric analysis of CP OCT images and TVUS data helps to identify pathological tissue changes in patients with PUPS.

Acknowledgements. The study was supported by the Russian Science Foundation, project No. 25-15-00530.

[1] E. Kiseleva, A. Moiseev, A. Kuyarov, M. Molvi, G. Gelikonov, A. Maslennikova and O. Streltsova, In vivo assessment of structural changes of the urethra in lower urinary tract disease using cross-polarization optical coherence tomography, J. Innov. Opt. Health Sci., vol.13, p. 2050024, (2020).

# Potential of Terahertz Sensing for diagnostics

**O. Cherkasova**[1,2,3]

*1- Institute of Automation and Electrometry, Siberian Branch of the Russian Academy of Sciences, 1 Academician Koptyug Ave., 630090 Novosibirsk, Russia*
*2- National Research Centre "Kurchatov Institute", 123182 Moscow, Russia*
*3- Institute of Laser Physics, Siberian Branch of the Russian Academy of Sciences, 630090 Novosibirsk, Russia*

*o.p.cherkasova@gmail.com*

Terahertz (THz) spectroscopy has shown significant potential for diagnostics due to its unique features, such as the non-invasive and label-free identification of biological molecules [1]. Molecular biomarkers are released into the blood and other body fluids at an early stage of disease development [2]. Its diagnosis using THz spectroscopy has already been demonstrated [3, 4]. Implementing plasmonic metamaterials or metasurfaces can improve the spectroscopy's sensitivity to biomarkers [5]. Metasurfaces are artificially structured planar metal-dielectric media composed of unit cells that are sized at subwavelength scales. The spectral response of THz metasurfaces is determined by the induced currents that depend on the geometry of the unit cells [6]. Terahertz sensors can be divided into two general types. The first are sensitive to the dielectric environment and change their spectral response in the presence of a certain volume of analyte. The second type resonantly interacts with the vibrational mode of the substance being detected and thus exhibits high selectivity and sensitivity to single molecules. It was these last sensors that we paid close attention to.

Often, the unit cell in the form of a split ring (split-ring resonator, SRR) and its modifications are used in the design of THz sensors [5, 6]. The geometry is convenient for modeling and allows for the easy tuning of plasmonic and magnetic resonances to the required frequencies corresponding to the molecular modes. In accordance with this approach, a sensor was developed consisting of square elements made of aluminum on a silicon substrate. The sensor exhibits selective sensitivity to the steroid hormone cortisol at a resonance frequency of 1.52 THz and can be used for its quantitative assay in the nanomol range [7].

Another approach to microresonator design can be based on a dipole antenna with a nanogap. The dipole configuration (strip) exhibits only electrical resonance, but the nanoscale gap between the antennas allows for greater localization of the electric field and, consequently, improved interaction efficiency with the analyte. According to this approach, we proposed a nanoantenna-based sensor optimized for the resonant frequency of 1.337 THz for detecting the oncology biomarker L-2-Hydroxyglutarate [8]. It represents an array of gold antennas with 100-nm gaps supported by Si substrate with $SiO_2$ nano sublayer. The sensor demonstrates the sensitivity of picomoles, which is sufficient for detection in biosamples. The report will discuss key ways to increase the sensitivity of THz sensors.

The author acknowledges the Shared Equipment Center "Spectroscopy and Optics" of the IA&E SB RAS and the Shared Research Center "VTAN" of the Novosibirsk State University.

This work was performed partly within the State Assignment of IA&E SB RAS (FWNG-2024-0025), ILP SB RAS (FWGU-2026-0005), NRC "Kurchatov Institute" (in terms of THz sensor design).

[1] O.A. Smolyanskaya, N.V. Chernomyrdin, A.A. Konovko et al, Terahertz biophotonics as a tool for studies of dielectric and spectral properties of biological tissues and liquids, Progress in Quantum Electronics, vol. 62, 1-77 (2018).
[2] D. Vrazhnov, A. Mankova, E. Stupak et al., Discovering Glioma Tissue through Its Biomarkers' Detection in Blood by Raman Spectroscopy and Machine Learning, Pharmaceutics, vol. 15, p. 203 (2023).
[3] M.R. Konnikova, O.P. Cherkasova, M.M. Nazarov, et al., Malignant and benign thyroid nodule differentiation through the analysis of blood plasma with terahertz spectroscopy, Biomed. Opt. Express, vol. 12, pp. 1020-1035 (2021).
[4] O. Cherkasova, D. Vrazhnov, A. Knyazkova, et al., Terahertz Time-Domain Spectroscopy of Glioma Patient Blood Plasma: Diagnosis and Treatment, Appl. Sci., vol. 13, pp. 5434 (2023).
[5] O. Cherkasova, Y. Peng, M. Konnikova, et al., Diagnosis of Glioma Molecular Markers by Terahertz Technologies, Photonics, vol. 8(1), p. 22 (2021).
[6] H. Wang, F. Zheng, Y. Xu et al. Recent progress in terahertz biosensors based on artificial electromagnetic subwavelength structure, TrAC. Trends Anal. Chem., vol. 158, pp. 116888 (2023).
[7] D.S. Ustiantseva, M.R. Konnikova, A.R. Shevchenko et al., Terahertz sensor for cortisol detection, Izvestiya Vuzov. Radiofizika, vol. 68, N12, pp. 1059-1071 (2025).
[8] O.P. Cherkasova, S.A. Kuznetsov, A.A. Rybak et al., Terahertz nanoantenna sensor for detection of biomarker L-2-Hydroxyglutarate, design optimization and testing, Opt. Quantum Electron., vol. 57, pp. 340 (1-14) (2025).

# Complementary optical and magnetic detection of cancer and cardiovascular biomarkers: from binding kinetics to non-invasive picogram-level quantification in saliva

**P.I. Nikitin[1], A.V. Orlov[1], N.A. Belyakov[1,2], V.V. Volkov[1,3], A.M. Skirda[1,2], J.A. Malkerov[1,3], B.G. Gorshkov[1]**

*1- Prokhorov General Physics Institute of the Russian Academy of Sciences, 38 Vavilov St, Moscow, Russia*
*2- Moscow Center for Advanced Studies, Moscow, Kulakova str. 20, Moscow, Russia*
*3- National Research Nuclear University MEPhI, 31 Kashirskoe shosse, Moscow, Russia*

*nikitin@kapella.gpi.ru*

For immunochemical in vitro diagnostics, saliva is an attractive biofluid because sample collection is non-invasive, patient-friendly, and associated with minimal risk. However, the concentrations of many informative protein biomarkers of cancer, heart diseases and small-molecules, are typically three orders of magnitude lower in saliva than in blood, so highly sensitive methods are still needed for analysis [1,2]. We present a complementary biosensing strategy that couples optical label-free interaction analysis with ultrasensitive magnetic detection, establishing a continuous pathway from the characterization of molecular recognition kinetics to picogram-level biomarker quantification.

Label-free spectral-phase interferometry (SPI) is employed for real-time analysis of antibody interactions with surface-immobilized antigens and bioconjugates [3,4]. SPI provides association and dissociation rate constants, as well as equilibrium binding parameters governing molecular recognition. These measurements enable the rational selection of bioconjugates, antibody pairs, and surface chemistries prior to assay development. We show that these kinetic data can be used not only to identify the most stable recognition elements, but also to engineer adaptive sensing interfaces whose analytical characteristics (the balance between detection limit, sensitivity and dynamic range) are reconfigured in situ, combining sub-picogram detection limits with dynamic ranges of up to ten orders of magnitude.

A central concept of this work is that practical assays operate far from equilibrium: the binding observed under controlled SPI flow does not translate directly into the diffusion-limited, time-constrained lateral flow rapid test. Guided by the measured kinetics, we therefore implement magnetic labels readout by magnetic particle quantification (MPQ) method, which exploits the nonlinear magnetization of labels [5,6]. In contrast to optical readout, MPQ interrogates the entire volume of the lateral flow membrane rather than only its surface, enhancing both sensitivity and dynamic range.

To overcome mass-transport limitations inherent to non-equilibrium binding, anisotropic magnetic nanochains are actuated using a low-frequency rotating magnetic field [6]. Functioning as nanoscale stirrers, the rotating nanochains accelerate antigen–antibody association kinetics and promote cooperative target capture within the detection zone while simultaneously reducing nonspecific background signals. This magnetically actuated, volumetrically detected assay format achieves picogram-level sensitivity across a broad dynamic range in a single rapid analytical step. The versatility of the approach is demonstrated using several cancer and cardiovascular biomarkers. For the cardio biomarker heart-type fatty acid-binding protein (H-FABP), the rotating-nanochain assay enables picogram-level detection within 6 minutes [6]. For folic acid, a small-molecule ligand associated with folate-receptor-positive cancers, the optical assay achieves detection limits of tens of pg/mL range over six orders of magnitude, while the magnetic assay enables direct quantification in artificial saliva, supporting the development of non-invasive diagnostic testing. The results establish a unified framework in which label-free optical kinetic characterization guides the development of motion-enhanced magnetic assays, providing a route toward rapid and non-invasive point-of-care diagnostics.

The research was funded by Russian Science Foundation, grant No 25-12-00373.

[1] A. Kudriavtseva et al., Microchimica Acta, vol. 192, p. 831 (2025).
[2] S. Jaric et al., Microchemical Journal, vol. 196, p. 109611 (2024).
[3] P. I. Nikitin et al., Quantum Electronics, vol.30, pp. 1099-1104 (2000).
[4] A. V. Orlov et al., Doklady Physics, vol. 67, pp. 193-196 (2022).
[5] A. M. Skirda et al., Biosensors, vol. 14, p. 607 (2024).
[6] J. A. Malkerov et al., Biosensors and Bioelectronics, vol. 297, p. 118346 (2026).

# Neurolymphaphotonics for revolutionary technologies of preventive medicine

**O. Semyachkina-Glushkovskaya**

*Saratov State University, Scientific Medical Center, Laboratory "Smart Sleep", Saratov, Russia*

*glushkovskaya@mail.ru*

Pharmacological treatment of brain diseases is hampered by the blood-brain barrier, which prevents the vast majority of drugs from reaching brain tissue. For this reason, the pharmaceutical industry is reluctant to invest in the development of new neurotropic drugs. This places a premium on the development of neuro-lymphaphotonics, which focuses on developing promising non-drug approaches to modulating the function of the meningeal lymphatic vessels (MLVs). MLVs play a key role in the removal of toxins and metabolites from the brain, as well as in the regulation of brain immunity. Because MLVs are located on the brain's surface, light penetrating the skull easily reaches the MLVs and influences their function. Thus, MLVs are ideal targets for photobiomodulation (PBM). Pioneering animal and clinical research has shown that PBM of MLVs is a promising approach for the treatment of many brain diseases, including Alzheimer's, Parkinson's, tumors, intracranial hemorrhages, and age-related or metabolic changes in neural tissue. Given that PBM is non-invasive and safe, and offers commercial advantages (portability, accessibility, ease of use, and low cost), neurolymphaphotonics offers promising prospects for the development of advanced technologies for effective non-invasive treatment of brain diseases[1,2].

This research was supported by the grant from the Russian Science Foundation 23-75-30001.

[1] Liu S, Semyachkina-Glushkovskaya O, Yu T et al. Neuro-lymphaphotonics opens new horizons of the future technologies for the therapy of brain diseases. Theranostics 16(2):776-793 (2026).
[2] Dong-Yu Li, Shao-Jun Liu, Ting-Ting Yu et al. Photostimulation of brain lymphatics in male newborn and adult rodents for therapy of intraventricular hemorrhage. Nat. Commun. 14, 6104 (2023).

# Laser measurement of the anomalous dispersion of dura mater

**M. Pinheiro[1,2], M. Carvalho[1,2], V. Tuchin[3,4], L. Oliveira[1,5]**

*1- Institute for Systems and Computer Engineering, Technology and Science (INESCTEC), Campus da FEUP, Rua Dr. Roberto Frias, 4200-465 Porto, Portugal*
*2- Department of Electrical and Computer Engineering, Faculty of Engineering of Porto University (FEUP), Rua Dr. Roberto Frias, 4200-465 Porto, Portugal*
*3- Institute of Physics and Science Medical Center, Saratov State University, 83 Astrakhanskaya str., Saratov 410012, Russian Federation*
*4- Laboratory of Laser Diagnostics of Technical and Living Systems, Institute of Precision Mechanics and Control of the FRC "Saratov Scientific Centre of the Russian Academy of Sciences," 24 Rabochaya, Saratov 410028, Russian Federation*
*5- Physics Department, School of Engineering, Polytechnic of Porto, Rua Dr. António Bernardino de Almeida n° 431, 4229-015 Porto, Portugal*

*lmo@isep.ipp.pt*

The development and optimization of in vivo light-based diagnostic and treatment procedures requires knowledge on the broadband optical properties of tissues [1]. One of those optical properties is the tissue dispersion, which when evaluated in its anomalous version contains information relative to the tissue components and their correspondent contents. The evaluation of the contents of certain tissue components, such as blood, lipids, or proteins may be useful to proceed with a diagnosis and identify certain pathologies [2,3]. In this work, six low-power lasers (5 mW) were used to measure the refractive index of the pig's dura mater at discrete wavelengths between 405 and 850 nm. Such data was fitted with a curve described by the Conrady dispersion relation [4]. By measuring the absorbance spectrum of the dura mater between 200 and 1000 nm, calculations were performed with the Kramers-Kronig relations [4], so that the anomalous dispersion could be estimated for this tissue. The calculated anomalous dispersion presented a good matching with the Conrady dispersion curve that was obtained from experimental refractive index measurements, allowing further to identify the components in the dura mater through their characteristic absorption bands. By obtaining such anomalous dispersion in such a broad spectral range, it will become possible to select the appropriate wavelengths to be used for diagnostic or treatment procedures to be applied to the dura mater.

[1] I.S. Martins, H.F. Silva, E.N. Lazareva, N.V. Chernomyrdin, K.I. Zaytsev, L.M. Oliveira and V.V. Tuchin, Measurement of tissue optical properties in a wide spectral range: a review [invited], Biomedical Optics Express, vol. 14, pp. 249-298, (2023).
[2] E.N. Lazareva, L. Oliveira, I.Yu. Yanina, N.V. Chernomyrdin, G.R. Musina, D.K. Tuchina, A.N. Bashkatov, K.I. Zaytsev and V.V. Tuchin, Handbook of Tissue Optical Clearing (CRC Press), Chapter 7, (2022).
[3] M.R. Pinheiro, L.E. Fernandes, I.C. Carneiro, S.D. Carvalho, R.M. Henrique, V.V. Tuchin, H.P. Oliveira and L.M. Oliveira, Optimized reconstruction of the absorption spectra of kidney tissues from the spectra of tissue components using the least squares method, J. Biophotonics, vol. 18, pp. e202300466, (2025).
[4] M.R. Pinheiro, M.I. Carvalho and L.M. Oliveira, Tutorial on the use of photon diffusion approximation for fast calculation of tissue optical properties, J. Biophotonics, vol. 18, e202400257, (2025).

# Multimodal OCT-based Approaches for Diagnosis in Critical Care and Oncology

**A. Plekhanov[1], E. Kiseleva[1], E. Gubarkova[1], P. Shilyagin[2], A. Sovetsky[2], I. Ryzhkov[3], S. Panfilov[4], D. Vorontsov[4], V. Zagainov[1,4], S. Gazhva[1], G. Grechkanev[1], V. Vlasov[1], L. Matveev[2], A. Potapov[1], M. Sirotkina[1], A. Matveyev[2], S. Gamayunov[4], E. Grigoriev[5], E. Zagaynova[6], G. Gelikonov[2], V. Zaitsev[2], N. Gladkova[1]**

*1- Privolzhsky Research Medical University, 10/1 Minin and Pozharsky sq., 603950 Nizhny Novgorod, Russia*
*2- A.V. Gaponov-Grekhov Institute of Applied Physics RAS, 46 Ulyanova st., 603950 Nizhny Novgorod, Russia*
*3- V.A. Negovsky Research Institute of General Reanimatology, Federal Research and Clinical Center of Intensive Care Medicine and Rehabilitology, 25/2 Petrovka st., 107031 Moscow, Russia*
*4- Nizhny Novgorod Regional Oncological Hospital, 11/1 Delovaya st., 603093 Nizhny Novgorod, Russia*
*5- Research Institute for Complex Issues of Cardiovascular Diseases, 6 Barbarash b., 650002 Kemerovo, Russia*
*6- Lopukhin Federal Research and Clinical Center of Physical-Chemical Medicine of Federal Medical Biological Agency, 1/3 Malaya Pirogovskaya st., 119435 Moscow, Russia*

*strike_gor@mail.ru*

This work demonstrates that multimodal optical coherence tomography (MM OCT) enables real-time tracking and monitoring of sublingual microcirculation as a marker of organ failure in critical conditions, while also accurately distinguishing precancerous/malignant lesions across various organs based on cross-polarization and elastic tissue characteristics. The resulting OCT biomarkers provide clinicians with objective metrics for decision-making in both intensive care and oncology settings.

Through innovative investigation of sublingual microvascular beds, we validate OCT-angiography (OCT-A) as a robust method for tracking patient status during surgery and in the postoperative period. We demonstrated the capability of OCT-A for imaging oral mucosa vessels and described the system adapted for this purpose. The technique provides continuous, real-time assessment of sublingual microcirculation, allowing estimation of key parameters (perfused vessel density and signal intensity distributions) that serve as indicators of compromised internal organ perfusion and progression to multiple organ dysfunction [1]. We have developed and validated a clinical OCT-A protocol for monitoring sublingual microcirculatory changes in patients in the operating room and intensive care unit. In practice, we were able to identify vasopressor-induced vasoconstriction and quantify a marked rise in sublingual microcirculation following a lung recruitment maneuver; moreover, a decline in sublingual microcirculation was clearly linked to worsening organ failure scores [2].

In recent years, OCT approaches have begun to demonstrate effectiveness in diagnosing and monitoring treatment response for various oncologic pathologies [3]. We show that microstructural assessment via cross-polarization OCT (CP-OCT) combined with stiffness mapping by compression OCT-elastography (C-OCE) yields strong diagnostic accuracy for identifying premalignant and malignant lesions across multiple sites, including the breast, prostate, colon, endometrium, and head & neck [4,5]. Analysis of the signal attenuation coefficient, speckle contrast coefficient, depolarization ratio, and nonlinear elasticity characteristics of the studied tissues enabled the identification of malignant tissue areas and the detection of metastatic lesions in sentinel lymph nodes by MM OCT. Consequently, the MM OCT-derived biomarkers introduced in this work represent powerful, actionable instruments to refine clinical judgment in both intensive care and oncologic practice.

The study was funded by the Russian Science Foundation, grant # 25-75-10160, https://rscf.ru/project/25-75-10160/

[1] A.A. Plekhanov et al, Microcirculation in critical care: current pathophysiology and place in the strategy of monitoring critical conditions as a monitoring technology, Complex Issues of Cardiovascular Diseases, 14(5), pp. 139-159, (2025).
[2] A.A. Plekhanov et al, Optical Coherence Tomography Angiography for Monitoring Sublingual Microcirculatory Changes: a Prospective Tool for Investigation of Tissue Hypoperfusion in Critical Care Medicine, Journal of Biomedical Photonics & Engineering, (2026).
[3] R. Leitgeb et al, Enhanced medical diagnosis for dOCTors: a perspective of optical coherence tomography, Journal of Biomedical Optics, 26(10), p. 100601, (2021).
[4] A.A. Plekhanov et al, Compression OCT-elastography combined with speckle-contrast analysis as an approach to the morphological assessment of breast cancer tissue, Biomedical Optics Express, 14(6), pp. 3037-3056, (2023).
[5] A.A. Plekhanov et al, Quantitative Assessment of Polarization and Elastic Properties of Endometrial Tissue for Precancer/Cancer Diagnostics Using Multimodal Optical Coherence Tomography, Diagnostics, 14(19), p. 2131, (2024).

# Dynamic speckle diagnostics of biological and technical objects: new objects and new results

**A.P. Vladimirov** [1,2,3]

*E.S. Gorkunov Institute of Engineering Science of the Ural Branch of the Russian Academy of Sciences, 34 Komsomolskaya str., Yekaterinburg, 620219, Russia*
*Ural Federal University named after B.N. Yeltsin, 19 Mira str., Yekaterinburg, 620002, Russia*
*FSRIVI « Virome» of Rospotrebnadzor, 23 Letnaya str., Yekaterinburg, 620039, Russia*

*vap52@bk.ru*

Previously, a new mechano-optical effect and a new shearography developed on its basis were successfully tested to study deformations occurring in turbulent flow, in living cells, and during high-cycle fatigue of solids [1,2]. The method is two orders of magnitude more sensitive and spatially resolved than existing optical methods for determining deformations, and for the first time makes it possible to quantify turbulent flows in real time. The disadvantage of the last two studies mentioned above was, respectively, the study of relatively slow intracellular processes and the identification of fatigue mechanisms of only three materials. Previously, the processes occurring in a monolayer of cultured cells for a time of about 10 seconds – a day were studied. The accumulation of fatigue damage in plexiglass, aluminum alloy and steel was studied. The aim of the new work was to study the contribution to cell activity of processes occurring over a period of about 1ms – 1s and to identify the mechanism of fatigue degradation of two composites: polymer–metal and fabric-polymer. To achieve these goals, optical systems have been upgraded: a high-speed camera with a maximum frame rate of about 1kHz and new software have appeared, and the field of view under study has been expanded. The recorded parameters were the digital value of the radiation intensity in camera pixels and the normalized temporal autocorrelation function $\eta(\tau)$ of this intensity, found by averaging over an image fragment. The parameter characterizing the activity of a group of cells, or a section of an individual cell, was the standard deviation $\sigma$ and relaxation time $\tau_0$ of the optical path difference $\Delta u$ of two waves probing cells at a distance of about 2 microns. In the composites, the components of the relative displacement vector $\Delta u$ of two surface points located at a distance of 2 microns were determined.

It is shown that as the frame input frequency increases from 0.1 Hz to 100 Hz, the value of $\sigma$ found for the same cells decreases. At a frequency of 1kHz, in a single cell, according to the distribution of the value of $\eta$, it was found that it has only a few active areas in which processes are taking place at different speeds. The presence of pulses of magnitude $\eta$ with duration of about 1ms seems to indicate the existence of faster-flowing processes. It is shown that the mechanisms of fatigue degradation of the two polymers are similar to those of damage in plexiglass, aluminum alloy, and steel. It is concluded that there is a single mechanism of degradation of materials under low-, high-, and giga-cycle fatigue. Based on the data obtained, it is proposed to create diagnostic and control methods of a new generation. The first applications of the method and the directions of further research are discussed.

The work was supported by grant of the Russian Science Foundation, No. 25-25-00517

[1] A. P. Vladimirov, New shearograpy: theory, experiments, and some applications, Diagnostics, Resource and Mechanics of materials and structures, Issue 6, pp. 268–293, (2024).
[2] A. P. Vladimirov, Dynamic speckle diagnostics of irreversible processes in biological and technical objects, Abstracts of the 31th International Conference on Advanced Laser Technologies – 2024, p.179, (2024).

# Optical Coherence Elastography and Brillouin Spectroscopy for Tissue Biomechanics

**K. Larin**

*University of Houston, Houston, USA*

*klarin@uh.edu*

Biomechanical properties of tissues play a critical role not only in disease development and progression but also in normal function and development. Several clinical conditions, such as Neural Tube Defects and keratoconus, presbyopia, and glaucoma of the eye, significantly alter these properties, making biomechanical assessment essential for understanding disease mechanisms and guiding clinical management. This talk will present recent advances in Optical Coherence Elastography and Brillouin Spectroscopy for noninvasive biomechanical evaluation of different tissues and cells. I will review progress in noncontact optical coherence elastography (OCE) – including quasi-static, dynamic, and reverberant approaches – and Brillouin microscopy for characterizing tissue stiffness. These methods enable high-resolution, depth-resolved measurements from the cornea and sclera to posterior structures, offering insights into the entire eye globe. I will demonstrate that OCE and Brillouin-based techniques represent a paradigm shift in tissue diagnostics, enabling noninvasive, quantitative evaluation of its biomechanics. Future directions include integration into clinical workflows and longitudinal studies to validate their predictive value.

# Real-time determination of substances penetration and associated skin dehydration using OCT-based osmotic-strain imaging

**A.A. Sovetsky[1], K.S. Petrova[2], M.A. Kulagina[1,2], A.L. Matveyev[1], L.A. Matveev[1], I.E. Pogodin[3], P.V. Kulagin[1,2], V.Y. Zaitsev[1]**

*1- A.V. Gaphonov-Grekhov Institute of Applied Physics, RAS, Nizhny Novgorod, Russia*
*2- N.I. Lobachevsky Research State University, Nizhny Novgorod, Russia*
*3- Institute of Traumatology and Orthopedics, Nizhny Novgorod, Russia*

*vyuzai@ipfran.ru*

In the reported study we utilize the recently proposed OCT-based approach to real-time visualization of diffusional fronts formed during the penetration of substances in the bulk of biological tissues, as well as the diffusional fronts of water outflow which may develop simultaneously with the front of the penetrating substance [1]. Unlike previous variants of OCT-based methods intended for studying diffusion processes, the principle of the applied method is elastographic; namely, we apply OCT for visualization of osmotic strains induced in biological tissues by penetrating liquids. An important advantage of the method is that it requires the access to the studied sample/region from one side only, which significantly simplifies the experimental realization. At the same time, since the strain visualization is based on the analysis of interframe phase variations, realization of *in vivo* measurements is challenging because high stabilization of the studied living tissue is required. In view of this presently the method shows the best operability using motionless excised samples.

The performed preliminary tests [1,2] of the method demonstrated good agreement of the results obtained using porcine cartilaginous samples and samples of porcine skin. The latter is often considered as quite an adequate model of human skin in biomedical research. However, similar tests with post-amputation samples of human skin demonstrated that their permeability is drastically lower than that of porcine skin, despite the fact that the latter mechanically is much more solid than human skin. Since for excised skin samples, the penetrating solution (e.g. water solution of glycerol) can readily be applied to any side of the sample, it was found that, when the glycerol solution was applied to the inner side of human skin samples, they demonstrated the permeability quite comparable with that for porcine samples. This indicates that the revealed strongly enhanced barrier function of human skin is due to very low permeability of the thin outer layer of stratum corneum. It was then directly verified that mechanical elimination of a few tens micrometers of the stratum corneum (50-80% of the total thickness) leads to drastic increase in permeability of human skin samples from the outer side. These results open promising prospects for detailed comparative studies of permeability of human skin for various substances, as well as for developing methods of the permeability enhancement, which is important for improvement of transdermal delivery of various medications and cosmetics.

The study was supported by RSF grant No 22-12-295-П.

[1] Y.M. Alexandrovskaya, et al "Visualizing Kinetics of Diffusional Penetration in Tissues Using OCT-Based Strain Imaging." *Advanced Drug Delivery Reviews* 217, 115484 (2025).
[2] V.Y. Zaitsev, et al. "Optical Coherence Elastography — A Novel Non-Invasive Optical Method for Real-Time Determination of Substances Penetration and Associated Skin Dehydration." *Cosmetics* 12,: 183(1-25) (2025).

# Multiscale Optoacoustic Tomography: from 3D Scanning Angiography to 5D Functional Real-Time Diagnostics

**P.V. Subochev**

*Laboratory of Ultrasound and Optoacoustic Diagnostics, Division of Radiophysics Methods in Medicine, A.V. Gaponov-Grekhov Institute of Applied Physics RAS, Nizhny Novgorod, Russia*

*pavel.subochev@gmail.com*

The synergy of pulsed laser excitation and ultrawideband acoustic detection [1] has established optoacoustic (photoacoustic) imaging as a scalable modality for biomedical diagnostics, combining optical absorption contrast with ultrasonic resolution. Yet clinical and preclinical translation still requires balancing imaging depth, spatial resolution, sensitivity, and the capability to capture rapid volumetric dynamics. In this invited talk, we present recent advances in multiscale optoacoustic technologies designed to address these constraints. First, we discuss piezopolymer-based (PVDF/PVDF-TrFE) acoustic detectors, including spherically focused ring-segment sensors optimized for cylindrical-wave detection, which extend the depth-of-field in optical-resolution optoacoustic angiography while preserving sensitivity [2]. We then consider calibrated detection and local fluence estimation as a route toward quantitative optical-resolution optoacoustic angiography [3]. Second, we demonstrate the transition from high-resolution structural 3D imaging to real-time 5D functional tomography (3D spatial + spectral + temporal) using an ultrawideband, high-density polymer-based spherical array integrated with multi-wavelength laser illumination [1]. This platform enables deep-tissue compositional mapping and simultaneous in vivo assessment of hemoglobin dynamics and oxygenation together with water, lipid, and collagen distributions. Finally, we highlight applications for monitoring tumor angiogenesis and therapy-induced vascular remodeling, including axitinib-induced changes in tumor vascularization and oxygenation assessed by combined optoacoustic angiography and diffuse optical spectroscopy [4]. The emphasis is placed on how detector bandwidth, sensitivity, and geometry define the practical route from single-element microscopy to real-time functional tomography.

Acknowledgment. The author acknowledges support from the Russian Science Foundation (RSF), grant No. 25-45-20023.

[1] P. V. Subochev, X. L. Dean-Ben, Z. Chen, M. B. Prudnikov, V. A. Vorobev, et al., "Ultrawideband high density polymer-based spherical array for real-time functional optoacoustic micro-angiography," Light Sci. Appl. 14, 239 (2025).
[2] A. Kurnikov, M. Prudnikov, D. Voitovich, A. Glyavina, A. Orlova, M. Sirotkina, et al., "Ring-segment piezopolymer sensor optimized for cylindrical-wave detection in optical-resolution optoacoustic angiography with extended imaging depth," Biomed. Opt. Express 16(10), 3988-4002 (2025).
[3] D. Voitovich, A. Kurnikov, A. Orlova, A. Petushkov, L. Shimolina, A. Komarova, et al., "Local laser fluence estimation in optical resolution optoacoustic angiography employing calibrated ultrasound detector," Photoacoustics 44, 100734 (2025).
[4] A. Orlova, K. Akhmedzhanova, A. Glyavina, A. Kurnikov, D. Khochenkov, Y. Khochenkova, et al., "Assessing axitinib-induced differential responses in tumor vascularization and oxygenation with combined optoacoustic angiography and diffuse optical spectroscopy," Neoplasia 76, 101303 (2026).

# Optoacoustic Methods for Vascular Imaging in Biomedical Applications

**A. Orlova[1], A. Glyavina[1], A. Kurnikov[1], D. Khochenkov[2], Yu. Khochenkova[2], K. Akhmedzhanova[1], K. Kim[1], A. Maslennikova[1,3], S. Nemirova[1,3], I. Turchin[1], P. Subochev[1]**

*1- A.V. Gaponov-Grekhov Institute of Applied Physics of RAS, 46 Ulyanov Str., Nizhny Novgorod, Russia*
*2- N.N. Blokhin National Medical Research Center of Oncology, 23 Kashirskoe highway, Moscow, Russia*
*3- Privolzhsky Research Medical University, 10/1 Minina i Pozharskogo Sq., Nizhny Novgorod, Russia*

*ag.orlova@mail.ru*

Assessment of vascular architecture and function provides important data for both disease diagnosis and evaluation of treatment efficacy. Hybrid optoacoustic (OA) imaging techniques provide label-free angiographic contrast at optical penetration depths while preserving ultrasonic spatial resolution [1]. Here, we present applications of OA systems equipped with wideband PVDF detectors [2] for the investigation of vascular characteristics of experimental tumors during growth and following treatment, as well as for the assessment of vascular alterations in human pathologies.

A multispectral optoacoustic tomography system incorporating a 256-element ultrasonic transducer array was used to compare experimental tumors growing at different implantation sites. OA imaging revealed higher hemoglobin content and more pronounced hypoxia in orthotopic tumor models compared to subcutaneous tumors.

Raster-scan OA angiography at 532 nm with a single-element detector [3] was employed to evaluate therapy-induced changes in tumor vascular architecture. Treatment with the antiangiogenic agent axitinib resulted in reduced vascular density and vessel diameter [4]. Radiation therapy also induced changes in vascular architecture, including reductions in vessel fraction and vessel size [5]. The clinical applicability of raster-scan OA angiography was demonstrated in patients with post-thrombotic syndrome of the foot [6]. In these patients, OA imaging revealed increased blood volume, vessel diameter, and vascular tortuosity relative to normal tissues.

These findings highlight the potential of optoacoustic imaging for *in vivo* evaluation of vascular structure and function in normal and diseased tissues, as well as for monitoring angiogenesis and vascular remodeling during therapeutic intervention.

The work was supported by the Russian Science Foundation (project 25-15-00238).

[1] N.T. Huynh, E. Zhang, O. Francies, F. Kuklis, T. Allen, J. Zhu, O. Abeyakoon, F. Lucka, M. Betcke, J. Jaros, S. Arridge, B. Cox, A. A. Plumb, P. Beard, A fast all-optical 3D photoacoustic scanner for clinical vascular imaging, Nat. Biomed. Eng., 9, 638-655 (2025).
[2] P.V. Subochev, X.L. Dean-Ben, Z. Chen, M.B. Prudnikov, V.A. Vorobev, A.A. Kurnikov, A.G Orlova, A.S. Postnikova, A.V. Kharitonov, M.D. Proyavin, R.I. Ovsyannikov, A.G. Sanin, M.Y. Kirillin, F.M. de Espinosa, I.V. Turchin, D. Razansky, Ultrawideband high density polymer-based spherical array for real-time functional optoacoustic micro-angiography, Light Sci Appl., 14, 239 (2025).
[3] A. Kurnikov, G. Volkov, A. Orlova, A. Kovalchuk, Y. Khochenkova, D. Razansky, P. Subochev, Fisheye piezo polymer detector for scanning optoacoustic angiography of experimental neoplasms, Photoacoustics, 31, 100507 (2023).
[4] A. Orlova, K. Akhmedzhanova, A. Glyavina, A. Kurnikov, D. Khochenkov, Y. Khochenkova, A. Korobov, A. Volovetskiy, A. Yudintsev, A. Nerush, A. Maslennikova, V. Vodeneev, I. Turchin, W. Liu, D. Razansky, P. Subochev, Assessing axitinib-induced differential responses in tumor vascularization and oxygenation with combined optoacoustic angiography and diffuse optical spectroscopy, Neoplasia 76, 101303 (2026).
[5] A. Orlova, K. Pavlova, A. Kurnikov, A. Maslennikova, M. Myagcheva, E. Zakharov, D. Skamnitskiy, V. Perekatova, A. Khilov, A. Kovalchuk, A. Moiseev, I. Turchin, D. Razansky, P. Subochev, Noninvasive optoacoustic microangiography reveals dose and size dependency of radiation-induced deep tumor vasculature remodeling, Neoplasia, 26, 100778 (2022).
[6] S. Nemirova, A. Orlova, A. Kurnikov, Y. Litvinova, V. Kazakov, I. Ayvazyan, Y.H. Liu, D. Razansky, P. Subochev, Scanning optoacoustic angiography for assessing structural and functional alterations in superficial vasculature of patients with post-thrombotic syndrome: A pilot study, Photoacoustics, 38, 100616, 2024.

# Optoacoustic and fluorescence lifetime bimodal visualization based on indocyanine green in phantoms

**T. Torokhov[1,2], S. Perkov[1,3], M. Mokrousov[1], E. Prikhozhdenko[4], M. Shlykov[5], E. Maksimov[6], I. Sergeev[1], V. Shcheslavskiy[7,8], D. Gorin[1]**

*1 - Skolkovo Institute of Science and Technology, Bolshoy blvd. 30, Moscow 121205, Russia*
*2 - Prokhorov General Physics Institute, Vavilova str. 38, Moscow, 119991, Russia*
*3 - Central University, Gasheka str., 7, Moscow, 123056, Russia*
*4 - Moscow Institute of Physics and Technology, Dolgoprudny, 141701, Russia*
*5 - Baikov Institute of Metallurgy and Materials Science, Leninsky Prospekt, 49, Moscow, 119334, Russia*
*6 - Department of Biophysics, School of Biology, Moscow State University, Leninskie Gory 1, building 12 Moscow, 119991 Russia*
*7 - Institute of Experimental Oncology and Biomedical Technologies, Privolzhsky Research Medical University, Minina i Pozharskogo Sq., 10/1, Nizhny Novgorod 603005, Russia*
*8 - Becker&Hickl GmbH, Berlin, Nunsdorfer Ring 7-9, Berlin, 12277 Germany*

*timothy.torokhov@skoltech.ru*

The integration of fluorescence lifetime imaging (FLIM) and optoacoustic (OA) tomography has the potential to provide complementary information on tissue physiology, metabolism [1], oxygenation and vascularization [2]. However, the development and optimization of combined OA–FLIM instrumentation requires tissue-mimicking phantoms capable of generating independently tunable contrast for both modalities [3].

To address this challenge, we developed bimodal gelatin phantoms based on indocyanine green (ICG) and its J-aggregate form (IJA). Monomeric ICG is a clinically approved near-infrared fluorophore producing strong fluorescence signals [4], IJA exhibits enhanced optoacoustic performance due to fluorescence quenching, nanoparticle formation, and a red-shifted absorption peak [5,6]. Since both forms of the dye suffer from limited stability, ICG and IJA were encapsulated into vaterite particles using a freezing-induced loading (FIL) method [7].

Gelatin phantoms containing Lipofundin as a scattering agent and varying ratios of ICG- and IJA-loaded vaterite particles were fabricated while maintaining a constant total dye concentration of 15 μM. The phantoms were characterized using the TriTom system combining optoacoustic and fluorescence tomography, the IVIS Spectrum CT fluorescence imaging platform, and a custom-built FLIM setup.

The results demonstrate that varying the ICG ratio enables modulation of both fluorescence and optoacoustic responses. Phantoms with higher IJA content generated stronger OA signals at 890 nm, whereas increased ICG content enhanced fluorescence intensity. FLIM measurements revealed systematic changes in fluorescence lifetime, increasing from approximately 300 to 550 ps with increasing IJA fraction. These findings demonstrate that vaterite-loaded ICG/IJA phantoms provide a stable and tunable platform for calibration, optimization, and validation of multimodal OA–FLIM imaging systems.

This work was supported by the Russian Science Foundation (RSF), Grant № 24-19-00618

[1] V.I. Shcheslavskiy, M. V. Shirmanova, K.S. Yashin, A.C. Rück, M.C. Skala, and W. Becker, "Fluorescence Lifetime Imaging Techniques—A Review on Principles, Applications and Clinical Relevance," J Biophotonics, (2025).
[2] G. Wissmeyer, M.A. Pleitez, A. Rosenthal, and V. Ntziachristos, "Looking at sound: optoacoustics with all-optical ultrasound detection," Light Sci Appl 7(1), 53 (2018).
[3] C.K. McGarry, L.J. Grattan, A.M. Ivory, F. Leek, G.P. Liney, Y. Liu, P. Miloro, R. Rai, A. Robinson, A.J. Shih, B. Zeqiri, and C.H. Clark, "Tissue mimicking materials for imaging and therapy phantoms: a review," Phys Med Biol, (2020).
[4] J.T. Alander, I. Kaartinen, A. Laakso, T. Pätilä, T. Spillmann, V. V. Tuchin, M. Venermo, and P. Välisuo, "A Review of Indocyanine Green Fluorescent Imaging in Surgery," Int J Biomed Imaging 2012, 1–26 (2012).
[5] C.A. Wood, S. Han, C.S. Kim, Y. Wen, D.R.T. Sampaio, J.T. Harris, K.A. Homan, J.L. Swain, S.Y. Emelianov, A.K. Sood, J.R. Cook, K. V. Sokolov, and R.R. Bouchard, "Clinically translatable quantitative molecular photoacoustic imaging with liposome-encapsulated ICG J-aggregates," Nat Commun 12(1), 5410 (2021)
[6] R. Liu, J. Tang, Y. Xu, Y. Zhou, and Z. Dai, "Nano-sized Indocyanine Green J-aggregate as a One-component Theranostic Agent," Nanotheranostics 1(4), 430–439 (2017).
[7] S.V. German, et al. «High-efficiency freezing-induced loading of inorganic nanoparticles and proteins into micron-and submicron-sized porous particles.» Scientific reports 8.1 (2018): 17763.

# Perceptual-Based Approach to Meso-scale Inhomogeneity Characterization in Optical Coherence Tomography (OCT) Scans

**L. Matveev[1], D. Nikoshin[1,2], D. Mikhailenko[2], N. Matveeva[2,1], A. Sovetsky[1], E. Kiseleva[3], M. Novgorodskaya[3], O. Streltsova[3], K. Petrova[4], M. Ryabkov[3], M. Kulagina[1,4], P. Kulagin[1,4], A. Matveyev[1], V. Zaitsev[1]**

*1- Institute of Applied Physics RAS, 46 Ulyanov Str., 603951 Nizhny Novgorod, Russia*
*2- HSE University, 25/12 Bolshaya Pecherskaya street, 603155 Nizhny Novgorod, Russia*
*3- Privolzhsky Research Medical University, 10/1, Minin and Pozharsky Sq., 603950 Nizhny Novgorod, Russia*
*4- N.I. Lobachevsky Research State University, 23 Gagarin Avenue, 603022 Nizhny Novgorod, Russia*

*lev@ipfran.ru*

OCT-based diagnosis heavily relies on the visual assessment of the layers and underlying tissue heterogeneity. Micro-scale inhomogeneity arises at speckle-scale [1], whereas, meso-scale inhomogeneity characterized by specific structural inclusions and can be isolated using SAM-based tools [2]. We propose an automated, context-aware hybrid framework to objectively quantify layers and stromal meso-scale inhomogeneity (Fig. 1 serves as the graphical abstract for this work). The pipeline integrates a fine-tuned MedSAM [3,4] to isolate macroscopic upper tissue layer and context-aware zero-shot SAM 2.1 [5] to isolate mesoscopic inclusions. The SAM2.1 context is defined by the determined size of inclusions and perceptual sensitivity, enabling the robust quantification of inhomogeneity. For further SVM-based classification we utilized upper layer area and stromal inclusion area. We validate this approach on two *in vivo* datasets: 1) private clinical dataset[1] with normal and inflamed urethral tissue and 2) public dataset [6,7] with "young" vs. "old" eye corner skin.

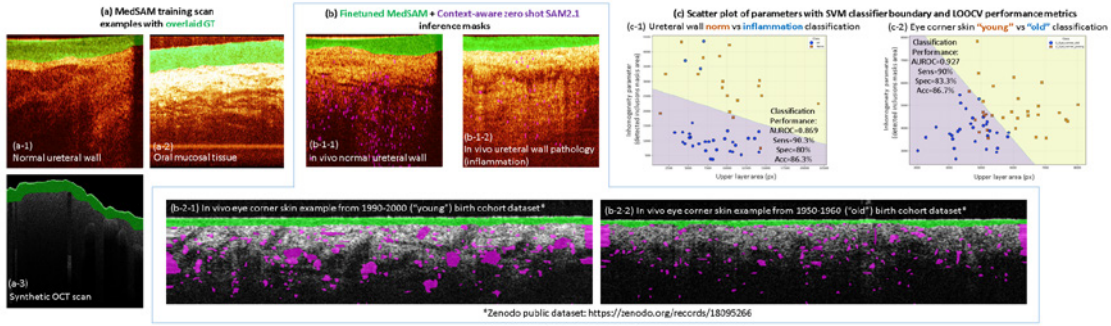


**Fig.1.** The proposed context-aware hybrid segmentation pipeline and its application to tissue classification. The MedSAM mask spatially restricting SAM 2.1 to the sub-epithelial stroma to reject structural artifacts. (a) Diverse fine-tuning data for the MedSAM model targeting the upper tissue layer (green mask), an examples: from 23 labeled urethral wall scans[1] (a-1); from 54 labeled oral mucosal tissue scans[1] (a-2); from 32 physics-based synthetic OCT scans from repository: github.com/OCTDigitalPhantoms/MICCAI_SASHIMI_2025 [4] (a-3). (b) Inference results combining the fine-tuned MedSAM (green) and zero-shot SAM 2.1 (purple inclusions) filtered by biological context (min. area=10 px, max. area=500 px for urethral tissues and min. area=1000 px, max. area=2000 px for skin). The method effectively captures the decrease in sub-epithelial heterogeneity during urethral inflammation (b-1-1 vs. b-1-2) and age-related structural changes in the skin (b-2-1 vs. b-2-2) at contextualized inhomogeneity scales. (c) Extracted biomarkers (upper layer area and inclusion area) provide a robust feature space for SVM classification. (c-1) Classification decision boundary and LOOCV performance for normal vs. inflamed ureteral tissue (Acc. = 86.3%). (c-2) Classification of eye corner skin scans into 1990-2000 ("young") and 1950-1960 ("old") birth cohorts (Acc. = 86.7%).

**Funding:** The study was solely funded by a joint grant from the Government of the Nizhny Novgorod Region and the Russian Science Foundation (RSF), project No. 25-12-20032.

[1] L. Matveev, A. Sovetsky, A. Matveyev, et al., Refined speckle contrast estimation in OCT based on compensation of scattering-related distortions of speckle pattern parameters, Laser Physics Letters, vol. 22(1), pp. 015601, (2025).
[2] D. Mikhailenko, D. Nikoshin, N. Matveeva, et al., Revealing tissue macro-structures by clustering of SAM-obtained foundational meso-segments from OCT attenuation maps, Proc. SPIE 13721, pp. 137211M, (2025).
[3] J. Ma, Y. He, F. Li, et al., Segment anything in medical images, Nature Communications, vol. 15, pp. 654, (2024).
[4] D. Nikoshin, D. Mikhailenko, A. Sovetsky, et al., From Tissue-Mimicking Phantoms to Physics-Based Scans: Synthetic OCT for Few-Shot Foundation Model Training, International Workshop on Simulation and Synthesis in Medical Imaging, pp. 44-51, (2025).
[5] N. Ravi, V. Gabeur, Y.-T. Hu, et al., SAM 2: Segment Anything in Images and Videos, arXiv preprint, arXiv:2408.00714, (2024).
[6] A. Sovetsky, K. Petrova, et al., Automated Segmentation and Skin-Layer Thickness Estimation by Extracting the Optical Scattering Coefficient and Speckle Contrast Parameter from Optical Coherence Tomography Scans, Skin Pharmacol Physiol, 000550613, (2026).
[7] L. Matveev, A. Sovetsky, K. Petrova, et al., In vivo Human Skin Optical Coherence Tomography (OCT) Dataset for Classification Benchmarking and Digital Phantom Generation (Version 1) [Data set], Zenodo, https://doi.org/10.5281/zenodo.18095266, (2025).

[1] Note: The private data were initially acquired during a separate research project (RSF Grant No. 25-15-00530), which does not fund the presented study. The development of the dataset and the ground truth annotation were performed under R&D contract No. K70-5 fully funded by RSF Grant No. 25-12-20032 solely for this project.

# Complementary Application Of LSCI, OCT And DRS For Comprehensive Assessment Of The Microvascular Bed: From Numerical Modeling To In Vivo Validation

**V. Perekatova, M. Kirillin, D. Kurakina, E. Sergeeva, K. Bylinskaya, Yu. Belozerov, A. Savelyev, I. Turchin**

*A.V. Gaponov-Grekhov Institute of Applied Physics of the Russian Academy of Sciences, 46 Ul'yanov Street, Nizhny Novgorod, 603950, Russia*

*Valeriya1000@yandex.ru*

The development of non-invasive methods for obtaining diverse information on the microcirculatory bed is a relevant challenge in biomedical diagnostics and personalised medicine. A comprehensive approach combining three complementary optical techniques is proposed: laser speckle contrast imaging (LSCI) [1] for large-scale perfusion mapping (fields up to cm); optical coherence tomography [2] for detailed 3D tissue structure at depths up to 1 mm; diffuse reflectance spectroscopy (DRS) [3] for quantitative assessment of chromophore content (hemoglobin, oxygenation, water, melanin).

A Monte Carlo modeling of photon trajectories for LSCI signal formation was developed. The LSCI MC model tracks per-photon parameters (weight, path length, exit coordinates, and scattering events on static/dynamic scatterers) during light propagation in layered tissues. An algorithm for vessel depth and radius, $r$, reconstruction from the spatial distribution of LSCI contrast was created and tested on synthetic data. For one (970 nm) or two wavelengths (655+970 nm), the depth reconstruction error is $\leq 25\%$ for large vessels $r \geq 0.2$ mm; adding a third wavelength (532 nm) reduced the minimum detectable radius to 0.1 mm.

For experimental validation, a solid tissue-mimicking phantom based on Elegoo White, Elegoo Translucent photopolymer resins and pigments (red, yellow, black) was developed. Numerical and experimental LSCI images of the phantom demonstrated quantitative agreement of contrast dependence on depth and radius.

Another task of microvascular bed investigation employed OCT+DRS measurements. The *in vivo* study involved 58 volunteers (4 age groups, 4 anatomical locations). OCT measurements allowed estimation of epidermal thickness (from 33±8 μm at the temple to 290±55 μm in the web space), which was used to correct the melanin content retrieved from DRS spectra, accounting for the predominant localization of melanin in the epidermal layer. DRS with a self-calibrating fiber-optic probe [3] and the refined model [4] enabled reconstruction of total hemoglobin volume fraction (0.12–0.93%), water volume fraction (30–90%), and melanin content (0.2–5 mg/g epidermis) after the aforementioned correction, values that agree with literature data. These results collectively demonstrate the potential of the complementary approach.

For the first time, a complementary LSCI+OCT+DRS approach provides multiscale information – from large-scale perfusion maps to local vessel morphology and quantitative chromophore content. The ability of multi-wavelength LSCI to assess vessel depth and of DRS to non-invasively measure hemoglobin, water and melanin content was experimentally confirmed.

The study is supported by the Russian Science Foundation (project No. 24-75-10068).

[1] D. Boas, and A. Dunn, Laser speckle contrast imaging in biomedical optics, Journal of biomedical optics, 15, 1, 011109-011109 (2010).
[2] M.Y. Kirillin, G. Farhat, E.A. Sergeeva, M.C. Kolios, A. Vitkin, Speckle statistics in OCT images: Monte Carlo simulations and experimental studies, Optics letters, 39 (2014) 3472-3475.
[3] V. Perekatova, A. Kostyuk, M. Kirillin, E. Sergeeva, D. Kurakina, O. Shemagina, A. Orlova, A. Khilov, I. Turchin, VIS-NIR diffuse reflectance spectroscopy system with self-calibrating fiber-optic probe: study of perturbation resistance, Diagnostics, 13 (2023) 457.
[4] E. Sergeeva, D. Kurakina, I. Turchin, M. Kirillin, A refined analytical model for reconstruction problems in diffuse reflectance spectroscopy, Journal of Innovative Optical Health Sciences, 17 (2024) 2342002.

# Optical-based approaches for PDT efficiency assessment

**V. Elagin[1], A. Komarova[1], P. Bureev[1,2], L. Shimolina[1], M. Sirotkina[1], E. Gubarkova[1], A. Plekhanov[1], P. Morozov[3]**

*1- Institute of Experimental Oncology and Biomedical Technologies, Privolzhsky Research Medical University, Nizhny Novgorod, Russia*
*2- Institute of Biology and Biomedicine, Lobachevsky State University of Nizhny Novgorod, Nizhny Novgorod, Russia*
*3- LLC "Superconducting Nanotechnology" (SCONTEL), Moscow, Russia*

*elagin.vadim@gmail.com*

Photodynamic therapy (PDT) is used clinically to treat a wide range of oncological and nononcological diseases and is recognized as a treatment strategy that is both minimally toxic and minimally invasive. PDT is based on interaction of three components: photosensitizer (PS), the light of the appropriate wavelength to excite the PS and molecular oxygen. Reactive oxygen species produced during PDT induce damages of various targets in biological tissues and cells that leading to elimination of pathological process. To monitoring of PDT efficiency noninvasive optical approaches are very useful. Fluorescence imaging is helpful to assess accumulation of a photosensitizer within tumor as well as its photobleaching immediately after PDT. A study conducted on experimental animals showed that photobleaching of at least 72% resulted in a 135% inhibition of tumor growth. However, tumor heterogeneity may effect it. Optical coherence tomography angiography may be used to monitor early tumor response to treatment. It was found that the absence of tumor blood flow 24 hours after PDT correlates with high value of tumor growth inhibition. Moreover, the damage of peri-tumor microvasculature is played the key role in determining the long-term PDT response. Compressional optical coherence elastography is able to visualize and quantify the tumor structure alterations (necrosis, edema, and viable tumor cells) after PDT. The pronounced differences in stiffness of tumor were revealed between responder group and both control group and non-responders at days 1, 2 and 6 post PDT. In responder tumor, areas with lower stiffness values appeared within 24 hours after PDT and increase in size over time. In responder tumor, areas with lower stiffness values are appearing within 24 hours after PDT and increase in size over time. Direct registration of singlet oxygen by its phosphorescence may be used to evaluate the effectiveness of the illumination regimen and the dose of the PS. Measurements performed on monolayer cancer cells culture and cell spheroids revealed that singlet oxygen formation rate depends on the concentration of the photosensitizer and increases linearly with increasing PS concentration. Doubling the laser power density results in a 10-fold increase in the singlet oxygen formation rate.

This work was supported by the Russian Science Foundation, project № 23-65-10005.

# Upconversion in High-Tech BioMedicine

**E. Khaydukov**

*Skolkovo Institute of Science and Technology, 121205, Moscow, Russia*
*Petrovsky National Research Centre of Surgery, 119991, Moscow, Russia*

*E.Khaydukov@skoltech.ru*

Nanoengineering enables the creation of special photoluminescent nanomaterials. Among the vast range of developed materials, inorganic nanocrystals doped with lanthanide ions occupy a special place. “Inverted” luminescence (anti-Stokes), which occurs during the upconversion process in such nanocrystals, is not typical of “living” nature, where light with higher energy is usually converted into photons with lower energy. Therefore, the physical phenomenon of upconversion, in which photons from the near-infrared spectrum are converted into visible and even ultraviolet light quanta, has opened up unique opportunities for researchers in the fields of biotechnology and medicine.

The aim of the report is to present an interdisciplinary, comprehensive approach to using the phenomenon of anti-Stokes luminescence in biomedicine. The report will examine: the results of research into photophysical processes in upconversion nanomaterials, the characteristics of their growth, the creation of biocompatible coatings on the surface of nanoparticles, the development of theranostic nanostructures, the advancement of bio-visualization methods, photodynamic and photothermal therapy of tumor tissues, as well as the use of nanocrystals in regenerative medicine. Attention will be drawn to the prospects for developing technologies for producing upconverting nanomaterials to transition into the second “window” of biotissue transparency (1000–1500 nm). New approaches to complicating the hierarchy of the nanoparticles being created will also be considered, with the aim of expanding the range of methods in nanoengineering in biotechnology and antimicrobial photodynamic therapy to address the problem of antibiotic resistance in microorganisms.

The final part of the report will present the results of the clinical testing of photodynamic therapy using Vitamin B2 for the treatment of wound infections and intraoperative visualization of pathologically altered biological tissues.

# Registration of changes in the tumor extracellular matrix during photodynamic therapy

**A.V. Ryabova[1,2,3], I.D. Romanishkin[1], I.V. Markova[1,2], D.V. Pominova[1,2], T.A. Savelieva[1,2], V.A. Tochilina[1,2], A.S. Moskalev[1]**

*1- Prokhorov General Physics Institute of the Russian Academy of Sciences, Moscow, Russia*
*2- National Research Nuclear University MEPhI, Moscow, Russia*
*3 - Peoples' Friendship University of Russia named after Patrice Lumumba, Moscow, Russia*

*nastya.ryabova@gmail.com*

One of the key obstacles to drug delivery is the increased rigidity and high mechanical stress in tumor tissue, which significantly reduces therapeutic efficacy [1]. Presented herein are the findings of an investigation into the effects of photodynamic therapy (PDT) on the tumor extracellular matrix (ECM) in order to reduce its rigidity.

The study used transplantable mouse mammary tumors with high levels of mechanical stress: EMT6 and a solid form of Ehrlich carcinoma (EC), as well as EMT6, EC and fibroblast cell cultures. The production of collagen by cells was studied using Sirius red/Fast green staining. The mechanical stress of the tumors was studied and the correlation with spectroscopic characteristics (diffuse reflectance spectroscopy (DRS) in the visible (VIS) and short-wave infrared (SWIR) ranges, speckle-contrast imaging, Raman scattering, and time-resolved fluorescence microscopy (FLIM)) was analyzed. To analyze the rate of photosensitizer accumulation and its distribution in tumor and stroma, fluorescence was recorded in real time after chlorin e6 (Ce6, 5 mg/kg) intravenous administration, including measurements before and after PDT (660 nm, 100 mW/cm$^2$, 50 J/cm$^2$). Laser scanning microscopy was used to study the cellular microenvironment composition, the type of cell death, and changes in the extracellular matrix structure.

The tumors used differed in stiffness, scattering, blood permeability, water and collagen content. This difference also affected the collagen distribution in the resulting tumor nodules *in vivo*: EMT6 cells form a dense tumor cell nodule with a distinct collagen border, while collagen content in EC tumors is higher, with more diffuse distribution from the center to the edges. The presence of collagen in EMT6 and EC tumor nodules *in vivo* correlates with their stiffness: 20 kPa and up to 50 kPa, respectively. The cellular metabolism type for tumor nodes *in vivo* for EC (NADH a1/a2 in the tumor center/edge are 6.98±2.03/11.49±5.03) is more glycolytic than for EMT6 (NADH a1/a2 in the tumor center/edge are 6.02±2.40/5.83±1.88). The Ce6 administration affects metabolism by blocking OXPHOS.

Ce6 accumulation was slower for stiffer tumors, which correlates with hypoperfusion and hypoxia. Within 5 min after administration Ce6 is observed in both the skin and tumor at a concentration of about 0.3 mg/kg. Subsequently, a decrease in Ce6 concentration is observed in the skin, while an increase in the tumor is observed due to the enhanced permeability and retention effect. The highest Ce6 accumulation in the EMT6 tumor occurs within 20-30 minutes after administration (0.45 mg/kg), and for the EC, the concentration continues to increase after 1 hour (0.55 mg/kg). Ce6 photobleaching after PDT was more intense for EMT6. The oxygenation reduction after PDT was approximately the same for EC and EMT6. However, the deoxygenation rate was significantly higher for EMT6 (2.1 s$^{-1}$) than for EC (1.7 s$^{-1}$) tumor. The decrease of scattering measured by DRS, as well as cell death and ECM damage confirmed by confocal microscopy, were observed after PDT.

In summary, EMT6 and EC tumors differed in their scattering (higher for stiffer tumors), blood permeability (lower for stiffer tumors), water content (lower for stiffer tumors), collagen content (higher for stiffer tumors), cellular respiration mode (shifted toward glycolysis for stiffer tumors), slower Ce6 accumulation for stiffer tumors, and photobleaching during PDT, which correlates with hypoperfusion and hypoxia. PDT reduced tumor stiffness due to cell death and ECM damage.

Funding. The study was supported by a grant from Russian Science Foundation No. 25-12-00436.

[1] K. Efendiev, A. Shiryaev, A. Rakhmanova, et al, Combined Photodynamic Therapy and Chemotherapy Using Local Intra-Arterial Intratumoral Administration of Chlorin e6 and Cisplatin: First Clinical Observations, Int. J. of Mol. Sc., vol. 26, № 17, pp. 8640 (2025).

# Method for assessing optical properties of multilayer biological tissues for personalization of laser-induced therapy

**A. Krivetskaya[1,2,3], T. Savelieva[1,2], D. Kustov[1], V. Levkin[4], I. Romanishkin[1], S. Kharnas[4], V. Loschenov[1,2]**

*1- Prokhorov General Physics Institute of the Russian Academy of Sciences, Vavilov str., 38, Moscow, Russia,119991*
*2- Institute of Engineering Physics for Biomedicine, National Research Nuclear University MEPhI, 31, Kashirskoe highway, Moscow, Russia, 115409*
*3- State Budgetary Healthcare Institution of the City of Moscow "S.S. Yudin City Clinical Hospital of the Moscow City Healthcare Department", Moscow, Russia, 117152*
*4 - I.M. Sechenov First Moscow State Medical University, Moscow, Russia, 119992*

*annakrivetskaya1998@gmail.com*

Currently, the layer-by-layer determination of the optical properties of biological tissues, such as the absorption coefficient, scattering coefficient and anisotropy factor, is carried out only on resected samples. One of the standard methods used for this task is to carry out measurements using integrating spheres [1-3]. Determination of the optical properties immediately before or during laser exposure during treatment will allow you to personalize this procedure. The purpose of this work was to develop a method for evaluating optical properties suitable for use in clinical settings in real time, by translating method of the measurements on integrating spheres to measurements using a fiber-optic spectrometer.

The initial determination of optical properties was carried out using a two-stream Kubelka-Munk model. For its application modified formulas for the dependence of Kubelka-Munk scattering and absorption parameters on optical properties have been developed. The layered assessment of optical properties was carried out using the developed method based on the inverse adding-doubling method. Verification of the developed algorithm for restoring the absorption coefficient, scattering coefficient and anisotropy factor was carried out using numerical modeling of light propagation in tissues using the Monte Carlo method, optical phantoms, and resected gastrointestinal tract samples. The method was also approbated on the diffuse reflection and transmission spectra recorded in clinical conditions.

According to the results of the research, the developed method for evaluating the optical properties of multilayer biological tissues has sufficient speed to be applied in clinical settings to personalize laser-induced therapy.

The work was funded by the Russian Science Foundation, grant No. 25-25-00516.

[1] A. Bashkatov, E. Genina, V. Kochubey, V. Rubtsov, E. Kolesnikova, V. Tuchin, Optical properties of human colon tissues in the 350 – 2500 nm spectral range, Quantum Electronics, vol. 44, p. 779, (2014).
[2] A. Bashkatov, E. Genina, V. Kochubey, A. Gavrilova, S. Kapralov, V. Grishaev, V. Tuchin, Optical properties of human stomach mucosa in the spectral range from 400 to 2000 nm: Prognosis for gastroenterology, Medical Laser Appli-cation, vol. 22. pp. 95-104, (2007).
[3] R. Marchesini, E. Pignoli, S. Tomatis, S. Fumagalli, A.E. Sichirollo, S. Di Palma, M. Dal Fante, P. Spinelli, A.C. Croce, G. Bottiroli, Ex vivo optical properties of human colon tissue, Lasers in surgery and medicine, vol. 15(4), pp. 351–357, (1994).

# Optically tunable tissue-mimicking phantoms for laser thermotherapy

**S.A. Mirzaeva[1], P.V. Aleksandrova[1], I.N. Dolganova[1,2], Yu.A. Suchkov[1], V.B. Tsvetkov[1], K.I. Zaytsev[1], D.G. Kochiev [1], A.K. Zotov[1]**

*1- Prokhorov General Physics Institute of the Russian Academy of Sciences, Moscow 119991, Russia*
*2- Osipyan Institute of Solid State Physics of the Russian Academy of Sciences, 142432, Chernogolovka, Russia*

*akzotov@hotmail.com*

Laser ablation is a minimally invasive oncological technique [1,2], enabling targeted thermal destruction of malignant tissues in various organs [3,4]. Treatment efficacy depends on the accurate calibration of operational parameters, including power density, laser pulse duration, cooling intervals, and exposure cycles. Suboptimal settings may cause excessive heat accumulation, leading to tissue carbonization, collateral neurovascular damage, or paradoxical tumor progression induced by sublethal heat stress (40–45°C) [5,6]. Preclinical validation of treatment protocols is therefore essential. Animal studies, however, are constrained by inter-subject variability in optical properties, inherent tissue heterogeneity, and ethical restrictions. Existing tissue-mimicking phantoms (TMPs) for soft and bone tissues mitigate several of these limitations but fail to simultaneously satisfy the thermal stability, optical fidelity, mechanical characteristics, and safety requirements necessary for optimizing laser ablation in osseous tumors and bone–soft tissue interfaces [7,8].

To model soft tissue, TMPs were developed using sodium alginate supplemented with $CuSO_4$ (as an optical absorber) and ovalbumin (to simulate scattering and thermal protein coagulation). These formulations replicate the optical, thermal, and mechanical behavior of liver tissue during laser thermotherapy for hepatocellular carcinoma at 1064 nm [9]. Phantoms containing 0.3–0.7 M $CuSO_4$ and 40–50 g/L ovalbumin exhibited optical attenuation coefficients and densities consistent with native liver. Irradiation with an Nd:YAG laser (General Physics Institute of the Russian Academy of Sciences, Russia; 1064 nm, 220 μs FWHM, 28.6 kW peak power, 1000 mJ pulse energy, 12.5 Hz) generated coagulation and ablation zones with morphological features comparable to those in bovine liver specimens. The biocompatibility of sodium alginate, combined with its thermal stability and adjustable parameters, establishes a reproducible platform for equipment calibration, operator training, and protocol optimization without reliance on biological tissues.

To mimic bone tissue, synthetic opals were fabricated from monodisperse $SiO_2$ particles using the Stöber method [9,10]. Optical properties were matched through $CuSO_4$ infiltration, while porosity and density were tuned via particle size control and thermal annealing [10]. The measured densities of the resulting opal structures closely matched those of native bone tissue. Infiltration with 0.3–0.7 M $CuSO_4$ solutions successfully replicated the near-infrared absorption of bone at 1064 nm. Laser ablation tests confirmed that the thermal damage patterns and acoustic emission profiles matched those of ex vivo human bone.

[1] A. Andavar, et al., "Current Research in Drug-Free Cancer Therapies," Bioengineering, vol. 12, 2025.
[2] Y. Fan, et al., "The State-of-the-Art and Perspectives of Laser Ablation for Tumor Treatment," Cyborg Bionic Syst., vol. 5, p. 62, 2024.
[3] C. Chen, et al., "Laser interstitial thermotherapy (LITT) for the treatment of tumors of the brain and spine: a brief review," J. Neurooncol., vol. 151, pp. 429–442, 2021.
[4] H. Adwan, et al., "Percutaneous Thermal Ablation Therapy of Hepatocellular Carcinoma (HCC): Microwave Ablation (MWA) versus LaserInduced Thermotherapy (LITT)," Diagnostics, vol. 12, p. 564, 2022.
[5] S. Thompson, et al., "Heat Stress-Induced PI3K/mTORC2-Dependent AKT Signaling Is a Central Mediator of Hepatocellular Carcinoma Survival to Thermal Ablation Induced Heat Stress," PLoS One, vol. 11, p. e0162634, 2016.
[6] E. Schena, P. Saccomandi, and Y. Fong, "Laser Ablation for Cancer: Past, Present and Future," J. Funct. Biomater., vol. 8, p. 19, 2017.
[7] M. Kulmaganbetov, "Advancements in Retinal Tissue-Mimicking Optical Coherence Tomography Phantoms: Materials, Properties, and Applications," BioChem, vol. 5, p. 6, 2025.
[8] A. J. R. Barcena, et al., "Emerging Biomedical and Clinical Applications of 3D-Printed Poly (Lactic Acid)-Based Devices and Delivery Systems," Bioengineering, vol. 11, p. 705, 2024.
[9] S. A. Mirzaeva, et al., "Sodium alginate-based tissue-mimicking phantom with tunable optical properties for laser thermotherapy," Biomed. Opt. Express 16, 5210-5220 (2025)
[10] V. M. Masalov, et al., "Mechanism of formation and nanostructure of Stöber silica particles," Nanotechnology, vol. 22, p. 275718, 2011.
[11] V. E. Ulitko, et al., "Nanoporous $SiO_2$ based on annealed artificial opals as a favorable material platform of terahertz optics," Opt. Mater. Express, vol. 10, p. 2100, 2020.

# Lanthanide-based MOFs for luminescent thermometry: design, synthesis, and application in laser surgery

**Utochnikova V.V.,[1,2] Koshelev D.S.,[1,2] Tselykh L.O.,[1,2] Orlova A.V.[1,2]**

*1- Lomonosov Moscow State University, Moscow, 119991, Russia*
*2- Center of Advanced Research, HSE, Russia*

The design of materials for luminescent thermometry is currently hindered not by a lack of sensitive sensors, but by the absence of rational design principles for compounds that would combine luminescence intensity, its temperature sensitivity, and photothermal stability. In our work, this problem is solved using heterometallic metal-organic frameworks (MOFs) based on lanthanides, primarily Eu-Tb and Nd-Yb pairs. To this end, series of new MOFs based on these pairs were obtained through directed synthesis, their crystal structures were determined, and the features of the formation of these compounds were studied. Along with the classical "Boltzmann" thermometry, we have proposed two fundamentally new mechanisms of reversible temperature dependence of luminescence: reversible phase transition and reversible dehydration of coordination compounds. As a result, a relative sensitivity exceeding 50 % $°C^{-1}$ was achieved, which is two orders of magnitude higher than typical values for Boltzmann systems.

The key result is the unsurpassed stability of the obtained MOFs. We have developed an automated protocol for cyclic measurements of luminescence and powder X-ray diffraction under conditions of simultaneous UV irradiation and heating up to 400 °C. The heterometallic MOFs withstand multiple cycles without any signs of phase degradation. In addition, for the first time, X-ray luminescent thermometry using MOFs under excitation by X-ray radiation has been demonstrated.

Thanks to this stability, a transition to practical application has been made: the fiber we developed, coated with an MOF-based material, enables real-time monitoring of tissue temperature during laser endovascular ablation. Thus, the directed synthesis of heterometallic lanthanide MOFs with controlled metal distribution across the nodes and unprecedented photothermal and radiative stability transforms luminescent thermometry from a laboratory method into an applied technology.

The work was supported by a grant from the Russian Science Foundation (25-43-20038).

# Gold Nanoparticles for Biomedical Application: Insight into Their Photodynamic and Catalytic Properties

**E. Solovyeva, E. Kolobova, K. Makarova, S. Aslanov, V. Sharoyko**

*Institute of Chemistry, Saint-Petersburg State University, Saint Petersburg, Russia*

*e.solovieva@spbu.ru*

Thorough understanding of surface phenomena, occurring on plasmonic nanoparticles under a local electromagnetic field, is crucial for research and development of their applications. This is of particular importance for the interface phenomena which involve gold nanoparticles and bioactive molecules since such systems may be intended for living cells or human body. Here, the comprehensive study of photodynamic and catalytic processes occurring on the gold nanoparticle surface is presented. Oxidative effect on the adsorbed bioactive compounds was investigated on bare and modified gold nanoparticles. Surface-enhanced Raman scattering, X-ray photoelectron spectroscopy, capillary electrophoresis, high performance liquid chromatography, and other methods were used to study the gold surface and solution on it (Fig. 1). To reveal a role of reactive oxygen species, the experiments were performed in the oxygen-saturated and oxygen-deficient gold nanoparticle dispersions. Effects of radical scavenger additives and pH of nanoparticle dispersion were also assessed.

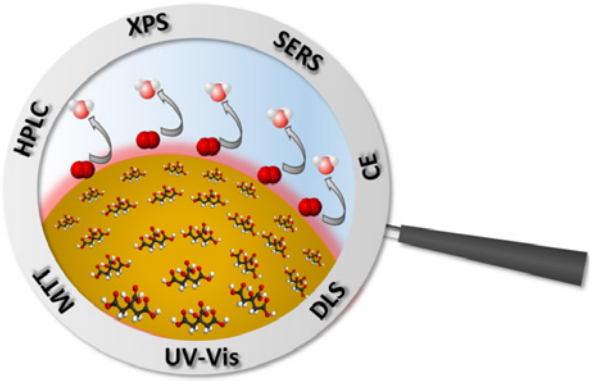


**Fig. 1.** Schematic representation of gold-assisted ROS generation and methods involved to the study of surface phenomena.

Catalytic oxidation of several bioactive molecules was revealed on the surface of citrate-stabilized gold nanoparticles [1] that may have important implications for further use of gold nanoparticles in bioanalysis and medicine. Overall, the study underscores the necessity of a rigorous analytical approach to evaluate drug-nanoparticle interactions, as understanding these catalytic transformations is paramount for ensuring the safety and therapeutic integrity of nanomedicine.

The work was supported by Saint-Petersburg State University, project № 122040800256-8. The authors would like to thank the Resource Centers of SPbU: “Optical and Laser Materials Research”, “Chemical Analysis and Materials Research”, «Physical Methods of Surface Investigation», and «Interdisciplinary Center for Nanotechnology».

[1] E.A. Kolobova, K.N. Makarova, E.V. Solovyeva, Plasmon-mediated N-dealkylation instead of chiral discrimination of the drug propranolol adsorbed on gold nanoparticles, Nanoscale, vol. 18, 2851, 2026.

# Laser assisted methods for studying the interactions between cellular components of blood and vessel endothelium

**A.V. Priezzhev, M.K. Maksimov, P.B. Ermolinskiy, A.E. Lugovtsov**

*Faculty of Physics, Lomonosov Moscow State University, 1-2 Leninskiye Gory, Moscow, Russia, 119991*

*avp@biomedphotonics.ru*

Blood microcirculation is largely determined by the parameters of the microrheology of its erythrocytes, in particular, their deformability and ability to aggregate. Microcirculation is essentially related to blood viscosity, which depends not only on erythrocytes but also on platelets and endothelial cells that line the inner surface of vessels. Changes in the parameters of these cells in diseases lead to a deterioration in tissue oxygen saturation, increased thrombogenesis and several other negative consequences. In particular, the adhesion of erythrocytes to endothelial cells may increase, as well as the aggregation of erythrocytes proper, i.e., their adhesion to each other. The interaction of cells is not limited to direct mechanical contact between them. It also includes cell-to-cell signaling, i.e., the transmission of signals by means of gasotransmitter molecules such as nitric oxide, hydrogen sulfide, and carbon monoxide. At the same time, endotheliocytes and erythrocytes are the main sources of gasotransmitters in blood vessels. It has been established that nitric oxide plays the greatest role in normalizing the deformability of erythrocytes and reducing their ability to aggregate.

Laser tweezers allow for using a sharply focused laser beam to trap living cells without mechanical contact and manipulate them *in vitro*. They also allow non-invasive measurement of the forces of intercellular interaction. In this work, we used two-channel laser tweezers based on a neodymium laser with a wavelength of 1064 nm in the transparency window of the cells under study, which prevents their heating and destruction. We measured the forces of reversible aggregation and disaggregation of paired erythrocytes, as well as the strength of interaction between one erythrocyte and a monolayer of endothelial cells lining the inner surface of a microvessel filled with a dilute suspension of erythrocytes in autologous plasma. The range of measured forces, depending on the experimental conditions, ranged from fractions to units of piconewtons.

The results obtained by us indicate that in the presence of endothelium previously incubated with the substrate of the nitric oxide synthase enzyme present in the endothelium - L-arginine, the forces of aggregation and disaggregation of erythrocytes decrease. Indeed, the addition of this substance to the endothelium stimulates an increase in the production of nitric oxide and, as a result, a decrease in the aggregation of red blood cells. This conclusion is supported by the fact that the effect disappeared after preliminary incubation of the endothelium with the nitric oxide synthase inhibitor L-NAME. The magnitude of the effect depends on the concentration of L-arginine, and this dependence is bell-shaped: the aggregation force is minimized at a concentration of 100 μM. A further increase in the concentration leads to an increase in the force up to the control value at 1000 μM. This dependence occurs due to the inhibition of nitric oxide synthase by its product at high concentrations. Under native (physiological) conditions, this circumstance prevents the toxic effect of this gasotransmitter at its high concentrations. Our results also show that the forces of interaction between a single erythrocyte and the endothelium, i.e., the monolayer of endothelial cells, grow monotonically with an increase in the concentration of fibrinogen in the environment. At the same time, they are comparable in magnitude to the forces of interaction between individual erythrocytes.

The study was supported by the RSCF grant No 26-15-00086.

# Observation and analysis of Luminescence of a colloidal-organized suspension of nanodiamonds

**A. Karmenyan[1], E. Perevedentseva [2], P. Badgujar[1], N. Melnik[2] and C-L. Cheng[1]**

*1- Department of Physics, National Dong Hwa University, Hualien, Taiwan*
*No 1, Sec. 2, Da Hsueh Rd., Shou-Feng, Hualien, 974, Taiwan*
*2- P.N. Lebedev Physical Institute of Russian Academy of Sciences, Moscow, Russia*

*artashes@gms.ndhu.edu.tw*

Colloidal photonic crystals (CPC) - organized structures with a periodicity of elements on the order of wavelength and the ability to control incident light - are currently being widely studied and used in various fields, particularly in biomedicine, as sensors, labels, specific carriers of compounds, drugs, etc. [1]. Such a system could be significantly more appealing for application development and possess greater capabilities if it has its own emission with the ability to be adjusted. Nanodiamonds (NDs), widely considered for various biomedical applications and possessing stable intrinsic emission across a broad spectral range, could be candidates for the creation of CPC and subsequent development of their applications. However, the formation of CPC typically requires high spatial homogeneity and ordering of the elements, which could pose a challenge. This study investigated the ability of aqueous suspensions of nanodiamonds synthesized by the high-pressure, high-temperature (HPHT) method to organize into colloidally ordered structures with unusual scattering and luminescence properties. CPC-like system based on detonation ND was first described in 2008 [2], but its spectral characteristics determined by both the inherent luminescence of the ND and the colloid structure have not been described so far.

In our study, the investigated structures were obtained using a method based on particles' sedimentation by repeated centrifugation, and their ordering was initially determined by the formation of rainbow layers in a centrifuge tube (inset Fig.1). Fragments of these colored layers were extracted to prepare ND samples for microscopic and spectroscopic studies. In addition to the formation of observed spectacular rainbow-colored layers, the excitation of microscopic ND samples at a wavelength of 488 nm revealed visible multicolored emission corresponding to various intervals within the full spectral range characteristic of ND (Fig.1).

By focusing exciting light on areas of a microscopic sample with varying structure, we can obtain emission with intensity modulation or a narrowed luminescence band.

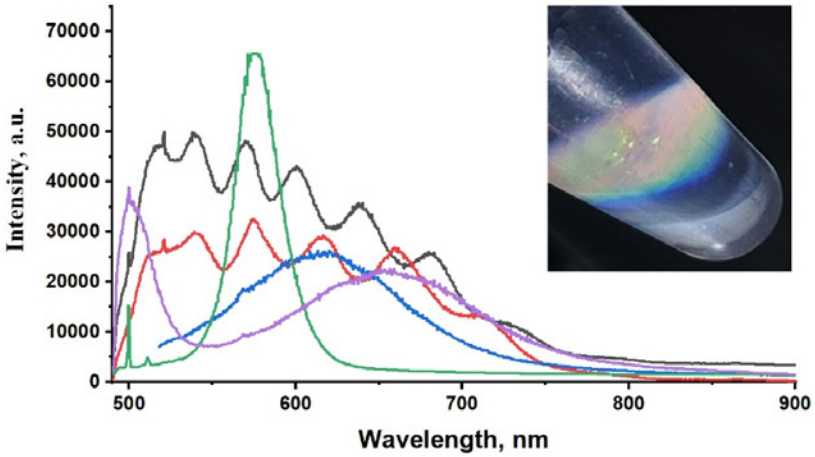


**Fig. 1.** Examples of emission spectra from CPC ND when excited at a wavelength of 488 nm. Inset: ND forming rainbow layers with floating CPC on their surface in a centrifuge tube.

The analysis of the spectra, along with the obtained microscopic images, demonstrates the ability of the used ND with heterogeneous in shape and size particles to form ordered structures ranging from a few microns upwards, exhibiting properties analogous to those of photonic crystals with intrinsic luminescence.

[1] W. Zhang, Y. Hu, P. Feng, Z. Li, etc., Structural Color Colloidal Photonic Crystals for Biomedical Applications, Advanced Science, 11, 2403173, (2024).
[2] V. Grichko, T. Tyler, V. Grishko, O. Shenderova, Nanodiamond particles forming photonic structures, Nanotechnology, 19, 225201, (2008).

# Design and characterization of luminescent nanoparticles for their application in bone regeneration and angiogenesis

**H.J. Velázquez-Castillo[123], P. Sengar[3], R. González[2], M. Marsal [4], E.J. Gualda, P. Loza-Alvarez[4], G. Hirata[3], P. Juárez[2]**

*1- Postgratuate Program in Nanotechnology, Ensenada Center for Scientific Research and Higher Education (CICESE), Ensenada, Baja California 22860, México.*
*2- Biomedical Innovation Department, Ensenada Center for Scientific Research and Higher Education (CICESE), Ensenada, Baja California 22860, México; erendira@cicese.edu.mx; pjuarez@cicese.mx*
*3- Center for Nanoscience and Nanotechnology, National Autonomous University of México (UNAM).*
*4- ICFO-Institut de Ciencies Fotoniques, The Barcelona Institute of Science and Technology, Av. Carl Friedrich Gauss, 3, 08860 Castelldefels, Spain*

Bone tissue is a dynamic and highly vascularized structure with an inorganic matrix composed primarily of hydroxyapatite (HAp) crystals, $Ca_5(PO_4)_3OH$. Synthetic Hap is osteoconductive, facilitating cartilage formation, hard tissue deposition, and blood vessel proliferation. These properties make it useful in nanomedicine for treating musculoskeletal disorders resulting from imbalances in the bone remodeling process, such as those caused by mechanical stress. The $Eu^{3+}$ ion is a particularly promising activator for the apatite family due to its stable luminescence, high thermal and chemical stability, as well as biocompatibility and applications in bioimaging. The purpose of this work was the synthesis and biological characterización of calcium phosphates doped with europium ions ($Eu^{3+}$) using hydrothermal and combustion methods, selected for their efficiency in obtaining particles with controlled structural and optical properties, as well as biocompatibility.

**Materials & Methods:** Physicochemical characterization was carried out using techniques such as scanning electron microscopy (SEM), transmission electron microscopy (TEM), X-ray diffraction (XRD), Fourier transform infrared spectroscopy (FTIR), energy-dispersive X-ray spectroscopy (EDS), photoluminescence (PL) and cathodoluminescence (CL) spectroscopy. For biological evaluation, *in vitro* assays were performed on different cell lines, including osteoblasts, using colorimetric cell viability tests, cellular internalization observed by confocal microscopy, and measurement of reactive oxygen species (ROS). In addition, *in vivo* studies were conducted using the zebrafish model (Danio rerio) at embryonic and larval stages, employing both WT and Fli strains.

**Results:** Luminescen nanoparticles presented the expected fisicochemical characteristic including size and luminicense. They were safe to use in vitro, got internalize to the cells and induced ROS. They were detected in Fli-zebra fish, and at low dosis did not induced mortality and malformations, in embryonic development, demostrated by internalization of the nanomaterials using confocal microscopy. The materials did not generate significant toxic effects, supporting their potential use in biomedical applications.

**Conclusion**: the synthesized luminescent materials exhibited optimal structural and optical properties, as well as biocompatibility in both *in vitro* and *in vivo* models. These results suggest that the developed materials are promising candidates for applications in regenerative medicine, particularly in bone tissue engineering (BTE) and angiogenesis promotion.

# Influence of NO synthesis modulation on peripheral skin blood flow regulation under local heating in db/db type 2 diabetic mice

**M. Severyukhina[1,2], A. Dyukina[1], A. Grinevich[1], A. Tankanag[1]**

*1- Institute of Cell Biophysics of Russian Academy of Sciences, Pushchino, Russia*
*2- Branch of Shemyakin-Ovchinnikov Institute of Bioorganic Chemistry RAS, Pushchino, Russia*

*tav@pbcras.ru*

Peripheral circulatory disorders in type 2 diabetes mellitus (T2DM) result from angiopathies characteristic of the pathology, which develop against the background of chronic hyperglycemia and insulin resistance. The aim was to evaluate changes in the regulation of cutaneous microhemodynamics of the hind limb in control mice and db/db mice, as a genetic T2DM model, in response to local heating during administration of Larginine (a substrate for nitric oxide (NO) synthesis) or metformin (a regulator of endothelial NO synthase activity).

Inbred male C57BL/Ksdb+/+m mice aged 12–14 weeks were used as a T2DM model. The db gene in the homozygous state causes T2DM accompanied by abnormal obesity, high blood sugar, reduced glucose utilization, and the absence of insulin deficiency. Animals of the C57BL/6J mice aged 12–14 weeks served as controls. Each group (T2DM and Control) was divided into three subgroups: water consumption without additives, with Larginine supplementation, or with metformin supplementation. Microcirculation dynamics were recorded in the skin of the hind paw of isoflurane-anesthetized animals using a laser Doppler flowmeter (LAKK01, wavelength 630 nm, laser power 0.5 mW). For analysis, two fragments were selected from each recording: 15 minutes at 32 °C (rest) and 15 minutes at 40 °C after temperature stabilization and to exclude fast transients corresponding to the axon reflex. Average skin blood perfusion (SBP) and relative spectral energies in the endothelial, neurogenic, myogenic, and Mayer frequency intervals were analyzed.

In the control mice, a significant increase in SBP during heating was observed in the Larginine subgroup, while in the T2DM group, a significant increase in SBP during heating was observed in the water and metformin subgroups. At the same time, in diabetic animals receiving Larginine, SBP **at rest** was higher compared to the water subgroup, whereas metformin administration in diabetic mice led to a decrease in SBP in response to heating relative to animals that consumed water without additives. Additionally, at rest, an increase in perfusion was found in T2DM mice receiving Larginine, and conversely, a decrease in mice receiving metformin, compared to the corresponding subgroups of control animals. In the control group, no significant changes were found between subgroups, nor between rest and heating. In diabetic animals, Larginine administration led to a significant decrease in the neurogenic component and an increase in the Mayer component both at rest and during heating, as well as a significant decrease in the myogenic component at rest compared to the water subgroup. In the subgroups of diabetic animals receiving water and water with metformin, a significant decrease in the myogenic component and an increase in the Mayer component of microcirculation regulation were observed in response to heating relative to rest.

Comparison of control and T2DM animals revealed differences only in the water and Larginine subgroups. In the water subgroups at rest, the contribution of the myogenic component to microhemodynamic regulation was higher in T2DM animals, whereas the contribution of the Mayer component was lower, compared to control animals. Larginine administration led to a decrease in the contribution of the myogenic component to microhemodynamic regulation at rest and a decrease in the contribution of the neurogenic component during heating in T2DM animals compared to control animals receiving Larginine.

Thus, it has been shown that stimulation of NO synthesis by Larginine consumption exerts a modulating effect on microhemodynamic regulation. The obtained results indicate the promise of strategies aimed at modifying NOmediated vasodilation for the correction of microcirculatory disorders in diabetes.

Animal experiments were carried out in compliance with the requirements of the Basel Declaration and legal acts of the Russian Federation. Experimental protocols were approved by the local Bioethics Committee (ID No. 2b/032024 dated March 1, 2024).

The study was supported by the Russian Science Foundation [grant number # 221500215P].

# Real-time Imaging Photoplethysmography for Intraoperative Perfusion Mapping: Synchronized iPPG-ECG System

**V.V. Zaytsev[1], S.V. Miridonov[2], V.A. Kashchenko[3,4,5], A.A. Kamshilin[1]**

*1- Institute of Automation and Control Processes, FEB RAS, Vladivostok, Russia*
*2- Centro de Investigación Cientfica y de Educación Superior de Ensenada, Ensenada, Baja California, Mexico*
*3- North-Western District Scientific and Clinical Center named after L.G. Sokolov, FMBI, St. Petersburg, Russia*
*4- Beloostrov Clinic, Vsevolozhsk District, Leningrad Region, Russia*
*5- Saint Petersburg State University, Saint Petersburg, Russia*

*zaytsevphoto@gmail.com*

Conventional imaging photoplethysmography (iPPG) is highly susceptible to motion artifacts, which complicates reliable assessment of tissue microcirculation, especially in a real surgical environment. We develop a hardware-software system for extracting a perfusion-index signal proportional to blood supply from video data heavily contaminated by motion artifacts. The key feature is high-precision hardware synchronization (microsecond timestamping) of iPPG and ECG via a shared clock and hardware interrupts, enabling the calculation of Pulse Arrival Time (PAT) in real time.

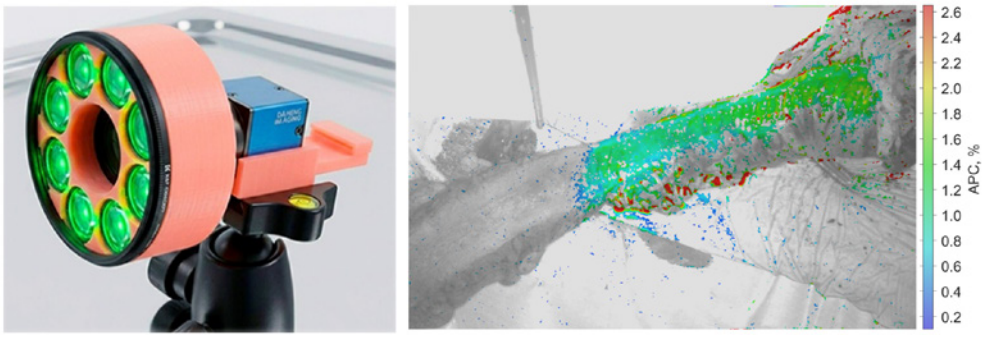


**Fig. 1** A general view of the imaging photoplethysmography module (left) and an example of intraoperative visualization of intestinal perfusion at the pre-incision stage (right).

The system employs a monochrome camera (50-150 fps) with green-light LED illumination module (525 nm) and a custom Arduino-based ECG module (AD8232, 1 kHz). Synchronous acquisition of video and ECG data using only computer's RAM allows real-time processing of image frames without recording any raw data to a hard disk. We developed an algorithm based on optical flow stabilization and spatial pixel averaging, which calculates two parameters for each pixel (or block of pixels) across five cardiac cycles: the Amplitude of the Pulsatile Component (APC, representing the perfusion index) and PAT. Unlike previous offline methods, the PAT parameter and its variability are used as a criterion to automatically identify and reject pixels corrupted by motion artifacts. This approach ensures that the resulting perfusion maps, generated and updated every few seconds, display only reliable data.

The clinical utility of the data processing algorithm was validated in a trial study using recordings from various abdominal surgeries. In a representative case of colon resection at the pre-incision stage, the perfusion mapping algorithm revealed a critical gradient in APC across the planned transection line. The PAT-filtered map precisely shows the boundary between viable tissue and the ischemic zone, which was visually undetectable. This feedback can guide surgeons in adjusting the transection line intraoperatively.

To our knowledge, this is the first real-time iPPG system capable of simultaneously mapping both amplitude (APC) and phase (PAT) parameters of the pulse wave. By using PAT variability to automatically reject pixels corrupted by motion artifacts, the method provides a clear differentiation between well-perfused and compromised tissue, thereby aiding intraoperative decision-making.

This study was supported by the Russian Science Foundation (Grant No. 25-15-00400).

# Sapphire Probes Based on Diffuse Reflectance Spectroscopy for Biomedical Applications

**A.A. Platonova[1], A.K. Zotov[1], D.G. Kochiev[1], V. N. Kurlov[2], I.N. Dolganova[2]**

*1- Prokhorov General Physics Institute of The Russian Academy of Sciences, Moscow, Russia,*
*2- Osipyan Institute of Solid State Physics of The Russian Academy of Sciences, Chernogolovka, Russia*

*platlina.hibou2001@yandex.ru, in.dolganova@gmail.com*

Optical methods are gradually integrated into clinical workflow to improve the efficiency of the performed procedures. Despite the variations of the applied techniques, most of them are basedthe detection of tissue optical parameters, especially refractive index, absorption and scattering coefficients, whose dynamic changes can indicate actual physiological and pathological processes in real time. These methods are commonly used for monitoring photodynamic therapy, to differentiate tumors, microcirculation disorders and others malignant conditions, for intraoperative control during surgical operations and cryodestruction processes. Among such methods, spatially resolved diffuse reflectance spectroscopy (SR-DRS), which is characterized by relatively simple hardware implementation, high sensitivity and rapid quantitative determination of tissue optical properties.

However, to implement SR-DRS into a single optical probe that can be used in various clinical circumstances, such as open and laparoscopic surgery, MRI control, laser or cryo ablation, such probe must meet a number of requirements. First of all, the probe should be non-toxic, stable to corrosion, resistant to sterilization and disinfection processes; secondly, it must have compact design, optical transparency in the operating wavelength range, precise light transport and detecting system. To satisfy these requirements, sapphire fiber-based probes can be used [1-4].

In this talk, we propose a sapphire SR-DRS compact probe with an outer diameter of 5 mm, with three working channels. A halogen light source is used for tissue illumination. To measure tissue properties, we involve a signal processing technique, based on the diffused reflectance estimation

$$I(\rho) = \frac{I_0}{4\pi\rho D} \cdot e^{-\mu_{\text{eff}}\rho}, \qquad (1)$$

where $\mu_{\text{eff}} = \sqrt{3\mu_a(\mu_a + \mu_s')}$ – effective attenuation coefficient, $\mu_a$, $\mu_s'$, $D$ – absorption, reduced scattering, and diffusion coefficients, $\rho$ is the source-detector distance.

Special attention in the talk is paid to experimental test of this probe. For this aim, several tissue-mimicking phantoms with varying optical properties were used. Advantages and drawbacks of the proposed probe and extraction of optical properties are discussed.

[1] G.M. Katyba et al., Sapphire shaped crystals for waveguiding, sensing and exposure applications, Prog. Cryst. Growth Charact. Mater., 64, 131-151, (2018).
[2] A.A. Platonova., P.V. Aleksandrova A.I. Alekseeva et al., Feasibility of Monitoring Tissue Properties During Microcirculation Disorder Using a Compact Fiber-Based Probe with Sapphire Tip, J Biophotonics, 17(11)., p. e202400368, (2024).
[3] A.A. Platonova., P.V. Aleksandrova, S.P. Kudryavtseva et al., Compact sapphire fiber-optic probe for intraoperative analysis of microcirculation disorders,Optica and Spectroscopy, 133(5), pp. 474-480, (2025).
[4] A.A. Platonova., A.K. Zotov, D.G. Kochiev et al., Estimation of two-layered media extinction by sapphire fiber probe and diffuse reflectance analysis,Optica and Spectroscopy, 133(12), pp. 1218-1223, (2025)

# Coarse-Grained Molecular Dynamics Simulation of Lipid Nanoparticle Self-Assembly for siRNA Delivery

**P.S. Trofimchuk[1], C.N. Grin[2], V.A. Dimitreva[1,2], V.A. Oleinikov[1,2], A.V. Zalygin[3]**

*1- National Research Nuclear University MEPhI, 31 Kashirskoe Highway, Moscow, 115409, Russia*
*2- Shemyakin-Ovchinnikov Institute of Bioorganic Chemistry, RAS, 16/10 Miklukho-Maklaya Street, Moscow, 117997, Russia*
*3- Lebedev Physical Institute, Troitsk Branch, Russian Academy of Sciences, Troitsk, 11 Physicheskaya Street, Moscow, 108840, Russia*

*zalygin.anton@gmail.com*

Lipid nanoparticles (LNPs) are the leading non-viral delivery platform for small interfering RNA (siRNA) therapeutics, enabling cytosolic delivery of nucleic acid cargo while protecting it from degradation. LNP performance – encapsulation efficiency, endosomal escape, and biodistribution – is governed by particle size and internal lipid organization, both of which are difficult to resolve experimentally at the nanometer scale. Coarse-grained (CG) molecular dynamics (MD) offers a computationally tractable route to studying the spontaneous self-assembly of multicomponent lipid mixtures capable of forming nanostructures and the effect of composition on the resulting nanostructure.

The composition under study followed a formulation reported for siRNA-delivery LNPs and included the ionizable lipid KC2, the helper phospholipid DSPC, cholesterol, and the PEGylated lipid PEG-DSPE, taken in a molar ratio of 50 : 10 : 37.5 : 2.5 (mol %) [1], corresponding to 100, 20, 75, and 5 molecules, respectively, per 25 nm cubic simulation box (200 lipid molecules in total, excluding water).

Initial structural files for each lipid were obtained from PubChem and geometry-optimized in Avogadro using the UFF force field; parameterized PDB files in the GROMOS 54A7 force field were then generated via the ATB service [2]. For each molecule individually, energy minimization and NVT/NPT equilibration were carried out in explicit water (SPC model) with NaCl (C = 0.15 M) in GROMOS 54A7 using GROMACS software. The molecules were subsequently converted to a coarse-grained representation semi-automatically, by mapping atoms to MARTINI 3 beads based on the force field's reference topologies [3] and generating the corresponding gro/itp files with PyCGTOOL.

The full system was then assembled in a cubic 25×25×25 nm box containing the required numbers of each lipid together with water and 0.15 M NaCl, under periodic boundary conditions, and equilibrated through sequential energy minimization, NVT (Bussi-Donadio-Parrinello, T = 298.15 K, 1 ns), and NPT (Parrinello-Rahman, p = 1 bar, 1 ns) stages. Production molecular dynamics was then run for 100 ns with a 9 fs integration step, and particle counts and radii of gyration were subsequently computed from the trajectory.

As a result, 21 distinct nanoparticles/aggregates were identified in the simulation box, with lipid tails oriented toward the aggregate core and polar head groups facing the surrounding water, and aggregation numbers ranging from 4 to 15 lipid molecules per aggregate (7 on average). The average radius of gyration was 1.07 ± 0.07 nm, far smaller than the 40-100 nm size range typical of real siRNA-delivery LNPs, indicating that, under the tested box size, lipid density, and 100 ns simulation timescale, the system underwent kinetically trapped nucleation into many small, compact micelle-like aggregates rather than coalescence into full-sized nanoparticles – a preliminary finding that points to the need for a higher lipid-to-box-volume ratio and/or a longer production run to reach realistic LNP dimensions.

[1] Jayesh A. Kulkarni et al., On the role of helper lipids in lipid nanoparticle formulations of siRNA, Nanoscale, vol. 11, 21733–21739 (2019).
[2] Stroet M. et al., Automated Topology Builder Version 3.0: Prediction of Solvation Free Enthalpies in Water and Hexane, J Chem Theory Comput. American Chemical Society, vol. 14 (11), pp. 5834–5845 (2018).
[3] Souza P.C.T. et al., Martini 3: a general purpose force field for coarse-grained molecular dynamics, Nat Methods, vol. 18 (4), pp. 382–388 (2021).

# Optical controlling multi-wavelength laser action on blood-containing tissue

**A.V. Belikov[1], V.Yu. Chuchin[1,2]**

*1- ITMO University, 49 Kronverksky Pr., 197101, Saint Petersburg, Russia*
*2- NPP VOLO LLC, 4−6 17th line V.O., 199034, Saint-Petersburg, Russia*

*avbelikov@gmail.com*

Laser treatments for vascular diseases based on the absorption of light by blood vessels. Currently, laser sclerotherapy uses single-wavelength laser systems emitting in the visible and near-infrared spectral ranges. The disadvantage of these systems is their low effectiveness in treating deep vessels.

The effectiveness of laser sclerotherapy of deep vessels can be increased by using multi-wavelength systems [1]. The basic principle of multi-wavelength systems is that exposure to laser radiation at one wavelength can specifically alter the condition of the target or surrounding tissue in such a way that subsequent or simultaneous exposure at a different wavelength will be more effective. However, it should be noted that for optimal implementation of the multi-wavelength method, not only a well-founded choice of working wavelengths is necessary, but also a feedback system that allows for real-time monitoring of changes in the condition of the blood and vessels and control of the parameters of working laser exposure, including the moment of switching between working wavelengths. In our study the theoretical and experimental principles of multi-wavelength laser action on blood-containing tissues and methods for controlling this action are discussed.

In the theoretical part of the study, optical computer modeling of the interaction of light with human skin and blood was performed [2], and absorption spectra were obtained in the range from 400 to 1100 nm for a layer of human blood at various concentrations of its main chromophores. Analysis of these spectra revealed that short-wavelength λ1 radiation (400-450 nm) is effectively absorbed by blood and can be used to preheat the skin to increase the transmittance of its blood-filled layers to long-wavelength λ2 radiation (830-1100 nm).

The experimental part of the study examined changes in the transmittance of a human capillary blood layer exposed to dual-wavelength laser radiation. The experiment demonstrated for the first time that transmittance at a wavelength of λ2=980 nm changes throughout the entire λ1=450 nm laser pulse and beyond. Therefore, it should be noted that for effective laser sclerotherapy of deep vessels, it is advisable to initiate the λ2=980 nm laser pulse at the moment of maximum blood optical clearing under λ1=450 nm. The time to achieve maximum optical clearance (increase of transmittance on λ2=980 nm) depends significantly on the thickness of the blood layer, which in turn varies for each individual and disease. Due to this dependence, the optimal moment for the action of radiation with working wavelength of λ2=980 nm is individual and can only be determined using optical feedback in a dual-wavelength laser system based on recording changes in the optical properties of blood using diagnostic laser radiation during irradiation with working laser radiation.

Thus, the work defines the spectral parameters of the working and diagnostic laser radiation of a dual-wavelength laser system with feedback for effective sclerotherapy of skin vessels and proposes a basic diagram and algorithm for its operation, consisting of searching for an enlarged vessel in the skin with subsequent controlled dual-wavelength laser therapeutic action on it.

[1] Trelles M.A. et al. Treatment of leg veins with combined pulsed dye and Nd: YAG lasers: 60 patients assessed at 6 months, Lasers in surgery and medicine, vol. 42, No. 9 pp. 769-774 (2010).
[2] Chuchin V.Y., Masharskaya A.A., Belikov A.V. Numerical study of the influence of oxyhemoglobin, deoxyhemoglobin, and methemoglobin content on the reflection, absorption, and transmission spectra of human blood, Optics and Spectroscopy, vol. 133. No. 5. pp. 551-559 (2025).

# Light-Activated STING Agonist Release for Macrophage Reprogramming

**O. Gusliakova[1,2], L. Mikhailova[3], O. Mayorova[1], B. Khlebtsov[4], M. Durymanov[5,6], M. Zyuzin[3], G. Sukhorukov[1,7], O. Sindeeva[1]**

*1- Center for Bio- and Medical Technologies, Skoltech, 30 Bolshoy Boulevard, Moscow 121205, Russia;*
*2- Science Medical Center, Saratov State University, 83 Astrakhanskaya str., Saratov 410012, Russia;*
*3- School of Physics and Engineering, ITMO University, 49A Kronverksky prospect, St. Petersburg 197101, Russia;*
*4- Institute of Biochemistry and Physiology of Plants and Microorganisms of the Russian Academy of Sciences, 13 Entuziastov ave., Saratov 410049, Russia;*
*5- Medical Informatics Laboratory, Yaroslav-the-Wise Novgorod State University, Veliky Novgorod, 173003, Russia;*
*6- Faculty of Chemistry, M.V. Lomonosov Moscow State University, Moscow, 119991, Russia;*
*7- Life Improvement by Future Technologies (LIFT) Center, Moscow, 121205, Russia;*

*olga.gusliakova17@gmail.com*

The tumor microenvironment (TME) of solid tumors is heavily characterized by immunosuppression, largely driven by tumor-associated macrophages (TAMs). These cells predominantly exhibit an M2-like phenotype, which actively supports tumor growth, angiogenesis, and metastasis [1]. Reprogramming TAMs from the anti-inflammatory M2 state toward the pro-inflammatory, anti-tumoral M1 phenotype represents a highly promising immunotherapeutic strategy. The Stimulator of Interferon Genes (STING) agonist (AgST) has emerged as a potent agent capable of driving this M1 polarization [2]. However, the systemic administration of free STING agonists is severely hindered by rapid clearance, low tumor accumulation, and the high risk of severe systemic side effects [3]. To address these limitations, biomedical photonics offers a powerful solution through the development of light-responsive drug delivery systems that enable spatiotemporally controlled, localized cargo release.

This presentation will report on the development and evaluation of internalizable, light-responsive polymeric carriers of two distinct size dimensions: micrometer (Mic, 4.1 μm) and sub-micrometer (Sub, 0.7 μm). To impart photothermal sensitivity, gold nanorods (AuNRs) were integrated into the polymeric walls of the carriers, enabling on-demand cargo release via the surface plasmon resonance effect. The carriers were loaded with a water-insoluble STING agonist. Photostimulation was performed using a near-infrared (NIR) laser operating at a power density of 1035 mW/cm². The presentation will outline the internalization and polarization efficiency of the carriers evaluated *in vitro* using RAW264.7 macrophage cell lines, followed by *in vivo* validation results conducted on a murine melanoma tumor model via direct intratumoral injection and localized NIR laser irradiation.

We have successfully developed a novel, laser-controlled delivery platform utilizing gold-nanorod-functionalized polymeric carriers for precise STING agonist release. Our findings highlight that optimization of carrier size (4.1 μm) is crucial for enhancing specific uptake by TAMs within the complex tumor architecture *in vivo*. This non-invasive, highly tunable biophotonic approach offers a powerful strategy to maximize anti-tumor immunity while eliminating systemic toxicity.

This report was prepared with the support of the Russian Science Foundation (project No. 23-75-10070-П).

[1] A. Christofides, L. Strauss, A. Yeo, C. Cao, A. Charest, V.A. Boussiotis, The complex role of tumor-infiltrating macrophages, Nat. Immunol. 23 (2022) 1148–1156, https://doi.org/10.1038/s41590-022-01267-2
[2] X. Li, S. Xu, Z. Su, Z. Shao, X. Huang, Unleashing the potential of metal ions in cGAS-STING activation: advancing nanomaterial-based tumor immunotherapy, ACS Omega 10 (2025) 11723–11742, https://doi.org/10.1021/acsomega.4c10865
[3] J. Mahin, X. Xu, L. Li, & C. Zhang, cGAS/STING in skin melanoma: from molecular mechanisms to therapeutics (2024). https://doi.org/10.1186/s12964-024-01860-y.

# Controlled Laser Treatment of Biological Tissues

**A.P. Sviridov**

*NCR"Kurchatov institute"*
*1 Kurchatov pl, Moscow, Russia 123182*

*sviridoa@gmail.com*

The ability of laser radiation to penetrate biological tissue and precisely modify it is widely used in various fields of medicine. Despite significant progress, issues related to ensuring the effectiveness, reliability, and safety of intense laser radiation on biological tissue remain pressing. The main problem is that laser radiation propagates in a highly inhomogeneous medium, the optical and thermophysical parameters of which can vary significantly depending on the tissue type, age, and race of the patient. Consequently, uncertainty arises in the choice of laser radiation parameters that ensure the safety and effectiveness of the treatment procedure. Most laser medical instruments leave the selection of exposure modes to the physician's discretion without objective indications. Experience and general recommendations for a specific procedure play a key role. Clearly, this approach carries a high risk of medical error. Therefore, objective prediction of the outcome of intense laser treatment and the search for optimal exposure parameters are crucial. Consequently, one of the most important tasks in developing precision laser-based surgical methods is predicting the results of laser treatment on a specific area of a patient's biological tissue.

The proposed approach combines preoperative measurement of the optical and thermophysical parameters of a specific tissue using attenuated radiation, numerical modeling of thermophysical processes in the tissue based on this data [1], and machine learning using neural networks for operational management of the treatment process. Measurement of the effective absorption coefficient, thermal diffusivity, and heat capacity of the tissue and acquisition of data on the thermophysical and optical characteristics of a given tissue area are proposed to be accomplished using laser thermography and optical reflectometry [2]. Using Monte Carlo simulation of light propagation in an optically inhomogeneous medium the spatial distribution of the light field intensity and the corresponding temperature field are calculated. This allows one to estimate the boundaries of thermal tissue modifications, such as protein coagulation or cell necrosis.

A number of medical procedures using lasers require tissue heating according to a specified scenario. For example, rapid tissue heating to a specified temperature and subsequent maintenance at this level is required for hyperthermia of malignant tumors. Such tasks can be accomplished using laser thermography combined with laser through feedback system. In this case, it is important to set the optimal parameters of the feedback system regulator for automatic control of laser radiation power [3]. Some examples of such heating is demonstrated.

[1]. Sedova Y.K., Sviridov A.P., Konovalov A.N., Zakharkina O.L., Ignatieva N.Y. Dynamics of the temperature field in biological tissues during local laser heating. Pisma JTP. vol. 51. pp. 20-24. (2025).
[2]. Kondyurin A.V., Sviridov A.P., Obrezkova M.V., Lunin V.V.. Contactless measurement of thermophysical and optical parameters of biological tissues and materials using laser IR radiometry. Sov J Phys Chem. vol. 83. pp. 1575-1584. (2009).
[3]. Sviridov A., Kondyurin A. Laser Thermography of Biological Tissues in: M. Diakides, J. Bronzino, D.R Peterson, Eds. "Medical Infrared Imaging. Principles and Practices" Ch29. CRC Press. (2012).

# Thermal Effect of Surface Plasmon and Its Biomedical Applications

**Xiangwei Zhao**

*State Key Laboratory of Digital Medical Engineering, School of Biological Science and Medical Engineering, Southeast University, Nanjing, 211189, China*

*xwzhao@seu.edu.cn*

After absorbing light energy, metal micro/nanostructures excite plasmons, which undergo non-radiative decay to generate hot carriers. These carriers dissipate energy through interactions with the lattice, converting light energy into heat. Constrained by the micro/nanostructures, this photothermal conversion process exhibits localized and tunable characteristics. Therefore, plasmonic photothermal effects hold broad application prospects in imaging, sensing, and particle manipulation. This work aims to explore and exploit their applications in cell manipulation and biodetection, thereby providing novel engineering tools for biomedicine. By designing and fabricating metal micro/nanostructures and selecting appropriate parameters (e.g., material, shape, and size), we achieve control over plasmon generation and propagation. For example, using a metal coating on a tapered optical fiber surface, we direct plasmon propagation to the tip and couple it with a photosensitive hydrogel to form a low-damage single-cell optical tweezer. Additionally, highly dispersed gold nanoparticles are modified onto fabric surfaces to create a plasmonic photothermal fabric that enables bulk heating of PCR systems for rapid nucleic acid amplification and detection. Our results show that plasmonic photothermal control of thermosensitive hydrogels allows for the manipulation of individual living or dead cells. Moreover, the plasmonic photothermal fabric enables photothermal PCR amplification of 40 cycles within 7 minutes and supports quantitative detection. These findings provide technical support for single-cell analysis and rapid nucleic acid detection. The plasmonic photothermal effect offers a unique means of energy conversion and regulation in biomedicine. Its core advantages include: (1) precise nanoscale thermal control, minimizing damage to biological entities such as cells; (2) compatibility with optical techniques, enabling high-sensitivity detection and real-time feedback; (3) potential for multifunctional integration, advancing personalized medical technologies with broad application prospects. Future efforts should focus on further optimizing material design and exploring multimodal effects (e.g., combining photothermal and photodynamic approaches) to enhance clinical translation.

[1] Lu Y, Liu C, Zhou QF, Huang Y, Yi JW, Jin W, Liu ZH, He BS*, Zhao XW*. Ultralow-cost personal PCRstrip with volumetric heating based on broadband absorption plasmonic fabric for POCT of pathogens. Nano Today, 65, 102868 (2025)
[2] Kang S, Nisar MS, Lu Y, Chang N, Huang Y, Haibin N, Novikov SM, Wang Y, Cui QN*, Zhao XW*. A 3D Biocompatible Plasmonic Tweezer for Single Cell Manipulation, Small Methods, 2201379 (2023,)

# Laser ablation and coagulation of soft biological tissues under exposure of microsecond pulsed laser

**P. Aleksandrova[1], A. Zotov[1], D. Pechenkin[1], Yu. Suchkov[1], D. Kochiev[1], A. Alekseeva[2], K. Zaytsev[1], I. Dolganova[1,3]**

*1- Prokhorov General Physics Institute of the Russian Academy of Sciences, Moscow 119991, Russia*
*2- Avtsyn Research Institute of Human Morphology of FSBSI "Petrovsky National Research Centre of Surgery", Moscow 117418, Russia*
*3- Institute of Solid State Physics of the Russian Academy of Sciences, Chernogolovka 142432, Russia*

*aleksandrovapolina98@gmail.com*

The dissemination and clinical implementation of treatment methods using pulsed laser radiation directly depend on the study level of the mechanisms of laser-biological tissue interaction. The key factor determining the effect of exposure and enabling differentiation between thermal and non-thermal regimes is the pulse duration [1]. Modes with pulse durations exceeding 1  predominantly induce thermal coagulation, whereas modes with shorter pulses provide tissue ablation [2]. Since the clinical outcome depends on the combination of laser radiation parameters (wavelength, energy density, and pulses duration) [3] and the intrinsic properties of biological tissue (composition, microstructure), one of the main tasks of modern laser surgery is still the optimization of generation modes and account of the processes occurring within the irradiated zone [4].

For this purpose, a comprehensive study of the effects of high-intensity pulsed laser radiation on liver tissues was conducted *ex vivo* and *in vivo* respectively. In the *ex vivo* study the dynamics of ablation and coagulation zones induced by pulsed laser radiation (λ ≈ 1.08 μm) were analyzed depending on the pulse train repetition frequency (ν=12.5;25; 50 Hz) (Fig. 1(a)). *In vivo* study was performed on Wistar rat models and aimed to compare two generation modes: free running (λ ≈ 1.064 μm) and pulse-train generation (λ ≈ 1.08 μm), both operated at a pulse/pulse-train frequency of 12.5 Hz and an exposure duration of 5 seconds (Fig. 1(b)). The analysis of the obtained results demonstrated that the pulse-train mode reduces the coagulation area and the dispersion of thermal damage compared to the free running mode, providing more predictable and controlled interaction with soft biological tissues.

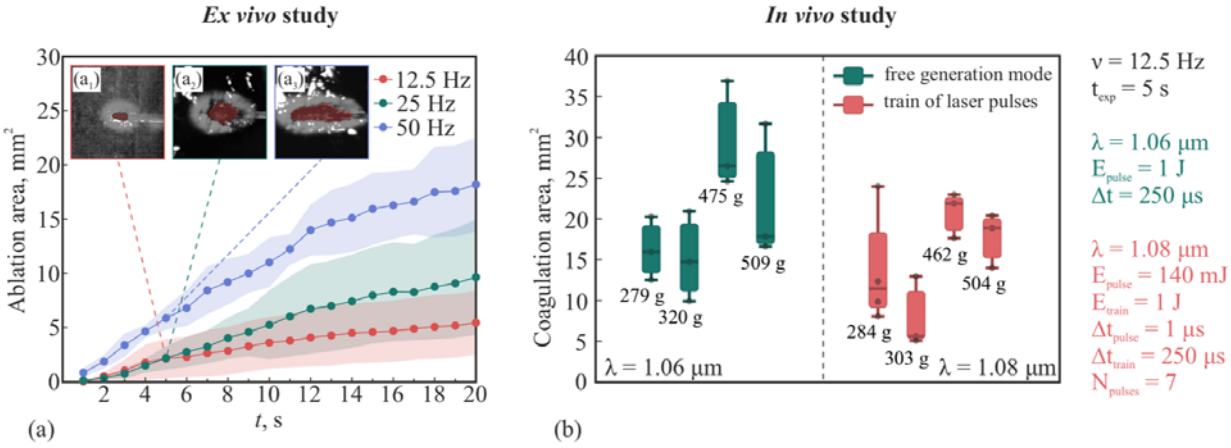


**Fig. 1.** Evaluation of soft biological tissue thermal damage. (a) *Ex vivo* study of the ablation area dynamics depending on the pulse train frequency: ($a_1$-$a_3$) are representative images of beef liver slices after laser 5 seconds exposure at the frequencies 12.5, 25, 50 Hz consequently; the ablation area mask colored in red. (b) *In vivo* study of the coagulation area of Wistar rat liver by comparing two generation modes: free running (green diagrams) and pulse-train generation (red diagrams).

[1] C. Chaki, L. De Taboada, K.M. Tse, Comparative analysis of pulsed and continuous wave modes in high-intensity laser therapy: implications for deep tissue treatment, J. Biophotonics, 18(7), e202400164, (2025).
[2] M.H. Niemz, Laser-tissue interactions: fundamentals and applications (Springer), (2024).
[3] M.S.H. Hutson, G.S. Edwards, Advances in the physical understanding of laser surgery at 6.45 microns, Proceedings of the 26-th Interantional FEL Conferences and 11-th FEL Users Workshop, 648-653, (2004).
[4] M. Hohmann, D. Kühn, D. Niet al., Relevant parameters for laser surgery of soft tissue, Sci Rep., 14(1), 1263, (2024).

# FLIM-Based Metabolic Profiling for Non-Invasive Assessment of Spheroids in Regenerative Medicine

**D. Kuznetsova, A. Mozherov, D. Kozlov, N. Kosheleva, P. Timashev**

*Institute for Regenerative Medicine, Sechenov First Moscow State Medical University (Sechenov University), 8-2 Trubetskaya Str., 119991 Moscow, Russia*

*kuznetsova_d_s@staff.sechenov.ru*

Evaluating the functional state, particularly the metabolic activity, of cellular spheroids is essential when using them as building blocks for biofabrication in tissue engineering and regenerative medicine. Standard approaches to studying cell metabolism come with notable drawbacks: they are often destructive, fail to provide real-time dynamic information, require lengthy protocols, and involve expensive reagents. A promising alternative is fluorescence lifetime imaging microscopy (FLIM), which allows label-free, non-invasive measurement of NADH fluorescence lifetimes - a reliable indicator of the balance between glycolytic and oxidative phosphorylation pathways. Our earlier work has already confirmed the value of FLIM for metabolic phenotyping across various cell systems and for tracking metabolism-related changes in multiple biomedical settings and experimental models [1–3]. Because FLIM is minimally invasive, it is particularly well-suited for assessing living spheroids without compromising their structure. Using two-photon NAD(P)H FLIM, we assessed the metabolic profiles of spheroids derived from different cell types and identified distinct metabolic signatures. These FLIM-based differences are functionally relevant for regenerative applications: spheroids with a more glycolytic phenotype may be better suited for avascular or poorly vascularized, whereas those with a more oxidative profile could support the formation of highly vascularized, metabolically active tissues. Thus, FLIM not only reveals intrinsic metabolic heterogeneity among spheroid populations but also provides a rationale for selecting specific spheroid types depending on the vascularization demands of the target tissue. Collectively, these findings position FLIM as a powerful, non-destructive metabolic quality-control platform that can guide the selection of optimal cell sources for personalized regenerative medicine strategies, ultimately improving the predictability and efficacy of spheroid-based biofabrication. The work was carried out with financial support from the Russian Science Foundation (RSF grant No. 25-45-20013).

[1] A. Ivleva, P. Bikmulina, V. Brumberg, A. Fayzullin, Z. Heydari, A. Mozherov, D. Krylov, D. Kuznetsova, F. de Sena Pereira, A. Solovieva, A. Svistunov, M. Vosough, A. Shpichka, P. Timashev, Bioprinted spheroid-based liver equivalents: Functionality and applicability in assessing pharmacodynamics, Bioprinting, vol. 54, e00467, (2026).

[2] S. Rodimova, A. Mozherov, V. Elagin, M. Karabut, I. Shchechkin, D. Kozlov, D. Krylov, A. Gavrina, V. Kaplin, E. Epifanov, N. Minaev, K. Bardakova, A. Solovieva, P. Timashev, E. Zagaynova, D. Kuznetsova, FLIM imaging revealed spontaneous osteogenic differentiation of stem cells on gradient pore size tissue-engineered constructs, Stem Cell Research & Therapy, vol. 14 (1), 81, (2023).

[3] A. Meleshina, V. Dudenkova, A. Bystrova, D. Kuznetsova, M. Shirmanova, E. Zagaynova, Two-photon FLIM of NAD (P) H and FAD in mesenchymal stem cells undergoing either osteogenic or chondrogenic differentiation, Stem Cell Research & Therapy, vol. 8 (1), 15, (2017).

# Method of detecting tissues of intracranial tumors using fiber optic laser spectroscopy *in situ*

**T. Savelieva[1,2], I. Romanishkin[1], K. Linkov[1], A. Borodkin[1], V. Yunanov[2], D. Yakovlev[1], A. Ospanov[2], S. Shugay[3], A. Kosyrkova[3], G. Pavlova[3,4], I. Pronin[3], V. Loschenov[1,2]**

*1- Prokhorov General Physics Institute of Russian Academy of Sciences, Moscow, Russia*
*2- National Research Nuclear University MEPhI (Moscow Engineering Physics Institute), Moscow, Russia*
*3- N.N. Burdenko National Medical Research Center of Neurosurgery, Moscow, Russia*
*4- Institute of Higher Nervous Activity and Neurophysiology of the Russian Academy of Sciences, Moscow, Russia*

*savelevat@nsc.gpi.ru*

Currently, there are a number of problems in neuro-oncology that can be solved using optical-spectral methods characterized by speed, accuracy, non-invasiveness, and a wide range of analyzed parameters. Primarily, this concerns intraoperative demarcation of tumor boundaries, as well as urgent biopsy during surgery. The use of optical-spectral methods for these tasks is called optical biopsy. Intraoperative diagnostic methods currently used in neurosurgery are primarily qualitative rather than quantitative and analyze a limited number of tumor markers. However, spectral methods can detect changes in parameters such as high proliferative status, hypoxia, high cell and nuclear density, myelin destruction, increased blood flow, changes in lipid and protein content in tumor tissue, and other molecular changes. An effective intraoperative optical biopsy strategy should include as many of these parameters as possible. In our work, we propose an integrated approach based on the use of fluorescence, diffuse reflectance, and Raman spectroscopy.

To develop a method for detecting intracranial tumor tissue using *in situ* laser optical spectroscopy, a prototype was created at the Cryoconservation laboratory of the N.N. Burdenko National Medical Research Center of Neurosurgery for recording fluorescence, diffuse reflectance and Raman spectra from tumor samples received at the laboratory. The prototype featured a distal end of optical probe consisting of the tip of a neurosurgical aspirator with embedded optical fibers at specified distances between their centers at the probe face to ensure optimal probing depth in various spectral recording modes. We conducted a sensitivity study of intracranial tumor tissue detection methods using laser optical spectroscopy at various wavelengths of laser radiation exciting fluorescence and Raman scattering on optical phantoms and intracranial tumor models in laboratory animals. As a result, an optimal set of laser excitation sources for fluorescence spectra was selected (405 nm for autofluorescence excitation, 632.8 nm for 5-ALA-induced protoporphyrin IX excitation, 785 nm for recording Raman spectra, as well as a broadband light source for recording diffuse reflectance spectra in the entire studied spectral range in order to use this information for normalizing the spectra obtained by laser excitation).

This work was supported by the Ministry of Science and Higher Education of the Russian Federation (the Federal Scientific-technical program for genetic technologies development for 2019–2030), agreement №075-15-2025-559

# Compartment-Resolved Monitoring of Cellular Metabolism by NAD(P)H FLIM

**I.A. Gorbunova[1], E.E. Nikonova[1], A. M. Mozerov [1], D.S. Kuznetsova[1], I.D. Grakhmez[2], Y.V.Afanasiev[2], M.V. Shirmanova[3], V.I. Shcheslavskiy[3], A.D. Komarova[3,4], I. N. Druzhkova[3], P.S. Timashev[1] , E.A. Shirshin[1,2]**

*1- Institute for regenerative medicine, Sechenov First Moscow State Medical University, Moscow, Russia*
*2- Faculty of Physics, M.V. Lomonosov Moscow State University, Moscow, Russia*
*3- Institute of Experimental Oncology and Biomedical Technologies, Privolzhsky Research Medical University, Nizhny Novgorod, Russia*
*4- Institute of Biology and Biomedicine, Lobachevsky State University of Nizhny Novgorod, Nizhny Novgorod, Russia*

*i.gorbunova@mail.ioffe.ru*

Fluorescence lifetime imaging microscopy (FLIM) is an effective and highly informative optical method for monitoring the metabolism of living cells and tissues [1, 2]. In FLIM, spatiotemporal photon-count histograms are recorded from endogenous or exogenous molecular probes in living cells and tissues, followed by analysis of fluorescence lifetime distributions and their relative contributions to the overall signal. One of the key challenges in this field is the monitoring of metabolism in different intracellular compartments, including mitochondria, endolysosomes, peroxisomes, cytosol, and nuclei, based on the fluorescence of the metabolic coenzymes NAD(P)H and FAD [3].

This work presents new approaches to the acquisition and analysis of FLIM images for compartment-resolved assessment of cellular metabolism. Several important results were obtained. First, it was shown that analysis of the fluorescence decay signals of intracellular NAD(P)H in the nuclei of HCT116 colorectal carcinoma cells enables evaluation of the cellular metabolic response to metabolic inhibitors and chemotherapeutic drugs. The key result is the identification of two cell subpopulations with distinct nuclear NAD(P)H fluorescence lifetime parameters after treatment with 5-fluorouracil. This finding indicates pronounced metabolic heterogeneity in the cellular response to chemotherapy. It was also demonstrated that changes in the fluorescence parameters of nuclear NAD(P)H correlate with changes observed in the cytoplasm, supporting a relationship between the nuclear and cytoplasmic pools of NAD(P)H. These results suggest that nuclear NAD(P)H fluorescence can be used to monitor metabolic alterations in cases where analysis of the cytoplasmic signal is challenging due to spectral overlap with exogenous fluorescent probes. A second important result is the demonstration of the relevance and significance of improving the FLIM temporal resolution by using an ultrafast detector with a response of approximately 15 ps. It was shown that fluorescence decay analysis performed with this detector makes it possible to resolve two decay components of free NAD(P)H both in solutions and directly in living cells. This substantially increases the information content of FLIM and opens the way to a more accurate determination of metabolic indices.

Authors are grateful to Russian Science Foundation (RSF) for financial support under the grant #25-79-10362

[1] V. I. Shcheslavskiy, M. V. Shirmanova, K. S. Yashin, A. C. Rück, M. C. Skala, W. Becker, "Fluorescence Lifetime Imaging Techniques—A Review on Principles, Applications and Clinical Relevance," Journal of Biophotonics, vol. 18, e202400450, (2025).
[2] B. Yakimov et al, Simultaneous assessment of NAD(P)H and flavins with multispectral fluorescence lifetime imaging microscopy at a single excitation wavelength of 750 nm, Journal of Biomedical Optics, vol. 29 (10), (2024).
[3] A. A. Zhikhoreva et al. "QPI-and FLIM-assisted multimodal analysis of the dynamics of morphological and physiological parameters of cells" Light: Advanced Manufacturing, vol. 6, pp. 1-13, (2025).

# FLIM-based metabolic monitoring of burn wound regeneration for early identification of burn wound conversion

**A. Mozherov, D. Krylov, A. Volovetsky, A. Fayzullin, P. Timashev, D. Kuznetsova**

*Institute for Regenerative Medicine, Sechenov First Moscow State Medical University (Sechenov University), 8-2 Trubetskaya Str., 119991 Moscow, Russia*

*mozherov_a_m@staff.sechenov.ru*

One of the key clinical challenges in superficial and indeterminate-depth burns is secondary deepening of the injury, known as burn wound conversion. According to Jackson's classical concept, a burn wound consists of three concentric zones: coagulation, stasis, and hyperemia [1]. The zone of stasis is of particular interest because it contains potentially viable cells required for spontaneous re-epithelialization and tissue regeneration [2]. The aim of this study is to investigate metabolic rearrangements and the structural and functional state of tissue during burn wound regeneration using FLIM, as well as to identify criteria associated with a high risk of burn wound conversion. FLIM imaging was performed using a two-photon microscopy system (Nikon Ti2-U, Japan) equipped with a time-correlated single-photon counting (TCSPC) FLIM module. Excitation was achieved using a femtosecond pulsed laser (Femto Fiber Ultra 780 Toptica, Germany) at 780 nm. Fluorescence detection was performed with a hybrid GaAsP detector (HPM-100-40, Becker & Hickl, Germany) covering a spectral range of 300–720 nm. A BP445/45 bandpass and an SP680 short-pass filter were employed to isolate NADH fluorescence. The average excitation power at the sample ranged from 5 to 10 mW, yielding a photon count rate of approximately 1–2 × $10^5$ photons per second.

**Table 1** NADH fluorescence lifetime parameters in the epidermis adjacent to the burn wound

| | R1 (3h) | R2 (24h) | R3 (48h) | Control |
|---|---|---|---|---|
| a1, % | 72.04 ± 1.44 | 70.46 ± 2.51 | 71.92 ± 3.09 | 66.84 ± 2.32 |
| t1, ps | 544.1 ± 24.0 | 530.4 ± 57.0 | 547.7 ± 52.0 | 610.8 ± 77.0 |
| t2, ps | 3028.0 ± 220.5 | 2895.3 ± 135.1 | 2894.6 ± 112.2 | 3000.5 ± 249.4 |
| tm, ps | 1231.2 ± 84.8 | 1224.3 ± 101.1 | 1218.6 ± 115.1 | 1390.4 ± 102.7 |

As shown in Table 1, the epidermis adjacent to the burn injury exhibits pronounced metabolic alterations according to NADH FLIM parameters. These changes suggest metabolic stress in the perifocal region, which may correspond to Jackson's zone of stasis. A decrease in mean NADH lifetime ($\tau m$) and the short component ($\tau_1$), together with an increased contribution of free NADH ($\alpha_1$), reflects a shift toward glycolytic metabolism. This shift is typical of hypoxia, ischemia, and inflammation, when cells switch from oxidative phosphorylation to less efficient but faster glycolysis. These changes are critical in the zone of stasis, where potentially viable cells are exposed to ischemic and inflammatory stress, determining tissue fate - recovery or progression of injury. Moreover, reduced $\tau m$ and $\tau_1$ may also indicate damage to the NADH protein microenvironment due to thermal injury, oxidative stress, and inflammation, leading to protein disorganization and mitochondrial dysfunction. Thus, FLIM parameters reflect both metabolic reprogramming and early structural damage. The observed NADH shifts in perilesional epidermis can serve as optical indicators of zone-of-stasis formation and potential markers of burn wound conversion risk. FLIM enables label-free detection of these changes and supports dynamic metabolic assessment during wound healing. These findings highlight FLIM's potential for identifying tissues at risk of secondary burn wound deepening. The work was carried out with financial support from the Russian Science Foundation (RSF grant No. 25-25-00623).

[1] D. Jackson, The diagnosis of the depth of burning. Br J Surg, 40(164), 588-596, (1953).
[2] P. Rousselle, F. Braye, G. Dayan, Re-epithelialization of adult skin wounds: Cellular mechanisms and therapeutic strategies, Adv Drug Deliv Rev, (2019).

# FLIM-based diagnosis of tumor metabolic state using endogenous NADH and FAD lifetime of tumor and immune cells

**D.V. Pominova[1,2], A.V. Ryabova[1,2], I.V. Markova[1,2], I.D. Romanishkin[1], A.S. Skobeltsin[1,2]**

*1- Prokhorov General Physics Institute of the Russian Academy of Sciences, Moscow, Russia*
*2- National Research Nuclear University MEPhI, Moscow, Russia*

*pominovadv@gmail.com*

Optical assessment of tumor metabolism is a promising route towards personalized therapy selection, because the balance between glycolysis, mitochondrial oxidation and redox state strongly influences sensitivity to photodynamic and metabolic treatments [1]. The aim of this work is to develop an *in vivo* approach for tumors metabolic state diagnosing using fluorescence lifetime imaging (FLIM) of endogenous coferments NADH and FAD for further prediction of treatment response.

Since the tumor microenvironment is highly heterogeneous and consists of both tumor and immune cells, as well as fibroblasts, at first step we characterized *in vitro* metabolic fingerprints of normal, tumor and immune cells. Vero and NIH/3T3 cells showed predominantly oxidative features, whereas EMT6, 4T1, HeLa and TRAMP-C2 cells demonstrated a more glycolytic phenotype. A correlation was observed between the activity of glycolysis and the obtained FLIM parameter values; for the TRAMP-C2 line, which has lower glycolytic activity, the NADH fluorescence lifetime value was higher, and a1/a2 was lower than in other studied cultures.THP-1-derived macrophages displayed polarization-dependent FLIM signatures: M1 cells were associated with activated glycolysis and pentose phosphate pathway (PPP), while M2 cells showed a larger contribution of oxidative phosphorylation and fatty-acid metabolism. It has been shown that the use of alternative metabolic pathways, such as the PPP and fatty acid oxidation, leads to changes in the lifetime of coenzymes and cannot be estimated using the simplified glycolysis-oxidative phosphorylation model. Thus, for cultures actively using the PPP (3T3, M1), a decrease in the average fluorescence lifetime and an increase in the NADH a1/a2 ratio are observed, caused by the accumulation of free NADH in the cytosol. For cultures using alternative metabolic pathways, it is necessary to analyze the full range of metabolic coefficients to accurately assess their state.

The sensitivity of cells to metabolic inhibitors was tested using oligomycin, rotenone/antimycin, CCCP, glucose and 2-deoxyglucose. Inhibition of mitochondrial respiration shifted the FLIM profile towards glycolysis, CCCP revealed the reserve of mitochondrial oxidation, glucose enhanced the glycolytic response, and 2-deoxyglucose suppressed it. Methylene blue produced a time-dependent effect: an early increase in glycolytic features was followed by partial compensation of glycolytic stress and recovery of a more oxidative profile after prolonged incubation. The response depends on the initial metabolic state.

Based on these *in vitro* calibration data, the approach is being transferred to *in vivo* tumor measurements in mouse tumor models. FLIM mapping of tumor tissue *in vivo* is used to evaluate endogenous fluorescence lifetime patterns before and after treatment and to relate them to the metabolic phenotypes established in cell culture. This workflow is intended to distinguish glycolytic and oxidative tumor regions, identify metabolically resistant areas, and support the selection of optimal therapeutic strategies, including photodynamic therapy and metabolic modulation.

The obtained results demonstrate the feasibility of using endogenous-cofactor FLIM for metabolic phenotyping and *in vivo* tumor diagnostics.

Acknowledgements. This work was supported by the Russian Science Foundation, project No. 22-72-10117-П.

[1] S.R. Alam, H. Wallrabe, Z. Svindrych et al., Investigation of mitochondrial metabolic response to doxorubicin in prostate cancer cells: an NADH, FAD and tryptophan FLIM assay, Scientific Reports 7, 10451, (2017). https://doi.org/10.1038/s41598-017-10856-3

# Comparison of LSCI-based flow velocity estimation methods in phantoms

**Y. Belozerov, A. Savelyev, E.Sergeeva, I. Turchin, V. Perekatova**

*A.V. Gaponov-Grekhov Institute of Applied Physics of the Russian Academy of Sciences,*
*46 Ul'yanov Street, Nizhny Novgorod, 603950, Russia*

*u.belozerov@ipfran.ru*

Quantitative estimation of blood-flow velocity in tissue-mimicking phantoms is an important step toward calibrated laser speckle contrast imaging (LSCI) systems for microcirculation studies. LSCI records temporal blurring and fluctuations of speckle patterns caused by moving scatterers; however, the relationship between speckle-derived parameters and flow velocity depends on exposure time, optical properties of the phantom and channel geometry. Therefore, phantom experiments with controlled flow are required to select an appropriate velocity estimation strategy.

In this work, three LSCI-based approaches were compared on the same phantom. The first approach was multi-exposure speckle imaging, where contrast-exposure curves acquired at exposure times from 100 μs to 20 ms were fitted to estimate the decorrelation time and reduce the influence of static scattering [1]. The second approach used empirical calibration of the speckle contrast level at selected exposure conditions against known reference velocities. [2]. The third approach was based on high-frame-rate image acquisition within a limited field of view of 10 × 100 pixels, corresponding to a physical area of 0.15 × 1.53 $mm^2$. The acquisition was performed at 2.5 kHz with an exposure time of 350 μs and an inter-frame delay of 50 μs. The obtained image sequences were used for temporal autocorrelation analysis of speckle intensity fluctuations between frames [3].

The protocol used a scattering tissue-mimicking phantom with embedded flow channels with a diameter of 1 mm and a controlled blood-mimicking liquid. LSCI measurements were performed at an illumination wavelength of 808 nm and imposed flow velocities of 0.63–6 mm/s. Each method was applied to identical regions of interest, allowing their comparison under the same optical and geometrical conditions. The main comparison parameters included monotonicity with velocity, repeatability, sensitivity to static components, dependence on exposure time or frame rate, and practical complexity of implementation.

A comparative analysis of these three strategies was aimed at selecting a robust calibration protocol for LSCI measurements in optical phantoms. This work enabled a systematic evaluation of the robustness of each method under different acquisition conditions and helped identify the approach most suitable for further translation from model media to biological tissues. This is essential for interpreting LSCI maps not only as qualitative perfusion images but also as quantitative indicators of microvascular dynamics.

The study is supported by the Russian Science Foundation (project No. 24-75-10068).

[1] A.B. Parthasarathy, W.J. Tom, A. Gopal, X. Zhang and A.K. Dunn, Robust flow measurement with multi-exposure speckle imaging, Optics Express, 16(3), pp. 1975-1989, (2008).
[2] Y. Wang, D. Wen, X. Chen, Q. Huang, M. Chen, J. Lu and P. Li, Improving the estimation of flow speed for laser speckle imaging with single exposure time, Optics Letters, 42(1), pp. 57–60, (2017).
[3] D.D. Postnov, J. Tang, S.E. Erdener, K. Kiliç and D.A. Boas, Dynamic light scattering imaging, Science Advances, 6(45), eabc4628, (2020).

# Multispectral optoacoustic localization of ICG-labeled sentinel lymph nodes: phantom study

D. Chekmareva[1], A. Kurnikov[1], E. Smolina[1], A. Glyavina[1], M. Kirillin[1], D. Gorin[2], I. Turchin[1], P. Subochev[1]

*1- Institute of Applied Physics, Russian Academy of Sciences, 603005 Nizhny Novgorod, Russia*
*2- Skolkovo Institute of Science and Technology, 121205 Moscow, Russia*

*darya_voytovich@mail.ru*

Sentinel lymph node mapping is clinically important, but optical localization at depth is limited by tissue scattering. This preliminary phantom study evaluates whether multispectral optoacoustic imaging can detect lymph-node-mimicking inclusions embedded in a tissue-like scattering medium. Model nodes containing indocyanine green (ICG) or ICG J-aggregates were used as near-infrared absorbing targets.

Compact lymph node models were placed at controlled depths in a Lipofundin-based tissue-mimicking liquid. Two contrast formulations were compared: conventional ICG and self-assembled ICG J-aggregates with a shifted near-infrared absorption band. The measurements were designed to assess detectability, depth dependence and spectral separability under simplified phantom conditions.

Optoacoustic measurements were performed with a custom 3D tomographic system based on ultrasound detection of laser-induced acoustic signals [1]. Excitation wavelengths covered the main spectral features of ICG and ICG J-aggregates [2]. Representative spectra and reconstructed projections of embedded lymph node models are shown in Fig. 1. The same phantom platform is compatible with complementary fluorescence readout.

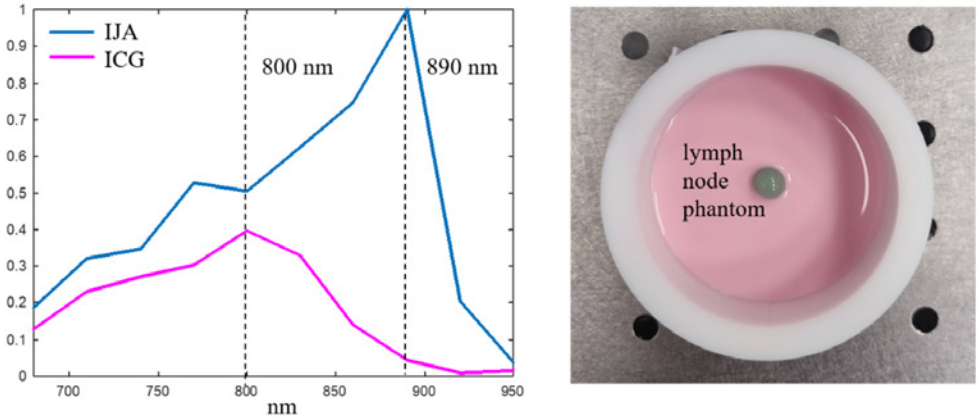


**Figure 1.** Preliminary phantom assessment of lymph-node-mimicking inclusions in a tissue-mimicking scattering medium: (a) optoacoustic spectra of ICG and ICG J-aggregate models; (b) photograph of a lymph node phantom in a tissue-simulating scattering medium.

Initial measurements indicate that both ICG- and J-aggregate-based inclusions can be detected optoacoustically in a scattering liquid, while their spectral responses provide a basis for multispectral discrimination. The signal decreases with depth, as expected, but the phantom experiments define a practical framework for estimating the useful spectral window and contrast formulation for sentinel lymph node localization.

The work was supported by the Russian Science Foundation, project No. 25-45-20023 (joint RSF-INSF project).

[1] Subochev, Pavel V., et al., Ultrawideband high density polymer-based spherical array for real-time functional optoacoustic micro-angiography, Light: Science & Applications 14.1, 239, (2025).
[2] T. Torokhov et al., Indocyanine Green-Based Test-Platform With Tunable Contrast for Optoacoustic and Fluorescence Lifetime Visualization, Laser & Photonics Reviews, 20.8, e02094, (2026).

# Proton Beam therapy technology

**M. Belikhin, D. Orlov, A. Chernykh**

*National Research Center "Kurchatov Institute",*
*123182 Russia, Moscow, Academician Kurchatov Square, Building 1*

*Chernykh_AN@nrcki.ru*

Proton and carbon therapy has seventy years of development firmly established itself as a highly effective cancer treatment. There are currently more 130 proton therapy centers and 17 ion therapy centers in the world. Additionally, 33 more centers are under construction, and 30 proton therapy centers are planned. There are three proton therapy centers in Russia, one of them using domestic equipment [1].

Currently, the Russian Federation, in accordance with Decree of the President of the Russian Federation No. 356 of July 25, 2019, is implementing the Federal Scientific and Technical Program for the Development of Synchrotron and Neutron Research and Research Activities for the Period from 2019 to 2030 and Further Growth, approved by the Government of the Russian Federation in March 2020 [2 - 4]. The leading scientific organization is the National Research Center "Kurchatov Institute".

As part of the program, a Scientific and Educational Medical Center of Nuclear Medicine is being established at the National Research Center "Kurchatov Institute" [5]. The structure of the Scientific and Educational Medical Center of Nuclear Medicine includes a number of specialized complexes: proton and ion (carbon) therapy, an onco-ophthalmological complex for proton therapy, as well as a radioisotope complex designed for the production of medical radionuclides.

The proton beam therapy complex being created at the National Research Center «Kurchatov institute». One of important part development of proton therapy complex is proton therapy technology. In the report will discuss the main technological stages of proton beam therapy, implemented using the technological equipment being developed.

[1] WWW.PTCOG (Particles Therapy Co-Operative Group), Online 2026.
[2] Decree of the President of the Russian Federation of July 25, 2019, No. 356 "On measures to develop synchrotron and neutron research and research infrastructure in the Russian Federation" http://publication.pravo.gov.ru/Document/View/0001201907250034 (date of the application: 19.08.2026) (In Russ.).
[3] Resolution of the Government of the Russian Federation of March 16, 2020 No. 287 "On Approval of the Federal Scientific and Technical Program for the Development of Synchrotron and Neutron Research and Research Infrastructure for 2019–2027" http://static.government.ru/media/files/7HOnpvIMtHyahEIAhzisATobIo9SKvkv.pdf (date of the application: 19.08.2026) (In Russ.).
[4] Resolution of the Government of the Russian Federation of March 23, 2024 No. 368 Moscow "On Amendments to Resolution of the Government of the Russian Federation of March 16, 2020 No. 287" http://static.government.ru/media/files/AHWpvvlPRRs8XtUMZdat3KvCiCJSOAJa.pdf (date of the application: 19.08.2026).
[5] Kovalchuk M.V., Naraikin O.S., Sergunova K.A., Dyakova Yu.A., Chernykh A.N. etc., The Kurchatov Institute's Distributed Nuclear Medicine Center: History, Current Status, and Development Prospects.Crystallography Reports, 2022, V.67, № 5, pp. 801 – 817 (In Russ.).

# Antibacterial photodynamic therapy in treatment of chronic urinary tract infection

**V. Elagin[1], P. Bureev[1,2], N. Ignatova[1], M. Birin[2], O. Streltsova[3]**

*1- Institute of Experimental Oncology and Biomedical Technologies, Privolzhsky Research Medical University, Nizhny Novgorod, Russia*
*2- Institute of Biology and Biomedicine, Lobachevsky State University of Nizhny Novgorod, Nizhny Novgorod, Russia*
*3- LLC "Superconducting Nanotechnology" (SCONTEL), Moscow, Russia*

*elagin.vadim@gmail.com*

The growing resistance of pathogenic microorganisms to the commonly used antibiotics has stimulated the development of alternative approaches that exhibit high antimicrobial activity. One such alternative approach is antimicrobial photodynamic therapy (aPDT). However, this approach is sometimes ineffective, due to the complex structure of their cell wall, and overexpression of efflux pumps. The non-ionic detergent Triton X-100 and emulsifier Tween 80 were tested to enhance an aPDT efficacy. Using Tween 80 at concentration of 10% provided an insignificant decreasing of bacteria viability after aPDT. Meanwhile, Triton X-100 increased the number of killing cells on 52%. The presence of an extracellular photosensitizer during illumination made it possible to reduce the number of living cells by 100 times. The efficacy of aPDT of *E. coli* incubated with photosensitizer and Triton X-100 achieved 52.5%. It was found that washing of the extracellular photosensitizer led to loss of the aPDT efficacy. The high sensitivity of *P. aeruginosa* to aPDT with extracellular photosensitizer significantly reduced after washing of the photosensitizer. The efficacy of aPDT of *P. mirabilis* did not change after washing of the extracellular photosensitizer. It was demonstrated that the aPDT efficacy depended on laser power in all studied species, excluded *K. pneumoniae*. The efficacy of *K. pneumoniae* treatment did not exceed 93%. The irradiation of other bacteria species with a power of 450 mW provided an aPDT efficacy of 99.99%. Analysis of damage of main biological macromolecule (lipids, proteins and DNA) revealed difference between bacteria treated with and without Triton X-100. Triton X-100 mediated aPDT induced strong fragmentation of genomic DNA as well as plasmids DNA. Regarding to lipid oxidation, a dose-dependent increasing a MDA level was observed in the absence of Triton X-100. Conversely, Triton X-100 led to a decrease in lipid damage. Evaluation of safety of bactericidal regimens of aPDT on laboratory animals did not reveal any alterations of renal pelvis morphology and abnormalities of renal function. Moreover, aPDT was allowed to destruct the original biofilm structure of uropathogenic S. aureus and E. coli on 97.7% and 96.5%, correspondingly. Intracystic aPDT was performed on patients with urinary tract infection. After two procedures performed alternate-day, no bacteria growth was detected for all patients. Furthermore, all patients reported a reduction in pain and an improvement in quality of life after the treatment, which lasted for 3 months. The experiment established that intraoperative photodynamic therapy is an effective and safe method of inactivating uropathogenic microorganisms, which allows it to be considered as an alternative to antibiotic therapy.

This work was supported by the Russian Science Foundation, project № 26-15-00182.

# Investigation of the structure of the vascular bed and the level of oxygenation of tumors in the combined treatment with antiangiogenic and radiation therapy

**A.M. Glyavina[1,2], D.A. Chekmareva[1], A.A. Kurnikov[1], Yu.A. Khochenkova[3], D.A. Khochenkov[3], A.V. Maslennikova[1,2], I.V. Turchin[1], P.V. Subochev[1], A.G. Orlova[1]**

*1- A.V. Gaponov-Grekhov Institute of Applied Physics RAS, 46 Ulyanov Street, Nizhny Novgorod, Russia*
*2- Lobachevsky State University of Nizhny Novgorod, 23 Gagarin Avenue, Nizhny Novgorod, Russia*
*3- N.N. Blokhin National Medical Research Center of Oncology, 23 Kashirskoye Highway, Moscow, Russia*

*annaglyavina@gmail.com*

Radiation therapy is a standard treatment method for malignant neoplasms, which uses high doses of ionizing radiation. Antiangiogenic therapy improves tumor oxygenation, enhancing the effect of radiotherapy, since oxygen prevents the repair of DNA damage. It also suppresses the restoration of blood supply, which makes the combined approach promising for treatment. In this study, we employed optoacoustic angiography (OA) and diffuse optical spectroscopy (DOS) to assess the vascular structure and oxygenation levels of experimental tumors. These modalities enable investigations at a comparable depth of approximately 2 mm [1] and facilitate the tracking of individual blood vessel development within the tumor nodule [2]. The study was conducted in female BALB/c nude mice bearing subcutaneous tumors derived from the human colon carcinoma cell line Colo320.

OA and DOS studies were performed starting from day 7 of tumor node growth with an interval of 3-7 days to 36 days of neoplasm growth. The tumor volume was measured every 3-7 days. The vascular endothelial growth factor tyrosine kinase receptor inhibitor Axitinib was administered orally from day 9 to 33 of the experiment daily every five days a week at a dose of 25 mg/ kg in Axitinib monotherapy group and 12.5 mg /kg in the combination therapy group. Radiation therapy was delivered at a dose of 5 Gy on the 11th day of neoplasm growth. The irradiation was performed on a Novalis Tx linear accelerator (Varian Medical Systems, USA).

OA and DOS assessments were conducted weekly from day 9 to day 37. OA imaging used a raster-scan system with a pulsed laser (532 nm, 1 ns, 2 kHz) and a wideband PVDF detector (IAP RAS) [3]. DOS employed a fiber-optic system with a broadband LED source and a spectrometer (IAP RAS) [4]. During the OA and DOS studies, animals under isoflurane anesthesia were fixed in a position on their side on a portable support plate with an opening for the study area above the OA sensor of the microscope.

At the end of the experiment, tumor volume was reduced by 2.4-fold in the Axitinib group, 4.6-fold in the radiation therapy group, and 8.8-fold in the combination therapy group compared with controls. The DOS study revealed a rapid decline in tissue oxygen saturation ($StO_2$) in untreated tumors and during Axitinib therapy. In contrast, radiation therapy alone and in combination with Axitinib induced a transient increase in $StO_2$.OA imaging demonstrated that radiation therapy, both alone and in combination with Axitinib, caused a decrease in vascular fraction by the 28th day of neoplasm growth.

The work was supported by the Russian Science Foundation, project No. 25-15-00238.

[1] K. G.Akhmedzhanova, A. A.Kurnikov, D. A.Khochenkov, Yu. A.Khochenkova, A. M.Glyavina, V. V.Kazakov, A. V.Yudintsev, A. V.Maslennikova, I. V.Turchin, P. V. Subochev, A. G.Orlova. In vivo monitoring of vascularization and oxygenation of tumor xenografts using optoacoustic microscopy and diffuse optical spectroscopy. Biomedical Optics Express, 13, 11, 5695 (2022)
[2] A.Glyavina, K.Akhmedzhanova, A.Kurnikov, D.Khochenkov, Y.Khochenkova, P. Subochev, A. Orlova. Optoacoustic angiography for noninvasive monitoring of experimental tumor angiogenesis. Laser Physics Letters. 20, 11, 115601 (2023)
[3] A.Kurnikov, G.Volkov, A.Orlova, A.Kovalchuk, Y.Khochenkova, D.Razansky, P.Subochev. Fisheye piezo polymer detector for scanning optoacoustic angiography of experimental neoplasms. Photoacoustics, 31, 100507 (2023)
[4] M.S.Kleshnin, and I.V.Turchin. Evaluation of oxygenation in the surface layers of biological tissues based on diffuse optical spectroscopy with automated calibration of measurements. Quantum Electron. 49, 7, 628–632 (2019)

# Onco-Ophthalmology System «OKO»: From Cyclotron Beam Formation to Treatment Planning Systems

**V.I. Maksimov, D.I. Granin, Zh.S. Lebedeva**

*Petersburg Nuclear Physics Institute named by B. P. Konstantinov of National Research Centre «Kurchatov Institute», 1 Orlova Roshcha Microdistrict, Gatchina, Leningrad Region 188300, Russia*

*granin_di@pnpi.nrcki.ru*

Proton therapy of intraocular tumours requires accurate integration of accelerator physics, beam delivery, patient positioning, and treatment planning. The clinical result depends on the consistency between the physical characteristics of the proton beam, the calculated dose distribution, and the actual position of the patient's eye during irradiation.

The «OKO» onco-ophthalmology system is intended to integrate a cyclotron-based proton source, beam transport and shaping systems, patient-specific field-forming devices, gaze fixation, X-ray navigation, patient positioning, and a treatment planning system (TPS). The cyclotron provides a proton beam with parameters suitable for therapy. Beam-shaping components, including a scattering system, collimator, range modulator, range shifter, and patient-specific compensator, are used to form the required field and depth-dose distribution.

The TPS is the central tool linking the physical beam characteristics to an individual treatment plan. CT simulation, MRI, ophthalmological data, and information on beam geometry are used to construct a patient-specific three-dimensional eye model. The model includes the tumour volume, critical ocular structures, and tantalum marker positions. The TPS calculates the dose distribution taking into account the beam parameters, target depth, field geometry, and individual beam-shaping devices.

Treatment planning includes selection of the beam entrance angle, patient position, and gaze direction; assessment of target coverage; and optimisation of doses to organs at risk. The plan is designed to minimise irradiation of the optic nerve, macula, lens, ciliary body, and healthy ocular tissues, while avoiding proton beam passage through tantalum markers.

For treatment setup verification, digitally reconstructed radiographs generated by the TPS are compared with X-ray images acquired in the treatment position. Gaze fixation, a mechanical fixation point, and X-ray navigation support reproducible positioning of the eye relative to the treatment-system isocentre. The «OKO» concept therefore connects cyclotron beam formation with patient-specific dose calculation and treatment verification.

**Keywords:** cyclotron, proton therapy, ocular oncology, treatment planning system, beam shaping, dose distribution, intraocular tumours, uveal melanoma.

# Modeling and Phantom Validation of Transcranial Ultrasound Detectors for Photoacoustic Microscopy

**A. Kurnikov, M. Loginova, D. Gubankova, P. Subochev**

*Federal research center A.V. Gaponov-Grekhov Institute of Applied Physics of the Russian Academy of Sciences, Nizhny Novgorod, Russia*

*daryagubankova@yandex.ru*

Brain conditions like stroke and neurodegeneration are intimately tied to alterations in cerebral blood vessels and neurovascular communication. Photoacoustic microscopy holds particular promise here because it merges optical absorption contrast with ultrasound detection, enabling label-free mapping of vascular networks. Yet the mouse cranium poses a major acoustic obstacle: it weakens, bends, and scrambles broadband photoacoustic waves, reducing both sensitivity and consistency in transcranial recordings.

This poster presents an approach to enhance photoacoustic sensing from the mouse cortex using two purpose-built transcranial ultrasound transducers. Optical access is achieved through a standard cranial window. A focused laser beam sweeps across this window, generating photoacoustic responses in cortical vessels, while the acoustic signals are captured by miniaturized transducers placed either on the skull exterior or, in later designs, partially inserted via small skull perforations. The overarching aim is to create implantable ultrasound sensors that stay mechanically anchored to the skull and boost the signal-to-noise ratio during long-term brain imaging studies.

Currently, our efforts center on physical modeling and phantom verification rather than a finished in vivo procedure. We model the travel of broadband photoacoustic waves across the mouse skull and examine how skull thickness, sensor placement, and the introduction of drilled apertures affect the received signal. In tandem, we conduct phantom trials using excised mouse skull bones. The laser is raster-scanned through an artificial cranial window, and the resulting ultrasound is captured either across intact skull areas or through fabricated openings with custom hydrophones and compact transducers. These tests aim to quantify the acoustic loss imposed by the skull, pinpoint sensor arrangements suited for transcranial reception, and inform the next project phase: implantable ultrasound detectors for more sensitive photoacoustic tracking of cortical blood vessels.

The work was supported by the Russian Science Foundation (project 25-45-02127).

# Determination of radiochemical purity of radiopharmaceuticals $^{177}$Lu-PSMA-617 and $^{177}$Lu-DOTA-TATE

**L. Khajiyev[2], I. Sadikov[1], A. Abdukayumov[2], Z. Usarov[2]**

*[1]Institute of Nuclear Physics Academy of Sciences of the Republic of Uzbekistan*
*[2]State Institution "Radiopreparat", Institute of Nuclear Physics, Academy of Sciences of the Republic of Uzbekistan,*

*hajiyev.lazizbek@mail.ru*

Today, nuclear medicine is widely used in the treatment and diagnosis of various types of cancer using radiopharmaceuticals. These include [$^{177}$Lu]-PSMA-617 and [$^{177}$Lu]-DOTA-TATE. These radiopharmaceuticals are used in the treatment of somatostatin receptor-positive prostate diseases and neuroendocrine tumors (NETs) using radionuclide therapy. The radiochemical purity of the radiopharmaceuticals determines the effectiveness of treatment and minimizes harmful effects on the patient.

The aim of this study is to develop rapid, highly sensitive and reliable methods for determining the radiochemical purity of radiopharmaceuticals [$^{177}$Lu]-PSMA-617 and [$^{177}$Lu]-DOTA-TATE produced at the State Institution "Radiopreparat".

The radiochemical purity of $^{177}$Lu-PSMA-617 and $^{177}$Lu-DOTA-TATE radiopharmaceuticals was determined by paper chromatography (PC). The mobile phase was a 1:1 mixture of ammonium acetate and methanol for the former and a 1:1 mixture of acetonitrile and distilled water for the latter. With this method, free lutetium ions $^{177}Lu^{3+}$ remain at the initial Rf line of 0.0-0.1, while the $^{177}$Lu-PSMA-617 complex migrates with the solvent to the final Rf line of 0.9±0.0.2, and $^{177}$Lu-DOTA-TATE migrates with an Rf value of ~0.8-0.9.

The radiochemical purity of a radiopharmaceutical is calculated using the following formula:

$$RCP = \frac{\sum A_{main.\ substance}}{\sum A_{chr}} \cdot 100\%$$

where:

$\sum A_{main.\ substance}$ - the sum of the number of pulses for the main zone of the substance;

$\sum A_{chr}$ - sum of pulses for the entire chromatogram.

The results obtained showed that the radiochemical purity of $^{177}$Lu-PSMA-617 and $^{177}$Lu-DOTA-TATE exceeds 99.5%. In conclusion, the developed methods can be applied to quality control of radiopharmaceuticals.

# Interaction of homodimer styrylcyanine dyes with human serum albumin

**A.Sh. Yarmukhamedov, E.N. Kurtaliev, I.D. Khairov, L.N. Rizakulova, N.Sh. Rakhmonova**

*Samarkand State University after Sharaf Rashidov. Uzbekistan, 140104, Samarkand, University blvd.,15*

*kurtaliev@rambler.ru*

Human serum albumin (HSA) is the most abundant extracellular plasma protein, serving as a transporter of exogenous and endogenous substances in the blood. Abnormal levels of albumin in blood plasma is associated with the development of various pathological processes in the human body [1]. Therefore, the early and accurate detection of HSA in human serum and other biological fluids is important in clinical analysis.

Fluorescence spectroscopy employing molecular probes is a highly sensitive and widely used technique for the detection of albumin and the investigation of its conformational changes. Although numerous organic dyes have been utilized as fluorescent probes in biomedical and biological studies [2], styrylcyanine dyes have recently attracted considerable attention as promising alternatives. Their distinctive property is a pronounced enhancement of fluorescence intensity upon binding to biopolymers, which is attributed to the restriction of intramolecular torsional motions and the consequent suppression of nonradiative relaxation pathways.

In this work, the interaction of a series of monomer (Sbt, Sbo, Sil) and homodimer (Dbt-10, Dbo-10, Dil-10) styrylcyanine dyes with HSA was investigated. Absorption spectra were recorded on Specord 50 SA spectrophotometer (Analytik Jena, Germany), and fluorescence spectra were measured using a FluoTime 300 spectrometer (PicoQuant, Germany). Fluorescence lifetimes were measured using the TCSPC technique with PicoHarp 300 system at excitation wavelengths of $\lambda_{ex}$=485 nm and $\lambda_{ex}$=510 nm. Molecular docking simulations were performed using AutoDock with the Lamarckian Genetic Algorithm (LGA) and the human serum albumin crystal structure (PDB ID: 1AO6) [3].

A substantial enhancement of fluorescence quantum yield, reaching up to 30-fold relative to the buffer solution, was observed for the homodimer dyes upon binding to HSA. This effect is attributed to the suppression of twisted intramolecular charge transfer (TICT) state formation following the immobilization of the dye molecules within the hydrophobic binding pocket of the protein. The resulting restriction of intramolecular torsional motions reduces the rate of nonradiative relaxation and leads to a pronounced increase in fluorescence efficiency. The binding constants ($K_s$) were determined and found to depend on the molecular structure of the probes. For the homodimer dyes, the binding constants ($K_s$) were determined to be $6.16\times10^4$ $M^{-1}$for Dbt-10, $4.57\times10^4$ $M^{-1}$ for Dbo-10, and $2.18\times10^4$ $M^{-1}$ for Dil-10. The observed dependence of Ks on the nature of the substituents can be attributed to the ability of the sulfur and oxygen heteroatoms in Dbt-10 and Dbo-10 to form additional hydrogen-bonding interactions with amino acid residues within the protein binding site. In contrast, the methyl substituent in Dil-10 contributes predominantly through hydrophobic interactions. Dbt-10 and Dbo-10 exhibit the highest affinity to HSA.

The preferential binding sites of the studied dyes within the HSA molecule were identified using competitive displacement experiments with ibuprofen and molecular docking analysis. The results revealed that the majority of the dyes preferentially bind to subdomain IIIA.The only exception was the monomer dye Sil, which was found to localize in subdomain IIA. The results of molecular modeling showed that hydrophobic interactions with residues Val 409, Lys 545, Arg 410 and hydrogen bonds with Ala 406 and Asn 405 play a key role in stabilizing the complexes.

[1] G. De Simone, R. Varricchio, T. F. Ruberto, A. di Masi, and P. Ascenzi, Heme Scavenging and Delivery: The Role of Human Serum Albumin, Biomolecules, vol. 13, no. 3, pp. 575, (2023).
[2] Y. Wang, F. Huo, and C. Yin, Development of Human Serum Albumin Fluorescent Probes in Detection, Imaging, and Disease Therapy, J. Phys. Chem. B, vol. 128, no. 5, pp. 1121–1138, (2024).
[3] S. Sugio, A. Kashima, S. Mochizuki, M. Noda, and K. Kobayashi, Crystal structure of human serum albumin at 2.5 Å resolution, Protein Engineering, vol. 12, no. 6, pp. 439–446, (1999).

# Promising targeted radiopharmaceuticals based on alphaemitter lead212

**K.A. Makoveeva, D.Yu. Chuvilin, I.N. Zavestovskaya, S.M. Deev, A.A. Artyukhov, T.M. Kuznetsova, P.D. Remizov, K.I. Nikiforova**

*National Research Center "Kurchatov Institute", 1 Akademika Kurchatov Square, Moscow, 123182, Russia*

*makoveeva_ka@nrcki.ru*

Currently, targeted radionuclide therapy is experiencing a rapid development, with extensive research and implementation of radiopharmaceuticals based on alpha- and beta-emitting radionuclides, primarily the beta-emitter lutetium-177 ($^{177}$Lu) and the alpha-emitter actinium-225($^{225}$Ac). At the National Research Centre "Kurchatov Institute", longstanding extensive work has been carried out on the production of lead-212 ($^{212}$Pb), which represents an effective alternative to $^{225}$Ac, as well as on the investigation of radiopharmaceuticals based on this radionuclide.

Among alphagenerating radionuclides, $^{212}$Pb stands out as particularly promising for targeted alpha therapy of small cancers and metastatic disease: although $^{212}$Pb is itself a betaemitter, its daughter nuclides ($^{212}$Po and $^{208}$Tl) undergo alpha decay, making it an in vivo generator of alpha particles. At the National Research Centre "Kurchatov Institute", extensive work has been carried out on the production of $^{212}$Pb and betaemitter $^{177}$Lu, as well as on the investigation of radiopharmaceuticals based on both radionuclides.

Two main approaches are currently considered for $^{212}$Pb production. The first is based on ionexchange chromatography by eluting $^{212}$Pb from a column containing $^{224}$Ra, though the short halflife of $^{224}$Ra limits effective column operation to 4–5 days. The second approach relies on emanation of gaseous $^{220}$Rn from a $^{228}$Thbearing source, followed by its transfer into a collection volume where it decays and the target $^{212}$Pb accumulates, offering the advantages of long generator lifetime (up to two years) and high radionuclide purity due to separation of solidstate parent radionuclides from the gaseous decay product. This emanation method enables a simple and efficient generator producing highpurity $^{212}$Pb without complex equipment, laborious steps or hazardous chemicals, and represents a promising route for effective $^{212}$Pb production.

The obtained $^{212}$Pb is used to investigate new chelators for improving stability and pharmacokinetic properties of radiopharmaceuticals.

Within the framework of these studies, an innovative agent based on an affibody targeting the HER2/neu antigen on the surface of tumour cells was obtained, which demonstrated satisfactory in vivo distribution in a breast tumour xenograft model, along with a clear therapeutic effect and toxicological safety.

A novel domestic agent based on a PSMA molecule for the therapy of metastatic castration-resistant prostate cancer, containing therapeutic $^{177}$Lu and $^{212}$Pb produced at the Kurchatov Institute, is currently at the preclinical trial stage.

# RBC deformability assessment via optical tweezers enhanced with deep learning

**M. Maksimov, A. Lugovtsov, A. Priezzhev**

*Faculty of Physics, Lomonosov Moscow State University, 1-2 Leninskiye Gory, Moscow, Russia, 119991*

*madoway@yandex.ru*

Red blood cells (RBC) are the most abundant blood cells, which govern the blood flow properties. To do so, RBC adapt in response to extracellular stimuli, such as signaling molecules, shear stress and oxygen saturation. The main cellular mechanisms of such adaptation are changes in RBC deformability and aggregability. At various pathologies blood microcirculation is impaired, which can lead to negative consequences. Thus, RBC deformability is critical at some diseases such as diabetes mellitus. Nowadays the RBC deformability is not included in common clinical tests, however, its assessment can lead to advances in diagnostics and treatment quality control. On the other hand, the mechanisms of cellular deformability are of fundamental interest.

To assess RBC deformability various approaches can be applied. Among the most common methods are optical microscopy combined with microfluidic systems, laser diffractometry and atomic force microscopy. Optical tweezers are also capable of cellular deformability assessment, its advantages include single cell manipulation *in vitro* without direct mechanical contact, relatively simple sample preparation and operating in fluid. The basic principle of optical tweezers is utilizing tightly focused laser beams (optical traps) to trap and manipulate nano- and microobjects.

In this work we enhance the cell deformability measurement method introduced by Fontes et al. with computer vision based on deep learning algorithm [1]. Basically, RBC are trapped and dragged at increasing velocities, which causes increasing shear stress applied to the cell, thus, increasing deformation. Visualization is achieved via CMOS camera-coupled microscope and the resulting images of deformed cells at certain velocities are analyzed. Cell segmentation is provided by Cellpose algorithm pretrained on vast dataset of various cell cultures [2]. To further increase the segmentation accuracy the model was additionally trained on manually created dataset of RBC trapped with optical tweezers.

This work was supported by the Russian Science Foundation (Grant No. 26-15-00086).

[1] M.M. Brandão, A. Fontes, M.L. Barjas-Castro, L.C. Barbosa, F.F. Costa, C.L. Cesar, S.T.O. Saad, Optical tweezers for measuring red blood cell elasticity: application to the study of drug response in sickle cell disease, Eur. J. Haematol., 70, pp. 207–211 (2003).
[2] C. Stringer, M. Pachitariu, Cellpose3: one-click image restoration for improved cellular segmentation, Nat. Methods, 22, 592–599 (2025).

# Special features of using fluorescence lifetime imaging microscopy for highly stiff tumors

**I. Markova[1,2], D. Pominova[1,2], I. Romanishkin[1], T. Savelieva[1,2], A. Skobeltsin[1,2], A. Ryabova[1,2]**

*1- Prokhorov General Physics Institute of the Russian Academy of Sciences, Moscow, 119991 Russia*
*2- National Research Nuclear University MEPhI, Moscow, 115409 Russia*

*12.inessa.markova@gmail.com*

Desmoplastic tumors, such as breast cancer subtypes, become stiff as they grow within the normal host tissue. Tissue stiffness is caused by the activation of cancer-associated fibroblasts (CAFs), which produce excessive extracellular matrix (ECM), primarily collagen and hyaluronic acid [1]. The ECM is a three-dimensional network of macromolecules that provide structural and biochemical support to the cell environment.

Changes in the mechanical properties of the ECM (increased stiffness) promote tumor growth and progression (angiogenesis, proliferation, migration and invasion of tumor cells) [2]. One of the reasons for these changes may be hypoxia within the tumour microenvironment, induced by CAFs. It is also known that ECM stiffness impedes drug penetration into the tumor site, causing tumors with a stiff matrix to be difficult to treat [3]. Thus, as the ECM is closely connected with dynamic changes in the tumor microenvironment, it plays a crucial role in modulating tumor immunity.

The formation of stiff and disordered ECM also affects the optical properties of the tumor: high heterogeneity, as well as increased scattering and absorption, can distort diagnostic data obtained using non-invasive spectroscopic methods and complicate the interpretation of the data obtained.

This study presents the results of an investigation into the fluorescence lifetimes of the endogenous coenzymes NAD(P)H and FAD in mouse tumor models with high ECM stiffness and varying collagen content (Ehrlich carcinoma, EC, and mammary carcinoma, EMT) using fluorescence lifetime imaging microscopy (FLIM). Laser-scanning confocal microscopy (LSM-710-NLO, Carl Zeiss, Germany) with a FLIM module (Becker&Hickl, Germany) was used to analyze cell metabolism. Autofluorescence of coenzymes was recorded under two-photon excitation with a 730 nm, 80 MHz femtosecond laser (Chameleon Ultra II, Coherent, USA). To assess the effect of stiffness on metabolism, EMT cell spheroids of various sizes were studied. The effect of collagen on cellular metabolism was also investigated in cultures of EMT tumor cells and 3T3 fibroblasts *in vitro*. Furthermore, model studies were conducted on the effect of scattering on measured fluorescence lifetime values using optical phantoms with varying intralipid content.

Results showed differences between the studied EMT and EC tumor models in terms of scattering levels (higher for stiffer EC tumors), blood content (lower for stiffer tumors), water content (lower for stiffer tumors) and collagen content (higher for stiffer tumors). A shift in the type of cellular respiration (towards glycolysis for stiffer tumors) was observed in both spheroids and *in vivo* tumor models.

Upon the addition of collagen, the metabolism of fibroblasts remained virtually unchanged ($t_m$ NADH – 1120 ps, NADH $a_1/a_2$ – 2.05); however, for tumor cells, we observed a marked shift towards glycolysis ($t_m$ NADH decreased from 770 ps to 610 ps, and NADH $a_1/a_2$ increased from 4.6 to 6.05). This suggests that collagen may act as a signaling factor in the interaction between CAFs and tumor cells.

Therefore, a correlation has been established between stiffness and the metabolic state of tumor cells, including a shift towards glycolysis under the influence of a stiff microenvironment and collagen content. It was also shown that high scattering can lead to distortion of data obtained using FLIM microscopy and for *in vivo* diagnostics it is advisable to perform additional scattering assessment using independent spectroscopic methods.

The work was supported by a grant from the Russian Science Foundation No. 25-12-00436.

[1] K.-X. Yu, W.-J. Yuan, H.-Z. Wang, et al. Extracellular matrix stiffness and tumor-associated macrophage polarization: new fields affecting immune exclusion, Cancer Immunol. Immunother., vol. 73, 115, (2024).
[2] X. Zhang, A. Al-Danakh, X. Zhu, et al. Insights into the mechanisms, regulation, and therapeutic implications of extracellular matrix stiff-ness in cancer, Bioeng. Transl. Med., vol. 10(1), e10698, (2025).
[3] B. Deng, Z. Zhao, W. Kong, et al. Biological role of matrix stiffness in tumor growth and treatment, J. Transl. Med., vol. 20, 540, (2022).

# Boron Neutron Capture Therapy at the National Research Centre «Kurchatov Institute»: Historical Overview and Future Prospects

**D.S. Petrunya[1,2], D.V. Andreev[1], M.N. Shushunov[1], A.N. Strepetov[1], Yu.E. Pesnya[1], G.A. Posypanova[1], E.Yu. Moskaleva[1], Ya.V. Razdrogova[3], S.M. Deyev[1], I.N. Zavestovskaya[1,2]**

*1- National Research Center "Kurchatov Institute", 1 Kurchatov Square, Moscow, Russia*
*2- Lebedev Physics Institute of the Russian Academy of Sciences, Leninsky pr. 53, Moscow, Russia*
*3- National Research Nuclear University "MEPhI", Kashirskoe shosse 31, Moscow, Russia*

*Petrunya_DS@nrcki.ru*

Boron Neutron Capture Therapy (BNCT) is one of the most promising modalities in radiotherapy for malignant neoplasms. The method is based on the selective accumulation of the stable isotope $^{10}B$ in tumour cells, followed by their irradiation with a low-energy neutron flux. As a result of the nuclear reaction $^{10}B(n,\alpha)^{7}Li$, which has a thermal-neutron capture cross-section of 3835 barns (b), high-energy α-particles and $^{7}Li$ recoil nuclei are produced, both characterised by high linear energy transfer. The range of the reaction products in biological tissue is approximately 5–10 μm, which is comparable to the typical diameter of mammalian cells (10–20 μm), thereby ensuring preferential destruction of malignant cells with minimal damage to surrounding healthy tissues. The successful implementation of BNCT requires: (1) a neutron source that fully meets clinical specifications; (2) a $^{10}B$-based agent capable of targeted delivery of the isotope to tumour cells; and (3) a dosimetric treatment planning system.

In recent years, global interest in BNCT has increased considerably. This surge is driven by advances in the development of compact and high-efficiency accelerator-based epithermal neutron sources that can be installed directly in clinical settings. In Japan, China, South Korea, and Finland, BNCT medical centres have already been commissioned or are currently entering routine operation. In the Russian Federation, an accelerator-based neutron source, VITA-IIβ, manufactured by the Budker Institute of Nuclear Physics of the Siberian Branch of the Russian Academy of Sciences, has been installed at the Federal State Budgetary Institution «N.N. Blokhin National Medical Research Center of Oncology» of the Ministry of Health of the Russian Federation. The facility is presently undergoing start-up and adjustment procedures, with the commencement of clinical trials scheduled for the first half of 2027.

Nevertheless, despite notable progress in the development of compact epithermal neutron sources, a number of unresolved issues remain that hinder the widespread implementation of BNCT. The principal challenges include the need for novel, more efficient boron-containing agents, as well as the development of reliable absorbed-dose monitoring methods and dosimetric treatment planning systems. Addressing these tasks necessitates comprehensive preclinical studies using cell cultures and laboratory animal models. Conducting such experiments on medical-grade neutron sources is difficult owing to regulatory constraints. Consequently, there is a requirement for dedicated research-grade neutron sources suitable for tackling the current physical, technical, and radiobiological challenges of BNCT.

The first experimental facility in the USSR for research in the field of BNCT was established in the 1980s on the basis of the tangential horizontal experimental channel (HEC) No. 7 of the IR-8 research nuclear reactor at the I.V. Kurchatov Institute of Atomic Energy (now the National Research Centre «Kurchatov Institute»). Effective experimental methodologies and real-time BNCT monitoring techniques were developed, relying on semiconductor spectrometry of prompt gamma radiation generated upon neutron interaction with irradiated targets. From the 1980s through 2004, the HEC-7 facility enabled over 10,000 in vitro measurements of $^{10}B$ concentration in various biological specimens, as well as the irradiation of more than 300 laboratory animals. By the end of 2004, the Kurchatov Institute surpassed any other country engaged in analogous research in terms of the total number of irradiated mice and the volume of data obtained on $^{10}B$ biodistribution in their organs and tissues.

At present, two research-grade neutron sources for BNCT are operational in the Russian Federation: the VITA™ accelerator-based neutron source at the Budker Institute of Nuclear Physics (SB RAS, Novosibirsk), and a radiobiological beamline based on the tangential HEC No. 1 of the IRT-T research nuclear reactor at Tomsk Polytechnic University. These facilities are insufficient to support a broad spectrum of preclinical studies, particularly given the high beam-time demand and their geographical remoteness from the leading research centres in the Moscow region. Consequently, expansion of the research infrastructure remains a pressing and critically needed objective.

The IR-8 research nuclear reactor at the National Research Centre «Kurchatov Institute» represents a promising platform for the development of a new radiobiological beamline that would meet modern beam-quality requirements. The specific configuration of the core and biological shielding provides a high neutron flux density at the exits of the horizontal experimental channels (HECs). In this respect, the IR-8 reactor ranks among the world's best medium-flux research reactors. The tangential HEC No. 7 is the most suitable channel for radiobiological studies, since the neutron

beam is formed outside the core, the neutron spectrum is softer, and the gamma-ray intensity is reduced compared to channels adjacent to the core.

This report presents the results of investigations into the spectral and spatial characteristics of the radiation field at the exit of HEC No. 7B, the development of novel boron-containing agents based on nanosystems produced via laser-based synthesis methods, and the first in vitro experimental results assessing their therapeutic efficacy. Furthermore, the prospects for the further development of the experimental facility based on HEC No. 7 of the IR-8 research nuclear reactor at the National Research Centre «Kurchatov Institute» are discussed.

Acknowledgements: The work was carried out within the framework of the state assignment of the National Research Centre “Kurchatov Institute.”

# Multi-wavelength Monte Carlo LSCI Modeling for Blood Vessel Depth Reconstruction

**A. Savelyev, D. Kurakina, V. Perekatova, Yu. Belozerov, I. Turchin, E. Sergeeva, M. Kirillin**

*A.V. Gaponov-Grekhov Institute of Applied Physics of the Russian Academy of Sciences, 46 Ul'yanov Street, Nizhny Novgorod, 603950, Russia*

*a.savelyev@ipfran.ru*

A crucial diagnostic parameter in biomedical applications (neuroscience, dermatology, and ophthalmology) is the localization and structural characterization of blood vessels in scattering biological tissues. Laser speckle contrast imaging (LSCI) is a widely used non-invasive technique for blood-flow visualization based on the analysis of spatial or temporal speckle contrast [1, 2]. Conventional LSCI is typically performed at a single wavelength and therefore provides limited information on vessel embedding depth.

This study presents a Monte Carlo model of multi-wavelength LSCI capable of estimating the depth of blood-vessel-like inclusions in a skin-mimicking medium. The approach exploits the wavelength dependence of tissue optical properties in the visible and near-infrared ranges inducing the variation of the effective probing depth and the relative contribution of photons scattered by superficial static tissue and moving scatterers inside the vessel. As a result, vessel contrast measured at several wavelengths can be used as a depth-dependent metric.

The Monte Carlo model simulates coherent light propagation in a two-layer skin-like medium with epidermis and dermis layers containing an embeded cylindrical vessel with moving scatterers. Optical properties were assigned for 455, 532, 655 and 970 nm according to literature data [3]. LSCI contrast maps were obtained from simulated backscattered-photon speckle patterns, with spatial speckle contrast calculated using a 7 × 7 pixel window.

The simulated contrast maps showedvessels as regions of reduced spatial contrast due to dynamic speckle blurring, while strong scattering in the superficial layer caused broadening of the apparent vessel image. For all considered wavelengths, global vascular contrast demonstrated a monotonic dependence on vessel depth and radius. The wavelength-specific dependancies in the depth-radius-contrast space, were used as a calibration dataset for vessel-depth reconstruction. For each test configuration, the vessel depth was estimated by minimizing the difference between its multi-wavelength contrast values and the interpolated Monte Carlo dataset.

The depth reconstruction error did not exceed 25% for vessels with radii larger than 0.1 mm using either a single wavelength of 970 nm or a dual-wavelength combination of 655 and 970 nm. Adding a third wavelength of 532 nm improved sensitivity for smaller vessels and reduced the minimum detectable radius to 0.1 mm. At the same time, radius reconstruction remained less reliable, indicating that the proposed approach is primarily suitable for depth-sensitive vascular mapping.

The obtained results demonstrate the feasibility of multi-wavelength LSCI as a basis for depth-sensitive visualization of subsurface blood vessels and provide a framework for further validation on tissue-mimicking phantoms and experimental LSCI data.

The study is supported by the Russian Science Foundation (project No. 24-75-10068).

[1] D.A. Boas and A.K. Dunn, Laser speckle contrast imaging in biomedical optics, Journal of Biomedical Optics, 15.1, 011109 (2010).
[2] Heeman, Wido, et al. Clinical applications of laser speckle contrast imaging: a review, Journal of biomedical optics 24.8, 080901 (2019).
[3] E.V. Salomatina, B. Jiang, J. Novak, and A.N. Yaroslavsky, Optical properties of normal and cancerous human skin in the visible and near-infrared spectral range, Journal of Biomedical Optics, 11.6, 064026 (2006).

# Immersion optical clearing of tissues in the THz range

**D.S. Ustiantseva[1], D.R. Il'enkova [1], V.V. Tuchin[2], N.V. Chernomyrdin[1], K.I. Zaytsev[1]**

*1- Prokhorov General Physics Institute of the Russian Academy of Sciences, 119991 Moscow, Russia*
*2- Saratov State University, 410012 Saratov, Russia*

*dasau9913@gmail.com*

The penetration depth of terahertz (THz) waves into hydrated biological tissues is limited by hundreds (or even tens) of microns due to their strong absorption by tissue water, which makes it possible to probe only the superficial tissues by the THz spectroscopy, imaging, and endoscopy [1-3]. Among the promising methods of increasing the THz-wave penetration depth is the immersion optical clearing (IOC) of tissues [3, 4]. The essence of this method is a replacement (reversible or irreversible) of free tissue water by hyperosmotic agent that features much less THz wave absorption. Such a replacement is carried out via the bimodal diffusion process – i.e., free water diffuses from tissues, while agent flows into them.

While IOC of tissues is widely used in the ultraviolet, visible, and infrared ranges [5], its potential in the THz gap is still to be comprehensively analyzed [1-3]. In fact, in the THz range, IOC agents should offer high diffusion ability and low THz-wave absorption, as compared to that of tissue water [1]. In our previous work, main attention was paid to independent studies of the THz optical properties and diffusion coefficient of different hyperosmotic agents, aimed at selecting the optimal ones for the THz applications [6, 7].

In this work, we continue our research on the tissue IOC in the THz range, with a focus on work with real biological tissues *ex vivo* and several *a priori* selected optimal hyperosmotic agents. For this, two laboratory setups were assembled.

- The first relies on the principles of reflection-mode backward wave oscillator spectroscopy [8], that allows to study evolution (during IOC) of the THz reflectivity of tissues *ex vivo* (those are handled at the shadow side of a reference window). THz optical properties of tissues are retrieved from the parameters of Fabry-Pérot resonances in the reflectivity spectra [9], while the diffusion coefficients – from the observed changes in these optical properties.
- The second allows to measure the collimated transmission spectra of tissues *ex vivo* in the visible range during IOC and then quantify the diffusion coefficients from these spectra. These data form a reference to verify the THz measurements.

Pilot studies of the tissue IOC using these two setups shows consistency of the diffusion coefficient retrieved from the visible and THz data, as well as considerable reduction of the THz-wave absorption of tissues upon IOC.

While these pilot results demonstrate high potential of IOC in THz range, a number of hyperosmotic agents and tissues types is still to be examined in our future studies. Meanwhile, the developed methods open broad prospects for systematic research on the tissue IOC in the THz range.

[1] K.I. Zaytsev, I.N. Dolganova, N.V. Chernomyrdin et al., The progress and perspectives of terahertz technology for diagnosis of neoplasms: a review, Journal of Optics, vol. 22(1), pp. 013001 (2020).

[2] O.A. Smolyanskaya, N.V. Chernomyrdin, A.A. Konovko et al., Terahertz biophotonics as a tool for studies of dielectric and spectral properties of biological tissues and liquids, Progress in Quantum Electronics, vol. 62, pp. 1–77 (2018).

[3] O.P. Cherkasova, D.S. Serdyukov, E.F. Nemova et al., Cellular effects of terahertz waves, Journal of Biomedical Optics, vol. 26(9), pp. 090902 (2021).

[4] V. Tuchin, Tissue Optics: Light Scattering Methods and Instruments for Medical Diagnosis (SPIE Press), 3rd edn, (2015).

[5] E.A. Genina, A.N. Bashkatov, V.V. Tuchin, Tissue optical immersion clearing, Expert Rev. Med. Devices, vol. 7(6), pp. 825–842 (2010).

[6] G.R. Musina, A.A. Gavdush, N.V. Chernomyrdin, Optical Properties of Hyperosmotic Agents for Immersion Clearing of Tissues in Terahertz Spectroscopy, Optics and Spectroscopy, vol. 128(7), pp. 1027–1034 (2020).

[7] G.R. Musina, I.N. Dolganova, N.V. Chernomyrdin et al., Optimal hyperosmotic agents for tissue immersion optical clearing in terahertz biophotonics, J. Biophotonics, vol. 13(12), pp. e202000297 (2020).

[8] G.A. Komandin, S.V. Chuchupal, S.P. Lebedev et al., BWO Generators for Terahertz Dielectric Measurements, IEEE Trans. Terahertz Sci. Technol., vol. 3(4), pp. 440–444 (2013).

[9] G.M. Katyba, S.P. Lebedev, A.S. Kucheryavenko et al., Terahertz refractometry of hard-to-access objects using the sapphire endoscope suitable for harsh environments, Appl. Phys. Lett., vol. 124(24), pp. 243703 (2024).

ALT INTERNATIONAL CONFERENCE
Advanced Laser Technologies

# LASER DIAGNOSTICS AND SPECTROSCOPY

# One and two photon PLE spectroscopy as a key to the interface properties of InP/ZnSe nanocrystals

**K.I. Russkikh, A.A. Golovatenko, A.V. Rodina**

*Ioffe Institute, Politechnicheskaya st. 26, 194021 St. Petersburg, Russia*

*anna.rodina@mail.ioffe.ru*

The spectroscopic studies of semiconductor colloidal nanocrystals (NCs) embedded in glass matrix or chemically synthesized solution started in early 80s of the past century led to a huge field of research and applications. Today, the importance of the NC research in requires no further justification following the Nobel Prize in Chemistry for their discovery awarded in 2023. The valuable information about the electronic structure and optical properties of NCs can be obtained from combining different spectroscopic methods such as one and two-photon absorption or photoluminescence excitation (1-PLE and 2-PLE) spectroscopy, Raman spectroscopy and nonlinear pump-probe spectroscopy.

While the most studied are the CdSe-based NCs, the InP-based NCs attract a lot of attention due to their lower toxicity. InP/ZnSe NCs with a ZnSe shell exhibit high quantum yields and a narrow, tunable photoluminescence spectrum, making them desirable for next-generation optoelectronic applications and the subject of active research. However, the analysis of the optical properties of the InP-based NCs is challenged by necessarily to consider the surface and interface effects. For example, the interface between InP core and ZnSe shell does not have of a common atom promoting the formation of interface electric dipoles (P-Zn and In-Se). The interface dipoles together with the elastic deformations caused by the difference of the lattice constants alter the values of conduction and valence band offsets expected due to the difference in electron affinity energies between InP and ZnSe. The uncertainty in the interface properties, in turn, makes it difficult to calculate the energy spectra theoretically.

We present a semi-analytical theoretical ***kp*** study of the energy structure and optical transitions in spherical core-shell InP/ZnSe nanocrystals [1]. The one- and two-photon absorption spectra are calculated as functions of the band offsets between the InP core and ZnSe shell and compared with the experimentally measured 1-PLE and 2-PLE spectra in thick-shell InP/ZnSe NCs [2]. We show that only the joint analysis of the one-photon and two-photon transitions between energy levels of different symmetry allows one to make the conclusions about the InP/ZnSe interface properties. We identify all exciton states responsible for the main features in the two-photon absorption spectra of InP/ZnSe NCs and predict the spectral dependence of the linear-circular dichroism. Further experimental studies of the linear-circular dichroism in the two-photon absorption or 2-PLE spectra can serve as an indicator of the symmetry of electron and hole states in InP/ZnSe NCs. Moreover, the joint analysis of the one-photon and two-photon transitions will provide access to the surface properties of thin-shell InP/ZnSe and bare-core InP NCs.

This work was supported by the Russian Science Foundation under Grant No. 23-12-00300-П.

[1] K.I. Russkikh, A.A. Golovatenko, A.V. Rodina, Band offsets in InP/ZnSe nanocrystals evaluated using two-photon transitions analysis, Nanoscale, published online 02 June (2026), DOI: 10.1039/d6nr01017b

[2] Respekta, P. Schiettecatte, L. Giordano, N. De Vlamynck, P. Geiregat, J. I. Climente and Z. Hens, ACS Nano 19, 19831 (2025).

# Tip-enhanced optical spectroscopy of one-dimensional nanostructures

**A.G. Milekhin[1], I.A. Milekhin[1,2], A.V. Taranenko[1,2], V.V. Fedorov[3], L.N. Dvoretckaia[3], I.S. Mukhin[3], V.S. Tumashev[1], A.E. Gayduk[1], A.V. Latyshev[1,2]**

*1- A.V. Rzhanov Institute of Semiconductor Physics, 630090, Novosibirsk, Lavrentjev av. 13, Russia*
*2- Novosibirsk State University, Novosibirsk, 630090, Pirogov str., 1, Russia*
*3- Alferov University, 8 Khlopina st., 194021, St. Petersburg, Russia*

*milekhin@isp.nsc.ru*

Tip-enhanced Raman scattering (TERS) is based on a combination of Atomic Force or Scanning Tunneling Microscopies (AFM or STM) and conventional Raman scattering allows studying the phonon and electron spectra of semiconductor nanostructures with nanometer spatial resolution [1,2].

Classical 1D object for TERS spectroscopy is a carbon nanotube which is used for estimation of TERS setup performance and spatial resolution in TERS experiment. However, information on TERS study of 1D semiconductor nanostructures (nanowires, nanocolunms etc.) is still scar.

Here, we present the results of experimental TERS and TEPL studies of single gallium phosphide (GaP) nanowires (NWs). The nanowires, with varying diameters and a gallium (Ga) catalyst droplet at the tip, were grown on Si(111) substrates via a self-catalyzed vapor-liquid-solid (VLS) mechanism. Formation of about 100nm-GaPAs insertion was controlled by As/P flux ratio. For optical characterization, single NWs were mechanically transferred on Si substrates covered with a thin Au layer.

AFM maps, TERS, TEPL spectra and images were obtained using an AFM AIST-NT coupled with a Raman spectrometer (Xplora, Horiba). All PL and Raman spectra were recorded under laser excitation with a wavelength of 532 and 638 nm using self-made TERS probes metallized with Au or Ag/Au.

It is shown that Ag-coated tip provides the maximal enhancement of TERS by optical phonons while probing GaP NWs with incident light at a wavelength of 532 nm. We detect background emission induced by gap plasmon inherent for joint system composed of Au cluster on the tip apex and Ga droplet of the NW using Au-coated TERS tip. TERS imaging enables us to track evolution of GaP phonon modes intensity along the NW with a spatial resolution of about 20 nm and to probe both the enhancement and quenching of TERS signal. Moreover, we manage to utilize phonon mode of $Ag_2S$ originated from the Ag-coated TERS tip, to scan the NW and construct TERS map which reproduces the peculiarities of the TERS image obtained for GaP TO phonon intensity.

TEPL images of single GaP nanowire with a direct bandgap GaPAs insertion with a spatial resolution of about 10 nm were obtained. Beside of intense interband TEPL band observed from the insertion near 720 nm, the Fabry-Perot (FP) resonance fringes modulate the PL band. Near-field optical images reveal an ordered pattern associated with the spatial localisation of the FP modes. The role of localized surface plasmon originated at metallized TEPL tip for spatial imaging of FP resonances in semiconductor nanostructures is discussed.

This work was supported by the Russian Science Foundation (project 22-12-00302 P).

[1] I.A. Milekhin, M. Rahaman, A.V. Tsarev, K.V. Anikin, E.E. Rodyakina, T.A. Duda, B.M. Saidzhonov, R.B. Vasiliev, A.G. Milekhin, A.V. Latyshev, D.R.T. Zahn, Applied Surface Science, v. 686, pp.162144, (2025).
[2] N.N. Kurus, V. Kalinin, N.A. Nebogatikova, I.A. Milekhin, I.V. Antonova, E.E. Rodyakina, A.G. Milekhin, A.V. Latyshev, D.R.T. Zahn, RCS Advances, 14, 3667-3674 (2024).

# Strong coupling of chiral light with chiral matter: a macroscopic study

**S.A. Dyakov[1], N.S. Salakhova[1], A. Demenev[2], O. Klimenko[1,3], V.D. Kulakovskii[2], V. Antonov[1], N.A. Gippius[1]**

*1- Skolkovo Institute of Science and Technology, Moscow, 121205, Russia*
*2- Osipyan Institute of Solid State Physics RAS, Chernogolovka, 142432, Russia*
*3- Lebedev Physical Institute of RAS, Moscow, 119991, Russia*

*s.dyakov@skoltech.ru*

The study of optical chirality is important for understanding the fundamental principles of light-matter interaction [1]] which may lead to advances in chiral molecule sensing and drug development. The feasibility of all these advancements depends on the successful design of affordable and effective resonators that support chiral electromagnetic eigenmodes.

We designed and fabricated a handedness-preserving mirror based on a one-dimensional grating of silicon stripes on a Bragg mirror, which maintains the handedness of both left and right circularly polarized incident light. The mirror demonstrates remarkable stability against deviations in geometric parameters and angle of incidence, while operating over a broad spectral range exceeding 100 nm. Experimental characterization of fabricated samples achieved 98% handedness conservation, even with non-optimal geometries, confirming the design's robustness. Furthermore, we theoretically studied a Fabry-Perot resonator formed by a pair of these mirrors. By placing a chiral material characterized by a Lorentz pole in its macroscopic parameters inside the cavity, we predict enantioselective strong coupling. This effect should manifest as distinct spectral signatures in transmission spectra depending on the handedness compatibility between the cavity modes and the chiral medium, enabling selective optical discrimination of molecular enantiomers. The findings of this study contribute to the development of techniques for the selective optical detection of chiral organic molecules, further advancing the field of chiral photonics.

This work was supported by the Russian Science Foundation Grant No. 25-12-00454.

[1] Baranov, D. G., Schafer, C., Gorkunov, M. V. (2023). Toward molecular chiral polaritons. ACS Photonics, 10(8), 2440-2455.
[2] Dyakov, S. A., Salakhova, N. S., Ignatov, A. V., Fradkin, I. M., Panov, V. P., Song, J. K., Gippius, N. A. (2024). Chiral light in twisted fabry–p′erot cavities. Advanced Optical Materials, 12(12), 2302502.
[3] Dyakov, S., Smagin, I., Salakhova, N., Blokhin, O., Baranov, D. G., Fradkin, I., Gippius, N. (2025). Strong coupling of chiral light with chiral matter: a macroscopic study. Optica, 12(9), 1406-1416.

# Chiral exciton engineering in hybrid structures based on atomically thin 2D $A^{II}B^{VI}$ semiconductors for photonics

**R.B. Vasiliev, D.A. Kurtina, M.Yu. Platonova, A.I. Lebedev**

*Lomonosov Moscow State University, Leninskie Gory119991, Moscow, Russia*

*romvas@inorg.chem.msu.ru*

Chirality refers to the asymmetry of objects that cannot be superposed on their mirror image. This paradigm exists in various scientific fields, ranging from biology, chemistry, and pharmacology to recent advances in chiral phonons, topological systems, and chiral materials, which have brought this topic to the forefront of interdisciplinary research. Chiral inorganic nanostructures strongly interact with circularly polarized light, absorbing or emitting left- or right-polarized photons [1]. The exhibiting of mirror asymmetry makes chiral nanostructures candidates for a number of important applications, including chiral sensing, asymmetric catalysis, enantiomeric separation, and circularly polarized photon emitters and detectors. We examine atomically thin (less than 1 nm thick) nanosheets of semiconductor cadmium and zinc chalcogenides grown in colloidal systems with precisely controlled thicknesses at the atomic plane level [2]. A distinctive feature of the synthesis method is the ability to hybridize with organic molecules. We used chiral compounds with various anchoring groups to induce chirality in the resulting nanostructures.

We discuss the results of circular dichroism, magnetic circular dichroism, and optical rotation for various examples of the obtained nanostructures and their relationship with the composition and helical shape of the synthesized 2D nanostructures. Atomically thin (less than 1 nm) nanostructures of cadmium and zinc chalcogenides were grown in colloidal systems [3, 4]. For the hybridization of nanostructures with chiral ligands, protocols were developed for replacing the native oleic acid ligand with stereoisomers of a number of chiral ligands. In the case of nanostructures based on cadmium selenide, enantiomers of N-acetyl-L-/D-cysteine were used, which were attached to cation-rich planes by a thiolate group, while the carboxyl group ensured colloidal stability. For zinc selenide-based nanostructures, enantiomers of L-/D-methylbenzylamine were used, anchored to neutral planes by an amino group. The resulting chiral nanostructures exhibited chiroptical properties with pronounced mirror-asymmetric bands corresponding to hh and lh excitons. The influence of ligand type, nanostructure size, and shape on the observed chiral transitions was analyzed. The contributions of helical shape, dissymmetric distortion of the crystal structure and dipole-dipole interaction are discussed. We hypothesize a dipole–dipole interaction between an exciton in the plane of the 2D nanostructure and a dipole involving the contribution of the asymmetric ligand center. This is confirmed by the influence of permittivity on the dissymmetry factor. On the other hand, chiral scattering indicates a contribution from the helical shape, leading to an increase in the dissymmetry factor with increasing lateral dimensions of the nanostructure. This may be attributed to helical distortions in stacks of flat zinc selenide nanostructures or folded cadmium selenide nanostructures. The proposed approaches to nanostructure engineering enable both the induction of chiral excitons or the enhancement of chiral scattering depending on type of nanostructures.

The demonstrated unique properties of chiral two-dimensional excitons with mirror asymmetry observed in chiral nanostructures of 2D II–VI compounds demonstrate their great potential for applications in photonics and optoelectronics.

This work was supported by the Russian Science Foundation (grant № 25-13-00416).

[1] Z. Nazir, N. Liu, M. A. Khan, et al., Chirality-Induced Spin Selectivity in II-VI and III-V Semiconductor Nanocrystals: Mechanism, Manipulation, and Application," Advanced Optical Materials 14, 02769 (2025)

[2] Kurtina D.A. et.al., Atomically Thin Population of Colloidal CdSe Nanoplatelets: Growth of Rolled-up Nanosheets and Strong Circular Dichroism Induced by Ligand Exchange, Chem. Mater., 31, 9652–9663, (2019).

[3] Kurtina, D.A. et al. Induction of Chirality in Atomically Thin ZnSe and CdSe Nanoplatelets: Strengthening of Circular Dichroism via Different Coordination of Cysteine-Based Ligands on an Ultimate Thin Semiconductor Core. Materials, 16, 1073 (2023).

[4] D.A. Kurtina et al., Solvent effect on chiroptical properties of chiral atomically thin CdSe nanoplatelets capped with enantiomeric ligands. Optical Materials, 158, 116483 (2025).

# Features of photoluminescence of porous anodic aluminum oxide

**E.V. Kytina[1], O.A. Shalygina[1], P.P. Shcherbakov[2,1], D.A. Dronova[2,1], E.A. Konstantinova[1]**

*1- Faculty of Physics, M.V. Lomonosov Moscow State University, Leninskie Gory 1/2, 119991 Moscow, Russia*
*2- National Research University of Electronic Technology – MIET, Shokina 1, 124498 Zelenograd, Moscow, Russia*

*kata13012002@mail.ru*

Currently, anodic aluminum oxide, which is an array of ordered nano-sized pores (por-$Al_2O_3$), is being actively studied by the world scientific community with the aim of creating optical biosensors for biomarkers [1, 2]. The main advantages of por-$Al_2O_3$ are the simplicity and low cost of synthesis, and a large specific surface area [1,2]. It is known that photoluminescence (PL) in por-$Al_2O_3$ is of a defect nature, but the question of the type of defects still remains open [3, 4]. The purpose of this work was to study the PL of por-$Al_2O_3$ obtained in both organic and inorganic acids at different synthesis temperatures and to identify the defects responsible for PL in this material.

The synthesis of por-$Al_2O_3$ was carried out by anodic oxidation in dilute solutions of oxalic (por-$Al_2O_3$-Ox), sulfuric (por-$Al_2O_3$-S) and selenic (por-$Al_2O_3$-Sel) acids in galvanostatic mode. The acid concentration was (0.45 or 1.5 M), the current density was 15 mA/cm$^2$, the synthesis temperature varied from t=5 to t=40°C. PL was excited by using a He-Cd laser (photon energy 3.8 eV, excitation power 5 mW). The laser beam was focused on the sample into a spot of 1 mm diameter. The PL signal was dispersed by a 50 cm monochromator and was detected by a CCD array (spectral region 1.1 - 2.2 eV). Spin centers (defects) were detected using the electron paramagnetic resonance (EPR) technique.

The PL of por-$Al_2O_3$-Ox consists of two bands with maxima at 2.2 eV (very low intensity) and 2.7 eV (very high intensity). The EPR signals of por-$Al_2O_3$-Ox represent a single isotropic line with a g-factor equal to 2.0024±0.0003, which refers to oxygen vacancies with an unpaired electron ($F^+$ spin centers) in aluminum oxide. According to XRD data, all samples have an amorphous structure. A correlation has been established between the intensity of the PL band at 2.7 eV and the defect concentration $N_s$, and thus it can also be assumed that $F^+$ centers contribute to the radiative recombination of photoexcited electrons and are responsible for the PL band at 2.7 eV. The intensity of the PL band at 2.2 eV does not correlate with the concentration of $F^+$ centers and, therefore, is due to radiative recombination of photoexcited electrons on nonparamagnetic centers, which were probably formed because of the introduction of molecular fragments of oxalic acid into the structure of the samples during anodization. The samples of por-$Al_2O_3$-S and por-$Al_2O_3$-Sel were characterized by extremely low PL intensity (at background level). Using the EPR technique, it was established that the concentration of $F^+$ centers in por-$Al_2O_3$-Ox is more than an order of magnitude greater than in por-$Al_2O_3$-S and por-$Al_2O_3$-Sel. At the same time, other defects (oxygen radicals and fragments of selenic and sulfuric acids) were recorded in por-$Al_2O_3$-Sel and por-$Al_2O_3$-S in high concentrations exceeding the concentrations for $F^+$ centers. Note that the presence of acid fragments in the composition of por-$Al_2O_3$ is confirmed by XPS data. Thus, PL in por-$Al_2O_3$, regardless of the synthesis conditions, occurs at $F^+$ centers. This is an important result, which makes it possible to eliminate the contradictions in literature in establishing the nature of the defects responsible for PL.

The data obtained can be used to create an optical sensor platform with controlled PL intensity. The study was supported by the Russian Science Foundation grant No. 24-19-00402, https://rscf.ru/project/24-19-00402/.

[1] A. Santos, T. Kumeria, D. Losic, Nanoporous anodic aluminum oxide for chemical sensing and biosensors, Trends Anal. Chem., vol. 44, pp. 25–38, (2013).
[2] A. Abd-Elnaiem, Z. Mohamed, S. Soliman, M. Almokhtar, Synthesis, characterization, and optical sensing of hydrophilic anodic alumina films, Opt. Mater., vol. 157, p. 116390, (2024).
[3] G. Khan, A. Singh, K. Mandal, Structure dependent photoluminescence of nanoporous amorphous anodic aluminium oxide membranes: Role of F+ center defects, J. Lumin., vol. 134, pp. 772–777, (2013).
[4] K. Staninski and M. Kaczmarek, Afterglow luminescence phenomena in the porous anodic alumina, Opt. Mater., vol. 121, p.111615, (2021).

# Life path of a molecular luminophore in hydrothermal synthesis of carbon dots

**A. Vervald[1,2], K. Laptinskiy[1,2], A. Korepanova[1], T. Dolenko[1,2]**

*1- Faculty of Physics, Lomonosov Moscow State University, 1, Building 2, Leninskie Gory, Moscow 119991, Russian Federation*
*2- Skobeltsyn Institute of Nuclear Physics, Lomonosov Moscow State University, 1, Building 2, Leninskie Gory, Moscow 119991, Russian Federation*

*alexey.vervald@physics.msu.ru*

The hydrothermal synthesis of carbon dots (CDs) begins with the mixing of precursors that then go through stages of polymerization, dehydration, carbonization, and possible graphitization [1,2]. In this process the reaction products obtain luminescence that changes from one synthesis stage to another. At stages prior to the massive graphitization, the main luminescence source is often determined to be the molecular luminophores. The life path of such luminophores – when and how they form, transform, and then de- or over-form, – is closely related to the changes in the properties of CDs being synthesized.

The present study analyses the life path of the luminophores during the hydrothermal treatment of an aqueous solution of citric acid (CA) and ethylenediamine (EDA). Under certain conditions this treatment produce structures with ultra-bright luminescence in the violet-blue region with a quantum yield up to ~100%. Most publications suggest that this luminescence is due to (and only) luminophore IPCA (5-oxo-1,2,3, 5-tetrahydroimidazo[1,2-a]pyridine-7-carboxylic acid) (Fig. 1) [3]. Our study [2] of 392 CA and EDA samples subjected to hydrothermal synthesis with varying EDA:CA ratio in the range of 0–20:1, temperature in 80–200 °C, and reaction time in 0.5–6 h, showed that the formation of samples' main luminophores starts with the polymerization of precursors, accelerates with the initial carbonization of the samples, while the stage of graphitizing carbonization – formation of CDs' cores – brings their partially destruction. The present study compares all these samples to the IPCA.

The luminescence of all CD samples is found to never fully repeat the luminescence of IPCA, however the difference at minimum is found to be lower than 3% (Fig. 1, middle map). Such low difference is typical for the samples with EDA:CA ratio ≤ 1:1 that have bright luminescence, while the bright samples with EDA:CA ratio ≥ 2:1 have shifted luminescence and thus not IPCA but its modification. The nature and dynamic of main and other luminescence peaks (see Fig. 1, right map) are analyzed. The fractionation of the bright samples via electrophoresis showed that despite the separation of sample to over 6 fractions with different optical properties, all of them contain IPCA-like luminescence.

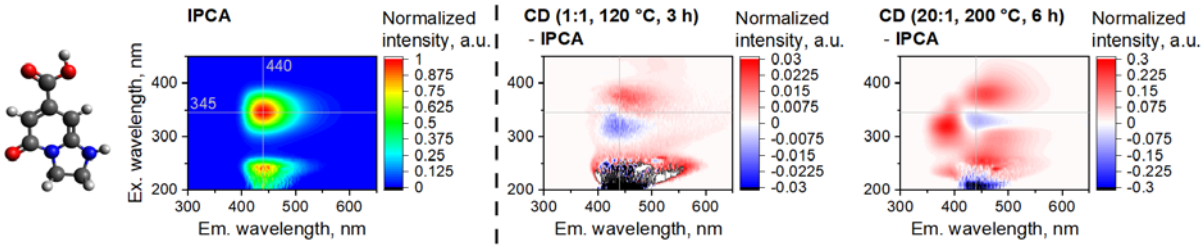


**Fig. 1.** Structure and excitation-emission map (EEM) of IPCA, difference EEMs of CDs and IPCA.

The study was supported by the grant from the Russian Science Foundation No. 22-12-00138-P, https://rscf.ru/en/project/22-12-00138/.

[1] N. Papaioannou, M.-M. Titirici, A. Sapelkin, Investigating the effect of reaction time on carbon dot formation, structure, and optical properties, ACS Omega, 4, pp. 21658-21665, (2019).
[2] A. M. Vervald, K. A. Laptinskiy, M. Yu. Khmeleva, T. A. Dolenko, Toward carbon dots from citric acid and ethylenediamine, part 1: Structure, optical properties, main luminophore at different stages of synthesis, Carbon Trends, 19, 100452, (2025).
[3] P. Duan, B. Zhi, L. Coburn, C. L. Haynes, K. Schmidt-Rohr, A Molecular fluorophore in citric acid/ethylenediamine carbon dots identified and quantified by multinuclear solid-state nuclear magnetic resonance, Magn. Reson. Chem., 58, pp. 1130-1138, (2020).

# Transfer Learning for Effective Increase of the Number of Simultaneously Determined Parameters in Solving Multi-Parameter Inverse Problems of Spectroscopy

**A. Mardanov[1], A. Guskov[1,2], I. Isaev[2], K. Laptinskiy[2], T. Dolenko[1,2], S. Dolenko[2]**

*1- Physics Department, M.V. Lomonosov Moscow State University, 1/2 Leninskie Gory, Moscow, 119991, Russia*
*2- D.V. Skobeltsyn Institute of Nuclear Physics, M.V. Lomonosov Moscow State University, 1/2 Leninskie Gory, Moscow, 119991, Russia*

*dolenko@srd.sinp.msu.ru*

In spectroscopy, the main challenge in terms of data processing is solving inverse problems (IPs), which involve reconstructing the target parameters of an object from its spectra. These problems often have known negative properties that make them difficult to solve: they are often ill-posed or even incorrect due to low stability and non-uniqueness of their solution.

An example of such a problem that is often encountered in practice is determination of concentrations of components in a multi-component mixture or solution by the shape of its spectrum, sensitive to the concentrations of the components. Various types of spectra may be used to perform this task: optical or IR absorption spectra, photoluminescence spectra, Raman spectra and others.

Spectroscopic IPs have several inherent properties that make them challenging to solve using conventional methods. Such problems usually have a high input dimension, with a large number of channels in the spectrum. They are typically non-linear (especially if the objects are liquids), which makes them computationally complex or even unsolvable with conventional IP solution methods.

To address these challenges, machine learning (ML) methods have emerged as an effective alternative. ML algorithms are well suited to handle the high dimensionality and non-linear nature of spectroscopic IPs. They can often provide solutions that are both accurate and computationally efficient.

However, along with their advantages, ML methods face some challenges, the most notable of which is the need for a large volume of data to train ML models effectively. This can be particularly problematic in the context of experimental spectroscopic data, which is often costly to obtain, requiring specialized equipment, expensive reagents, and qualified personnel, making data acquisition an expensive endeavor.

Moreover, each possible combination of components (e.g. ions in the solution) requires its own dataset to train ML models. If the component composition of the object (solution) is changed, it is necessary to re-collect the data and to retrain the ML models on new data. At the same time, adapting the already trained models to another component composition may require less experimental spectra (reducing experimental costs) and less computational resources.

Transfer learning (TL) [1] is a special approach allowing efficient transfer of a model trained on one dataset (source domain) to another dataset (target domain), if both domains describe similar problems. TL may be effectively applied also in solving IP [2, 3].

In this study, we consider the IP of determining concentrations of 6 types of ions (heavy metal cations ($Cu^{2+}$, $Ni^{2+}$, $Al^{3+}$, $Co^{2+}$, $Cr^{3+}$) and $NO_3^-$ anion) in water solutions by the shape of photoluminescence 2D spectrum of carbon dots (CD) (synthesized by hydrothermal method from ethylenediamine and citric acid) added to the solution. This 6-parameter (6P) IP is the source domain, and the target domain is a similar problem with possible presence of one more cation $Pb^{2+}$ (7P IP). The IPs are solved by artificial neural networks, gradient boosting and other ML methods. We compare various implementations of TL.

It is demonstrated that correct use of TL provides solution of the 7P IP (target domain) with comparable quality at less computational cost and using a smaller number of patterns (spectra obtained in experiment) than direct re-training of the models in the target domain.

This study has been conducted at the expense of Russian Science Foundation grant no. 24-11-00266, https://rscf.ru/en/project/24-11-00266/.

[1] J. Wang, Y. Chen, Introduction to Transfer Learning (Springer Nature), (2023).
[2] A. Guskov et al., Transfer Learning for Neural Network Solution of an Inverse Problem in Optical Spectroscopy, Moscow University Physics Bulletin, vol.78, pp. S115–S121, (2023). https://doi.org/10.3103/S0027134923070111
[3] M.Shaleev et al., Transfer Learning for Neural Network Solution of Inverse Problems in Exploration Geophysics with Limited Data, Studies in Computational Intelligence, vol.1241, pp. 477-486, (2026). https://doi.org/10.1007/978-3-032-07690-8_38

# Raman and Fluorescence Spectroscopy of Interactions of Carbon Nanoparticles with Ions in Multicomponent Solutions

**S. Burikov[1], A. Vervald[1], K. Laptinskiy[1,2], K. Kozhushnyi[1], L. Utegenova[1], G. Chugreeva[1], I. Plastinin[1,2], T. Dolenko[1,2]**

*1- Department of Physics, Lomonosov Moscow State University, Leninskiye Gory 1/2, 119991 Moscow, Russia*
*2- Skobeltsyn Institute of Nuclear Physics, Lomonosov Moscow State University, Leninsky Gory 1/2, 119991 Moscow, Russia*

*tdolenko@mail.ru*

The relevance of developing optical nanosensors of environmental parameters is due to active development of science and industry, where the issue of controlling the composition of various substances in multicomponent media is becoming increasingly acute. Currently, one of the most promising bases for such sensors are carbon dots (CD). CD have intensive photoluminescence (PL) sensitive to environmental parameters, which makes it possible to develop sensors of these parameters based on CD.

In our study, the objects of research were CD obtained by hydrothermal synthesis from citric acid and ethylenediamine. The effect of $Fe^{3+}$, $Cr^{3+}$, $Al^{3+}$, $Co^{2+}$, $Cu^{2+}$, $Pb^{2+}$, $Zn^{2+}$, $Ni^{2+}$, $Mg^{2+}$ ions in water on the PL of our CD was found. It turned out that all the ions studied extinguish the PL of carbon dots in water to varying degrees. Based on this, luminescent multimodal CD-nanosensors capable of simultaneously detecting the concentrationd of 8 ions were developed using machine learning methods [1]. However, to increase the sensitivity and to make the use of CD-nanosensors more effective in specific tasks, it is necessary to study the various interactions of ions and water molecules with the CD surface and to understand the mechanisms of the influence of these interactions on the PL of nanoparticles.

For this purpose, the interactions of $Co^{2+}$, $Zn^{2+}$, $Ni^{2+}$, $Al^{3+}$, $Li^{+}$, and $NO_3^-$ ions with each other, with water molecules and with CD functional surface groups in multicomponent solutions were studied experimentally and theoretically.

Based on the results of laser Raman macro- and microspectroscopy, it was found that the differences in the effect of the studied ions on the network of hydrogen bonds in water and on the vibrations of water molecules in multicomponent solutions are due to the competition of the formation of ion hydrate shells of different strengths, their ability to form contact or solvate-separated ion pairs, as well as differences in the steps of hydrolysis of ionic complexes.

With the help of the discovered competitive processes occurring between the studied ions and water molecules in solutions, the mechanisms of interaction of ion complexes with the surface functional groups of CD and the degree of influence of ions on their fluorescence were explained. The conclusions were confirmed by the results of calculations of ion interactions with the CD surface in multicomponent solutions using molecular dynamics.

The results obtained are extremely important for the targeted development of fluorescent nanosensors based on CD for various environments. Knowledge of the mechanisms of influence of environmental parameters on the PL of carbon nanomaterials allows solving fundamental problems of nanotechnology and materials science.

The research was carried out at the expense of the grant from the Russian Science Foundation no.22-12-00138-P, https://rscf.ru/en/project/22-12-00138/.

[1] G.N. Chugreeva, K.A. Laptinskiy, A.A. Guskov, G.A. Kupriyanov, I.V. Isaev, S.A. Dolenko, T.A. Dolenko. Machine Learning Methods for Designing a Carbon Dot Based Photoluminescent Multimodal Nanosensor. Scientific Reports, 2026, V.16, art. 11808. DOI 10.1038/s41598-026-38266-4.

# CARS of rotational GHz resonances of ortho- and para-$H_2O$ in water: ortho/para ratio 1:1

**S.M. Pershin, A.F. Bunkin, E.V. Stepanov**

*Prokhorov General Physics Institute of the Russian Academy of Sciences.*
*119991, Vavilov str. 38, Moscow, Russia*

*pershin@kapella.gpi.ru*

On the 100th anniversary of the birth of Academician R.V. Khokhlov, a pioneer and founder of nonlinear optics [1], we note the significant contribution of nonlinear optics to the discovery of new properties of materials. Undoubtedly, CARS, which was first implemented by the staff of R.V. Khokhlov's department [2], is one of these. Thus, for the first time [3], to our knowledge, we discovered the rotation of $H_2O$ molecules in the GHz range with giant absorption in water using low-frequency CARS developed by A.F. Bunkin. The first recorded rotational resonances were attributed to the spin isomers of ortho-$H_2O$ and para-$H_2O$ in accordance with the international HITRAN database. Fig.1 (circles) shows a fragment of the spectrum in the vicinity of two lines: ($4_{04} - 3_{13}$) and ($4_{14} - 3_{03}$) para- and ortho-, respectively. From Fig.1 it is evident that in water the ortho/para ratio = 1:1, while in air it is 1:3 (HITRAN) [4]. Note the peculiarity of ortho- and para-$H_2O$ spin isomers – selectivity of interaction with proteins in aqueous solutions due to continuous rotation of ortho-$H_2O$ (there is no zero rotational level [5]). From Fig.1 (squares) it is evident that the intensity of the para-$H_2O$ monomer line (79.8 cm-1) is absent in the α-hymotrypsin protein solution, which indicates a noticeable decrease in the concentration of para-$H_2O$ isomers due to the formation of hydration shells of the protein [6]. It should be noted that the presence of monomers in water is confirmed by lines in the vicinity of 3700 $cm^{-1}$ of the OH band in the experiments of Y. Shen et al. [7] (see Fig.2). The question remained open: where do $H_2O$ molecules rotate in water? Rotation of $H_2O$ molecules with a size of ~0.27 nm can occur in ice-like channels with a diameter of ~0.3 nm [8], as in aquaporin channels [9], with the possibility of tunneling [10]. Recently [11], the ortho/para ratio of 1:1 in water was confirmed by diode spectroscopy of H2O spin isomers during forced fragmentation of water with an ultrasonic fountain without the thermal evaporation phase.

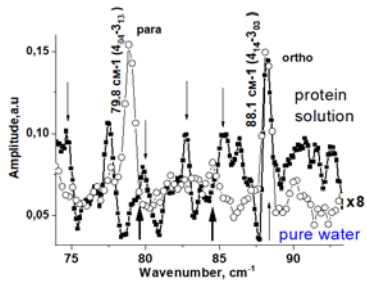


Fig.1

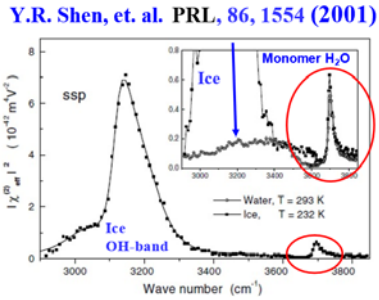


Fig.2

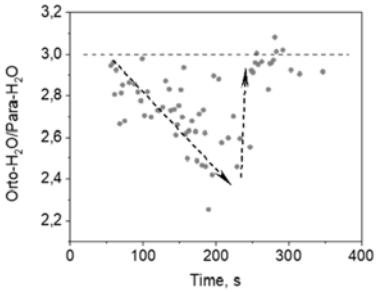


Fig.3

This work was supported by the Russian Science Foundation (project No. RSF-23-42-10019)

[1] S. A. Akhmanov and R. V. Khokhlov, Problems of Nonlinear Optics: Electromagnetic Waves in Nonlinear Dispersive Media (Akad. Nauk, Moscow, 1964; Gordon and Breach Science, London, 1972).
[2] С. А. Ахманов, В. Г. Дмитриев, А. И. Ковригин, Н. И. Коротеев, В. Г. Тункин, А. И. Холодных. Метод нелинейной спектроскопии комбинационного рассеяния, использующий перестраиваемые параметрические генераторы света, Письма в ЖЭТФ, том 15(10), 600, (май, 1972).
[3] A. F. Bunkin, A. A. Nurmatov, S. M. Pershin, "Coherent four-photon spectroscopy of low-frequency molecular librations in a liquid", UFN, 176:8 (2006), 883–889; Phys. Usp., 49:8 (2006), 855–861. DOI: https://doi.org/10.3367/UFNr.0176.200608h.0883
[4] S. M. Pershin and A. F. Bunkin, "Temperature evolution of the relative concentration of the H2O ortho/para spin isomers in water studied by four-photon laser spectroscopy," Laser Phys. 19, 1410 (2009). https://doi.org/10.1134/S1054660X0907007X
[5] L. D. Landau and E. M. Lifshitz, Quantum Mechanics, 3rd ed. (Pergamon, Oxford, 1981).
[6] A.F. Bunkin, S.M. Pershin, and A.A. Nurmatov, Four-photon spectroscopy of ortho/para spin-isomer H2O molecule in liquid water in sub-millimeter range, Laser Phys. Lett. 1–3 (2006) / DOI 10.1002/lapl.200610007
[7] Y.Shen et al., Surface vibrational spectroscopic study of surface melting of ice, Phys. Rev. Lett., 86(8), 1554 (2001)/
[8] S.M. Pershin et al., A.F. Bunkin, & V.L. Golo, H2O monomers in channels of icelike water structures. J. Exp. Theor. Phys. 115, 1008 (2012). https://doi.org/10.1134/S1063776112130109
[9] P. Agre et al., Structural determinants of water permeation through aquaporin-1, Nature, 407(6804), 599-605 (2000), doi:10.1038/35036519
[10] A. I. Kolesnikov et al., Quantum Tunneling of Water in Beryl: A New State of the Water Molecule, Phys. Rev. Lett. 116, 167802 (2016)
[11] E. V. Stepanov, S. M. Pershin, and D. A. Gerashchenko, "Laser analysis of the nonequilibrium ratio of the ortho and para H2O number density in vapor by the ultrasonic vaporization of water," Opt. Lett. 50, 7492 (2025). https://doi.org/10.1364/OL.575896

# Applications of Raman Spectroscopy in Earth Sciences: A Case Study of Deep-Seated Xenoliths from the "Eclogite" Pipe (Eastern Pamir)

**A.V. Korsakov[1], S.P. Demin[1], E.E. Podgolnikova[1,2], D.S. Mikhailenko[3], Sh.A. Odinaev[4,5], M.L. Gadoev[5]**

*1- V.S. Sobolev Institute of Geology and Mineralogy SB RAS, Novosibirsk, 630090, Koptyiga 3, Russia*
*2- Novosibirsk State University, Novosibirsk, 630090, Pirogov st., 1, Russia*
*3- A.N. Zavaritsky Institute of Geology and Geochemistry IGG UB RAS, Yekaterinburg, 620110, Akademika Vonsovskiy st., 15, Russia*
*4- Guangzhou Institute of Geochemistry, Chinese Academy of Sciences (GIG CAS), Guangzhou, Kehua st., 511, China*
*5- Institute of Geology, Earthquake Engineering and Seismology, National Academy of Sciences of Tajikistan, Dushanbe, 734063, Ayni st., 267, Tajikistan*

*korsakov@igm.nsc.ru*

Raman spectroscopy, including Raman mapping, is increasingly used in the Earth sciences to address a wide range of geological problems. Traditionally, the technique has been applied to characterize the composition and structure of fluid, melt, and solid inclusions, providing critical constraints on geological processes. While solid inclusions can often be analyzed by complementary methods, fluid and gas compositions can only be retrieved from unopened inclusions. Opening such inclusions results in the loss of volatiles and, consequently, of invaluable information required to understand deep-Earth processes and the formation of strategic mineral deposits. The small size of fluid and melt inclusions (typically 10–15 μm) adds further complexity, making Raman spectroscopy an essential tool for their investigation.

Here we present results of Raman mapping of melt inclusions in minerals from high-pressure xenoliths recovered from the Eclogitovaya diatreme (Eastern Pamir). These samples are remarkable due to their rapid ascent from depths exceeding 90 km — on the order of days in geological terms — which favored the preservation of relict minerals from high-pressure, high-temperature parageneses [1].

Melt inclusions identified in various minerals were found to contain glass and a coexisting fluid phase. Raman spectra of the glass allowed estimation of the water content in the original melt and reconstruction of the fluid composition. In most samples, the fluid phase is dominated by $CO_2$, with only rare cases showing significant methane. Graphite inclusions were also identified [2]; their well-ordered structure, as revealed by Raman spectroscopy, points to formation at high temperatures. Despite thorough investigation, no diamond inclusions were observed, suggesting that pressures during crystallization were below the diamond stability field.

This work was supported by the Russian Science Foundation (grant No. 24-17-00164).

[1] Korsakov A. V. et al. Melt Inclusions in Minerals of Granulitic Xenoliths from Diatremes of Eastern Pamir, Tajikistan: Evidence of Incongruent Melting at the Crustal–Mantle Boundary. Doklady Earth Sciences. 2025. Vol. 520, No. 1. P. 13.
[2] Podugolnikova E. E. et al. Raman Spectroscopic Study and Isotopic Composition of Graphite Inclusions in HP Xenoliths From "Eclogitovaya" Pipe (The Eastern Pamir). Journal of Raman Spectroscopy, 2025. Vol. 56, No. 11. P. 1178–1187.

# Stimulated Brillouin Scattering Spectral and Temporal Characteristics Dependence on Water Salinity

**M. Karpov, A. Kudryavtseva, T. Mironova, A. Skrabatun, N. Tcherniega, S. Umanskaya**

*P. N. Lebedev Physical Institute of the Russian Academy of Sciences, Leninskii pr. 53, 119991, Moscow, Russia*

*akudr@lebedev.ru*

The state of water in the world's oceans has a huge impact both on the climate of our planet and on the formation of weather conditions in various regions. Different industries and economic activities are associated with the seas and oceans: oil production from offshore fields, shipping, fishing, aviation over the seas and oceans, etc. Many kinds of geological processes occur on the seabed, such as shifts in the regions of the earth's crust, eruptions of underwater volcanoes, and earthquakes. All this makes it necessary to monitor sea water and study water characteristics depending on different conditions (temperature, salinity, pressure). Sea water monitoring is carried out both directly at the measurement site and remotely. One of important methods to detect sea water characteristics is stimulated Brillouin scattering (SBS). SBS gives a possibility to obtain useful information, for instance, the speed of sound, because Brillouin frequency shift depends on its value. A lidar method based on Brillouin scattering allows not only to carry out remote sensing of sea water in the upper ocean mixed layers, but also to obtain water characteristics profile at the depths up to 100 m. In [1] spaceborne Brillouin lidar was used for sea water study in different seas both in the day and in the night. The dependences of the frequency shift and the speed of sound on the temperature in clean water and sea water with different salinity have been experimentally measured [2]. Both temperature and salinity lead to an increase of the SBS frequency shift and linewidth [3,4]. Salinity is very important characteristic of a sea water. Salt presents in micro- and nanodrops of water over the sea, which influences atmospheric processes, which form weather conditions in the definite regions. Despite the more and more important role of the remote sensing of the sea water characteristics, laboratory studies of sea water are also important. In this work we investigated SBS spectral and temporal characteristics dependencies on the salinity of water with NaCl and seawater from different seas and oceans.

For SBS excitation we used Nd:YAG laser 2$^{nd}$ harmonic ($\lambda$ = 532 nm, $\tau$ = 11 ns, $E$ = 0.2 J, frequency 10 Hz). Laser light was focused into a cell with a sample through its open upper surface. Focusing lens had focal length 7 cm. For experiments we used bidistilled water with definite amount of NaCl. We also registered SBS frequency shift in the water samples obtained from different seas: Baltic sea, Black sea (Gagra and Sevastopol), Japan sea. SBS spectra were registered with the help of Fabri-Perot interferometer. Temporal characteristics were measured with the help of high-speed diode connected with oscilloscope Tektronix 8 GHz.

We measured following characteristics of SBS in water with different salinity: SBS frequency shift, full width at half maximum (FWHM), pulse duration and SBS pulse time shift relative to the exciting laser pulse. The results showed that the SBS frequency shift increases with the increase of salinity almost linearly. FWHM increases up to concentration of 1 %, then decreases. As for temporal characteristics, both SBS pulse duration and its time shift relative to the laser pulse decrease with the sample's salinity up to 15-20%, then increase.

Results obtained in this study may be used for creating of methods and schemes for remote sensing and monitoring of seawater with the help of Brillouin lidars.

[1] Dapeng Yuan, Peng Chen, Zhihua Mao, and Zhenhua Zhang, Potential of spaceborne Brillouin scattering lidar for global ocean optical profiling, Optic Express, 29, 43049, (2021).

[2] C. C. Leroy, S. P. Robinson, M. J. Goldsmith, A new equation for the accurate calculation of sound speed in all oceans, The Journal of the Acoustical society of America, 124, 2774-2782, (2008).

[3] . Fen Hu, Gangning Guo, Jin Xu, Ningning Luo, Jiulin Shi, Xingdao He, Measurment of sound veloci ty in water based kn Stimulated Brillouin scattering, Proc. of SPIE, 11427, 114273Y (2020).

[4] D. Koestel, T. Walther, The Brillouin linewidth in water as a function of temperature and salinity: the missing empirical relationship, Applied Physics B, Lasers and Optics, 130:53, (2024).

# Infrared Tracking of Copper-Bound Water and Thermal Transformations in Eumelanin

**P.A. Abramov, K.A. Motovilov**

*Center for Photonics and 2D Materials, Moscow Institute of Physics and Technology, Moscow, Russia*

*abramovpa33@gmail.com*

Hydration is a functional component of eumelanin rather than a passive environmental variable. Water participates in proton transport and shifts the redox equilibrium of the polymer, but the intensity of the broad O-H absorption alone does not indicate how much of this water remains mobile. This distinction is especially important for copper-containing eumelanin: $Cu^{2+}$ increases hydration while the complex conductivity can nevertheless decrease [1-3]. Here, stepwise vacuum thermal treatment followed by cooling to room temperature and FTIR measurement was used to track dehydration, decarboxylation, and other thermally induced transformations, while distinguishing weakly adsorbed water from water retained in the local coordination environment of copper.

Room-temperature mid-infrared spectra were recorded after each vacuum-heating step for synthetic eumelanin (EUM), Cu-doped eumelanin (EUM-Cu), partially decarboxylated eumelanin (EUM-D), and polydopamine (PDA). The comparison of chemically different samples allowed changes in the O-H envelope to be distinguished from spectral changes associated with decarboxylation, redistribution of carbonyl and nitrogen-containing groups, and higher-temperature evolution of the polymer matrix. X-ray photoelectron spectroscopy was used as a complementary probe of the copper-induced changes in the chemical states of oxygen- and nitrogen-containing functional groups in eumelanin. These changes were interpreted as a redistribution of the oxidized tautomeric forms of eumelanin.

The O-H response exhibits two clearly different trends with increasing treatment temperature. Absorption in the 3400-3700 $cm^{-1}$ range, associated predominantly with weakly bound hydroxyl species, is almost eliminated after heating to 80-100 °C. The broader 2400-3200 $cm^{-1}$ contribution decreases over the entire heating sequence and therefore represents a more strongly hindered hydrogen-bonded population. After treatment above 100°C, EUM-Cu retains the largest fraction of this low-frequency O-H absorption. Its persistence is consistent with water molecules being constrained within copper ions' coordination complexes rather than simply occupying readily exchangeable sorption sites.

In the fingerprint region, thermal treatment produces a gradual redistribution of existing bands rather than new dominant vibrational features. The evolution of the carbonyl contribution identifies decarboxylation of DHICA-derived groups and shows that copper binding does not substantially protect them against thermal loss. At higher treatment temperatures, additional changes reflect broader transformation of the polymer matrix, whereas PDA displays the smallest overall spectral variation. The XPS data reveal increased carbonyl-related O 1s and C 1s contributions together with a shift of N 1s intensity toward less protonated $R_2N$ environments. These changes support stabilization of the quinone tautomer relative to quinone-imine and quinone-methide configurations in the dry Cu-containing matrix.

The combined results show that copper changes not only the quantity of retained water but also its spectroscopic and transport-relevant state, while leaving the principal sequence of thermally induced chemical transformations largely intact. A significant part of the additional hydration becomes coordinatively trapped and is therefore poorly connected to the extended proton-transfer network. Together with coordination-induced localization of semiquinone sites, this provides a consistent explanation for the lower charge mobility of hydrated EUM-Cu. More generally, room-temperature IR spectroscopy after controlled stepwise thermal treatment provides a practical way to distinguish water release, decarboxylation, and functional-group redistribution in heterogeneous bioorganic conductors.

This work was supported by the Russian Science Foundation (project No. 25-12-00134).

[1] K. Motovilov and A.B. Mostert, *Soft Matter*, 20, 5635-5651 (2024).
[2] A.B. Mostert et al., *Proc. Natl. Acad. Sci.*, 109, 8943-8947 (2012).
[3] P.A. Abramov et al., *Phys. Chem. Chem. Phys.*, 25, 11601-11612 (2023).

# Random Laser Generation - Fundamental and Applied Aspects

**N. Tcherniega**

*P.N. Lebedev Physical Institute, 119991 Russia, Moscow, Leninskii pr.53*

The paper that pioneered the concept of random lasers was written by V. S. Letokhov in 1967 [1]. In his paper Letokhov considered a system of many particles with a negative absorption index (gain), where photon propagation was described by diffusion equations and the mean free path was much smaller than the size of the scattering medium. It was shown that even if light propagation is described in terms of a diffusion equation that completely ignores its wave nature and carries no phase information, laser-like behavior can be observed, characterized by a threshold, spectral line narrowing, attenuation, and other hallmarks of laser radiation. Examples of random laser generation in the diffuse regime include generation in powders. The first such studies were conducted by Lebedev Physics Institute researchers [2,3[. In these papers stimulated Raman scattering (SRS) in stilbene powders as a function of laser energy and temperature was studied. Raman random lasers based on the SRS effect represent a separate class of random lasers with their own unique characteristics. Firstly, due to the narrow gain line in Raman-active media, a broad spectral line will not be observed in the output radiation. Secondly, due to the small gain range, a random laser is more likely to operate in a diffuse mode, since a small number of modes will be formed by a coherent closed photon scattering trajectory. Thus, in Raman lasers the presence of non-resonant feedback affects only the behavior of the intensity of the fundamental Raman mode, while the spectral composition remains unchanged. Thirdly, since SRS depends not on the electronic levels of the system, but on vibrational ones, it is possible to tune the emission wavelength by changing the pump wavelength. Thus, for specific purposes, it is possible to select the desired frequency of high-intensity radiation by choosing the wavelength at which the absorption of the active medium is minimal. Although this area of research has been developing for quite some time, interest in it is growing primarily due to its many practical applications.. Indeed, the availability of practical applications stimulates research in this area. Random laser sources (including Raman lasers) are widely used in many fields of science and technology due to their low manufacturing cost, the ability to vary the operating wavelength over a wide spectral range, and the ability to create active media of various shapes. Given that the working medium of such sources is typically a system consisting of particles, it is relatively easy to create systems with specified spatial characteristics by varying their size and shape. For example, such laser sources can be created as coatings of varying thickness and shape. Given that the properties of such laser systems are highly temperature-dependent, their use as remote temperature sensors is very promising. Other important properties of random lasers for applications include low spatial coherence and the absence of speckle structure. This feature of random lasers makes them ideal illumination sources for visualization applications. A random SRS laser based on barium nitrate powder has been created with a record-high efficiency of pump-to-first Stokes SRS conversion, amounting to 30% in all directions. A study of the temperature dependence of SRS emission parameters in $Ba(NO_3)_2$ powder revealed that lowering the sample temperature to liquid nitrogen leads to an increase in SRS signal intensity and a decrease in the random lasing threshold. In addition to a decrease in the lasing threshold at low temperatures, a narrowing of the first Stokes SRS component line by a factor of 1.5 was observed. A study of the temporal dynamics of the first, second, and anti-Stokes SRS components in $Ba(NO_3)_2$ powder demonstrated SRS compression and a delay of all Stokes components relative to the pump. For the first Stokes component, a linear dependence of the delay time relative to the pump power density was found.

[1] V. S. Letokhov. Generation of light by a scattering medium with negative resonance absorption. Sov. Phys. JETP 26, 835–840 (1967).
[2] V. A. Zubov, G. V. Peregudov, M. M. Sushchinskii, V. A. Chirkov & I. K. Shuvalov. Observation of stimulated Raman scattering of light in crystalline powders. Sov. J. Exp. Theor. Phys. Lett. 5, 188–189 (1967).
[3] Peregudov G. V., Ragozin E. N. & Chirkov V. A. Energy and Time Characteristics of Stimulated Raman Scattering of Light in a Disperse Medium at Various Temperatures. Sov. J. Exp. Theor. Phys. 63, 421–430 (1972).

# Plasmonic enhancement of optical processes: expectations and reality

**T.A. Vartanyan**

*International Scientific and Educational Center for Physics of Nanostructures, ITMO University, St. Petersburg, Russia*

*tavartanyan@itmo.ru*

Since the discovery of the Surface Enhanced Raman Scattering (SERS) effect in 1973, modifications of varied optical processes taking place in close proximity of objects possessing plasmon resonance were described and studied. These changes were interpreted as caused either by an enhancement of the near field, or by an acceleration of radiative decay, or, as in the case of SERS, by both simultaneously. As metals are most suitable materials for plasmon excitation in the visible range, a number of metal-enhanced effects like metal-enhanced absorption, metal-enhanced photoluminescence, metal-enhanced chemiluminescence, and so on have been reported. Despite of very optimistic estimations of the possible improvements in chemical and biological sensors performance, based on the plasmon effects [1], real-world applications are limited.

I will describe our efforts to optimise the conditions for observation and registration of tiny amount of reactive oxygen species that are produced by neutrophils and other immune cells in response to bacterial penetration into the living body [2]. Luminol was used as a chemiluminescence probe that gives blue light after oxidation. We have compared different methods of luminol mixing with sodium hypochlorite chosen as a representative oxidiser produced by immune cells. In particular, the conventional droplet-in-a well method was compared to the novel method of reagents mixing in the microfluidic chip [3]. The chip construction was optimized to provide for the possibility to introduce silver nanoparticles for plasmonic enhancement of luminol chemiluminescence [4]. We find moderate chemiluminescence intensity growth as well as the shift of the chemiluminescence spectrum maximum in the direction of plasmon band spectrum maximum [5]. On the other hand, general consideration of the interrelated and competing processes of chemiluminescence enhancement via resonant interaction with the localized surface plasmons brought in the system by metal nanoparticles and the simultaneous absorption and scattering of the chemiluminescence light by the same metal particles required an introduction of two different enhancement factors. The first one is the conventional extinction efficiency equal to the ratio of the extinction cross section to the geometrical cross section of the nanoparticle. The second one is the ratio of the chemiluminescence enhancement factor integrated over the outer space of the nanoparticle to its volume. It appears that the usefulness of the nanoparticle addition to a macroscopic cell depends on the ratio of these two enhancement factors.

We explored also different possibilities to improve the performance of metal nanoparticles via control of the distance between the chemiluminescent molecule and the plasmonic nanoparticle that may be achieved by their strong binding together.

This work was financially supported by the Russian Science Foundation (Project 23-72-00045).

[1] Daler R. Dadadzhanov, I.A. Gladskikh, M.A. Baranov, T.A. Vartanyan, A. Karabchevsky, Self-organized plasmonic metasurfaces: The role of the Purcell effect in metal-enhanced chemiluminescence (MEC), Sensors & Actuators: B. Chemical, vol. 333, 129453 (2021).

[2] S.N. Pleskova, N.A. Bezrukov, E.D. Nikolaeva, Yu.A Zamazkina, Differences Between Oral Neutrophils and Neutrophils Isolated From the Blood of Healthy Donors, Molecular Oral Microbiology, https://doi.org/10.1111/omi.70025, (2026).

[3] G.R. Simonenko, A.S. Bukatin, L.N. Borodina, D.R. Dadadzhanov, N.B. Leonov, E.I. Naumov, A.A. Tiushkevich, T.A. Vartanyan, Chemiluminescence sensors of oxidative stress: Microfluidic chip versus droplet-in-well method of detection, Microchemical Journal, vol. 221, pp. 117003, (2026). https://doi.org/10.1016/j.microc.2026.117003

[4] A. Karabchevsky, A. Mosayyebi, A.V. Kavokin., Tuning the Chemiluminescence of a Luminol flow using Plasmonic nanoparticles, Light Sci. Appl. 5 (11) (2016) e16164, https://doi.org/10.1038/lsa.2016.164.

[5] L.N. Borodina, A.V. Palekhova, D.V. Kononov, S. Pinamyan, D.R. Dadadzhanov, A.V. Veniaminov, T.A. Vartanyan, Chemiluminescence enhancement in the course of luminol oxidation in the presence of metal ions and plasmonic nanoparticles, Optics and Spectroscopy, 2025, vol. 133, 1140-1143 (2026) DOI: 10.61011/EOS.2025.11.62923.8201-25

# Probing of resonant states in dielectric resonators by light-emitting structures with Ge(Si) self-assembled nanoislands

**A.V. Novikov[1,2], A.N. Yablonskiy[1], V.E. Zaharov[1,2], S. A. Dyakov[3], A.V. Peretokin[1], M.V. Stepikhova[1], D.V. Yurasov[1], M.V. Shaleev[1], E.E. Rodyakina[4], Z.F. Krasilnik[1]**

*1- Institute for Physics of Microstructures RAS, 7 Academicheskaya St., Afonino v., Nizhny Novgorod, Russia*
*2- Lobachevsky State University of Nizhny Novgorod, 23 Gagarin ave., Nizhny Novgorod, Russia*
*3- Skolkovo Institute of Science and Technology, Bolshoy Boulevard, 30, bld. 1, Moscow, Russia*
*4 - Institute of Semiconductor Physics of SB RAS, 13 pr. Lavrentieva, Novosibirsk, Russia*

*anov@ipmras.ru*

Today various dielectric resonators, including photonic crystals (PhCs), have been actively used to increase the power and reduce the size of semiconductor lasers. The wide range of PhC parameters allows for tuning their properties to address specific problems, but also complicates the search for the optimal set of PhC parameters. This paper demonstrates that structures with Ge(Si) self-assembled nanoislands are a convenient system for studying the dependence of various PhC resonant states on the their parameters.

The formation of PhCs on structures with Ge(Si) nanoislands grown by MBE on silicon-on-insulator (SOI) substrates allows for an increase in the intensity of their photoluminescence (PL) signal at room temperature in the wavelength range of 1.3–1.55 μm by several orders of magnitude due to the interaction of the islands with high-quality the bound states in the continuum (BIC) [1]. It was shown that control of the spectral position and quality factor of BIC states is possible by changing both the shape of the holes that make up the PhC and the symmetry of their arrangement [2]. By using a technique with separation of excitation and collection regions for PL signal, the features of the propagation of states with different Q factors realized at different values of the wave vector were revealed. Possibilities for reducing the impact of non radiative recombination associated with the formation of PhC by using PhC with an unprocessed central region were identified [3].

The obtained results were used to form light-emitting diodes (LEDs) and transistors on structures with Ge(Si) islands imbedded into PhC [4, 5]. Spatial non-uniformity of the electroluminescence signal distribution in the obtained LEDs was revealed, which is caused by the spatial localization of holes in islands [5]. Applying a voltage to SOI substrate allows the formation of an additional conductivity channel at the boundaries of the structure with buried oxide, and thus changing the spatial distribution of the EL signal [5]. Due to the compatibility of the developed technology with silicon integrated technology, the obtained LEDs can be used for testing silicon photonic circuits.

The work was funded by the Russian Science Foundation (Grant No. 25-12-00367) and was carried out using the facilities using of the multiple access centers “Physics and technology of micro- and nanostructures” (IPM RAS).

[1] S.A. Dyakov, M.V. Stepikhova, A.A. Bogdanov, et al., “Photonic bound states in the continuum in Si structures with the self-assembled Ge nanoislands”, Laser & Photonics Reviews 15(7), 2000242-13 (2021)
[2] .V. Yurasov, S.A. Dyakov, I.A. Smagin, et al., “Symmetry breaking of bound states in continuum in luminescence response of photonic crystal slabs with embedded Ge nanoislands”, Appl. Phys. Lett. 125, 021105(6) (2024)
[3] A.N. Yablonskiy, V.E. Zakharov, D.V. Yurasov, et al., “Enhanced emission of Ge nanoislands in two-dimensional photonic crystals with an unpatterned central region”, Appl. Phys. Lett. 128, 031103-7 (2026)
[4] V.B. Shmagin, A.N. Yablonskiy, M.V. Stepikhova et al., «Room-temperature light-emitting diodes with Ge(Si) nanoislands embedded in photonic crystals», Nanotechnology 35(16), 165203 (9) (2024).
[5] A.N. Yablonskiy, V.B. Shmagin, V.E. Zakharov, et al., “Silicon-based light-emitting transistor with Ge(Si) nanoislands embedded in a photonic crystal: control of the spectrum and spatial distribution of the emission”, Appl. Phys. Lett 125, 231103 (2024)

# Topological nanocavities: possibilities to control the light-emission properties of SiGe structures

**M. Stepikhova[1], E. Smolina[2], I. Chuprin[3], A. Peretokin[1], M. Shaleev[1]**
**A. Bespalov[1], D. Shengurov[1], A. Novikov[1]**

*1- Institute for Physics of Microstructures RAS, GSP-105, Nizhny Novgorod, 603950, Russia*
*2- Federal Research Center A.V. Gaponov-Grekhov Institute of Applied Physics RAS, Nizhny Novgorod 603950, Russia*
*3- Higher School of General and Applied Physics, Lobachevsky State University of Nizhny Novgorod, Nizhny Novgorod 603950, Russia*

*mst@ipmras.ru*

Photonic crystals (PCs) and metasurfaces have recently attracted considerable attention from researchers due to new opportunities for manipulating radiation at the nanoscale, managing information flows in integrated photonics circuits, the prospects for creating radiation sources for next-generation quantum computers, and others [1]. Of particular interest here are the ideas of topological photonics, which studies states of light that are not subject to local small-scale perturbations [2,3].

This paper examines the problem of creating topological defects that enable control of radiation and its interaction with the active medium in a limited space of wave vectors [4]. We discuss defects of the «grain boundary loops» type, formed in a photonic crystal by rotating one of its segments. Such defects were first proposed by us in [5]. In this work, we will show the possibility of realizing topological defects in photonic crystals of two types: a) - with a triangular lattice of holes and b) - with a honeycomb-type lattice of holes. The main difference between such PCs is the presence or absence of a forbidden gap in their zone structure. In this paper, topological defects will be discussed in comparison with the so-called «trivial» defects formed in photonic crystals by the omission of an appropriate number of holes.

Both the results of theoretical calculations and data from experimental studies of the luminescent response of topological and trivial defects in photonic crystals formed on silicon structures with Ge(Si) nanoislands will be presented. We will show that topological defects in PCs can be characterized by high Q-factors ($Q \sim 5\times10^3$), significantly exceeding the Q-factor of «trivial» defects, and provide a high degree of localization of the electromagnetic field in defect. As the calculation results show, for modes localized in the defect, the mode volume can be comparable to and even smaller than the radiation wavelength in material $(\lambda/n_{Si})^3$. Of interest here are also the polarization features of the radiation modes of the proposed topological defects in the far field. Based on the results of experimental and theoretical studies, it will be shown that in such defects it is possible to form modes characterized by both linear and vortex polarization of radiation with a topological charge q = 1 and q = -2. The consequence of the strong localization of the electromagnetic field in the defect and its interaction with the active medium is an increase in the emissivity of the structures we are considering. According to experimental studies, localization of the electromagnetic field in topological defects can provide an enhancement of the luminescent response of the studied structures with Ge(Si) nanoislands by more than an order of magnitude.

The work was funded by the Russian Science Foundation (grant # 25-22-00386).

[1] S.A. Schulz, R.F. Oulton, M. Kenney et al., Roadmap on photonic metasurfaces, Appl. Phys. Lett., vol. 124, p. 260701 (2024).
[2] L. Lu, J. D. Joannopoulos, M. Soljačić, Topological photonics, Nat. Photon., vol. 8, pp. 821-829 (2014).
[3] H. Price, Y. Chong, A. Khanikaev, et al., Roadmap on topological photonics, J. Phys. Photonics, vol. 4, p. 032501 (2022).
[4] X. Zhang, F. Zangeneh-Nejad, Z.-G. Chen, M.-H. Lu, J. Christensen, A second wave of topological phenomena in photonics and acoustics, Nature, vol. 618, pp. 687-697 (2023).
[5] E.O. Smolina, M.V. Stepikhova, Loop defects in honeycomb photonic crystals, Physica Status Solidi (RRL) - Rapid Research Letters, p. 2400247 (2024).

# 1.5 μm laser linewidth diagnostics and narrowing by silicon photonic integrated circuits

**D.M. Zhigunov, D.S. Zemtsov, A.S. Smirnov, A.K. Zemtsova, K.N. Garbuzov, S.S. Kosolobov, and V.P. Drachev**

*Skolkovo Institute of Science and Technology, Bolshoy Boulevard 30, bld. 1, 121205 Moscow, Russia*

*d.zhigunov@skoltech.ru*

Modern optical systems, especially those in the telecommunication C-band (1530-1565 nm), rely heavily on lasers with exceptional coherence. The performance of these systems, in terms of sensitivity and resolution, is dictated by the laser frequency stability, spectral linewidth, and noise characteristics. In coherent optical communication, the laser spectral linewidth is a key determinant of signal phase stability, demodulation quality, and maximum data rates. Furthermore, when generating spectrally pure microwave signals via photonic means, the laser phase noise restricts the achievable spectral purity of the output radio frequency signals.

Distributed feedback (DFB) semiconductor lasers are attractive for their small size, energy efficiency, and cost-effectiveness, coupled with respectable optical power. Their compatibility with fiber and photonic integrated circuit (PIC) platforms is a notable benefit. However, a significant drawback is their typical spectral linewidth of hundreds of kilohertz to few megahertz. The laser cavity length, a low Q factor, and noise from current and temperature fluctuations all impede further enhancements in output coherence by compromising frequency stability, which in turn limits their utility.

To address these constraints, one can utilize the laser self-injection locking capability. This effect is achieved by directing a portion of the laser output through a high-Q external resonator. This resonator functions as a filter, selecting a specific frequency. When this filtered light is returned to the laser, it lowers the lasing threshold at the resonant frequency. Once this frequency lock is established, any slow alteration in the resonator mode, such as from temperature changes, will result in a simultaneous adjustment of the lasing frequency. The stability of the laser operating mode in the self-injection locking regime is determined by the power and phase stability of the wave entering the laser.

Microring resonators based on PICs can be used as external resonators. They offer a high quality factor ($10^6$ and above), a compact design, and robust stability. Their compatibility with standard complementary metal-oxide-semiconductor (CMOS) technology allows for large-scale production. It was shown that such resonators, fabricated from $Si_3N_4$ or silica, can narrow the laser linewidth to a few hertz [1, 2].

In this work, we demonstrate the narrowing of the 1.5 μm DFB laser linewidth via self-injection locking using an external integrated microring resonator implemented on a silicon-on-insulator platform. The spectral width of the laser line was measured using a self-heterodyne interferometer with a delay [3]. The minimal achieved width of the narrowed by an external resonator laser line was about 150 Hz, while initial DFB laser linewidth was about 90 – 150 kHz. These results open up new possibilities for the creation of compact narrowband lasers suitable for coherent multiplexed data transmission, low-noise microwave signal generation, high-resolution spectroscopy, and precision optical sensor technology.

This work was supported by the Russian Science Foundation (grant #23-91-06301).

[1] W. Jin, Q.-F. Yang, L. Chang, B. Shen, H. Wang, M. A. Leal, L. Wu, M. Gao, A. Feshali, M. Paniccia, K. J. Vahala, J. E. Bowers, Hertz-linewidth semiconductor lasers using CMOS-ready ultra-high-Q microresonators, Nature Photonics, 15, 346–353 (2021).
[2] G. Zhang, Q. Cen; T. Hao; X. Yin; X. Zi; N. Shi, Self-injection locked silica external cavity narrow linewidth laser, Journal of Lightwave Technology, 41 (8), 2474-2483, (2023).
[3] T. Okoshi, K. Kikuchi, A. Nakayama, Novel method for high resolution measurement of laser output spectrum, Electronics letters. 16 (16), 630–631 (1980).

# Mapping Nanoscale Heterogeneity in Copolymer Composites Using FLIM

**U. Saidvaliev[1], D. Fixler[1], V. Zherdeva[2], A. Likhov[2]**

*1- School of Biomedical Engineering, Faculty of Engineering, Jan Koum Center for Nanoscience and Nanotechnology, Tel-Aviv University, Ramat Aviv 6997801, Israel*
*2- Research Center of Biotechnology RAN, AN Bach Institute of Biochemistry, Moscow, Russian Federation*

Copolymer-based materials are widely utilized in medicine and biotechnology for implants, prostheses, drug delivery systems, and biosensors. Combining Magnetic Resonance Imaging (MRI) with Indocyanine Green (ICG)-labeled Fluorescence Lifetime Imaging Microscopy (FLIM) enables in vivo tracking of tissue responses. This approach yields a precise quantitative or semi-quantitative assessment of composite degradation.ICG is an optimal dye for deep-tissue visualization. Its inherent instability can be reduced by incorporating the dye into hydrophobic polymer carriers. Furthermore, changes in the fluorescent properties of ICG—driven by environmental parameters such as viscosity, pH, and protein concentration—serve as a valuable tool for monitoring polymer degradation.

Methodology

In this work, the fluorescence lifetime (FLT) of ICG within copolymer-based materials was measured using both frequency-domain (FD) and time-domain FLIM.Frequency-Domain (FD) FLIM: Measurements were performed using a LIFA system (Groningen, The Netherlands) attached to an Olympus IX-81 inverted microscope with a 10× (NA = 0.4) objective (Olympus, Tokyo, Japan). The excitation source was a modulated multi-light emitting diode (LED) system controlled by a signal generator (Prior OptiScan II). Three scanning frequencies were utilized for sample excitation: 30 MHz, 40 MHz, and 50 MHz. Time-Domain FLIM: Measurements were conducted using an inverted two-channel laser scanning confocal microscope system (DCS 120, Becker & Hickl GmbH, Berlin, Germany). FLIM images and data analysis were processed using SPCImage software (version 3.9.4/5.3, Becker & Hickl GmbH, Berlin, Germany).

Results and Discussion

The FLT of ICG in a polymer matrix typically ranges from 0.4 to 2.2 nanoseconds, depending on the specific polymer type, temperature, and concentration. Our experimental results demonstrate that the copolymer's FLT remains relatively consistent across all tested environmental conditions. However, the fluorescence intensity (FI) varied significantly. The original copolymer sample exhibited the highest FI. Conversely, the lowest FI was observed when the copolymer was placed beneath mouse skin prior to optical clearing (OC). Applying the OC agent successfully restored the FI by enhancing skin transparency, which allowed more excitation light to reach the copolymer. While the copolymer maintains a stable FLT under diverse conditions, placing it under mouse skin reduced the overall FI and slightly elevated the measured FLT due to the tissue's intrinsic optical properties. Crucially, neither the OC solution nor the skin introduced background fluorescence that distorted the final FLIM data, confirming the reliability of this imaging approach.

Conclusions

In conclusion, ICG-labeled copolymer materials demonstrate high fluorescence lifetime (FLT) stability across diverse environmental conditions, while their fluorescence intensity (FI) remains highly sensitive to microenvironmental changes, making this system a powerful tool for monitoring polymer degradation. The application of an optical clearing (OC) agent successfully restores fluorescence intensity by enhancing skin transparency. Crucially, neither the skin nor the OC solution introduces confounding background fluorescence, confirming that FLIM imaging approach provides highly reliable, artifact-free data for in vivo tissue tracking.

[1] Zherdeva V.V., Likhov A.R., Saidvaliev U.A. et al. Enhanced fluorescence imaging of implants based on polyester copolymers in combination with MRI. Journal of Biophotonics. 2025; 18(12): e202400147. DOI: 10.1002/jbio.202400147.

# Estimation of average values over intensity distribution wavelength spectra of light field using bandpass filters

**D.V. Nesterenko, N. V. Polevoy**

*Samara National Research University; Molodogvardejskaya 151, Samara, 443001 Russia*

*nesterenko@ssau.ru*

Evaluation of wavelength spectra of light fields is one of the main tasks of spectroscopy. Traditional experimental approaches include implementation of diffractive structures [1], sets of light filters [2], and tunable resonators [3]. The existing solutions are relatively noncompact, require precise fabrication techniques, slow post-processing, or address a limited number of characterized wavelength bands. Optical absorptive bandpass filters transmit light within a certain wavelength range and absorb light outside this wavelength range. Following the need in compact, fast and non-expensive solutions we focus on implementation of conventional thin-film absorptive bandpass filters for characterization of more than two wavelength bands.

In the evaluation problem of field spectral intensity $I(\lambda)$, consider an absorptive thin-film filter with a finite thickness $d$ and the refractive index $n(\lambda)=n'(\lambda)+in''(\lambda)$. Suppose that a plane wave is incident on the filter under a certain incidence angle $\theta^{in}$. A transmission coefficient of the filter can be expressed as $\tau(\lambda,\theta)=\tau_0(\lambda)exp\{-4\pi n''(\lambda)d)/[\lambda\cos\theta(\lambda)]\}$, where $\tau_0(\lambda)$ is the transmission coefficient for normal incidence, $\theta$ is an angle between the wavevector of plane wave propagating inside the filter and the normal to the filter surface that corresponds to $\theta^{in}$. For collimated incident light field with spectral intensity $I(\lambda)$ the transmission through the filter oriented under the incidence angle $\theta^{in}$ is approximately transformed as $I^t(\lambda,\theta)=I(\lambda)\tau(\lambda,\theta)$. In experiments, a broadband detector registers the transmitted flux $\Phi(\theta)=\int I^t(\lambda,\theta)\,d\lambda$ for particular $\theta$. When $\tau_0(\lambda)$ is given by discrete values $\tau_0(\lambda_k)$, where $k$ scans wavelength values in the overall wavelength band $\Lambda$, a discretization of the average spectral intensity over wavelength spectra $I^t(\lambda_k,\theta)$ can be also implemented, so

$$\Phi(\theta) = \Lambda \sum I^{t}(\lambda_k, \theta). \quad (1)$$

To simplify the numerical problem and reduce the number of unknowns, split $\Lambda$ into $n$ subbands $\Lambda_p, p=\overline{1,n}$. In each subband $\Lambda_p$, piecewise linear approximation of $\tau(\lambda,\theta)$ can be obtained as $\tilde{\tau}_p(\lambda_k,\theta)=a_p(\theta)\lambda_k+b_p(\theta)$, $\lambda_k \epsilon \Lambda_p$, where $a_p$ and $b_p$ are the approximation coefficients. Substituting $\tilde{\tau}_p(\lambda_k,\theta)$ into Eq. (1) provides the following approximation

$$\Phi(\theta) = \Lambda \sum_{p=1}^{n} [a_p(\theta) y_p + b_p(\theta) x_p], \quad (2)$$

where $x_p=\sum_{\lambda_k \epsilon \Lambda_p} I(\lambda_k)$ is the average spectral intensity over subband $\Lambda_p$ and $y_p=\sum_{\lambda_k \epsilon \Lambda_p} I(\lambda_k)\lambda_k$.

A system of $2n$ linear algebraic equations with $2n$ unknowns can be formed for $2n$ measurements at the angles $\theta_j$ as follows

$$\Phi(\theta_j) = \Lambda[\sum_{p=1}^{n} a_p(\theta_j) y_p + \sum_{p=1}^{n} b_p(\theta_j) x_p], j = \overline{1,2n}. \quad (3)$$

Solving the system (3), the average spectral intensity values $x_p$ are found in each subband $\Lambda_p$.

We present and discuss our results on study of the efficiency of this approach for colored glass bandpass filters. The calculated average intensity in corresponding subbands demonstrated relative error values of less than 5 %.

This work was carried out within the state assignment of the Ministry of Education and Science of the Russian Federation (No. FSSS-2024-0014).

[1] A. Li, Y. Fainman, On-chip spectrometers using stratified waveguide filter, Nat. Commun. 12, 2704 (2021).
[2] J.R. Shakya, F.H. Shashi, A.X. Wang, Plasmonic color filter array based visible light spectroscopy, Sci Rep 11, 23687 (2021).
[3] Z. Chang, Z. Luo, S. Cao, K. Ouyang, K. Ge, and Z. Wan, Narrow-band tunable optical filters based on cascaded Fabry-Perot cavities, Opt. Express 30, 13864-13874 (2022).

# Spatial light modulator development for laser wavefront shaping

**S.V. Mutilin**

*A.V. Rzhanov Institute of Semiconductor Physics, 630090, Novosibirsk, Lavrentjev av. 13, Russia*

*mutilin@isp.nsc.ru*

Phase-only liquid crystal on silicon spatial light modulators (LCoS SLMs) operating in the visible range are essential components in modern optical systems. They allow dynamic shaping of the laser wavefront, providing spatial structure of light in real time. Originally developed for display applications—such as image projectors and augmented/virtual reality (AR/VR) systems—LCoS SLMs have now been widely adopted in optical information processing and transmission. This includes areas like optical computing, neuromorphic systems, quantum optics, and telecommunications [1].

In most LCoS SLMs, electro-optical cells operate based on the S-effect in nematic liquid crystals and have a sandwich-type structure consisting of a transparent top electrode (glass coated with a transparent conductive layer), a liquid crystal (LC) layer, and a silicon substrate containing an array of individually addressable reflective pixels [2]. Their operating principle relies on controlling the orientation of LC molecules using an electric field. By adjusting the voltage distribution across the pixel matrix, the desired phase profile of the wavefront can be generated in real time.

Here, we present recent advances in the development of LCoS SLMs, including operating principles, manufacturing technologies, and calibration methods. The main focus is on presenting our latest results in the development and research of phase-only LCOS SLM with megapixel resolution. The LCoS SLM prototype includes an LC-cell based on a very-large-scale integrated (VLSI) circuit matrix with a resolution of 1024 × 1024 pixels (15 μm pitch, 14 × 14 $\mu m^2$ pixel size). The prototype is designed for operation in the visible wavelength range from 450 to 700 nm. The phase change of the reflected light ranges from 0 to 2π (at $\lambda = 532$ nm). Power consumption is approximately 15 W. To ensure dynamic display of the obtained phase profiles on the LCD cell matrix, the system supports the reception of grayscale images from a PC at a frequency of 60 Hz. The possibility of forming complex phase profiles through individual control of pixels has been experimentally confirmed.

This study was conducted within the framework of the scientific program of the National Center for Physics and Mathematics, section 1 «National Center for Research on Supercomputer Architectures». Stage 2026-2027 and the Ministry of Science and Higher Education of the Russian Federation.

[1] Talukder R. et al. A spiking photonic neural network of 40,000 neurons, trained with latency and rank-order coding for leveraging sparsity //Neuromorphic Computing and Engineering. – 2025.

[2] Lazarev G., Chen P.-J., Strauss J., Fontaine N., Forbes A. Beyond the display: phase-only liquid crystal on Silicon devices and their applications in photonics [Invited] // Optics Ex-press. - 2019. - Vol. 27. - No. 11. - P. 16206.

# Nonlinear metal-organic framework crystals for light conversion and generation

**V.A. Milichko**[1,2]

*1- School of Chemistry, Dalian University of Technology, Dalian 116024, China*
*2- New Uzbekistan University, Tashkent 100007, Uzbekistan*

*v.milichko@newuu.uz*

Metal–organic frameworks (MOFs) represent a versatile class of crystalline hybrid materials composed of metal-containing nodes interconnected by organic linkers [1]. Owing to the vast diversity of available building blocks and synthetic approaches, MOFs offer exceptional flexibility in tuning their architecture, topology, and physicochemical properties, making them highly attractive for a broad range of photonic and optoelectronic applications [2].

In recent years, considerable attention has been directed toward the optical properties of MOFs in the form of bulk crystals, powders, and thin films. These materials can exhibit both efficient photoluminescence (PL) and a wide variety of nonlinear optical (NLO) phenomena. Reported examples include second- and third-harmonic generation (SHG, THG), lasing, optical limiting, birefringence, optical switching, and sensing. The remarkable optical functionality of MOFs arises from the ability to tailor framework geometry while incorporating molecular building blocks with strong nonlinear responses. As a result, MOFs have emerged as promising alternatives to conventional inorganic NLO crystals, while offering additional advantages associated with their modular design, structural tunability, and synthetic versatility.

Here, we discuss a series of MOFs spanning dimensionalities from three-dimensional (3D) to two-dimensional (2D) and one-dimensional (1D) architectures, as well as morphologies ranging from bulk crystals to ultrathin nanosheets. These MOF crystals exhibit nonlinear optical properties comparable to, and in some cases exceeding, those of established inorganic NLO counterparts. We examine a broad spectrum of nonlinear processes, including conventional SHF/THG, sum- and difference-frequency generation, as well as broadband coherent supercontinuum generation enabled by the simultaneous contribution of $\chi^{(2)}$ and $\chi^{(3)}$ nonlinearities [3,4]. In addition, we explore nonlinear PL control, including multiphoton upconversion [5], and discuss dynamic transmission responses relevant to applications in all-optical data processing, optical communications, and neuromorphic photonics [6-9].

Throughout this discussion, MOFs are evaluated as a new generation of NLO crystals within the framework of their highly tunable chemistry, which enables precise optimization of crystal structures, framework topologies, and optical performance. Particular attention is given to key parameters such as operating spectral range, nonlinear conversion efficiency, and long-term stability..

[1] A. V. Desai, S. Canossa, E. A. Chernova, S. M. Vornholt, K. Stracke, J. D. Evans, E. E. Petersen, S. Wuttke, R. Ettlinger. Retrospective Review on Reticular Materials: Facts and Figures Over the Last 30 Years, Adv. Mater. 37, 2414736 (2025).
[2] L. R. Mingabudinova, V. V. Vinogradov, V. A. Milichko, E. Hey-Hawkins, A. V. Vinogradov. Metal–organic frameworks as competitive materials for non-linear optics, Chem. Soc. Rev. 45, 5408-5431 (2016).
[3] N. Zhestkij, S. Povarov, S. Shipilovskikh, I. D. Yushina, J.-F. Pierson, V. Milichko. Highly Nonlinear Metal-Organic Framework Microcrystal for Ultrabroadband and Multiwavelength Coherent Light Emission, Laser. Photon Rev. 20, e01152 (2026).
[4] N. A. Zhestkij, A. S. Efimova, Y. Kenzhebayeva, M. V. Dmitriev, A. S. Novikov, I. D. Yushina, A. Krylov, M. V. Timofeeva, A. N. Kulakova, N. V. Glebova, A. A. Krasilin, S. A. Shipilovskih, V. A. Milichko. Nonlinear Metal–Organic Framework Crystals for Efficient Multicolor Coherent Optical Emission, Adv. Opt. Mater. 11, 2300881 (2023).
[5] X. Yu, Z. Zhou, N. Zhestkij, Y. Kenzhebayeva, S. A. Povarov, J. Chen, D. I. Pavlov, N. A. Burzak, A. R. Knyazeva, S. S. Lazarev, V. A. Dyachuk, A. S. Potapov, L. Sun, V. A. Milichko, V. P. Fedin. Mixed-Lanthanide Metal–Organic Frameworks for Near-Infrared-I Bioimaging and Near-Infrared-III Four-Photon Upconversion, J. Am. Chem. Soc. 148, 14197–14204 (2026).
[6] V. A. Milichko, S. V. Makarov, A. V. Yulin, A. V. Vinogradov, A. A. Krasilin, E. Ushakova, V. P. Dzyuba, E. Hey-Hawkins, E. A. Pidko, P. A. Belov. van der Waals Metal-Organic Framework as an Excitonic Material for Advanced Photonics, Adv. Mater. 29, 1606034 (2017).
[7] N. K. Kulachenkov, D. Sun, Y. A. Mezenov, A. N. Yankin, S. Rzhevskiy, V. Dyachuk, A. Nominé, G. Medjahdi, E. A. Pidko, V. A. Milichko. Photochromic Free MOF-Based Near-Infrared Optical Switch. Angew. Chemie Int. Ed. 59, 15522-15526 (2020).
[8] N. Kulachenkov, M. Barsukova, P. Alekseevskiy, A. A. Sapianik, M. Sergeev, A. Yankin, A. A. Krasilin, S. Bachinin, S. Shipilovskikh, P. Poturaev, N. Medvedeva, E. Denislamova, P. S. Zelenovskiy, V. V. Shilovskikh, Y. Kenzhebayeva, A. Efimova, A. S. Novikov, A. Lunev, V. P. Fedin, V. A. Milichko. Dimensionality Mediated Highly Repeatable and Fast Transformation of Coordination Polymer Single Crystals for All-Optical Data Processing, Nano Lett. 22, 6972–6981 (2022).
[9] S. V. Bachinin, A. Marunchenko, I. Matchenya, N. Zhestkij, V. Shirobokov, E. Gunina, A. Novikov, M. Timofeeva, S. A. Povarov, F. Li, V. A. Milichko. Metal-organic framework single crystal for in-memory neuromorphic computing with a light control, Commun. Mater 5, 128 (2024).

# Cavity-assisted THz waveform control via optically reconfigurable carrier layers in GaAs

**T.V. Dolgova, M.A. Kiryanov, I.A. Novikov, V.I. Stadnichuk, A.A. Fedyanin**

*Faculty of Physics, Lomonosov Moscow State University, Moscow, 119991 Russia*

*dolgovatv@my.msu.ru*

Terahertz (THz) radiation interacts with matter through mechanisms inaccessible at other frequencies: phonon resonances, carrier dynamics on picosecond timescales, and low-energy collective excitations. Despite this, practical tools for shaping THz waveforms in real time are still quite limited compared to available in the visible and near-infrared. There are two reasons for this. First, the long wavelength of THz radiation (100-1000 μm) makes conventional phase-accumulation optics physically bulky. Second, the photon energy (~1-10 meV) is too small for most nonlinear optical mechanisms that work well in the near-infrared. Femtosecond-laser-induced carrier generation in semiconductors offers a way around both of these problems. It creates a transient medium whose optical properties at THz frequencies can be switched on a picosecond timescale and tuned from weakly perturbative to fully metallic simply by changing the pump fluence. In this sense, the approach fits naturally into the broader framework of optical pulse shaping and coherent control, but at wavelengths three orders of magnitude longer.

In this work, we report new waveform shaping effects like trapezoidal envelope and control over the rising edge observed in optically pumped sub-millimeter GaAs plates. We extend our previous study of femtosecond-laser-induced THz pulse shaping in gallium arsenide (GaAs) by exploiting Fabry-Perot interference within sub-millimeter GaAs plates as a controllable degree of freedom. To support the experimental observations, we develop an analytical time-domain model of THz reflection from the photoexcited layer, which avoids the standard transition to the frequency domain and gives a closed-form expression for the reflected waveform as a function of carrier density and relaxation time.When a photoexcited carrier layer is generated near the front surface by an optical pump pulse, it acts as a partially reflective mirror whose reflectivity and temporal response are controlled by the pump fluence. The THz probe pulse undergoes multiple round trips within the photoexcited plate, and the interference between the directly reflected component and the round-trip echoes produces a rich variety of waveforms, including temporally sculpted pulses.

Experimentally, we study THz reflection from optically pumped GaAs plates in a modified time-domain spectroscopy setup. By varying the pump fluence from the sub-metallization to the strongly metallic regime, we observe systematic changes in the amplitude and temporal profile of the Fabry-Perot echo structure. At intermediate fluences, the interference between the carrier-reflected and boundary-reflected contributions can produce waveforms with a trapezoidal envelope and allows selective control over the rising edge of the THz pulse. To describe the reflection analytically, we work in the time domain and treat the carrier layer as a thin conducting sheet, since its thickness (~1 μm) is much smaller than the THz wavelength. The sheet current is governed by a time-domain Drude equation, and the self-consistent field inside the layer is found. The model captures both interfering contributions to the reflected field: radiation from the carrier current and reflection from the semiconductor-air boundary.

This work was supported by Russian Science Foundation (24-12-00210).

# Light control with optical surface states in one-dimensional photonic crystals

**V.O. Bessonov, A.A. Popkova, A.A. Fedyanin**

*Faculty of Physics, Lomonosov Moscow State University, Moscow 119991, Russia*

*bessonov@nanolab.phys.msu.ru*

Optical surface states arise in one-dimensional photonic crystals (PCs) due to the breaking of translation symmetry at PC edges. When PC borders a dielectric, such as air, the optical surface states called Bloch surface waves (BSW) are excited at frequencies belonging to the photonic band gap, with the BSW wave vector exceeding the wave vector of light in air. Due to these two conditions, the BSW electric field decays exponentially inside the PC and in the air, thereby localizing on the PC surface. The all-dielectric nature of BSW ensures their centimeter-scale propagation length and wide spectral flexibility making BSW attractive for the use in integrated photonics. In this work we demonstrate light control in the microscale range by directionally exciting and guiding BSW using dielectric waveguides, microprisms, resonant nanoparticles and perovskite nanolasers. We also show that BSW can be combined with 2D materials such as graphene monolayer to enhance the graphene-light interaction for all-optical switching applications.

The PCs under study consist of 5-10 pairs of alternating $SiO_2/Ta_2O_5$ layers designed to sustain BSW in the wavelength range from 500 nm to 800 nm. BSW are visualized using leakage radiation microscopy combined with fourier plane analysis. First we show that two-photon laser lithography technique can be applied for printing polymer BSW waveguides on the PC surface. We systematically study the multimode interference of BSW in waveguides and use it to develop integrated optical splitters and Mach-Zehnder interferometers based on BSW [1]. We also propose a method of highly efficient unidirectional BSW excitation based on the microscale prism Otto configuration. Polymer microprisms with a submicrometer air gap are printed by two-photon lithography on the PC surface and transfer 40 - 54% of the incident light energy into BSW in the experiment and 73% in theory [2].

Since a significant part of the BSW field is concentrated in the air near the PC surface, nanoscale light sources placed in this region should effectively excite BSW. A directional BSW excitation with an efficiency of over 16% is demonstrated by perovskite ($CsPbBr_3$) nano- and microlasers deposited on the PC surface. BSW beams exhibit high in-plane directivity, down to 9°, and can be steered by varying the pumping laser beam position [3]. The mechanism of BSW generation using light scattered by a single Mie-resonant silicon nanoparticle on the PC surface is also studied. The BSW excitation direction can be switched from forward to backward within the 30 nm spectral range with its central wavelength corresponding to the magnetic dipole resonance of the nanoparticle [4]. A BSW excitation efficiency of 8% is estimated for tightly focused pump beams, which considerably outperform the efficiency of the Kretschmann scheme for such beam sizes.

In addition to localizing light, BSW can control the light reflected from the PC by leveraging the high-quality BSW resonance in the reflectance spectrum. We use these two features to enhance the ultrafast reflectance modulation of the graphene monolayer by an order of magnitude while maintaining its inherent subpicosecond dynamics. A pump-probe experiment shows a maximum reflection change of 0.3% at a fluence of only 40 μJ $cm^{-2}$ for the BSW resonance wavelength [5].

[1] Safronov, K. R. et al. Multimode Interference of Bloch Surface Electromagnetic Waves. ACS Nano 14, 10428–10437 (2020).
[2] Safronov, K. R. et al. Miniature Otto Prism Coupler for Integrated Photonics. Laser Photon. Rev. 16, 2100542 (2022).
[3] Safronov, K. R. et al. Efficient Emission Outcoupling from Perovskite Lasers into Highly Directional and Long-Propagation-Length Bloch Surface Waves. Laser Photon. Rev. 16, 2100728 (2022).
[4] Gulkin, D. N. et al. Mie-driven directional nanocoupler for Bloch surface wave photonic platform. Nanophotonics 10, 2939–2947 (2021).
[5] Popkova, A. A. et al. Bloch Surface Wave-Assisted Ultrafast All-Optical Switching in Graphene. Adv. Opt. Mater. 10, 2101937 (2022).

# Optical second harmonic generation spectroscopy of antiferromagnets

**V.V. Pavlov**

*Ioffe Institute, Politekhnicheskaya 26, St. Petersburg, Russia*

*pavlov@mail.ioffe.ru*

Antiferromagnets constitute the vast majority of magnetically ordered materials and exhibit a wide range of unique physical properties. Among nonlinear optical phenomena, second-harmonic generation (SHG) is the simplest process associated with light frequency conversion. This effect is described by a second-order nonlinear susceptibility tensor, making it exceptionally sensitive to the details of both crystal and magnetic structure [1, 2].

This talk focuses on nonlinear magneto-optical phenomena related to SHG in several antiferromagnetic (AFM) crystals with different symmetries. To systematize these materials, it is convenient to use a classification based on symmetry operations acting on the antiferromagnetic vector [3-5]. According to this classification, antiferromagnets are divided into three classes: I. *magnetoelectrics*, in these materials the spontaneous spin order breaks the inversion symmetry (classic example is AFM $Cr_2O_3$); II *ordinary antiferromagnets*, these AFM's retain the inversion center (e.g., NiO); III *altermagnets* represent a new class with unique features in their electronic structure (e.g., $CoF_2$).

In the electric dipole (ED) approximation, SHG is allowed only in materials without an inversion center. In magnetoelectric $Cr_2O_3$ below the Néel temperature $T_N$ the inversion symmetry is broken, allowing ED-SHG to be observed in the antiferromagnetic phase [6]. Furthermore, in such systems, a new SHG mechanism induced by an external magnetic field and directly related to the linear magnetoelectric effect is possible.

In centrosymmetric media, SHG can arise from higher-multipole contributions, such as magnetic dipole (MD) or electric quadrupole (QD). In centrosymmetric AFM NiO SHG is related to the MD-type nonlinear susceptibility, enabling the study of a magnetic structure that does not violate spatial inversion [7]. Altermagnetic AFM $CoF_2$ obeys a new nonlinear optical susceptibility of the QD type, reflecting the specific symmetry of this state, which is both predicted and observed [8].

Support by the Russian Science Foundation (project No. 24-12-00348) is acknowledged.

[1] M. Fiebig, V. V. Pavlov, and R. V. Pisarev, Second-harmonic generation as a tool for studying electronic and magnetic structures of crystals: Review, J. Opt. Soc. Am. B **22**, 96-118 (2005).
[2] M. Fiebig, *Nonlinear Optics on Ferroic Materials* (Wiley-VCH, Weinheim, 2023).
[3] L. Šmejkal, J. Sinova, and T. Jungwirth, Beyond conventional ferromagnetism and antiferromagnetism: a phase with nonrelativistic spin and crystal rotation symmetry, Phys. Rev. X **12**, 031042 (2022).
[4] L. Šmejkal, J. Sinova, and T. Jungwirth, Emerging research landscape of altermagnetism, Phys. Rev. X **12**, 040501 (2022).
[5] A. V. Kimel, Th. Rasing, and B. A. Ivanov, Optical read-out and control of antiferromagnetic Néel vector in altermagnets and beyond, J. Magn. and Magn. Mater. **598**, 172039 (2024).
[6] V. V. Pavlov, M. A. Semina, J. Mund, P. A. Usachev, D. R. Yakovlev, R. V. Pisarev, and M. Bayer, Time-space symmetry breaking on Frenkel excitons in the antiferromagnet $Cr_2O_3$ revealed by second harmonic generation, Phys. Rev. B, **111**, 174405 (2025).
[7] M. Fiebig, D. Fröhlich, Th. Lottermoser, V. V. Pavlov, R. V. Pisarev, and H.-J. Weber, Second harmonic generation in the centrosymmetric antiferromagnet NiO, Phys. Rev. Lett. **87**, 137202 (2001).
[8] P. A. Usachev, R. V. Pisarev, and V. V. Pavlov, Nonlinear optical probing of ferroic-octupolar order parameter in collinear altermagnet, to be published, (2026).

# Technology of phytosanitary control of plant diseases based on SERS spectroscopy

**V. Novikov[1,2], S. Kuznetsov[1,2], E. Zavyalova[1,3], A. Sibirev[1], A. Gulyaev[1], M. Moskovskiy[1]**

*1- Federal Scientific Agro-Engineering Center VIM, 109428 Moscow, Russia*
*2-Prokhorov General Physics Institute of the Russian Academy of Sciences, 119991 Moscow, Russia*
*3- Chemistry Department, Lomonosov Moscow State University, 119991 Moscow, Russia*

*maxmoskovsky74@yandex.ru*

Early detection of plant diseases is critically important for ensuring global food security, minimizing crop losses, and reducing the need for extensive chemical treatments. Rapid and reliable diagnostic methods enable timely intervention, thereby improving both yield quality and agricultural sustainability. In this context, non-destructive optical techniques are of particular interest due to their potential for in situ and real-time monitoring. As an illustrative example, this work focuses on the investigation of infection processes in cereal crops.

We have developed a technology for the early detection of Fusarium infections in plants, enabling diagnosis at stages prior to the appearance of visible symptoms, and potentially allowing timely fungicide application to suppress further fungal growth and spore dissemination. The proposed approach is based on surface-enhanced Raman scattering (SERS) spectroscopy using silver nanoparticles in combination with a coagulant.

Experimental results demonstrate that fungal contamination leads to the emergence of characteristic spectral features associated with pathogenic activity. Measurements were carried out using a portable EnSpectr spectrometer with an excitation wavelength of 532 nm. The methodology has been adapted for different plant growth stages, from early seedling emergence—where suppression of fungal development in the root zone is particularly critical—to later stages such as ear formation in wheat. Additionally, the possibility of post-harvest infection detection has been confirmed. The study includes both naturally infected plants, including those with visible symptoms, and artificially infected field plots isolated from surrounding areas and inoculated with a known strain of Fusarium graminearum.

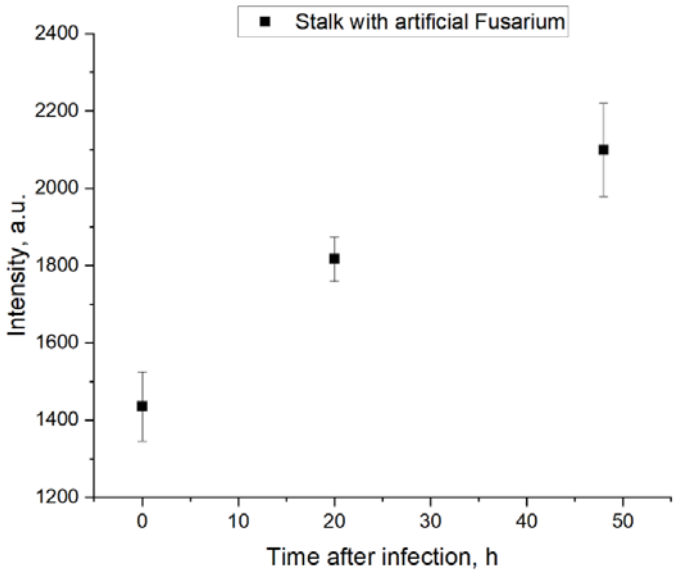


**Fig. 1.** Determination of mycotoxins in wheat stems using a SERS aptasensor at different times after artificial infection under real agrocenosis conditions.

This research was funded by a grant of the Ministry of Science and Higher Education of the Russian Federation for large scientific projects in priority areas of scientific and technological development (subsidy identifier 075-15-2024-540).

# Advanced Bragg gratings based on photo-thermo-refractive glasses for laser technologies

**N. Nikonorov[1], V. Popova[1], A. Eshbekov[2], S. Srajev[2]**

*1- ITMO University, 197101, Kronverksky av., 49, St. Petersburg, Russia,*
*2- Samarkand State University named after Sharof Rashidov. University Boulevard, 15, Samarkand, Uzbekistan*

*Nikonorov@oi.ifmo.ru*

Photo-thermo-refractive (PTR) glasses are a new class of photosensitive materials designed for holographic recording of volume Bragg gratings, which are in high demand in the photonics market today. The abbreviation PTR refers to the fact that photo-irradiation and subsequent heat treatment in the irradiated region of the PTR glass causes a change in the refractive index. This change is caused by the formation of metallic silver nanoparticles and the growth of silver halides and sodium fluoride nanocrystals on them in the irradiated region due to photo-thermo-induced (PTI) crystallization. The change in refractive index in the irradiated region compared to the unirradiated region enables the recording of phase volume Bragg gratings [1-2].

To date, a wide range of next-generation photonics elements and devices has been developed: ultra-narrow-band spectral filters for laser systems, chirped Bragg gratings for light pulse compression, multichannel spectral multiplexers with high spectral resolution, laser light combiners for increasing the output power of laser systems, holographic prisms for calibration and testing of rocking platforms, holographic waveguides for augmented reality glasses, holographic optical elements for collimation sights, and non-linear limiters for protecting photodetectors from pulsed laser radiation. Doping of PTR glass with neodymium, ytterbium and erbium allows it to be used simultaneously as a laser and holographic medium, i.e., opens up the possibility of creating lasers with Bragg mirrors and lasers with distributed feedback based on active PTR glass.

In this paper, two technologies for modifying the surface of PTR glasses are proposed: low-temperature ion exchange and photo-chemical etching. A combination of these technologies with PTI glass crystallization is also presented. This modification allows for increasing the mechanical, thermal, and optical strength of Bragg gratings based on PTR glass, as well as creating 3D hollow microstructures and waveguides. All the listed characteristics of PTR glass allow it to be classified as an advanced polyfunctional material for photonics.

It can be concluded that PTR glasses have great potential as holographic media, which can be modified by ion exchange and photochemical etching to improve their performance. In addition, PTR glasses are a polyfunctional medium that can be used for monolithic integration of volume Bragg gratings, waveguides, sensors, and 3D hollow structures on a single substrate.

The work was carried out with the financial support of the Russian Science Foundation (project No. 24-43-20020).

[1] N.V. Nikonorov, S.A. Ivanov and E.S. Musikhina, Photo-thermo-refractive glass: a promising photonics material, Journal of Optical Technology, vol. 90(3), pp. 142-160. (2023), https://doi.org/10.1364/JOT.90.000142.
[2] N. Nikonorov et al., New photo-thermo-refractive glasses for holographic optical elements: properties and applications, Holographic Materials and Optical Systems, pp. 435-461 (2017), https://doi.org/10.5772/66116.

# Combined nano- and microsecond laser ablation for elemental profiling of coated steel samples by laser induced breakdown spectroscopy

**Sdvizhenskii P.A., Lednev V.N., Rogachevskaya A.V.**

*Prokhorov General Physics Institute, Russian Academy of Science, Moscow, Russia*

*pausdw@gmail.com*

In modern steel industry an express monitoring of the steel chemical composition is a critical stage that determines the quality of the final product and the process economic efficiency. However, real time elemental analysis of steel objects faces the problem that sample surface is covered by a layer of scale or metal coating, making direct analysis impossible. Conventional analytical methods require mechanical sample preparation. Laser induced breakdown spectrometry (LIBS) technique is a good candidate to provide express multielemental analysis of coated samples including depth resolved measurements. A combination of nano- and microsecond laser pulses has been suggested for ablation and LIBS elemental profiling up to 2 mm depth for metal samples. LIBS setup scheme and oscillogram of the temporal profile of the combined microsecond and nanosecond laser pulses are presented in Fig.1.

A combination of micro- and nanosecond pulses also enables the analysis of steel samples through a scale layer with analytical performance comparable to the results obtained for a polished metal surface. The approach was successfully validated for steel grades identification including heated (up to 800 C) and movable samples. It confirms potential of combination nano- and microsecond laser ablation for implementation in real-time analytical control in metallurgical production.

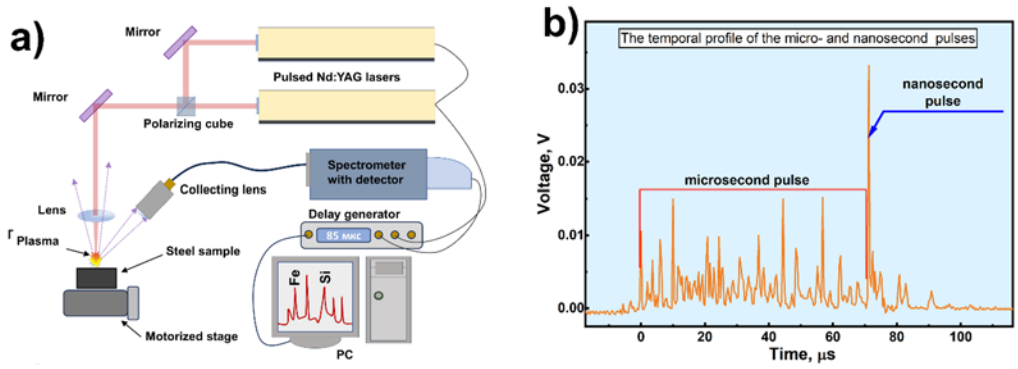


**Fig. 1.** Laser induced breakdown spectrometry (LIBS) setup scheme (a) for elemental profiling analysis of steel samples through a scale layer; oscillogram (b) of the temporal profile of the combined microsecond and nanosecond laser pulses

The authors gratefully acknowledge financial support from the Russian Science Foundation (RSF) (agreement № 25-79-00356), https://rscf.ru/en/project/25-79-00356/

# In situ analysis of bulk technological fluid by double-pulse laser induced breakdown spectroscopy

**V.N. Lednev, P.A. Sdvizhenskii1, A.V. Rogachevskaya**

*Prokhorov General Physics Institute of the Russian Academy of Sciences, Moscow, Russia*

*lednev@kapella.gpi.ru*

In situ chemical analysis of technological fluids without any interruption is in a high demand in the nuclear industry, automotive and aerospace engineering. Remote measurements are convenient to monitor the status of hard-to-reach equipment and especially important when working with chemically hazardous liquids. A good solution to perform remote and in situ chemical sensing is to utilize double-pulse laser-induced breakdown spectroscopy (LIBS) technique. However, up to now this technique have been utilized only for bulk water analysis.

For the first time, a double pulse LIBS technique has been implemented for non-water liquids (ethanol, acetone, oil, gasoline) chemical analysis. To optimize chemical analysis laser-induced bubble dynamics have been studied in details by high-speed shadowgraph imaging to estimate the impact of laser pulse energy, and liquid temperature, density and viscosity on the bubble dynamics. It was found that the laser-induced bubble expansion does not depend on the liquid nature, while the bubble collapse dynamics are different for water, gasoline, and engine oil samples. The effect of bubble dynamics on the plasma properties (temperature and electron density) induced inside a cavity has been demonstrated. To obtained spectra with the highest signal-to-noise ratio for chemical element of interest, one should control the delay between bubble generation and second plasma induction. The chemical analysis performance (accuracy and sensitivity) by double pulse LIBS has been estimated by calcium quantification in a bulk engine oil.

Delayed localized boiling of a bulk fluid near a laser-induced bubble has been observed for the first time (Fig. 1). The boiling starts 50-70 μs after the laser bubble induction and explained by pressure drop near bobble of the low heated liquid.

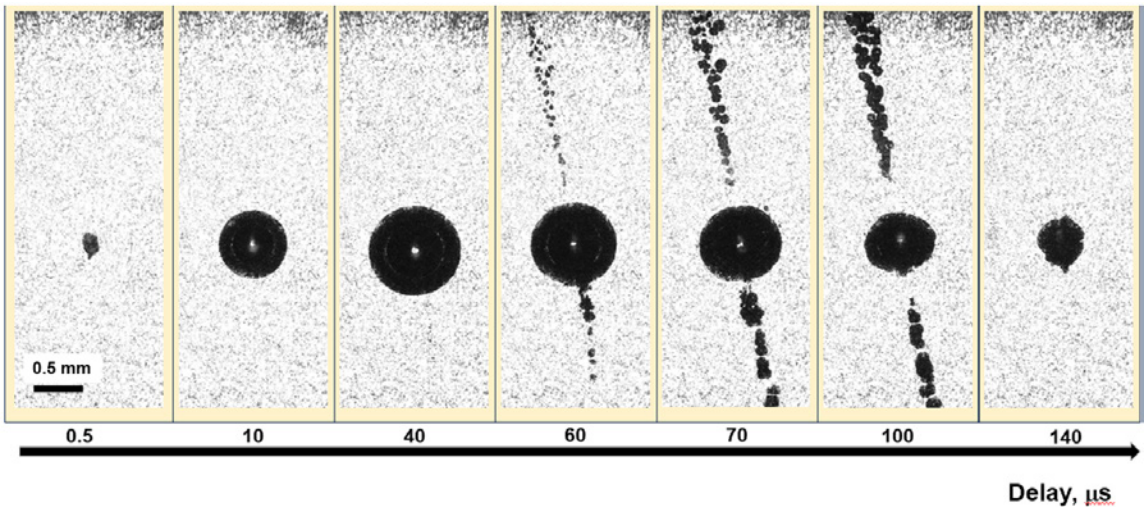


**Fig. 1** High-speed shadowgraphs of the expansion and collapse of a laser-induced bubble in gasoline.

The authors gratefully acknowledge Russian Science Foundation for the financial support of the study (project 25-29-00835). https://rscf.ru/project/25-29-00835/

# Creation of a carbon nanosensor with controlled luminescent properties

**G. Chugreeva[1], A. Guskov[1], G. Kupriyanov[1,2], K. Laptinskiy[1,2], S.A. Dolenko[1,2], T. Dolenko[1,2]**

*1- Faculty of Physics, M.V. Lomonosov Moscow State University, Russia*
*2- D.V. Skobeltsyn Institute of Nuclear Physics, M.V. Lomonosov Moscow State University, Russia*

*chugreeva.gn17@physics.msu.ru*

Carbon dots (CD) are carbon nanoparticles exhibiting intense, stable, environment-sensitive photoluminescence (PL), making them promising optical nanosensors and medicine agents [1]. While most studies predict PL properties from known synthesis conditions [2,3], the more challenging "synthesis-properties-application" problem -- determining synthesis conditions that yield nanoparticles with PL most sensitive to change of specific environmental parameters -- remains largely unresolved.

In this study, we demonstrate the feasibility of determining CD hydrothermal synthesis parameters (precursor ratio, temperature, time) for obtaining nanoparticles with PL most sensitive to both $Cu^{2+}$ and $Co^{2+}$ cations using artificial neural networks. A set of 74 CD was synthesized from ethylenediamine (ED) and citric acid (CA) with varying precursor ratios (CA:ED from 1:1 to 1:20), temperatures (100-200 °C, 20 °C step), and reaction times (30-360 min). For each CD type, 100 aqueous solutions (fixed CD concentration 5 mg/L, variable $Cu(NO_3)_2$ and $Co(NO_3)_2$ from 0 to 6 mM) were prepared (7400 solutions), and excitation-emission matrices of PL each of them were recorded.

A 2D convolutional neural network (two convolutional and two fully connected layers) was applied to each dataset to determine ion concentrations from PL spectra, generating a database of mean absolute errors (MAE) for each CD type. Subsequently, a fully connected neural network, approximation model, was trained to identify optimal synthesis conditions based on MAE. The most sensitive CD nanosensors for $Cu^{2+}$ and $Co^{2+}$ are synthesized at CA:ED ratios of 1:2 and 1:2, temperatures of 120 °C and 160 °C, and reaction times of 240 min and 240 min, respectively.

Thus, using convolutional and fully connected neural networks for experimental data provided a successful solution of the "synthesis-properties-application" problem of creating a carbon nanosensor most sensitive to the content of $Cu^{2+}$ and $Co^{2+}$ cations in an aqueous solution (Fig.1).

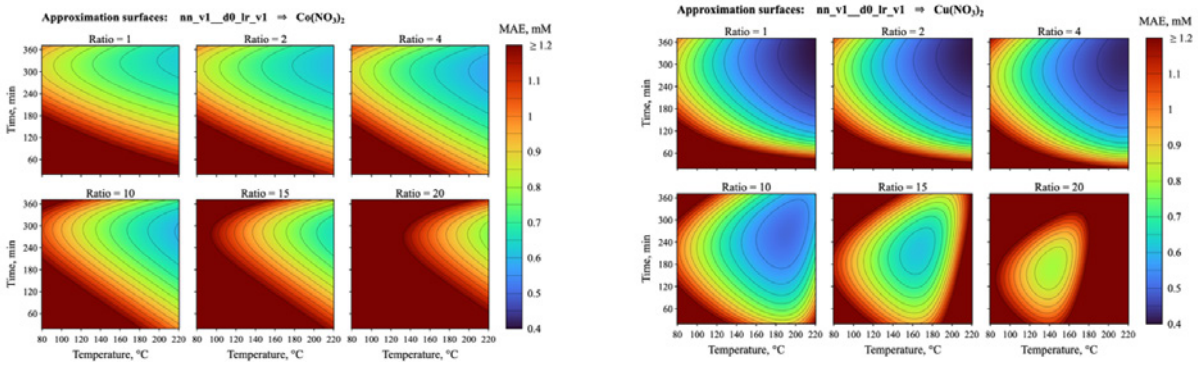


**Fig. 1.** The result of training the approximation model

The study was supported by the grant from the Russian Science Foundation No. 22-12-00138-P, https://rscf.ru/en/project/22-12-00138/.

[1] A.M. Vervald, K.A. Laptinskiy, G.N. Chugreeva, S.A. Burikov, T.A. Dolenko. Quenching of Photoluminescence of Carbon Dots by Metal Cations in Water: Estimation of Contributions of Different Mechanisms // J. Phys. Chem. C, vol. 127, pp. 21617-21628, 2023.
[2] Q. Hong, X.-Y. Wang, Y.-T. Gao, J. Lv, B.-B. Chen, D.-W. Li, R.-C. Qian Customized Carbon Dots with Predictable Optical Properties Synthesized at Room Temperature Guided by Machine Learning // J. Mater. Chem., vol. 34(3), pp. 998-1009, 2022.
[3] A. Goldstein, A. Kapelner, J. Bleich, E. Pitkin Peeking Inside the Black Box: Visualizing Statistical Learning With Plots of Individual Conditional Expectation // J. Comput. Graph. Stat., vol. 24(1), pp. 44-65, 2015

# Traps in diamonds and wide-band luminescent materials

**E.V. Dementeva[1], K.N. Orekhova[1], G.A. Gusev[1], P.A. Demenetev[1], S.N. Bocharov[2], M.V. Zamoryanskaya[1]**

*1- Ioffe Institute st. Polytekhnicheskaya 26, Saint-Petersburg, Russia*
*2- Crystallyne ltd, 29L, ul. Marshala Govorova, St. Petersburg, 198097, Russia*

*dementeva@mail.ioffe.ru*

Carrier traps can significantly affect the luminescence and scintillation properties of wide-bandgap materials, LEDs based on semiconductor nanoheterostructures, and other luminescent functional materials. The presence of traps in some cases leads to a deterioration in properties (reduced luminescence yield for phosphors, scintillators, and LEDs). However, in other cases, they can play a positive role, for example, in the development of memory devices (hopping conductivity in thin dielectric layers). The phenomenon of thermoluminescence, which is used in the creation of thermoluminescent sensors of ionizing radiation, is based on the capture of charge carriers by deep trap levels. Therefore, the study of trapped states is relevant and has not only fundamental but also practical significance. Thermoluminescence is currently the primary method for studying trapped states. This method allows one to determine the activation energy of traps and the frequency factor, but provides no information on the rate of charge carrier capture by traps (charge localization on traps), the type of traps, or their number. These problems can be solved by studying the dynamics of cathodoluminescence intensity and absorbed current during prolonged irradiation of samples with an electron beam [1, 2]. Such studies can be performed using an electron microscope. In many cases, the slow change in cathodoluminescence intensity and absorbed current during continuous irradiation with an electron beam is associated with trap states, which, in turn, can be luminescence centers or affect the excitation of luminescence centers as a result of excitation energy transfer from electrons of the primary electron beam. The nature of the absorbed current dynamics allows one to determine the trap type (electron or hole capture, or both processes simultaneously). The dependence of the absorbed current and cathodoluminescence intensity on the excitation density (electron beam current density) provides information on the rate of charge carrier capture by traps. The temperature dependence of the cathodoluminescence intensity dynamics allows one to estimate the trap activation energy. The relative change in the intensity of the cathodoluminescence bands and the absorbed current is related to the content of traps in the region irradiated by the electron beam. Studying the kinetics of the cathodoluminescence bands in irradiated and non-irradiated regions of the sample allows one to determine the interaction of traps with luminescence centers. Studying the nature of trap states, their interaction with luminescence centers, and determining their activation energy using local cathodoluminescence opens up new possibilities for the application of scanning electron microscopy to the study of wide-bandgap materials.

This method has been used to study diamonds, YAG, YSZ-YSH activated by rare earth ions. The study was supported by grant No. 26-19-00562 from the Russian Science Foundation, https://rscf.ru/project/26-19-00562/

[1] P.A. Dement`ev, E.V. Ivanova, M.V. Zamoryanskaya, Traps in the Nanocomposite Layer of Silicon-Silicon Dioxide and Their Effect on the Luminescent Properties. Phys. Solid State, v.61, 8, p. 1394 – 1400 (2019)
[2] E.V. Dementeva, P.A. Dementev, M.A. Yagovkina, M.V. Zamoryanskaya, ACS Appl. Nano Mater. v.6, 16212 (2023)

# Study on the cathodoluminescent properties of NV-containing diamonds as a function of the growth sector

**G.A. Gusev[1], M.V. Tokarev[1], E.A. Vasilev[2], B.E. Burakov[1], K.N. Orekhova[1], E.V. Dementeva[1], M.V. Zamoryanskaya[1]**

*1- Ioffe Institute, 26 Politekhnicheskaya St., St. Petersburg, 194021, Russian Federation*
*2- St. Petersburg Mining University, 199106, St. Petersburg, Russian Federation*

*ggusev@mail.ioffe.ru*

One approach to utilizing long-lived radionuclides (e.g., $^{241}$Am or $^{14}$C) is their incorporation into stable dielectric matrices containing efficient luminescence centers. In this case, the high-energy radiation generated during radioactive decay is converted into visible light directly within the material volume, providing a self-glowing effect [1, 2]. Such materials can serve as elements of optocouplers or, in combination with a photodetector, be used to create low-power sources of electrical energy.

Diamonds have been investigated as functional materials for more than 50 years. Their luminescent properties are determined by point defects, of which more than 300 different types can exist in diamond. Among the brightest emitting defects are NV defects. This center consists of a nitrogen atom in a carbon substitutional position and a vacancy in an adjacent lattice site. The center exists in negative ($NV^-$) and neutral ($NV^0$) charge states, distinguished by zero-phonon lines at 637 and 575 nm, respectively [3]. $NV^-$ centers can be used for magnetometry and also as spin qubits for quantum information processing and quantum metrology devices. There are reports that $NV^0$ centers are promising for the creation of lasers. At the same time, these defects do not possess optically detected spin resonance. However, they are the principal emission centers under high-energy excitation. For the creation of a self-glowing diamond with the addition of $^{14}$C, the total luminescence intensity and self-absorption of NV defects, regardless of their charge state, are of particular importance. These properties directly depend on the defect concentration in diamond.

The aim of this work is to determine the concentration and analyze the cathodoluminescence of NV defects in diamond as a function of the growth sector.

The object of investigation was a diamond synthesized by the HPHT (High Pressure High Temperature) method, subjected to electron irradiation with an energy of 3 MeV and annealing at 1200 °C to form NV defects. The point defect concentrations in the sample were determined by IR spectroscopy. The total nitrogen content was measured by secondary ion mass spectrometry (SIMS). In combination with optical absorption data in the visible range, this made it possible to estimate the NV defect content. Using local cathodoluminescence (beam energy ~20 keV), the emission spectra were studied in detail in various growth sectors differing in impurity composition.

As a result of the work, the dependence of the NV defect concentration on the diamond growth sector was established, and the influence of this concentration on the cathodoluminescence intensity was revealed. The obtained data are of interest for the creation of self-glowing diamonds containing defects of this type.

The study was supported by grant No. 26-19-00562 from the Russian Science Foundation, https://rscf.ru/project/26-19-00562

[1] M. Zamoryanskaya, E. Dementeva, K. Orekhova, V. Kravets, A. Trofimov, G. Gusev, I. Ipatova, B. Burakov, Self-glowing crystals – radioactive decay energy converters into optical emission, Mater. Res. Bull., 142, 111431 (2021).
[2] S.N. Bocharov, B.E. Burakov, A.I. Isakov, K.N. Orekhova, E.V. Dementeva, M.V. Zamoryanskaya, P.A. Dementev, B.Y. Ber, D.Yu. Kasantsev, M.V. Tokarev, Y.Yu. Petrov, Self-glowing single crystal diamond activated with carbon-14: First synthesis and characterization, Diam. Relat. Mat., 141, 110650 (2024).
[3] Z.W. Zheng, X.N. Li, C.X. Li, N. Zhou, C.Y. Ma, Q.Y. Zhang, C. Zhang, Z. Yi, Vibronic property of $NV^-$ and $NV^0$ centers in diamond and the thermal behavior of zero-phonon lines, Diam. Relat. Mat., 161, 113081 (2026).

# Analysis of the Concentration Behavior of the Landau–Placzek Ratio at the Peculiar Point of Aqueous Solutions

**L.M. Sabirov, F.R. Ismailov, G.N. Umarova, Kh.Sh. Omonov, Kh.Sh. Djumaniyazov**

*Samarkand State University, University Boulevard 15, Samarkand 140104, Uzbekistan*

*lazer.fizika@gmail.com*

The structural properties of aqueous solutions of γ-picoline attract considerable interest due to the presence of anomalous thermodynamic behavior and concentration singularities. In the present work, the temperature and concentration dependences of the Landau–Placzek ratio were investigated by means of molecular light scattering spectroscopy. The Landau–Placzek ratio characterizes the relationship between the central Rayleigh component and the Mandelshtam–Brillouin side components and provides valuable information about density fluctuations, compressibility, and structural transformations in liquids.

Measurements were carried out using a double-pass Fabry–Perot interferometer with a contrast of $4 \times 10^5$ and a finesse of approximately 40. A frequency-stabilized single-mode He–Ne laser served as the excitation source. Aqueous γ-picoline solutions with molar fractions ranging from 1.0 to 0.06 were studied within the temperature interval of 10–80°C.

The experimental results revealed a pronounced dependence of the Landau–Placzek ratio on both concentration and temperature. For concentrated solutions (0.8–0.4 molar fractions), the ratio remained relatively small and exhibited only weak temperature dependence. In contrast, dilute solutions (0.2–0.06 molar fractions) demonstrated a significant increase in the ratio accompanied by characteristic temperature anomalies. A singularity temperature close to 50°C was identified, separating two distinct regimes of behavior. Above this temperature, the observed increase in scattering intensity is associated with the approach to the lower critical point of phase separation, whereas below 50°C the behavior is influenced by structural transformations within the hydrogen-bonded water network.

Calculations based on the experimental Landau–Placzek ratios showed that the isothermal compressibility increases dramatically with decreasing γ-picoline concentration. For solutions near 0.06 molar fractions, the compressibility exceeds that of concentrated solutions by more than one order of magnitude. This behavior indicates enhanced structural organization of water molecules and the formation of extended hydrogen-bonded networks. The observed growth of the background scattering intensity is attributed to the development of stable molecular aggregates and increased density fluctuations.

The obtained results demonstrate that the Landau–Placzek ratio is a sensitive probe of structural heterogeneity in aqueous γ-picoline solutions and provides evidence for concentration-induced restructuring processes in the vicinity of singular states.

[1] L.M. Sabirov, F.R. Ismailov, Sh.A. Kadirov, and Sh.E. Karshibaeva, Temperature and Concentration Dependences of the Landau–Placzek Ratio in Aqueous Solutions of γ-Picoline, Opt. Spectrosc., 129, 51–55 (2021).
[2] I.L. Fabelinskii, Molecular Scattering of Light (Springer, New York, 1968).
[3] N.F. Bunkin, V.S. Gorelik, L.M. Sabirov, D.I. Semenov, and Kh.S. Khaydarov, Quantum Electron., 40, 817–821 (2010).

# Study of CH··· π intermolecular interactions in the meta-xylene and chloroform system based on raman spectroscopy and mep maps

**A. Jumabaev, A. Absanov, H. Hushvaktov, Sh. Umidullaev, M. Shoimov**

*Samarkand State University after Sharaf Rashidov. Uzbekistan, 140104, Samarkand, University blvd.,15*

*jumabaev2@rambler.ru*

The study of Raman spectra shows that the formation of molecular complexes through any type of intermolecular interaction, including intermolecular hydrogen bonding, leads to changes in the spectral parameters of interacting molecules [1–2]. Investigating the interaction of aromatic hydrocarbons with proton-donor solvents is of great importance for understanding the mechanisms of intermolecular bonding. In particular, the π-electron system of an aromatic ring can form weak intermolecular interactions with proton-donor molecules. Raman spectroscopic studies have reported that CH···π interactions in solutions of aromatic compounds are associated with shifts in spectral bands [3].

The Raman spectra of mixtures of meta-xylene and chloroform were investigated at room temperature and atmospheric pressure, and the spectra of the solutions were compared with those of the pure substances. In this study, mixtures of meta-xylene and chloroform with mole fractions of 0.9, 0.7, 0.5, 0.3, and 0.1 were prepared, and their Raman spectra were analyzed. The results showed that the symmetric stretching vibrations of the $CH_3$ groups in the meta-xylene molecule shifted toward higher frequencies as the amount of chloroform in the solution decreased. This phenomenon was explained by the CH···π intermolecular interaction occurring between the hydrogen atom of the CH group in chloroform and the π-electrons of the aromatic ring in meta-xylene. It was determined that this intermolecular interaction causes changes in the vibrational frequencies.

In the Raman spectrum, the band observed around 2919 $\mathbf{c}m^{-1}$ shifted toward higher frequencies, which was found to be associated with the solvation effect of the solvent medium. As a result of the interaction between the C–H dipole of chloroform and the π-electron system of meta-xylene, strengthening of the C–H bond and shortening of the bond length were observed, leading to an increase in the vibrational frequency. In addition, molecular electrostatic potential (MEP) maps were constructed to determine the electronic distribution of the molecules. Through MEP analysis, regions of high and low electron density within the molecules were identified, and the possible active centers of intermolecular interactions between meta-xylene and chloroform were evaluated.

[1] M. Nishio, Y. Umezawa, J. Fantini, M. S. Weiss, and P. Chakrabarti, CH–π hydrogen bonds in biological macromolecules, Physical Chemistry Chemical Physics, vol. 16, no. 25, pp. 12648-12683, (2014).
[2] A. Jumabaev, A. A. Absanov, B. B. Khudaykulov, and Z. I. Ernazarov, Investigation of intermolecular interactions in butyl acetate using vibrational spectroscopy and non-empirical calculations, Uzbek Physics Journal, vol. 25, no. 4, (2023).
[3] S. Suzuki, P. G. Green, R. E. Bumgarner, S. Dasgupta, W. A. Goddard, and G. A. Blake, Benzene forms hydrogen bonds with water, Science, vol. 257, no. 5072, pp. 942-945, (1992).

# Nature of halogen bonding in PhX-DMF (X=Cl, Br, I) complexes: experimental and theoretical (DFT) consistency

**A. Jumabaev, A.A. Absanov, U.A. Holikulov, B.B. Khudaykulov, J.N. Sulaymonov**

*Samarkand State University after Sharaf Rashidov. Uzbekistan, 140104, Samarkand, University blvd.,15*

*jumabaev2@rambler.ru*

Halogen bonding (HB) has been widely recognized in recent years as an important and independent type of noncovalent interaction. Similar to hydrogen bonding (HB), halogen atoms can also act as electrophilic centers that interact with electron-donating centers [1]. Politzer et al. [2] demonstrated that halogen bonding is noncovalent in nature and argued that its essence is manifested in the competition between the electrophilic region of the halogen atom, i.e., the σ-hole, and the electron-rich (nucleophilic) center of the neighboring molecule.

In this work, the intermolecular interactions in binary mixtures of chlorobenzene (PhCl), bromobenzene (PhBr), and iodobenzene (PhI) formed with dimethylsulfoxide (DMF) were studied in a comprehensive manner using infrared (IR) spectroscopy and density functional theory (DFT, ωB97X-D/def2-TZVP) methods.

In Fig. 1(a,b,c), systematic frequency shifts in the region of the C-X valence (X-sensitive) vibrations [3] characteristic of halobenzenes were observed in the experimental infrared spectra. The largest blue shift observed in the experiment was observed in the PhI-DMF system (+6 $cm^{-1}$), followed by the PhBr-DMF system (+4 $cm^{-1}$), and the smallest shift was observed in the PhCl-DMF system (+3 $cm^{-1}$). The observed pattern is consistent with the increasing polarizability of iodine, bromine and chlorine atoms and the σ-hole intensity.

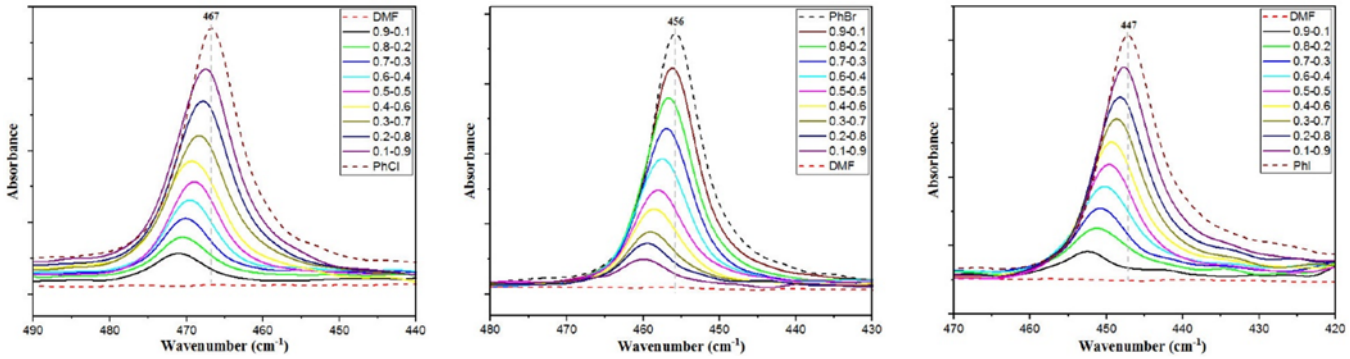


*a)* *b)* *c)*

**Figure 1.** Experimentally obtained infrared spectra of binary mixtures
a) PhCl-DMF, b) PhBr-DMF and c) PhI-DMF in the corresponding ranges

These binary systems, when studied using DFT, showed that during the complex formation process, the C-X (X = Cl, Br, I) bond shortening (Δr) and, accordingly, the valence vibration frequencies undergo an unusual blue shift (Δν). The orbital interactions and second-order stabilization energies ($E^{(2)}$) in the complexes were evaluated using NBO analysis. It was found that the stabilization energy due to the charge transfer $n$O(DMF)→σ*(C-X) increases sharply when going from the chlorine complex to the iodine complex ($\sum E^{(2)}$ from 0.62 kcal/mol in chlorine to 4.30 kcal/mol in iodine).

While the blue shift of the C-X vibrational frequency was observed to increase in the order PhCl < PhBr < PhI in the experiment, the harmonic frequency calculations at the ωB97X-D/def2-TZVP level gave the trend PhCl ≈ PhBr > PhI. This discrepancy can be explained by the fact that the calculations were performed for an isolated 1:1 complex model, the solvent environment and multi-particle associations were not taken into account, and the limitations of the harmonic approximation.

[1] Legon, A. C. (2010). The galogen bond: an interim perspective. *Physical Chemistry Chemical Physics*, *12*(28), 7736-7747.
[2] Politzer, P., Murray, J. S., & Clark, T. (2010). Galogen bonding: an electrostatically-driven highly directional noncovalent interaction. *Physical Chemistry Chemical Physics*, *12*(28), 7748-7757.
[3] Whiffen, D. (1956). 273. Vibrational frequencies and thermodynamic properties of fluoro-, chloro-, bromo-, and iodo-benzene. *Journal of the Chemical Society (Resumed)*, 1350-1356.

# Morphology and Optical Properties of SERS-Active Substrates with Silver Nanoparticles Deposited on Single-Crystal and Porous Silicon Surfaces

**V.V. Tregulov[1], A.I. Ivanov[1], D.S. Kostsov[2], N.N. Melnik[2], E.V. Perevedentseva[2], K.O. Aiyyzhy[3], E.V. Barmina[3]**

*1- Ryazan State University named for S.A. Yesenin, Svobody str. 46, 390000, Ryazan, Russia*
*2- P.N. Lebedev Physical Institute of the Russian Academy of Sciences, Leninsky Prospekt, 53, 119991 Moscow, Russia*
*3- Prokhorov General Physics Institute of the Russian Academy of Sciences, Vavilova str. 38, 119991 Moscow, Russia*

*d.kostzov@lebedev.ru*

In this paper, new active substrates for surface-enhanced Raman scattering (SERS) spectroscopy based on silver nanoparticles deposition on surface of semiconductor structures: monocrystal n-Si (Ag/n-Si) or on porous Si film (Ag/por-Si/n-Si) are presented. For the Ag/n-Si structure, Ag nanoparticles were deposited directly onto the front surface of a single-crystal silicon wafer using a chemical method. For the Ag/por-Si/n-Si structure, a porous silicon (por-Si) film was first grown on a single-crystal silicon wafer using anodic electrochemical etching in an alcoholic hydrofluoric acid solution, and then Af nanoparticles were deposited onto it. The morphology, optical properties and Raman enhancement ability were characterized and compared for two types of the SERS-agents to estimate the optimal conditions of their applications. Scanning electron microscopy (SEM), reflectance spectroscopy, and Raman spectroscopy were used for the characterization.

SEM image analysis revealed that the por-Si film thickness was 0.5 μm, and the average Si crystallite size was 49 nm and that the Ag/por-Si/n-Si structure contains smaller Ag particles compared to the Ag/n-Si structure. The reflectance spectra of the front surface of the substrates demonstrate a blue shift of the plasmon resonance for the Ag/por-Si/n-Si structures relative to Ag/n-Si, which corresponds to the observed difference in Ag nanoparticle sizes. We conclude that the Ag nanoparticles size is determined by the conditions of formation of Ag nanoparticles either directly on the surface of single-crystal Si with slight Si dissolution (in the case of Ag/n-Si), or on the nanostructured surface of silicon crystallites separated by pores (Ag/por-Si/n-Si), which leads to a decrease in the Ag particle size.

The potential of using Ag/n-Si and Ag/por-Si/n-Si substrates for SERS spectroscopic measurements was assessed using Methylene blue solution as an analyte. SERS observations revealed that the Ag/por-Si/n-Si structure provides a higher enhancement of Raman scattering intensity compared to Ag/n-Si. The alteration in the size of silver particles, as well as of their arrangement relatively Si surface, primarily influences the intensity and distribution of the electromagnetic field of the exciting light, which is modified by the ensemble of particles. This allows for the adjustment of the enhancement factor and facilitates a discussion regarding the predominant mechanism of SERS within this system.

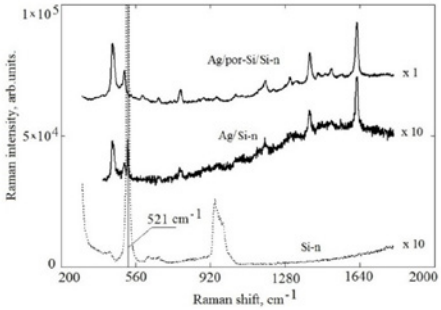


**Fig. 1.** Raman spectra of the Si-n substrate, as well as Ag/por-Si/Si-n and Ag/Si-n with methylene blue

# Near- and middle-IR range laser generation of refractive index gratings in gases to detect weak absorption by molecular species or small amounts of absorbers

**D.N. Kozlov**

*Prokhorov General Physics Institute of the Russian Academy of Sciences,*
*38 Vavilov Str., 119991 Moscow, Russia*

*dnk@kapella.gpi.ru*

The technique employing laser-induced gratings (LIGs) of the refractive index [1], generated by pulsed NIR- or MIR-range laser radiation in gases and probed by diffracting continuous wave laser light, allows for temporally- and spatially-resolved detection of extremely weak molecular absorption or small amounts of absorbing molecules present in gas mixtures. In the latter case, using LIGs it is also possible to determine several parameters of the gas, such as the speed of sound, temperature, and thermal diffusivity, in a single laser shot.

Pulses from a Q-switched $Nd^{3+}$-YAG laser at 1064 nm are used to generate LIGs in neat $O_2$ at ambient temperature by photoexcitation of molecular species. LIGs are created within the extremely weak $O_2(a\ ^1\Delta_g, v = 1) \leftarrow O_2(X\ ^3\Sigma_g^-, v = 0)$ absorption band of $O_2$ monomers over a wide pressure range (1-130 bar) [2]. The proposed modeling of the signal temporal profiles suggests that at small delays (0-2 μs) LIGs are formed, in addition to electrostriction, by "instantaneous" collisional energy exchange with the environment of the $O_2$-$O_2$ dimols, excited due to collision-induced absorption, and the subsequent breakdown of the laser-excited species, with the emergence of electronically and vibrationally excited $O_2$ monomers. At large delays (20-1000 μs), LIGs are created by the "slow" collisional relaxation of the produced excited monomers.

Pulses of 3-μm tunable narrowband radiation obtained by difference-frequency mixing of radiations from a Q-switched $Nd^{3+}$-YAG laser at 1064 nm and from a tunable dye laser at 800 nm in a $LiNbO_3$ crystal are used to generate LIGs at resonant excitation of a selected rovibrational transition of the strong $\nu_3$ band of $CH_4$ molecules, contained in different buffer gases at very low molar concentration (down to ~50 ppm, or 0,005 % in $N_2$) [3]. The LIG signal temporal profiles are formed as a result of a multi-stage collisional energy exchange between the vibrationally excited $CH_4$ molecules and the environment, occuring at different rates. The specific features of the LIG signal temporal profiles related to the mixture composition, pressure, and temperature of a selected buffer gas are studied in terms of their application to determination of these characteristics. The results show that the LIG technique with resonant mid-IR excitation allows the measurement of low concentrations of $CH_4$ in gases in a broad range of pressures. In addition, the signal temporal profiles in gas mixtures with low concentrations of $CH_4$ can be effectively used for sensitive local determination of gas parameters.

[1] H.J. Eichler, P. Günter, D.W. Pohl, Laser-induced dynamic grating (Springer, Berlin, 1986).
[2] D.N. Kozlov, Near-IR range laser generation of refractive index gratings in $O_2$ gas: role of mono- and bimolecular absorption and collisional relaxation, Chemical Physics, 593, 112619, (2025). https://doi.org/10.1016/j.chemphys.2025.112619.
[3] A.-L. Sahlberg, D. Hot, Z. Li, D. Kozlov, Mid-infrared generated laser-induced grating signal profiles in methane-containing gas mixtures as indicators of gas composition, pressure, and temperature, Applied Spectroscopy, 78(4), pp. 423-437, (2024). https://doi.org/10.1177/00037028241230340.

# Neuromorphic Reservoir Computing Based on Distributed Random Fiber Laser Dynamics

**D. Kudashkin**

*Novosibirsk State University, Novosibirsk, Russia, Pirogova str. 2, 630090*

*d.kudashkin@g.nsu.ru*

Modern computing paradigms face severe bandwidth and energy-efficiency constraints, a bottleneck inherent to the von Neumann architecture [1]. Photonic reservoir computing offers a promising alternative, enabling the processing of temporal optical signals directly within a high-dimensional physical state space with low latency and low energy consumption. Random fiber lasers (RFLs), which utilize distributed Rayleigh backscattering and nonlinear optical amplification, serve as a robust hardware platform for physical reservoir computing due to their complex spatio-spectral dynamics [2, 3].

In this work, we theoretically validate the feasibility and computational capabilities of a reservoir architecture based on an all-fiber random laser with distributed feedback, employing a system of power balance equations. The system modeled consists of a semi-open random fiber laser cavity into which the input optical signal and pump radiation are injected via an open input port (Fig. 1). By numerically solving the system of coupled power balance equations (both steady-state and dynamic) for the pump and the spectral power distribution along the fiber length $z$, we simulate nonlinear state-space transformations upon optical signal injection. Simulation results confirm that the distributed feedback and nonlinear mode interactions within the random laser provide the necessary fading memory and data mapping into a high-dimensional state space. Specifically, the system achieves a total memory capacity TMC≈ 26 and demonstrates high accuracy on chaotic time-series prediction tasks, yielding a Normalized Mean Square Error as low as $4 \times 10^{-4}$ for the Mackey-Glass benchmark. These quantitative metrics establish the all-fiber random laser system as a highly efficient physical hardware candidate for neuromorphic optical platforms.

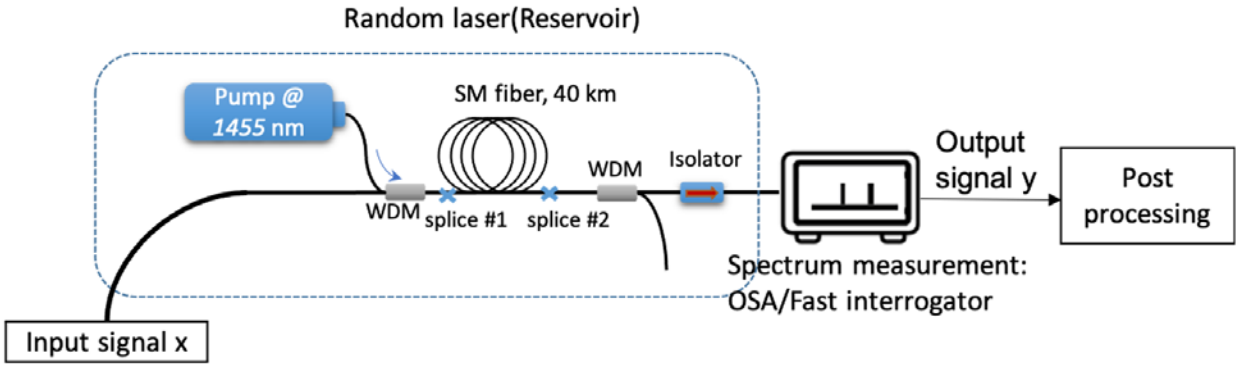


**Fig. 1.** Schematic diagram of the random laser reservoir computing architecture

The study was supported by the Russian Science Foundation (24-12-00432), https://rscf.ru/en/project/24-12-00432/

[1] B. J. Shastri, A. N. Tait, T. Ferreira de Lima, W. H. P. Pernice, M. Bhaskaran, C. D. Wright, and P. R. Prucnal, Photonics for artificial intelligence and neuromorphic computing, *Nature Photonics*, vol. 15, pp. 102–114, (2021).
[2] D. V. Tsarev, P. V. Zakharenko, and A. P. Alodjants, Complex networks for random lasers and photonic computing, *Physical Review A*, vol. 112, 033508, (2025).
[3] S. K. Turitsyn, S. A. Babin, A. E. El-Taher, P. Harper, D. V. Churkin, S. I. Kablukov, J. D. Ania-Castañón, and E. V. Podivilov, Random distributed feedback fibre laser, *Nature Photonics*, vol. 4, pp. 231–235, (2010).

# Wavelength Tuning and Acoustic-Thermal Noise Suppression in a Random Fiber Laser Locked to an Active SNAP Microresonator

**D. Kudashkin, I. Vatnik**

*Novosibirsk State University, Novosibirsk, Russia, Pirogova str. 2, 630090*

*d.kudashkin@g.nsu.ru*

Random Random fiber lasers (RFLs) based on distributed Rayleigh backscattering offer unique spectral properties, high power scalability, and cavity-free operation [1]. Achieving narrow-linewidth single-mode generation and agile wavelength control in RFLs is essential for high-precision sensing and spectroscopy. Integrating a microresonator based on the Surface Nanoscale Axial Photonics (SNAP) platform into the laser cavity allows for highly selective mode injection locking, establishing stable single-mode lasing [2].

In this work, we propose and demonstrate dynamic wavelength tuning and acoustic-thermal noise suppression in a random fiber laser locked to a SNAP microresonator fabricated on an optical fiber with an active Erbium-doped core. The SNAP platform provides ultra-low optical loss and precise axial mode control [3]. As demonstrated in our previous work [4], optical pumping directed directly into the active core modulates the local refractive index via thermo-optic effects and population inversion dynamics. By adjusting the auxiliary pump power in the Er-doped core, the resonant frequencies of the SNAP microresonator shift continuously, allowing smooth and precise wavelength tuning of the locked random laser without mechanical components.

Furthermore, we analyzed the thermal stability and spectral performance of the laser output under continuous core heating. The steady-state internal heat dissipation within the active core establishes a localized thermal gradient, which buffers the microresonator against ambient thermal drift and stabilizes output mode position. Experimental characterization of the tuning agility, spectral linewidth, and power stability demonstrates the strong potential of active-SNAP-controlled RFLs for stable photonic light sources.

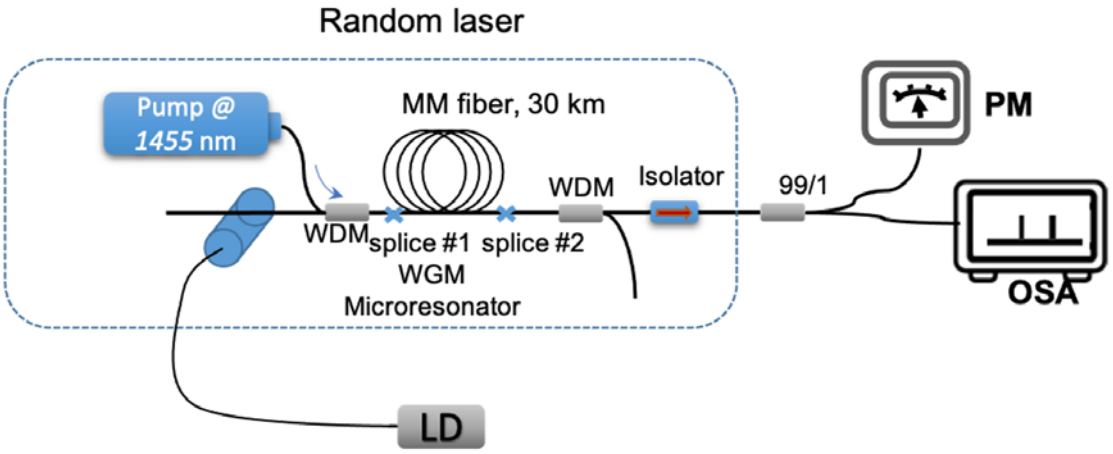


**Fig. 1.** Schematic diagram of the random laser with ab embedded SNAP microcavity with external heating by laser diode

The study was supported by the Russian Science Foundation (24-12-00432), https://rscf.ru/en/project/24-12-00432/

[1] S. K. Turitsyn, S. A. Babin, A. E. El-Taher, P. Harper, D. V. Churkin, S. I. Kablukov, J. D. Ania-Castañón, and E. V. Podivilov, Random distributed feedback fibre laser, Nature Photonics, vol. 4, pp. 231–235, (2010).
[2] D. V. Kudashkin, O. A. Gorbunov, I. D. Vatnik, and D. V. Churkin, Single-mode generation in the random fiber laser with an embedded microcavity, Optics Letters, vol. 49, pp. 3120–3123, (2024).
[3] M. Sumetsky and J. M. Fini, Surface nanoscale axial photonics, Optics Express, vol. 19, no. 27, pp. 26470–26485, (2011).
[4] D. V. Kudashkin, S. V. Khorev, and I. D. Vatnik, Self-stabilization by negative feedback of whispering gallery mode resonators based on optical fiber with active core, Journal of Lightwave Technology, vol. 40, no. 22, pp. 7351–7357, (2022).

# New optical properties of nanodiamonds synthesized from hydrocarbons

**O. Kudryavtsev[1], R. Bagramov[2], D. Pasternak[1], V. Filonenko[2], I. Vlasov[1]**

*1- Prokhorov General Physics Institute of the Russian Academy of Sciences, Moscow, Russia.*
*2- Vereshchagin Institute of High Pressure Physics of the Russian Academy of Sciences, Moscow, Russia.*

*leolegk@gmail.com*

Pure diamond with a hydrogen-terminated surface, as a semiconductor, has two unique properties: negative electron affinity and p-type surface conductivity. The occurrence of this conductivity is explained using the model of electrochemical "transfer doping", in which electron density is transferred from the diamond surface to the near-surface layer of an electrolyte, for example, adsorbed water [1]. The thickness of the electron-depleted diamond layer is ~ 1 nm, and the concentration of free holes in it can reach $10^{19}$-$10^{20}$ $cm^{-3}$. Until now, only the electrical properties of "hydrogenated" diamonds have been studied. For these purposes, macro-sized diamond structures such as films and plates have mainly been used. We have developed methods for the synthesis of diamond nanoparticles from various hydrocarbons, in particular, from adamantane, under high pressure and temperature (the HPHT method), which has made it possible to efficiently obtain "hydrogenated" nanodiamonds directly during their synthesis. Diamond sizes can vary depending on the synthesis parameters, and as they decrease, the volume fraction of the material containing free charge carriers increases. As a result, for diamond nanoparticles 3–30 nm in size, we were able to detect for the first time the interaction of a continuum of hole states induced by transfer doping with optical phonons of the diamond lattice. This interaction manifests itself as a narrow transparency peak at 1328 $cm^{-1}$, associated with destructive Fano interference, in the IR absorption spectra of nanodiamonds [2]. The Fano effect we discovered initiates the study of plasmon-phonon interactions in undoped semiconductors and demonstrates the potential for the use of hydrogen-terminated nanodiamonds as a new optical material with induced transparency in the infrared optical range.

[1] F. Maier and M. Riedel, Origin of Surface Conductivity in Diamond, Phys. Rev. Lett., vol. 85, pp. 3472-3475, (2000).
[2] O. Kudryavtsev, R. Bagramov, I. Vlasov, Fano-type effect in hydrogen-terminated pure nanodiamond, Nano Letters, vol. 22, pp. 2589–2594, (2022).

# Concentration-dependent structural changes in water–isopropanol systems studied by dynamic light scattering

**L.M. Sabirov, D.I. Semenov, F.R. Ismoilov, Y.T. Juraev, M.A. Khasanov, Kh.Sh. Omonov, G.N. Umarova, Kh.Sh. Djumaniyazov**

*Institute of Engineering Physics, Sharof Rashidov Samarkand State University, Samarkand, Uzbekistan*

*xumoyunomonov125@gmail.com*

Aqueous alcohol solutions are widely used as model systems for studying hydrogen bonding and structural heterogeneity in liquids. The addition of alcohol modifies the three-dimensional hydrogen-bond network of water, leading to clustering, concentration fluctuations, and microheterogeneity whose properties strongly depend on composition [1–4]. Despite extensive research, the mechanisms responsible for these structural transformations remain under discussion.

In this work, concentration-dependent structural changes in water–isopropanol mixtures were investigated by dynamic light scattering (DLS). Solutions with isopropanol mole fractions $0.001 \leq x \leq 0.1$ were studied using a Photocor Complex analyzer equipped with a 637.4 nm semiconductor laser (25 mW). Measurements were performed at a scattering angle of 90° and a temperature of $20.0 \pm 0.1$ °C. Hydrodynamic radii were determined from diffusion coefficients obtained from intensity autocorrelation functions using the Stokes–Einstein equation.

The results reveal pronounced nonmonotonic concentration dependences of both scattering intensity and characteristic size. At $x \approx 0.001$, structures with hydrodynamic radii of 120–180 nm were detected. In the range $0.01 < x < 0.04$, the scattering intensity increased while the characteristic size remained nearly constant, indicating the formation of an increasing number of nanoscale heterogeneities. A distinct structural transition occurred at $x > 0.05$, where the average radius increased sharply and reached approximately 540 nm at $x \approx 0.1$. At the same time, the scattering intensity decreased, indicating a transition from many small scattering centers to fewer but substantially larger aggregates.

The concentration dependence of the scattering intensity exhibits two maxima, suggesting a two-stage mechanism of structural evolution. The first maximum corresponds to the formation of nanoscale heterogeneities, whereas the second reflects their further aggregation and reorganization. The observed anticorrelation between scattering intensity and aggregate size at higher concentrations indicates a decrease in the number density of scattering centers as mesoscale domains develop. The results demonstrate that structural evolution in water–isopropanol mixtures is governed by the competition between water–water, water–isopropanol, and isopropanol–isopropanol interactions. Rearrangement of the hydrogen-bond network plays a key role in the emergence and transformation of microheterogeneous structures, providing new insight into concentration-induced heterogeneity in aqueous alcohol solutions.

[1] Franks F. Water: A Comprehensive Treatise. New York: Plenum Press, 1972.
[2] Rodnikova M.N., Chumaevskii N.A. Three-dimensional net of hydrogen bonds in liquids and solutions. Journal of Structural Chemistry. 2006;47(Suppl.):S151–S158.
[3] Dixit S., Crain J., Poon W.C.K., Finney J.L., Soper A.K. Molecular segregation observed in a concentrated alcohol–water solution. Nature. 2002;416:829–832.
[4] Tang H., Cai J., Zhu C.-Y., Chen G.-J., Wang X.-H., Sun C.-Y. Review on the clustering behavior in aqueous solutions. Journal of Molecular Liquids. 2022;367:120382.
[5] Berne B.J., Pecora R. Dynamic Light Scattering: With Applications to Chemistry, Biology, and Physics. New York: Wiley, 1976.

# Luminescence of defects in IIb diamond grown by the HPHT method using a precursor enriched with $BaCO_3$

**K.N. Orekhova[1], V.A. Kravets[1], S.N. Bocharov[2], B.E. Burakov[1], E.V. Dementeva[1], G.A. Gusev[1], P.A. Dementev[1], M.V. Tokarev[1], E.A. Vasilev[1], M.V. Zamoryanskaya[1]**

*1- Ioffe Institute, 26 Polythekhnicheskaya St., St. Petersburg, 194021, Russian Federation*
*2- Crystallyne ltd, 29L, ul. Marshala Govorova, St. Petersburg 198097, Russian Federation*

*orekhova.kseniia@gmail.com*

The synthesis of large diamond crystals characterized with intensive luminescence is an urgent task for obtaining chemically and mechanically durable materials to be applied in microelectronics.

One of the possible applications is related to the production of environmentally safe low-power energy source based on self-glowing diamonds activated with beta-emitter carbon-14. Previous study demonstrated that typical commonly available chemical form of $^{14}C$ to be used in starting precursor is $BaCO_3$. Taking into consideration that diamond synthesis by the HPHT method using precursor enriched with $BaCO_3$ has not been developed in detail before, additional studies of defects, composition and luminescence properties of such diamonds are needed. The method of local cathodoluminescence is very efficient for studying inhomogeneities and point defects in diamonds. This method also makes it possible to clarify in detail the luminescent properties of various growth sectors. Such an information is important for optimizing synthesis, improving the functional characteristics of diamonds, and expanding their applications in electronics, quantum technologies, and optoelectronics, including the production of self-glowing radioactive diamonds.

The purpose of this work was to study the features of cathodoluminescence, the content of impurities, and the charge carriers' diffusion length in various growth sectors of a diamond single crystal grown by the HPHT method using $BaCO_3$-enriched precursor as typical chemical form of radioactive isotope carbon-14. It is shown that the addition of $BaCO_3$ does not lead to significant changes in the optical properties of the obtained artificial diamonds although the distribution of nitrogen and boron impurities in the growth zones {111} and {100} is different. It is shown the impurity content impact on the cathodoluminescent (CL) properties of diamond growth zones and the charge carriers' dissipation length. It has been observed that the shape of the CL bands, their intensity, and the decay time depend on content of impurities. In addition, it has been demonstrated that an increase of boron content supports the luminescence intensity by an order of magnitude. At the same time boron admixture causes blue coloring of diamond matrix, which is related to absorption of CL. The results obtained can be used to optimize synthesis of self-glowing radioactive diamonds activated with boron and carbon-14.

The purpose of this work was to study in detail the growth zones of diamond crystal obtained by HPHT method and using precursor enriched with non-radioactive $BaCO_3$. The impurity contents, their impact on the luminescent properties and dissipation length of charge carriers are discussed.

The results obtained demonstrate that the addition of $BaCO_3$ does not lead to significant changes in the optical properties of artificial diamond, although the distribution of nitrogen and boron in different growth zones in diamond varies in a broad range. In the {111} growth sector the average content of boron was up to 1.3 ppm; nitrogen – up to 0.2 ppm. In the {100} growth sector the impurity content is significantly lower: boron – 0.09 ppm, nitrogen – 0.05 ppm. It is shown that the impurity content leads to the dissipation lengths of charge carriers: 60 and 140 microns in sectors {111} and {100}, respectively.

The study was supported by grant No. 26-19-00562 from the Russian Science Foundation, https://rscf.ru/project/26-19-00562/

# CARS-diagnostics of temperature during combustion of composite fuels

**K. Aiyyzhy, E. Barmina, V. Kobtsev, D. Kozlov, S. Kostritsa, S. Orlov, A. Saveliev. V. Smirnov**

*Prokhorov General Physics Institute of the Russian Academy of Sciences,*
*38 Vavilov Str., 119991 Moscow, Russia*

*orlov@kapella.gpi.ru*

Coherent anti-Stokes Raman spectroscopy (CARS) is widely used for local non-intrusive investigations of reactive flows and, in particular, for the diagnostics of combustion. In the present study, CARS local temperature measurements were applied, for the first time to our knowledge, to investigation of diffusion combustion of composite hydrocarbon fuels - *n*-decane or isopropanol seeded with aluminum or boron nanoparticles (NPs). It is established that NPs of materials with a high calorific value added to hydrocarbon fuels can significantly intensify their combustion. In this case, local temperature distribution in a flame can serve as an indicator of combustion efficiency.

The study was conducted using a continuous flow burner, with an oxygen-free heater-evaporator of liquid fuel droplets atomized by a nitrogen flow. The vapor was injected, through a 2 mm×4 mm slot nozzle, into a co-flow of oxygen, resulting in a stable flat laminar diffusion flame with a well-defined flame front position. Mounting the burner on a 3D-movable table allowed the flame to be positioned relative to the CARS probe volume with an accuracy of ± 10 μm. Flame temperatures, in the range up to 2600 K, were obtained from rovibrational CARS spectra of $N_2$ probe molecules. Measurements were taken in a direction perpendicular to the flame axis, at several distances from the nozzle edge.

The first set of measurements was accomplished using isopropanol seeded with amorphous B NPs (0.5 wt%) produced by a nanosecond pulsed laser fragmentation of boron powder in isopropanol. The distribution of NPs was bimodal: most (99%) of the boron mass was contained in large particles (≈ 750 nm in diameter), and most NPs had a diameter of 10 nm. It was found that during combustion, the temperature in the flame front region is higher for the composite fuel than for pure isopropanol, while the temperature differences increase with the distance from the nozzle edge and reach ≈ 150°K at a temperature of ≈ 2500 K [1]. This indicates that B NPs actively influence the development of combustion in a diffusion flame. It is estimated to be most likely due not to an increase in heat generation during the combustion of NPs, but to their intensification of the oxidation reactions.

The second set of measurements was performed using *n*-decane or isopropanol seeded with oxidized (0.10-0.15 wt%) Al NPs. These NPs were produced by fragmentation of initially large NPs (mean diameter of ≈ 450 nm) in isopropanol using two different nanosecond lasers. The resulting NPs were added to *n*-decane or isopropanol in the required concentrations. In *n*-decane, the largest number of NPs were ≈ 10 nm in diameter, while the majority of Al mass (85%) was concentrated in NPs with a diameter of ≈ 400 nm, and the mass of NPs with a diameter of 10-40 nm amounted to only 0.015 wt%. In isopropanol, the mass of small NPs (3-30 nm in diameter) was 87%. CARS temperature measurements showed that combustion of both fuels with Al NPs also leads to higher flame front temperatures compared to the combustion of pure fuels. The addition of NPs can provide temperature difference up to 250 K at flame temperatures of ≈ 1850-2250 K. The magnitude of this difference and its dependence on the distance from the nozzle edge for each fuel are defined by the mass concentration of nanoparticles and their distributions by diameters and masses [2].

The obtained results allow us to numerically model the combustion processes in a similar way to how it was done in [3].

[1] E. Barmina, M. Zhilnikova, K. Aiyyzhy, V. Kobtsev, D. Kozlov, S. Kostritsa, S. Orlov, A. Saveliev, V. Smirnov, N. Titova, G. Shafeev, Experimental Study of the Diffusion Combustion of Suspension of Boron Nanoparticles in Isopropanol, Doklady Physics, v. 67 (2), pp. 39-43, (2022).
[2] E. Barmina, V. Kobtsev, S. Kostritsa, S. Orlov, V. Smirnov, M. Zhilnikova, O. Uvarov, G. Shafeev, Laser synthesis of nanocomposite hydrocarbon fuel and CARS diagnostics of its combustion flame, Quantum Electronics, v. 52 (1), pp. 100-104, (2022).
[3] A.M. Savel'ev, V.V. Smirnov, N.S. Titova, D.A. Yagodnikov, Diffusion combustion of *n*-decane with unpassivated aluminum nanoparticles additives: Analysis of mechanism and numerical simulation, Combustion and Flame, v. 236, 111761, (2022).

# Dependence of the reflected radiation spectra on the preplasma conditions in the relativistic femtosecond laser interaction regime

**A.R. Poletaeva[1], N.D. Bukharskii[1,2], Ph.A. Korneev[1,2], I.P. Tsygvintsev[3]**

*1- National Research Nuclear University MEPhI, Moscow, Russia*
*2- P. N. Lebedev Physical Institute, Moscow, Russia*
*3- KIAM RAS, Moscow, Russia*

*anro.poletaeva@gmail.com*

A laser pulse of relativistic intensity is accompanied by a nanosecond-duration prepulse (amplified spontaneous emission, ASE) with an intensity sufficient to create a plasma layer. Consequently, when irradiating a solid target, the main pulse at its peak intensity interacts with a cloud of preformed plasma (preplasma). The parameters of the preplasma influence the mechanisms of laser energy absorption, which determine the generation of fast particles and secondary radiation [1].

In this work, we investigate the influence of the preplasma on the process of high-order harmonic generation for a laser pulse with a peak intensity of $I_0 = 5 \cdot 10^{21}$ W/cm², which is achieved at the J-Karen laser facility [2]. Several contrast values $C = I_0 / I_p$ in the range from $10^{-11}$ to $3 \cdot 10^{-9}$ were considered, where $I_p$ is the intensity of the prepulse on the nanosecond timescale. Three-dimensional hydrodynamic simulations of the prepulse interaction with the target were carried out using the 3DLINE code [3]. The obtained density profiles were subsequently used in two-dimensional kinetic simulations performed with the Particle-In-Cell (PIC) code SMILEI [4]. From these simulations, the angular distributions of harmonics at multiples of the fundamental laser frequency were obtained.

The obtained spectra exhibit a transition from one absorption mechanism to another due to the influence of the preplasma. This allows for a qualitative determination of the contrast value. Based on the results of the analysis, conclusions are made about a diagnostic method that relies on the distinctive features of the spectra of the reflected multiple harmonics.

[1]. Ivanov K. A., Shulyapov S. A., Gorlova D. A., Mordvintsev I. M., Tsymbalov I. N., and Savel'ev A. B. Quantum Electronics 51 (9) 768-794 (2021).
[2]. Kiriyama H., Pirozhkov A. S., Nishiuchi M., Fukuda Y., Ogura K., Sagisaka A., et al. Optics Letters 43 (11) 2595-2598 (2018).
[3]. Krukovskiy A. Yu., Novikov V. G., and Tsygvintsev I. P. Mathematical Models and Computer Simulations 9 (1) 48-59 (2017).
[4]. Derouillat J., Beck A., Perez F., et al. Computer Physics Communications 222 351-373 (2018).

# Abnormally high second harmonic generation signal in spherulitic lead zirconate titanate thin films

**I. Pronin[1], S. Senkevich[1], E. Kaptelov[1], A. Elshin[2], E. Mishina[2], M. Staritsyn[3], V. Pronin[4]**

*1- Ioffe Institute, Politechnicheskaya str., 26, St.-Petersburg, 194021 Russia*
*2- MIREA – Russian Tecnological University, Vernadsky Ave., 78, Moscow 119454 Russia*
*3- National Research Centre "Kurchatov Institute" – Shpalernaya str., 15, St.-Petersburg, 191015 Russia*
*4 - Herzen State Pedagogical University of Russia, Moika River Emb., 48, St.- Petersburg, 191186 Russia*

*Petrovich@mail.ioffe.ru*

The development of the growth technology of ferroelectric lead zirconate titanate (PZT) thin layers allows these to be considered as promising materials for the creation of memory elements, piezoelectric energy converters, microelectromechanical devices, infrared radiation sensors, etc. [1]. Incorporation of the obtained thin PZT layers (with submicron and micron thicknesses) in CMOS and MEMS technologies usually requires these films to be deposited on silicon substrates.

In the work, nonlinear optical microscopy techniques have been used to study the orientation of ferroelectric polarization in mechanically strained spherulitic 500 nm thick PZT films deposited on $Pt/TiO_2/SiO_2/Si$ substrate by means of RF magnetron sputtering. Due to target–substrate distance variation in the range of D = 30-70 mm, the block spherulitic sizes changed from 40-45 to 15-20 μm. The abnormally high change in lateral polarization $P_L$ which is proportional to the square of second harmonic generation signal was revealed in the films of large size blocks (Fig. 1, curve 1) [2]. The normalized factors ($P^N_L$) responsible for the observed strong variation in lateral polarization projection included a) structural factor $P^N_{L1}$, curve 2, b) orientational factor $P^N_{L2}$ , curve 3, and c) induced factor $P^N_{L3}$, curve 4. The structural factor concernes the changes in remanent polarization measured from polarization hysteresis loops (P-V) of the films. The orientational factor deals with polarization reorientation under the action of lateral mechanical stresses in the directions as close as possible to film plane in separate spherulitic blocks differ in <100>, <110>, and <111>- growth orientations. And the third one induced factor defines as polarization induced by lateral mechanical stresses ($P^N_{L3}$) measured from P-V loops. It is shown that The sum contribution of these factors in lateral polarization (curve 5) shows a good agreement with the experiment [3].

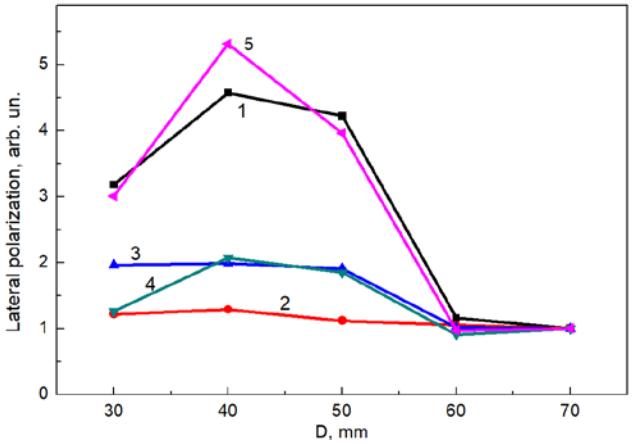


**Fig. 1.** Contributions of different factors ((2) $P^N_{L1}$, (3) $P^N_{L2}$, (4) $P^N_{L3}$) to the change in the normalized lateral polarization projection ((1) $P^N_L$, experiment, (5) $P^N_{L1}*P^N_{L2}*P^N_{L3}$, calculation) in thin PZT films deposited at different target–substrate distances D

[1] N. Izyumskaya, Y-I. Alivov, S-J. Cho, H. Morkoç, H. Lee, Y-S. Kang. Processing, structure, properties, and applications of PZT thin films. Critical Reviews in Solid State and Materials Sciences, vol. 32, iss. 3-4, pp. 111–202. (2007).
[2] M.V. Staritsyn, V.P. Pronin, I.I. Khinich., S.V. Senkevich, E.Yu. Kaptelov, I.P. Pronin, A.S. Elshin, E.D. Mishina. Microstructure of spherulitic lead zirconate titanate thin films. Physics of the Solid State, vol. 65, iss. 8, pp. 1312-1318 (2023).
[3] A.S. Elshin, E.D. Mishina, A.R. Valeeva, S.V. Senkevich, M.V. Staritsyn, E.Yu. Kaptelov, I.P. Pronin. Anomalously high lateral polarization in spherulitic thin films of lead zirconate titanate. Crystallography Reports, vol. 70, iss. 7, pp. 1201–1207 (2025).

# Laser induced breakdown spectrometry for online elemental analysis of scale-coated steel

**A.V. Rogachevskaya, P.A. Sdvizhenskii, V.N. Lednev**

*Prokhorov General Physics Institute of the Russian Academy of Sciences, Vavilova Street 38, Moscow Russia*

*rogachevskaya.alexa@gmail.com*

Elemental analysis of alloys and melts and the prompt deviations detection are most important in metallurgy for high-quality production and cost minimization. To determine the zone of change in metal composition is of interest specifically in continuous casting processes of slab and billet production and online measurements are particularly useful in this case. However, online analysis is a complex task, as an alloy usually has a layer of oxide slag with different chemical composition and is in constant movement.

In this study we successfully applied laser induced breakdown spectrometry (LIBS) analysis for quantitative analysis of silicon in steel under a slag coat by a combination of pulses of different durations. The microsecond laser pulse removes the scale on the steel surface, and nanosecond pulse generates LIBS plasma on the cleaned surface area for spectral analysis. This approach resulted in the detection accuracy on scale-coated steel comparable to polished steel without oxide layer (coefficient of determination $R^2$ from calibration curves equaled 0.964). The high efficiency of the method was experimentally demonstrated on moving samples with scale coat (Fig.1)

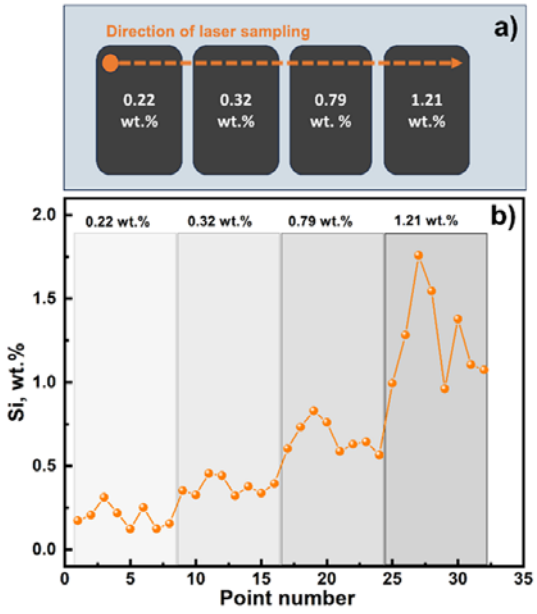


**Fig. 1.** Schematic diagram (a) of the silicon content measurement in moving steel samples with scale coat; the silicon content in different zones of moving samples (b)

This work was supported by the Russian Science Foundation (grant 25-79-00356, https://rscf.ru/project/25-79-00356/).

# Diagnostics of the polarized state of a ferroelectric calcium orthovanadate crystal using modulated IR laser radiation

**O. Sergeeva[1], A. Solnyshkin[1], A. Tsilich[1], L. Ivleva[2], I. Voronina[2], E. Dunaeva[2]**

*1- Tver State University. 33Zhelyabova street, Tver,170100, Russia*
*2- Prokhorov General Physics Institute of the Russian Academy of Sciences*
*38 Vavilov street, Moscow, 119991, Russia*

*o_n_sergeeva@mail.ru*

In this work, modulated IR laser radiation was used to diagnostic the polarized state of ferroelectric calcium orthovanadate (CVO) crystals grown by the Chokhralsky method from the melt in General Physics Institute. Samples of polar and non-polar cuts both nominally pure and doped with thulium ions were studied. For measurements, a dynamic pyro effect method was used in which an infrared laser with rectangular output pulses was used as a heating source. Heating/cooling of the polar cut samples at different frequencies induced a pyroelectric current. The current direction was determined by the natural unipolarity vector due to changes in spontaneous polarization with temperature. If the polarization distribution in the sample volume is uniform and stationary thermal state is achieved, the shape of pyroelectric response coincides with the shape of modulated IR-radiation with the same modulation frequency. It was shown [1] that CVO crystal doping by thulium ions at concentration of 0.5 wt% leads to polarized state stabilization and increased polarization distribution homogeneity in the sample volume (Fig.1).

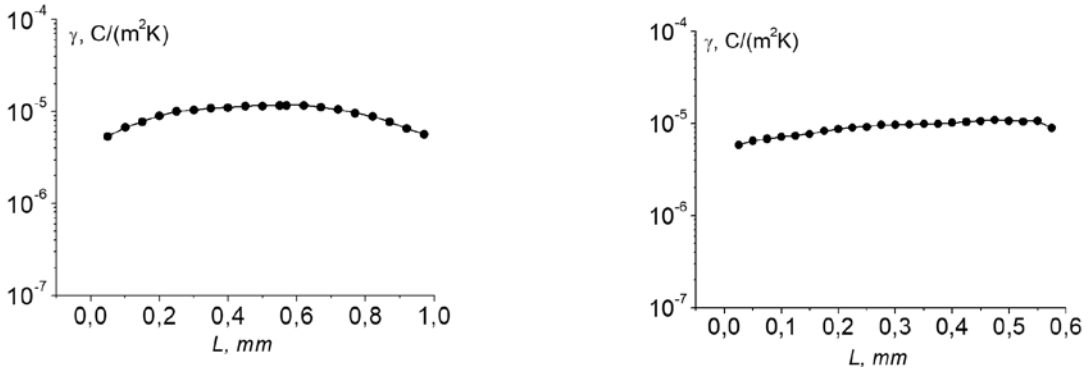


**Fig.1.** Distribution of the pyroelectric coefficient in CVO crystals: a –nominally pure, b - doped with 0.5% thulium ions.

In nonpolar-cuts, the spontaneous polarization vector should lie in the sample's plane, so in this geometry a pyroelectric response should not be observed. After etching a nonpolar-cut thulium doped CVO (CVO + 0.5% Tm) sample in acetic acid, a distinct boundary appeared across the entire sample separating regions with different etch rates. However, when different areas and sides of this sample were irradiated with a modulated heat flux, a pyroelectric current was observed in the same direction. This effect could be assigned to spontaneous polarization projection onto the normal direction of this sample due to the presence of an irregular three-dimensional labyrinth of rounded domains with charged walls slightly inclined relative to the polar direction [2]. The same direction of polarization of the sample's different sides could be attributed to the existence of the positively charged boundary. The obtained results are discussed. A model for charge source at the etching boundary is proposed.

[1]A. D. Tsilikh, A. V. Solnyshkin, O. N. Sergeeva, L. I. Ivleva, E. E. Dunaeva, I. S.Voronina, D. A. Kiselev, A. M. Kislyuk & T. S. Ilina The polar properties of calcium orthovanadate crystals doped with manganese and thulium ions Ferroelectrics, Vol. 591, pp.201–210. (2022).
[2] E.Shishkina, V.Yuzhakov, M.Nebogatikov, E.Pelegova, E.Linker, L.Ivleva, V. Shur As-Grown Domain Structure in Calcium Orthovanadate Crystals. Crystals. Vol.11. (12). pp.1508-1515. (2021).

# From Ag Nanopillar–Nanoflower Arrays to Endotaxial Ag Nanoparticles in Si: Periodic Ordering via Lithographically Controlled Galvanic Displacement

**Yu.A. Zharova[1], E.S. Fedorova[1,2], D.P. Markov[1], A.A. Ermina[1], N.S. Solodovchenko[1,3], V.O. Bolshakov[1], K.V. Prigoda[1], A.O. Larin[3]**

*1- Ioffe Institute, Polytechnicheskaya street 26, 194021, St. Petersburg, Russia*
*2- Peter the Great Saint-Petersburg Polytechnic University, Polytechnicheskaya street 29, 195221, St. Petersburg, Russia*
*3- ITMO University, Kronverksky Prospect 49, building A, 197101, St. Petersburg, Russia*

*piliouguina@mail.ioffe.ru*

Excitation of localized plasmon resonance (LPR) in metallic nanostructures is accompanied by strong localization of the electromagnetic field near the surface of nanoparticles, as well as a pronounced enhancement of the absorption and scattering of light at the resonant frequency [1]. These effects lead to a unique optical response of plasmonic nanostructures and underlie a wide range of applications, including sensorics [2], energy [3], nonlinear optics [4], surface-enhanced Raman scattering (SERS), and biosensors [5–6]. The spectral position and intensity of LPR significantly depend on the material, size, shape of nanoparticles (NPs), and the surrounding medium. Therefore, controlling the morphology and spatial arrangement of metallic nanoparticles is one of the key approaches to tuning their optical response. Unlike disordered arrays, where the «hot spots» distribution and spectral response are poorly reproducible, ordered arrays provide more controllable optical properties and can support high-Q collective lattice resonances [7].

To create such structures, we proposed for the first time a lithographically controlled galvanic displacement (LCGD) method, which enables the reproducible formation of ordered Ag nanostructures on a Si(100) substrate with controlled morphology. The developed approach combines (i) electron beam lithography, which defines the structure's topology, and (ii) a galvanic displacement reaction from an $AgNO_3$/HF solution, which ensures the growth of the metallic nanostructure. In this study, three types of ordered Ag nanostructures were created on Si: «nanoflowers,» «nanopillars,» and endotaxial pyramidal AgNPs. A mask made of electron-beam resist or a thermally grown $SiO_2$ layer served as a physical template guiding the growth of Ag. Ordered arrays of nanostructures were thus obtained, ranging from «nanoflowers» (with diameters (d) ranging from 50 to 300 nm) to vertical nanopillars (with d ~ 50 nm and a height of ~ 200 nm). Subsequent high-temperature annealing of the Ag «nanoflowers» in a humid atmosphere (at 1000 °C) allowed the creation of ordered endotaxial AgNPs in the shape of tetrahedral «pyramids». The morphology of the resulting structures was studied using scanning electron microscopy. Their optical properties were investigated using spectroscopic ellipsometry and elastic scattering spectroscopy in dark-field geometry. The potential application of the created structures as SERS substrates for detecting low concentrations of triphenylmethane brilliant green dye was also explored. The developed LCGD method is characterized by its technological simplicity and reproducibility. It is of interest for scaling to smaller periods and sizes of nanoparticles, and also opens up new possibilities for forming nanostructures with a given topology and shape. However, potential limitations on minimum characteristic dimensions will most likely be determined by the maximum resolution of electron-beam lithography.This work was supported by the Ministry of Science and Higher Education of the Russian Federation under a state assignment (project no. FFUG-2024-0017).

[1] U. Kreibig, M. Vollmer. Optical properties of metal clusters (Berlin, Springer, 2013).
[2] M. Pan, J. Yang, K. Liu, Z. Yin, T. Ma, S. Liu, L. Xu, S. Wang, Noble Metal Nanostructured Materials for Chemical and Biosensing Systems, Nanomaterials, 10(2), 209 (2020).
[3] H. A. Atwater, A. Polman, Plasmonics for improved photovoltaic devices, Nat. Mater., 9, 205-213 (2010).
[4] Z.-W. Yang, L. Meng, J.-S. Lin, W.-M. Yang, 3D Hotspots Platform for Plasmon Enhanced Raman and Second Harmonic Generation Spectroscopies and Quantitative Analysis, Adv. Opt. Mater., 7(23), 1901010 (2019).
[5] J. Aizpurua, R. Hillenbrand. Localized surface plasmons: basics and applications in field-enhanced spectroscopy (Berlin, Springer, 2012).
[6] A.A. Ermina, N.S. Solodovchenko, K.V. Prigoda, V.S. Levitskii, V.O. Bolshakov, M. Yu. Maximov, Y.M. Koshtyal, S.I. Pavlov, V.A. Tolmachev, Y.A. Zharova, Silver particles embedded in silicon: The fabrication process and their application in surface enhanced Raman scattering (SERS), Appl. Surf. Sci, 608, 161771 (2023).
[7] Wurtz G.A., Dickson W., O'Connor D., Atkinson R., Hendren W., Evans P., Pollard R., Zayats A.V. Guided plasmonic modes in nanorod assemblies: strong electromagnetic coupling regime // Opt. Express. 2008. V. 16. № 10. P. 7460–7470.

ALT INTERNATIONAL CONFERENCE
Advanced Laser Technologies

# LASER SYSTEMS AND MATERIALS

# Self-injection locking stabilization mechanisms in low-noise CW and pulsed fiber laser configurations

**V.A. Ribenek, I.S. Panyaev, P.A. Itrin, G.V. Tertyshnikova, M.V. Pribylov, D. P. Kachalkin, A.I. Abanin, D.A. Korobko, A.A. Fotiadi**

*Ulyanovsk State University, 42 Leo Tolstoy Street, Ulyanovsk, 432970, Russian Federation*

*fotiadi@mail.ru*

Self-injection locking is a powerful physical mechanism for improving the spectral purity, temporal stability and noise performance of laser systems without relying exclusively on high-bandwidth electronic stabilization. In this talk, we discuss two apparently different classes of fiber laser configurations - continuous-wave narrow-linewidth semiconductor lasers locked to external fiber resonators and passively mode-locked soliton fiber lasers stabilized by optoacoustic resonances - and show that both can be understood within a unified self-locking framework.

In the continuous-wave case, a standard DFB laser is coupled to a high-Q polarization-maintaining fiber ring cavity. The frequency-selective resonant feedback from the external cavity locks the semiconductor laser to a cavity mode and strongly narrows its emission linewidth. A fully spliced PM configuration suppresses polarization-related instabilities, while a low-bandwidth optoelectronic feedback loop controls the phase delay in the feedback path and prevents mode hopping. Recent experiments demonstrated a Lorentzian linewidth of about 20 Hz, output power of about 8 mW, reduced phase and intensity noise, and a frequency drift of about 0.5 MHz/min under thermal control [1, 2]. Thus, self-injection locking provides a practical route from a low-cost DFB diode to a highly coherent source suitable for microwave photonics, coherent optical systems and distributed fiber sensing.

In pulsed fiber lasers, an analogous stabilization principle appears when the pulse repetition rate is locked to an optoacoustic resonance of the cavity fiber. The circulating pulse train resonantly excites a long-lived acoustic mode through guided acoustic wave Brillouin scattering. The acoustic vibration, in turn, acts back on the optical field as a narrow-band phase modulation mechanism and stabilizes the pulse timing. When a harmonic of the laser cavity frequency coincides with an acoustic resonance, the acoustic mode can define the elementary step for pulse repetition rate tuning. This leads to double harmonic mode-locking, where the pulse repetition rate is locked to integer multiples of the optoacoustic resonance rather than to successive harmonics of the fundamental cavity frequency. In soliton fiber ring lasers, this mechanism enabled pulse repetition rates up to about 12 GHz, supermode suppression exceeding 40 dB, and improved timing jitter and relative intensity noise [3, 4].

The comparison of these CW and pulsed systems highlights a common stabilization scenario: a laser with many degrees of freedom becomes locked to a narrow-band resonant subsystem with a long memory time. In CW SIL lasers, this subsystem is an external optical fiber ring cavity; in harmonically mode-locked lasers, it is a fiber acoustic mode resonantly driven by the pulse train. In both cases, the resonant feedback reduces the number of accessible dynamical states and transforms a sensitive laser configuration into a more stable oscillator. This unified view suggests new strategies for designing low-noise fiber lasers, optomechanical oscillators and compact photonic sources where optical, acoustic and electronic feedback mechanisms are deliberately combined.

The work was funded by the Russian Science Foundation (23-79-30017).

[1] A. A. Fotiadi, D. A. Korobko, and I. O. Zolotovskii, "Brillouin Lasers and Sensors: Trends and Possibilities," Optoelectron Instrument Proc. 59(1), 66–76 (2023).
[2] I. S. Panyaev, P. A. Itrin, D. A. Korobko, and A. A. Fotiadi, "Sub-100-Hz DFB laser injection-locked to PM fiber ring cavity," Journal of Lightwave Technology 42, 2928–2937 (2024).
[3] V. A. Ribenek, P. A. Itrin, D. A. Korobko, and A. A. Fotiadi, "Double harmonic mode-locking in soliton fiber ring laser acquired through the resonant optoacoustic coupling," APL Photonics 9, 056105 (2024).
[4] A. Sudin, I. Volkov, et al., "Enhancing high-order harmonic mode-locking in Er/Yb-doped fiber lasers with sub-MHz fundamental frequency via optoacoustic resonance," Optical Fiber Technology 88, 104028 (2024).

# Cladding-pumped Bismuth-doped Fiber Lasers and Amplifiers: Current Status and Future Perspectives

**M.A. Melkumov**

*Prokhorov General Physics Institute of the Russian Academy of Sciences, Dianov Fiber Optics Research Center, 38 Vavilov str., 119333 Moscow, Russia*

*melkoumov@fo.gpi.ru*

Core pumped Bi-doped fiber amplifiers (BDFAs) and lasers (BDFLs) possess unique properties such as broadband amplification and a wide wavelength tuning range. Depending on the glass composition and pump wavelength they can operate in the wavelength range of 1.1 to 1.8 μm. Until recently, such devices required complex and expensive single-mode pump sources, such as single-mode laser diodes and Raman fiber lasers. In 2022, it was demonstrated for the first time [1] that Bi-doped fibers could be pumped through the cladding using commercially available pump sources. Using this approach, several lasers and amplifiers based on double clad (DC) Bi-doped fibers with phosphosilicate, low-germanium and high-germanium-doped core glasses were demonstrated (see Fig. 1). The laser output powers ranged from 0.05 W to 1 W. It was shown that such lasers can reach 0.8–1.0 W of output power in the 1.3–1.47 μm range [2,3], and about 0.15 W near 1.75 μm [4], when pumped near 0.793, 0.808 and 0.915 μm, respectively. Additionally, DC BDFAs demonstrate levels of gain and noise figure (NF) similar to those of core-pumped BDFAs. Furthermore, they allow the combination of gain of different bismuth active centers (BAC) within a single fiber using specially designed fibers and pump sources at different wavelengths, thus providing ultrawideband amplification [5]. The main advantage of such schemes is the simplicity of the pump source, which consists of inexpensive multimode laser diode. The main limitation of the cladding-pumped scheme for Bi-doped fibers is the low power conversion efficiency (PCE), which is typically in the 1–5% range, whereas core-pumped counterparts can achieve maximum efficiency of 30–70%. The main reasons for this low PCE are large quantum defect, the high transition rate from the pump level to the ground state, and the high level of unsaturated loss at the pump wavelegth. Nevertheless, such fiber sources hold great potential for use in telecommunications, metrology, biomedicine and many other applications.

This work was supported by the Russian Science Foundation (grant 22-19-00708-P).

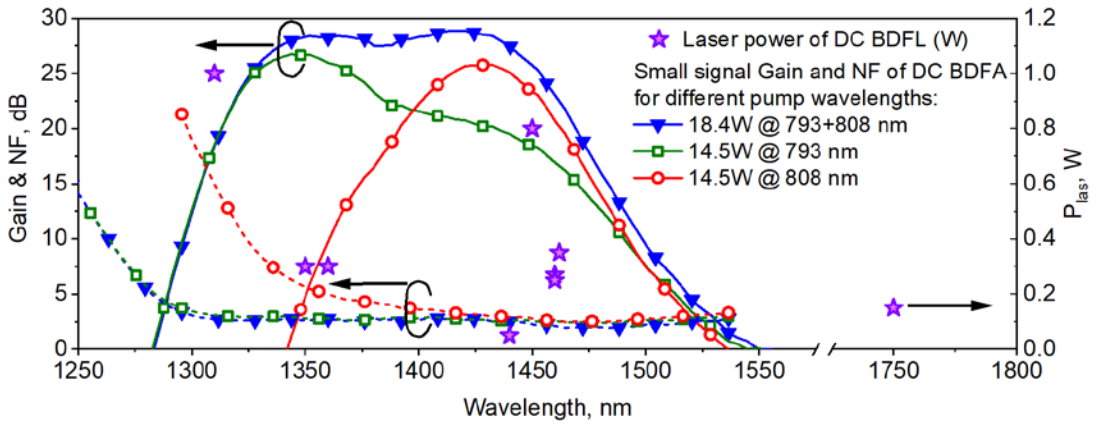


**Fig. 1.** Normalized gain (solid lines), noise figures (dash lines) of various DC BDFAs and output powers of DC BDFLs (stars).

[1] S.V. Firstov, et al., "Cladding-pumped bismuth-doped fiber laser," Opt. Lett., vol. 47(4), pp. 778-781, (2022).
[2] A.S. Vakhrushev, et al., "Watt-level cladding-pumped bismuth-doped fiber laser operating near 1.31 μm," Opt. Laser Technol., vol. 180, pp. 111526, (2025).
[3] A.S. Vakhrushev, et.al., "Cladding-pumped laser and amplifier for E- and S-bands based on multimode bismuth-doped graded-index fibers: toward "watt-level" output power," Opt. Lett. 49, 1828-1831 (2024)
[4] D.S. Serenkov, Afanasyev F.V., "School-conference of young scientists "Prokhorovsky weeks", Moscow, (2026).
[5] A.S. Vakhrushev, et al., "Cladding pumped bismuth-doped fiber amplifiers operating in O-, E-, and S-telecom bands," Opt. Lett., vol.48(6), pp. 1339-1342, (2023).

# Scattering lensed optical fibers with a concave end surface obtained by volumetric chemical etching

**L.O. Zhukov, D.A. Kornilin, R.S. Ponomarev**

*Perm State University, Integrated photonics laboratory, Perm, Russia*

*leonidgp@bk.ru*

The forming of microstructures on the end-faces of optical fibers, particularly diverging lenses, is a promising approach for the optical trapping and manipulation of micro-objects [1]. This paper presents a modified technique for manufacturing concave axicons via bulk chemical etching at the interface between HF and a xylene buffer layer [2].

The key features of the proposed approach are the precision positioning of the fiber end-face using optical reflectometry and strict thermal stabilization of the process, which prevents geometric distortion caused by thermogravitational convection. Scanning electron microscopy (SEM) analysis revealed that a complex end-face topology – a parabolic cavity with a central conical protrusion – forms within just 5 to 10 minutes. This is driven by intense downward flows of the etchant, which etch away not only the germanium-doped core but also the adjacent regions of the silica cladding.

Numerical simulations of light propagation in COMSOL Multiphysics, combined with experimental beam profile measurements using an infrared camera, confirmed that the resulting geometry ensures the formation of a toroidal output beam profile in the far field.

The developed technology enables the rapid and reproducible fabrication of diverging microstructures, which are in high demand for the development of fiber-optic tweezers.

The study was funded by the Russian Science Foundation grant No. 24- 91-21001.

[1] Piccirillo F. et al. (INVITED)Miniaturized lenses integrated on optical fibers: Towards a new milestone along the lab-on-fiber technology roadmap // Results in Optics. Elsevier. 2022 Vol. 6 P. 100203 https://doi.org/10.1016/j.rio.2021.100203

[2] Woźniak A., Łakomski M., Niedzielski P. Lensed Chemically Etched Optical Fibers for Free-Space Coupling of Multicore Fibers // Materials. 2026. Vol. 19, № 5. P. 1013. https://doi.org/10.3390/ma19051013

# Supercontinuum generation in GRIN MM fiber: nonlinear dynamics of modal content

M.D. Gervaziev[1,2], N. Bochkarev[1,2], D.S. Kharenko[1,2], S.A. Babin[1,2], S. Wabnitz[1,3]

*1- Novosibirsk State University, 1 Pirogova str., 630090, Novosibirsk, Russia*
*2- Institute of Automation and Electrometry SB RAS, 1 Ac. Koptyug ave., 630090, Novosibirsk, Russia*
*3- DIET, Sapienza University of Rome, Via Eudossiana 18, 00184 Rome, Italy*

*gervaziev.m@gmail.com*

Supercontinuum (SC) sources are extremely helpful for biomedical imaging, metrology, and spectroscopy [1]. While photonic crystal fibers enabled visible spectral broadening, they often suffer from limited power handling. Recently, gradedindex multimode fibers (GRIN MMFs) have reemerged as a scalable platform for highpower SC generation, exploiting intermodal nonlinear interactions such as geometric parametric instability (GPI) and fourwave mixing [2,3]. Efficient generation of visible SC was demonstrated in a GRIN MMF pumped at 1064 nm, attributing the shortwavelength components to GPI induced by periodic selfimaging [3]. However, the modal dynamics of different spectral components during SC generation have not been investigated experimentally. In particular, it remains unknown how the fundamental mode and higherorder modes contribute to the formation of new frequencies and how Kerr beam selfcleaning (KBSC) accompanies the spectral broadening.

Here we report on visibleextended SC generation in a standard 11m long GRIN MMF with 50μm core, pumped by a Qswitched microchip laser delivering 435ps pulses at 1064 nm. The coupling efficiency was 85%. Output spectra were measured as a function of average power up to 85 mW (Fig. 1a)). At low power, selfphase modulation and the first Stokes line dominate. With increasing power, discrete peaks appear at 730, 840, and 930 nm due to GPI [2]. At maximum power, these peaks merge into a smooth supercontinuum spanning from 450 nm to beyond 1500 nm (more than one octave).

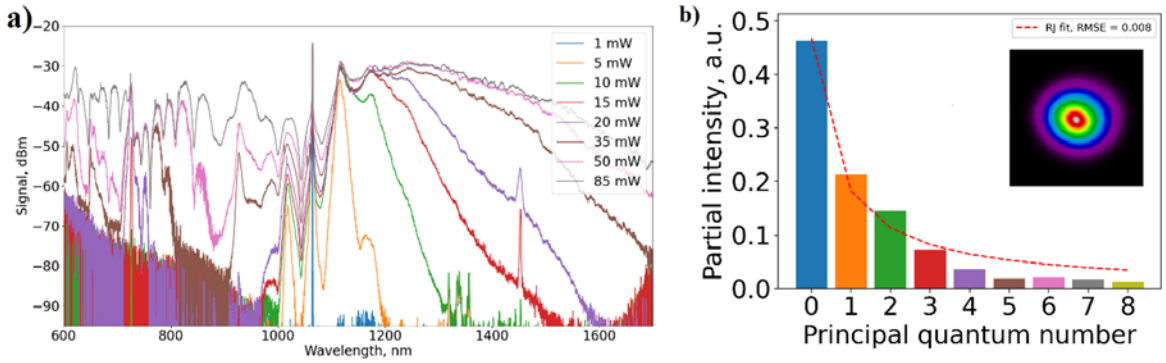


**Fig. 1.** a) – optical spectra of SC for different input power,
b) – modal content of the beam filtered with long-pass filter (1150 nm) with Rayleigh-Jeans fit (red line).

To analyze the modal content, we performed mode decomposition [4] after spectral filtering (bandpass at 1064 nm; longpass at 1100 and 1150 nm (Fig. 1b)). The fundamental mode ($LG_{00}$) carries ~68% of the energy at low input power at the pump wavelength. With increasing power, its fraction first decreases due to energy transfer to higherorder modes, then recovers as KBSC takes effect. The first and secondorder Stokes components exhibit high fundamentalmode content from their onset, indicating that stimulated Raman scattering predominantly starts in the fundamental mode. Importantly, the modal distribution obeys the RayleighJeans statistics [5], confirming that KBSC accompanies SC generation.

The work was supported by Russian Science Foundation (Grant No. 25-72-31018)

[1] J. M. Dudley, G. Genty, and S. Coen, Rev. Mod. Phys. 78, 1135-1184 (2006).
[2] L. G. Wright, S. Wabnitz, D. N. Christodoulides, and F. W. Wise, Phys. Rev. Lett. 115, 223902 (2015).
[3] G. Lopez-Galmiche, Z. Sanjabi Eznaveh, M. A. Eftekhar, et. al., Opt. Lett. 41, 2553-2556 (2016).
[4] Gervaziev, M. D., Zhdanov, I., Kharenko, D. S., et al. Las. Phys. Let. 18, 015101 (2021).
[5] F. Mangini, M. Gervaziev, M. Ferraro, et. al., Opt. Exp. 30, 10850-10865 (2022).

# Simplified design of vibration-induced sweeping Erbiumdoped fiber laser

**E. Kashirina, I. Lobach, S. Kablukov**

*Institute of Automation and Electrometry, Siberian Branch of the Russian Academy of Sciences, 1 Ac. Koptyug Ave., Novosibirsk 630090, Russia*

*kashirina@iae.nsk.su*

A new method for wavelength tuning in a single-frequency laser by modulating the optical length of the cavity – referred to as vibro-sweeping – was recently demonstrated [1,2]. This method relies on a dynamic population grating (DPG) that ensures stable single-frequency lasing. The spectrum of this DPG can shift under the influence of vibrations, leading to mode hops [1]. The approach was implemented in a figure-of-nine cavity comprising a ring section and a linear section, each containing an active fiber. In the ring section, the active fiber provides amplification, while in the linear section it serves as an adaptive DPG-based filter. In this paper, we propose a simplified tunable laser design that requires only a single fiber segment in the ring section of the cavity (Fig. 1a). We found that stable single-frequency lasing is observed even without a separate absorbing fiber in the linear section. We hypothesize that this effect is related to the length of the erbium-doped fiber in the ring section, which acts simultaneously as both the amplifying and absorbing medium. In this study, we investigated the effect of pump wavelength on the pumping efficiency of the active fiber.

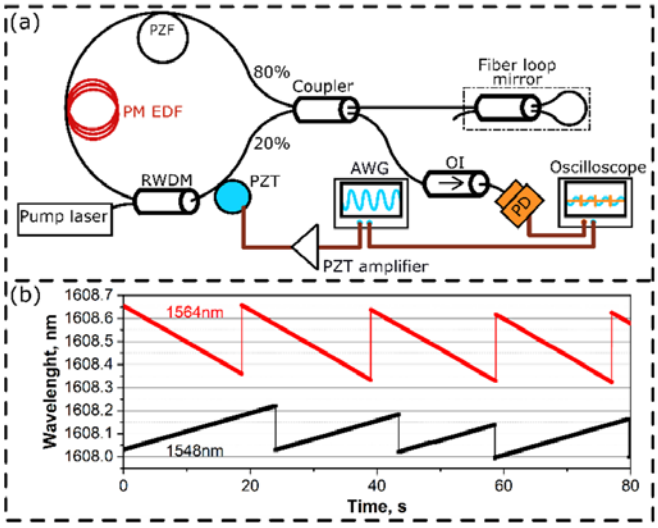


**Fig. 1.** (a) Scheme of the erbium-doped fiber laser with vibration-induced wavelength sweeping; (b) Laser wavelength dynamics over time at pump wavelengths of 1548 nm (black line) and 1564 nm (red line).

For wavelength tuning in this design, we employed optical path length modulation using a piezoelectric element (PZT). A positive sine wave at a frequency of 100 Hz, generated by an arbitrary waveform generator (AWG), was used as the control signal and applied to the PZT. Upon application of the modulation signal, wavelength sweeping commenced. The sweeping rate, direction, and tuning range depended on the pump power and wavelength. For example, at a pump wavelength of 1548 nm, direct sweeping (from shorter to longer lasing wavelengths) was observed (Fig. 1b, black curve), with a tuning range of approximately 0.2 nm and a sweeping rate of 7.8 pm/s. At a pump wavelength of 1564 nm, reverse sweeping was observed (Fig. 1b, red curve), with a tuning range exceeding 0.3 nm and a sweeping rate of 15.6 pm/s. Further details on the power characteristics, intensity dynamics, and measured reflectance spectra of the DPG in the ring section of the cavity at different pump wavelengths will be presented in the report.

The study was supported by the grant of the Russian Science Foundation No. 25-12-00186, https://rscf.ru/project/25-12-00186/. In the presented work, the equipment of the Multiple-access center «High-resolution spectroscopy of gases and condensed matters» in IA&E SB RAS, was used.

[1] E. Kashirina, I. Lobach, S. Kablukov, Vibration-induced sweeping operation in fiber lasers, Photonics, Vol. 11. No. 8, p.731. MDPI, (2024).
[2] E. Kashirina, I. Lobach, S. Kablukov, Active wavelength control in a single-frequency fiber laser via modulation of dynamic population grating, Optics & Laser Technology, 199, p. 115058. (2026).

# Picosecond high-frequency laser based on a regenerative amplifier for optical-laser systems

**Akentev, V. Nenadovich, A. Sokolov, Yu. Roy, K. Tokarev**

*Joint-stock Company "receach-and-Production Corporation "Precision Systems and instruments", Moscow, Aviamotornaja, 53*

*alsokolov@bk.ru*

This paper presents the results of a study on a developed picosecond high-frequency laser for optical-laser systems. Precision range measurements for geodetic and navigation spacecraft equipped with laser retroreflector systems, are performed for the purposes of determining the orbits of geodetic spacecraft, the geocentric coordinates of ground points, and their current changes; determining the parameters of the Earth's rotation; establishing and maintaining global geocentric coordinate systems and so on [1].

It is demonstrated that a regenerative amplifier provides amplification of picosecond pulses with an energy 1 pJ from a master oscillator to 2.5 mJ at a pulse repetition rate of up to 1000 Hz.

The laser uses a picosecond DFB laser diode controlled by current pulses and featuring low jitter (~200 ps). The pulse repetition rate is determined by the electrical pulse repetition rate and can be adjusted from single pulses to 250 MHz. The lasing wavelength, $\lambda$ = 1064 nm, is precisely tuned to the center of the Nd:YAG gain line by varying the diode's temperature. In gain modulation mode, the laser diode generates transform-limited pulses with a stable, symmetrical, bell-shaped shape. The lasing spectrum width is $\lambda \sim 0.1 - 0.2$ nm. To achieve a second harmonic pulse energy of >2.5 mJ, a pulse energy of ~5 mJ at a wavelength of 1064 nm is required. The required gain is achieved in a regenerative amplifier (RA), which is a resonator into which the master oscillator's radiation is injected.

After the pulse is emitted from the master oscillator, the resonator is "closed" using an optical switch. The master oscillator's radiation is amplified many times in the RA resonator. When the pulse energy reaches its maximum value, the resonator "opens" and the amplified pulse is emitted. This approach allows for a high integral gain of $G > 10^9$ with a relatively low unsaturated gain of $G_0 \sim 3$.

According to the study, the laser is capable of operating in a temperature range from -20°C to +40° C. The laser will be used in optical-laser systems for measuring the range of spacecraft, particularly at the International Space Center in Maidanak (Republic of Uzbekistan).

[1] B. A. Borisov, S. I. Donchenko, Yu. A. Roy and others. Development of "Tochka" Radio-Laser of Space Geodesy and Navigation Issues // Photonics Russia. V. 16. № 5. P.370 – 391. 2022.

# Optical Frequency Comb Generation in Fiber Lasers with an Integrated High-Q Resonator

**Y. Gladush[1], A. Netrusova[1], M. Mishevskiy[1], A.A. Mkrtchyan[1], A. Hegai[2], S. Firstov[2], M.A. Melkumov[2], N. Dmitriev[3], D.A. Chermoshentsev[3], I.A. Bilenko[3], A.G. Nasibulin[1]**

*1- Skolkovo Institute of Science and Technology, Bolshoy Boulevard 30, Moscow, Russian Federation*
*2- Prokhorov General Physics Institute of the Russian Academy of Sciences, Scientific Center of Fiber Optics, Vavilova 38, Moscow, Russian Federation*
*3- Russian Quantum Center, Bolshoy Boulevard 30, Moscow, Russian Federation*

*y.gladush@skoltech.ru*

An optical frequency combs - is a spectrum consisting of narrow, equally spaced lines - are widely used in optical clocks, coherent communications, optical coherence tomography, dual-comb spectroscopy, and related applications. Conventional comb sources are mode-locked lasers, where the line spacing is determined by the cavity length and are typically in range from few to tens of megahertz. In contrast, high-Q integrated ring microresonators pumped by a continuous-wave laser can provide comb spacings from about 50 GHz to 1 THz, but they often suffer from low conversion efficiency, the need for expensive tunable lasers, and limited stability.

One of the promising ways to overcome these limitations is to integrate the microresonator directly into a fiber-laser cavity [1]. In this work a fiber laser with an integrated optical ring microresonator acting as a nonlinear output mirror is investigated. The proposed configuration uses a two-port integrated microresonator as a reflective element in the laser cavity: a metallic (gold) mirror is placed on one side, while the integrated ring microresonator coupled to the fiber through a bus waveguide is located on the other side. Under active-fiber pumping, the micro-ring modes form a frequency comb; owing to Rayleigh scattering, part of this energy is transferred to a counter-propagating comb and returned to the fiber cavity, thereby providing optical feedback. Experimentally, the scheme provides stable self-starting soliton comb generation with a total spectral span exceeding 500 nm, which is significantly broader than the gain bandwidth of standard erbium-doped fiber. In the time domain, the coherent comb corresponds to a train of femtosecond pulses with a 1 ps spacing, as confirmed by autocorrelation measurements.

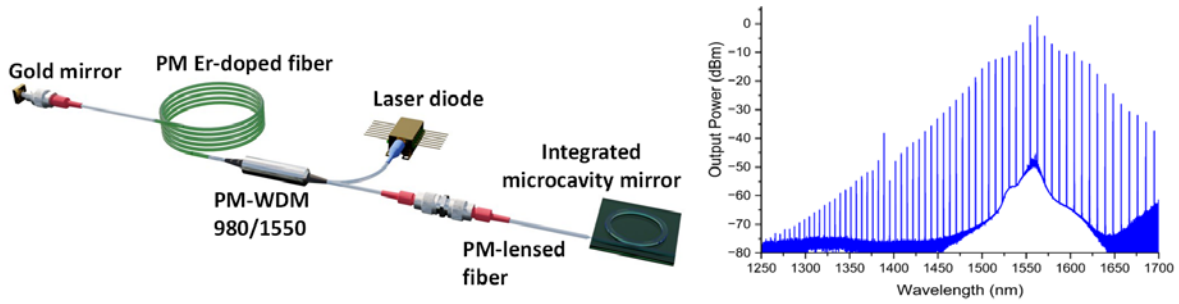


**Fig. 1.** Scheme of the fiber laser with integrated microresonator (left) and spectrum of optical frequency comb (righ)

The applicability of the approach to different active fibers and microresonators is also demonstrated. In particular, the scheme is shown to operate with bismuth-doped active fiber, which offers a broad gain bandwidth in the near-infrared range. Operation with normal dispersion integrated microresonator and toroidal multimode microresonator is also discussed.

The proposed approach combines the advantages of nonlinear microresonator comb generation with the stability of fiber-laser systems, making it promising for practical optical frequency comb sources in metrology, spectroscopy, and telecommunications.

This work was supported by the Russian Science Foundation (No. 25-22-00388).

[1] H. Bao, A. Cooper, M. Rowley, et al. Laser cavity-soliton microcombs, Nature Photonics, 13(6), pp. 384-389, (2019).

# 5-μm terbium fiber laser with Bragg grating

**V.V. Koltashev[1], M.V. Sukhanov[2], V.V. Likhov[1], B.I. Denker[3], B.I. Galagan[3], S.E. Sverchkov[3], E.N. Lashmanov[2], A.P. Velmuzhov[2], V.G. Plotnichenko[1], A.G. Okhrimchuk[1]**

*1- Prokhorov General Physics Institute of the RAS, Dianov Fiber Optics Research Center, Moscow, Russia;*
*2- Devyatykh Institute of Chemistry of HighPurity Substances of the RAS, Nizhny Novgorod, Russia;*
*3- Prokhorov General Physics Institute of the RAS, Moscow, Russia;*

*kvv@fo.gpi.ru*

Modern technology for producing chalcogenide glasses activated by rare-earth ions has enabled the development of a new class of bulk and fiber lasers operating in the mid-infrared range. Laser oscillations has been demonstrated using transitions between the first excited and ground levels of $Ce^{3+}$, $Pr^{3+}$, $Nd^{3+}$, and $Tb^{3+}$ ions in the spectral range from 4.5 μm to 6.2 μm.

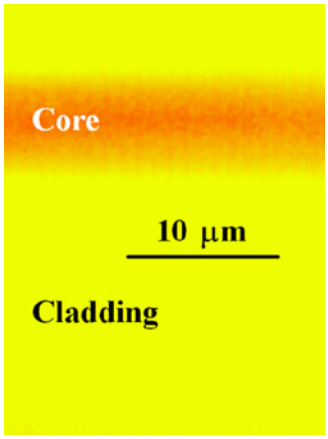


**Fig. 1.** Photo of the grating in chalcogenide fiber core.

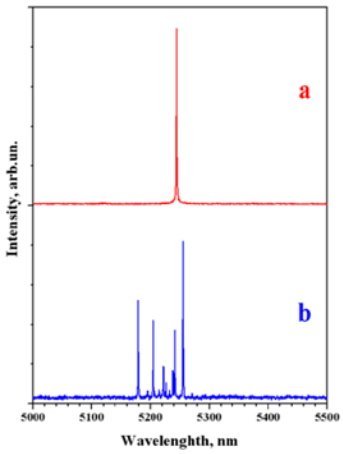


**Fig. 2.** Output lasing spectrum with (a) and without (b) Bragg grating.

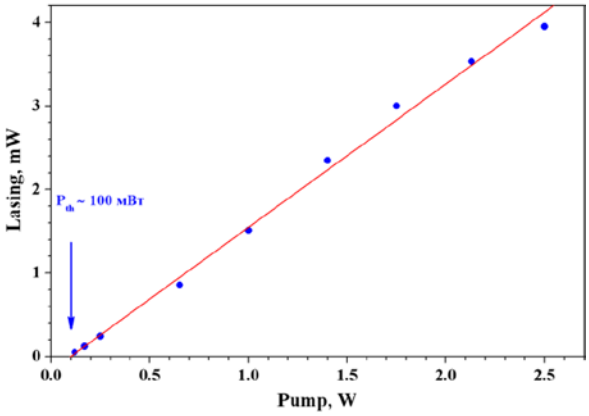


**Fig. 3.** Output power of chalcogenide fiber laser.

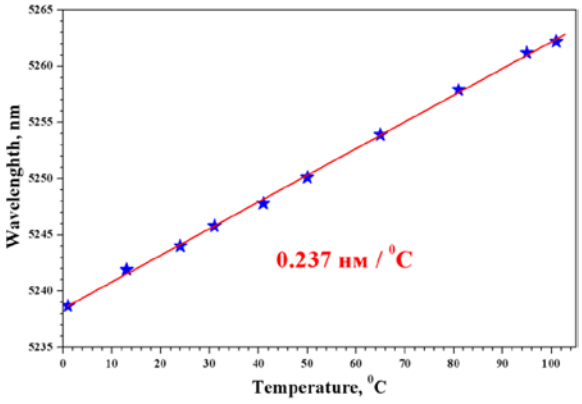


**Fig. 4.** The lasing wavelength vs the temperature.

An original method of Bragg grating inscription in chalcogenide fibers by 1030 nm femtosecond laser beam was proposed and demonstrated. The grating was embedded in the core of a few-mode $Tb^{3+}$-doped chalcogenide fiber, Fig. 1. The chalcogenide fiber laser output characteristics (output lasing spectrum and output power) are shown in Figs. 2 and 3. The registered spectral width of the laser emission (w = 0.13 $cm^{-1}$) was limited by the resolution of the spectrometer. The temperature derivative of the emission wavelength is about 20 times greater than that in silica fibers, Fig. 4 [1].

The investigation was supported by Russian Science Foundation grant 25-22-00552.

[1] V.V. Koltashev, M.V. Sukhanov, V.V. Likhov, B.I. Denker, B.I. Galagan, S.E. Sverchkov, E.N. Lashmanov, A.P. Velmuzhov, V.G. Plotnichenko, A.G. Okhrimchuk, 5-μm terbium fiber laser with Bragg grating, Infrared Physics and Technology, vol. 155, 106455 (2026).

# The peculiarities of heavily erbium-doped fiber lasers for extended L-band operation

**M.P. Bazakutsa[1,2], A.M. Smirnov[1,2,3], A.V. Dorofeenko[1,2,4,5], O.V. Butov[1]**

*1- Kotelnikov Institute of Radioengineering and Electronics of RAS, Mokhovaya 11-7, Moscow 125009, Russia*
*2- Moscow Institute of Physics and Technology, 19 Institutskiy pereulok, Dolgoprudny 141700, Russia*
*3- Faculty of Physics of Lomonosov Moscow State University, Leninskie Gory 1-2, Moscow 119991, Russia*
*4- Institute for Theoretical and Applied Electromagnetics RAS, 13 Izhorskaya, Moscow 125412, Russia*
*5- Dukhov Research Institute of Automatics, 22 Suschevskaya, Moscow 127055, Russia*

*alsmir1988@mail.ru*

Heavily erbium-doped fiber lasers with short cavities are of considerable interest for compact narrow-linewidth laser systems operating in the telecommunications spectral range. However, the increase in erbium concentration leads to ion clustering and strong up-conversion processes, which significantly affect the lasing dynamics and result in passive Q-switched generation regimes. Earlier, thermal switching between pulsed and continuous-wave (CW) generation regimes in heavily erbium-doped fiber lasers was demonstrated and attributed to the temperature dependence of the up-conversion process probability due to phonon-assisted energy matching [1]. Further studies revealed universal power-law dependences of pulse frequency, duration and peak intensity near the lasing thresholds with critical indices weakly dependent on cavity parameters [2,3].

In this work, we investigate lasing features of heavily erbium-doped fiber lasers operating in the L-band spectral region near 1600–1620 nm. Fabry-Perot cavities were fabricated in the active fiber using point-by-point femtosecond fiber Bragg grating inscription technology. It was experimentally demonstrated that stable CW operation at room temperature can be achieved in the 1600–1610 nm spectral region despite the decreasing energy mismatch in the up-conversion process for erbium ion pairs at the lasing wavelength. In this spectral range, both gain and absorption of erbium ions decrease significantly, which substantially modifies the balance between amplification and nonlinear ion-pair interaction processes. A fundamentally new lasing regime was observed at liquid nitrogen temperature (77 K). In contrast to previously studied erbium-doped fiber lasers operating in the 1530–1580 nm spectral range, this regime exhibited giant pulses with substantially modified temporal characteristics. The pulse repetition frequency decreased by more than two orders of magnitude, accompanied by a reduction of the pulse duration by approximately one order of magnitude, while the pulse peak intensity increased by nearly four orders of magnitude.

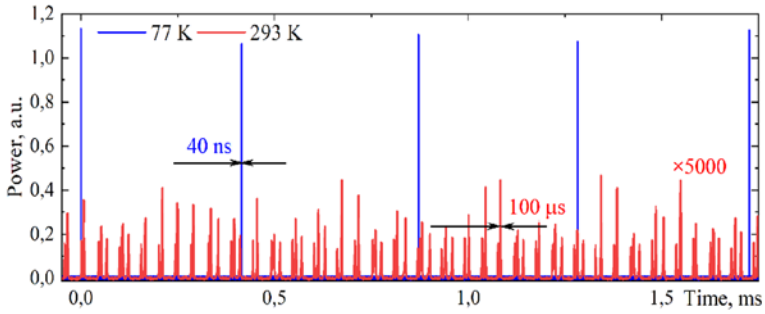


**Fig. 1.** Time dependence of lasing intensity at different operation temperatures.

Additionally, the critical indices describing the power-law behavior of pulse parameters were found to differ significantly from those previously reported for erbium pulsed lasers operating in the 1530–1580 nm spectral range [2], whereas for the newly observed giant-pulse regime near 1620 nm at 77 K the indices changed to $\beta \approx 0.85$, $\delta \approx -0.13$ and $\chi \approx 0.30$. The obtained results indicate a substantial modification of the nonlinear dynamics and suggest the emergence of another type of critical behavior in heavily erbium-doped fiber lasers operating in the extended L-band. The observed effects demonstrate that the extended L-band region near 1620 nm represents a distinct regime of erbium laser operation, where the interplay between reduced gain, weakened phonon-assisted up-conversion and cavity temperature lead to qualitatively new lasing dynamics.

[1] Smirnov A. M., Bazakutsa A. P., Chamorovskiy Y. K., Nechepurenko I. A., Dorofeenko A. V., Butov O. V. Thermal Switching of Lasing Regimes in Heavily Doped $Er^{3+}$ Fiber Lasers, ACS Photonics 5, 12, 5038–5046 (2018).
[2] A.M. Smirnov, A.A. Rybaltovsky, I.A. Nechepurenko, A.V. Dorofeenko, O.V. Butov, Critical behavior of erbium fiber lasers in pulsed and relaxation oscillations regimes, Optics and Laser Technology, Volume 181, Part B, 111823 (2025)
[3] Smirnov A. M., Butov O. V. Pump and Thermal Impact on Heavily Erbium-Doped Fiber Laser Generation, Optics Letters 46, 1, 86–89.

# Pump mechanisms of 5÷6 μm $Nd^{3+}$: fiber lasers

**S.E. Sverchkov[1], M.V. Sukhanov[2], R.D. Blagin[2], B.I. Denker[1] B.I. Galagan[1], V.V. Koltashev[3], T.V. Kotereva[2], E.N. Lashmanov[2], A.S. Lobanov[2], V.G. Plotnichenko[3], A.P. Velmuzhov[2]**

*1- Prokhorov General Physics Institute of the Russian Academy of Sciences, Moscow, Russia*
*2- Devyatykh Institute of Chemistry of High-Purity Substances of the Russian Academy of Sciences, Nizhny Novgorod, Russia*
*3- Prokhorov General Physics Institute of the Russian Academy of Sciences, Dianov Fiber Optics Research Center, Moscow, Russia*

*glasser@Lst.gpi.ru*

Rare earth doped selenide glasses have become a new class of solid-state materials for bulk and fiber lasers operating at λ>4μm unattainable for oxide and fluoride hosts. Laser action is already demonstrated in Tb, Ce and Pr-doped fibers. $Nd^{3+}$ in selenide glasses is also an interesting active ion which is notable for the long lasing wavelengths approaching 6 μm. Unfortunately, $Nd^{3+}$ absorption bands that are observable in selenide glasses (1.7 μm, 2.4 μm and 5 μm) are not too convenient for direct optical pumping for the lack of common lasers with such wavelengths. This communication describes our attempts to overcome this difficulty. The experiments were held with newly developed Ge–Sb–Se glasses and fibers whose relatively low-labor fabrication technique was described in [1]. The feature of these glasses is the limited rare earth doping capacity (<$3\times10^{18}$ $cm^{-3}$) excluding the usage of radiationless interactions between the active ions.

One of our approaches was the use of 1.7 μm CW bismuth fiber laser for direct excitation of $^4I_{15/2}$ $Nd^{3+}$ level with further cascade of **radiative** transitions to the upper laser level $^4I_{11/2}$. Another approach was the **intracavity pumping** of $Nd^{3+}$ ions by $Tb^{3+}$ ions in a fiber co-doped with both of them. The advantage of $Tb^{3+}$ is the presence of absorption bands (at ~2 μm and ~3 μm) convenient for optical pumping by $Tm^{3+}$ or $Er^{3+}$ lasers. $Tb^{3+}$ in selenide glasses is able to lase at 4.8÷5.55 μm while its spontaneous emission ranges from 4.3 μm to 5.7 μm (Fig. 1). The $Nd^{3+}$ absorption band corresponding to the $^4I_{9/2}\rightarrow{}^4I_{11/2}$ transition occupies the spectral interval from 4.5 μm to 6.1 μm. It can be seen, that $Tb^{3+}$ spontaneous and stimulated emission bands well overlap with $Nd^{3+}$ absorption band. This is the feature we were going to use.

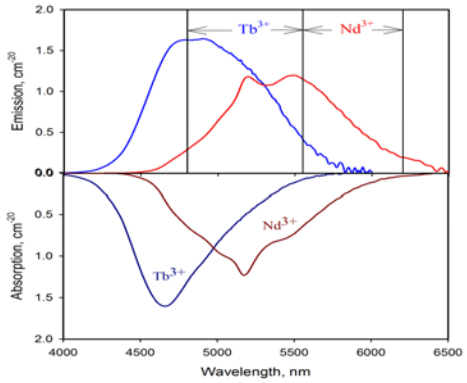


**Fig. 1.** $Tb^{3+}$ and $Nd^{3+}$ absorption and emission cross-sections in selenide glass. The spectral intervals where these ions generate laser radiation are also indicated.

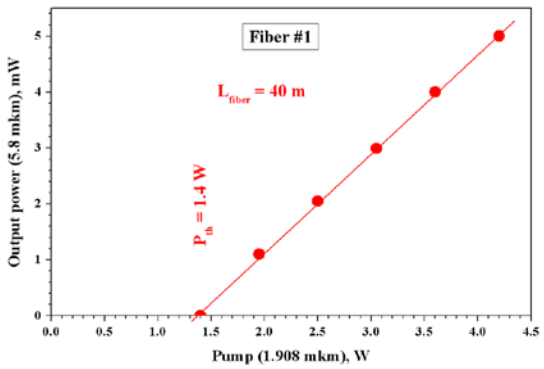


**Fig. 2.** $Nd^{3+}$ 5.8 μm laser input/output characteristic. Pumping into $Tb^{3+}$ absorption band by $Tm^{3+}$ fiber laser. $Tb^{3+}$ ions are **not** lasing in this case.

Both approaches gave positive results and enabled to demonstrate CW $Nd^{3+}$ lasing at λ=5.7÷5.9 μm in chalcogenide glass fibers. An interesting unexpected effect was the possibility to pump a neodymium laser by **spontaneous** emission of terbium ions trapped in the co-doped fiber (Fig. 2).

The investigations were supported by Russian Science Foundation (grant 25-13-00245).

[1] M. Sukhanov, E. Lashmanov, T. Kotereva, A. Velmuzhov, V. Shiryaev, Continuous 5.22–5.31 μm wavelength lasing in optical fiber based on $Tb^{3+}$-doped gallium-free selenide glass, Optical Materials, 167, 117314 (2025).

# Effect of standing wave visibility on the fiber laser generation regime

**N.R. Poddubrovskii, I.A. Lobach, S.I. Kablukov**

*Institute of Automation and Electrometry SB RAS, Academician Koptyug Avenue, 1, Novosibirsk, Novosibirsk region, Russia, 630090*

*pod_nikita@iae.nsk.su*

Fiber lasers have numerous advantages, including wide variety of possible generation regimes. The formation of a standing wave in the laser active medium can cause the formation of dynamic population gratings (DPGs) [1]. DPGs act as adaptive spectral filters: their formation in unpumped fibers (absorption DPGs) results in stable single-frequency generation [2], while their formation in pumped fibers (gain DPGs) may cause wavelength self-sweeping effect [3]. It is known that the DPGs positioning in the cavity and their type strongly influence the lasing. In current study we consider a new approach of the generation regime control - by actively changing the visibility of the standing wave forming the DPG.

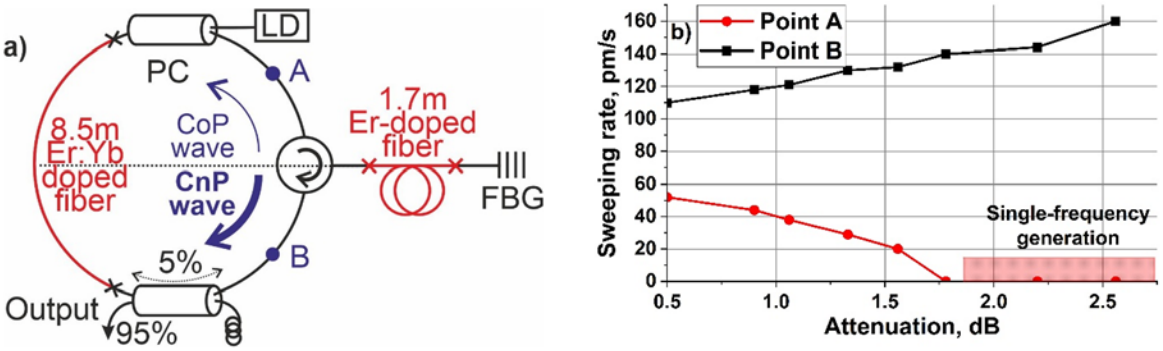


**Fig. 1.** a) Laser experimental setup, b) Sweeping rate dependence on attenuation.

An Er-doped sigma-cavity fiber laser was studied (Fig. 1(a)). An unpumped fiber was placed in the linear section of the cavity, enabling absorption DPG formation. The pumped fiber was located in the ring section. Two sections were connected via a circulator. The circulator selected the main direction of the generation propagation in the ring section of the cavity - counter-propagating with pump (CnP wave, see bold blue arrow in Fig. 1a)). However, the isolation of the circulator was ~37dB, meaning that a weak wave co-propagating with pump (CoP wave, see thin blue arrow in Fig. 1(a)) could exist in the ring section of the cavity. It was the CoP wave that enabled the gain DPG formation in the ring section of the laser. The competition between two DPGs in the laser resulted in the continuous-wave self-sweeping [3]. It was found that by introducing attenuation at point A, the contribution of the gain DPG could be reduced, resulting in wavelength stabilization (see the red line in Fig. 1(b)). In contrast, if additional attenuation was introduced at point B, the amplitudes of two waves became comparable, making it possible to increase the gain DPG formation efficiency and increase the sweeping rate (black line in Fig. 1(b)). Thus, introducing intracavity losses makes it possible to control the generation regime and the laser sweeping rate. More details about the laser operation, including numerical simulation results, will be given in the report. The results may prove useful for the development of stable single-frequency and tunable lasers based on DPGs with desired generation characteristics.

The study was supported by the grant of the Russian Science Foundation No. 25-12-00186, https://rscf.ru/project/25-12-00186/. In the presented work, the equipment of the Multiple-access center “High-resolution spectroscopy of gases and condensed matters” in IA&E SB RAS, was used.

[1] S. Stepanov, Dynamic population gratings in rare-earth-doped optical fibres, Journal of physics D: applied physics, 41, 224002 (2008)
[2] N.P. Poddubrovskii, R.V. Drobyshev, I.A. Lobach, S.I. Kablukov, Fiber lasers based on dynamic population gratings in rare-earth-doped optical fibers, Photonics, 9, 613 (2022)
[3] N.P. Poddubrovskii, I.A. Lobach, S.I. Kablukov, Regular mode-hopping dynamics in Erbium-doped ring fiber laser with saturable absorber, Optics&Laser Technology, 156, 108568 (2022)

# New applications of semiconductor optical amplifier

**S.K. Turitsyn**

*Aston Institute of Photonic Technologies, Aston University, UK*

*s.k.turitsyn@aston.ac.uk*

The semicondutor optical amplifier (SOA) is an important practical device developed for optical communication systems. It exhibits many attractive characteristics, including compactness, low power consumption, wide gain bandwidth and the possibility of direct gain modulation by controlling the injection current [1]. Beyond direct applications as an amplifier, SOA is used in all-optical signal processing, and applications such as radio over fiber and modulators [2]. SOA transformed the field of nonlinear optical techniques for data processing at high sed, and it can operate at 100 Gb/s and higher [3]. Semiconductor pulsed lasers are used in various applications, ranging from wave-division-multiplexing telecommunication systems to metrology. In laser applications, optical injection locking or feedback is used to stabilize the highly nonlinear dynamics of light in SOA methods. I will discuss our recent work [4] on the application of an optical power-seeded electronic feedback to stabilize a pulsed laser system with an SOA. The proposed concept is examined for a simple laser system based on SOA with the feedback implemented by an electrically modulating amplifier current that uses a fraction of the output optical power.

SOA is also an example of a physical system with interesting nonlinear properties, often considered by engineers as a drawback and undesirable feature of the device. However, rich nonlinear dynamic characteristics of SOA make it a promising component of neuromorphic photonic systems [5,6]. SOA can be utilsied as a nonlinear element allowing mapping of input optical signals to a high-dimensional space that is a critical concept in various computing paradigms. I will disucss deisgn of the reservoir computing based on upsampling and modulation, utilizing a SOA and photodetector as nonlinear elements without conventionally used delay loop and extreme learning machine computing approach using commercially available SOA and telecom technologies developed for high-speed optical data transmission.

[1] G. P. Agrawal and N. A. Olsson, Self-phase modulation and spectral broadening of optical pulses in semiconductor laser amplifiers IEEE J. Quantum Electron. 25, 2297-2306 (1989).
[2] R. J. Manning, A. D. Ellis, A. J. Poustie, and K. J. Blow, Semiconductor laser amplifiers for ultrafast all-optical signal processing, J. Opt. Soc. Am. B 14, 3204-3216 (1997)
[3] D. Cotter *et al.* Nonlinear Optics for High-Speed Digital Information Processing, Science, 286,1523-1528 (1999).
[4] D. Khudozhitkova, A. Bednyakova, S. Boscolo, S. K. Turitsyn, Laser systems with a SOA and optical-power-to-electrical-current feedback, Optics Letters, 50(24), 7552-7555 (2025)
[5] E. Manuylovich, A. E. Bednyakova, D. A. Ivoilov, I. S. Terekhov, and S. K. Turitsyn SOA-based reservoir computing using upsampling, Opt. Lett. 49, 5827-5830 (2024)
[6] E. Manuylovich, D. Stoliarov, D. Saad, and S.K. Turitsyn, Optical neuromorphic computing via temporal up-sampling and trainable encoding on a telecom device platform, Nanophotonics, 14(16) 2761 (2025)

# Mid-infrared photoluminescence in a core-clad chalcogenide fiber doped with terbium ions

**E.A. Romanova[1], M.V. Sukhanov[2], V.V. Koltashev[3]**

*1- Saratov State University, Astrakhanskaya 83, 410012 Saratov, Russia*
*2- Devyatykh Institute of Chemistry of High-Purity Substances of Russian Academy of Sciences, Nizhny Novgorod, Russia*
*3- Prokhorov General Physics Institute of the Russian Academy of Sciences, Dianov Fiber Optics Research Center, Moscow, Russia*

*romanovaelena@sgu.ru*

Fiber-optic spectroscopic sensors for real-time IR spectroscopy are in demand in various fields of industry, agriculture, ecology, and healthcare [1]. The lack of compact and inexpensive broadband radiation sources in mid-IR is slowing the implementation of such sensors. In addition to supercontinuum generation and tunable lasing, excitation of mid-IR emission in rare-earth doped chalcogenide fibers is considered as an option for creating the broadband radiation sources [2]. Photoluminescence in rear-earth doped chalcogenide fibers has already been studied in theory [3], but without taking into account the specifics of light propagation in an optical fiber.

In this work, a theoretical study of the luminescent radiation excitation in a core-clad chalcogenide fiber with a core made of Ge-Ga-Sb-Se glass doped with terbium ($Tb^{3+}$) ions and an undoped cladding made of Ge-As-Sb-S glass was carried out, and the obtained results were assessed by comparison with experimental data. In the experiment, 100 mW pump radiation at a wavelength of 1.98 μm from a single mode silica fiber excited guided modes at the input facet of the few-mode chalcogenide fiber doped with $10^{19}$ $cm^{-3}$ of $Tb^{3+}$ions. Luminesence spectra in the 46 μm spectral range were recorded at various distances from the input facet, from several meters to several centimeters.

In the developed theoretical model, propagation of luminescent radiation was considered separately in the core and in the cladding of the chalcogenide fiber. Calculations have shown that at the pump wavelength, predominantly the fundamental mode with a large confinement factor is excited. Part of the mode's power is then transferred to luminescent radiation propagating in the fiber core. However, due to the incoherence of spontaneous emission, some part of the luminescent radiation penetrates through the core-cladding boundary into the fiber cladding and propagates there with a low confinement factor.

The change in the luminescence spectra along the fiber was investigated using a numerical model including steady-state kinetic equations for the population of a three level system of $Tb^{3+}$ ions and differential equations for the pump and emission powers [4].

The results of calculations showed a growth and subsequent decay of the emission power in the fiber core over some distance that depended on the pump power. The luminescent radiation in the cladding peaked and then decayed over much longer distance of several meters along the fiber, as it was absorbed by the undoped glass matrix in the cladding rather than by the rear-earth ions in the core. A comparison with the measured luminescence spectra showed good quantitative agreement.

Thus, cladding modes can transmit luminescent radiation over long distances. This opens the way to combining the functions of a broadband radiation source and a sensing element in a single fiber. Practical implementations of such components for fiber-optic spectroscopic sensors are discussed.

[1] C. Boussard-Pl´edel, Chalcogenide waveguides for infrared sensing. In: Chalcogenide Glasses. Preparation, Properties and Applications. 1st ed., J.- L. Adam, X. Zhang (Eds.), Woodhead Publishing, pp. 381–410 (2014).
[2] V. Nazabal, J-L. Adam, Infrared luminescence of chalcogenide glasses doped with rare earth ions and their potential applications, Opt. Mater.: X, 15 (2022) 100168.
[3] S. Sujecki, L. Sojka, E. Pawlik, K. Anders, R. Piramidowicz, Z. Tang, D. Furniss, E. Barney, T. Benson, A. Seddon, Numerical analysis of spontaneous mid-infrared light emission from terbium ion doped multimode chalcogenide fibers, J. of Luminescence 199 (2018) 112–115.
[4] E.A. Romanova, N.D. Parshina, V.S. Shiryaev, The influence of the mode intensity profile on the population kinetics of terbium ion levels and the excitation of luminescence in a few-mode chalcogenide fiber, Bull. of the Lebedev Phys. Inst., 50 (2023) S1225-S1239.

# Vibration-induced frequency sweeping in a Yb-doped fiber laser

**Yu. Tkachenko, I.A. Lobach, S.I. Kablukov**

*Institute of Automation and Electrometry, Siberian Branch of the Russian Acade*
*Ac. Koptyug ave. 1, Novosibirsk, 630090 Russia*

*tkachenko@iae.nsk.su*

18:30-18:45 *Tkachenko Alina*
*Institute of Automation and Electrometry, Siberian Branch of the Russian Academy of Sciences*
Vibration-induced frequency sweeping in a Yb-doped fiber laser

Self-sweeping fiber lasers (SSFLs) are attractive for practical applications as simpl sers, the wavelength tuning occurs over time due to internal processes involving the for gratings [1]. Several applications have already been demonstrated using SSFLs as straig However, signal processing in practical applications remains challenging because the pulse positions are not equidistant in time. Recently, vibration-induced frequency tuning was reported for an erbium-doped fiber laser [3], enabling the locking of mode-hopping events to a specific phase of external vibrations. In this work, we extend this approach to an ytterbium-doped fiber laser. The key difference between Er- and Yb-doped fiber laser lies in the shorter upper-level lifetime (and consequently, the shorter dynamic grating lifetime) in the Yb-doped system.

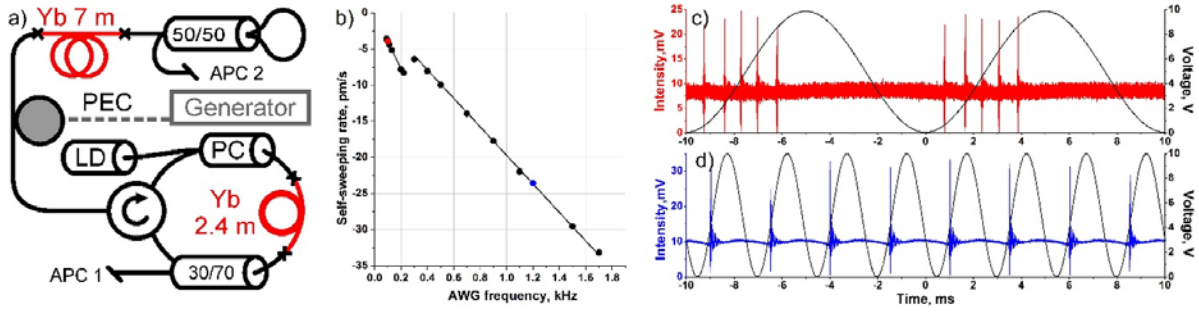


**Fig. 1.** (a) Schematic of a sigma-cavity Yb-doped fiber laser with vibration-induced sweeping; (b) Sweeping rate as a function of external modulation frequency at a fixed modulation amplitude of 10 V; (c) Intensity dynamics at a modulation frequency of 100 Hz and amplitude of 10 V; (d) Intensity dynamics at 1200 Hz and 10 V.

In the demonstrated sigma-cavity fiber laser (Fig. 1a), cavity length oscillations were induced using a piezoelectric ceramic (PEC) with 2 m of PM fiber placed in the linear arm. Both the oscillation amplitude and frequency were controlled using an arbitrary waveform generator (AWG) with a positive sine wave function. It should be noted that in the absence of length modulation, the laser operates in a single longitudinal mode without self-sweeping. Varying the modulation frequency from 80 Hz to 1.7 kHz at a fixed amplitude of 10 V vibration-induced sweeping from longer to shorter wavelengths. The sweeping rate increased nearly linearly with the external modulation frequency (Fig. 1b): a slope of 3.9 pm/(s·kHz) in the 80–220 Hz range, and a slope of 1.9 pm/(s·kHz) in the 300–1700 Hz range. A sudden drop in the sweeping rate is observed at 300 Hz. Furthermore, different operating regimes were identified in the intensity dynamics, characterized by a varying number of bursts (each burst corresponds to a mode hop by one free spectral range of the cavity). In the burst-group regime, between 2 and 6 bursts were observed. Figures 1c and 1d show the intensity dynamics at 100 Hz (red line) and 1200 Hz (blue line), with the corresponding sweeping rates marked by red and blue dots in Fig. 1b. Further details will be presented in the report.

The study was supported by the grant of the Russian Science Foundation No. 25-12-00186, https:// rscf.ru/project/25-12-00186/. In the presented work, the equipment of the Multiple-access center “High- resolution spectroscopy of gases and condensed matters” in IA&E SB RAS, was used.

[1] N. Poddubrovskii, R. Drobyshev, I. Lobach, S. Kablukov, Fiber lasers based on dynamic population gratings in rare-earth-doped optical fibers, Photonics, vol.9, No.9, p. 613, (2022).
[2] A.Yu. Tkachenko, I.A. Lobach, S.I. Kablukov, Coherent optical frequency reflectometry based on a fiber self-scanning laser: current status and development prospects (Review), Instruments and Experimental Techniques, vol.66, , pp. 730-736, (2023).
[3] E.K. Kashirina, I.A. Lobach, S.I. Kablukov, Active wavelength control in a single-frequency fiber laser via modulation of dynamic population grating, Optics and Laser Technology, vol. 199, p. 115058, (2026).

# Polarization analysis of quantum-optical systems for satellite laser ranging

**A. Akentev, A. Sokolov, Yu. Roy, K. Tokarev**

*Joint-stock Company "Receach and Production Corporation "Precision Systems and instruments", Moscow, Aviamotornaya, 53*

*akentev_as@npk-spp.ru*

Currently, laser satellite ranging is used to solve tasks of satellite geodesy and frequency-time support for global navigation satellite systems [1]. Transmission of laser beam between a ground-based optical-laser station and a spacecraft is associated with difficulties such as: atmospheric turbulence and changes in its refractive index, the need to maintain a target at high angular velocity, significant losses in the receiving optical system, disruption of the polarization structure of laser radiation, etc. These problems are primarily random in nature. However, there are also systematic errors such changes of the polarization state of the laser radiation output from the transmitting optical-laser system. Polarization losses also depend on the direction of the laser beam in space. The theoretical phenomenon of this process is presented in [2]. So experimental studies of the polarization characteristics of laser beam guidance systems are relevant. The aim of this work is to experimentally investigate the advantage of circularly polarized light over linearly polarized light.

As a result of the conducted experiments, it was determined that the laser beam guidance system to an arbitrary point on the celestial hemisphere does not maintain the spatial orientation of the laser radiation polarization plane and leads to elliptical polarization of the laser terminal radiation. In the case of a linear state of beam polarization at the input, the polarization azimuth of the output beam when moving along the "parallel" of the celestial sphere changes linearly with a period of 180°. Polarization losses also depend significantly on the beam direction. In the case of a right-hand circular polarization of the beam at the input of the guidance system, a left-hand elliptical polarization state is observed at the output, while the deviation of the ellipticity angle from 45° can reach 13°. The magnitude of polarization losses in the case of a circular polarization state does not depend on the orientation of the output beam, but is determined only by the phase and amplitude anisotropy of the mirrors of the guidance system [3]. The analysis showed that circularly polarized light reflected from corner-cube reflector forms a far-field diffraction pattern, which has an advantage over linear polarization.

The results of the conducted research are of practical significance and have been used in the development of quantum-optical systems for satellite ranging, research into methods for determining the spatial orientation of spacecraft with retroreflector systems, and the development of high-speed laser communication terminals.

[1] B. A. Borisov, S. I. Donchenko, Yu. A. Roy and others. Development of "Tochka" Radio-Laser of Space Geodesy and Navigation Issues // Photonics Russia. V. 16. № 5. P.370 – 391. 2022.
[2] A.S. Akentyev, A.L. Sokolov, M.A. Sadovnikov, G.V. Simonov. Polarization Analysis of the Beam-Steering Device of Quantum Optical Systems. «Optics and Spectroscopy». June 2017, Vol. 122, № 6, pp. 1044–1050.
[3] Sokolov A.L., Akentev A.S., Nenadovich V.D. Polarization analysis of quantum-optical systems for space laser communications using a modified BB84 protocol [in Russian] // Opticheskii Zhurnal. 2026. V. 93. № 1. P. 69–79. http://doi.org/10.17586/1023-5086-2026-93-01-69-79.

# Dual Assistance on Glioma Surgery: Tumor resection and histological support

**P. Ricci[1,2,+], E. Conti[2,3,+], I. Costantini[2], D. Di Meo[2], L. Perego[2], J. Ramazzotti[2], G. de Vito[1], E. Baria[1], Ch. Caredda[4], I. Ezhov[5], L. Giannoni[6], D. Nardini[1,2], A. Toaha[1,2], J. Lucchesi[1,2], B. Montcel[4], Daniel Rueckert[5,7,8], I. Tachtsidis[6], F.S. Pavone[1,2,3]**

*1- Department of Physics and Astronomy, University of Florence, Sesto Fiorentino, Italy;*
*2- European Laboratory for Non-Linear Spectroscopy, Sesto Fiorentino, Italy;*
*3- National Institute of Optics, National Research Council, Sesto Fiorentino, Italy;*
*4- Université Claude Bernard Lyon, Lyon, France;*
*5- Klinikum rechts der Isar, Technischen Universität München, Munich, Germany;*
*6- Department of Medical Physics and Biomedical Engineering, University College London, London, UK;*
*7- Imperial College London, Department of Computing, London, United Kingdom*
*8- Munich Center for Machine Learning (MCML), München, Germany*
*+ Co-first authors contributed equally*

*pietro.ricci@unifi.it*

Accurate characterization of gliomas requires imaging strategies able to bridge intraoperative decision-making, pathological evaluation, and a deeper understanding of tumor architecture. In this talk, we will present our recent advances in optical imaging approaches designed to address these complementary needs.

First, we will discuss hyperspectral imaging as a label-free platform for neurosurgery and anatomopathology. By extracting spatially resolved spectral signatures from brain tissue, this approach enables tumor border delineation, tissue classification, and assessment of metabolic and vascular heterogeneity. Particular emphasis will be placed on glioma-related biomarkers derived from intrinsic optical contrast, including NADH/FAD-based metabolic readouts, oxygenation-sensitive signals, and hemodynamic imaging. I will also show in vivo measurements in mouse models, demonstrating the potential of hyperspectral imaging to monitor dynamic brain oxygenation and activity-related vascular changes.

Second, we will present light-sheet fluorescence microscopy of optically cleared tumor samples as a complementary three-dimensional strategy to reconstruct the glioma microenvironment. These volumetric datasets reveal the spatial organization of cellular, vascular, structural, and molecular features, including markers linked to proliferation, tissue architecture, and therapy resistance. Such multiscale reconstructions provide a richer representation of tumor heterogeneity and may support more informed diagnostic interpretation and personalized therapeutic planning.

Together, these results outline an integrated optical imaging framework that connects real-time functional assessment with high-resolution 3D pathology, opening new perspectives for precision neurosurgery and patient-tailored glioma management.

# Potential of Light in Neurosurgery – Fluorescence - PDT - DLT

**R. Sroka[1,2], M. Aumiller[1,2], A. Rühm[1,2]**

*1- Laser-Forschungslabor, LIFE-Zentrum, Hospital of LMU Munich, Fraunhoferstr 20, 82152 Planegg, Germany*
*2- Department of Urology, Hospital of LMU Munich, Marchioninistr 15, 81377 Munich, Germany*

*Ronald.sroka@med.uni-muenchen.de*

Neurosurgery suffered from discrimination of tumor to normal tissue during surgical tissue resection, but also for selective treatment of GBM. The application of photoactive drugs and their use for fluorescence guided resection, optical guided biopsy and photodynamic therapy in neurosurgery could support such requests [1,2,3]. Latest research includes directly 1O2-excitation by NIR-illumination offering new treatment strategies. Besides the medical needs and boundary conditions, the physics and technical research and developments will be presented. Different clinical aspects of photodynamic therapy (PDT), like treatment planning [4,5], treatment and dosimetry protocols [5,6], spectral on-line-monitoring (SOM) [7] as well as follow-up evaluation of clinical outcome [8,9], are of interest regarding further iPDT developments. Preliminary study results as well as the potential of optical dosimetry concepts based on light-tissue interaction and light-photosensitizer interaction are included summarizing the latest developments in this field.

**Keywords:** brain tumor, glioma, 5-ALA, interstitial photodynamic therapy, PDT, online monitoring, direct light therapy (DLT).

[1] Schwartz, C. et al. (2015) Interstitial Photodynamic Therapy for De-Novo Glioblastoma Multiforme WHO IV: A Feasibility Study, In: Proceedings of the 66th Annual Meeting of the German Society of Neurosurgery (DGNC) (Karlsruhe, Germany, 7-10 June 2015), DOI:10.3205/15dgnc304
[2] Quach, S. et al. Interstitial photodynamic therapy for untreated glioblastoma. 2023 submitted to
[3] Lietke, S. et al. (2021) Interstitial Photodynamic Therapy Using 5-ALA for Malignant Glioma Recurrences, Cancers 13:1767, DOI:10.3390/cancers13081767
[4] Beck, T.J. et al. (2007) Interstitial photodynamic therapy of nonresectable malignant glioma recurrences using 5-aminolevulinic acid induced protoporphyrin IX, Lasers Surg Med 39:386-393, DOI:10.1002/lsm.20507
[5] Aumiller, M. et al. (2021) Investigation of Changes of Optical Tissue Properties up to 50°C, OSA Technical Digest (Optica Publishing Group, 2021), JW1A.6, DOI:10.1364/BODA.2021.JW1A.6
[6] Yassine, A.-A., et al. (2019) Optimizing interstitial photodynamic therapy with custom cylindrical diffuser, J Biophotonics 12(1):e201800153, DOI:10.1002/jbio.201800153
[7] Rühm, A., et al. (2014) 5-ALA based photodynamic management of glioblastoma, Proc SPIE 8928:89280E, DOI:10.1117/12.2040268
[8] Aumiller, M. et al. (2022) Interrelation between Spectral Online Monitoring and Postoperative T1-Weighted MRI in Interstitial Photodynamic Therapy of Malignant Gliomas, Cancers 14:120, DOI:10.3390/cancers14010120
[9] Foglar, M. et al. (2023) Interstitial Photodynamic Therapy of Glioblastomas: A Long-Term Follow-up Analysis of Survival and Volumetric MRI Data Cancers 2023, 15, 2603. DOI: 10.3390/cancers15092603

# Multispectral Skin Sensing for Psychological Stress Detection

**V. Barygina[1], E. Baria[1], A.M. Monciatti[2], F.S. Pavone[1,3,4]**

*1- Dept. of Physics and Astronomy, University of Florence, Italy;*
*2- Conservatory of Music L. Cherubini, Italy;*
*3- LENS - European Laboratory for Non-Linear Spectroscopy, Italy;*
*4- The National Institute of Optics (CNR-INO), Italy*

*victoria.barygina@unifi.it*

Human skin hosts multiple biochemical and structural matrices—including tissue, interstitial fluid, blood-derived constituents, and sweat—that can provide insight into both physiological and psychological states. Traditional methods for probing these biomarkers are often invasive, labor-intensive, costly, or restricted to a narrow panel of molecular targets. This study explores the potential of a high-throughput, multimodal optical sensing platform for non-invasive monitoring of psychological stress via skin spectroscopy.

Raman, reflectance, fluorescence, and spectrally resolved fluorescence-lifetime signals were collected from palmar and dorsal forearm skin of healthy volunteers using a multimodal fiber-optic probe. Psychological stress was elicited through the Montreal Imaging Stress Task (MIST), which combines cognitive load, time pressure, and social evaluative challenge. Stress induction was validated with electrodermal activity and heart-rate-derived physiological measures recorded via wearable biosensors. Spectral datasets were pre-processed to correct for instrumental artefacts and analyzed using principal component analysis combined with supervised classification algorithms. The multimodal integration of optical modalities demonstrated superior discriminative performance compared to single techniques. On palmar skin, after excluding one participant without an electrodermal stress response, the multimodal classifier achieved 100% accuracy and 100% AUC in differentiating "no-stress" from "stress" conditions. Measurements from the dorsal arm confirmed the robustness of stress-related spectral detection, with multimodal classification also reaching 100% performance.

To investigate the molecular underpinnings of the observed spectral changes, a reference library of stress-associated biomolecules was constructed. Candidate markers, including cortisol, interleukins, TNF-α, neuropeptide Y, and sodium lactate, were characterized in both solid and diluted forms using the same multimodal optical platform. Preliminary spectral unmixing analyses revealed stress-related modulations in specific molecular signatures, including significant differences in IL-1α-associated Raman components between baseline and stress states.

These findings support the feasibility of multispectral optical skin sensing as a rapid, non-invasive strategy for detecting psychological stress and probing its molecular correlates. The approach holds promise for development into portable or wearable systems for mental health monitoring, stress assessment in high-responsibility occupations, and biomarker-driven investigations in clinical research.

# Ultraviolet laser systems on $Ce^{3+}$-based active media and photodynamic processes

**A. Nizamutdinov[1], D. Makarova[1], A. Shavelev[1], A. Varlamov[1], V. Semashko[1,2], S. Korableva[1]**

*1- Kazan Federal University, 420008, Kremlevskaja str., 18, Kazan, Russian Federation*
*2- FRC Kazan Scientific Center of RAS, Zavoisky Physical-Technical Institute, Sibirsky tract, 10/7, Kazan, Russian Federation*

*anizamutdinov@mail.ru*

Today technologies express demand on lasers oscillating in ultraviolet (UV) spectral range and having short pulse duration [1]. Main methods of obtaining UV laser radiation are nonlinear and parametric conversion of non-UV laser radiation. These methods can be technically difficult and it takes a lot of space. But on the other hand one can obtain UV lasing by use of fluoride crystals doped by $Ce^{3+}$ ions as active media [2]. Among the trivalent lanthanide ions the ion of $Ce^{3+}$ has minimal energy of 5d configuration with the value of about 50000 $cm^{-1}$ [3]. And ultraviolet laser radiation in Ce-doped fluoride crystals is driven by stimulated emission resulting from interconfigurational 5d-4f transitions in $Ce^{3+}$ ions excited by UV laser pump. Fluoride crystals doped by ions $Ce^{3+}$ allow us to obtain short pulses with duration from several to tens of nanoseconds and even in subnanosecond time domain.

Here we discuss developments in design of practical laser systems based on $LiCaAlF_6$ and $Li(Lu,Y)F_4$ crystals doped with $Ce^{3+}$ ions. These are solid state active media capable to generate laser light in the range of 280-340 nm [4,5]. The discussed advantages are wide wavelength tuning for intracavity spectroscopy or selective tissue treatment, and also possibility to manage the output characteristics inside the cavity [6].

At the same time there are photodynamic processes in UV active medium resulting in formation of color centers [7]. Color centers in there turn absorb energy of laser radiation and cause losses in active medium [7,8]. Level of losses due to color centers depends on amount of laser radiation inside the cavity and doesn't remain constant during experiment [7,8]. This gives an opportunity to utilize the color center losses for arrangement the modulation of Q-factor of the cavity or even mode-locking. Here we discuss additional light and temperature approach for control of UV laser output characteristics. For example, Laser oscillation was obtained in active medium $Ce:LiLu_{0.7}Y_{0.3}F_4$ in a pulse mode at the wavelength $\lambda = 311$ nm as single pulse with duration $t = (400\pm10)$ ps in the low Q-factor cavity. We expect that shortening of the pulse duration was achieved by passive Q-switch, which is caused by bleaching of color centers in the volume of the active medium absorbing the laser radiation. Thus measured contrast of losses level dependence on pump energy appeared to be 1,8 and methods of Q-switch control are change of pumping energy, output mirror reflection and additional illumination intensity.

[1] A. Saliminia, A. Proulx, R. Vallée, Optics Communications, 333, 133-138, (2014).
[2] M. Dubinskii, V. Semashko, A. Naumov, R. Abdulsabirov, S. Korableva, J. Mod. Opt., 40, 1-5, (1993).
[3] L. Brewer, JOSA, 61, 1666–1682, (1971).
[4] A. Shavelev, A. Nizamutdinov, A. Shakirov, S. Korableva, D. Zverev, A. Rodionov, E. Lukinova, V. Semashko, Bulletin of the Russian Academy of Sciences: Physics, 88, S600-S608, (2024).
[5] A. Nizamutdinov, L. Nurtdinova, V. Semashko, S. Korableva, Optics and Spectroscopy, 116, 732-738, (2014).
[6] D. Makarova, A. Nizamutdinov, A. Shavelev, T. Minnebaev, Bulletin of the Russian Academy of Sciences: Physics, 88, S651-S653, (2024).
[7] A. Shakirov, A. Nizamutdinov, A. Shavelev, S. Batygov, S. Kuznetsov, V. Semashko, Bulletin of the Russian Academy of Sciences: Physics, 88, S609-S614, (2024).
[8] V. Semashko, M. Dubinskii, R. Abdulsabirov, S. Korableva, A. Naumov, A. Nizamutdinov, M., Zhuchkv, M.S., Proceedings of SPIE, 4766, 119-126, (2002).

# Detection of DNA hybridization with alkyne-labelling and Raman spectroscopy

M. Veres[1], H.V. Nguyen[2], J. Fossey[2], J. Tucker[2], R. Holomb[1]

*1- HUN-REN Wigner Research Center for Physics, Konkoly-Thege M. str. 29-33., Budapest, Hungary*
*2- bUniversity of Birmingham, Birmingham, UK*

*veres.miklos@wigner.hun-ren.hu*

DNA hybridization is a technique used in molecular biology to measure the degree of genetic similarity between DNA sequences. It involves the mixing of a known single-stranded probe DNA sequence with the sample DNA; followed by the denaturation of the sample DNA and the re-establishment of the hydrogen bonds (hybridization) with the probe strand. Successful hybridization means that the probe and sample strands are complementary, and it is a clear confirmation that the sequence in question is present in the sample DNA. In most cases, hybridization is detected by well-known polymerase chain reactions and other techniques.

Here we report on a Raman spectroscopy-based method in which the probe strand is labeled with an alkyne group and the hybridization is detected through the changes in the parameters of the alkyne Raman peak, occurring during the hydrogen bond formation [1].

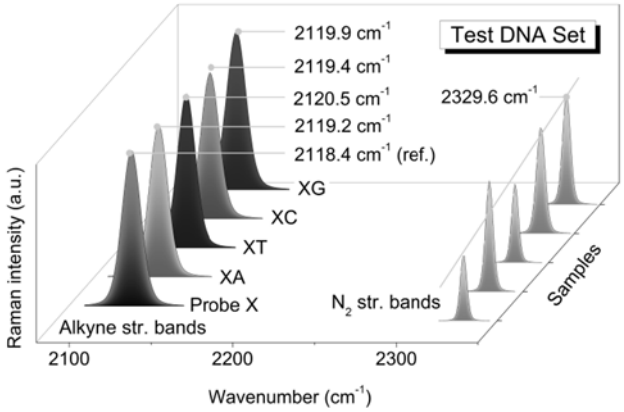


**Fig. 1.** Curve-fitted alkyne Raman bands (C≡C stretching vibrations) of the DNA set for SNV detection, and molecular nitrogen Raman bands (N≡N stretching vibrations) used as an internal reference (N2 gas). The data for the fitting are obtained from baseline-corrected experimental Raman spectra of the oligonucleotides.

It was found that the variation of the peak position allows the distinction between the complete and imperfect hybridizations of the probe and sample DNA strands, and so the identification of mutations in the sample strand (Figure 1). Therefore, our method is capable of the detection of single-nucleotide variants or SNVs (substitution of a single nucleotide at a specific position in the DNA sequence). On the other hand, probes tagged with different alkyne groups having distinct Raman signals can be used for simultaneous detection of multiple DNA sequences in the sample.

The work was supported by the EU H2020 FET-Open 712821 NEURAM project, and the NKFIH-468-3/2021 NAPLIFE, VEKOP-2.3.3-15-2016-00002 and TKP2021-NVA-04 grants of the National Research, Development and Innovation Office of Hungary.

[1] R. Holomb, H.van Nguyen, F. Allabush, A.S. Quy, A. Sik, F. Müller, L. Himics, T. Váczi, J.H.R. Tucker, M. Veres, J.S. Fossey, Detection of single nucleotide variants in nucleic acid biomarkers using Raman spectroscopy, Biosensors and Bioelectronics 304, 118574 (2026)

# Additive-Free vdW Nanoparticle Inks via Femtosecond Laser Ablation for Aerosol Jet Printing

**I.S. Kazantsev[1], G.V. Tikhonowski[1], Z.Sofer[2], G.I. Tselikov[1], A.V. Arsenin[1], V.S. Volkov[1]**

*1-Emerging Technologies Research Center, XPANCEO, Dubai Investment Park First, Dubai, United Arab Emirates*
*2-Department of Inorganic Chemistry, University of Chemistry and Technology Prague, Technická 5, 166 28 Prague 6, Czech Republic*

*Main author email address: kazantsev.is@xpanceo.com*

Van der Waals (vdW) nanoparticles (NPs) represent a versatile class of functional nanomaterials with tunable optical, electronic, and mechanical properties, making them attractive for advanced additive manufacturing. In a recent study, single-step femtosecond pulsed laser ablation in liquids (fs-PLAL) was used to synthesize spherical, additive-free vdW nanoparticles exhibiting exceptional colloidal stability across diverse solvents, including water. This laser-based approach was used by Tselikov et al. to enable the synthesis of nanoparticles from more than 50 different vdW materials, underscoring its universality and scalability [1]. This stability arises from an intrinsic surface charging mechanism, providing strong electrostatic repulsion that prevents agglomeration without the need for chemical surfactants. The ability to prepare pure, stable colloids expands opportunities for environmentally friendly additive manufacturing workflows and ensures compatibility with chemically sensitive substrates. We demonstrate the direct use of these vdW nano-inks in high-resolution aerosol jet printing (Fig. 1), achieving uniform, well-defined patterns on multiple substrates with no sedimentation of inks during prolonged operation [2]. The spherical morphology of the nanoparticles ensures reliable jetting and consistent deposition quality, which is essential for precision patterning applications. Using this approach, we also printed SERS-active substrates on various materials, including aluminum foil, paper, and PET, and evaluated their performance, confirming their functionality for sensing applications. Beyond advanced printing, the exceptional stability enables integration into simple writing tools, such as marker pens, facilitating rapid, equipment-free prototyping of functional surfaces.

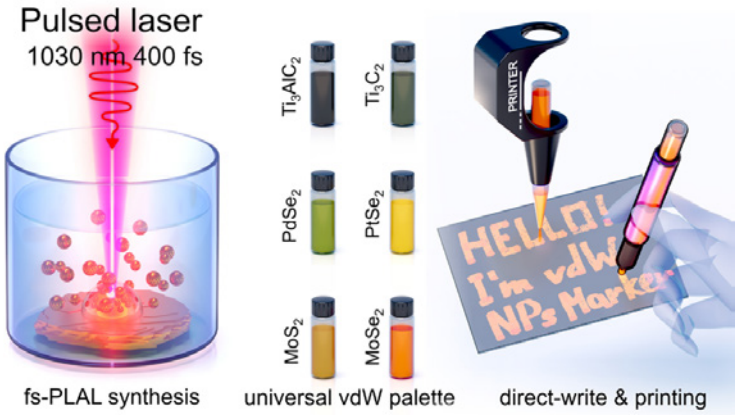


**Fig. 1.** Laser ablation of vdW materials for inks synthesis

[1] Tselikov, G. I., Minnekhanov, A. A., Ermolaev, G. A., Tikhonowski, G. V., Kazantsev, I. S., Dyubo, D. V., ... & Volkov, V. S. Tunable Nanostructuring for van der Waals Materials, ACS nano, (2025).
[2] Kazantsev, I. S., Tikhonowski, G. V., Ermolaev, G. A., Minnekhanov, A. A., Slavich, A. S., Solovei, V. R., ... & Volkov, V. S. Printable van der Waals Nanoparticles for Additive Technologies, Nano Letters, (2026).

# Laser Hollow Beams Generated by Acousto-Optical Spatial Frequency Filters for Optical Trapping Applications

**V. Molchanov, K. Yushkov, A. Chizhikov**

*Acousto-Optical Research Center, National University of Science and Technology MISIS, 4 Leninsky Prospekt, Moscow, 119049, Russia*

*v.ya.molchanov@gmail.com*

The research is devoted to the study the spatial-frequency properties of acousto-optic noncollinear filters based on a $TeO_2$ single crystal for the generation of bottle laser beams promising for capturing, holding, and transporting ensembles of cold atoms [1] by controlling the phase distribution of a piezoelectric transducer.

AO spatial frequency filters (AOSFs) allow filtering the angular spectrum of a laser beam [2]. The spatial transfer function of the AOSF is a function with one argument – frequency. Control of the transfer function can by expanded by adding the second argument – transducer phase distribution. Antiphase control an AOSF was first reported using $\Delta\phi=\pi$ a PPLN transducer [3]. Now, the transfer function of the AOSF for an arbitrary phase difference $\Delta\phi$ is investigated theoretically and experimentally. The phenomenon of transfer function splitting is shown in Fig. 1. Custom noncollinear AOSF based on $TeO_2$ crystal with two transducers for independent phase $\Delta\phi$ control was developed and manufactured, Fig. 2 [4].

2D ring transfer functions (photograph on the screen) of the phase-controlled AOSF at relevant ratio of frequencies $f$ and phase difference $\Delta\phi$ demonstrate wall splitting, Fig. 3 (top). Top row: $f$=153.6 MHz, bottom row: $f$=154.0 MHz. (1) In-phase operation, $\Delta\phi=0$; (2) $\Delta\phi=\pi/2$; (3) antiphase operation of the sections, $\Delta\phi=\pi$; (4) $\Delta\phi=3\pi/2$, $\lambda$=633 nm.

3D intensity distribution of a split cylindrical laser field (like a thermos) for a dark trap was obtained using a motorized CCD camera and a Ti:sapphire laser in free-running mode, Fig. 3 (bottom) at $f$=117.2 MHz, $\lambda$=799 nm, $\Delta\phi$=240°. Top row: 2D intensity distribution of the annular laser field along the Z axis, middle row: cross-section of the laser field by the Y=0 plane, bottom row: cross-section of the laser field by the X=0 plane. The extent of the thermos region is important for dynamic manipulation of cold atoms: the ratio of the thermos length to the diameter is 10:1.

The research was supported by RSCF Project 20-12-00348-P.

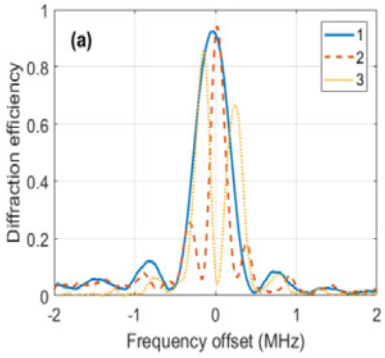


**Fig. 1.** Transfer function splitting: 1 – single transducer, 2 – two transducers, $\Delta\phi=0.3\pi$, 3 – two transducers, $\Delta\phi=1.3\pi$

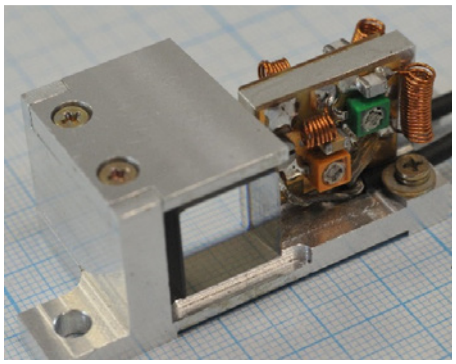

**Fig. 2.** Home-made noncollinear $TeO_2$ AO spatial frequency phase controlled filter

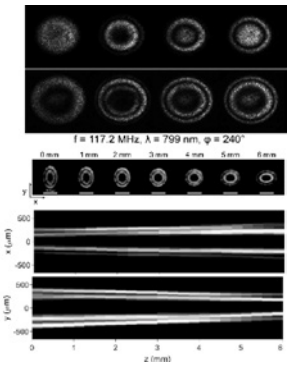

**Fig. 3.** 2D (top) and 3D (bottom) cross-sections of the laser beam intensity distributions

[1] F.K. Fatemi et al., Dynamic high-speed spatial manipulation of cold atoms using acousto-optic and spatial light modulation, Opt. Express, vol. 15, pp. 3589-3596 (2007).
[2] V.I. Balakshy. Application of acousto-optic interaction for holographic conversion of light fields, Opt. Laser Technol., vol. 28, pp. 109-117 (1996).
[3] V.Ya. Molchanov, Acousto-optic TeO2 devices using regular domain structure transducers, Acta Physica Slovaca, vol. 46, pp. 715-720 (1996).
[4] K.B. Yushkov, A.I. Chizhikov, D.V. Obydennov, V.Ya. Molchanov. Phase-tuned acousto-optic spatial filter. Opt. Lett., vol. 49, pp. 3866-3869 (2024).

# A high-energy, mid-infrared solid-state coherent source based on a $BaGa_2GeS_6$ optical parametric oscillator–amplifier system

**E. Erushin[1], S. Sere[1], M. Vostrikova[1], A. Boyko[1], G. Shevyrdyaeva[2], A. Karapuzikov[3], D. Badikov[2], N. Kostyukova[1]**

*1- Institute of Laser Physics of the SB of the RAS, Russia, 630090, Novosibirsk, 15B, prosp. Ac. Lavrentiev*
*2- Kuban State University, Russia, 350040, Krasnodar, 149 Stavropolskaya Str.*
*3-Special technologies, Ltd, Russia, 630060, Novosibirsk, 1/3 Zelenaya Gorka Str.*

*n.duhovnikova@gmail.com*

Expanding the spectral range and improving the conversion efficiency of mid-infrared radiation sources remains an important challenge. Research into barium chalcogenides is yielding key insights, as these crystals offer a broad transparency range, strong nonlinearity, and a high laser-induced damage threshold [1]. The $BaGa_2GeS_6$ (BGGS) crystal, in particular, has emerged as a material of significant interest within the barium chalcogenides. Very recently, we demonstrated optical parametric oscillation in the aforementioned crystal with idler wavelength tuning across the 3.4–12.6 μm range [2] and and achieving pulse energies exceeding 2 mJ at 6.45 μm [3].

In this work, a two-stage scheme was implemented, comprising optical parametric oscillation and subsequent amplification of the generated radiation at a wavelength of 6.45 μm using a BGGS nonlinear crystal. The pump source was a diode-pumped, Q-switched Nd:YAG laser producing pulses with an energy of up to 320 mJ, a duration of 11 ns, and a repetition rate of 10 Hz. In the first stage, a single-pass optical parametric oscillator (OPO) was realized using a 13.29 mm long BGGS crystal with cut angles $\varphi = 17.3°$ and $\theta = 33.9°$ serving as the nonlinear element. Subsequently, the idler radiation was separated from the pump and signal waves by filtering and coupled into a second BGGS crystal (20.15 mm in length, cut angles $\varphi = 17°$, $\theta = 37.4°$), which was also pumped by the same Nd:YAG laser. The two crystals were positioned such that the phase-matching conditions in both stages coincided and corresponded to the idler wavelength of 6.45 μm. Thus, an optical parametric amplifier (OPA) was realized.

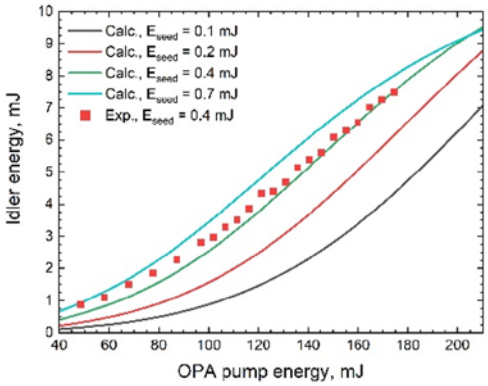


**Fig. 1.** Idler OPA energy at 6.45 μm vs. pump energy

Consequently, an increase in pulse energy by more than a factor of 3.5 was achieved. The maximum output energy at a wavelength of 6.45 μm was 7.5 mJ at a pump energy of 175 mJ, which corresponds to a conversion efficiency of 4.1% and a quantum efficiency of 24.8%. These findings suggest that the BGGS crystal is a promising candidate for nonlinear down-conversion applications. The development of the OPA was carried out under the State Assignment of ILP SB RAS, grant No. FWGU-2026-0005.

[1] N. Kostyukova, et al., Barium Chalcogenide Crystals: A Review, Photonics, vol. 11, p. 281 (2024).
[2] E. Erushin, et al., Widely tunable mid-infrared $BaGa_2GeS_6$ optical parametric oscillator pumped at 1064 nm by Nd:YAG laser, Optical Materials, vol. 169, pp. 117610 (2026).
[3] E. Erushin, et al., An optical parametric oscillator based on $BaGa_2GeS_6$ with energy exceeding 2 mJ at 6.45 μm Infrared Physics & Technology, Vol. 154, pp. 106393 (2026).

# DFB-laser based on a quasirelativistic-momentum-law HgCdTe quantum well structure with a third-order Bragg grating

**S.V. Morozov[1], M.A. Fadeev[1], V.V. Utochkin[1], A.A. Razova[1], V.V. Rumyantsev[1], K.A. Mazhukina[1], A.A. Yantser[1], A.A. Dubinov[1], V.Ya. Aleshkin[1], D.V. Shengurov[1], N.S. Gusev[1], E.E. Morozova[1], N.N. Mikhailov[2], S.A. Dvoretskii[2], V.R. Baryshev[3], E.D. Egorova[3], N.S. Ginzburg[3], A.M. Malkin[3], G.S. Sokolovskii[4], V.V. Dudelev[4], A.Yu. Egorov[4], V.I. Gavrilenko[1]**

*1- The Institute for Physics of Microstructures of the RAS, Nizhniy Novgorod, Russia*
*2- Rzhanov Institute of Semiconductor Physics Siberian Branch of RAS, Novosibirsk, Russia*
*3- A.V. Gaponov-Grekhov Institute of Applied Physics of the RAS, Nizhniy Novgorod, Russia*
*4- A. F. Ioffe Physical-Technical Institute of the RAS, Saint Petersburg, Russia*

*more2009@yandex.ru*

Compact mid-indfrared (IR) radiation sources remain in demand for a number of fundamental and applied problems related to the spectroscopy of gases and solids. Among semiconductor lasers, quantum cascade lasers (QCLs) currently demonstrate the best performance in terms of power and operating temperatures in the mid-IR range. Interband lasers based on narrow-gap HgCdTe/CdHgTe heterostructures with quantum wells (QWs) [1] can serve as alternative compact sources. Achieving optical amplification and generation of electromagnetic radiation in such materials has been proven possible due to the suppression of the main loss mechanism associated with non-radiative Auger recombination for charge carriers with a quasirelativistic dispersion law [2]. Due to the known difficulties of p-doping of HgCdTe QW structures and the resulting difficulties in implementing laser diodes, it seems reasonable to consider such compact lasers with optical pumping by near-IR diode lasers or the aforementioned IR QCLs [3, 4]. It is of particular interest to implement a laser with distributed feedback (DFB) providing high frequency stability, which is of priority for a number of applications. The concept of such a laser based on HgCdTe/CdHgTe QWs with optical pumping was proposed in [5].

The waveguide structure with five 7.4-nm thick $Hg_{0.89}Cd_{0.11}Te/Cd_{0.66}Hg_{0.34}Te$ QWs was grown by molecular beam epitaxy on a GaAs-substrate (013). The fabrication of the DFB laser involved the direct etching of a one-dimensional dielectric grating into the structure surface. The grating period was set to 7,5 μm, and the process was carried out using ion etching. Optical pumping was provided by various sources. A pulsed QCL (8 μm, ~4 W in a beam diameter of ~2.5 mm), pulsed or continuous-wave CO2 lasers (lasing wavelength of 10.6 μm), and a continuous-wave fiber laser (lasing wavelength of 1.9 μm) were used.

Single-frequency lasing at a wavelength of 13.5 μm was demonstrated from a waveguide structure with HgCdTe QWs pumped by QCL with 8 μm wavelength. Importantly, due to the effective refractive index of 2.89 in HgCdTe for this frequency range, which is atypical for semiconductor materials, it is possible to simultaneously provide DFB and grating-outcoupling at an angle of 21° to the surface using a third-order Bragg grating. The studied DFB-laser exhibited narrow-band lasing with a FWHM < 0.15 $cm^{-1}$ (4.5 GHz) at a wavelength of ~13.5 μm. The laser frequency exhibited temperature stability, typical for DFB-lasers, and the emission spot size at a distance of 15 cm did not exceed 3 mm, confirming small beam divergence.

This work was supported by Russian Science Foundation grant # 22-12-00310.

[1] A. A. Razova, M. A. Fadeev, V. V. Rumyantsev, et al., "Whispering gallery mode HgCdTe laser operating near 4 μm under Peltier cooling," Appl. Phys. Lett., vol. 123, № 16, pp. 161105, (2023).
[2] S. V. Morozov, V. V. Rumyantsev, M. S. Zholudev, et al., "Coherent Emission in the Vicinity of 10 THz due to Auger-Suppressed Recombination of Dirac Fermions in HgCdTe Quantum Wells," ACS Photonics, vol. 8, № 12, pp. 3526−3535, (2021).
[3] A. A. Razova, V. V. Rumyantsev, K. A. Mazhukina, et al., "Microdisk HgCdTe lasers operating at 22–25 μm under optical pumping," Appl. Phys. Lett., vol. 126, № 12, pp. 121102, (2025).
[4] V. V. Rumyantsev, K. A. Mazhukina, V. V. Utochkin, et al., "Optically pumped stimulated emission in HgCdTe-based quantumwells: Toward continuous wave lasing in very long-wavelength infrared range," Appl. Phys. Lett., vol. 124, № 16, pp. 161111, (2024).
[5] V. R. Baryshev, E. D. Egorova, N. S. Ginzburg, et al., " Development of a single-mode DFB heterolaser with inclined radiation output," Semiconductors, vol. 57, № 5, pp. 349–354, (2023).

# Precise characterization of dispersion and birefringence in a photonic crystal fiber using spontaneous vector four-wave mixing

**I.V. Fedotov[1,2], A.A. Voronin[1,2], A.V. Gladyshev[3], M.A. Smirnov[4], S.A. Moiseev[4], A.B. Fedotov[1,2]**

*1- Lomonosov Moscow State University, Physics Faculty, Moscow 119991, Russia*
*2- Russian Quantum Center, Skolkovo, Moscow Region, 143025 Russia*
*3- Prokhorov General Physics Institute of RAS, Moscow 119991, Russia*
*4- Kazan National Research Technological University , Kazan, 420015, Russia*

*a.b.fedotov@physics.msu.ru*

Chromatic dispersion is a key characteristic of optical fibers because it strongly affects the propagation of optical signals in scientific, industrial, and telecommunications applications. For this reason, methods for measuring chromatic dispersion are covered by international standards. These standards include several established approaches, such as phase-shift techniques, spectral group-delay measurements in the time domain, differential phase-shift methods and interferometry.

The ability to control dispersion is particularly important for photonic crystal fibers (PCFs), whose microstructure allows phase-matching conditions to be engineered. One important application of photonic crystal fibers is their use generation of quantum states of light through spontaneous four-wave mixing (SFWM) based on third-order nonlinearity. Photon-pair generation in SFWM is governed by the laws of energy conservation and phase matching and the latter is mainly determined by the dispersion properties of the fiber [1 -3]. When generating entangled photon pairs and selecting and analyzing the conditions for their formation, the dispersion properties of optical fibers are typically assumed to be known and specified. This is a separate and challenging task when using new types of fibers, therefore, the development of methods for precisely determining the chromatic dispersion of fibers is of great importance, including for the design of a quantum fiber biphoton source.

In this work, we demonstrate the inverse approach for determining the dispersion and birefringence of a fiber from experimentally obtained spectra of photon pairs generated by vector SFWM. The measurement setup essentially followed the generally accepted approach and our earlier work [4-6], A femtosecond Ti:Sapphire laser with a tunable wavelength, pulse duration of approximately 200 fs, and repetition rate of 76 MHz was used as the pump source. The pump spectral bandwidth, pulse energy, and polarization were controlled before the beam was coupled into a highly nonlinear birefringent NL-PM-750 NKT photonic crystal fiber using an aspherical lens. The central wavelengths of the generated signal and idler photons in different polarization configurations are governed by the phase-matching conditions and therefore by the fiber dispersion. In the proposed inverse procedure, scalar polarization configurations are used to retrieve the dispersion of the fast and slow modes, whereas vector configurations provide access to the group-delay difference and birefringence. Compared with approaches based on group-delay measurements, this avoids numerical differentiation, which can amplify experimental noise. Since the spectra are measured in the spontaneous, low-gain regime, pump-power-dependent nonlinear phase shifts have a negligible effect on the extracted phase-matching wavelengths.

The proposed technique enables accurate reconstruction of the dispersion of both polarization modes over a broad spectral range using a limited pump-tuning range. In our experiment, pump tuning over 690–815 nm allowed the fiber dispersion to be reconstructed over 450–1800 nm and the birefringence to be retrieved. This approach can be used for the design of fiber-based photon-pair sources and, more generally, for precision characterization of dispersion properties in fibers with different architectures.

The work was supported by Russian Science Foundation grant # 25-12-00211.

[1]. L. J. Wang, C. K. Hong, and S. R. Friberg, "Generation of correlated photons via four-wave mixing in optical fibres," J. Opt. B: Quantum Semiclass. Opt. **3**, 346 (2001).
[2]. M. Fiorentino, P. L. Voss, J. E. Sharping, and P. Kumar, "All-fiber photon-pair source for quantum communications," IEEE Photonics Technology Letters **14**, 983–985 (2002).
[3] K.Garay-Palmett, H.McGuinness, O.Cohen, J. Lundeen, R.Rangel-Rojo, A. Uren, M. Raymer, C. McKinstrie, S.Radic, I.Walmsley, Photon pair-state preparation with tailored spectral properties by spontaneous four-wave mixing in photonic-crystal fiber, Optics express 15, 14870 (2007).
[4] K. Garay-Palmett, D. B. Kim, Y. Zhang, F. A. Dom´ınguez-Serna, V. O. Lorenz, and A. B. URen, Fiber-based photon-pair generation: tutorial, Journal of the Optical Society of America B 40, 469 (2023).
[5] N. L.Petrov, A. A. Voronin, A.B.Fedotov, and A. M. Zheltikov, "Ultrahigh-contrast cross-polarized entangled photon pairs from a strongly birefringent photonic-crystal fiber," Appl. Phys. B **125**, 54 (2019).
[6]. M. A. Smirnov, I. V. Fedotov, A. M. Smirnova, A. F. Khairullin, A. B. Fedotov, and S. A. Moiseev, "Bright ultra-broadband fiber-based biphoton source," Opt. Lett., OL **49**, 3838–3841 (2024).

# Optofluidic laser filled with perovskite nanocrystals

**D. Gagarinova[1], D. Gets[1], L. Zelenkov[1,4], E. Menshikov[1], F. Kuzikov[1], A. Pryamikov[2], A. Kosolapov[2], V. Velmiskin[2], A. Pushkarev[3], A. Kokhanovskiy[1]**

*1- School of Physics and Engineering, ITMO University, 197101 Saint Petersburg, Russia*
*2- Prokhorov General Physics Institute of RAS, 119991 Moscow, 38 Vavilov street, Russia*
*3- Hybrid Photonics Laboratory, Skolkovo Institute of Science and Technology, 121205 Moscow, Russia*
*4- Harbin Engineering University, 150001 Harbin, 145 Nantong Street, Nangang District, China*

*a.kokhanovskiy@itmo.ru*

Optofluidic lasers integrate seamlessly with microfluidic systems and integrated photonic circuits, providing a versatile platform for energy-efficient coherent light sources within a small volume [1]. Colloidal halide perovskite nanocrystals (NCs) $CsPbX_3$ are attractive gain media owing to their high optical gain, low lasing threshold and size- and composition-tunable emission across the visible range [2]. Their main limitation is sensitivity to moisture and oxygen; encapsulating the NC solution inside a hollow optical fiber simultaneously protects the perovskite and provides a low-loss waveguiding resonator [3].

Here we demonstrate multiband lasing of $CsPbBr_3$ NCs infiltrated into a purpose-designed hollow-core silica fiber. The fiber was drawn from Suprasil F300 tubes by a two-stage capillary-stack technique, forming a 20-μm hollow core surrounded by eleven petal-like cavities (outer diameter ≈ 89 μm). Both the core and the petals were filled with a 100 mg/mL toluene solution of 15.6-nm $CsPbBr_3$ NCs (photoluminescence near 532 nm), yielding measured linear losses of 3.72 and 3.84 dB/m at 480 and 532 nm. The sample was side-pumped by 290-fs, 480-nm pulses at a 10-kHz repetition rate, and the emission was collected from the fiber facet.

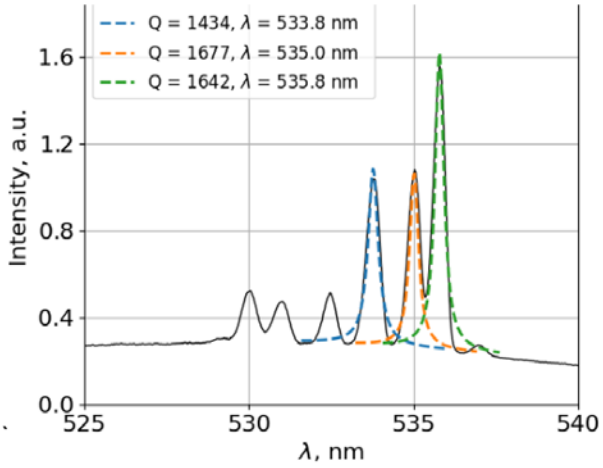


**Fig. 1.** Photoluminescence spectrum at maximum pump fluence (≈ 17 μJ/cm²) near the output facet, showing five lasing lines with Q = 1434–1677.

By shifting the femtosecond pump spot along the fiber, the lasing wavelength, linewidth and quality factor are reconfigured without any structural modification of the device. Near the output facet, five lines spaced by ≈ 1–1.5 nm appear with Q-factors of 1434–1677 and a threshold of 12.22 μJ/cm² (Fig. 1), whereas mid-fiber excitation yields dual-line emission (≈ 2 nm spacing, Q = 1166–1481) with an even lower threshold of 9.83 μJ/cm². Finite-element modelling attributes the spectra to low-index cladding-ring modes ($n_{eff}$ = 1.451–1.453) propagating in the silica behind the peripheral cavities. The device thus provides spatially reconfigurable, multiband green lasing across a 528–537 nm tuning range, a promising step toward compact lab-on-fiber sources for on-chip spectroscopy and sensing.

[1] X. Yang, C. Gong, C. Zhang et al., Fiber optofluidic microlasers: structures, characteristics, and applications, Laser & Photonics Reviews, vol. 16, p. 2100171, (2021).
[2] L. Protesescu, S. Yakunin, M. Bodnarchuk et al., Nanocrystals of cesium lead halide perovskites ($CsPbX_3$, X = Cl, Br, and I), Nano Letters, vol. 15, pp. 3692–3696, (2015).
[3] X. Li, P. Zeng, Q. Ou, S. Zhang, Fabrication of perovskite film-coated hollow capillary fibers using a fast solvent exchange method, Nanomaterials, vol. 11, p. 1483, (2021).

# Growth, spectroscopy and laser operation of disordered Tm,Ho:NaGd(MoO$_4$)$_2$ crystal

**Y.S. Didenko[1,2], K.A. Subbotin[1,2], G.Z. Elabedine[3], Z. Pan[4], P. Loiko[4], K. Eremeev[5], P. Camy[5], A. Braud[5], S. Slimi[3], R.M. Solé[3], M. Aguiló[3], F. Díaz[3], W. Chen[6,7], W. Griebner[6], V. Petrov[6], X. Mateos[3]**

*1- Prokhorov General Physics Institute of RAS, Vavilova St. 38, 119991 Moscow, Russia*
*2 - Mendeleev Russian University of Chemical Technology Miusskaya Sq. 9, 125049 Moscow, Russia*
*3 - Universitat Rovira i Virgili (URV), 43007 Tarragona, Spain.*
*4 - School of Information Science and Engineering, Shandong University, Qingdao 266237, China*
*5 - Université de Caen Normandie, Boulevard Maréchal Juin 6, 14050 Caen Cedex 4, France*
*6 – M.Born Institute for Nonlinear Optics, Max-Born-Str. 2a, 12489 Berlin, Germany*
*7 - Fujian Institute of Research on the Structure of Matter, CAS, Fuzhou, 350002 Fujian, China*

*ia.didenko@yandex.ru*

A $Tm^{3+}$,$Ho^{3+}$-codoped disordered NaGd(MoO$_4$)$_2$ crystal (5.55 at.% Tm, 0.43 at.% Ho) was grown by the Czochralski method. The crystal has the tetragonal Scheelite-type structure (space group $I4_1/a$), refined by the Rietveld method with lattice parameters $a$ = 5.237(5) Å and $c$ = 11.443(6) Å. The structure disorder, arising from the statistical distribution of $Na^+$ and $Gd^{3+}$ cations over the same lattice site, leads to significant inhomogeneous broadening of $Tm^{3+}$ and $Ho^{3+}$ spectral lines. Polarized Raman spectroscopy has revealed the dominant high-frequency mode at 883 $cm^{-1}$ due to symmetric stretching vibrations of $[MoO_4]^{2-}$ groups.

The complex of spectroscopic studies of the crystal has been performed (Fig. 1). For $Ho^{3+}$, the stimulated-emission cross-section for the $^5I_7 \rightarrow {}^5I_8$ transition reaches $1.84\times10^{-20}$ $cm^2$ at 2043 nm (π-polarization), with an exceptionally broad emission bandwidth of 66 nm for σ-polarized light. Low-temperature (12 K) spectroscopy enabled determination the energy positions of Stark sub-levels for the $^3H_6$ and $^3F_4$ manifolds of $Tm^{3+}$ and for the $^5I_8$ and $^5I_7$ manifolds of $Ho^{3+}$. The parameters of the $Tm^{3+} \rightarrow Ho^{3+}$ energy transfer were found, yielding a thermal equilibrium decay time of 3.8 ms for the coupled $^3F_4(Tm^{3+})$ and $^5I_7(Ho^{3+})$ manifolds, indicating highly efficient energy transfer.

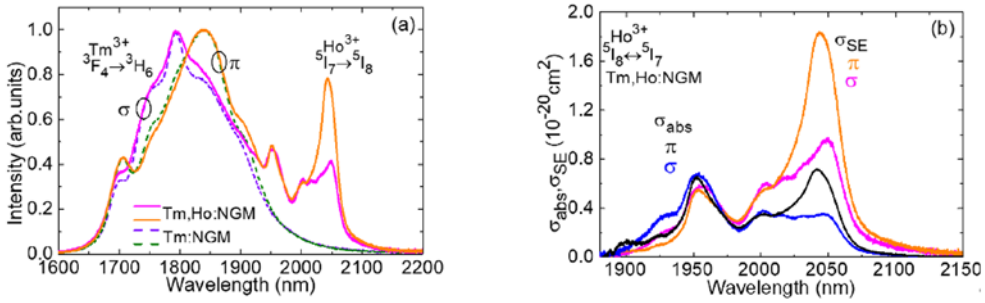


**Fig. 1.** (a) luminescence spectra of a codoped crystal (solid curves), the spectra for a singly $Tm^{3+}$-doped one (dashed curves) are given for comparison; (b) $\sigma_{abs}$ and $\sigma_{SE}$ for the $^5I_7 \rightarrow {}^5I_8$ $Ho^{3+}$ transition in Tm,Ho:NaGd(MoO$_4$)$_2$,.

A continuous-wave laser operation was realized at the $Tm^{3+}$,$Ho^{3+}$:NaGd(MoO$_4$)$_2$ crystal using an $a$-cut active element pumped by a Ti:Sapphire laser at 795 nm. The laser generated a maximum output power of 548 mW at 2045–2055 nm with a slope efficiency of 32.4% and a very low laser threshold of 98 mW. The emission was linearly polarized (π-polarization). For high output coupling (≥5%), co-lasing at both $Tm^{3+}$ (1.92 μm) and $Ho^{3+}$ (2.04 μm) transitions was observed. Preliminary experiments with diode-pumping at 788 nm yielded 130 mW laser action at 2048 nm, demonstrating the potential for compact pump sources.

The combination of broad, smooth gain profiles (gain bandwidth of up to 35 nm for σ-polarization at β=0.4), efficient energy transfer, low laser threshold, and strong polarization anisotropy makes Tm,Ho:NaGd(MoO$_4$)$_2$ a very promising gain medium for broadly tunable and mode-locked ultrafast lasers operating in the eye-safe 2-μm spectral region.

# Graphene-Inspired 2D-Grown Ultrathin Metal Films: Transferable Platform for Flexible Optoelectronics and Sensing

**D.I. Yakubovsky[1], M.S. Mironov[2], T.A. Kochetkov[1,2], G.A. Ermolaev[1,2], D.V. Grudinin[2], A.S. Slavich[2], A.V. Arsenin[1,2], V.S. Volkov[2]**

*1- Center for Photonics and 2D Materials, Moscow Institute of Physics and Technology, Dolgoprudny, Russia*
*2- Emerging Technologies Research Center, XPANCEO, Dubai Investment Park First, Dubai, United Arab Emirates*

*dmitrii-y@mail.ru*

The emerging field of transparent conductive materials focuses on developing fabrication techniques for 2D metallic layers of varying dimensions and characterizing their unique properties. Recent milestone achievements have produced two-dimentional (2D) and even monolayer metals [1–3], but the resulting materials are limited to micrometer-scale flakes or require encapsulation or stabilizing layers, precluding their use as large-area, open-surface components in wafer-scale technologies. Consequently, a general strategy to produce continuous, transferable, and technologically relevant ultrathin metals has remained elusive.

Here, we resolve this challenge by the adaptation of the graphene technology to produce transferrable wafer-scale adhesion-free ultrathin metal films, merging techniques from two different fields: template stripping and polymer-assisted transfer from 2D materials technology. Initially, our approach leverages upon template stripping to fabricate an atomically smooth wafer-scale copper foil, which allows to overcome the thermodynamic barrier for the 2D growth of ultrathin metals, guiding the physical vapour deposition into continuous films. We then employ a robust, graphene-inspired transfer-process to cleanly delaminate this ultrathin metal film, rendering it a freestanding, handable layer that can be integrated with arbitrary substrates [4]. The suggested two-step process results in a film formation that unites the previously mutually exclusive goals of atomic-scale thickness and large-area transferability. We validate the versatility of this approach by fabrication of atomically smooth and continuous ultrathin gold and platinum films, less than 8 nm thickness, exhibiting highest optoelectronic performance: transparency-conductance trade-off and flexibility. The functionality of the films was demonstrated through different applications, including organic light-emitting diodes (OLEDs) and transferrable electronic sensing devices.

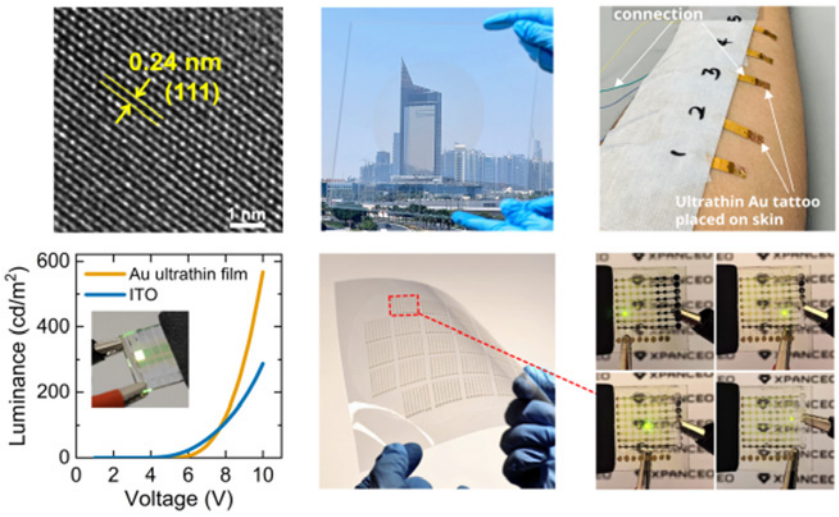


**Fig. 1.** Crystalline structure, transparency, wafer scalability of the transferred ultrathin gold films, and devices demonstration based on them.

The presented study is supported by the grant №24-72-10039 from the Russian Science Foundation.

[1] C. Pan, et al., Large area single crystal gold of single nanometer thickness for nanophotonics, Nat. Commun., 15, 2840 (2024).
[2] J. Zhao, et al., Realization of 2D metals at the ångström thickness limit, Nature, 639, 354–359 (2025).
[3] S. Kashiwaya, et al., Synthesis of goldene comprising single-atom layer gold, Nat. Synth., 3, 744–751 (2024).
[4] M. Mironov, D. Yakubovsky, et al., Graphene-Inspired Wafer-Scale Ultrathin Gold Films, Nano Lett., 24, 16270–16275 (2024).

# Micro- and nano- structuring of optical materials with a femtosecond laser beam: applications

A.G. Okhrimchuk[1], V.S. Tsarev[1], V.V. Likhov[1], G.K. Alagashev[1], A.E. Levchenko[1], I.S. Glebov[2]

*1- Prokhorov General Physics Institute of the Russian Academy of Sciences, 38 Vavilova Str. Moscow, Russia*
*2- Mendeleev University of Chemical Technology, Miusskaya sq. 9, Moscow 125047, Russia*

*a.okhrim@yandex.ru*

In the 90s of the last century the femtosecond laser became a reliable laboratory instrument for research. It was then discovered that there is an energy range of an ultrashort laser pulse in which a laser beam tightly focused in the glass volume can produce the controlled local change of the refractive index (RI) around the beam waist, rather than destroying the material. As a result, a discipline has emerged for creating waveguide three-dimensional structures (optical chips) and encoding data in a volume of silicate or phosphate glass, called direct laser writing (DLW)[1,2]. In fact, DLW is in some cases a cheaper alternative to traditional planar lithography, which is also used to produce optical chips. Examples of DLW applications in the production of photonics elements are splitters, filters, lanterns, laser resonators and amplifiers. DLW has proved to be extremely important in prototyping optical quantum computers, since the optical chips created by this method are able to maintain controlled inter-mode phase differences for a long time [3].

Later, it was found that repeated exposure to ultrashort laser pulses leads to the formation of nanogratings in silica glass – nearly flat nanofractures in the glass net [3]. The region of glass containing nanogratings is birefringent and is etched in hydrofluoric acid at a rate several orders of magnitude higher than unirradiated glass. The first property was the basis of a 5D optical memory, and the second is used in the creation of microfluidic devices and sensors used deformations [4,5].

DLW is used in nanostructuring of fibers, both at their ends and in writing Bragg gratings in the fiber core. Such gratings are more resistant to elevated temperatures than traditional "ultraviolet" gratings. But the most important thing is that the DLW method allows to write Bragg gratings in glasses of any composition, for this it does not require special photosensitive properties. This advantage was manifested in fabrication of Bragg mirrors for infrared fiber lasers based on fluoride and chalcogenide glasses [6,7].

In the early 2000s, it was found that DLW is also applicable to crystals. But unlike glasses, in which, depending on the chemical composition and writing mode, both an increase and a decrease in IR is observed, in crystals, with rare exceptions, PP decreases in the area of laser exposure. Therefore, a depressed cladding architecture with parallel modification tracks is usually used to inscribe waveguides [8]. Another way to write a waveguide in a crystal is to form a deformation region adjacent to one or two parallel tracks of modification of the crystal lattice [9]. Waveguide micro-lasers operating in various generation modes, optical frequency doublers, and electro-optical modulators based on the Mach-Zander interferometer are demonstrated in crystals.

A promising research line in DLW is creation of helical waveguide structures in the volume of glasses and crystals capable of generating beams carrying an orbital angular momentum [10,11].

[1] K. M. Davis, K. Miura, N. Sugimoto, and K. Hirao, Opt. Lett. **21**, 1729 (1996).
[2] E. N. Glezer, M. Milosavljevic, L. Huang, R. J. Finlay, T.-H. Her, J. P. Callan, and E. Mazur, (1996), **21**.
[3] Y. Shimotsuma, P. G. Kazansky, J. Qiu, and K. Hirao, Phys. Rev. Lett. **91**, 247405 (2003).
[4] J. Zhang, M. Gecevičius, M. Beresna, and P. G. Kazansky, Phys. Rev. Lett. **112**, 033901 (2014).
[5] Y. Bellouard, A. A. Said, and P. Bado, Opt. Express **13**, 6635 (2005).
[6] M. Bernier, D. Faucher, R. Vallée, A. Saliminia, G. Androz, Y. Sheng, and S. L. Chin, Opt. Lett. **32**, (2007).
[7] V. V. Koltashev, M. V. Sukhanov, V. V. Likhov, B. I. Denker, B. I. Galagan, S. E. Sverchkov, E. N. Lashmanov, A. P. Velmuzhov, V. G. Plotnichenko, and A. G. Okhrimchuk, Infrared Phys. Technol. **155**, (2026).
[8] A. G. Okhrimchuk, A. V Shestakov, I. Khrushchev, and J. Mitchell, Opt. Lett. **30**, 2248 (2005).
[9] V. Apostolopoulos, L. Laversenne, T. Colomb, C. Depeursinge, R. P. Salathé, M. Pollnau, R. Osellame, G. Cerullo, and P. Laporta, Appl. Phys. Lett. **85**, 1122 (2004).
[10] A. G. Okhrimchuk, V. V. Likhov, S. A. Vasiliev, and A. D. Pryamikov, Journal of Lightwave Technology **40**, 2481 (2022).
[11] V. Likhov, S. Vasiliev, G. Alagashev, and A. Okhrimchuk, Opt. Lett. **49**, 1217 (2024).

# Nonlinear spatio-spectral control of laser beams in multicore fibers

**S.A. Babin[1,2], A.G. Kuznetsov[1], A.Y. Kolesnikova[1,2], A.V. Dostovalov[1], M.D. Gervaziev[1,2], N.V. Bochkarev[1,2], D.S. Kharenko[1,2], E.V. Podivilov[1,2]**

*1- Institute of Automation and Electrometry SB RAS, Novosibirsk 630090, Russia*
*2- Novosibirsk State University, Novosibirsk 630090, Russia*

*babin@iae.nsk.su*

Multicore fibers (MCFs) are considered now as promising means of generating, amplifying, and delivering high power / energy continuous wave (CW) / pulsed radiation, which overcome limitations of conventional singlemode large-mode-area (LMA) fibers [1]. Implementation of fiber Bragg grating (FBG) arrays inscribed in MCFs by femtosecond laser pulses with high spatial resolution over transverse and longitudinal coordinates offers new opportunities in 3D shape sensing, as well as in new designs of fiber laser cavities [2].

Here we review our recent experimental and theoretical studies on the spatio-spectral control of CW and pulsed beams in multicore fibers either generated in laser cavities involving FBG arrays or just propagating in MCFs with uncoupled or weakly coupled cores.

The selective inscription of FBGs with individual parameters in different cores allows to control spatio-spectral characteristics of output beam in CW fiber lasers based on active MCFs (e.g. Yb-doped) pumped by laser diodes. The individual cores may generate independently delivering multiple uncoupled beams at different wavelengths defined by individual FBGs with broad total spectrum. However, separate core generation spectra collapse into a single narrow and stable line at strong optical coupling between the cores [3]. The developed model [4] shows that the collapsed spectrum linewidth depends on the number of cores, their coupling strength, geometric-mean reflection width of individual FBGs. It is revealed that physical mechanisms and quantitative features of linewidth broadening are defined by spatial-hole-burning and Kerr effects are sufficiently modified in comparison with single-core singlemode fiber lasers [1]. A performed comparison of the theory with experiment in the 7-core MCF demonstrates a fairly good correspondence of key characteristics, namely generation wavelength, spectrum shape and its linewidth value depending on power. An extreme linewidth narrowing is predicted for a high-power multicore fiber laser with greatly increased number of cores and their coupling strength. The same spectral behavior is observed at pulsed operation of the 7-core Yb-doped fiber laser obtained by intra-cavity AOM Q-switching [5], where maximum energy of microsecond pulses up to 15 μJ at 1 kHz repetition rate is achieved. The lasing spectrum is hybridized so that the laser line maxima of each core is nearly the same having a negligible spread relative to each other, which is much lower than the wavelength shifts between individual FBGs in the cores. At the same time, the generated power is nearly the same in all the cores. However, with increasing power beyond the SRS threshold, the spectra in the cores become more different and less stable and the output power becomes mainly concentrated in one of the cores, whereas the pulse shortens significantly to a sub-microsecond duration (300 ns). It should be noted that in a CW LD-pumped 4-core Yb-doped fiber with FBGs fs-inscribed in each core, where the core coupling is induced via strong bending, the fiber output power concentration in one core have also been observed [6].

Besides, the effect of spatiotemporal beam stirring between weakly coupled cores is observed for subnanosecond narrowband pulses of several kW peak power propagating in ~10 m long 7-core fiber [7]. In contrast to the low-power domain where the output power distribution in the cores is random with large fluctuations sensitive to fiber disturbances, at high power of the input pulse injected in the central core the output power becomes equalized between the cores with fluctuations reduced to <5% being insensitive to disturbances. Similar behavior is observed in cut-back experiments showing that equi-partition is approached at a distance of ~5 m. The performed modeling describes well the experimental results and clarifies mechanisms of the new effect caused by a large nonlinear phase shift changing along the pulse and thereby resulting in statistical averaging over the pulse length of multidirectional power transfer processes between cores, thus leading to the robust equilibrium. At the same time, the combined output beam measured in a far field takes a stable bell-shaped profile instead of speckled beam at low powers, similar to the beam self-cleaning effect in multimode fibers [8].

The details of these studies and potential application will be presented at the conference.

This work is supported by Russian Science Foundation (№21-72-30024-П).

[1] C. Jaregui, J. Limpert, & A. Tünnermann, High-power fibre lasers, Nature Photonics, vol. 7, pp. 861–867 (2013).
[2] A. Wolf, A. Dostovalov, K. Bronnikov, M. Skvortsov, S. Wabnitz, and S. Babin, Advances in femtosecond direct writing of fiber Bragg gratings in multicore fibers: technology, sensor and laser applications, Opto-Electronic Advances, vol. 5, 210055 (2022).
[3] A. G. Kuznetsov, A. A. Wolf, O.N. Egorova et al.. Spectrum collapse in a 7-core Yb-doped fiber laser with an array of fs-inscribed fiber Bragg gratings. Opt. Lett., vol.48, pp.3603-3606 (2023)..

[4] A.Yu. Kolesnikova, A.G. Kuznetsov, E.V. Podivilov, S.A. Babin. Spectrum collapse in a 7-core fiber laser with wavelength-shifted FBGs: modeling and comparison with experiment. High Power Laser Sci. and Eng., early posting https://doi.org/10.1017/hpl.2026.10157.
[5] A.G. Kuznetsov, A.V. Dostovalov, S.A. Babin. Q-switched pulse generation in a multicore fiber laser with femtosecond-laser inscribed FBG array. Photonics (in press).
[6] A. A. Wolf, M. I. Skvortsov, I. A. Lobach, A. V. Dostovalov, and S. A. Babin, Bending induced output power concentration in a core of a 4-core Yb-doped fiber laser, Opt. Exp., vol. 30, pp. 7580-7590 (2022).
[7] A.Y. Kolesnikova, M.D. Gervaziev, N.V. Bochkarev, D.S. Kharenko, E.V. Podivilov, S.A. Babin. Spatiotemporal beam stirring in a multicore fiber. Opto-Electronic Advances (in press).
[8] K. Krupa, A. Tonello, B.M. Shalaby et al. Spatial beam self-cleaning in multimode fibres. Nature Photonics vol.11, pp. 237-241 (2017).

# Phase transitions in spatio-temporal mode locking of multimode fiber laser

**K. Stefanska[1], V. Cecconi[1], K. Krupa[2], L. Zhou[1,3], J.A. Alvarez-Chavez[4], S.G. Murdoch[5,6], F. Mangini[7], S. Wabnitz[1,8]**

*1- Department of Information Engineering, Electronics and Telecommunications, Sapienza University of Rome, 00184 Rome, Italy*
*2- Institute of Physical Chemistry, Polish Academy of Sciences, 01-224 Warsaw, Poland*
*3- College of Communication Engineering, Jilin University, Changchun 130012, China*
*4- The Hague University of Applied Sciences, Lectoraat Fotonica, Rotterdamseweg 137, 2628AL Delft, The Netherlands*
*5- Department of Physics, University of Auckland, Auckland 1010, New Zealand*
*6- The Dodd-Walls Centre for Photonic and Quantum Technologies, Auckland, New Zealand*
*7- Department of Engineering, Niccolò Cusano University, Via Don Carlo Gnocchi 3, 00166 Rome, Italy*
*8- Novosibirsk State University, Pirogova 1, Novosibirsk 630090, Russia*

*stefan.wabnitz@uniroma1.it*

Passive mode-locked fiber lasers provide a reliable source of ultrashort pulses, making them essential tools in many applications. These pulses emerge as dissipative solitons, resulting from a balance between dispersion, nonlinearity, gain, and loss. Among the various passive mode-locking mechanisms, nonlinear polarization evolution (NPE) remains one of the most widely used. In parallel, multimode graded-index fibers (GIF) have attracted widespread research interest due to their unique nonlinear response, large mode area, and high damage threshold. Their low modal dispersion and periodic self-imaging enable rich a spatiotemporal dynamics.

The transitions between spatiotemporal mode-locking [1] (STML) and noise-like pulse (NLP) generation [2] in multimode fiber lasers—and the mechanisms governing them—have largely remained unexplored. In this talk, we present a systematic experimental study of these transitions in an Yb-doped multimode fiber laser. We show that intracavity spectral filtering drives the system from disordered NLP emission to stable STML, and that an optimal balance between chromatic and modal dispersion—tuned by adjusting the GIF length—maximises pulse compressibility. At the GIF length of 5.2 m, pulses are compressed to 170 fs. Numerical simulations validate this dispersion-balance picture. We further establish that Kerr spatial self-cleaning [3] at the output of the GIF ($M^2 \approx 1.5$) is a consequence of high peak powers, and is not a prerequisite for mode-locking.

Our results provide practical design guidelines for ultrashort-pulse multimode fiber sources [4]. Controllable switching between coherent STML and broadband NLP emission from a single cavity is directly relevant to optical coherence tomography, multiphoton imaging, and material processing, where temporal coherence, peak power, and beam quality must be tailored. More broadly, these results advance the understanding of multimode laser dynamics and open new avenues for spatiotemporal light engineering in fiber systems.

S.W. ackowledges support by the Russian Science Foundation (RSF) grant 25-72-31018.

[1] L. G. Wright, D. N. Christodoulides, and F. W. Wise, "Spatiotemporal mode-locking in multimode fiber lasers," Science 358, 94–97 (2017)
[2] Y. Meng, O. Ougrige, F. Bessin, et al., "Broadband noise-like pulses in fiber laser based on a filter," Appl. Phys. Lett. 124, 201104 (2024)
[3] K. Krupa, A. Tonello, B. M. Shalaby, et al., "Spatial beam self-cleaning in multimode fibres," Nat. Phot. 11, 237–241 (2017)
[4] K. Stefańska, V. Cecconi, K. Krupa, L. Zhou, J. A. Alvarez-Chavez, S. G. Murdoch, F. Mangini, and S. Wabnitz, «Transitions between mode-locked and noise-like pulsed states in a multimode fiber laser,» Opt. Lett. 51, 3229-3232 (2026)

# Direct Current Modulation of Power Semiconductor Lasers at High Frequency by Self-Oscillating Avalanche Diodes

**A.V. Rozkhov, P.B. Rodin**

*Ioffe Institute, 194021 St. Petersburg, Russia*

*rodin@mail.ioffe.ru*

Direct current modulation of lasers by short current pulse trains is widely used for formation of subnanosecond power lasers pulses. This method imposes strict requirements on a semiconductor driver that generates short current pulses at high repetition frequency, but allows one to use commercially available lasers instead of specially designed ones, as it is generally required when phase locking and Q-modulations methods are used. Here we demostrate experimentaly that direct high-frequency (2-2.4 GGz) modulation of laser radiation with peak power up to 5.5 W can be achieved by using a single self-oscillating avalanche diode as driver. These high-frequency limit cycle oscillations spontaneously appear in both GaAs and Si avalanche diodes [1]. Unlike the case of common IMPATT-diodes, such oscillations do not require external microwave resonantor [2].

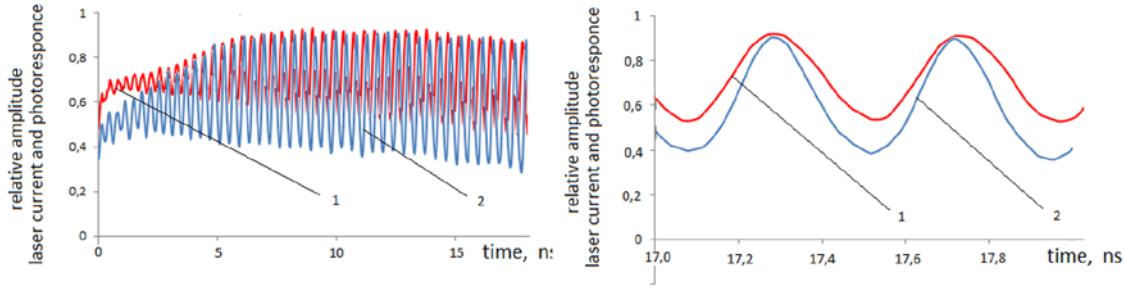


**Fig. 1.** Direct current modulation at 2.4 GHz: the current in the laser supply circuit (red curve1) and the photoresponce (blue line 2) in small (left panel) and enlarged (right panel) time scales.

The experimental setup includes GaAs diode, fabricated at Ioffe Institute, with limit-cycle oscillation frequency 2.4 GHz, diameter 500 μm and breakdown voltage 380 V connected in-series with SPLPL_90_3 commercially available laser (emission maximum at wavelength 905 nm) and 50 Ω load via coplanar microwave strip line. Quasi-rectangular reverse-polarity pulses with duration from 20 to 200 ns were applied to the input of this line at repetition frequency up to 10 kHz. GaAs photodiode served as laser radiation detector. The currents in the laser supply circuit and in the photodiode circuit were recorded simultaneously by Tektronix DPO 70404C digital dual-channel 4 GHz oscilloscope.

Fig.1 shows the respective oscilloscope records for a pulse duration of 20 ns. We observe deep high-frequency modulation of laser radiation in-phase with laser current. The half-width of the laser pulse was 180 ps at the repetition frequency 2.4 GHz. The relative photo response value and watt-ampere characteristic of SPLPL90_3 laser were used to evaluate the pulse power. Peak optical signal power of 5.5 W was achieved at current 2.0 A. Radiation power increased significantly under high frequency current pumping, presumably due to the resonance with laser relaxation oscillations frequency.

Combined with detector tuned to gigahertz carrier frequency, nanosecond trains of quasi-harmonic pulses may be used for laser ranging and detection as well as amplitude, phase and frequency modulation in combined radio-over-fiber communication lines. Due to the absence of external microwave resonator a low inductive stack assembly of the self-oscillating avalanche diode and semiconductor laser is possible. We compare our results with results achieved previously using bipolar transistors, *S*-diodes and HEMT GaN transistors (see [1] for respective references) as current drivers.

[1] A.V. Rozhkov, P.B. Rodin, Direct modulation of high-power semiconductor lasers by high-frequency limit-cycle oscillations in avalanche gallium arsenide diodes. Techn. Phys. Lett., vol.52, No 1, pp. 35 – 37 (2026).
[2] A.V. Rozhkov, M.S. Ivanov, P.B. Rodin, Self-excitation of the microwave-range auto-oscillations in avalanche GaAs, Techn. Phys. Lett., vol. 50, No 10, pp. pp. 91 – 94 (2024).

# III-N nanostructures on h-BN: From selective growth of AlN nanowires to InN quantum dots

**A.M. Dautov[1-4], P.A. Alekseev[5], M.E. Popov[5], K.P. Kotlyar[1-3], V.V. Lendyashova[1,2], Melnichenko I.A.[6], T. Shugabaev[1,2], G.E. Cirlin[1-3], V.O. Gridchin[1-3]**

*1 – Faculty of Physics, St. Petersburg State University, Universitetskaya Embankment 13B,199034 St. Petersburg, Russia*
*2 – Laboratory of epitaxial nanotechnologies, Alferov University, Khlopina 8/3, 194021 St. Petersburg, Russia*
*3 – Institute for Analytical Instrumentation of the Russian Academy of Sciences, Ulitsa Ivana Chernykh, 31-33, lit. A, St. Petersburg, Russia, 198095*
*4 – Moscow Centre for Advanced Studies, Kulakova St., 20, building 1, 123592, Moscow, Russia*
*5 – The Ioffe Physical-Technical Institute of the Russian Academy of Sciences, Polytekhnicheskaya st., 26, 194021, St. Petersburg, Russia*
*6 - HSE University, 20 Myasnitskaya Ulitsa, Moscow, 101000, Russia*

*amdautov24@gmail.com*

The use of two-dimensional materials such as hexagonal boron nitride (h-BN) for van der Waals epitaxy of III-N compounds (InN, GaN, AlN) overcomes the fundamental limitation of lattice mismatch, enables efficient elastic strain relaxation, and facilitates integration with silicon platforms. Owing to their direct band structure and the possibility of continuously tuning the band gap from 0.7 to 6eV, these materials are highly demanded in optoelectronics. Among the various quasi-low-dimensional structures, AlN nanowires (NWs) and InN quantum dots (QDs) are of particular interest [1]. However, the nucleation and evolution of such structures on h-BN surfaces remain poorly understood. In particular, the role of h-BN topography and the effect of preliminary surface nitridation on the density, size, and morphology of the nanostructures are still unclear.

Here, we report on experimental studies of AlN NWs and InN QDs grown on h-BN layers. The synthesis was performed in a Riber Compact 12 plasma-assisted molecular beam epitaxy system using h-BN flakes mechanically exfoliated onto $SiO_x$/Si(111) substrates. For the AlN growth series, an artificial topography in the form of geometric patterns was additionally created on the flake surface by probe-based friction lithography. The growth temperature (pyrometer readings with calibration correction) was set to 810–850 °C for AlN NWs and 335 °C for InN islands. All growth runs were conducted under N-rich conditions: 2 hours for AlN NWs and 15 to 120 seconds for InN islands. The morphology and crystalline quality were examined by scanning electron microscopy (SEM), atomic force microscopy (AFM), and Raman spectroscopy.

Based on the experimental series, we established correlations between the morphology of the resulting structures and the growth temperature for AlN NWs, and between the morphology and growth time for InN QDs. The characteristic geometric parameters of AlN NWs vary systematically with the growth temperature. Raman spectroscopy confirms the high crystalline quality of AlN NWs, as evidenced by a full width at half maximum of the $E_2$(high) mode as low as 4.38 $cm^{-1}$. The diameter of InN QDs (typical height h∼5 nm) exhibits a more nonlinear dependence on growth time, resulting in a broad size distribution ranging from a few to tens of nanometers.

A key finding is the decisive role of the h-BN surface topography in the formation mechanisms of III-N nanostructures. In particular, when the height of h-BN steps reaches about five monolayers, a growth-mode transition occurs – from isolated NWs to continuous nanowalls. Furthermore, we determined the influence of preliminary nitridation of the h-BN surface on the distribution density of InN islands, the nucleation probability across the surface, and the average island size.

The obtained results demonstrate the feasibility of controlled formation of AlN nanowires and InN quantum dots on h-BN, laying the groundwork for laser heterostructures on silicon. The topographic control provided by the h-BN surface further opens a pathway towards laser-patterned growth and on-chip integration of III-N laser sources.

The work was carried out with the support of the St.-Petersburg State University for a research project No. 116524353.

[1] Wu, Yuanpeng, et al. "Van der Waals quantum dots on layered hexagonal boron nitride." Proceedings of the National Academy of Sciences 122.9 (2025): e2417859122.

# Broadband 2 um Faraday Isolator

**A. Starobor, E. Mironov, O. Palashov**

*Federal Research Center A.V. Gaponov-Grekhov Institute of Applied Physics of the Russian Academy of Sciences (IAP RAS) 46 Ul'yanov Street, Nizhny Novgorod, 603951, Russia*

*astarobor@ipfran.ru*

The creation of broadband optical Faraday isolators for the 2 micron range is an urgent task of modern laser physics, which is associated with a wide range of applications of ultrashort or/and broadband lasers in this range. The range of 1.9–2.1 microns is actively being developed thanks to thulium (Tm) and holmium (Ho) lasers. These sources have high power (tens of watts) and are used in medicine (lithotripsy, soft tissue surgery), in material processing and as pumping for the mid-IR range. However, high-power lasers are extremely sensitive to back reflections (from the metal being welded, biological tissue, etc.). Without an isolator, the reverse wave destabilizes the frequency, generates spurious peaks, and physically destroys the pumping laser diode.

Commercial 2-um Faraday isolators (Fis) are mainly based on various iron garnets, which have relatively high absorption and are not suitable for use in high-power lasers. The mentioned obstacles have led to the attention of pure semiconductor materials as magnetic active media for FIs in the mid-infrared range. Their main advantage over media containing rare earth metal ions is that their absorption band is limited by interband transitions only in the short wavelength region and by phonon absorption in the long wavelength region. Another important feature of semiconductors is their ability to produce a Faraday effect that is comparable in magnitude to that associated with transitions between levels in rare earth metal ions [1].

Previously, it was proposed to use silicon (Si [2]) and zinc selenide (ZnSe [3]) to create FIs in the region of 2 microns. However, these media have a relatively low Verdet constant (15 rad/T/m and 7 rad/T/m at a wavelength of 1.94 um, respectively). We suggest using gallium arsenide (GaAs) as such a magnetooptical medium. It has a relatively high Verdet constant (23 rad/T/m @1.94 um), which makes it possible to use relatively compact magnetic systems. The transmission spectrum of the medium is very wide ~1-18 microns, where there are no absorption peaks, which makes it possible to implement broadband devices.

We have implemented an FI on GaAs with a Verdet dispersion compensator using crystalline quartz. The optimal rotation angle of this quartz rotator has been determined, as a result of which it is possible to implement a device with a working band of 1.8-2.05 micrometers, limited by coatings applied to optical elements and quartz transmission. With an available power of up to 10W, no thermal effects could be detected in the FI.

Thus, the presented approach is promising for creating powerful FIs in the mid-IR range.

Acknowledgements: This work was supported by Russian Science Foundation No. 23-12-00199-П (https://rscf.ru/en/project/23-12-00199-П).

[1]. E. A. Mironov, I. L. Snetkov, A. Starobor, and O. V. Palashov, "A perspective on Faraday isolators for advanced lasers," Appl. Phys. Lett. 122, (2023).
[2]. I. Snetkov and A. Yakovlev, "Faraday isolator based on crystalline silicon for 2-μm laser radiation," Opt. Lett. 47, 1895 (2022).
[3]. E. A. Mironov, O. V. Palashov, I. L. Snetkov, and S. S. Balabanov, "ZnSe-based Faraday isolator for high-power mid-IR lasers," Laser Phys. Lett. 17, 125801 (2020).

# The influence of Tm and Li concentrations on the spectroscopic, luminescent, laser, and EPR properties of Tm,Li:$ZnWO_4$ crystals

**Y. Zimina[1,2], K. Subbotin[1,2], D. Lis[1], A. Titov[1], A. Popov[3], V. Vazhenin[4], M. Artemov[4], A. Potapov[4], A. Fokin[4], P. Loiko[5], K. Eremeev[5], P. Volkov[5], V. Petrov[7], O. Lis[1]**

*1 - Prokhorov General Physics Institute RAS, 38 Vavilova St., Moscow, Russia*
*2- Mendeleev University of Chemical Technology of Russia, 9 Miusskaya Sq., Moscow, Russia*
*5 - Institute of Theoretical and Applied Electrodynamics RAS, 13 Izhorskaya St., Moscow, Russia*
*4 - Ural Federal University, 48 Kuybysheva St., Ekaterinburg, Russia*
*5- National Research Center «Kurchatov Institute» IREA, 1 Academician Kurchatov Square, Moscow, Russia*
*6 - Universit´e de Caen Normandie, 6 Boulevard Mar´echal Juin, Caen, Cedex 4, France*
*7- Max Born Institute for Nonlinear Optics and Short Pulse Spectroscopy, Max-Born-Str. 2a, Berlin, Germany*

*yulia_zimina@inbox.ru*

In recent years, monoclinic $ZnWO_4$ crystals doped with rare-earth ions have attracted considerable attention as promising active laser media for visible and infrared spectral ranges [1]. Here we report on the investigation of the spectroscopic, laser and EPR characteristics of Tm,Li:$ZnWO_4$ single crystals.

The series of Tm,Li:$ZnWO_4$ single crystals was grown by the Czochralski method in air using a Pt crucible. The actual concentrations of the dopants were determined by ICP-MS. It was shown that the introduction of $Li^+$ as a charge compensator raise the $Tm^{3+}$ segregation coefficient from 0.2 to 0.4.

Polarized optical absorption spectra of the crystals were measured at room temperature for all possible orientations of the electric and magnetic fields relative to the optical indicatrix axes (Fig. 1). The absorption bands are rather broad and smooth that is favorable for diode pumping of laser media. The influence of the lithium presence in the crystal on the shape of the absorption spectra was determined.

The emission spectra are also smooth and broad, extending beyond 2 μm (Fig. 2) due to relatively large total Stark splitting of the $Tm^{3+}$ ground-state, $\Delta E(^3H_6) = 644$ $cm^{-1}$. The luminescence lifetime of the $^3F_4$ level of $Tm^{3+}$ is 1.57 ms at 300K, the peak emission cross-section is $0.77\times10^{-20}$ $cm^2$ at 2015 nm for $E||N_p$ polarization.

The 2 μm CW laser operation was demonstrated at the sample with the actual concentration of $Tm^{3+}$ 1.6 at. % with a maximum output power of 282 mW and a slope efficiency of 14.7% (Fig. 3).

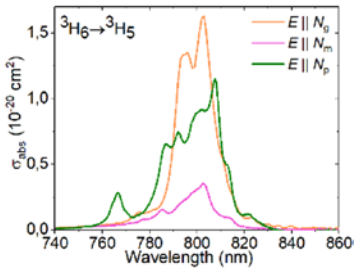


**Fig. 1.** Absorption cross-sections for the $^3H_6 \rightarrow ^3H_4$ transition of $Tm^{3+}$ in $ZnWO_4$

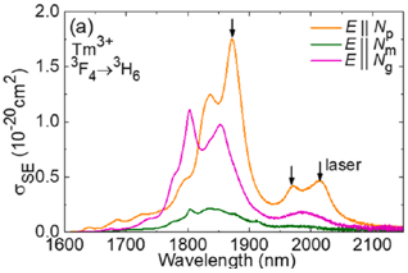


**Fig. 2.** Stimulated emission cross-sections for the $^3F_4 \rightarrow ^3H_6$ transition of $Tm^{3+}$ in $ZnWO_4$

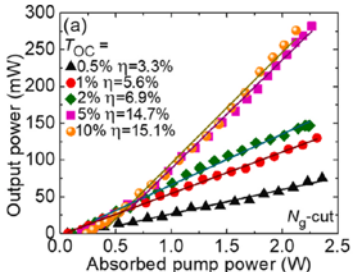


**Fig. 3.** Tm,Li:$ZnWO_4$ laser input-output dependences

The modest laser performance is caused by too low actual Tm concentration. The cross-relaxation ($^3H_4 \rightarrow ^3F_4$; $^3H_6 \rightarrow ^3F_4$) efficiency was calculated for this sample to be only 54%. To determine this value, the luminescence decay kinetics near 800 nm ($^3H_4 \rightarrow ^3H_6$) was measured 300 K. The efficiency of cross-relaxation in the sample with the highest achieved $Tm^{3+}$ concentration is 80%.

EPR spectra of accidental $Fe^{3+}$, $Cr^{3+}$, $Gd^{3+}$ and $Mn^{2+}$ impurities were detected at room temperature at the $ZnWO_4$ single crystal doped with Tm ions. The introduction of Li was found to suppress the formation of zinc-vacancy related centers. Instead, Tm-Li associates form.

The microhardness and fracture toughness of the crystals along the principal optical indicatrix axes were measured by the indentation method. It was shown that introduction of $Li^+$ into Tm,Li:$ZnWO_4$ crystal leads to improvement in mechanical strength characteristics due to disappearance of Zn vacancies.

[1] A. Volokitina, S. P. David, P. Loiko et. al., Monoclinic zinc monotungstate $Yb^{3+}$,$Li^+$:$ZnWO_4$: Part II. Polarized spectroscopy and laser operation, J. Lumin. 231, 117811 (2021).

# Optical and nonlinear optical properties of $TlFeS_2$ and $TlFeSe_2$ magnetic semiconductors: theory and experiment

**Z.I. Badalova[1], Z.A. Jahangirli[1,2], Yu.A. Abdullayev[1], S.S. Ragimov[2,1], Kh. A. Hidiyev[1], T. G. Mammadov[1], N.A. Abdullayev[1,2]**

*1- Institute of Physics of the Ministry of Science and Education, H. Javid av., 131, AZ1073, Baku, Azerbaijan*
*2- Baku State University, Z. Xalilov str., 33, AZ1148, Baku, Azerbaijan*

*zibchik1964@gmail.com*

Despite extensive research on the magnetic properties of $TlFeS_2$ and $TlFeSe_2$ crystals, there is virtually no data in the literature on the optical properties of $TlFeS_2$ and $TlFeSe_2$ crystals. This article presents the results of an experimental and theoretical study of the optical properties of $TlFeS_2$ and $TlFeSe_2$ compounds. Spectral ellipsometry, a precise (exact) method for determining the optical characteristics of crystals, was used for the experimental studies.

The spectral dependences of the optical conductivity and reflectivity of TlFeS2 and TlFeSe2 crystals were studied experimentally using spectral ellipsometry, as well as theoretically from first principles using density functional theory (DFT).

Good agreement was obtained between the experimentally obtained spectral dependences of the real and imaginary parts of the optical conductivity (Fig. 1), as well as the refractive index, extinction, and absorption coefficients, and the calculated results. An estimate of the band gap width $E_g$ of $TlFeS_2$ crystals from experimental data yields a value of ~1 eV (Fig. 1a), and from theoretical calculations from first principles, ~1.1 eV (Fig. 1b), while in $TlFeSe_2$ - $E_g$ is equal to ~0.7 and 0.9 eV, respectively.

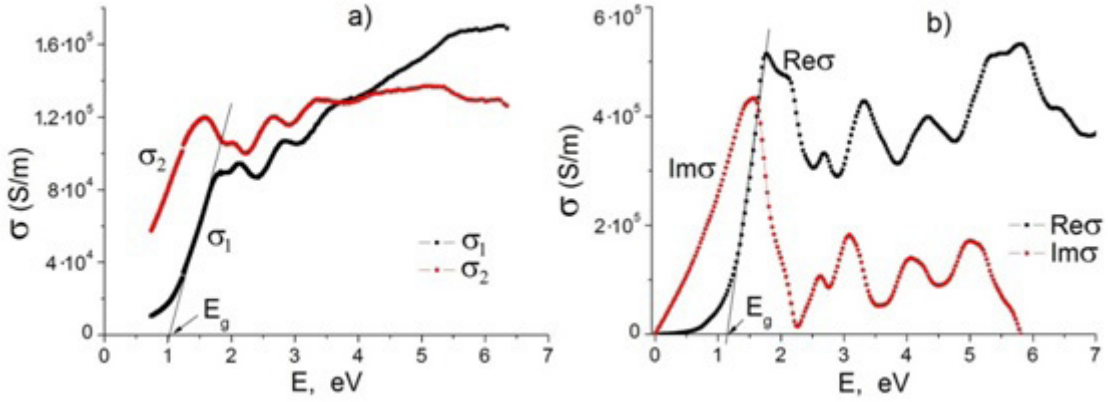


**Fig. 1.** Spectral dependences of the components of the complex optical conductivity of $TlFeS_2$ crystals, calculated experimentally (σ1, σ2) from ellipsometry data (a) and theoretically (Reσ, Imσ) from first principles (b)

Changes in the absorption coefficient and skin depth of the crystal as a function of energy were studied, and the plasma frequency and carrier density-to-effective mass ratio in $TlFeS_2$ and $TlFeSe_2$ crystals were estimated. Using the single-effective-oscillator model, the single-oscillator energy $E_{SO}$ and the dispersion energy $E_d$ in $TlFeS_2$ and $TlFeSe_2$ crystals were calculated. Taking into account the experimentally determined static value of the refractive index of the crystal $n_0$ = 2.45 for the TlFeS2 crystal and $n_0$=2.95 for the $TlFeSe_2$ crystal, the values of the nonlinear refractive index $n_2$, nonlinear susceptibilities of the first $\chi^{(1)}$ and third order $\chi^{(3)}$ were calculated, which turned out to be equal to $6.8x10^{-11}$ esu, 0.4 esu, $4.4x10^{-12}$ esu for the TlFeS2 crystal, and $3.1x10^{-10}$ esu, 0.61 esu, $2.4x10^{-11}$ esu, respectively, indicating the prospects for integrating the compound into various nonlinear optical systems.

# Ultraviolet Luminescence of Crystals and Nanoceramics of $CaF_2$–$SrF_2$:$YbF_3$ Solid Solutions

**M.Kh. Ashurov, I. Nuritdinov, S.T. Boyboboeva**

*Institute of Nuclear Physics of the Academy of Sciences of the Republic of Uzbekistan,*

*izzatilloh@yahoo.com; sohibaboyboboeva@gmail.com*

Fluoride materials based on $CaF_2$, doped with ytterbium ions, are of considerable interest for optoelectronic and scintillation applications due to their low phonon energy and high quantum efficiency of luminescence [1,2]. Ultraviolet emission in these systems arises from the $4f^{14} \rightarrow 4f^{13}5d$ transitions of $Yb^{2+}$ ions, which are highly sensitive to the local crystal field and the defect structure of the lattice [3,4].

In this work, the photoluminescence of single crystals and nanoceramics of $CaF_2$–$SrF_2$:$YbF_3$ solid solutions was investigated at room temperature. Under excitation in the 230–240 nm range, a broad emission band is observed in the 200–450 nm region, resulting from the superposition of several components associated with different types of Yb-related centers. The main contribution to the spectrum arises from isolated centers (≈290–320 nm), $Yb^{2+}$ centers with a distorted local environment (≈320–380 nm), and paired $Yb^{2+}$–$Yb^{3+}$ centers (≈400–430 nm) [4].

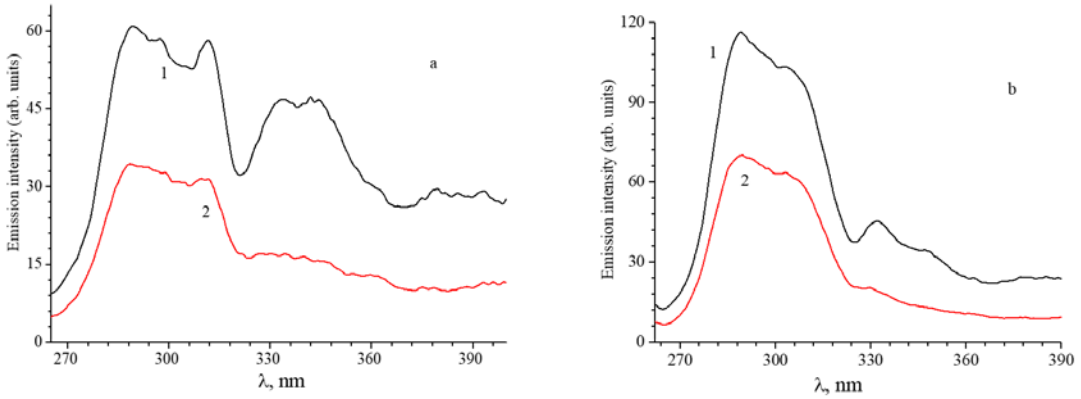


**Fig. 1.** Luminescence spectra of an unirradiated $CaF_2$:$SrF_2$:$YbF_3$ crystal (1) and nanoceramic (2) at room temperature under excitation at 230 nm (a) and 242 nm (b).

Comparative analysis shows that the shapes of the luminescence spectra for the crystals and nanoceramics are nearly identical, indicating a common nature of the emitting centers. However, the luminescence intensity in the nanoceramics is significantly lower, particularly in the 330–360 nm region. This reduction is attributed to the presence of grain boundaries, a higher defect density, and enhanced nonradiative processes typical of condensed media with a developed defect structure [3]. A comparison with the $CaF_2$:$YbF_3$ system indicates that the incorporation of $Sr^{2+}$ leads to modifications of the lattice parameter and the local crystal field, resulting in shifts of the excitation bands and a redistribution of luminescence intensity, in agreement with the experimental data [5]. Furthermore, in $CaF_2$–$SrF_2$:$YbF_3$ solid solutions, the effect of concentration quenching—characteristic of $CaF_2$:$YbF_3$ at high ytterbium concentrations—is reduced. This behavior is attributed to a more uniform distribution of $Yb^{3+}$ ions and a lower probability of cluster center formation [3].

Thus, the ultraviolet luminescence in the $CaF_2$–$SrF_2$:$YbF_3$ system is governed by the contributions of different types of $Yb^{2+}$ centers and is strongly dependent on the material's microstructure. Matrix modification through the incorporation of $SrF_2$ enables effective control over energy transfer processes and suppresses concentration quenching, making these materials promising for ultraviolet-emitting and scintillation applications.

[1] Henderson B., Imbusch G.F. Optical Spectroscopy of Inorganic Solids. Oxford, 2006.
[2] Payne S.A. et al. Yb-doped laser materials // IEEE J. Quantum Electron., 1992.
[3] Dorenbos P. 5d-level energies of lanthanides in inorganic compounds// J. Lumin., 2000.
[4] McClure D.S. Optical spectra of rare earth ions // J. Chem. Phys., 1959.
[5] M.Kh. Ashurov et al. Luminescence of $CaF_2$:$YbF_3$ and the effect of $YbF_3$ concentration. // Application of Nanoscale Systems in Modern Semiconductor Microelectronics and Photovoltaics, Andijan, 2025.

# Hybrid MOPA Source of Femtosecond Pulses with Spectrum Optimization of a Chirped Fiber Bragg Grating Stretcher

**A.S. Burkov[1], N.V. Tereshchenko[2], I.V. Obronov[2], D.V. Myasnikov[2]**

*1- Moscow Institute of Physics and Technology, Institutskiy pereulok 9, Dolgoprudny, Russia*
*2- VPG Laserone, Vvedenskogo sq. 1, Fryazino, Moscow Region, Russia*

*burkov.as@phystech.edu*

The aim of this study is to develop a hybrid fiber-solid-state laser source with high peak power utilizing chirped pulse amplification (CPA). This work focuses on optimizing the parameters of a stretcher based on a chirped fiber Bragg grating (CFBG) for optimal pulse compression after amplification in a Yb:YAG crystal.

A fiber stretcher based on a chirped fiber Bragg grating was inscribed. A key feature is that the grating was designed and used in the normal dispersion regime rather than the anomalous one. During such radiation propagation, the spectrum becomes distorted due to losses. This was mitigated by adjusting the inscription parameters: the study showed that reducing the stretcher's reflection coefficient, along with modifying the beam focusing ratio and exposure, minimizes spectral distortion. To achieve a shorter pulse, the grating was inscribed with a broader spectral width, a shifted central wavelength, and a spectral filter was used in the CPA scheme to select the flattest part of the spectrum. This allows obtaining a shorter pulse compared to a distorted spectrum. The optimal spectral width, considering the spectral shape features, was determined based on modeling the entire CPA scheme.

After stretching and pre-amplification in the fiber amplifier, the signal was amplified in the Yb:YAG crystal. The output pulse duration was measured using an autocorrelator. The autocorrelation function is shown in Fig. 1. As a result, an average power of 35 W was achieved at a repetition rate of 400 kHz, with a pulse duration of 700 fs, corresponding to a peak power of 125 MW.

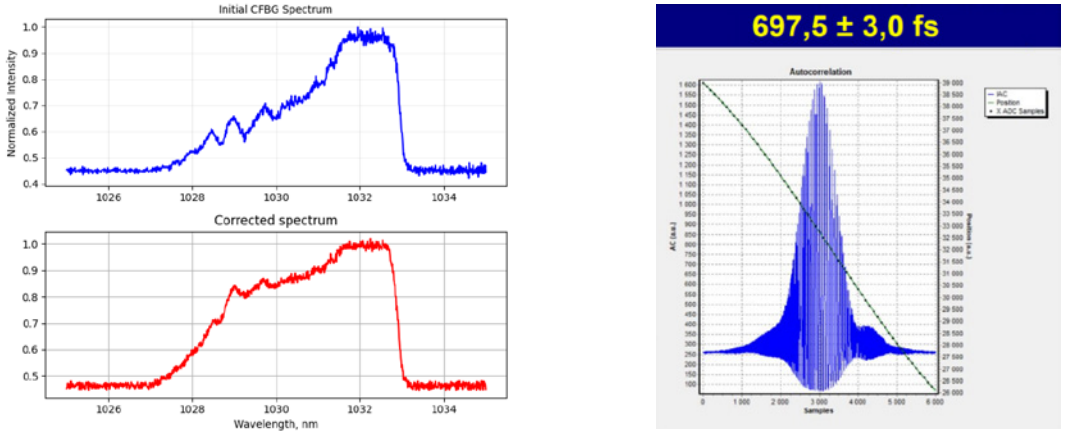


a) b)

**Fig. 1.** a) CFBG spectrum before and after distortion correction, b) autocorellation function.

[1] S. Lei, X. Zhao, X. Yu, A. Hu, S. Vukelic, M. B. G. Jun, H. E. Joe, Y. L. Yao, and Y. C. Shin., Ultrafast laser applications in manufacturing processes: a state-of-the-art review, Journal of Manufacturing Science and Engineering, vol. 142, pp. 031005, (2020).
[2] G. Huber, C. Kränkel, and K. Petermann, Solid-state lasers: status and future, Journal of the Optical Society of America B, vol. 27, pp. B93-B105, (2010).

# Numerical Modeling of Kerr-Enhanced Raman Beam Cleaning in a Short Multimode GRIN Fiber

**O.S. Sidelnikov[1], E.V. Podivilov[2], S.A. Babin[2], M.P. Fedoruk[1]**

*1- Novosibirsk State University, 2 Pirogova str., Novosibirsk 630090, Russia*
*2- Institute of Automation and Electrometry SB RAS, 1 Ac. Koptyug ave., Novosibirsk 630090, Russia*

*o.sidelnikov@g.nsu.ru*

Beam cleaning in multimode graded-index (GRIN) fibers has attracted considerable attention over the last decade due to its ability to transform low-brightness multimode radiation into high-brightness laser emission. While Kerr self-cleaning and Raman beam-cleaning phenomena have been extensively studied in multimode fibers [1], the interplay between Kerr nonlinearity, stimulated Raman scattering and cavity mode selection in short multimode Raman lasers remains insufficiently explored.

In this work, we numerically study stimulated Raman scattering and beam cleaning in a 110-m-long GRIN fiber using a coupled-mode model derived from the multimode nonlinear Schrödinger equation [2]. The model includes Raman gain, Kerr nonlinearity, fiber losses, and random linear mode coupling, caused be fiber imperfections. To reproduce the experimental cavity configuration, a multi-pass simulation scheme was employed. The fiber Bragg grating was modeled as a mode-selective spatial filter providing stronger feedback for the fundamental mode than for higher-order modes. After each cavity round trip, the resulting Stokes field was used as the input for the next pass, while the results were averaged over multiple realizations of random modal phases.

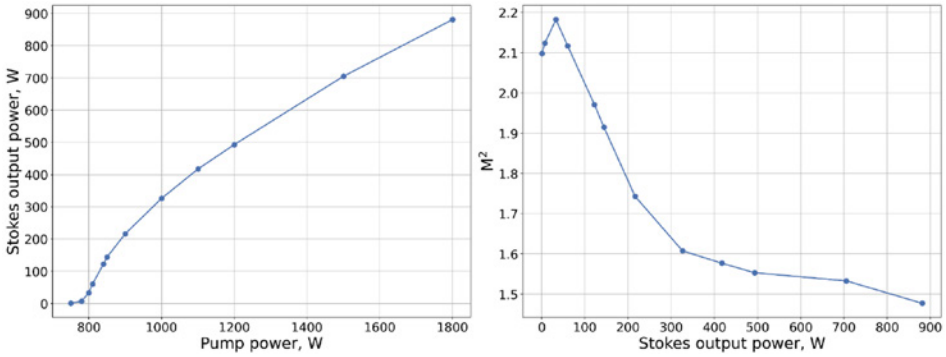


**Fig. 1.** The output Stokes as a function of the initial pump power (left) and the M2 of the Stokes beam as a function of the output Stokes beam power (right).

Fig. 1 (left) shows the dependence of the output Stokes power on the pump power. The calculated Raman threshold is approximately 750 W, and the Stokes power reaches nearly 900 W at the highest pump level considered. Fig. 1 (right) presents the evolution of the beam quality parameter $M^2$. As the Stokes power increases, $M^2$ decreases from 2.15 to 1.48, demonstrating efficient nonlinear beam cleaning in the multimode cavity. In addition to the improvement of the beam quality factor, the simulations reveal a progressive redistribution of optical power toward low-order spatial modes. As the Stokes power increases, the combined action of Raman amplification and Kerr nonlinearity promotes concentration of power in the fundamental mode, indicating that nonlinear beam cleaning becomes the dominant mechanism governing the spatial dynamics of the Raman field.

The obtained results are in good qualitative agreement with experimental observations and confirm that the combined action of Kerr nonlinearity, Raman amplification, and mode-selective cavity feedback leads to progressive concentration of optical power in the fundamental mode.

This research was supported the Russian Science Foundation (grant no. 25-61-00010, https://rscf.ru/project/25-61-00010/)

[1] K. Krupa et al., Spatial beam self-cleaning in multimode fibres, Nature Photon, vol. 11(4), pp. 237-241 (2017).
[2] O.S. Sidelnikov et al., Transverse mode distribution in multimode diode-pumped Raman fiber laser, J. Opt. Soc. Am. B, vol. 40(12), pp. 3269-3275 (2023).

# Fast Sixth-Order Padé Schemes Based on the Joukowski Transform and Chebyshev Polynomials for the Direct Zakharov–Shabat Problem

**I. Chekhovskoy, S. Medvedev, I. Vaseva, M. Fedoruk**

*1- Federal Research Center for Information and Computational Technologies, 6 Lavrentyev Ave., Novosibirsk, 630090, Russia*
*2- Novosibirsk State University, 1 Pirogova St., Novosibirsk, 630090, Russia*

*mifester@gmail.com*

The direct Zakharov–Shabat spectral problem is a basic computational step of the nonlinear Fourier transform (NFT). In optical applications, it is often necessary to compute the scattering coefficients for a large number of real spectral parameters. This motivates high-order schemes that have a rational or polynomial structure and therefore admit fast multiplication algorithms.

Previously, fast sixth-order schemes were constructed using rational Padé approximations together with a generalized Cayley transform [1]. These schemes provide high accuracy and efficient computation of the continuous spectrum. However, the Cayley-type mapping is adapted to the whole real spectral axis, while in practical computations the spectrum is usually evaluated only on a finite interval. For relatively coarse grids this parametrization may become poorly balanced, and the numerical evaluation of the scattering coefficients may lose robustness.

We propose fast sixth-order exponential schemes (ES6) with Padé approximants for matrix exponential computation based on the Joukowsky transform and Chebyshev polynomial representation. The spectral parameter is restricted to a finite interval and written as $\zeta=c+Hx$, $x\epsilon[-1,1]$. The Joukowski transform $x=(w+w^{-1})/2$ maps the unit circle to this interval. Instead of explicitly working with Laurent polynomials in , we represent the local matrix numerators and scalar denominators directly in the Chebyshev basis. This avoids artificial doubling of the local polynomial degree and preserves a compact representation of the transition matrices.

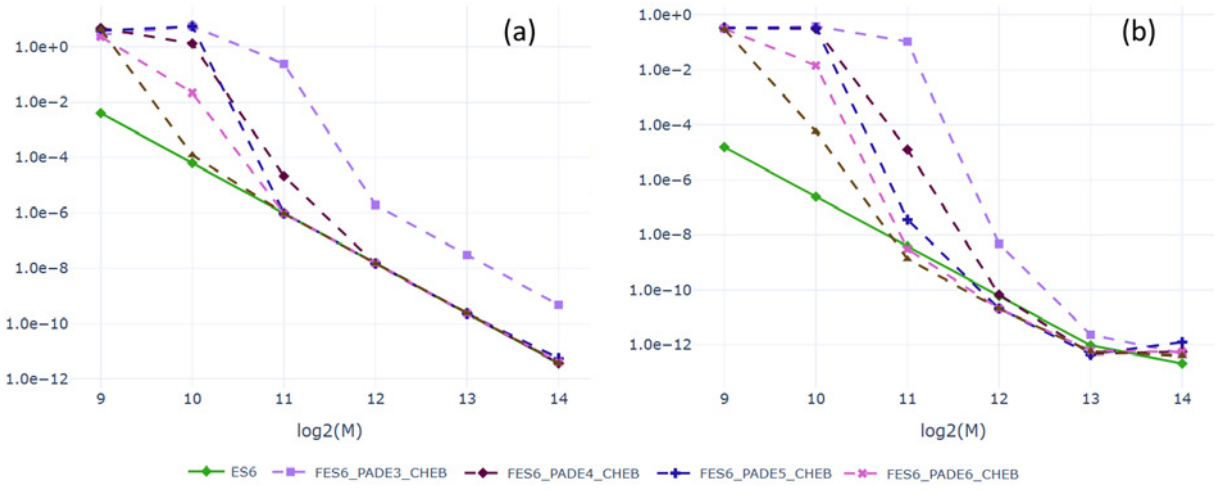


**Fig. 1.** Normalized mean square errors of the scattering coefficients: (a) $a(\xi)$ and (b) $b(\xi)$ for the chirped hyperbolic secant potential.

For each grid node, the local transition matrix is written as $T_n(x)=N_n(x)/d_n(x)$, where $N_n(x)$ and $d_n(x)$ are expanded in Chebyshev polynomials. The global transfer matrix is obtained by a product tree for matrix numerators and scalar denominators, keeping the complexity $O(N \log^2 N)$ with respect to the number of samples of the potential. Numerical tests for a chirped hyperbolic secant potential show regular convergence of the proposed schemes. The error in $b(\xi)$ decreases very stably and reaches the level of $10^{-12}$-$10^{-13}$ on refined grids; the error in $a(\xi)$ is more sensitive on coarse grids, but the best schemes also reach a near-machine-accuracy plateau after refinement.

[1] S. Medvedev, I. Chekhovskoy, I. Vaseva, M. Fedoruk, Fast sixth-order algorithm based on the generalized Cayley transform for the Zakharov-Shabat system associated with nonlinear Schrodinger equation, Journal of Computational Physics, vol. 448, 110764, (2022).
[2] S. Wahls and H. V. Poor, Fast numerical nonlinear Fourier transforms, IEEE Transactions on Information Theory, vol. 61, pp. 6957-6974, (2015).

# Spectroscopy of chromium ions in high temperature diffusion doped ferroelectric thin films

**M. Doroshenko[1], I. Voronina[1], A. Tumarkin[2], L. Ivleva[1]**

*1-Prokhorov General Physics Institute of the Russian Academy of Sciences, Moscow 119991, Russia*
*2- Saint Petersburg Electrotechnical University "LETI", Saint Petersburg 197022, Russia*

*ivleva@lst.gpi.ru*

Functional oxide materials doped with TM or RE ions can be considered as multifunctional systems, which combine light emission with other intrinsic properties such as ferroelectricity, piezoelectricity, and electro-optic properties. Much attention is currently paid to the processes of doping thin films in order to improve their functional properties or to obtain structures with new ones. In our work we demonstrate the luminescence of chromium-doped thin ferroelectric films: barium stannate-titanate (BSnT), strontium -barium niobate (SBN:75) and strontium titanate (STO). All films were grown on poly or single crystal alumina substrates using RF magnetron sputtering method and then successfully doped with chromium ions by a newly developed high-temperature diffusion technique from chromium oxide powder. Room temperature absorption, fluorescence and excitation spectra as well as decay curves of chromium ions in diffusion doped thin films were measured. Elemental analysis of the samples investigated shows that the distribution of chromium ions in the doped thin films is nearly uniform with the concentration of about 12 at% in BaSn0.2Ti0.8O3:Cr/ alumina composite; 8 at% in Sr0.75Ba0.25Nb2O6:Cr/ alumina composite; or 5 at% in SrTiO3:Cr film on sapphire substrate. Fluorescence and excitation spectra of chromium ions were measured at room temperature under selective short pulse laser excitation using time-resolved technique. Experimental results have shown that chromium ions in all types of thin films demonstrate a set of quite different spectroscopic properties. These wide variation of properties was attributed not only to the fact that chromium ions are incorporated in thin films in different valence state but also to their trend to occupy positions with different local symmetry. It should be noted that absorption and fluorescence lines characteristic for $Cr^{3+}$ ions in octahedral and $Cr^{4+}$ ions in tetrahedral coordination were detected in all types of thin films despite the fact that $SrTiO_3$ initially does not have positions with tetrahedral local symmetry. In BSnT film additionally chromium ions in 5+ valence state were also revealed. It was also noticed that in case of polycrystalline substrate a part of chromium ions can incorporate also into such substrate via diffusion doping process. Narrow fluorescence lines attributed in literature to R and N-lines of $Cr^{3+}$ ions in $Al_2O_3$ were observed in this case.

In the report results of thorough measurements of chromium ions spectroscopic properties will be presented. Influences of surface effects and structure peculiarities of thin ferroelectric films on chromium ions properties will be analyzed. Probable reciprocal effect of chromium ions diffusion doping on thin films composition will be discussed.

# Investigation of non-stoichiometry of ZnS for mid-IR lasers

**K. Kim, M. Zykova, E. Mozhevitina, E. Voronina, I. Avetissov**

*Mendeleev University of Chemical Technology of Russia,*
*125047, Moscow, Miusskaya Square, 9, Russia*

*karina.kim.2002@inbox.ru*

Zinc sulfide (ZnS) is a promising optical material for mid-infrared laser systems, particularly for ZnS doped $Cr^{2+}$ and $Fe^{2+}$ lasers operating in the 2–3 μm spectral range [1]. The optical and luminescent properties of ZnS crystals are largely determined by the type and concentration of structural defects. Therefore, the investigation and control of structural defects are important factor in producing high-optical-quality ZnS crystals [2].

This work presents the results of a study of bivariant equilibria on the sulfur-excess in ZnS samples at temperatures of 1173 K and 1223 K, using the "high-temperature equilibrium quenching method" (Fig. 1a). The purity of the ZnS preparation was studied using inductively coupled plasma mass spectrometry (ICP-MS) (Nexion 300D, Perkin Elmer Inc, USA). It was composed 99.999 wt.%.

The study of the concentrations of excess component by the "extraction" method (Fig. 1, b) annealing temperature of 923 K by extracting the superstoichiometric component to the "cold" end of ampoule. The analysis of excess sulfur was carried out by ICP-MS.

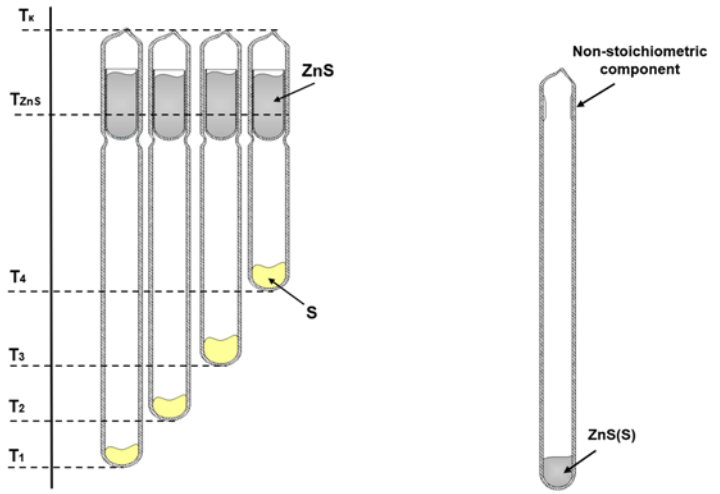


**Fig. 1** Picture of ampoules a) for the synthesis of non-stoichiometric ZnS preparations under conditions of bivariate equilibria; b) for the "extraction" method

Solubility isotherms of excess sulfur in zinc sulfide at 1173 and 1223 K were constructed based on the obtained experimental data. Luminescence spectra of stoichiometric and nonstoichiometric samples were obtained. It is assumed that defects form in the ZnS structure during synthesis in sulfur vapor.

This research was funded by the Ministry of Science and Higher Education of Russia through the project FSSM-2025-0006. The authors are grateful to the National Analytic Certification Laboratory of Mendeleev Center of D. Mendeleev University of Chemical Technology of Russia for the ICP-MS measurements.

[1] E. F. Kustov and I. S. Kurchatov, Investigation of spectral and luminescent characteristics of IR (1.5–3 μm) lasers based on AIIBVI semiconductors doped with $Fe^{2+}$, $Co^{2+}$ and $Ni^{2+}$ ions, Alternative Energy and Ecology (ISJAEE), no. 10–11, pp. 174–175, (2015).
[2] N. K. Morozova and V. A. Kuznetsov, Zinc Sulfide: Synthesis and Optical Properties, Nauka, 199 pp., (1987).

# Paratellurite crystals growth and their application in photonics

**A.E. Kokh, V.S. Shevchenko, D.A. Kokh**

*Sobolev Institute of Geology and Mineralogy Siberian Branch Russian Academy of Sciences*
*630090, Novosibirsk, Akad. Koptyug pr., 3, Russia*

*a.e.kokh@igm.nsc.ru*

Paratellurite ($TeO_2$) is one of the most well-known acousto-optic materials. Paratellurite crystals grown from melt by the Czochralski method at vertical temperature gradients of approximately 10°C/cm are characterized by a relatively high dislocation density (at a level of $10^3$-$10^4$ $cm^{-2}$ or more) and significant residual thermoelastic stresses, characterized by induced optical biaxiality, especially in the peripheral regions of the crystals. Typically, only the central regions of such high-gradient crystals are used in acousto-optic devices. These crystals lack external faceting and have a nearly cylindrical shape in cross-section perpendicular to the growth axis.

Growth of $TeO_2$ crystals by the Czochralski method under low-gradient thermal conditions (1-2 deg/cm) in the [110] direction allows for the production of partially faceted crystals with low residual thermoelastic stresses. The horizontal cross-section of the crystals becomes polygonal with tetragonal prismatic {110} faces appearing on the lateral surface of the boules. A photograph of such a crystal, weighing 1616 g, is shown below.

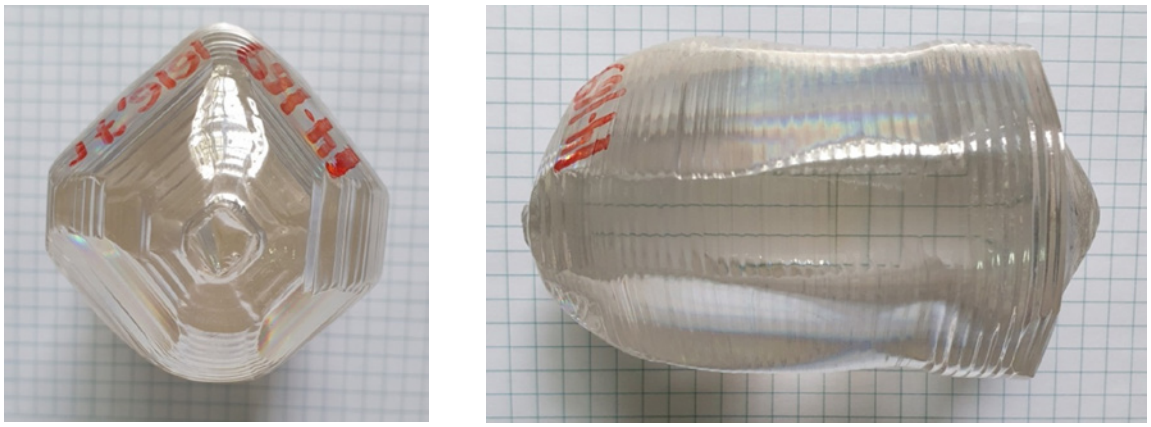

**Fig.** Paratellurite crystal weighing 1616 g: top view (left); side view (right)

A specific feature of low-gradient crystals is the presence of noticeable scattering of the laser beam at wavelengths of 532 and 633 nm. The formation of scattering centers is likely associated with the layer-by-layer crystallization mechanism at low temperature gradients. Nevertheless, the high structural perfection of low-gradient crystals has enabled their application in linear optics in the IR range as a highly birefringent material for the fabrication of Glan prisms and others. Such crystals are also finding application in acousto-optics [1].

Work is done on state assignment of IGM SB RAS (№ FWZN-2026-0005).

[1] V.Ya. Molchanov, Yu.I. Kitaev, A.I. Kolesnikov, et al., Theory and Practice of Modern Acousto-Optics (Moscow: MISiS), 459 p., (2015).

# Features of measuring the optical properties of dielectric ionic crystals taking into account gyrotropy

**N. Kozlova, E. Zabelina**

*National University of Science and Technology «MISIS», 119049, Russia, Moscow, Leninsky pr., 4, b. 1*

*kozlova_nina@mail.ru*

The group of dielectric ion crystals is currently actively used for the development and creation of electro-optical devices with active elements from these crystals. However, such materials possess the property of rotating the plane of polarization or natural optical activity (gyrotropy). These properties are not always immediately visible and their nature can not be immediately understood. All these properties are directly related to the structure and the presence of structural point defects that have arisen during crystal growth. At the same time, growth defects significantly affect the properties and technological parameters of crystals, which is poorly noticed and presented in publications. Rotation of the plane of polarization or optical activity is the ability of certain substances to rotate the plane of polarization when light passes through them. Optical activity can be detected only by measurements, and it occupies a special place among the physical properties of substances, including optical single crystals. There is a need to quantify such properties as optical activity values (gyration coefficients). It is very important to study their dispersions. Otherwise, it is possible to obtain inadequate results or misunderstand them. This leads to major errors in the development and manufacture of products, elements for electronic and microelectronic technology. [1] The coefficients of gyration strongly depend on the crystal structure. Currently, experimental results have been investigated and obtained for more than 100 crystalline materials. [2]

The lithium iodate α-$LiIO_3$ crystal of hexagonal modification, which has been studied quite well in our laboratory, has a record rotation of the polarization plane. Its coefficient of gyration varies from ρ = 1052.9 degrees/mm at λ = 0.286 μm to ρ = 489.47 degrees/mm at λ = 0.339 μm, and ρ =95.27 degrees/mm at λ = 0.600 μm. [2, 3]

In the last decade, significant improvements have been achieved in the optical quality of crystals of the langasite group: lanthanum-gallium silicate $La_3Ga_5SiO_{14}$ (LGS), lanthanum-gallium tantalate $La_3Ga_{5.5}Ta_{0.5}O_{14}$ (LGT) and calcium-gallotantalate silicate $Ca_3TaGa_3Si_2O_{14}$ (CTGS). In the work [4] the results of studies of the gyrotropic properties of these crystals are presented. The gyration coefficients of these crystals at λ = 0.630 μm are: for LGS, ρ = 3.0 deg/mm, for LGT ρ = 15.0 deg/mm and for CTGS, ρ =29.0 deg/mm. These results indicate that even with similar structures, the coefficients of gyration can vary significantly. This depends on elemental composition. All this makes it possible to consider these crystals as nonlinear crystals for tunable lasers, matrices for doping with rare earth elements, a material for generating optical harmonics, as well as scintillation crystals as a material for quantum and nonlinear optics, but it is necessary to first evaluate the contribution of gyrotropy to the measured values.

The studies were carried out in the accredited testing laboratory «Single crystals and stock on their base» NUST MISIS with financial support from the Ministry of Education and Science of Russia within the framework of the state assignment to Universities FSME-2023-0003.

[1] N.S. Kozlova, E.V. Zabelina, V.M. Kasimova, Features of Testing and Monitoring Optical Qualities of Dielectric Single Crystals, Measurement Standards. Reference Materials, vol. 21, pp. 72-85, (2025).

[2] V.A.Kizel, V.I.Burkov, Gyrotropy of crystals (Moscow, Nauka), 1980.

[3] E.V. Zabelina, R. Shahin, N.S. Kozlova, V. M. Kasimova, Determination of the polarization plane specific rotation in gyrotropic crystals of the middle category by the spectrophotometric method. Russian Microelectronics, 52(8), 757-763, (2023).

[4] E.V. Zabelina, N.S. Kozlova, O.A. Buzanov, Optical properties of crystals of the langasite family: $La_3Ga_5SiO_{14}$, $La_3Ga_{5.5}Ta_{0.5}O_{14}$, $Ca_3TaGa_3Si_2O_{14}$.Optics and Spectroscopy, vol. 131, pp. 634-641, (2023).

# Suppression of thermal effects in composite optical elements by using a thin layer of adhesive

**D.A. Kuzin, A.V. Starobor, I.I. Kuznetsov, O.V. Palashov**

*Federal Research Center A.V. Gaponov-Grekhov Institute of Applied Physics of the Russian Academy of Sciences (IAP RAS), 46 Ul'yanov Street, Nizhny Novgorod, 603950, Russia*

*d.kuzin@ipfran.ru*

Composite optical elements hold a firm position in modern laser engineering practice. Composite optical elements occupy a firm position in contemporary laser engineering practice. They enable mitigation of parasitic thermal effects (thermal lensing, thermally induced birefringence, depolarization [1]) and the amplified spontaneous emission effect [2], which hinder energy scaling in solid-state lasers. Several fundamentally different methods are used to assemble composite optical elements, such as diffusion bonding [3], surface-activated bonding (direct optical contact) [4], and the use of optical adhesive materials. Diffusion bonding and direct optical contact offer significant advantages, including negligible influence on radiation transmitted through the joint and on heat transfer; however, they are complex to manufacture, impose high requirements on the quality of the mating surfaces, and are costly. Contacting dissimilar elements is also problematic, especially when heating is required. Differences in coefficients of thermal expansion then produce mechanical stresses on cooling, which degrade the transmitted beam quality.

Optical adhesive, in turn, does not require the same high polish quality of the surfaces as diffusion bonding or optical contact, which makes production of composite elements considerably faster and cheaper. For this reason, photo-curable adhesives remain relevant for the manufacture of active laser elements (AE) and magneto-optical elements (MOE) for Faraday isolators. However, adhesives have a number of significant drawbacks: they affect heat transfer from the AE/MOE to the heatsink (the thermal resistance of the adhesive layer depends directly on its thickness), and the refractive index of most adhesives is lower than that of the commonly used AE materials for solid-state lasers, which leads to reflection of amplified spontaneous emission back into the element and increased losses. To overcome these shortcomings, precise control of the adhesive-layer thickness at the subwavelength level is required. This approach minimizes thermal resistance and suppresses parasitic reflections while preserving the technological simplicity of adhesive assembly.

We developed a method to control the adhesive-layer thickness in the range 0.1–1 μm by exploiting the effect of frustrated total internal reflection [5]. We demonstrate the feasibility of producing subwavelength adhesive layers (100–300 nm) that allow effective removal of heat and amplified spontaneous emission through them. Measurements of thermally induced depolarization in test composites indicate no measurable absorption in the adhesive layers and no mechanical stresses introduced by bonding. The adhesive withstands continuous-wave intensities up to 0.5–1 MW/cm$^2$ without visible damage.

A composite magneto-optical element composed of terbium aluminium garnet (TAG) ceramic and sapphire was implemented, which enabled efficient heat extraction from the TAG end face under high-power laser irradiation, thereby reducing the mean temperature and the resulting mechanical stresses. In such a composite magneto-optical element, while preserving the degree of isolation, the operating power can be increased by a factor of 1.6

Acknowledgements: This work was supported by Russian Science Foundation No. 23-12-00199-П (https://rscf.ru/en/project/23-12-00199-П).

[1] W. Koechner, *Solid-state laser engineering*, Sixth revised and Updated edition. New York, NY: Springer, 2006.
[2] I. Kuznetsov, A. Pestov, I. Mukhin, M. Volkov, M. Zorina, N. Chkhalo, and O. Palashov, "Composite Yb:YAG/sapphire thin-disk active elements for high-energy high-average power lasers," *Opt. Lett.*, vol. 45, no. 2, p. 387, Jan. 2020.
[3] H.-C. Lee, P. L. Brownlie, H. E. Meissner, and E. C. Rea, Jr., "Diffusion-bonded composites of YAG single crystals," presented at the Laser-Induced Damage in Optical Materials: 1991, 1992, pp. 2–10.
[4] H. Ichikawa, K. Yamaguchi, T. Katsumata, and I. Shoji, "High-power and highly efficient composite laser with an anti-reflection coated layer between a laser crystal and a diamond heat spreader fabricated by room-temperature bonding," *Opt. Express*, vol. 25, no. 19, p. 22797, Sept. 2017.
[5] S. Zhu, A. W. Yu, D. Hawley, and R. Roy, "Frustrated total internal reflection: A demonstration and review," *American Journal of Physics*, vol. 54, no. 7, pp. 601–607, July 1986.

# EPR observation of reversible rechange of paramagnetic iron centers in $ZnWO_4$ crystals under the influence of visible radiation

**D.A. Lis[1], M.Yu. Artyomov[2], V.A. Vazhenin[2], A.P. Potapov[2], K.A. Subbotin[1], Yu.I. Zimina[1]**

*1- Prokhorov General Physics Institute, Russian Academy of Sciences, 38 Vavilova St., 119991 Moscow, Russia*
*2- Ural Federal University (Institute of Natural Sciences and Mathematics), Yekaterinburg, Russia*

*lisdenis@mail.ru*

Interest to zinc tungstate ($ZnWO_4$) single crystals is caused by the favorable combination of its properties such as high scintillation efficiency, good thermal conductivity, thermal and radiation stability, and mechanical strength, as well as the ability to grow this crystal using the Czochralski method. This crystal is promising for use in high-energy physics, space exploration, industry, and medicine as an ionizing radiation detector, including cryogenic scintillation detectors. One of the most important negative issues, concerning, to some degree, almost all scintillation crystals, including $ZnWO_4$, is afterglow. It typically results from the presence of electron and/or hole traps in the crystal's band gap, which capture some of free electrons and/or holes formed in the crystal during its interaction with high-energy particles or quanta. Thus, optimizing the technology for growing of scintillating single crystals to minimize their afterglow by reduction the concentration of the corresponding trapping centers in their composition is the actual problem.

This report presents the results of study the visible light with $ZnWO_4$:Tm single crystal containing an uncontrolled iron impurity at the ppm level. It was found by the electron paramagnetic resonance measurements that such irradiation at low temperatures leads to recharging of iron ions $Fe^{2+} \rightarrow Fe^{3+}$. The extent and the velocity of such transition strongly depend on a temperature (see fig. 1). When stopping the irradiation, the reverse recharging process $Fe^{3+} \rightarrow Fe^{2+}$ begins, and the concentration of $Fe^{3+}$ gradually reaches its initial level (see fig. 2). Therefore, $Fe^{2+}$ ions can be considered as the hole traps in $ZnWO_4$ crystal, and their concentration should be as low as possible for the obtaining of good scintillating characteristics. The data of decay kinetics of $Fe^{3+}$ concentration at different temperatures allowed us to calculate the depths of the electron traps taking part in the electron-hole recombination processes, into which iron ions are involved in $ZnWO_4$ crystal.

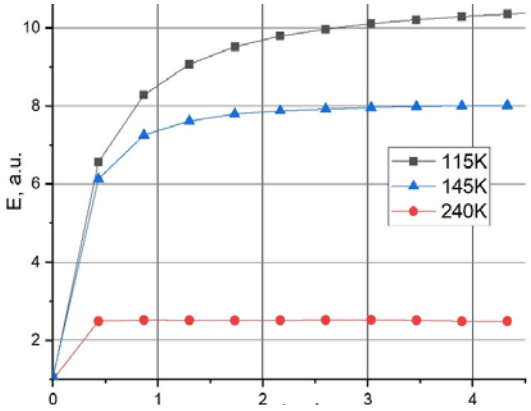


**Fig 1.** Dependence of the peak intensity of the EPR absorption signal of $Fe^{3+}$ centers in the Tm:$ZnWO_4$ crystal (B||Nm, frequency 9432 MHz) on time during irradiation of the sample with a violet LED ($\lambda_{max}$ = 397 nm) at different temperatures.

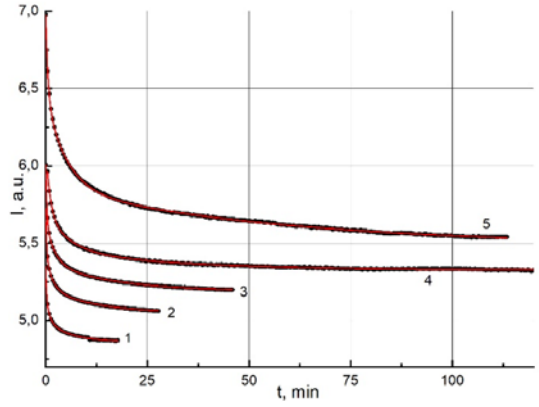


**Fig 2.** Relaxation kinetics of the $Fe^{3+}$ EPR signal intensity at temperatures of 115–145 K after irradiation with a LED with a peak wavelength of 397 nm. Points represent the experiment, curves represent the results of fitting the approximation: 1 – 145K, 2 – 140K, 3 – 135K, 4 – 125K, 5 – 115K.

# Growth of mixed magnesium-zinc tungstate $Zn_xMg_{1-x}WO_4$ single crystals of high optical quality with optimal Zn concentration for the Czochralski growth

**O.N. Lis[1], Y.I. Zimina[1,2] , K.A. Subbotin[1,2], D.A. Lis[1], L.D. Ishakova[1] , V.A. Agakhanova[1] , V.V. Voronov[1] , P.A. Popov[3] ,Y.S. Didenko[1,2]**

*1- Prokhorov General Physics Institute of the Russian Academy of Sciences, Moscow, Russia*
*2- D.I. Mendeleev Russian University of Chemical Technology, Moscow, Russia*
*3- Bryansk State Academician I.G. Petrovski University, Bryansk, Russia*

*ozaytceva@mail.ru*

The concentration series of the promising scintillating and laser crystals $Zn_xMg_{1-x}WO_4$ (x = 0–1) has been grown. The least zinc atomic fraction required for the possibility of Czochralski growth of these crystals was revealed to be $x$ = 0.15-0.2. Using the energy-dispersive microprobe analysis, the actual cations distribution along the crystal boules length has been measured and segregation coefficients of the cations between the crystals and the melts have been calculated by the Gulliver-Pfann equation. It was shown that the segregation coefficient of $Mg^{2+}$ substantially exceeds unity, whereas the segregation coefficient of $Zn^{2+}$ is substantially less than unity in whole the studied range of the mixed crystals.

The parameters of the monoclinic unit cell were calculated from the results of X-ray powder diffraction analysis, and the hydrostatic densities of the crystals were measured. The obtained results on the unit cell parameters and on the hydrostatic densities made it possible to calculate the actual molar weights of the crystals, which appeared to be very close to the molar weights of the same samples calculated from the measured cation compositions. It indicates about high correctness of determination the actual crystals compositions. It was shown that $Zn_xMg_{1-x}WO_4$ crystals with the nominal $x$ values of 0.5 and 0.7 contain the pronounced amount of vacancies in ($Mg^{2+}$ + $Zn^{2+}$) sites and the corresponding amount of oxygen vacancies. The values of thermal conductivity of the crystals along three principal directions were measured using the steady-state heat flow method. It was shown that substitution 20 at.% of magnesium with zinc leads to a sharp decrease in thermal conductivity compared to $MgWO_4$, and reaches the level of thermal conductivities of $ZnWO_4$. The mechanical strength characteristics (microhardness and fracture toughness) of the crystals were measured by the indentation method. Like the case of thermal conductivities, the values of mechanical strength characteristics crucially depend on the measurement direction. The crystals micro-hardness almost linearly reduces with increase the $Zn^{2+}$ fraction, whereas the dependence of fracture toughness on the crystals composition passes through a gentle minimum.

# Optical and nonlinear optical properties of $TlInS_2$ crystals of the hexagonal modification: theory and experiment

**I.A. Mamedova[1], N.A. Abdullayev[1,2], Z.A. Jahangirli[1,2], S.S. Osmanova[3], A.I. Najafov[1], Kh.A. Hidiyev[2], V.B. Aliyeva[1], T.G. Mammadov[1]**

*1- Institute of Physics of the Ministry of Science and Education, H. Javid av., 131, AZ1073, Baku, Azerbaijan*
*2- Baku State University, Z. Xalilov str., 33, AZ1148, Baku, Azerbaijan*
*3- Azerbaijan Technical University, H. Javid av., 25, AZ1073, Baku, Azerbaijan*

*irada_mamedova@yahoo.com*

The compound $TlInS_2$ is a member of the class of ternary thallium dichalcogenides, crystallizing in five polymorphic modifications: hexagonal (HM), tetragonal, orthorhombic, monoclinic, and triclinic. However, only the monoclinic (space group C62h) and hexagonal (space group D46h) modifications of $TlInS_2$ can be obtained by crystallization of the stoichiometric composition. The physical properties of $TlInS_2$ crystals with hexagonal symmetry have been poorly studied.

The electronic band structure, the origin of energy states, the spectral dependences of optical functions for various polarizations of incident light, and the partial densities of states projected onto atoms were studied using first-principles calculations for $TlInS_2$ crystals with hexagonal symmetry. The linear and nonlinear optical properties of this compound were experimentally studied in the photon energy range of 0.7-6.5 eV using spectral ellipsometry. Good agreement was obtained between the experimentally obtained spectral dependences of the imaginary and real parts of the dielectric function (Fig. 1), optical conductivity, as well as the refractive index, extinction and absorption, and the calculation results.

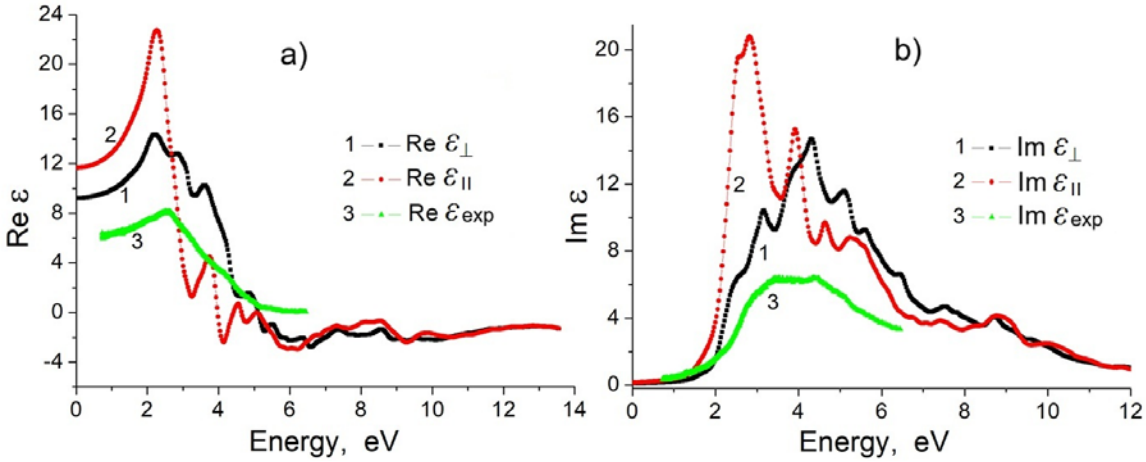


**Fig. 1.** Real (Re ε) (a) and imaginary (Im ε) (b) parts of the dielectric function of $TlInS_2$ GM crystals (1, 2 – theory: 1 – perpendicular to the hexagonal axis c (⊥), 2 – along the hexagonal axis c (II); 3 – experiment)

The changes in the absorption coefficient and skin depth of the crystal as a function of energy were studied. Using the single-effective oscillator model, the energy of a single oscillator $E_{SO}$ = 4.1 eV and the dispersion energy $E_d$ = 20.6 eV, the plasma frequency of $5.07\times10^{15}$ rad/s and the carrier density to effective mass ratio of $8.86\times10^{57}$ $m^{-3}\cdot kg^{-1}$ were calculated. Taking into account the experimentally determined static value of the refractive index of the crystal $n_0$ = 2.45, the values of the nonlinear refractive index $n_2$, the first-order $\chi^{(1)}$ and the third-order $\chi^{(3)}$ nonlinear susceptibilities were calculated and found to be equal to $6.8\times10^{-11}$ esu, 0.4 esu, $\chi^{(3)} = 4.4\times10^{-12}$ esu, respectively. These results indicate the prospects for integrating the compound into various nonlinear optical systems.

# Pulsed Nd:YAG DPSSL with intracavity SHG emitting 100 W at 10 kHz

**D. Kostritsa, D. Mashkovsky, S. Klimentov, S. Kostritsa, V. Derzhiev, D. Mamonov**

*DMK Laser Microsystems, Moscow, 129085 Russia, 101 Mira Avenue, bld. 1, loc. 1/4*

*dlaser@mail.ru*

A diode-pumped quasi-CW Nd:YAG laser with intracavity second harmonic generation was developed delivering the average power of more than 100 W at 10 kHz. The pulsewidth of 43 ns was measured at the wavelength of 532 nm. An active crystal with an isotropic longitudinal axis, 250 mm long and 5 mm in diameter, was side-pumped by CW LDs at the power of up to 1.9 kW. Type 2 room temperature phase matched LBO with the dimensions of 5x5x15 mm was used for efficient intracavity second harmonic generation. Q-switched operation was enabled by an AOM controlled by "Quantum-Ray Labs" driver (N. Novgorod) and the silica cell manufactured by L. Magdich from "Polyus" Institute.

The laser cavity parameters were optimized by measuring the thermal focal lengths (dependent on the input pump power) under nonlasing conditions, using HeNe laser radiation and a "Spiricon" beam profiler. Simultaneously, aberrations arising from the thermally induced refractiveindex profile in the laser rod were carefully monitored. The obtained data were used to validate our numerical calculations of the cavity stability range and mode size distribution along the cavity, both as functions of the pump level and cavity length. Notably, several techniques are available to compensate for laser beam aberrations and thermal focal lengths in the rod, such as employing a phaseconjugate cavity mirror [1].

It has long been recognized [2] that a major challenge in using crystals with an isotropic axis aligned along the radiation generation direction (e.g., Nd:YAG) for high power applications is the occurrence of depolarization and bi-focusing effects. These arise from thermally induced birefringence and are very difficult to compensate. This also leads to a deterioration of beam quality, while the issue of a short stability range persists. A widely adopted solution is to design a laser with two separate crystals positioned sequentially (one behind the other), with their spacing determined by the pump parameters to achieve mutual birefringence compensation [3]. In this configuration, however, the cavity becomes excessively long, resulting in laser pulsewidth exceeding 200 ns which is unsuitable for many technological applications. Consequently, we opted for a solution featured by single crystal. A shorter cavity length allowed us to achieve a recordbreaking duration of pulses for this class of lasers, i.e. below 50 ns.

[1] M. Ostermeyer, A. Heuer, and R. Menzel,, 27-W average output power with 1.2*DL beam quality from a single-rod Nd:YAG laser with phase-conjugating SBS mirror, IEEE J. Quantum Electron. v. 34, 372–377, (1998).
[2] W. Koechner, Solid-State Laser Engineering (Springer), Chapter 5, (2006).
[3] N. Hodgson, H. Weber, Laser Resonators and Beam Propagation, (Springer), Chapter 14, (2004).

# Development of All-Dielectric Magneto-Optical Transducer

**D. Neznanov, T. Dolmatov**

*Prokhorov General Physics Institute of the Russian Academy of Sciences, 38, Vavilov street, Moscow, 119991, Russia*

*neznanov.daniil@yandex.ru*

For the measurement of rapidly varying magnetic fields in pulsed power engineering and power electronics, the development of a fully dielectric fiber-optic transducer is an important scientific and technical task. Conventional magnetic field sensors contain metallic elements and semiconductor structures, which lead to distortions of the measured field [1]. To solve this problem and ensure high-accuracy measurements, magneto-optical transducers based on the Faraday effect are used.

In this work, a reflective dielectric probe structure is proposed. The optical path includes a laser source, a fiber-optic coupler, a polarizer, a quarter-wave plate, a sensitive magneto-optical material, and a reflective element. To shift the operating point into the linear region of the dependence of radiation intensity on the polarization plane rotation angle, the quarter-wave plate is oriented at an angle of 22,5 with respect to the polarizer axis. In the ideal case, when the propagation axis of the radiation coincides with the optical axis of the crystal, the transfer function of the system obtained by the authors is described by the following equation:

$$I=\frac{I_0}{2}\cdot[1+\sin\cdot(4\cdot\theta)],$$

where θ is the polarization plane rotation angle (Faraday rotation angle).

To experimentally determine the characteristics of the magneto-optical transducer, an experimental setup was developed, including a longitudinal pulsed magnetic-field generator based on a thyratron and an induction coil controlled by a delay generator. A CeF3paramagnetic crystal was selected as the magneto-optical material, and a 405 nm laser was used as the radiation source. The transition to the violet spectral range provides an increase in the Verdet constant, which is a quantitative characteristic of the Faraday effect, and improves the sensitivity of the system [2]. Practical implementation is limited by the intrinsic linear anisotropy of the selected material, which, when the light beam deviates from its optical axis, leads to distortions of the detected signal [3].

At the current stage of the work, it is necessary to eliminate the influence of the above-described linear anisotropy on the recorded signal in order to experimentally evaluate the magneto-optical characteristics of the cerium fluoride sample used. In this regard, the authors are developing an alignment procedure for the free-space optical system based on conoscopic inspection. The experiment is aimed at the quantitative determination of pulse-shape distortions caused by controlled angular deviations from the optical axis of the crystal. Establishing numerical alignment tolerance limits will make it possible to isolate the useful signal from the influence of crystal anisotropy, which is necessary for the further development of an efficient fiber-optic measuring probe.

[1] J. Zhang, C. Wang, Y. Chen, Y. Xiang, T. Huang, P. P. Shum, and Z. Wu, “Fiber structures and material science in optical fiber magnetic field sensors,” Frontiers of Optoelectronics, vol. 15, no. 1, pp. 34, (2022).

[2] P. Molina, V. Vasyliev, E. G. Víllora, and K. Shimamura, “CeF3 and PrF3 as UV-visible Faraday rotators,” Optics Express, vol. 19, no. 12, pp. 11786-11791, (2011).

[3] J. H. Lacy, G. E. Patenotte, A. C. Kinney, and P. K. Majumder, “Broadband High-Precision Faraday Rotation Spectroscopy with Uniaxial Single Crystal CeF3 Modulator,” Photonics, vol. 11, no. 4, pp. 304, (2024).

# Effect of oxygen impurity on the properties of zinc telluride

**V.A. Petrova, E.N Mozhevitina, A.V. Khomyakov, A.A. Pythcneko, I.Ch Avetisov**

*Department of Chemistry and Technology of Crystals, D. Mendeleev University of Chemical Technology of Russia (MUCTR), Moscow 125480, Russia;*

*frogpvahka@mail.ru*

Zinc telluride has gained popularity due to its semiconductor properties. These properties depend largely on the concentration of impurity elements in the material. ZnTe doped with metals and chalcogens has already found widespread practical application. Notable examples of application include materials with halogens, which enable the production of ZnTe with n-type conductivity [1], and materials with metals, which are useful in photocatalysis [2]. Iron-doped ZnTe crystals are used to create IR lasers [3]. However, in addition there is a group of gas-forming impurities whose influence on the properties of ZnTe has not been fully studied. This is primarily due to the fact that instruments that measure the concentration of these impurities are relatively expensive, rare, and difficult to interpret. In today's world, studying gas-forming properties has become more accessible. One accessible method is the extraction of impurities into a carrier gas [4]. The main limitation of research on the influence of gas-forming impurities on the properties of substances is the ability to work in a controlled gas atmosphere to prevent premature oxidation of the compounds, particularly by atmospheric oxygen. This is supported by a study showing that the presence of oxygen enabled the formation of efficient emission centers in ZnTe [5].

In that work using vacuum sublimation, a high-purity sample of roughly stoichiometric composition with minimal oxygen content was obtained from a commercial ZnTe sample. Based on this sample, non-stoichiometric ZnTe samples with both excess zinc and excess tellurium were synthesized. Samples of both stoichiometric composition and those with excess of each component were annealed in an oxygen atmosphere. The effect of oxygen impurity on the spectral properties of zinc telluride was assessed.

This research was funded by the Ministry of Science and Higher Education of Russia through the project FSSM-2025-0006.

The authors are grateful to the National Analytic Certification Laboratory of Mendeleev Center of D. Mendeleev University of Chemical Technology of Russia for the ICP MS measurements.

[1] Y.J. Jang, M. D. Bhatt, J. Lee, S. H. Choi, B. J. Lee, J. S. Lee. Metal, Free Artificial Photosynthesis of Carbon Monoxide Using N-Doped ZnTe Nanorod Photocathode Decorated with N-Doped Carbon Electrocatalyst Layer // Advanced Energy Materials. 2018. – V. 8. – № 20. – P. 1702636.

[2] E.O. Karpova, I.Yu. Nagibina, and A. S. Makarova, "The synthesis, x-ray diffraction, and optical properties of the CdS–ZnTe semiconductor system," Journal of Optical Technology. 82(6), 388-392 (2015).

[3] Yucheng Wei, Pengfei Xie, Hao Lei, Zeyu Lu, Changyou Liu, Bin-Bin Zhang, Wenhui Yang, Wanqi Jie Luminescence and optical properties of $Fe^{2+}$:ZnTe crystal grown by temperature gradient solution method // Journal of Alloys and Compounds. 2019. – V. 805. – № 15, P. 774-778.

[4] E.S. Kartashova, D.A. Danilov, I.B.Polovov Development of a method for determining the oxygen content in a mixture of lithium and beryllium fluorides , Physics. Technologies. Innovations. 2021. – - Yekaterinburg, P. 409-417.

[5] N.K. Morozova, I.A. Karetnikov, V.V. Blinov, V.K. Komar, V.G. Galstan , V.S. Zimogorskii, Dependence of the properties of Cd1-xZnxTe crystals on the type of intrinsic point defects and forms of oxygen presence , Physics and Technology of Semiconductors. – 1999. – V. 33. – No. 5. – P. 569-573.

# Measuring water concentration in LBO

**A.A. Pythcneko, K.I. Runina, E.N. Mozhevitina, I.Ch. Avetisov**

*Department of Chemistry and Technology of Crystals, D. Mendeleev University of Chemical Technology of Russia (MUCTR), Moscow 125480, Russia;*

*pytchenkoaa@mail.ru*

Lithium triborate ($LiB_3O_5$/LBO) is the one of the nonlinar borate crystals, which was found as material for nonlinar optical elements for second harmonics generation (SHG). Usually, in growth industry engineers use $Li_2CO_3$ and $H_3BO_3$ for synthesis LBO [1]. However, in growing process, water and carbon dioxide can be dissolved in melt, and affect the properties of crystals [2]. Moreover, in process of polishing [3], water can concentrate in scratches, pores and cracks [4]. Later in process of SHG water can vaporize and damage the surface of crystal leading to destruction affect quality of nonlinar optical element.

Nowadays there are a lot of different variants, how to measure amounts of water in solid samples, such as coulometric Karl Fischer titration, gravimetric methods, near-infrared spectroscopy. These methods often are expensive, have high limits of determination of amount of water or don't have standards for calibration.

As a consequence, our research group create laboratory setup for thermogravimetric analysis, that was cheaper and easier than other variants, that can be found as commercial products. This method of analysis can be used for solid materials such as boron oxide or borate crystals, in way of determination absorbed and bound water. In fact, the amount of water this method can detect is in range from 0,001 till the 0,1 weight %.

In that work LBO was used as material for samples for analysis. For the experiments quartz ampoules was used as sealed container for annealing process, which prevent process of losing water vapor in heating part of analysis. Moreover, ampule had 2 parts: top part of ampule with big diameter and low one with small diameter which was called capillary. Capillary was used for condense water vapor in cold part of ampule, that was cooled by liquid nitrogen. After the process of heating, capillary was cut and weighed The optimal annealing conditions for thermogravimetric analysis were selected for effective extraction surface and bounded water from lithium triborate samples. Worth-noting, that heating part of analyses didn't have to harm the nonlinar optical element.

Moreover, we studied the correlation between water concentration and IR absorption spectra by using dehydrated samples (after thermogravimetric analysis), that were hydrated in controlled conditions in spectrophotometers chamber.

This research was funded by the Ministry of Science and Higher Education of Russia through the project FSSM-2025-0006.

The authors are grateful to the National Analytic Certification Laboratory of Mendeleev Center of D. Mendeleev University of Chemical Technology of Russia for the ICP MSmeasurements.

[1] Z. Shuqing, H. Chaoen, Z. Hongwu, Crystal growth and properties of lithium triborate , Journal of Crystal growth., №. 1,T. 99, P.805-810, 1990.
[2] H. Franz, Solubility of water vapor in alkali borate melts, Journal of the American Ceramic Society, T. 49, №. 9,P. 473-477, 1966.
[3] J. Li,Y. Zhu, D. Zuo, Y. Zhu, C. Chen., Optimization of polishing parameters with Taguchi method for LBO crystal in CMP, Journal of Materials Sciences and Technology, T. 25, №. 05, P. 703, 2009.
[4] N.G. Korobeishchikov, I.V. Nikolaev, M.A. Roenko, V.V. Yakovlev, Formation of Anomalous Craters upon Bombardment of the Surface of a Lithium-Triborate Single Crystal by Cluster Ions, Journal of Surface Investigation: X-ray, Synchrotron and Neutron Techniques, T. 17., №. 1, P. 163-167, 2023.

# Photoinduced Residual Losses in Directly Diode-Pumped Ti:Sapphire Lasers

K. Reznikov[1,2], M. Esaulkov[1], A. Naumov[2,3]

*1- AVESTA Ltd., 108840 Troitsk, Moscow, Russia*
*2- P.N. Lebedev Physical Institute of the Russian Academy of Sciences, Troitsk Branch, 108840 Moscow, Russia*
*3- Institute of Spectroscopy of the Russian Academy of Sciences (ISAN), 108840 Troitsk, Moscow, Russia*

*k.reznikov@avesta.ru*

Direct blue diode pumping has significantly improved the compactness and optical-to-optical efficiency of Ti:sapphire laser systems. At the same time, continuous blue excitation may activate photoinduced processes in the crystal that introduce additional optical losses and limit laser performance, particularly near the edges of the Ti:sapphire tuning range.

One possible origin of these losses is photoinduced absorption associated with intervalence charge transfer (IVCT) involving $Ti^{3+}/Ti^{4+}$ centers and intrinsic or impurity-related defects [1]. Although IVCT processes have been discussed for titanium-containing oxide crystals, their contribution to the operation of directly diode-pumped Ti:sapphire lasers remains insufficiently understood. Their experimental identification is complicated by the fact that blue excitation simultaneously produces optical gain and may induce additional absorption.

To separate these contributions, the temporal response of a Ti:sapphire laser was studied during controlled switching of the blue pump. The laser was operated at selected wavelengths within the Ti:sapphire emission band, while its output power was recorded with a fast photodetector and a digital oscilloscope. Immediately after switching off the blue excitation, the laser power decreased below its pump-free stationary level and subsequently recovered on a millisecond time scale. Since the optical gain produced by the blue pump disappears immediately after switching, the delayed recovery is attributed to a transient residual loss persisting in the crystal after excitation.

A pronounced spectral dependence of the effect was observed. Measurements performed at different crystal temperatures also revealed a complex recovery kinetics containing fast and slow components, indicating that more than one relaxation process may contribute to the observed transient absorption.

The obtained results provide evidence for a long-lived photoinduced loss mechanism in blue-excited Ti:sapphire. Its spectral and temporal properties are consistent with an IVCT-related process, although further measurements are required for an unambiguous microscopic assignment. Quantitative measurements of the induced loss spectrum, its dependence on intracavity intensity, temperature, and excitation wavelength are currently in progress.

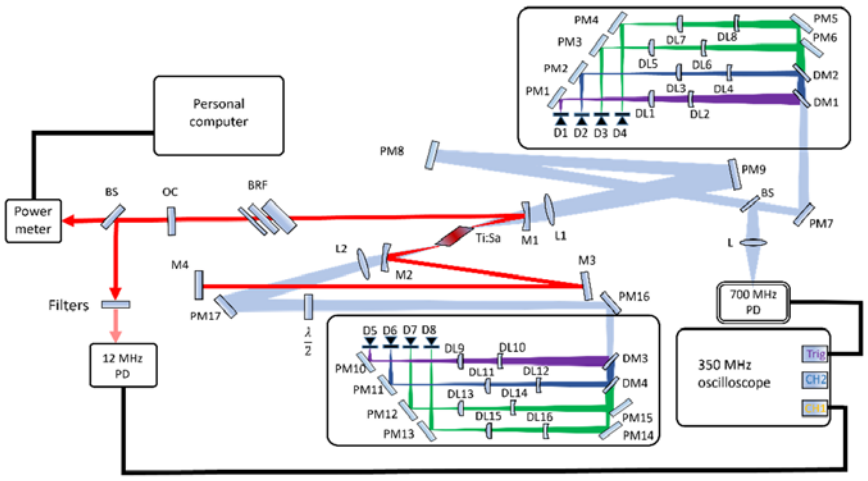


**Fig. 1.** Experimental arrangement for studying photoinduced residual losses in a Ti:sapphire laser. Blue excitation is periodically switched on and off, while the laser output at a selected wavelength is continuously recorded to resolve the transient response after pump extinction.

[1] Sawada, R., Tanaka, H., Sugiyama, N., & Kannari, F., Applied Optics, 56(6), 1654-1661 (2017).

# Design of 4 μm mid-Infrared laser based on $Ho^{3+}$ ions with commercial diode pumping

A. Senchurova[1, 2], A. Sirotkin[1], Yu. Kalachev[1]

*1- Prokhorov General Physics Institute of the Russian Academy of Sciences, Moscow, Russia*
*2- Moscow Institute of Physics and Technologies, Russia*

*Senchurova.av@phystech.edu*

Mid-infrared laser radiation (λ ~ 2.7–5 μm) lies within atmospheric transparency windows, overlaps strong molecular absorption bands (e.g., $CO_2$, $CH_4$, and $CH_2O$ in the 3.9–4.1 μm region [1, 2]), and coincides with the water absorption peak. $Ho^{3+}$-doped crystals can provide 4 μm lasing via the $^5I_5 \rightarrow {}^5I_6$ transition. Although 3.9 μm lasing in $Ho^{3+}$:BYF has been demonstrated with ~889 nm diode pumping [3, 4], the absence of a commercially available pump source at this wavelength hinders practical 4 μm laser development. To overcome this, we explore the potential of co-doping $KGd(WO_4)_2$:Ho with $Nd^{3+}$ ions as a dual sensitizer – both to populate the upper $Ho^{3+}$ level ($^5I_5$) and to depopulate the lower $Ho^{3+}$ level ($^5I_6$) – thus resolving the self-terminating nature of the laser transition.

In the present work, a KGW:Ho,Nd crystal was investigated as a potential active element. Transmission spectra were obtained, demonstrating that, unlike a holmium-only doped crystal (which requires pumping near 885 nm), the co-doped crystal can be pumped using commercially available radiation sources at 795 nm or 810 nm. Using a purpose-designed experimental setup, luminescence spectra in the 2 μm, 3 μm, and 4 μm regions were recorded. The result is shown in figure 1.

To estimate the lifetimes of the excited states, the luminescence decay kinetics were investigated. The measured lifetimes of the $Ho^{3+}$: $^5I_5$ and $^5I_6$ levels were found to be 7.9 μs ± 0.3 μs and 27.4 μs ± 0.7 μs, respectively. It was shown that the lifetime of the $Nd^{3+}$: $^4F_{3/2}$ level in a KGW:Nd crystal is approximately two times longer than that of the same level in the KGW:Ho,Nd crystal with the same Nd concentration, indicating depopulation of this level in the co-doped crystal and suggesting efficient energy transfer from $Nd^{3+}$ to $Ho^{3+}$ ions.

The result of our study demonstrates that the chosen material is a promising gain medium for 4 μm laser emission.

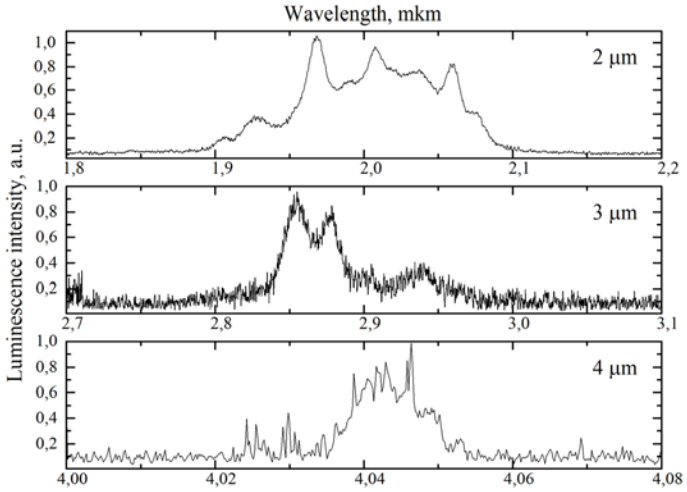


**Fig. 1.** Luminescence spectra of KGW:HoNd crystal

[1] Krebbers R. et al. Mid-infrared supercontinuum-based Fourier transform spectroscopy for plasma analysis //Scientific reports. – 2022. – V. 12. – №. 1. – P. 9642.
[2] Paterova A.V. et al. Broadband Quantum Spectroscopy at the Fingerprint Mid-Infrared Region //ACS Photonics. 2022 V. 9 P. 2151–2159
[3] Chaoqun Ma, et al. A 3.9 μm Ho3+:BaY2F8 laser directly pumped by laser diodes // ELECTRONICS LETTERS 2021 V. 57 No. 20. P. 779.
[4] R. Stutz, H. Miller, K. Dinndorf High-pulse-energy 3.9-μm lasers in Ho: BYF // Proc. of SPIE V. 5332 P. 111.

# Tunable upconversion luminescence of $Er^{3+}$, $Tm^{3+}$-doped bismuth-germanate glasses for NIR-visualization applications

**K. Serkina[1], E. Sektarov[2]**

*1- D. Mendeleev University of Chemical Technology of Russia, Moscow, Russia*
*2- Institute of Spectroscopy RAS (ISAN), Troitsk, Moscow, Russia*

*serkina.k.s@muctr.ru, sektarov_es@mail.ru*

Laser beam visualization is essential for advancing laser technology. IR beam visualizers are used in laser beam monitoring systems, optical system alignment, security systems, accelerator IR stations, and scientific research, including thermography [1]. Bismuth-germanate (BGO) glasses doped with erbium and thulium were prepared in this study. BGO glasses can visualize laser IR radiation (from 800 nm) via rare-earth ions upconversion luminescence. This type of luminescence has not previously been detected in bulk optically transparent glasses and has only been demonstrated for nanoscale objects.

Glasses of the molar composition $10Bi_2O_3$-$85GeO_2$-$5Na_2O$ doped with $Er^{3+}$ and $Tm^{3+}$ were synthesized by the classical melt-quenching method. The resulting samples were manufactured as 2x2x2 mm cubes with opposite plane-parallel polished faces of optical quality. Registration of the obtained samples visible luminescence spectra was performed using OpticInsight USB2000+ fiber optic spectrometer with 200 μm slit and 10 nm optical resolution at room temperature. The excitation source was 808 nm diode laser with optical power from 2 mW to 1600 mW. The laser beam (1 mm diameter, 1600 mW power) provided a power density of 204 W/cm².

Upconversion luminescence spectra (fig. 1) consists of $Er^{3+}$ emission bands 525 nm ($^2H_{11/2} \rightarrow {}^4I_{15/2}$), 550 nm ($^4S_{3/2} \rightarrow {}^4I_{15/2}$) 650 nm ($^4F_{9/2} \rightarrow {}^4I_{15/2}$) and $Tm^{3+}$ 790 nm emission band ($^3H_4 \rightarrow {}^3H_6$) [2, 3]. Furthermore, variations in the excitation power lead to a redistribution of the PL bands and a subsequent change in the emission color. The upconversion luminescence color shifts from pale red to bright green with increasing IR laser power.

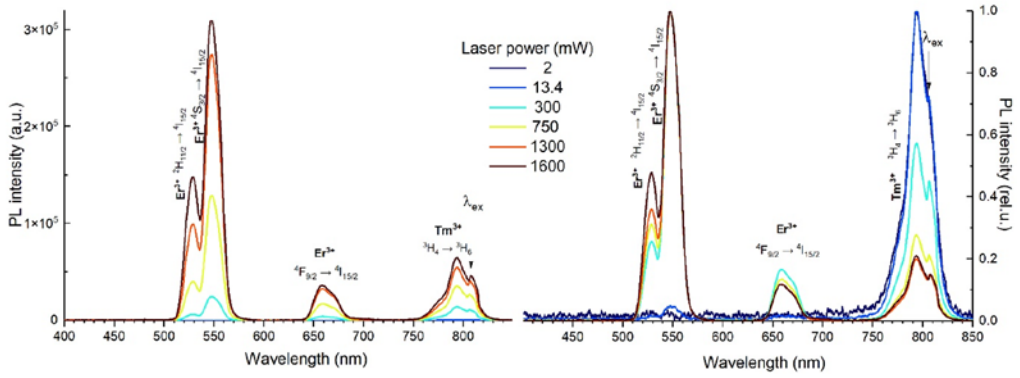


**Fig. 1.** Original emission spectra of synthesized glass (left) and spectra normalized to their maximum intensity (right) under 808 nm laser excitation with different power.

The research was financially supported by the Ministry of Science and Higher Education of the Russian Federation (FSSM-2025-0006), luminescence measurements, the study was carried out within the framework of the state assignment of the Institute of Spectroscopy of the Russian Academy of Sciences (#FFUU-2024-0004 – E. S. Sektarov).

[1] Y. Choi, J. Pak, K. Seo, S, Jeong, T. Lim, S. Ju Realization of infrared display images using infrared laser projection method, Opt. Lasers Eng., vol. 145, Article No. 106677, (2019)
[2] W. Lozano, C. Araújo, Y. Messaddeq Enhanced frequency upconversion in $Er^{3+}$ doped fluoroindate glass due to energy transfer from $Tm^{3+}$, J. of Non-cryst. Sol., vol. 311, pp. 318-322, (2015).
[3] T. Grzyb, I. R. Martín, R. Popescu The use of energy looping between $Tm^{3+}$ and $Er^{3+}$ ions to obtain an intense upconversion under the 1208 nm radiation and its use in temperature sensing, J. Nanoscale, vol. 16, pp. 1692-1702, (2024).

# Laser-optical systems for ultrafast processes registration

**V. Simonova, A. Dormidonov, A. Bychkov, V. Kamenev, P. Kubasov, A. Savvin, A. Tikhov, V. Turkin**

*Dukhov Automatics Research Institute, Federal State Unitary Enterprise,*
*22, Suschevskaya st., Moscow, 127055, Russia*

*vas@optoacoustics.ru*

This paper presents the latest developments of the VNIIA FSUE in laser-optical systems and measuring instruments designed to initiate ultrafast processes and study object parameters in gas-dynamic experiments.

A high-power subnanosecond diode-pumped solid-state laser is demonstrated. This laser is designed for shadow recording of rapidly moving objects and for plasma dynamics research. A key feature of this laser system is its ability to operate in the field over a wide range of operating temperatures, from minus 50 to plus 50°C.

The key characteristics of unique multichannel laser interferometric systems designed to record the velocity (PDV) and surface coordinates (LIDAR) of rapidly moving objects with ultra-high temporal resolution are presented. These systems operate by measuring the beat frequency of a reference laser beam and the laser beam reflected from the object being studied.

A digital camera with a mirror scanning is presented, which performs photochronographic and multi-frame recording of fast processes with nanosecond resolution, accompanied by optical radiation.

# Synthesis of high purity calcium fluoride for optical element for photolithography

**A.A. Sokolov, A.A. Sycheva, M.P. Zykova, R.I. Avetisov**

*Mendeleev University of Chemical Technology of Russia*

*sokol090619999@gmail.com*

Calcium Fluoride is very important material for laser optics, especially nowadays [1,2]. Historically, lenses for photolithography were made from calcium fluoride, because it has high transparency in ultraviolet range. This material includes some impurities which lead to scatter of laser beam. Commercial produced monocrystals of $CaF_2$ have less impurities quantity (about 99.99 mass% of $Ca^{2+}$) then natural crystals, but it is not enough [3]. In this work we tried to obtain the calcium fluoride with purity about 99.9999 %mass. Synthesis of high purity $CaF_2$ starts from filtration of solution of calcium nitrate with followed deposition of calcium carbonate [4,5]. Next stage is reaction of calcium carbonate with formic acid to produce calcium formate. After that we tried different ways of recrystallisation and chose the best of them. Recrystallisation with EDTA at 80˚C showed the result of 99.9995 mass% purity of $Ca^{2+}$. Analysis was carried out using ICP MS for 65 impurities. Important impurities present on Fig. 1. The most difficult part of purification is minimizing the amount of strontium and iron impurities. Hydrofluoric acid was chosen as fluoridation agent. Distilled high purity hydrofluoric acid was used in this work. Purity of obtained calcium fluoride is 99.999 mass%. Also, Calcium flouride powder includes oxygen impuruties. Additional fluoridation is necessary to minimise the amount of oxygen.

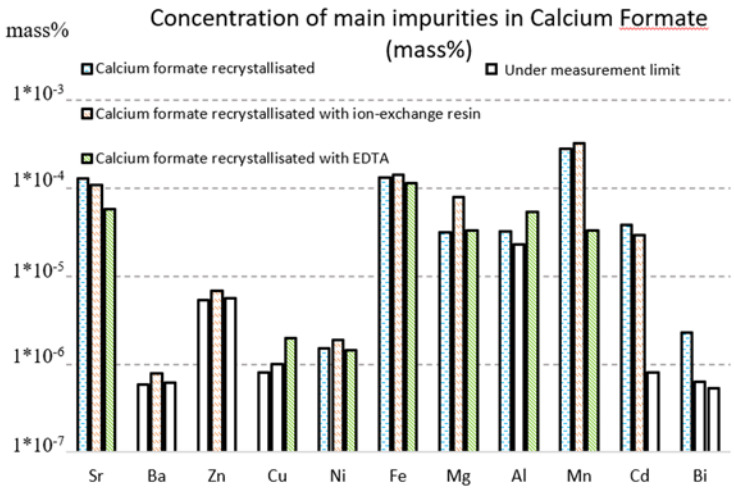


**Fig. 1.** Concentration of main impurities in calcium formate

[1] Zverev V.A., Krivopustova E.V., Tochilina T.V., Optical materials. Vol 1. Training manual for constructors of optical systems and devices (SPbGU ITMO) (2009).
[2] Banshchikov A.G., Vexler M.I., Ivanov I.A., Illarionov Yu.Yu., Sokolov N.S., Suturin S.M., Calcium fluoride films with 2−10 nm thickness on Silicon-(111): growth, diagnostics, study of the through current transport, Semiconductors, Vol.56. - №9, pp. 670-674, (2022).
[3] Kuznetsov S.V., Alexandrov A.A., Fedorov P.P., Fluoride optical nanoceramics, Inorganic materials, vol 56, № 6, pp. 583-607, (2021).
[4] Safronihin A.V., Lisichkin G.V., Production of calcium fluoride nanoparticles by two-jet chemical precipitation, Russian journal of applied chemistry, №7, pp. 924-931, (2022).
[5].Abiev R.Sh. Synthesis of nanosized calcium fluoride particles in a microreactor with intensely swirling flows, journal of inorganic chemistry, vol. 66, №7, pp. 929-934, (2021).

# Determination of the orientation of nonlinear optical crystals of the Li-Na-Mo-O system on a modern single crystal diffractometer

**D. Sychkova[1,2], V. Grigorieva[1,2], A. Sykhikh[1,2], V. Komarov[2,3], P. Serebrennikova[1,2]**

*1 – Novosibirsk National Research State University, 1 Pirogova Street, 630090, Novosibirsk, Russia*
*2 – Nikolaev Institute of Inorganic Chemistry, Siberian Branch of the Russian Academy of Sciences, 3 Acad. Lavrentiev Avenue, 630090, Novosibirsk, Russia*
*3 – Siberian Circular Photon Source (SKIF), Koltsovo, 630559, Russia*

*d.sychkova@g.nsu.ru*

Crystals based on the $LiNa_5Mo_9O_{30}$ structure, due to the absence of a center of symmetry (space gr. *Fdd*2), are of interest as nonlinear optical materials and acousto-optic elements [1]. The possibility of their application as crystalline polarizers is confirmed by the recorded large birefringence [2]. In [3], it was shown that the optimal second harmonic generation efficiency is observed for the $Li_{2.2}Na_{3.8}Mo_9O_{30}$ crystal, i.e., upon introducing $Li^+$ into the structure.

Using the low-gradient Czochralski method (LTG Cz) on unoriented seeds, we grew two crystals of this system. The $Li_{2.66}Na_{3.34}Mo_9O_{30}$ crystal (1), close in composition to that in [3], had linear dimensions of ~3 cm. It was faceted with a concave crystallization front and exhibited visible defects along its entire length. Nonlinear optical properties have been recorded for it, such as the effect of second harmonic generation. The composition of the crystal was determined by quantitative chemical analysis and Xray structural analysis (XSA). When attempting to grow a stoichiometric crystal of composition $LiNa_5Mo_9O_{30}$, the formation of a solid solution $Li_{1.27}Na_{4.73}Mo_9O_{30}$ (2) was established. This crystal (linear dimensions ~7 cm) had a blocktype structure, which led to the formation of a nonplanar parallel crystallization front.

Crystal quality determines their applicability in nonlinear optics. Furthermore, due to the anisotropy of properties, the optical properties of the material depend on the crystal orientation. Knowledge of the crystal orientation is necessary to achieve phase matching in second harmonic generation. To obtain large crystals of high structural perfection by the LTG Cz method, it is necessary to select the seed orientation. The most accurate methods for determining seed orientation are Xray methods.

The use of a powder diffractometer in the BraggBrentano geometry to determine the orientation of an arbitrary cut requires a threecircle goniometer, while the use of singlecrystal diffractometers for large single crystals is complicated by significant absorption in the “transmission” geometry and the lack of specialized holders. In this connection, using single crystals 1 and 2 as an example, we developed a method for determining the orientation of large samples (from 5 mm) using a laboratory singlecrystal diffractometer (Bruker D8 Venture) in the “reflection” geometry. To implement this method, a special holder for a standard goniometer head was fabricated. Based on the orientation matrix obtained from ωscanning, we were able to determine the indices of the most developed faces of the grown single crystals: the [0 1 0] direction in both cases. The misorientation angle for the two seeds is within 5°, which satisfies the requirements imposed on seed orientation in the lowgradient Czochralski technique to ensure stable layerbylayer growth. The obtained result correlates with the indices determined in the BraggBrentano geometry and with the faceting model from XSA data, which shows the most developed face to be (0 2 0). The Jackson criterion value is maximum for the plane perpendicular to the [0 1 0] direction.

The work was supported by Russian Science Foundation (Grant No. 25-73-00328)

[1] V.A. Sukharev, A.P. Sadovskiy, and E.A. Sukhanova, Crystal growth and luminescent properties of $LiNa_5Mo_9O_{30}$, Journal of Crystal Growth, vol. 519, pp. 35-40, (2019).
[2] W. Zhang, H. Yu, and J. Cantwell, $LiNa_5Mo_9O_{30}$: crystal growth, linear, and nonlinear optical properties, Chemistry of Materials, vol. 28, pp. 4483-4491, (2016).
[3] V.Z. Vuksan, Y. Cheng, and S. Park, Second-harmonic generation effect enhanced by Li substitution for Na in Li1 ($Li_XNa_{5-X}$) $Mo_9O_{30}$, Journal of Solid State Chemistry, vol. 339, pp. 124920, (2024).

# Luminescence properties of erbium-doped novel lead germanate oxybromide glasses

**A. Terekhova, A. Dybenko, K. Serkina, O. Petrova**

*D. Mendeleev University of Chemical Technology, Miusskaya Sq. 9, 125047 Moscow, Russia*

*nastt2001@mail.ru*

Glasses based on heavy metal oxides – for example, PbO–$GeO_2$ – are promising for IR photonic applications due to a number of properties. Among these, one can highlight a broad transparency range and a high refractive index [1]. To extend the transparency range of the oxide lead-germanate glass, as well as to reduce the phonon energy, which in turn improves the spectral-luminescent properties, the present work proposes introducing lead bromide into the glass matrix. $PbBr_2$ has a maximum phonon energy of 141 $cm^{-1}$ and an IR transmission cutoff reaching 30 μm [2, 3].

In this work, glasses of the system $x$PbBr$_2$–(50–0.5$x$)PbO–(50–0.5$x$)$GeO_2$ ($x$ = 0–25 mol%, step 5 mol%) were synthesized. Based on the comprehensive physicochemical characteristics, the optimal composition for doping with rare-earth ions $Er^{3+}$ (0.05, 0.1, 0.15, and 0.2 mol%) was selected: 20$PbCl_2$–40PbO–40$GeO_2$. The glass matrix exhibited a crystallization stability (ΔT) of 104°C, a transparency range of 398–6320 nm, a refractive index $n_d$ of 2.14829, an Abbe number of 15.3, a density of 6.494 g/$cm^3$, and a Vickers microhardness of 284 kg/$mm^2$. Vibrational spectroscopy revealed that the maximum phonon energy of the matrix is 796 $cm^{-1}$.

Figure 1 shows the absorption and luminescence spectra of oxybromide lead–germanate glasses doped with erbium ions. Photographs of the synthesized glasses are shown as insets in Fig. 1.

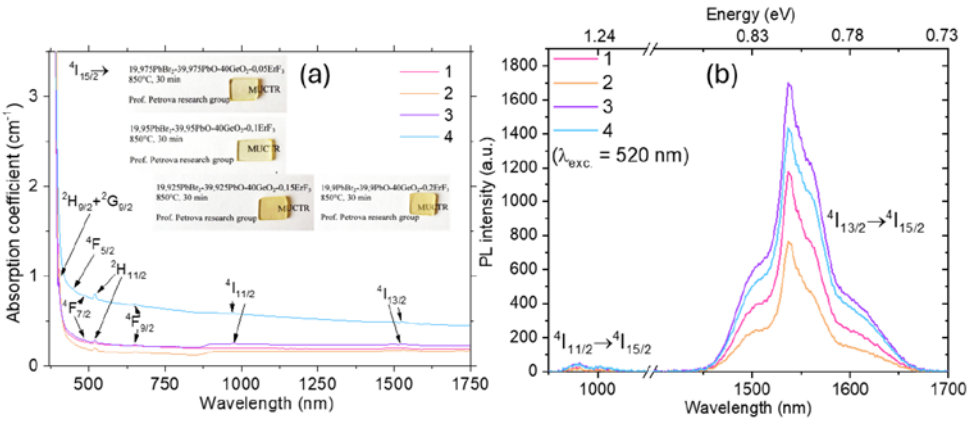


**Fig. 1.** Absorption (a) and luminescence (b) spectra of oxybromide lead-germanate glasses (1 – 19.975PbBr$_2$–39.975PbO–40$GeO_2$–0.05$ErF_3$, 2 – 19.95PbBr$_2$–39.95PbO–40$GeO_2$–0.1$ErF_3$, 3 – 19.925PbBr$_2$–39.925PbO–40$GeO_2$–0.15$ErF_3$, 4 – 19.9PbBr$_2$–39.9PbO–40$GeO_2$–0.2$ErF_3$)

In the presented spectra, we observe the absorption and luminescence bands typical for erbium (0.98 and 1.54 μm).

In this work, oxybromide lead-germanate glasses doped with $Er^{3+}$ ions were synthesized and studied for the first time. It is shown that doping with rare-earth ions, particularly $Er^{3+}$, makes them promising luminescent and laser materials.

[1] Sigaev V. N. Structure of lead germanate glasses by Raman spectroscopy / V. N. Sigaev, I. Gregora, P. Pernice, B. Champagnon, E. N. Smelyanskaya, A. Aronne, P. D. Sarkisov // Journal of Non-Crystalline Solids. 2001. V. 279, № 2-3. P. 136-144.
[2] Singh N. B. et al. Growth and characterization of lead bromide crystals //Journal of crystal growth. – 1992. – V. 123. – №. 1-2. – P. 221-226.
[3] Carabatos-Nédelec C., Bréhat F., Wyncke B. Lattice vibrations in lead bromide and chloride //Infrared physics. – 1991. – V. 31. – №. 6. – P. 611-619.

# Chromium-doped $SrBaNb_2O_6$ thin films: fabrication and structural properties

**I. Voronina[1], M. Doroshenko[1], A. Tumarkin[2], I. Novikov[1], V. Voronov[1], L. Ivleva[1]**

*1- Prokhorov General Physics Institute of the Russian Academy of Sciences, Moscow 119991, Russia*
*2- Saint Petersburg Electrotechnical University "LETI", Saint Petersburg 197022, Russia*

*avtumarkin@yandex.ru*

Metal-ion doped functional oxide hosts can be considered as multifunctional systems, which combine light emission with other intrinsic properties of the host such as ferroelectricity, magnetism, piezoelectricity, and electro-optic properties. A very promising class of materials, which could be used as multifunctional systems, is luminescent-ion doped ferroelectric thin films. Since both luminescent and ferroelectric properties coexist in metal-doped ferroelectrics, this class of materials has significant potential for the development of multifunctional devices due to coupling between physical parameters, such as polarization, dielectric nonlinearity, losses and luminescence. In particular, solid solutions of strontium barium niobates (SBN), which belong to the relaxor ferroelectrics, are of great interest for optoelectronic applications, for the development of efficient tunable electronic devices, for the creation of tailored domain structures for manufacturing of electric field controllable diffractive optical elements, for the development of new laser media operating on different wavelength in visible and near IR diapasons due to their large electro-optical coefficients and high dielectric nonlinearity. In our work, the high temperature diffusion technique was used to obtain Cr-doped $Sr_{0.75}Ba_{0.25}Nb_2O_6$ thin film on alumina substrate. In the work we consider the film processing conditions, the composition of the film, thin-film structure configuration, and luminescent properties of Cr-doped SBN thin film.

The SBN thin films were synthesized by RF magnetron sputtering. Polycrystalline aluminum oxide plates were used as substrates. The film deposition conditions were as follows: pure oxygen was used as the working gas with pressure ranged from 2 to 10 Pa; the temperature of the substrate during the deposition was 900 ◦C; SBN films were deposited for 4 h, the thickness of the films was 500 nm. The high-temperature diffusion process was applied for formation chromium doped SBN thin film on alumina substrate. Chromium oxide Cr2O3 powder was used as a solid state diffusant. The process was carried out in isolated zone of resistance furnace heated up to 1000-1300 ◦C. The exposure time was 24 h, followed by cooling up to room temperature with the heater turned off.

To study the real structure and composition of the films formed, we used the methods of scanning electron microscopy (SEM), X-ray diffraction analysis (XRD) and optical spectroscopy.

The results of studies of doped samples show that high-temperature action in a powdered chromium oxide environment leads to active diffusion of chromium into the SBN film and, to a much lesser extent, into the substrate. Elemental analysis of the samples investigated demonstrates the concentration of chromium ions in the doped films varied from 3 to 5 at.% depending on doping temperature. High-temperature diffusion doping with chromium affects the surface morphology, elemental composition, and structure of the SBN film. In the doped film, the component composition of the solid solution and the unit cell parameters change due to recrystallization of the film under the action of high temperature and the introduction of chromium ions into the SBN structure. Absorption and fluorescence spectra attributed to chromium ions in 3+, and 4+ valence states are observed. Possible position of chromium ions in different valence state in SBN structure is suggested.

# Physical origin of the short-circuit currents in the langasite family crystals

**V. Umylin[1], N. Kozlova[1], E. Zabelina[1], A. Korchagin[1], A. Mololkin[1,2], O. Buzanov[2]**

*1- University of Science and Technology MISIS; Leninsky prospect, 4, Moscow, Russia, 119049*
*2- JSC «Fomos Materials»; Buzheninova street, 16, Moscow, Russia, 107023*

*v.umylin@mail.ru*

Crystals of the langasite family, in particular: lanthanum gallium silicate $La_3Ga_5SiO_{14}$ (LGS), lanthanum gallium tantalate $La_3Ga_{5,5}Ta_{0,5}O_{14}$ (LGT) and calcium tantalum gallium silicate $Ca_3TaGa_3Si_2O_{14}$ (CTGS) belong to the one of the groups of functional piezocrystals, including for high-temperature applications. Point group of symmetry 32 ($L_33L_2$). Due to the absence of ferroelectric properties, pyroelectric effect, and phase transitions up to melting temperatures, these crystals are promising piezoelectrics for devices operating in a wide temperature range. These materials are used to manufacture filters in mobile communication systems, temperature sensors, devices operating on surface and bulk acoustic waves, as well as pressure, vibration, and weight sensors operating on the direct piezoelectric effect. The elements used in such devices must exhibit stable functional characteristics during their operation lifetime. The stability of such elements depends on the equilibrium state of the crystal. Non-equilibrium state may depend on the internal characteristics of the material, its prehistory, and under the external stimulations - electric fields or elevated temperatures. Processes that change properties of crystals can appear even without external influences. For example, the application of conductive coatings on the surface of polar cuts of dielectric ionic crystals can significantly effect the electrophysical, dielectric, mechanical properties and phase stability of the material, thereby resulting in their aging and degradation. These processes cause unreliability of the readings transmitted by the devices and a reduction in their operation lifetime up to destruction. The origin and mechanisms of the processes that occur when conductive coatings applied on the surfaces of polar cuts are poorly studied.

Therefore, the investigation of the influence of near-electrode processes on the characteristics of short-circuit currents (SCC) in samples of polar cuts of the langasite family is an important task.

The crystals were grown by JSC «Fomos-Materials» (Moscow, Russia) by the Czochralski method from iridium crucibles in an argon atmosphere with the addition of oxygen. Sample of polar cut (cut perpendicular to the axis 2) with dimensions of 10×10 mm and thickness of 1.3 mm were prepared. Indium foil with 40 μm thickness was used to form symmetric (identical) conductive coatings on the opposite surfaces of the samples. The polarity of the sample was determined using a «PCH041P» piezotester. The samples were heated in an air atmosphere from 25 to 450 °C in a linear automatic mode at a rate of 2 degrees per minute, and cooling was done naturally with the cooling the furnace. The registration of CSS was carried out using the special hardware complex with the specialized software (Certificate of State Registration of the Computer Program No. 2025615960), developed in our laboratory.

The temperature dependences of the SCC were obtained. The currents have a non-linear behavior with several extrema. There is a change in the direction of the flow of the current in the temperature range of 260-280 °C. On the LGS and LGT samples the maximum current up to 0.1 pA at 400 °C, and on the CTGS up to 28 nA at 434 °C.

The studies were carried out in the accredited testing laboratory «Single crystals and stock on their base» NUST MISIS with financial support from the Ministry of Education and Science of Russia within the framework of the state assignment to Universities FSME-2023-0003.

# Purity analysis of facilities for VGF method growth GaAs

**E.N. Voronina, E.N. Mozhevitina, O.A. Nefedov, I.Ch. Avetissov**

*Department of Chemistry and Technology of Crystals, D. Mendeleev University of Chemical Technology of Russia (MUCTR), Moscow 125480, Russia*

*lenavoronina8@gmail.com*

Gallium arsenide (GaAs) is one of the most popular materials used in semiconductor lasers. GaAs is a direct-band-gap semiconductor and possesses a high rate of radiative transitions. However, the presence of impurities in GaAs negatively affects laser properties. Scattering by impurity defects leads to losses in the laser [1].

In the course of this work, a methodology has been developed that allows for the monitoring of impurities that may enter a GaAs single crystal during the growth process. The methodology was tested on systems for producing GaAs single crystals by the Vertical Gradient Freeze (VGF) method [2], both single-crucible and multi-crucible. Cubes made of carbon-carbon composite materials (CCCM) were used as collectors for impurities released from the structural materials of the systems thermal zones. Before use, the collector cubes underwent preparation. The preparation consisted of repeated extraction of impurity elements with concentrated high-purity acids and deionized water upon heating. Following the final extraction, the solution was analyzed by inductively coupled plasma mass spectrometry (NexION 300D, PerkinElmer, USA). The values obtained from the analysis were taken as the blank.

The produced collecting cubes are placed in various parts of the hot zones of growth systems. Systems without high-purity raw materials are brought into a growth mode. Under high temperatures and in an atmosphere of process gases, the system is maintained according to a predetermined growth regime. For GaAs crystal growth, the typical conditions are as follows: a 1300 °C maximum temperature in a hot zone, vacuum at the start of the process up to $10^{-3}$ Pa, and argon pressure during the growth process of 10 bar. All the experiments in the present research were conducted under these conditions. After that the collecting cubes are removed for analysis of trace impurities by extraction into high-purity acid, followed by the impurities' determination by ICP-MS.

This research was funded by the Ministry of Science and Higher Education of Russia through the project FSSM-2025-0006.

[1] W. W. Chow and S. W. Koch, Semiconductor-Laser Fundamentals: Physics of the Gain Materials (Springer), Ch. 1, (1999).
[2] Freiberger Compound Materials GmbH, 2025. Freiberger Compound Materials: GaAs Wafer. [online] Available at: https://freiberger.com/ (accessed on 01 June 2026).

# Specificity of the origin of color-related defect centers in langasite ($La_3Ga_5SiO_{14}$), langatate ($La_3Ga_{5,5}Ta_{0,5}O_{14}$) and catangasite ($Ca_3TaGa_3Si_2O_{14}$) crystals

**E. Zabelina[1], N. Kozlova[1], O. Buzanov[2]**

*1- National University of Science and Technology «MISIS», 119049, Russia, Moscow, Leninsky pr., 4, b. 1*
*2 - FOMOS-Materials, 107023, Russia, Moscow, Buzheninova st., 16*

*zabelina.ev@misis.ru*

Langasite ($La_3Ga_5SiO_{14}$, LGS), langatate ($La_3Ga_{5.5}Ta_{0.5}O_{14}$, LGT) and catangasite ($Ca_3TaGa_3Si_2O_{14}$, CTGS) are the most perspective crystals of the langasite family. All these crystals refer to the point group of symmetry 32. The symmetry of crystals determines the possibilities of manifestation of properties in them [1,2]. But the physical properties of real crystals are determined by their defect structure [3,4]. Defects can arise during the crystal growth in dependence on growth atmosphere, as a result of technological features of growth processes and other environmental factors, in case of elements with a different possible oxidation states, with impurities and dopants, etc. Optical properties are extremely sensitive to crystal defect structure.

The aim of this work was a comprehensive study of the growth atmosphere and isomorphic substitution on the optical properties and defect formation in LGS, LGT and CTGS crystals.

LGT, LGS, CTGS crystals were grown in «FOMOS-Materials» by the Czochralski method in Ir crucibles in an argon-oxygen atmosphere; also LGT crystals were grown in an atmosphere with different oxygen contents.

Discrete values of the principal refractive indices No and Ne of these crystals were measured using the prism goniometric method; all crystals are optically positive. The obtained values were approximated by the Sellmeier equation.

The spectral dependences of the transmittances T were measured on the UV-Vis-NIR spectrophotometer «Cary-5000» with universal measurement accessory «UMA» in the wavelength range of 200-800 nm taking dichroism into account: To for ordinary wave, Te for extraordinary wave.

Based on the obtained T values, the spectral dependences of the linear dichroism Δ and the absorption coefficients α were calculated, and, taking into account the refractive indices, the spectral dependences of the attenuation coefficients μ were calculated. All spectral dependences of T, α, μ revealed absorption bands in the same regions at λ~290, 360, (460 - 480) nm; however, the intensity ratio of these bands in these spectral dependences is not the same. The most reliable way to estimate the absorption band intensities is to calculate the dispersion dependences of μ, since the calculation of μ takes into account the processes of reflection and light scattering from the samples.

The cause of the appearance of defect centers that lead to coloration in LGS, LGT, and CTGS crystals is the volatilization of gallium oxide during crystal growth. The intensity of the crystal color and the corresponding absorption band at λ~(460-480) is determined by the partial pressure in the growth chamber and the content of volatile components in the case of each crystal. The absorption band at λ~(460-480) nm can be reliably attributed to F-centers. The nature of the absorption bands at λ~290 nm and λ~360 nm remains to be established.

The studies were carried out in the accredited testing laboratory «Single crystals and stock on their base» NUST MISIS with financial support from the Ministry of Education and Science of Russia within the framework of the state assignment to Universities FSME-2023-0003.

[1] M.P. Shaskolskaya, Crystallography (Moscow: Higher School), 1984.
[2] I.S. Zheludev Physics of crystalline dielectrics (Moscow: Nauka), 1968.
[3] A.A. Blistanov, Features of structural defects in ionic crystals (dielectrics), News of Higher educational institutions. Electronic equipment materials, vol. 4, pp. 4-15, (2005).
[4] N.S. Kozlova, E.V. Zabelina, V.M. Kasimova, Features of Testing and Monitoring Optical Qualities of Dielectric Single Crystals, Measurement Standards. Reference Materials, vol. 21, pp. 72-85, (2025).

# Low-coherence illumination system for shadow characterization of fast processes

**E. Zaloznaya, A. Savvin, A. Bychkov, A. Dormidonov**

*Dukhov Automatics Research Institute, Federal State Unitary Enterprise,*
*Suschevskaya str., 22, Moscow, 127055, Russia*

*ed.zaloznaya@physics.msu.ru*

One of the methods for recording the parameters of fast-moving objects, including the dispersed phase, which makes it possible to visualize micron-sized particles with ultra-high temporal resolution, is the optical shadow method [1]. The principle of this method is to record on a photosensitive element a shadow image of an object formed by scattered illumination light [2]. In the recorded photo, the shadow of the object contrasts with the bright background formed by the light of illumination system, which allows one to determine the shape, the size and the spatial position of the studied object.

For visualization of fast-moving objects in gas-dynamic experiments one need an illumination system with high brightness and short pulse duration, therefore modern picosecond and femtosecond lasers act as a good source for illumination for shadow method. However high coherence of laser light is an adverse factor leading to a noise speckle pattern appearance in the registered picture [3,4]. We propose a megawatt sub-nanosecond $NV^-$ microchip laser with low temporal coherence as an illumination source in shadow registration method for illumination of speckle distortions associated with interference noise.

The report presents the results of shadow registration of a cloud of particles in a dispersed phase formed by an electric explosion of a copper wire bridge illuminated by a low-coherence $NV^-$ laser. To demonstrate an increase in the resolution of shadow method when using a low-coherence illumination source we also present the results of shadow registration of the same cloud illuminated by a pulse of the second harmonic of the $Nd^{3+}$:YAG laser.

The experimentally demonstrated increase in the spatial resolution of shadow photos due to illumination of the objects under investigation with a low-coherence $NV^-$ laser is confirmed by the results of qualitative analysis.

[1] Huang C., Zhang X., Han R., Fan J., Jiang H., Zhang Y., Yu J., Wang J., Chen Y.,Sun J. Techniques and Advances in Ultrafast Photography // Advanced Photonics Research. – 2025. – V. 6, № 12. – P. e202500184.
[2] Edgerton H.E. Shock wave photography of large subjects in daylight // Review of Scientific Instruments. – 1958. – V. 29, № 2. – P. 171-172.
[3] Malone R., Flurer R., Frogget B., Sorenson D., Holmes V.,Obst A. Shadowgraph illumination techniques for framing cameras // Digest of Technical Papers. 11th IEEE International Pulsed Power Conference (Cat. No. 97CH36127). – 1997. – P. 454-459.
[4] Biasiori-Poulanges L.,El-Rabii H. High-magnification shadowgraphy for the study of drop breakup in a high-speed gas flow // Optics Letters. – 2019. – V. 44, № 23. – P. 5884-5887. DOI: 10.1364/OL.44.005884.

ALT INTERNATIONAL CONFERENCE
Advanced Laser Technologies

# LASER-MATTER INTERACTION

# Formation of surface atomic scale structures by multy-pulsed laser induced diamond photochemical etching and thin film coating.

**V. I. Konov, V. V. Kononenko, N. D. Kurochitsky, V. P. Pashinin, P. A. Pivovarov**

*Prokhorov General Physics Institute of the Russian Academy of Sciences, Moscow, Russia*

*vik@nsc.gpi.ru*

Basing on the results of laser induced diamond processing studies, the technology that allows to fabricate surface nanostructures with extremely small (atomic scale) relief amplitude has been developed. Realization of the novel technology requires low intensity multiple pulsed irradiation in chemically active medium (gases). It differs from the traditional physical (thermal) methods of laser materials processing where the amplitude of the produced structures is determined by the length of laser pulsed thermal action. In the proposed technology the result of each laser pulse treatment depends on the thickness of the adsorbed layer formed by chemically active gas molecules on the material surface to be irradiated. This layer can completely or partially react in the cause of each pulse forming a coating. Between laser pulses the thickness of the adsorbed layer can be restored if the delay time between pulses is high enough.

When laser stimulated surface chemical reaction leads to formation of volatile products or products that can be deleted by additional treatment, such a regime is named laser nanoablation because in this case atomic scale material layer can be removed. If in each laser pulse deposition from the gas of the material different from the substrate material is initiated, we speak about CVD (chemical vapor deposition) growth of a thin film. Thus, by selecting the composition and pressure of gas mixture, parameters of laser pulses and beam focusing on the sample surface one can vary the height (depth) of the deposited (ablated) surface structures.

The results of the experiments with nano, pico and femto second laser pulses will be presented. Atomic scale surface structures on single crystal diamond will be demonstrated. Two regimes of laser induced surface chemical treatments were investigated: (i) diamond nanoablation by photoetching in oxidizing environment (air at atmospheric and lowered pressure); (ii) deposition on diamond surface of silicon based thin films from $SiH_4$:$H_2$ gas mixture. In both cases for radiation intensity below the diamond surface graphitization threshold, the rates of nanorelief formation turned out to be extremely low $10^{-2}$-$10^{-8}$ nm/pulse. The minimal produced structure amplitude could reach 1-10 nm. The necessary condition to produce and observe such ultra-small structures was application of lasers with extremely high pulse repetition rate $\leq 10^6$ Hz.

This work is supported by RSF Grant № 24-12-00137.

# New innovative technologies for laser additive manufacturing based on artificial intelligence

**Yu.N. Kulchin**

*Institute of Automation and Control Processes FEB RAS*

*Kulchin@iacp.dvo.ru*

Today, the entire world is living in the Fourth Industrial Revolution, which involves a new approach to production based on the widespread adoption of information technology in industry, the large-scale automation of business processes, and the proliferation of artificial intelligence. The technologies of the Fourth Industrial Revolution represent a wide range of innovative solutions that enable the digital transformation of production. These technologies contribute to increased productivity, improved worker safety by reducing hazardous working conditions, enhanced competitiveness, the development of groundbreaking products, and more.

Additive manufacturing technologies for metal parts, which are part of the Fourth Industrial Revolution's Industry Technologies, are recognized as the future of the manufacturing industry due to their capabilities: manufacturing complex shapes; significantly reducing the weight of products and shortening the time required for prototype production; improving the efficiency of material utilization. Since the 1990s, there has been a lot of buzz surrounding additive manufacturing. However, it is only now that companies feel ready to adopt it as a practical production method. However, along with the undeniable advantages of implementing additive technologies, there are barriers that seriously hinder their active use in real production.

The main problem is the need to take into account the influence of a large number of factors and technological parameters of laser processing on the elemental composition of the deposited layers, on the formation of various types of defects (cracks, pores, delaminations, delamination, etc.) and on the microstructure of the part material, as well as on the physical and mechanical characteristics of the part that has undergone the necessary post-processing of the resulting product. Currently, as a rule, acceptable modes of laser fusion of metal materials are often selected by trial and error. This approach to the design of additive manufacturing processes is very resource- and time-consuming. In this context, there is a lack of intellectual support for process engineers in the design (planning) of additive processes, which is closely related to the difficulty of scaling technological solutions for the production of metal products using direct energy and material deposition.

The listed problems determine the relevance of creating a viable intelligent decision support system for engineering technologists involved in the process of laser additive processing of materials. This intelligent system should provide the technologist with recommendations on setting the modes of operation of laser robotic equipment suitable for a specific practical application, which will allow to exclude the human factor as much as possible, i.e. to move to robotics and artificial intelligence.

One of the common approaches to the creation of software systems is the design, development and engineering of software based on ontologies (OBSE/ODSE, Ontology-Based Software Engineering). The purpose of this report is to present the works aimed at creating an ensemble of ontological models that form the basis of an intelligent decision support system for engineering technologists in the field of Laser Additive Manufacturing of metal parts using DED-LB technology.

# Micro and Nano 3D Printing Using Light

**M. Farsari**

*FORTH/IESL, N. Plastira 100, 70013, Heraklion, Greece*

Light-based micro and nano 3D printing has established itself as a transformative manufacturing technique for producing intricate structures with exceptional accuracy and virtually unlimited design flexibility. Within this family of technologies, Multiphoton Polymerization (MPP) represents a particularly sophisticated fabrication approach, capable of generating true three-dimensional constructs at the micro- and nanoscale. The technique works by directing tightly concentrated femtosecond laser pulses into photosensitive materials, triggering highly confined polymerization reactions that allow complex geometries to be written directly with sub-micrometer precision.

This distinctive capability has unlocked new possibilities across numerous fields [1]. In the area of integrated photonics, light-based 3D printing sidesteps the limitations inherent to traditional planar manufacturing, enabling the realization of fully three-dimensional optical components and circuits. Waveguide arrays, vertical coupling elements, photonic crystal structures, and on-chip micro-optical components can be produced within a unified platform, substantially broadening the design space for telecommunications, optical sensing, and emerging applications in quantum and neuromorphic computing.

In the biomedical domain, light-driven micro and nano 3D printing has shown considerable promise for constructing tissue engineering scaffolds and other biologically inspired architectures. Its outstanding spatial resolution and geometric adaptability make it well-suited for reproducing the hierarchical, porous structures characteristic of natural tissues, thereby enabling cell organization, tissue repair, and sophisticated biofabrication workflows. Consequently, these technologies are playing a growing role in advancing regenerative medicine, organ-on-chip systems, and the next generation of biomedical devices.

[1] M. Farsari, «Advances in 3D and 4D multi-photon printing for micro and nano photonics Invited,» *Optical Materials Express,* vol. 15, no. 11, pp. 2770-2791, Nov 1 2025, doi: 10.1364/ome.558798.

# Controlling the Allotropic State of Boron and Selenium Nanoparticles by Nanosecond Laser Fragmentation in Liquids

**K.O. Aiyyzhy[1], E.V. Barmina[1,2]**

*1- Prokhorov General Physics Institute of the Russian Academy of Sciences, 38 Vavilov St., Moscow, Russia*
*2- Lebedev Physical Institute of the Russian Academy of Sciences, 53 Leninsky Prospekt, Moscow, Russia*

*aiyyzhy@phystech.edu*

Directed control over the allotropic state of nanoparticles (NPs) is one of the key yet still unsolved challenges of laser synthesis. The extreme conditions of nanosecond laser ablation in liquids (PLAL) — temperatures of ~$10^4$ K, pressures up to several GPa, heating rates of ~$10^{10}$ K/s and cooling rates exceeding $10^8$ K/s [1] — offer a unique opportunity to address this challenge by enabling non-equilibrium structural transformations, including directed allotropic transitions in covalent elements, which have remained virtually unexplored to date.

The importance of controlling allotropic modification stems from the fact that the allotropic state (amorphous or crystalline) largely determines key NP characteristics such as reactivity, bioavailability, and toxicity [2,3]. This work presents the results of a systematic study of laser-induced allotropic modification of boron and selenium NPs, demonstrating a universal approach to tailoring the functional properties of nanomaterials through phase-state control.

Thus, upon nanosecond laser fragmentation with a Nd:YAG laser (1064 nm, 3.6 ns), the initial βrhombohedral phase of boron micropowder transforms into an amorphous state with nanocrystalline inclusions (fig 1, a)[4]. Likewise, under exposure to a copper vapor laser (510.6/578.2 nm, 10 ns) during nanosecond laser fragmentation, crystalline selenium becomes fully amorphized (fig 1, b) [5]. The role of pulse duration, fluence, and wavelength in governing these transitions has been established.

Consequently, controlling allotropic modification during PLAL paves the way for the targeted synthesis of functional nanomaterials with tailored properties for biomedicine, energy, and agricultural technologies.

This work was supported by Russian Science Foundation, Grant № 24-62-00018.

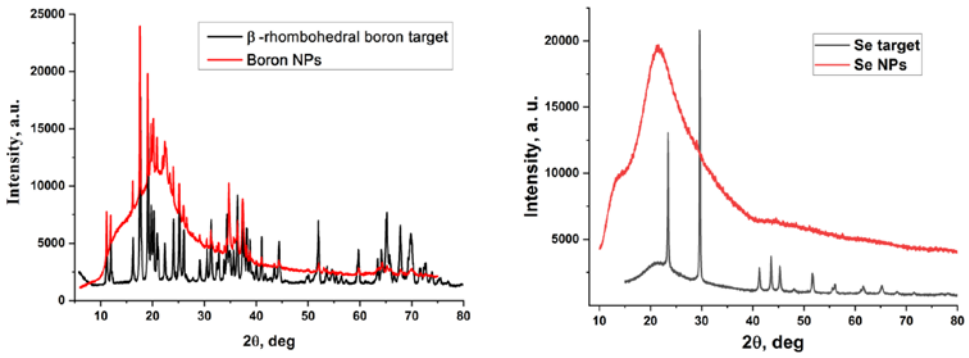


a b

**Fig 1.** X-ray diffraction patterns of the initial Boron target and generated Boron NPs (a); the initial Selen target and generated Selen NPs (b).

[1] D. Zhang, B. Gökce, S. Barcikowski, Laser synthesis and processing of colloids: fundamentals and applications, *Chem. Rev.*, 117, 3990–4103 (2017).
[2] K. Li, J. Li, S. Zhang et al., Amorphous structure and crystal stability determine the bioavailability of selenium nanoparticles, *J. Hazard. Mater.*, 465, 133287 (2024).
[3] W. Ao, J.H. Zhou, J.Z. Liu, W.J. Yang, Y. Wang, Effects of particle size and crystalline form on the ignition and combustion characteristics of boron particles, *Chin. J. Energ. Mater.*, 21, 800–805 (2013).
[4] K.O. Aiyyzhy, E.V. Barmina, D.I. Kobtsev, G.A. Shafeev et al., Laser ablation and fragmentation of Boron in liquids, *Opt. Laser Technol.*, 155, 108393 (2022).
[5] K.O. Ayyyzhy, E.V. Barmina, G.A. Shafeev et al., Laser fabrication and fragmentation of selenium nanoparticles in aqueous media, *Phys. Wave Phenom.*, 27, 113–118 (2019).

# Laser synthesis of amorphous $PdSe_{2-x}$ for high-performance photonics, catalysis and photothermal applications

**A. Ushkov, N. Belozerova, D. Dyubo, I. Martynov, S. Novikov, A. Vyshnevyy, A. Arsenin, A. Syuy**

*Moscow Institute of Physics and Technology, Dolgoprudny, Russia*

*Alsyuy271@gmail.com*

Transition metal dichalcogenides (TMDCs) exhibit remarkable optoelectronic properties, yet their functionality is predominantly governed by thermodynamically stable crystalline phases. Accessing metastable amorphous phases with engineered defects could unlock novel functionalities, but conventional synthesis methods struggle to stabilize such states.

Femtosecond pulsed laser ablation in liquid (fs-PLAL) was employed to ablate bulk $PdSe_2$ crystals in deionized water. The resulting colloids were characterized by TEM/SAED, Raman spectroscopy, EDX, XPS, and photoluminescence. Photothermal conversion efficiency (PCE) was measured under NIR-I illumination (830 nm). SERS performance was evaluated using model dyes (Rh6G, RhB, CV, MO). Photocatalytic activity was assessed via methylene blue degradation under simulated solar irradiation.

We demonstrate a single-step, ligand-free strategy using femtosecond pulsed laser ablation in liquid (PLAL) to transform crystalline, stoichiometric palladium diselenide ($PdSe_2$) into highly stable, amorphous, non-stoichiometric nanoparticles ($PdSe_{2-x}$, with $x \approx 1$). This laser-driven amorphization creates a high density of selenium vacancies and coordinatively unsaturated sites, unlocking emergent functions absent in the crystalline precursor. The synthesized $PdSe_{2-x}$ nanoparticles exhibit plasmon-free surface-enhanced Raman scattering with an enhancement factor exceeding $10^6$ for crystal violet, a 50-fold increase in photocatalytic activity for methylene blue degradation under simulated solar irradiation, and near-infrared photothermal conversion efficiency reaching 83% at 830 nm. Structural characterization via TEM, SAED, Raman spectroscopy, and XPS confirms the amorphous nature and defect-rich composition (Pd:Se ≈ 1:1) of the nanoparticles. The superior functional performance is attributed to synergistic mechanisms: resonant charge transfer facilitated by defect-state energy levels, enhanced molecular adsorption at coordinatively unsaturated surface sites, and plasmon-free electromagnetic hotspots in nanoparticle aggregates. Our findings establish laser-induced amorphization as a powerful top-down approach for defect-engineered transition metal dichalcogenides, advancing their practical usage in plasmon-free sensing, photocatalysis, and nanomedicine applications.

Laser-induced amorphization via fs-PLAL establishes a powerful top-down approach for defect engineering in TMDCs. The resulting amorphous $PdSe_{2-x}$ nanoparticles represent a versatile, multipurpose platform for advanced applications in plasmon-free sensing, photocatalysis, and nanomedicine, demonstrating that controlled disorder can be harnessed to surpass the performance of ordered crystalline counterparts [1-3].

The study was supported by the Ministry of Education and Science of the Russian Federation, FSMG-2024-0014.

[1] A. Ushkov, N. Belozerova, D. Dyubo, et al., Laser-Synthesized Amorphous $PdSe_{2-x}$ Nanoparticles: A Defect-Rich Platform for High-Efficiency SERS, Photocatalysis, and Photothermal Conversion, Advanced Materials Interfaces, vol. 13, pp. e00902, (2026).
[2] G.I. Tselikov, G.A. Ermolaev, A.A. Popov, et al., Transition Metal Dichalcogenide Nanospheres for High-Refractive-Index Nanophotonics and Biomedical Theranostics, Proceedings of the National Academy of Sciences, vol. 119, pp. e2208830119, (2022).
[3] T. Jena, M.T. Hossain, U. Nath, et al., Evidence for Intrinsic Defects and Nanopores as Hotspots in 2D $PdSe_2$ Dendrites for Plasmon-Free SERS Substrate with a High Enhancement Factor, npj 2D Materials and Applications, vol. 7, pp. 8, (2023).

# Laser-synthesized spherical $Ti_3C_2$ mxene nanoparticles for in vivo photothermal therapy of cancer

**G.V. Tikhonowski, G.I. Tselikov, I.S. Kazantsev, A.V. Arsenin, V.S. Volkov**

*Emerging Technologies Research Center, XPANCEO, Dubai Investment Park First, Dubai, United Arab Emirates*

*tikhonowski@xpanceo.com*

MXenes, a family layered transition-metal carbides and nitrides, have emerged as a promising platform for biomedicine owing to their metallic conductivity, hydrophilicity, and strong near-infrared (NIR) absorption arising from interband transitions (NIR-I) and localized surface plasmon resonances (NIR-II). For light-to-heat conversion, the efficiency of MXenes such as $Ti_3C_2$ can surpass that of gold nanorods, making them attractive sensitizers for photothermal therapy (PTT) [1-3].

The clinical translation of MXene-based photothermal agents remains constrained by their morphology because conventional synthesis through selective etching, delamination, and exfoliation yields heterogeneous nanosheets with broad size distributions and irregular sharp edges. Since nanoparticle (NPs) size, shape, and surface chemistry ultimately govern biodistribution, cellular uptake, and clearance, precise morphological control of MXenes represents a decisive yet unsolved step toward safe and effective PTT.

To overcome these limitations, we employed femtosecond laser fragmentation of MXene powder in liquid to produce spherical $Ti_3C_2$ NPs. Ultrashort pulses induce rapid, localized energy deposition and material disintegration, while fast cooling in the liquid medium preserves the crystalline structure and internal optical properties of the initial material. By tuning the fragmentation medium and irradiation conditions, we gained control over particle size, morphology, and crystallinity, obtaining nanospheres that were stabilized with a polyacrylic acid coating ($Ti_3C_2$@PAA).

The resulting crystalline $Ti_3C_2$ nanospheres retained strong optical absorption in both the NIR-I and NIR-II biological transparency windows and achieved superior photothermal conversion efficiencies of 68% and 63% under 808-nm and 1064-nm laser irradiation, respectively. In contrast to nanosheets, the NPs induced neither photodynamic effects nor ROS generation, and demonstrated negligible toxicity *in vitro* across and *in vivo* in healthy mice. Upon laser irradiation the nanospheres produced potent photothermal cytotoxicity. When applied for PTT, systemic administration of $Ti_3C_2$@PAA followed by 808-nm irradiation inhibited tumor growth and prolonged the median survival of animals 1.4-fold [4].

Taken together, these findings introduce spherical MXenes as a new class of biocompatible nanomaterials and provide the first demonstration of their safety and therapeutic applicability. Laser fragmentation transforms irregular nanosheets into uniform, crystalline nanospheres that combine favorable morphology, retained optical functionality, enhanced NIR-I photothermal conversion, and an improved safety profile.

[1] G. Tselikov, et al., Tunable nanostructuring for van der Waals materials, ACS nano, 19, 25 (2025).
[2] G. Tselikov, et al., Transition metal dichalcogenide nanospheres for high-refractive-index nanophotonics and biomedical theranostics, Proceedings of the National Academy of Sciences, 119, 39 (2022).
[3] I. Kazantsev, et al. Printable van der Waals Nanoparticles for Additive Technologies, Nano Letters (2026).
[4] J. Babkova, et al., Shaping Ti3C2 MXene Nanospheres for Precision Near-Infrared Photothermal Therapy, Advanced Functional Materials, 24090, (2026).

# Ablation-free pulsed laser nanotexturing for photonics and optoelectronics

**A. Kuchmizhak**[1,2]

*1- Institute of Automation and Control Processes, Far Eastern Branch, Russian Academy of Science, Vladivostok 690041, Russia*
*2- Far Eastern Federal University, Vladivostok, Russia, 10 Ajax Bay, Russky Island, Vladivostok 690091, Russia*

*alex.iacp.dvo@mail.ru*

Laser technologies provide practically unlimited pathways for material patterning at practically attractive throughput. However, ablation process associated with the material removal in a liquid phase accompanied by formation and redeposition of the nanoparticles introduces a certain degree of uncontrollability into the fabrication process reducing fabrication accuracy and resolution as well as the quality of the produced patterns. In this presentation, several laser processing approaches, where unique combination of material properties perfectly matching the ultrashort laser pulse durations, are presented demonstrating direct laser nanofabrication with sub-100 nm precision. Examples include thermomechanical sculpturing of thin noble metal films [1], sublimative processing of halide perovskites [2] and thermochemical laser-induced periodic surface structuring [3,4]. Applications of the developed technologies for structural coloring, sensing as well as fabrication of the plasmonic and optoelectronic devices will be also discussed.

[1] D. Pavlov, et.al., Nonlinear light conversion and infrared photodetection with laser-printed plasmonic metasurfaces supporting bound states in the continuum. Light: Science & Applications 15 (1), 23 (2026)
[2] A. Zhizhchenko, et.al., Polarization-dependent direct laser nanostructuring of halide perovskites, Photonics and Nanostructures-Fundamentals and Applications 66, 101408 (2025)
[3] V. Ladipas, et.al., Structural coloration on titanium films by direct femtosecond laser patterning empowered by neural networks, ACS Applied Materials & Interfaces 17 (10), 16122-16131 (2025).
[4] V. Ladipas, et.al., Full-Color Femtosecond Laser Painting on Titanium Films at 35000 DPI Resolution, The Journal of Physical Chemistry Letters 17, 2654-2660 (2026).

# Pioneering pulsed laser synthesis of colloids

**A. Fojtik**

*Faculty of Biomedical Engineering, Czech Technical University, Prague, Czech Republic (CR)*

*fojtiant@fbmi.cvut.cz*

During the past several decades, "small-particle" research has become quite popular in various fields of physics and chemistry. By "small particles" are meant clusters of atoms or molecules of metals, semiconductors and others materials, ranging in size between single atoms or molecules and bulk materials.

In the year 1991 it has been assumed, that all substantial facts and technologies regarding nanoparticles were already known.

We have been using methods: Pulls radiolysis, Stop flow techniques, and chemical synthesis in liquid system, in solutions, chemical dissolution of big particles to small nanostructures.

What more was left besides tuning of existing manufacturing technologies and developing clever applications?

**Could lasers be put to a good use?**

Attempts were made, but without any particular breakthrough...

At that time, we aimed to new type of nanostructures and we really had not expected that usage of lasers could bring us something revolutionary.

**But there was a surprize waiting around the corner...**

We hoped that by an absorption of intense laser beam by a solid state material, producing temperature of plasma of many thousands kelvins [1] (similar like in sonochemistry, where several thousand kelvins are reached in oscillating gas bubbles in a liquids [2]), similar effects could be reached. Nothing more, nothing less.

Initiating plasma by a focused laser beam (694nm Ruby laser flash) to thin film of solid state material thus creates conditions similar to a plasma discharge and cause ablation condition. When some liquid surrounds „hot plasma spot", evaporated products are very quickly cooled down and very small nanoparticles can be produced. We hoped that maybe under these conditions new colloidal particles and clusters could be produced. Perhaps even some new form of nanostructures?

First attempt was realised in a small 1 cm quartz cuvette. Filled by water,

Inside with a strip of metal. Cuvette was placed into the laser beam focused on the metal foil.

All was working.

After several pulses…. show through potholes to the cuvette.

Very small, microscopic leak…..But was there.

In order to exclude this undesirable effect from happening, it was necessary to use a very short focal lens.

Reason: to avoid thermal destruction of cuvette walls.

What we had learnt from this experiment? We concluded that smaller particles are formed with increasing laser energy. Smaller particles reacted more quickly with each other (case of silver oligomers) and some small metallic particles reacted with water and oxidized (in the case of Si nanoparticles).

Relatively broad size distribution was found in all experiments at laser synthesis of colloids.

(At that time we did not expect that this idea would have such an enthusiastic following)

Presently, situation for such a field of research, i.e., „Nanoparticle Generation by Lasers in Liquids", is becoming a much hotter topic due to availability of picosecond and femtosecond lasers. Shorter time for energy deposition causes less problems with high temperature, narrowing the size distribution, with possible applications in biological systems.

**Where are we now and what's next?**

Open the research mainly for biomedical and biomedicine applications.

For example, only this way can be prepare Fe /Ag magnetic nanoparticles, with high purity, which are at top interest for research against HIV virus and strategically defence against gram-positive batteries like anthrax (our attempt).

**See the lecture….**

[1]. Fojtik A., Henglein A.: Laser Ablation of Films and Suspended particles in a Solvent: Formation of Cluster and Colloid Solutions; Ber. Buns.Phys.Chem.Vol.97, No.9, 1993, p.252,

[2]. Hart E. J., Fischer Ch.-H., and Henglein A., J. Phys. Chem. 94, 284 (1990).

**Laser, small-particle, clusters of atoms, Pulls radiolysis, Stop flow techniques**

# Enhanced Efficiency and Improved Nanoparticle Size Control in Laser Ablation of Gold in Water by GHz-Burst Irradiation

**M. Spellauge[1], R. Auer[1], V. Taebling[1], A. Ziefuss[2], D. Förster[1], S. Barcikowski[2], H. P. Huber[1]**

*1- Laser Center HM, Munich University of Applied Sciences HM, Lothstr. 34, 80335 Munich, Germany*
*2- Technical Chemistry I and Center for Nanointegration Duisburg-Essen (CENIDE), University of Duisburg-Essen, Universitätsstr. 7, 45141 Essen, Germany*

*maximilian.spellauge@hm.edu*

Laser ablation in liquids (LAL) enables the generation of nanoparticles from a broad range of materials but remains limited in productivity, which must reach the g/h scale to compete with chemical synthesis routes [1]. This limitation arises from loss mechanisms, including nonlinear losses in the liquid, redeposition of ablated material, cavitation bubble shielding, and shielding by persistent microbubbles and nanoparticles [1]. While cavitation bubble shielding and persistent microbubble and nanoparticle shielding can be mitigated by fast scanning and flow-through reactors, respectively, up to 80% of the ablated material can be redeposited, rendering redeposition a major mechanism limiting productivity [2]. To mitigate redeposition, temporal pulse shaping has been proposed, where subsequent pulses interact with the ablated material [2]. As cavitation bubble formation occurs on a timescale of 1 ns to 2 ns after pulse impact [3], the laser energy must be delivered before cavitation bubble emergence to avoid shielding, making GHz-bursts with inter-pulse spacing of hundreds of picoseconds a promising approach. However, whether this approach enhances nanoparticle generation efficiency without increasing cavitation bubble shielding or compromising nanoparticle quality remains unclear.

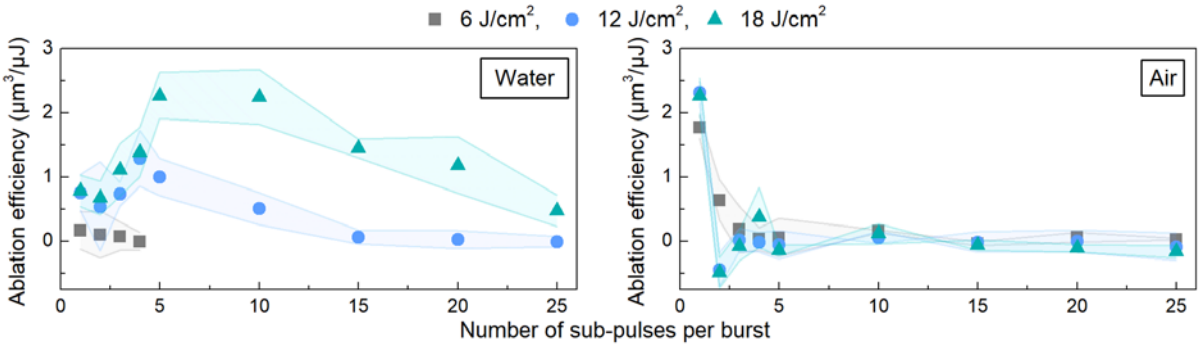


**Fig. 1.** Ablation efficiency in dependence of the number of pulses per burst in water (left) and air (right) for various peak fluences.

Here, we compare single-pulse and GHz-burst ablation (205 ps inter-pulse delay) of Au in water. Splitting the total pulse energy into 5 to 10 sub-pulses enhances the ablation efficiency by a factor of approximately 3, from 1.3 µm³/µJ in single-pulse to 4.1 µm³/µJ in GHz-burst mode (Fig. 1, left). Higher pulse numbers lead to an efficiency decrease attributed to the onset of cavitation bubble shielding. Since GHz-burst ablation in liquid reaches the air ablation efficiency (Fig. 1, right), it is hypothesized that temporal pulse shaping mitigates redeposition. Furthermore, the cavitation bubble generated by a GHz-burst has a 10% smaller radius and collapses 10% earlier than in single-pulse ablation, indicating that no additional constraints on scalability are introduced. Finally, nanoparticle size distribution analysis shows that GHz-burst produces a 2.5 times narrower distribution compared to single pulse LAL, indicating that nanoparticle quality is improved. These results demonstrate that GHz-burst laser ablation in liquids is a promising approach for advancing laser-based nanoparticle production toward an industrial scale.

[1] I. Khairani Y, G. Mínguez-Vega, C. Doñate-Buendía, B. Gökce, Green nanoparticle synthesis at scale: a perspective on overcoming the limits of pulsed laser ablation in liquids for high-throughput production, Physical Chemistry Chemical Physics, 25, 19380-19408 (2023)
[2] M. Spellauge, D. Redka, A. Podhrazsky, K. Eckmann, C. Eulenkamp, O. Koepp, C. Doñate-Buendia, B. Gökce, S. Barcikowski, H. P. Huber, Mechanisms of Laser Ablation in Liquids and Their Impact on the Efficiency of Nanoparticle Generation, Laser & Photonics Reviews, 20, 0:e01348, (2025)
[3] S. Dittrich, M. Spellauge, S. Barcikowski, H. P. Huber, B. Gökce, Time resolved studies reveal the origin of the unparalleled high efficiency of one nanosecond laser ablation in liquids, Opto-Electronic Advances, 5, 210053-210053, (2022)

# A new type of optoacoustic metamaterial and elastoplastic phenomena associated with weak nanosecond pulses

**N. Inogamov[1], S. Romashevskiy[2], Y. Petrov[1], V. Khokhlov[1]**

*1- L.D. Landau Institute for Theoretical Physics of Russian Academy of Sciences, 142432, Moscow Region, Chernogolovka, Akademika Semenova av., 1A, Russia*
*2- Joint Institute for High Temperatures of the Russian Academy of Sciences, 125412 Moscow, Izhorskaya 13, Bd. 2, Russia*

*nailinogamov@gmail.com*

The proposed report discusses a range of relatively weak laser effects. The first part of the report presents results that will be of interest to specialists in optoacoustics and nanophotonics/metamaterials. In this part, we work with ultra-short pump and probe pulses with durations of 10s-100s fs; induced pressures are less than 10 GPa. The objects used are ultra-thin films with a thickness of 10s nm on dielectric substrates; in our work, the substrates are made of glass and silicon. The report summarizes the results of [1-5]. It reports the discovery of a class of metamaterials based on structured nickel films, which, along with their spectral properties (extraordinary transmission), also function as an optoacoustic transducer. Due to the extraordinary transmission, we observe the propagation of an acoustic wave in a glass or silicon substrate through a thick (up to 7 skin-layer thicknesses) nickel film.

In the second part, the effect of a nanosecond pulse (10 ns) on a polycrystalline copper sample is analyzed. As mentioned, the effects are sufficiently weak in amplitude. The analysis is limited to a range of temperatures below those at which evaporation begins to have a significant impact on the evolution of the thermal field. The results are presented in articles [6-8], which were carried out in collaboration with co-authors on experiments and large-scale molecular dynamics simulations. At nanosecond exposure, the amplitude of acoustic radiation is much smaller, if compared with ultra-short pulses at the same absorbed energy. Analyzed how such radiation is formed in the absence of contribution from vapor pressure. There is, firstly, a contribution from solid-state thermal expansion with amplitudes less than 100 atmospheres. Secondly, a peculiar contribution to the acoustic field is made by the process of melting and crystallization. Detecting this radiation on the back side of the plate using a piezoelectric element and comparing it with the developed physical model will allow us to quantify what happens during nanosecond exposure. In particular, it will become clear how fast the rates of melting and crystallization can be.

[1] Yu. Petrov, S. Romashevsiy, A. Dyshlyuk et al.,, Abnormal light transmission through optically thick nickel films that are optoacoustic transducers (in Russian), ZhETF, vol. 167, No. 5, pp. 645-671, (2025).
[2] A. Dyshlyuk, S. Romashevskiy, Yu. Petrov et al., Simulation of Brillouin Oscillations Generated by a Metamaterial Based on a Nanostructured Nickel Film, JETP Letters, vol. 123(3), pp. 158-188, (2026).
[3] A. Dyshlyuk, N. Inogamov, O. Vitrik, Optical Properties of the Substrate-Buried Spherical Dipole Nanoantenna, Bulletin of the Russian Academy of Sciences: Physics, Vol. 88, Suppl. 3, pp. S450–S456 (2024).
[4] N. Inogamov, V. Khokhlov, S. Romashevskiy, et al., Strong excitation of the gold electronic subsystem by an ultra-short laser pulse and relaxation processes near the melting point (in Russian), ZhETF, vol. 165(2), pp. 165-190 (2024).
[5] A. Dyshlyuk, N. Inogamov, O. Vitrik, FEATURES OF BACKSCATTERING OF LIGHT BY PLASMONIC DIPOLE NANOANTENNS SUBMERGED IN A METAL SUBSTRATE (in Russian), Opticheskii Zhurn. Vol. 23, No. 3, pp. 7-17, (2026).
[6] I. Nelasov, S. Manokhin, Yu. Kolobov, et al., Evolution of the microstructure of the copper surface layer during thermocycles with nanosecond laser pulses (in Russian), ZhETF, vol. 167(6), pp. 782-797 (2025).
[7] V. Rogalin, V. Zhakhovsky, N. Inogamov et al., Thermal cycling of the copper surface in preablation mode when heated by ultraviolet laser nanosecond pulses (in Russian), Physics of the Solid State (FTT), vol. 67, No. 12, pp. 2371--2375, (2025).
[8] I. Nelasov, S. Manokhin, Yu. Kolobov et al., Thermoplastic modification of polycrystalline copper surface microstructure by nonmelting nanosecond laser pulses, J. Appl. Phys., sent to journal.

# Engineering chiral metal nanostructures via continuous and pulsed laser irradiation

**D.R. Dadadzhanov[1,2], D. Feferman[2], N.S. Petrov[1], V.D. Babaylova[1] V.S. Tuchin[1], I.A. Gladskikh[1], T.A. Vartanyan[1], G. Markovich[2]**

*1- International Research and Education Centre for Physics of Nanostructures, ITMO University, 49 Kronverksky Pr., St. Petersburg 197101, Russian Federation*
*2- School of Chemistry, Raymond and Beverly Sackler Faculty of Exact Sciences, Tel Aviv University, Tel Aviv 6997801, Israel*

*daler.dadadzhanov@gmail.com*

The report at the conference will present experimental and theoretical results on the formation of linear and circular dichroism in silver and gold plasmonic nanostructures under continuous-wave and pulsed laser irradiation [1–3]. Laser methods for controlling the optical response of initially achiral nanostructures will be considered, including spectral hole burning, photoinduced oxidation–reduction reactions, and plasmon-induced radical polymerization. The mechanisms responsible for dichroism formation will be discussed, with emphasis on the relative contributions of photochemical processes, plasmonic near-field enhancement, hot-carrier generation, and thermally induced structural transformations. Several types of plasmonic systems will be described, including self-organized silver and gold nanoparticle films obtained by vacuum deposition and subsequent thermal treatment, as well as chemically synthesized core–shell nanostructures consisting of gold nanorods and silver shells. The appearance of circular dichroism under circularly polarized irradiation and linear dichroism under linearly polarized irradiation will be analyzed in relation to laser-induced modification of plasmonic resonances. A separate part of the report will be devoted to the application of plasmon-induced radical polymerization for site-selective deposition of polymer in the near field of nanoparticles. The use of artificial intelligence technologies for rapid visualization and prediction of near-field distributions around plasmonic nanostructures will also be demonstrated.

This work was supported by the Russian Science Foundation (Project 22-72-10057-П).

[1] D.R. Dadadzhanov, N.S. Petrov, I.A. Gladskikh, D. Feferman, N.A. Toropov, L. Gu, P. Yu, Z. Wang, T.A. Vartanyan, A.O. Govorov, G. Markovich, Chiral Transformation of a Nanostructured Silver Film by Illumination with Circularly Polarized Light, ACS Nano, Vol. 20, p. 9516–9525, (2026).
[2] I.A. Gladskikh, N.A. Toropov, D.R. Dadadzhanov, M.A. Baranov, A.A. Gladskikh, G. Mirzoyan, G. Markovich, T.A. Vartanyan, Laser-Based Reshaping of Self-Organized Metasurfaces of Supported Ag Nanoparticles for Encoding Tunable Linear Dichroism Patterns, ACS Applied Nano Materials, Vol. 7, p. 11342–11349, (2024).
[3] A.A. Sapunova, Y.I. Yandybaeva, R.A. Zakoldaev, A.V. Afanasjeva, O.V. Andreeva, I.A. Gladskikh, T.A. Vartanyan, D.R. Dadadzhanov, Laser-Induced Chirality of Plasmonic Nanoparticles Embedded in Porous Matrix, Nanomaterials, Vol. 13, p. 1634, (2023).

# Ultrashort-Pulse Laser Crystallization of a-Ge:H Films and a-Ge/a-Si Nanolayers: The Role of Pulse Duration and Non-Thermal Mechanisms

**Y. Cheng[1], F.A. Samokhvalov[2], I.E. Nazarova-Merkulova[2], S.V. Starinsky[2], V.A. Volodin[1,3]**

*1- Novosibirsk State University, Pirogova street, 2, 630090, Novosobirsk, Russia.*
*2- S.S. Kutateladze Institute of Thermophysics SB RAS, Lavrentyev Ave. 1, 630090, Novosibirsk, Russia.*
*3- A.V. Rzhanov Institute of Semiconductor Physics SB RAS, Lavrentyev Ave. 13, 630090, Novosibirsk, Russia.*

*chengyuzhu9@gmail.com*

Pulsed laser annealing is an effective technique for crystallizing amorphous semiconductor films on non-refractory substrates. Polycrystalline and nanocrystalline Si and Ge films and nanostructures based on them are used in flexible electronics and sensors [1,2].

The samples were produced using plasma-enhanced chemical vapor deposition (PECVD) on a non-refractory glass substrate at 160°C. A 240-nm-thick Ge film was obtained, along with three structures consisting of five pairs of Ge/Si layers. The Si layers were 20 nm thick, while the germanium layers varied in thickness—10, 5, and 3 nm. Pulsed laser annealings (PLA) were carried out using Avesta TETA-3/200-HE infrared (IR) laser, characterized by a fundamental wavelength of $\lambda$=1035 nm and an adjustable pulse duration ($\tau$) from 220 fs to 10 ps. The phase composition of the germanium films was investigated by the analysis of Raman spectra (RS).

RS of the samples showed that the initial films contained only amorphous germanium and silicon. For the germanium-on-glass sample, the influence of pulse duration on the crystallization process during PLA was observed: at $\tau$ = 220 fs, the crystallization start threshold was 46 mJ/cm², but at $\tau$ = 2 ps and 10 ps, no indications of crystalline phase nucleation or growth were seen. At a fluence of 74 mJ/cm² or more, practically complete crystallization was attained for all $\tau$ values, with the crystalline phase exceeding 60%.

After PLA of the Ge (10 nm)/Si (20 nm) multilayer structure at a fluence of 46 mJ/cm² and a duration of 220 fs, selective partial crystallization of germanium occurred, but the silicon layers remained amorphous. At $\tau$ = 2 ps and 10 ps, the entire structure remained in an amorphous state. With a further increase in fluence, silicon crystallization was initiated; at significantly higher fluences, the germanium and silicon layers intermixed to form a crystalline GeSi solid solution. The crystallization kinetics were consistent with those reported previously [2].

It was estimated that at a fluence of 46 mJ/cm², the energy absorbed in the film is insufficient for its complete melting. This makes the classical liquid-phase crystallization via complete melting unlikely. The absorbed photons energize the electron subsystem, resulting in the electron being excited from the valence band to the conduction band, breaking the valence bond. It is known that the energy transfer duration between electrons and phonons is 1-2 ps; immediately following the pulse, the electron temperature markedly surpasses that of the atomic lattice. Consequently, with femtosecond PLA, the atomic lattice stays at a low temperature upon the conclusion of the pulse. This melting mechanism, presumably arising in our instance from non-thermal factors, is referred to as “cold” annealing, “plasma” annealing, or “cold” melting [3].

Accordingly, the PLA regimes for the complete crystallization of a germanium film and for the selective crystallization of germanium within a multilayer structure were identified, and a crystalline GeSi solid solution was successfully obtained. These results may be applied to the fabrication of films and nanostructures for flexible electronics and sensing applications.

[1] S. Suzuki and A. Hara, Evaluation of extremely thin polycrystalline germanium films and their TFT performance fabricated at 400 °C by Cu-induced crystallization on a glass substrate, Japanese J Appl Phys, 63., 051001, (2024).
[2] V.A. Volodin, Y. Cheng, A.V. Bulgakov, Single-shot selective femtosecond and picosecond infrared laser crystallization of an amorphous Ge/Si multilayer stack, Opt Laser Technol, 161., 109161, (2023).
[3] J. Bok, Effect of electron-hole pairs on the melting of silicon, Phys. Lett. A, 84, pp. 448–450, (1981).

# High-repetition-rate time-resolved X-ray diffraction for probing laser-induced structural dynamics

E.I. Mareev[1,2], A.G. Kulikov[1], F.S. Pilyak[1], N.N. Obydennov[1,2], V.F. Efremenko[1], Yu.V. Pisarevskii[1], F.V. Potemkin[1,2]

*1- National Research Centre "Kurchatov Institute", Moscow, 123182 Russia*
*2- M.V. Lomonosov Moscow State University, Moscow, 119991 Russia*

*mareev.evgeniy@physics.msu.ru*

We developed a new class of setups for timeresolved optical pump – Xray probe experiments at the KISIKurchatov synchrotron [1]. The key innovation is hardware averaging implemented inside a FPGAbased ADC, which eliminates data transfer bottlenecks and allows operation at repetition rates up to 10 kHz. Compared to conventional schemes, the signaltonoise ratio is increased by a factor of 50, enabling the detection of rocking curve shifts with an accuracy of about 1 arcsecond and relative amplitude changes as low as 0.1 %, all with subnanosecond temporal resolution.

Using this setup, we studied the response of Si and Fe:$LiNbO_3$ to nanosecond laser impact (532 nm, 4 ns) over a range of fluences. By measuring several Bragg reflections, we added spatial resolution to the experiments, allowing spatiotemporal mapping of laserinduced processes. For silicon, we analysed reflections 111, 333 and 555, which correspond to extinction depths of 1.5, 8.1 and 27.8 μm, respectively. The depthdependent dynamics reveal a clear threestage behavior: rapid energy transfer and partial amorphisation (<100 ns), propagation of a shock wave (0.1–10 μs, pressures 10–40 GPa), and finally thermal relaxation (>10 μs) [2]. Near the surface the diffracted intensity drops sharply, while at larger depths it increases up to 2.25 times due to lattice chirping caused by temperature gradients.

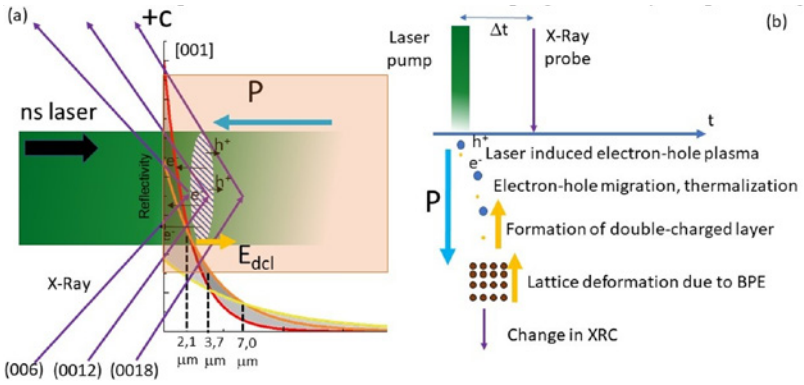


**Fig.1.** Dynamics of laser-induced double charged layer formation in Fe-doped $LiNBO_3$.

In Fedoped $LiNbO_3$, laserinduced charge separation generates an electric double layer via the piezophotovoltaic effect [3]. Using reflections 006, 0012 and 0018 (extinction depths 2.1–7.1 μm), we determined the depth of this charge layer. For positive crystal polarity the layer forms at 4–5 μm below the surface, whereas for negative polarity it is localised in the nearsurface region (<1 μm). The deformation front associated with the layer migrates at a velocity of about 120 m/s, consistent with hole drift. The charge storage capacity is limited; breakdown occurs at a threshold charge of $3 \cdot 10^{-10}$ C, causing an abrupt change in lattice parameter. These results demonstrate that the highrepetitionrate, hardwareaveraging setup provides a powerful and quantitative tool for studying fast, reversible lattice deformations in functional crystals [4].

[1] N. Marchenkov, E. Mareev, A. Kulikov, et al. *Optics*, 5(1), 110, (2024).
[2] F. Potemkin, E. Mareev, et al., *Appl. Surf. Sci.*, 178 164890, (2025).
[2] F.S. Pilyak, E.I. Mareev, A.G. Kulikov, et al., *Phys. Rev. B*, 110, L100302, (2024).
[4] M.V. Kovalchuk, E.I. Mareev, A.G. Kulikov, et al., "*Crystallogr. Rep.*, 69(2), 221229, (2024).

# Plasmon-enhanced up-conversion photoluminescence in $NaGdF_4$: Yb, Er nanoparticles using plasmonic gold dendritic nanostructures

**A.N.B.T. Pham[1], B.G. Arzumanyan[1], C.A. Burko[2], D.H. Bandarenka[2], E.A. Dauletbekova[3], F.L.T.K. Giang[4]**

*1- Joint Institute for Nuclear Research, Laboratory of Neutron Physics, Sector of Raman Spectroscopy, Dubna, Russia*
*2- Applied Plasmonics Laboratory, Belarusian State University of Informatics and Radioelectronics, Minsk, Belarus*
*3- Department of Technical Physics, L.N. Gumilyov Eurasian National University, Astana, Kazakhstan*
*4- Institute of Materials Science, Vietnam Academy of Science and Technology, 18 Hoang Quoc Viet Road, Cau Giay District, Hanoi, Vietnam*

*pnbaotri@gmail.com; arzuman@jinr.ru; h.bandarenka@bsuir.by*

The intense electromagnetic fields localized on noble metal nanostructures exhibit potential applications in particular surface-enhanced spectroscopy. The coupling between surface plasmons and emitters can dramatically modify emission characteristics, known as plasmon-enhanced luminescence phenomenon. Here, we coupled $NaGdF_4$:$Yb^{3+}$, $Er^{3+}$ Up-conversion nanoparticles (UC NPs) with gold dendritic nanostructures (AuDNs) fabricated on porous silicon *via* drop-casting method.

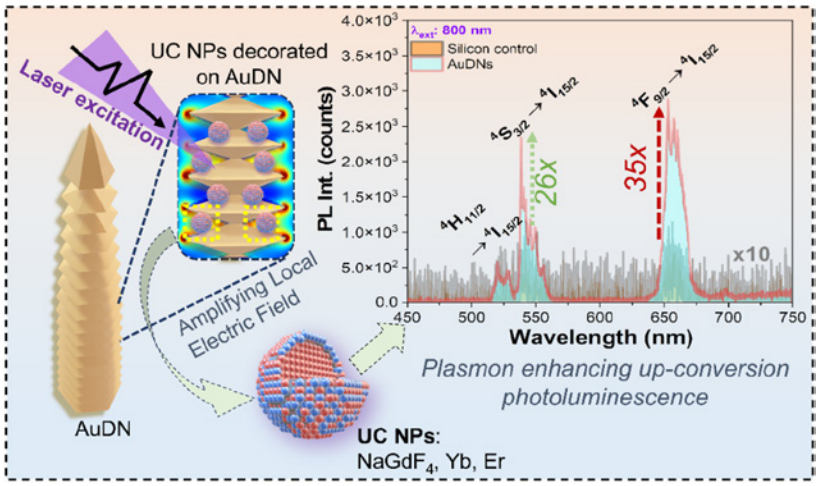


**Fig. 1.** Schematic illustration of plasmon-enhanced up-conversion photoluminescence in $NaGdF_4$:$Yb^{3+}$, $Er^{3+}$ UC NPs decorated on AuDN under 800 nm excitation. The simulated electromagnetic field distribution exhibits intense confinement at branch tips and inter-branch gaps ("hot spots"). Comparative UCPL spectra of UC NPs decorated on silicon (control) and AuDNs, demonstrating enhancement factors of 26× for green and 35× for red emission.

Fig. 1 illustrates a remarkable photophysical phenomenon: plasmon-enhanced up-conversion photoluminescence in UC NPs decorated on AuDNs. Upon 800 nm excitation, collective oscillations of free electrons in AuDNs generate intensified electromagnetic fields at sharp branch tips and sub-10 nm inter-branch gaps. Such near-field amplification increases the local density of optical states, thereby promoting $Er^{3+}$ radiative transitions and $Yb^{3+}$ excitation. The resulting hybrid architecture delivers substantial photoluminescence enhancement both under resonant excitation and across a broad excitation window (780-990 nm), effectively overcoming intrinsic limitations of UC NPs, such as low quantum yield and small absorption cross-sections [1,2]. This approach opens broad prospects for applications in bioimaging, solar energy conversion, solid-state lighting, and display technologies.

This work was supported by the Joint Institute for Nuclear Research (project # 1147-1, "NANOBIOPHOTONICS") and the Science Committee of the Ministry of Science and Higher Education of the Republic of Kazakhstan (Grant No AP23487881).

[1] Q. Luu, A. Hor, J. Fisher, R. B. Anderson, S. Liu, T.-S. Luk, H. P. Paudel, M. Farrokh Baroughi, P. S. May, and S. Smith, Two-Color Surface Plasmon Polariton Enhanced Upconversion in NaYF4:Yb:Tm Nanoparticles on Au Nanopillar Arrays, J. Phys. Chem. C **118**, 3251 (2014).
[2] F. Auzel, Upconversion and Anti-Stokes Processes with f and d Ions in Solids, Chem. Rev. **104**, 139 (2004).

# Diffraction-Limited Dynamic Beam Shaping for Advancing Laser Materials Processing

**E. Skoulas, P. Yadav, S. Shevchik, I. Elia, P. Hoffmann**

*EMPA Swiss Federal Laboratories for Materials Science and Technology, Laboratory for Advanced Materials Processing, Feuerwerkerstrasse 39, Thun CH-3602, Switzerland*

*evangelos.skoulas@empa.ch*

Laser-based manufacturing is central to modern production workflows, spanning subtractive machining, micro-drilling, additive manufacturing support processes, and surface texturing for functional performance[1,2]WGPs is the only available polarizing optical element. Herein, we demonstrate a method for the realization of polarizing plates exclusively via laser structuring. We find that laser induced, periodic surface structures (LIPSS. For decades, control of laser–matter interaction has been dominated by a limited set of "global knobs" such as laser power, wavelength, polarization, and exposure time (or pulse duration), with process outcomes often tuned through extensive parametric studies involving scan speed and temporal modulation (CW versus pulsed operation). Beam shaping has broadened the available processing space, but many approaches either sacrifice diffraction-limited focusing, require re-optimization of optics when modes change, or introduce instability in spot placement and repeatability.

In this work, we introduce dynamic drill-bit-inspired beam modes that preserve diffraction-limited focusing while enabling rapid modulation of the spatial energy distribution at the workpiece. The core concept is realized via vectorial polarization filtering, which allows programmable formation of high-purity structured beams. Using this method, we demonstrate (i) $HG_{01}$ beams with controlled spinning dynamics, and (ii) instantaneous mode shifting between HG01 and $LG_{01}$. Crucially, these transitions are achieved while maintaining constant spot size and stable pointing, making the technique practical for high-throughput scanning systems and precision drilling operations.

We evaluate the approach through three use cases spanning CW and pulsed laser regimes. First, on bulk metallic specimens, the drilling-inspired beams substantially improve material removal, consistent with enhanced coupling and more effective melt ejection dynamics. Second, we show improved machining consistency when using lower-power CW sources, indicating that dynamic energy delivery can compensate for limited peak intensity by promoting more favorable melt flow and removal pathways. Third, in thin metallic foils, drilling efficiency increases by up to approximately sixfold, highlighting the advantage of distributing energy in a way that reduces recast and accelerates breakthrough. Beyond removal rate, the dynamic modes can intentionally induce hydrodynamic melt motion, enabling the mitigation or elimination of porosity; this mechanism is validated using in situ synchrotron X-ray observations, directly visualizing melt behavior and defect suppression in real time.

Finally, the proposed beam dynamics provide a new degree of freedom for laser surface texturing: by programming the beam mode evolution during simple linear scanning, it becomes possible to generate controllable, repeatable macroscopic texture patterns without complex toolpaths. Overall, this work establishes dynamic vectorially filtered mode control as a robust route to improved drilling performance, defect reduction, and programmable surface structuring.

[1] Skoulas, E., Tasolamprou, A. C., Kenanakis, G. & Stratakis, E. Laser induced periodic surface structures as polarizing optical elements. *Applied Surface Science* **541**, 148470 (2021).

[2] Papadopoulos, A., Skoulas, E. *et al.* Biomimetic Omnidirectional Antireflective Glass via Direct Ultrafast Laser Nanostructuring. *Advanced Materials* **31**, 1901123 (2019).

# Table-top generation of ultra-broadband coherent radiation: a unified source from soft x-rays to terahertz and its transformative role in modern photonics

F.V. Potemkin[1,2]

*1- Faculty of Physics Lomonosov Moscow State University, Moscow*
*2- National Research Center NRC Kurchatov Institute*

*potemkin@physics.msu.ru, potemkinfv@my.msu.ru*

We present a groundbreaking platform for the generation of ultra-broadband, coherent radiation spanning from the extreme ultraviolet (EUV) and soft X-ray range to the terahertz (THz) domain, all from a compact, table-top laser system (see Fig.1) [1]. This achievement is made possible by pioneering advances in the efficient nonlinear conversion of near-IR radiation into the THz range within molecular crystals, coupled with precise dispersion control near molecular absorption bands during high-power mid-IR propagation. The resulting source delivers ultrashort pulses across an unprecedented spectral breadth, integrated with highly efficient conversion circuits—achieving remarkable efficiencies from 0.001% in the EUV to 1% in the THz and up to 10% in the mid-IR ranges [1]. This unified multispectral platform enables ultrafast, coherent manipulation of matter with exceptional temporal and spectral control, opening new frontiers in the physics of ultra-strong light fields and attosecond science.

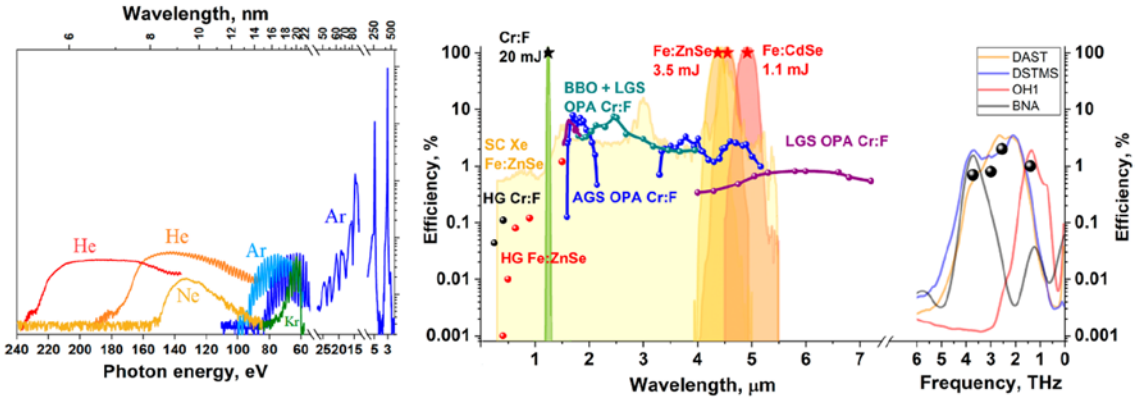


**Fig. 1.** The source of extremely broadband coherent radiation from EUV to THz frequency range.

Using the developed source, the possibility of controlling the symmetry and nonlinearity of a medium by applying a strong THz field was experimentally demonstrated for the first time [2]. We observe generation of the even harmonics along with suppression of the odd ones (see Fig.2 a,b). Our results show that application of the THz field is an efficient method for controlling nonperturbative light-matter interactions [3].

High harmonic generation spectrum obtained in helium [4] by optimizing the target geometry made it possible to carry out the first experiments on the spectroscopy of the sulfur hexafluoride (SF6) molecule in the soft X-ray range near the L-absorption edge of sulfur atoms (160 – 200 eV). In the experiment, three lines of resonance electron absorption from the 2p-subshell of sulfur atoms to high-lying energy levels were recorded (Fig. 2 (c), blue curve) – 173 eV, 184 eV and 196 eV, which also opens up possibilities for coherent diffraction imaging and time-resolved X-ray spectroscopy.

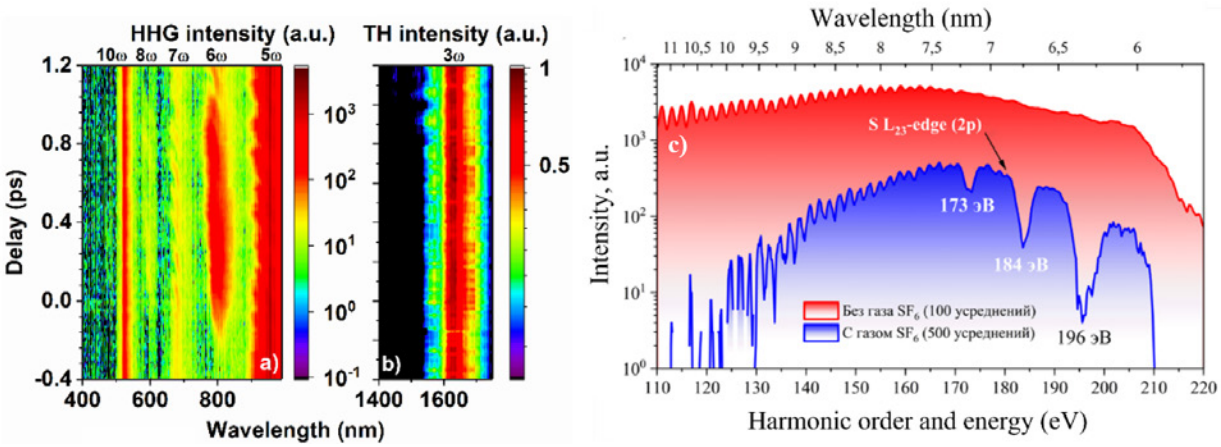


**Fig. 2.** High harmonic (a) and third harmonic (b) spectra from the mid-infrared pulse as a function of delay between THz and generation pulses in CdS. (c) X-ray absorption spectroscopy of L edges of the SF6 molecules.

In summary, this ultra-broadband coherent source not only pushes the limits of attosecond physics and strong-field phenomena but also bridges fundamental research with high-impact applications in nanotechnology, photonics, and transformative medical technologies, fostering synergy between science, education, and cutting-edge industry.

This work was supported by Russian Science Foundation Project № 25-22-00084.

[1] A. Pushkin, E. Migal, D. Suleimanova, E. Mareev, and F. Potemkin, Photonics 9, 90 (2022)
[2] E.A. Migal, A.V. Pushkin, F.V. Potemkin, Phys. Rev. B 110, 005200 (2024)
[3] E.A. Migal, D.Z. Suleimanova, M.A. Andreeva, A.V. Pushkin, F V. Potemkin, Journal of Physics Condensed Matter, 38, 1-6 (2026)
[4] B. V. Rumiantsev, A. V. Pushkin, P. A. Shulyndin, E. A. Migal, F. V. Potemkin, Phys. Rev. A 112, 063107 (2025)

# Ultrafast Dynamics in Hybrid Nanoparticles with a Metal Core

**A. Povolotskiy[1], E. Chebanova[1], Z. Tang[1], D. Soldatova[2], A. Del Carpio Rocha[1], A. Konev[1]**

*1- Saint-Petersburg State University, Saint-Petersburg, Peterhof, Ulianovskaya str. 5, 198504, Russia*
*2- Peter the Great St. Petersburg Polytechnic University, St. Petersburg, 195251, Russia*

*alexey.povolotskiy@spbu.ru*

In recent years, considerable progress has been made in the development of novel hybrid nanostructures for applications across various fields of science, industry, medicine, and environmental monitoring. Such nanostructures serve as luminescent markers, optical sensors for measuring temperature, pH, oxygen concentration, and heavy metals, as well as agents for photothermal and photodynamic therapy, among many other roles. Notably, hybrid systems exhibiting synergistic effects enable a substantial increase in the performance of the developed materials, including through the enhancement of Raman scattering signals and luminescence in the field of localized surface plasmons [1], the simultaneous measurement of multiple parameters via a multimodal approach [2], and the ability to achieve controlled heating while monitoring the temperature of heaters in real time [3]. Many of these phenomena are associated with interactions between plasmons and excitons, the metallic core lattice, the solid-state shell, and the solvent. Investigating the mechanisms of such interactions is practically impossible using steady-state measurement techniques, as the relaxation times lie in the femto- to picosecond range. This temporal range is accessible through femtosecond spectroscopy methods such as differential absorption and up-conversion luminescence. The present work is aimed at a fundamental study of the mechanisms of ultrafast processes in hybrid nanostructures with a metallic core using femtosecond spectroscopy.

Ultrafast relaxation processes following pulsed excitation have been investigated for both individual components and hybrid nanostructures. The differential absorption and emission spectra of metallic nanoparticles (gold, silver, copper, and alloys thereof), as well as the kinetic curves, have been experimentally measured and validated using theoretical models. The obtained differential absorption data are well described by the two-temperature model within the framework of Mie theory. The differential absorption spectra of gold and gold–silver alloy nanoparticles are determined by the dielectric permittivity of the surrounding medium and the temperature of the conduction electrons. The influence of inorganic shells on the relaxation rate of the system after pulsed plasmon excitation has been demonstrated. The interaction of plasmons with organic luminophores in electronically excited states has been investigated. In particular, energy transfer processes have been observed both from organic luminophores to the metallic core and in the reverse direction, depending on the structure of the hybrid nanostructure. A fluorescence enhancement effect of organic luminophores due to stimulated processes arising from plasmon interaction has been detected. The localized surface plasmon resonance effect can significantly increase the fluorescence quantum yield of an organic luminophore through the enhancement of the local electromagnetic field, which ultimately leads to an increase in fluorescence intensity.

This study was performed at the Center for Optical and Laser Materials Research and the Interdisciplinary Resource Centre for Nanotechnology (Research Park, Saint-Petersburg State University). The work was supported by Saint-Petersburg State University, project No 122040800256-8.

[1] A.V. Povolotskiy, D.A. Soldatova, A.A. Smirnov, A.V. Povolotckaia, D.A. Lukyanov, A.S. Konev, E.V. Solovyeva, Photophysical Properties of Hybrid Nanoparticles Based on Water-Soluble Porphyrin, Gold Core, and Polymer Shell, Russian Journal of General Chemistry, vol. 94(11), pp. 3023-3032, (2024).
[2] A.V. Povolotskiy, A.V. Mozzhukhina, E.S. Chebanova, D.A. Lukyanov, A.S. Konev, Multimodal water-soluble luminescent sensors based on hybrid nanostructures for simultaneous temperature and pH measurement, Optical and Quantum Electronics, vol. 58(1), 26, (2026).
[3] A.V. Povolotskiy, O.S. Smirnova, D.A. Soldatova, D.A. Lukyanov, A.V. Povolotckaia, High-Precision Optical Excited Heaters Based on Au Nanoparticles and Water-Soluble Porphyrin, Metals, vol. 13(11), 1851, (2023).

# Laser-generated metal-semiconductor nanohybrids for near-IR light-to-heat conversion

**A. Amosov[1], S.Gurbatov[1,2], A. Kuchmizhak[1,2]**

*1- Institute of Automation and Control Processes, Far Eastern Branch, Russian Academy of Science, Vladivostok 690041, Russia*
*2- Far Eastern Federal University, Vladivostok, Russia, 10 Ajax Bay, Russky Island, Vladivostok 690091, Russia*

*alex.iacp.dvo@mail.ru*

Noble metal nanoparticles (NPs) are widely used as nano-agents for theranostic applications, including photothermal cancer therapy, yet plasmon-mediated absorption of such NPs is typically confined to the visible range, resulting in poor light-to-heat conversion efficiency within the near-infrared (NIR) wavelengths matching biological transparency windows. Here, we present a rapid, laser-driven synthesis of NIR-absorbing hybrid nano-agents comprising gold (Au) combined with common semiconductors—silicon (Si) [1,2], germanium (Ge), and titanium dioxide ($TiO_2$) [3]. The synthesis procedure typically utilized irradiation of commercial nanopowders of mentioned semiconductors with pulsed laser radiation in the presence of the tetrachloroauric acid, resulting in generation of hybrid metal-semiconductor nanoparticles. Our studies systematically connect the observed laser-induced morphological transformations of the nanoparticles with their optical response as well as light-to-heat conversion performance weighted with practically relevant near-IR laser wavelengths. We systematically correlate the laser-induced morphological evolution of these nanoparticles with their optical response and NIR photothermal conversion performance. Furthermore, we demonstrate the theranostic potential of the laser-synthesized nanohybrids by evaluating their intrinsic cytotoxicity, cellular uptake, drug-loading capacity, compatibility with bioimaging agents, and efficacy in photothermal therapy against cancer cells.

[1] S. Gurbatov, et.al., Multigram-Scale Production of Hybrid Au-Si Nanomaterial by Laser Ablation in Liquid (LAL) for Temperature-Feedback Optical Nanosensing, Light-to-Heat Conversion, and Anticounterfeit Labeling. ACS Applied Materials & Interfaces (2023)
[2] S. Gurbatov, et.al., Au–Si Nanocomposites with High Near-IR Light-to-Heat Conversion Efficiency via Single-Step Reactive Laser Ablation of Porous Silicon for Theranostic Applications, ACS Applied Nano Materials, 7, 10779-10786, (2024).
[3] A. Amosov, et.al., Ultrafast Laser Synthesis of NIR-Absorbing Au-$TiO_2$ Nanoagents for Photothermal Theranostics, Colloids and Surfaces B: Biointerfaces, 259, 115359 (2026).

# The Application of New Nitrogen-Containing Flux-Cored Wires in Laser Directed Energy Deposition

**N. Soboleva[1], A. Berezovskiy[1], N. Davydova[1], I. Bakhteev[2], V. Veselova[1], A. Mushnikov[1]**

*1- Institute of Engineering Science, Ural Branch of the Russian Academy of Sciences, 34 Komsomolskaya St, Yekaterinburg 620049, Russia*
*2- Ural Federal University Named After the First President of Russia B. N. Yeltsin, 19 Mira St., Yekaterinburg 620002, Russia*

*natashasoboleva@list.ru*

Experimental compositions of flux-cored wires of the Fe-C-Cr-Mn-Ni-Mo-Cu-N alloying system with a nitrogen content of more than 0.3% were developed. These wires provide an austenitic-ferritic phase composition in the deposited metal structure. The most promising of them have previously used for wire arc additive manufacturing, as well as for welding of high-strength steels and duplex steels. The purpose of this work was to establish the possibility of using the developed wire feedstock materials in laser additive manufacturing.

The laser directed energy deposition was performed using a system based on an LS-5 laser (yttrium-doped fiber laser with a power of up to 5 kW) and a Kuka KR60 HA robot. The first stage of the work consisted in the selection of laser cladding modes (laser radiation power, cladding speed, diameter of the laser spot on the surface), to ensure that there were no cracks in the deposited material or the fusion zone between clad and base material, and to prevent the formation of macropores or non-melting regions between layers.

Using the selected parameters, laser directed energy deposition of "wall" type parts was performed. The formed products were characterized by continuity and uniform distribution of properties across the cross section. Microstructural studies, mechanical and corrosion tests were conducted to evaluate the properties of the materials. The developed wires can be used in laser additive manufacturing applications.

The research was carried out with the support of a grant from the Russian Science Foundation (RSF) No. 24-19-20059 (https://rscf.ru/en/project/24-19-20059/) and the Government of the Sverdlovsk Region.

# Non-thermal anti-Stokes photoluminescence in metal halide perovskites

**E. Battalova, A. Minibaev, S. Kharintsev**

*Department of Optics and Nanophotonics, Institute of Physics, Kazan Federal University, Kremlevskaya, 16, Kazan, 420008, Russia*

*elbatt@rambler.ru*

Metal halide perovskites represent a highly promising class of semiconductors for next-generation photovoltaics and optoelectronics. To date, the primary strategies to enhance perovskite device efficiency rely on layered architectures and precise defect passivation [1]. However, the inherent structural softness of these materials induces dynamic disorder and lattice fluctuations, creating dynamic defects that are notoriously difficult to passivate using conventional approaches [2].

In this work, we demonstrate that these dynamic defects, rather than being suppressed, can be harnessed to significantly enhance light-matter interactions. By applying a pulsed DC bias to pristine $CsPbBr_3$ crystals, we intentionally induce localized structural transformations, creating topological boundaries termed disorder-order interfaces (DOIs). We reveal that spatial confinement and long-range structural fluctuations at these DOIs facilitate extreme electron-photon interaction. This mechanism drives electronic light scattering (ELS), establishing it as the dominant light-matter interaction pathway in these disordered and spatially confined regions [3].

We show that ELS process enables indirect optical transitions, efficiently detrapping charge carriers from the mid-gap defect states into the conduction band, even when thermal phonon energy is insufficient. Consequently, this mechanism yields robust photocurrent generation and pronounced non-thermal, single-photon anti-Stokes photoluminescence (aS-PL) under sub-bandgap excitation, featuring anomalous spectral shifts exceeding 400 meV. These findings highlight a paradigm shift in utilizing structural disorder unlock novel optoelectronic functionalities in metal halide perovskites.

This work is supported by the Russian Science Foundation (Grant No. 26-12-00321).

[1] J. Ye, M. Byranvand, C. Martínez, R. Hoye, M. Saliba, L. Polavarapu, Defect passivation in lead-halide perovskite nanocrystals and thin films: toward efficient LEDs and solar cells, Angew. Chem. Int. Ed., 60, 21636-21660, (2021).
[2] B. Wang, W. Chu, Y. Wu, W. Saidi, O. Prezhdo, Sub-bandgap charge harvesting and energy up-conversion in metal halide perovskites: ab initio quantum dynamics. npj Comput Mater, 11, 11, (2025).
[3] S. Kharintsev, E. Battalova, I. Matchenya, A. Nasibulin, A. Marunchenko, A. Pushkarev, Extreme Electron-Photon Interaction in Disordered Perovskites, Advanced Science, 11, 2405709, (2025).

# Spatial light modulator–assisted femtosecond laser processing: from bulk writing to surface patterning

**V. Fedyaj[1,2], Zh.E. Munkueva[1,2], P.A. Elizarova[1,2], A. Kokhanovsky[3], A. Revjakin[1,2] , A. Simanchuk[1], S, Babin[1,2], A.Yakubov[5], P. Lazarenko[5], A. Kuchmizhak[4,6], A. Dostovalov[1,2]**

*1- Institute of Automation and Electrometry SB RAS, Novosibirsk 630090, Russia*
*2- Novosibirsk State University, Novosibirsk, Novosibirsk 630090, Russia*
*3- ITMO University, Saint-Petersburg, Russia*
*4- Institute of Automation and Control Processes of the FEB RAS, 5 Radio St., 690041 Vladivostok, Russia*
*5- National Research University of Electronic Technology, Zelenograd 124498, Russia*
*6- Far Eastern Federal University, 690041 Vladivostok, Russia;*

*dostovalov@iae.nsk.su*

Femtosecond laser micromachining is considered today a mature technique for fast, precise, and cost-effective direct materials processing across a variety of industrial manufacturing applications. These include cutting fragile and brittle materials [1], producing debris-free medical stents and implants [2], and enabling stress-free trenching and wafer dicing of semiconductors [3]. Furthermore, due to the nonlinear absorption mechanism of femtosecond pulses in transparent materials, this approach enables refractive index changes within the bulk of non-photosensitive materials, allowing the fabrication of various photonic elements, most notably, fiber Bragg gratings in optical fibers [4]. Spatial beam shaping of ultrafast lasers is further expanding the capabilities of femtosecond laser micromachining.

In this study, we review our recent results on spatial light modulator–assisted femtosecond laser writing of both regular and random refractive index change structures in optical fibers. In the first case, we demonstrate a new approach for writing fiber Bragg gratings in a static optical fiber [5]; in the second, we present Rayleigh point-reflectors featuring random distribution along the fiber and a ring-shaped cross-section [6].

Moreover, femtosecond laser patterning of metal thin films (Ti, Cr) and phase-change materials $Ge_2Sb_2Te_5$ (GST) under structured light impact was demonstrated. In the first case, the combination of multibeam irradiation with cross-polarized light and the self-organization effect, namely laser-induced periodic surface structures (LIPSS), leads to the formation of two-dimensional sub-wavelength periodic structures within a single beam scan. In the case of phase-change materials, SLM-based techniques are employed to dynamically shape the beam and write predefined periodic arrays (e.g., L-shapes, cross-shapes). Finally, we present a direct, scalable method for metasurfaces fabrication based on LIPSS, which is promising for the development of tunable and rewritable spectral filters in integrated photonic systems.

The work was supported by the Russian Science Foundation grant (No. 21-72-20162-P). In the research, we used the equipment of the following Multiple-Access Centres (MAC): MAC of the Far Eastern Federal University (FEFU), MAC "High-resolution spectroscopy of gases and condensed matters" at IAE SB RAS, MAC of the Novosibirsk State University (NSU).

[1] E. Mottay et al, "Femtosecond Laser Processing for Mobile Display Manufacturing," in CLEO: 2014, OSA Technical Digest (online) (Optica Publishing Group, 2014), paper AM1L.3.
[2] M. Maroof et al, "A Morphological Study on Femtosecond Laser Machining of Thin NiTi Sheet for Biomedical Application: Parameter Optimization to Device Fabrication", Adv. Eng. Mater., 28 (2026).
[3] S. Cai et al, "Damage-Free Full-Thickness Dicing of Ultra-Thin GaAs Wafers Using a Femtosecond Laser with Low Residual Stress." Adv. Sci.13, 7 (2026).
[4] A.V. Dostovalov et al., "Femtosecond point-by-point inscription of Bragg gratings by drawing a coated fiber through ferrule," Opt. Express, 24, 16232-16237 (2016)
[5] A. Dostovalov, A. Kokhanovskiy, E. Golikov, A. Revyakin, Zh. Munkueva, D. Kharenko, and S. Babin, "Fiber Bragg grating inscription assisted by a spatial light modulator," Opt. Lett. 49, 1077-1080 (2024).
[6] Zh. Munkueva et al, "Femtosecond laser inscription of artificial Rayleigh reflectors inside a fiber core using a spatial light modulator", Optics & Laser Technology, 196, 114734 (2026).

# Thermophysical mechanisms of laser printing and deposition: diagnostics, modeling, and optimization

**Samokvalov F.A., Starinskiy S.V.**

*Kutateladze Institute of Thermophysics SB RAS,*
*1 Academician Lavrentiev Avenue, Novosibirsk, 630090, Russia*

As the cost of quantum generators continues to decrease steadily, laser-induced processes are being increasingly and actively considered as viable alternatives to traditional methods of chemical synthesis or lithography in various technological fields. However, in the majority of existing approaches to fabricating structures using laser radiation, the key parameters such as wavelength, pulse duration, intensity, and beam energy are still selected empirically rather than on the basis of predictive physical models. Over the several decades that followed the invention of lasers, successful physical and mathematical models describing the processes associated with laser-matter interaction were indeed proposed. Nevertheless, as the understanding of the underlying phenomena has gradually deepened, research in this area has increasingly become reduced to brute-force parameter sweeping. In this context, what appears particularly problematic is that phenomena occurring in the surrounding environment, including ambient gas composition, pressure conditions, and fluid dynamics, are very often systematically ignored or considered only superficially. The present study demonstrates that a detailed analysis of hydrodynamic, gas-dynamic, and heat-and-mass transfer processes can significantly advance the field by enabling the achievement of unique regimes for material synthesis that are unattainable under purely empirical approaches. More specifically, a detailed analysis of the laser plume expansion dynamics during pulsed deposition makes it possible to achieve a unique and finely balanced ratio between the kinetic energy of the ablated particles and the intensity of the substance flow. This optimal balance, in turn, creates the necessary conditions for the growth of ultrathin, transparent, and conductive coatings based on gold when using nanosecond pulsed laser deposition (PLD). Furthermore, analogous thermophysical approaches are equally applicable to the challenges of laser direct writing. In this context, it is proposed to employ standard thermohydrodynamic diagnostic techniques such as planar laser-induced fluorescence (PLIF) and particle image velocimetry (PIV) in order to analyze the dynamics of processes occurring within a liquid medium and to determine the thermal regimes at the liquid-solid interface during femtosecond laser printing of gold and silver from their respective salts dissolved in a suitable carrier medium. As a result of such a systematic analysis, it becomes possible to understand whether existing technological methods can be substantially improved. For instance, one may consider combining laser tweezer technologies with direct laser writing to achieve ultra-precise printing, an approach that has already been successfully demonstrated for the laser cutting of thin films. In addition, this framework allows clarifying both the precise role of boiling during the printing process and the fundamental possibility of either controlling or completely eliminating boiling from the technological workflow. Thus, a comprehensive and detailed analysis of the aforementioned hydrodynamic, thermal, and mass-transfer processes will enable substantial progress in the synthesis of novel and promising functional materials for a wide range of modern applications, particularly in the fields of microelectronics and renewable energy technologies.

The work was supported by the Russian Science Foundation (Grant No. № 24-79-10070, https://rscf.ru/project/24-79-10070/);

# Laser-induced periodic surface structures on thin films: mechanisms and applications

**D.A. Sinev, A.A. Masharskaya, A.S. Khramov, M.D. Vasilev, R.M. Mukhsinova, V.A. Domakova, K.M. Arbuzova, E.A. Shakhno**

*Institute of Laser Technologies, School of Physics and Engineering, ITMO University, Kronverksky Pr. 49, bldg. A, St. Petersburg, 197101 Russia*

*sinev@itmo.ru*

Laser-induced periodic surface structures (LIPSS) form on bulk metal substrates usually as oriented perpendicular to the plane of polarization of the incident radiation with period close to λ (type I low spatial frequency LIPSS, LSFL-I). In this research we show both theoretically and experimentally (Figure 1) that LIPSS obtained on thin metal films indicate the formation of type II structures (LSFL-II), oriented parallel to the plane of polarization of the incident radiation and having a period of the order of the wavelength divided by the refractive index of the substrate $\lambda/n_{sub}$ (unusual for metals, but typical for dielectrics) [1]. Combination of laser-induced backward transfer technique (LIBT) with subsequent LIPSS formation with periods down to 660 ± 54 nm allows structural coloration of glass substrates (Figure 2) [2]. Research was financially supported by Russian science foundation, project #24-79-10230, https://rscf.ru/en/project/24-79-10230/.

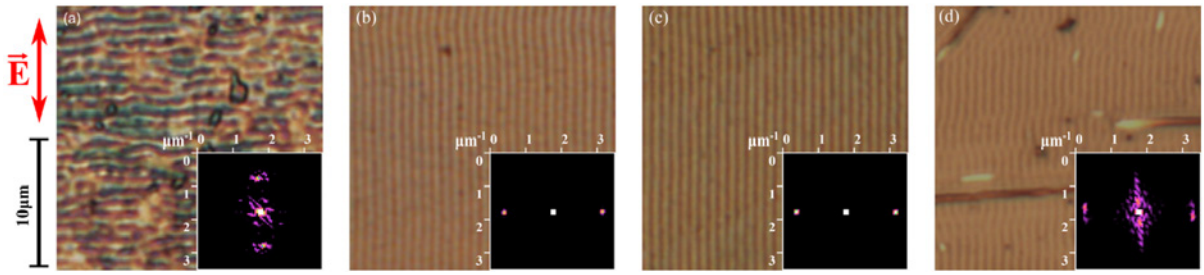


**Fig. 1.** Optical micrographs of LIPSS recorded on a) 1.5 mm thick bulk Ti, and 30 nm thick Ti films on b) BK7, c) JGS1, d) PI substrates. Corresponding 2D-FFT images are shown in the insets. **E** is the orientation of the polarization plane of the laser radiation [1].

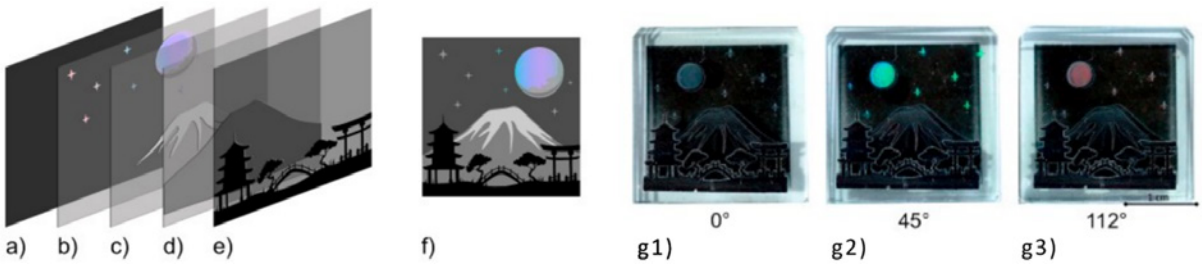


**Fig. 2.** a)-e) Arrangement diagram of images on glass plates created by LIBT and LIPSS methods; f) The final image when combining layers, front view; g) recorded image, front view, the angles of illumination relative to the object are g1) θ=0° (no color response is observed), g2) θ=45° and g3) θ=112° [2].

[1] A.S. Khramov, M.D. Vasilev, A.A. Masharskaya, R.M. Mukhsinova, A.S. Loshachenko, D.A. Sinev, E.A. Shakhno, Abnormal period of laser-induced periodic surface structures on thin metal films impacted by substrate optical properties, Next Materials, vol.11, P. 101704, (2026).
[2] V.Domakova, K.Arbuzova, A.Ramos-Velazquez, D.Polyakov, D.Sinev, V.Veiko, Laser-Induced Backward Transfer and Laser-Induced Periodic Surface Structures: New Horizons for Visual Arts and Design, Journal of Laser Micro/Nanoengineering, vol.20, pp. 297-301, (2025).

# The Mechanism of Nanoparticles Formation due to Pulsed Laser Ablation of Thin Metallic and Semiconductor Films in Liquids: Numerical Study

**D.S. Ivanov[1], A.A. Fronya[1], M.S. Grigor'eva[1], S.Yu. Lukashenko[2], E.I. Mavreshko[1], I.N. Zavestovskaya[1,3], A.V. Kolobov[1], A.V. Kabashin[3]**

*1- Lebedev Physical Institute of the Russian Acad. Sci., Leninskiy Pr. 53, 119991 Moscow, Russia*
*2- Institute for Analytical Instrumentation, Russian Academy of Sciences, St. Petersburg, 198095 Russia*
*3- National Research Nuclear University "MEPhI", Kashirskoe sh. 31, 115409 Moscow, Russia*

Currently, the synthesis of non-toxic colloidal solutions with a controlled nanoparticle (NP) size distribution is of extreme importance for biomedical applications [1]. Among various synthesis techniques, pulsed laser ablation in liquids (PLAL) has emerged as a promising tool in biomedical fields, enabling the production of chemically pure NPs. For instance, laser-synthesized metal and semiconductor NPs are widely utilized as contrast agents for bioimaging, effective sensitizers of radiofrequency hyperthermia for cancer theranostics, agents in photodynamic therapy, and carriers of therapeutic radionuclides in nuclear nanomedicine [2]. However, due to a number of complex and interconnected processes induced in the material by short-pulse laser irradiation, the final characteristics of the resulting NPs remain challenging to control, and the produced colloidal solutions often exhibit broad and multimodal size distributions [3]. Consequently, fabricating a colloidal solution with NPs of prescribed properties requires a robust understanding of the material ablation mechanism to enable its precise control. To investigate the mechanism of laser-induced NP formation in a liquid, this work performs large-scale molecular dynamics (MD) simulations of the laser irradiation interaction with a 20 nm gold and silicon film immersed in a liquid (Fig. 1). A comparative analysis is carried out between the ablation mechanisms of metals and semiconductors responsible for the formation of colloidal solutions with the required characteristics. The resulting NPs were subsequently characterized by shape, size, and morphological properties. Finally, a conclusion is formulated regarding the relative contribution of various laser-induced processes within the material to the overall mechanism of NP generation.

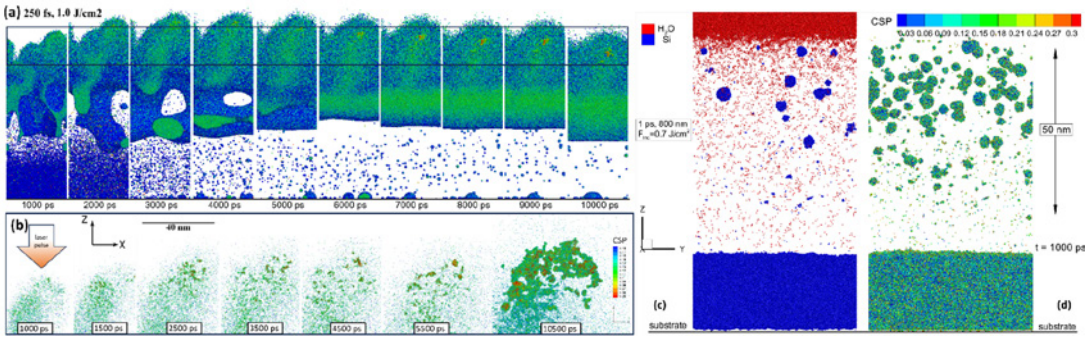


**Fig. 1:** The process of NPs generation due to PLAL is shown for 20 nm Au film in (a) and the rectangular area is zoomed in (b) for a better visual analysis. The water molecules are blanked. The CSP value of 0.03 was chosen as a threshold value between liquid and crystal phases. The final atomic configuration at t= 1000 ps for NPs generation due to PLAL is shown for 20 nm Si in (c) and for Si atoms only in (d).

[1] M. Nikzamir et. al,"An overview on nanoparticles used in biomedicine and their cytotoxicity", J. Drug Deliv. Sci. Technol. 61, 102316 (2021).
[2] A.V. Kabashin et. al,"Laser Processed Nanosilicon: A Multifunctional Nanomaterial for Energy and Health Care", ACS Nano 13, 9841–9867 (2019).
[3] D.S. Ivanov et. al, "Numerical Investigation of Ultrashort Laser-Ablative Synthesis of Metal Nanoparticles in Liquids Using Atomistic-Continuum Model", Molecules 25, 67 (2020).

# Direct laser thermochemical synthesis of functional $SrTiO_3$-based coatings

**X. Egorova[1], F. Gorensky[1], O. Mayorova[1], A. Loshachenko[2], M. Zhukov[3], E. Khairullina[4], D. Sinev[1]**

*1- Institute Laser Technology, University ITMO, Kronverksky avenue 49, St. Petersburg, 197101, Russia*
*2- Interdisciplinary Resource Center for Nanotechnology, Research Park, St. Petersburg State University, 199034 St. Petersburg, Russia*
*3- Laboratory of Scanning Probe Microscopy and Spectroscopy, Institute for Analytical Instrumentation of the Russian Academy of Sciences (IAI RAS), 198095 St. Petersburg, Russia*
*4- Institute of Automation and Control Processes, Far Eastern Branch, Russian Academy of Sciences, 690041 Vladivostok, Russia*

*x_egorova@itmo.ru*

The interaction of pulsed laser radiation with materials under confined conditions enables effective control of the surface structure of a material. The proposed approach is inspired by the concept of laser shock processing (LSP) [1, 2] and involves irradiation of an absorbing layer placed beneath a transparent confinement layer. Unlike conventional LSP, which is mainly used for surface strengthening, the present approach focuses on processes within the absorbing layer, leading to the formation of a functional coating directly on the titanium surface.

Extending the previously proposed approach for laser modification of titanium surfaces [3] was the investigation of the possibility of forming functional piezoelectric structures [4, 5]. In this work, the possibility of forming a functional coating on titanium by laser processing of a two-component $SrCO_3$–$TiO_2$ powder system was investigated.

The phase composition of the obtained structures was analyzed by X-ray diffraction (XRD). The XRD patterns showed diffraction peaks corresponding to the $SrTiO_3$ phase, indicating the synthesis of strontium titanate during laser processing. In addition, piezoelectric force microscopy (PFM) measurements revealed a detectable reverse piezoelectric response, and the recorded electromechanical hysteresis exhibited a characteristic butterfly-shaped behavior typical of piezoelectric materials, providing further evidence for the formation of a functional SrTiO3-containing structure. The mechanical properties of the modified surface were also evaluated. The results showed an increase in the surface hardness compared with the initial titanium substrate.

The results demonstrate the possibility of simultaneously forming a strontium titanate-based functional coating and strengthening the titanium surface within a single technological process [6]. The proposed approach is promising for the development of multifunctional biomedical materials and implants with improved performance characteristics.

Research was financially supported by Russian science foundation, project #24-79-10230, https://rscf.ru/en/project/24-79-10230/

[1] D. Weiwei, et al. Progressive developments, challenges and future trends in laser shock peening of metallic materials and alloys: A comprehensive review. International Journal of Machine Tools and Manufacture, vol.191, 104061, (2023).
[2] S. Bovid, et al. Pressure amplification and modelization in laser shock peening of Ti-6Al-4V and AA7085 with adhesive-backed opaque overlays, J. Mater. Process. Technol. vol. 299, 117381, (2022).
[3] X. Egorova, et al. Hardness enhancement by laser modification of titanium under an auxiliary graphite layer. Applied Physics A vol. 129, p. 855, (2023).
[4] B. Tandon, et al. Piezoelectric materials as stimulatory biomedical materials and scaffolds for bone repair. Acta Biomaterialia vol. 73, pp. 1–20, (2018).
[5] C. Wu, et al. A novel structure design of barium strontium titanate piezoelectric coating on titanium surface enhanced its response to low-intensity pulsed ultrasound. Surface and Coatings Techology vol. 479, p. 130497, (2024).
[6] X. Egorova, et al. Formation of Piezoelectric Coatings on Titanium by Laser Processing with TiO2/SrCO3 Powder. Technologies vol. 14, p. 226, (2026).

# Residual stresses induced by laser formation of catalytically active surfaces on $Al_2O_3$ ceramics

**A. Shchekin[1,2], E. Ishkinyaev[1,2], A. Sviridova[2,3], A. Shapova[2], A. Ayrapetov[2], Ya. Sadovskiy[2], A. Nefedov[1], O. Nefedov[1]**

*1- LLC LASSARD, Russia, Moscow, Volgogradsky Prospekt, 42, Bldg. 5, Room 5H, 109316*
*2- National Research Nuclear University "MEPhI", Russia, Moscow, Kashirskoe Highway, 31, 115409*
*3- LLC Scientific and Production Center "Lasers and Equipment TM", Moscow, Zelenograd, pr-d 4922, 4, building 4*

*a.shchekin@lassard.ru*

Using laser radiation for catalytic activation of dielectric surfaces makes it possible to create conductive layer on their surface by electroless deposition. This technology is relevant for the automotive, electronics, and medical industries. However, the main mechanism of formation of the catalytically active surface and the influence of laser irradiation on the mechanisms of copper adhesion to the substrate remain not fully understood. In this work, we present experimental results on elucidating the role of residual stresses formed under various laser treatments of $Al_2O_3$ ceramics.

Experimental processing was carried out using a fiber

laser with a pulse duration of 4–200 ns and pulse energy up to 1 mJ. The treatment with this source enabled local material evaporation for subsequent analysis and metallization with a copper layer on the surface. For non-thermal processing by laser shock peening, an industrial LASSARD laser with a pulse duration of 15 ns and pulse energy up to 30 J was used

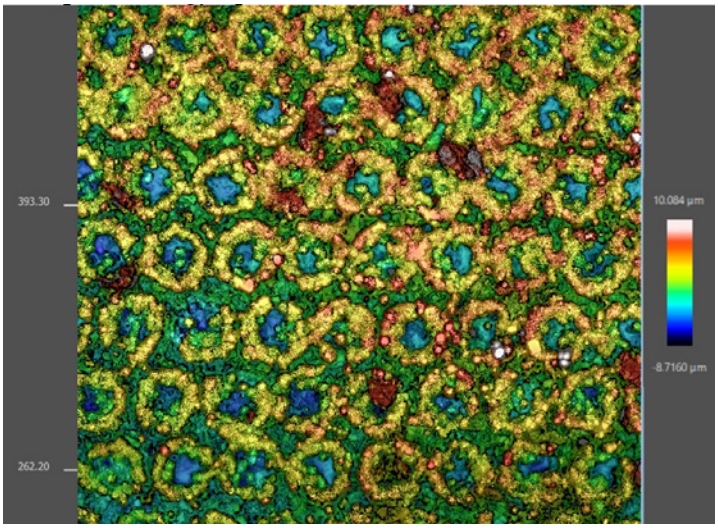


**Fig. 1.** Morphology of the metallized surface after treatment with a fiber ytterbium laser

The influence of the processing type and laser parameters on the formation of residual stresses and on the metallization mechanism of the ceramics after treatment was analyzed in this work. Residual stresses were determined using Raman spectroscopy, while the composition of the metallization layer was studied by EDX spectroscopy, and the surface morphology was examined with a confocal microscope (Figure 1).

[1] N. K. Kim, S. M. Kang, T. Kim, S. Kim, G. H. Kim. Electroless Plating on Polymer Surfaces: Comprehensive Review of Mechanism, Process, Analysis, and Future Applications. Adv. Mater. Interfaces, 12, 2400931, (2025),
[2]G. A. Shafeev. Laser Activation and Metallisation of Insulators. Quantum Electron., 27(12), 1104–1110, (1997).

# Laser synthesis of carbyne-enriched thin films for sensor devices

**A. Kucherik[1], V. Samyshkin[1], A. Abramov[1], A. Lelekova[1], A. Povolotskiy[2], A. Osipov[1]**

*1- Department of Physics and Applied Mathematics, Stoletov Vladimir State University, 600000 Gorkii street, Vladimir, Russia*
*2- Institute of Chemistry, St. Petersburg State University,198504, Ulianovskaya str. 5, St. Petersburg, Russia*

Carbon materials are a versatile platform for exploring new possibilities in material science and engineering, with applications in a wide range of fields, including the production of conductive polymers, chemical and optical sensors, high frequency optoelectronics, and alternative energy.

Recently, there has been a lot of interest in carbyne, the fully one-dimensional carbon allotrope with sp-hybridization, because of its ultimate one-atom thinness, which suggests possible uses in next-generation molecular electronics. This unconventional arrangement gives the material exceptional thermal stability, great electrical conductivity, and exceptional mechanical strength. When compared to graphene and CNTs, carbyne has some distinct benefits that make it an intriguing material for many uses, one of which being sensor.

Carbyne-based sensors have a number of advantages, including a large surface area and high electrical conductivity, which makes them sensitive to external influences. This allows them to detect gases with high accuracy and selectivity. The unique structure and chemical stability of carbine make it an ideal material for sensor devices, as it is durable and stable in various conditions. This opens up the possibility of creating sensors with increased sensitivity and accuracy for a wide range of applications such as medicine, industry and environmental protection. In this context, it is important to understand the various methods of synthesis of carbon nanomaterials, especially carbine, as they allow us to control their structure, size, shape and properties. A variety of synthesis methods provide a wide range of possibilities for producing carbon nanomaterials with special characteristics, opening up new possibilities for their use in various fields.

The work was supported within the framework of the state assignment in the field of RNF-grant #26-12-20015 (https://rscf.ru/project/26-12-20015/).

# Tunable Nanostructuring for van der Waals Materials

**G. Tselikov, G. Tikhonowski, I. Kazantsev, G. Ermolaev, A. Arsenin, V. Volkov**

*Emerging Technologies Research Center, XPANCEO, Emmay Tower, Dubai, United Arab Emirates*

*celikov@xpanceo.com*

Two-dimensional (2D) van der Waals (vdW) materials, including transition metal dichalcogenides (TMDCs) and MXenes have emerged as a cornerstone for next-generation nanophotonic and optoelectronic devices due to their extraordinary electronic and optical characteristics [1]. However, the wider adoption of these materials is often hindered by the limitations of traditional nanostructuring techniques, which are typically material-specific and involve complex lithographic processes [2].

In this work, we present a universal and high-throughput approach for the fabrication of colloidal vdW nanoparticles (NPs) using femtosecond laser ablation and fragmentation in liquids (PLAL/PLFL) [3]. Our method enables the synthesis of nanostructures from a diverse library of over 50 different vdW precursors while maintaining their crystalline integrity. We demonstrate precise control over the morphology and size of the resulting NPs, ranging from nanospheres and nanocubes to fullerene-like and pyramidal structures.

A key advantage of our laser-based platform is the ability to finely tune the NP dimensions. We report the synthesis of TMDC nanospheres with diameters selectively adjustable from 5 to 250 nm [4]. By combining laser treatment with auxiliary ultrasonic processing, we further extend this control to the quantum-sized regime, producing both 2D and 3D vdW quantum dots with tunable, excitation-dependent photoluminescence [5, 6].

Beyond geometric control, we demonstrate the ability to manipulate the chemical composition and oxidation state of the nanoparticles. Specifically, by adjusting the laser irradiation parameters, we achieved a controlled transformation of MoS2 into sub-stoichiometric molybdenum oxides MoO3-x, which allows for the continuous tuning of the dielectric response and a significant enhancement of photothermal efficiency [7].

The functional potential of these laser-synthesized vdW NPs is showcased through their application in Surface-Enhanced Raman Scattering (SERS). We show that WSe2 NPs produced via LFL provide a SERS signal enhancement an order of magnitude higher than that of bulk flakes, offering a promising platform for sensitive, plasmon-free molecular sensing [8]. Our findings establish laser-ablative synthesis as a versatile and powerful tool for engineering functional vdW nanostructures with tailored properties for advanced nanophotonics, sensing, and theranostics.

[1] Q. Wang, K. Kalantar-Zadeh, A. Kis, J. N. Coleman, M. S. Strano, Electronics and optoelectronics of two-dimensional transition metal dichalcogenides, Nature Nanotech, vol. 7, pp. 699–712, (2012).

[2] A. A. Popkova, I. M. Antropov, G. I. Tselikov, G. A. Ermolaev, I. Ozerov, R. V. Kirtaev, S. M. Novikov, A. B. Evlyukhin, A. V. Arsenin, V. O. Bessonov, V. S. Volkov, A. A. Fedyanin, Nonlinear Exciton-Mie Coupling in Transition Metal Dichalcogenide Nanoresonators, Laser & Photonics Reviews, vol. 16, pp. 2100604, (2022).

[3] G. I. Tselikov, A. A. Minnekhanov, G. A. Ermolaev, G. V. Tikhonowski, I. S. Kazantsev, D. V. Dyubo, D. A. Panova, D. I. Tselikov, A. A. Popov, A. B. Mazitov, S. Smirnov, F. Lipilin, U. Ahsan, N. D. Orekhov, I. A. Kruglov, A. V. Syuy, A. V. Kabashin, B. N. Chichkov, Z. Sofer, A. V. Arsenin, K. S. Novoselov, V. S. Volkov, Tunable Nanostructuring for van der Waals Materials, ACS Nano, vol. 19, pp. 25, (2025).

[4] G. I. Tselikov, G. A. Ermolaev, A. A. Popov, G. V. Tikhonowski, A. S. Taradin, A. A. Vyshnevyy, A. V. Syuy, S. M. Klimentov, A. B. Evlyukhin, A. V. Kabashin, A. V. Arsenin, K. S. Novoselov, V. S. Volkov, Transition metal dichalcogenide nanospheres for high-refractive-index nanophotonics and biomedical theranostics, PNAS, vol. 119, pp. e2208830119, (2022).

[5] A. V. Prokhorov, A. S. Chernikov, G. I. Tselikov, A. V. Shesterikov, M. Y. Gubin, I. S. Kazantsev, A. V. Syuy, A. A. Pelyovin, A. A. Popov, O. A. Shalygina, K. S. Khorkov, D. A. Kochuev, D. S. Kitkov, A. V. Arsenin, V. S. Volkov, Tunable photoluminescence on 2D WS 2 quantum dots, Nanoscale, vol. 17, pp. 19243–19252, (2025).

[6] A. V. Prokhorov, A. S. Chernikov, G. I. Tselikov, A. V. Shesterikov, M. Y. Gubin, I. S. Kazantsev, A. V. Syuy, I. A. Zavidovskiy, E. S. Zhukova, A. A. Popov, K. S. Khorkov, D. A. Kochuev, A. V. Arsenin, V. S. Volkov, Photoluminescence of 2D and 3D quantum dots synthesized by laser-ultrasonic treatment on van der Waals materials, Nanoscale Advances, vol. 8, pp. 135–144, (2026).

[7] A. S. Chernikov, G. I. Tselikov, M. Yu. Gubin, A. V. Shesterikov, K. S. Khorkov, A. V. Syuy, G. A. Ermolaev, I. S. Kazantsev, R. I. Romanov, A. Markeev, A. A. Popov, G. V. Tikhonowski, O. O. Kapitanova, D. A. Kochuev, A. Yu. Leksin, D. I. Tselikov, A. V. Arsenin, A. V. Kabashin, V. S. Volkov, A. V. Prokhorov, Tunable optical properties of transition metal dichalcogenide nanoparticles synthesized by femtosecond laser ablation and fragmentation, J. Mater. Chem. C, vol. 11, pp. 3493–3503, (2023).

[8] A. Ushkov, D. Dyubo, N. Belozerova, D. Yakubovsky, A. Syuy, D. Tselikov, G. Ermolaev, A. Popov, A. Chernov, A. Bolshakov, S. Novikov, A. Vyshnevyy, A. Arsenin, A. Kabashin, G. Tselikov, V. Volkov, Femtosecond laser ablation and fragmentation for TMDC nanoparticles synthesis: A comparative study, Applied Surface Science, pp. 163547, (2025)

# Synthesis of Porous Silicon-Based SERS Substrates with Noble Metal Particles obtained through Laser-Induced Transfer for the investigation of SERS of biological materials

**D.S. Kostsov[1], N.N. Melnik[1], E.V. Perevedentseva[1], V.V. Tregulov[2], A.I. Ivanov[2], A.A. Nastulyavichus[1], E.V. Ulturgasheva[1], S.P. Babina[1], S.I. Kudryashov[1]**

*1- P.N. Lebedev Physical Institute of the Russian Academy of Sciences, Leninsky Prospekt, 53, 119991 Moscow, Russia*
*2- Ryazan State University named for S.A. Yesenin, Svobody str. 46, 390000, Ryazan, Russia*

*d.kostzov@lebedev.ru*

This work presents synthesis and study of properties of crystalline and porous silicon structures decorated with noble metal particles and using these structures for observation and investigation of surface-enhanced Raman scattering (SERS).

Porous silicon films were fabricated by anodic electrochemical etching of p-type silicon substrates with a resistivity of 12 Ω·cm and a (111) crystallographic orientation. Samples for the Noble particles deposition were produced at different current densities during porous layer formation.

Noble metal particles (Ag, Au) were deposited onto the crystalline or porous Si samples using the laser-induced forward transfer (LIFT) technique. For particle transfer, a metal film was first deposited onto a separate glass substrate by magnetron sputtering. This substrate served as a source of metallic particles. The particle source was placed in close proximity to the Si sample, and laser irradiation was used to ablate and transfer the material onto the sample surface. This approach enables the formation of localized regions containing silver or gold particles on the sample surface.

We are examining the potential of such structures based on porous silicon with noble metal particles as active SERS substrates for spectroscopic applications. SERS was observed using An aqueous solution of methylene blue as a probe molecule. Interest in this research area is driven by the significant potential of porous silicon as a platform for SERS substrates and the need to explore diverse approaches for forming plasmon active layers with pronounced resonance properties.

# A Modern Approach to Enhancing the Fatigue Strength of Metal Alloys by Laser Shock Peening

**E. Ishkinyaev[1,2], A. Shchekin[1,2], A. Demidchik[1], O. Pagaev[1], A. Nefedov[1], O. Nefedov[1]**

*1- LLC LASSARD, Russia, Moscow, Volgogradsky Prospekt, 42, Bldg. 5, Room 5H, 109316*
*2- National Research Nuclear University "MEPhI, Russia, Moscow, Kashirskoe Highway, 31, 115409*

*ishkinyaev.emil@gmail.com*

This paper presents the results of generating high compressive residual stresses in titanium alloy Ti-6Al-4V using laser shock peening (LSP). This surface material processing technology can be employed to enhance the fatigue strength of critical components subjected to high-cycle fatigue stresses [1]. The main advantages of LSP over traditional shot peening methods include deeper penetration of compressive stresses with lower surface deformation [2].

Experimental processing was performed using an industrial laser manufactured by LASSARD, with a pulse duration of 15 ns and a pulse energy of up to 30 J. This energy level enables a power density exceeding 5 GW/cm² within a spot diameter of up to 7 mm, which ensures the formation of compressive residual stresses exceeding 500 MPa on the material surface.

This study analyzes the influence of power density and laser spot diameter on the magnitude and depth of residual stresses. The effects of the degree of overlap and the number of pulses per spot on the stress field distribution in the treated region are demonstrated. The results of mechanical tests to determine the fatigue strength limit of specimens before and after laser shock processing are presented.

In conclusion, ongoing work on upgrading the laser source to improve performance, reduce energy consumption, and increase reliability is presented. A transition is being made to a new generation of amplifiers with fully diode-pumped active elements up to 30 mm in diameter.

[1] Y. Ye, et. al. A Critical Review of Laser Shock Peening of Aircraft Engine Components. Adv. Eng. Mater., 25, 2201451, (2023)
[2] A.K. Gujba, M. Medraj. Laser Peening Process and Its Impact on Materials Properties in Comparison with Shot Peening and Ultrasonic Impact Peening. Materials, 7, 7925-7974, (2014)

# Nanosecond Laser-Textured Silicon Surfaces for Controlling Droplet Boiling Regimes on Superheated Substrates

**M. Vasilev[1], N. Miskiv[1], N. Smirnov[1], V. Sulyaeva[2], V. Terekhov[1], E. Starinskaya[1], S. Starinskiy[1]**

*1- S.S. Kutateladze Institute of Thermophysics SB RAS, Novosibirsk, Russia*
*2- Nikolaev Institute of Inorganic Chemistry SB RAS, Novosibirsk, Russia*

*vasilevmik.arck@gmail.com*

The interaction of liquid droplets with heated and superheated surfaces is a key process in spray cooling, thermal management of electronic devices, power engineering, metallurgy, and aerospace applications [1]. Previous studies have shown that droplet impact dynamics are governed not only by liquid properties, impact velocity, and surface temperature, but also by surface morphology and wettability [2,3]. Micro- and nanostructured surfaces can affect droplet spreading, vapor bubble nucleation, transition to film boiling, and the Leidenfrost temperature [4]. Therefore, the development of controllable surface engineering methods is important for passive regulation of boiling and cooling regimes. Laser texturing is a promising approach for producing functional surfaces with controlled micro- and nanoscale morphology. In particular, nanosecond pulsed laser ablation enables localized surface modification without masks or multistep chemical processing and can be used to tailor wettability, optical absorption, and thermophysical properties [5]. In this work, nanosecond laser processing of silicon is considered both as a method for fabricating hierarchical surface structures for passive control of droplet interaction regimes on superheated substrates.

Silicon wafers were textured using pulsed Nd laser radiation at a wavelength of 1064 nm. The laser fluence was found to be the key parameter governing the resulting morphology. Depending on the processing regime, four characteristic types of laser-modified silicon surfaces can be obtained: low-fluence modified silicon, black silicon (BlackSi), gray silicon (GraySi), and high-fluence modified silicon. The functional relevance of such laser-engineered surfaces was demonstrated using the example of water droplet impact on superheated silicon substrates. Laser-textured GraySi and BlackSi surfaces were compared with bare silicon. Experiments were performed over a wide range of surface temperatures and Weber numbers, allowing temperature–Weber number regime maps to be constructed. The results show that laser-induced surface morphology substantially changes droplet boiling dynamics. On bare silicon, droplet breakup and atomization are dominant over a broad range of conditions. In contrast, the hierarchical topography of BlackSi promotes localized vapor generation and directional jet formation. Thus, nanosecond laser processing provides a flexible method for tailoring silicon surface morphology and wettability. The obtained results demonstrate a direct link between laser processing parameters, surface micro/nanostructure, and droplet interaction regime maps, which is important for the design of passive heat-transfer and spray-cooling surfaces.

The work was supported by the Russian Science Foundation (grant No. 24-19-00664).

[1] G. Liang and I. Mudawar, Review of spray cooling – Part 1: Single-phase and nucleate boiling regimes, and critical heat flux, International Journal of Heat and Mass Transfer, vol. 115, pp. 1174–1205, (2017).
[2] J. Kim, Spray cooling heat transfer: The state of the art, International Journal of Heat and Fluid Flow, vol. 28, pp. 753–767, (2007).
[3] M. Visaria and I. Mudawar, Application of two-phase spray cooling for thermal management of electronic devices, IEEE Transactions on Components and Packaging Technologies, vol. 32, pp. 784–793, (2009).
[4] S.H. Kim, G. Lee, H.M. Kim and M.H. Kim, Leidenfrost point and droplet dynamics on heated micropillar array surface, International Journal of Heat and Mass Transfer, vol. 139, pp. 1–9, (2019).
[5] S.V. Starinskiy, A.A. Rodionov, Y.G. Shukhov, A.I. Safonov, E.A. Maximovskiy, V.S. Sulyaeva and A.V. Bulgakov, Formation of periodic superhydrophilic microstructures by infrared nanosecond laser processing of single-crystal silicon, Applied Surface Science, vol. 512, pp. 145753, (2020).

# Laser processing in liquid for alloying, fragmentation and surface nanomaterial modification

**N. Tarasenka[1,2], V.Kornev[1], N. Tarasenko[1]**

*1- B.I. Stepanov Institute of Physics, 68-2 Nezalezhnasti Ave., 220072 Minsk, Belarus*
*2- University of Strathclyde, Glasgow, UK*

*n.tarasenko@ifanbel.bas-net.by*

Laser processing of materials in liquids has gained an increased interest in the field of laser-matter interactions aiming targeted changes of materials properties. Laser processing involves focusing of pulsed laser beams onto a target material submerged in a liquid inducing synthesis, alloying, fragmentation, or nanomaterials (NMs) surface modification that makes laser-induced processing in liquids a relevant topic in the last decades [1, 2]. This paper discusses the potential of a number of combined approaches based on laser ablation/processing in liquids for the synthesis of alloy nanoparticles (Ge-Sn, Si-Sn), composite perovskite nanoparticles ($CsPbBr_3$), and multicomponent nanostructured high-entropy alloys (CuMoFeZnMn and CuFeZnMnNi). Multicomponent NMs have a wide range of promising applications in different fields, including catalysis, magnetism, biomedical science, photovoltaics, etc. However, preparation of compositionally complex nanostructures with attaining a composition control poses a persistent challenge.

For complex, homogeneous composite NMs fabrication, pulsed laser processing under liquid layer can be used in different ways: for example, utilizing multi-component bulk targets, laser irradiation of the colloidal mixtures, laser ablation of one material inside the colloidal solution of another, or laser processing of the deposited multilayered films in a surface scanning mode, that results in a fabrication of multielemental nanostructured films on a substrate (Fig. 1). By varying laser parameters a precise control of NMs structure and surface composition can be achieved. As a laser source, the beams of the second and forth harmonic (wavelength 532 and 266 nm, respectively) of the Nd:YAG laser (LOTIS TII, LS2134D) were used for laser-induced modification. The laser operated at repetition rate 10 Hz and pulse duration 10 ns. The phase composition, morphology, structure and optical properties of the prepared nanostructures were investigated. In the conditions created during laser irradiation, the formation of multielemental phases proceeds via generation of thermal energy by photoexcitation, followed by co-melting, and re-solidification processes at high cooling rates under optimized laser processing parameters. The results obtained demonstrated that laser processing of nanomaterials (NMs) in liquids provides unique possibilities for the fabrication of multicomponent nanostructures including high-entropy alloys with a control over their composition.

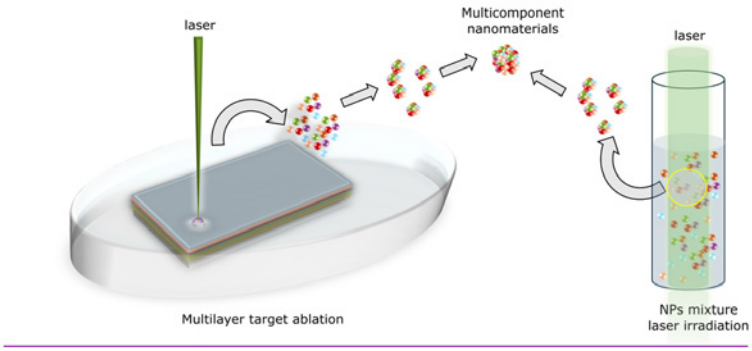


**Fig. 1.** A principal schemes of laser assisted synthesis and modification experiments used for compositionally complex nanomaterials preparation performed with colloids and thin films

The work was supported by the National Academy of Sciences of Belarus under project Convergence 2.2.07 and by the Belarusian Foundation for Fundamental Researches under Grant F25RNF-054.

[1] N. Tarasenka, Laser ablation in liquids for shape-tailored synthesis of nanomaterials: status and challenges, Beilstein J. Nanotechnol., 16, pp.1963–1997, (2025).
[2] C. D. Buendia, B. Gökce, L.V. Zhigilei, Laser–material interactions in liquids for the synthesis of nanomaterials: current status and perspectives, Beilstein J. Nanotechnol., 17, pp.571–575, (2026).

# Damage model for silicon irradiated by high-intensity X-ray laser pulse

**S. Grigoryev, V. Zhakhovsky, N. Inogamov**

*Dukhov Research Institute of Automatics, 22 Sushchevskaya street, 127030 Moscow, Russia*

*grigorev@phystech.edu*

The advent of hard X-ray free-electron lasers (XFELs) has opened unique opportunities for studying nonlinear optical phenomena and for developing advanced focusing optics with sub-10 nm resolution. However, the unprecedented peak brilliance and ultrashort pulse duration of these sources impose extreme radiation loads on optical components and structural materials. Silicon, being the widely used in X-ray mirrors, beamsplitters, and substrate elements, as well as a key construction material in many experimental facilities, requires deeper understanding of its damage mechanisms under high-fluence X-ray irradiation. While the empirical damage thresholds have been reported for various coatings and bulk materials, the underlying physical processes in silicon remain insufficiently clear in the hard X-ray regime. The primary goal of this work is to develop a predictive and physically transparent model of silicon damage that could serve both for optimizing X-ray optics and for prediction of the integrity of silicon-based components in intense FEL environments.

To address this challenge, we constructed a damage model for brittle materials irradiated by high-intensity XFEL beam similar to lithium fluoride presented in our previous work [1]. The validation of the model was performed against a series of well-controlled shock-wave experiments covering a wide range of strain rates from relatively low-speed impact loading to ultra-fast laser-driven shock compression. The simulated and experimental velocity profiles obtained by a line-imaging velocity interferometer demonstred a good agreement, thereby confirming the model's capability to describe silicon failure under extreme dynamic conditions. Subsequently, the validated model was applied to the quantitative analysis of experimental data on silicon optics damage under focused hard XFEL irradiation, including the results reported for single-layer silicon samples and silicon covered by platinum thin films. We reproduced well the measured damage thresholds as a function of fluence and identified the dominant damage mechanism for both types of samples. The model successfully explained the observed typical damage picture under extremely high intensities – deep cavity accompanied by a crater in a free surface. These findings not only confirm the robustness of the proposed modelling approach but also offer practical guidelines for the optimization of radiation-resistant silicon optics and for the interpretation of XFEL damage experiments. The developed framework thus represents a step towards reliable predictive capabilities for materials performance under next-generation X-ray sources.

[1] S. Makarov, V. Zhakhovsky, S. Grigoryev et al., Formation of high-aspect-ratio nanocavity in LiF crystal using a femtosecond X-ray free-electron laser pulse, Nature Communication, 16, 11504 (2025).

# Dual-fiber optical tweezers

**A.I. Gordeeva[1], L.O. Zhukov[1], A.S. Khanzhin[1], A.Yu. Kokhanovskiy[2], R.S. Ponomarev[1]**

*1- 614068 Russia, Perm, Bukireva St. 15, Perm State University*
*2- 197101, Russia, St. Petersburg, Kronverksky Pr. 49, bldg. A, ITMO University*

*Gordeeva@psu.ru*

The effect of focused laser radiation on the trajectory of objects suspended in hydrodynamic systems are experimentally investigated. A system has been designed and technically implemented on the basis of two tapered fibre probes, which makes it possible to manipulate nano- and microscale particles. The particles are controlled and manipulated using an optical trap, which is formed in the area of action of two interfering laser beams. To focus the radiation on the end of the fiber, a lens is formed using a combination of chemical etching, electric arc reflows, and/or precision polishing. A variation of the methods makes it possible to obtain lenses with the required numerical aperture and the position of the focal length relative to the end of the fiber.

At work [1] is shown that the optical properties of the lens significantly affect the field intensity distribution and the position of stable optical traps. Two lenticular fibers located opposite to each other, taking into account changes in the focal length and aperture in the liquid under study, support stable trap of particles in a wide range of their sizes and hydrodynamic flow rates.

To validate the numerical model and identify operational patterns, experiments were conducted using a single fiber and a system of two tapered fibres. An optical tweezer module with two fibers was assembled using a fiber optics ferrule to achieve maximum lens alignment. The studies were carried out with neutrally buoyant fluorescent and polyamide particles ranging from 1 to 5 μm in size, suspended in water. The installation allowed controlled pumping of liquid through a channel with a rectangular cross-section of 1×2 mm at a set speed. The recovery of the trajectory of particles in the field of laser radiation with varying input parameters of the experiment was carried out using PIV methods. Three configurations of relative lens positioning were considered.

During the experiment, it was found that in the case when the distance between the lenses exceeded the sum of their focal lengths, the particles, falling into the area of the laser beam, deviated from the original trajectory in an orthogonal direction at a speed several times higher than the flow velocity. In the case of a single fiber, the particles moved strictly away from the waveguide. While using a two-lens system, the particle initially, attracted to one of the waveguides, froze, after which it accelerated away from it into the region of the main hydrodynamic flow. In the case when the distance between the lenses was equal to or less than the sum of the foci, the particles, falling into the area of the optical trap, were held in it. Varying the power in the module arms allowed for smooth particle displacement in the direction orthogonal to the flow. It is important to note that after the particle is fixed, the laser radiation power can be significantly reduced while maintaining the velocity of the hydrodynamic flow.

The research carried out in the future will make it possible to develop compact fiber-optic tweezers or create microfluidic cells for working with nano- and micro-scale particles with a high refractive index in complex multifunctional systems.

This work was supported by the Ministry of Education and Science of Russia (FSNF 2024-0001 project).

[1] N.A. Kostina, A.Yu. Kokhanovskiy, L.O. Zhukov, R.S. Ponomarev, Modeling particle trapping using focused radiation of an optical fiber mode, Bulletin of the Lebedev Physics Institute, vol. 52, No.11, pp. S1217-S1223, (2025).

# Nanostructures for control over luminescence in 2D materials

**A. Bolshakov**[1,2]

*1- Centre for Photonics and Two-Dimensional Materials,*
*Moscow Institute of Physics and Technology, 141701 Dolgoprudny, Russia*
*2- Alferov University, 194021, St Petersburg, Russia*

*bolshakov@live.com*

Two-dimensional (2D) materials have emerged as a fascinating and technologically promising class of materials, fundamentally reshaping modern solid-state physics. Among them, Transition Metal Dichalcogenides (TMDs) in their monolayer geometry hold a unique place due to their direct bandgap structure. This exceptional electronic property allows for efficient radiative recombination of excitons, positioning TMDs as prime candidates for the next generation of optoelectronics and photonics. Notably, these materials are actively being explored for the fabrication of atomically thin light-emitting diodes (LEDs), nano-scale lasers, valley-polarized light sources, and single-photon emitters for quantum information processing.

However, the atomic-scale thickness that grants these materials their novel properties also introduces significant challenges. A critical drawback is the intrinsically low optical absorption cross-section and short optical path length. Because a monolayer is only a few angstroms thick, it interacts poorly with incident light, leading to weak light-matter interactions. This fundamental limitation severely restricts light-harvesting efficiency and quantum yield, acting as a major bottleneck for practical device applications where high brightness and efficient photon extraction are required.

In this presentation, we address these challenges by discussing the optical properties of hybrid structures that synergistically combine 2D materials with engineered nanostructures, specifically focusing on plasmonic platforms and semiconductor nanowires. We demonstrate that integrating 2D TMDs with metallic plasmonic nanostructures enables strong near-field enhancement and efficient coupling of excitons to surface plasmon polaritons. This facilitates sub-diffractional light confinement, significantly boosting the spontaneous emission rate and overall luminescence intensity. Complementarily, we explore the integration of semiconductor nanowires, which act as highly efficient waveguides and mode converters. These hybrid nanowire/2D architectures allow for precise control over light propagation direction, enabling directional emission and enhanced photon extraction efficiency.

By leveraging these advanced nanostructure designs, we show a viable pathway to overcome the intrinsic absorption and emission limitations of atomically thin materials. Our results establish a robust framework for controlling light at the nanoscale, paving the way for high-efficiency, ultra-compact, and tunable light-emitting devices for future nanophotonic systems.

This research was funded by the Ministry of Science and Higher Education of the Russian Federation, agreement 075-15-2024-560.

# Influence of Electron Density on Self-Regulated Crater Evolution in Molybdenum Plasma Induced by Picosecond Nd:YAG Laser Irradiation

**M.M. Akhmedov, J.O. Sadullayev, M.E. Vapaev, I.Y. Davletov**

*Department of Technique, Urgench State University, Kh. Alimjan Str. 14, Urgench, 220100, Uzbekistan.*

*munisbek95@urdu.uz*

Surface modification of Mo using picosecond laser irradiation has attracted considerable attention in recent years. Three distinct ablation regimes non-thermal, thermally dominated, and phase explosion - were identified during 35 ps laser ablation of Mo bulk, with crater morphology characterized by SEM and confocal microscopy [1]. Picosecond laser treatment of Mo and other metal surfaces, combined with profilometry and SEM analysis, was also used to fabricate structured surfaces with controlled wettability [2].

In the field of LIBS diagnostics, time-resolved measurements showed that electron temperature and density in picosecond-regime plasmas of W and Mo are lower than in the nanosecond regime [3]. Experiments on aluminum foil using a picosecond Nd:YAG laser ($\lambda = 1064$ nm, $\tau = 28$ ps) revealed a strong linear correlation ($R = 0.96$) between crater diameter and electron density, highlighting the potential of LIBS for minimally destructive surface analysis [4]. It has further been established that plasma shielding via inverse bremsstrahlung absorption is a key mechanism in picosecond and nanosecond ablation, enabling the plasma to absorb up to 30% of the incident laser energy [5, 6].

Despite these advances, a quantitative description of the negative correlation between electron density and crater diameter, along with the self-regulating plasma behavior during picosecond laser ablation of Mo, has not been reported in the literature. The present study addresses this gap.

The surface modification of molybdenum induced by picosecond laser irradiation was comprehensively studied, focusing on the relationship between plasma characteristics and the morphology of the resulting ablation craters. Experiments were carried out using a picosecond Nd:YAG laser with a wavelength of 1064 nm and a pulse duration of 28 ps. Molybdenum targets were irradiated at laser fluences of 34.06, 36.59, and 38.02 J/cm$^2$. The effectiveness of the ablation process was assessed through measurements of crater diameters obtained by surface profilometry, while the corresponding surface features were analyzed using scanning electron microscopy (SEM).

To characterize the laser-produced plasma, laser-induced breakdown spectroscopy (LIBS) was applied. The analysis revealed that the electron temperature remained within a relatively narrow interval of 12,263-12,781 K. In contrast, the electron density gradually decreased from $0.55 \times 10^{18}$ cm$^{-3}$ to $0.40 \times 10^{18}$ cm$^{-3}$ as the laser fluence increased. Statistical evaluation demonstrated a pronounced negative correlation ($r \approx -0.99$) between electron density and crater diameter, suggesting that plasma shielding plays a major role in restricting material removal at elevated fluences.

A significant outcome of this study is the experimental identification of a self-regulating plasma behavior during picosecond laser ablation of molybdenum. In this regime, inverse bremsstrahlung absorption together with plasma expansion acts as a feedback mechanism that moderates variations in plasma properties and stabilizes crater growth. To the best of our knowledge, such a quantitative relationship linking electron density, plasma absorption, and crater formation has not previously been reported for molybdenum under picosecond laser irradiation. These findings contribute to a deeper understanding of laser-plasma-material interactions and offer valuable insights for the optimization of precision laser micromachining processes involving refractory metals with high melting temperatures.

[1] D. Zhao et al., Investigation of laser ablation features of molybdenum bulk for picosecond laser-based techniques in fusion devices, Fusion Eng. Des. 151 (2020) pp.111379.
[2] C. Corsaro et al., Graining and texturing of metal surfaces by picosecond laser treatment, Materials 18 (2025) pp.1398.
[3] A. Marín Roldán et al., LIBS investigation of metals suitable for plasma-facing components: characteristics and comparison of picosecond and nanosecond regimes, Fusion Eng. Des. 172 (2021) pp.112898.
[4] M. Akhmedov et al., Picosecond-pulsed laser ablation of aluminum foils: crater morphology and plasma parameters, Eng. Res. Express 7 (2025) pp.035362.
[5] E.H. Kwapis et al., Laser ablation plasmas and spectroscopy for nuclear applications, Appl. Spectrosc. 78 (2024) pp.9–55.
[6] Z. He et al., Coupling effect of evaporation-plasma shielding and its influence on femtosecond laser ablation, Appl. Phys. A 130 (2024) pp.935.

# Interference Power Flows and Energy Exchange between Sources in Absorbing Media

**L.A. Apresyan[1], V.I. Krasovsky[2]**

*Prokhorov General Physics Institute of the Russian Academy of Sciences, Moscow*

*leon_apresyan@mail.ru*

A complex form of the duality lemma is considered, which generalizes the energy conservation law to the case of field superposition from several coherent sources in media with dielectric and magnetic losses. The lemma makes it possible to describe active (time-averaged) and reactive power flows, while separating the flows from each individual source and the interference flows arising from the superposition of fields from different sources. In the absence of absorption, during propagation between sources, the total interference flow of active power is conserved, whereas the reactive part of the interference flow is not conserved due to the contribution of evanescent waves. In the integral form, a natural separation of complex powers into symmetric and antisymmetric (with respect to source indices) parts is introduced. It is shown that the antisymmetric component directly accounts for the nonradiative (Förster) energy transfer between sources in the near field, while the symmetric component accounts for the total radiative losses of the system. Simple examples demonstrate how the lemma simplifies the analysis of energy balance in scattering problems, separating the contributions from the interaction with the driving currents and from absorption by the medium. The considered approach admits generalization to any quadratic field integrals of motion that satisfy a continuity equation.

# Laser-induced graphitized wires in diamond for photoconductive antennas

**T. Kononenko, K. Ashikkalieva, M. Komlenok**

*Prokhorov General Physics Institute of the Russian Academy of Sciences, Moscow, 119991 Russia*

*Ashikkalieva_KK@nsc.gpi.ru*

Photoconductive antennas (PCAs) are popular laser-based THz sources. A typical PCA includes a DC biased metal dipole antenna patterned on a semiconductor substrate. An ultrashort pulse being incident on the antenna gap is absorbed inside the semiconductor, generating photocarriers. The photocarriers are accelerated in the DC bias field, which produces a transient photocurrent. This photocurrent drives the dipole antenna and, as a result, reemits as a THz frequency pulse.

Among all semiconductors tested for THz generation with PCAs (ZnO, GaN, GaAs, etc.), diamond seems to be the best choice for an intense THz radiation generation. It possesses a much larger bandgap (5.5 eV) and can withstand the record-high electric field of 2000·kV/cm. Typically, PCAs on the basis of various materials, including diamond, consist of multiple interdigitated surface electrodes with a reduced interelectrode distance.

It is known that the optical excitation of diamond (as well as the THz generation) occurs in a relatively thick layer (>0.5 mm). Obviously, if the layer thickness is much larger than the interelectrode distance, the surface electrodes cannot form a homogeneous bias field over the entire excited layer. This is why, in the case of diamond, the electrode design should be modified essentialy to reduce considerably the interelectrode distance. It can be achieved by formation of the electrodes penetrating deep into diamond. A promising technique for the formation of buried electrodes is a laser microstructuring of diamond bulk based on the local phase transition of diamond into graphite. Recently, this technique was used for developing 3D graphite electrodes inside HPHT diamond: a series of PCAs with various electrode interspaces was formed and tested [1].

Here, we report on a new tecnique of 3D graphite electrode formation in diamond for PCAs. Picosecond laser irradiation ($\tau$=10 ps, $\lambda$=532 nm, f=1 kHz) was focused into a HPHT diamond crystal mounted on an XYZ translation stage. The laser microstructuring was performed in two stages. First, laser-induced wires were formed inside the diamond crystal using a well-known laser writting technigue: the laser radiation was oriented perpendicularly to the (100) face of the diamond crystal. Initially, the laser focus was positioned beyond the rear (100) face of the crystal, so that the initial optical breakdown occurred precisely at the rear side of the diamond sample. We scanned the sample by shifting it away from the laser along the beam. By varying the sample scanning velocity and the pulse energy, a series of wires running through the crystal were obtained. Second, the obtained wires were additionally modified by the laser irradiation focused through the (110) crystal face. In this case, the laser beam waist passed along the existing wires leading to their thickening and improving their structural uniformity. We have studied a dependence of the wire electrical characteristics and their transverse sizes (diameters) on the number of the laser passes along the wires. The morphology of the wires was examined with an optical microscopy.

This work was supported by the Russian Science Foundation (project no. №25-19-00796).

[1] T. Kononenko, K. Ashikkalieva, V. Kononenko, E. Zavedeev, M. Dezhkina, M. Komlenok, E. Ashkinazi, V. Bukin, V. Konov, Diamond Photoconductive Antenna for Terahertz Generation Equipped with Buried Graphite Electrodes, 10, 10010075 (2023)

# Laser synthesis of boron nanoparticles for BNCT

**E.V. Barmina[1,2], K.O. Aiyyzhy[1], A.I. Kasatova[2,3], O.I.Kichakova[4], P.A.Kotelnikova[2,5,6], L.D.Romanenko[4], S.Yu. Taskaev[2,3], E.L.Zavjalov[4], I.N. Zavestovskaya[2,6]**

*1- Prokhorov General Physics Institute of the Russian Academy of Sciences, 38 Vavilov St., Moscow, Russia*
*2- Lebedev Physical Institute of the Russian Academy of Sciences, 53 Leninsky Prospekt, Moscow, Russia*
*3- Budker Institute of Nuclear Physics of the Siberian Branch of the Russian Academy of Sciences, 11 Lavrentyeva Prospekt, Novosibirsk, Russia;*
*4- Institute of Cytology and Genetics, Siberian Branch of the Russian Academy of Sciences, 10 Lavrentyeva Prospekt, Novosibirsk, Russia;*
*5- Shemyakin-Ovchinnikov Institute of Bioorganic Chemistry, Russian Academy of Sciences, 16/10 Miklukho-Maklaya St., Moscow, Russia;*
*6- National Research Centre "Kurchatov Institute", 1 pl. Kurchatova, Moscow, Russia;*

*barminaev@gmail.com*

The development of effective boron 10 - containing materials is a crucial task for boron neutron capture therapy (BNCT) of cancer [1-3]. One of the promising areas is laser synthesis of colloidal solutions of boron nanoparticles (B NPs) enriched with the $^{10}$B isotope. In this work, we study the production of B NPs by nanosecond laser fragmentation of boron micropowder enriched with the isotope $^{10}$B in isopropanol in a flow cell. A solid-state Nd:YAG laser with a wavelength of 1064 nm, a pulse duration of 4 ns, a pulse repetition rate of 1 kHz, and a pulse energy of 2.8 mJ was used as a source of laser radiation in our experiments. The initial boron particles consisted of irregular fragments ranging from several hundred nanometers to several micrometers. Laser fragmentation led to the formation of spherical nanoparticles. Transmission electron microscopy revealed an average particle size of 50 nm. X-ray diffraction analysis confirmed that the resulting B NPs are amorphous. Secondary ion mass spectrometry showed a $^{10}$B isotopic content of 85.1 %. To improve colloidal stability and biocompatibility, the B NPs were functionalized with polyethylene glycol.

The generated B NPs were tested in BNCT experiments both *in vitro* and *in vivo*. Using the breast carcinoma cell line BT474, clonogenic assay demonstrated that the fraction of surviving cells after BNCT was less than 1 %, indicating high therapeutic efficacy. *In vivo* studies on female SCID mice revealed that BNCT with the obtained B NPs exhibited a pronounced inhibitory effect on BT-474 human breast tumor xenografts, reaching up to 75% tumor growth inhibition.

This research was funded by Russian Science Foundation, Grant № 24-62-00018.

[1] R.F. Barth; A.H. Soloway; R.G. Fairchild, Boron neutron capture therapy for cancer, Scientific American, 263, 100-107 (1990).
[2] V. Torresan, et al., Biocompatible iron–boron nanoparticles designed for neutron capture therapy guided by magnetic resonance imaging, Advanced Healthcare Materials, 10, 2001632, (2021).
[3] I.N. Zavestovskaya, et al., Laser-Synthesized Elemental Boron Nanoparticles for Efficient Boron Neutron Capture Therapy, International Journal of Molecular Sciences, 24, 17088, (2023).

# Power scaling through the geometry of channel Cr:ZnS waveguide lasers

**M. Demesh[1], N. Gusakova[1], N. Tolstik[1,2], E.Sorokin[3], I.T. Sorokina[1,3]**

*1- Department of Physics, Norwegian University of Science and Technology, N-7491 Trondheim, Norway*
*2- ATLA lasers AS, Richard Birkelands vei 2B, 7034 Trondheim Norway*
*3- Institut für Photonik, TU Wien, Gusshausstrasse 27/387, A-1040 Vienna, Austria*

*maksim.demesh@ntnu.no*

Mid-IR laser sources emitting in the region of 2-5 µm are highly desired for a variety of scientific, defence and medical applications. Examples include environmental monitoring, targeting of molecular "fingerprint" absorption bands, laser radar systems, and medical diagnostic are key factors driving research efforts to create smaller, tunable, and high-power mid-IR laser systems [1,2].

Nowadays technology goes to miniaturization and integration of a lasers thus there is a growing interest to waveguide compact lasers which possess lower laser thresholds, higher beam quality and maintenance of a high gain over longer propagation distances [3]. For Cr:ZnS, utilizing a waveguide structure, can also help reduce issues related to thermal lensing within the gain medium. Ultrafast laser inscription has been reported as a versatile method for waveguide fabrication offering the advantage of easily modifying the structure's geometry, which subsequently affects the laser output characteristics of the waveguide laser [4]. Therefore, optimizing the recording process and finding the favorable parameters for femtosecond-written waveguides in TM-doped II-VI host materials remain areas of significant interest.

In this work we present the fabrication and performance of a Cr:ZnS depressed cladding waveguide lasers operating between 2240 and 2300 nm, achieving a maximum output power of 436 mW so far. Ultrafast laser inscription was employed to create waveguides with circular and ear-like geometries, featuring diameters of 30 µm, 40 µm, and 50 µm in a 34-mm long polycrystalline Cr:ZnS sample. Here we investigated the effect of waveguide geometry on the spectral, power, and spatial characteristics of Cr:ZnS waveguide lasers, as well as how writing conditions – such as pulse energy and step size – along with waveguide geometry, influence laser performance.

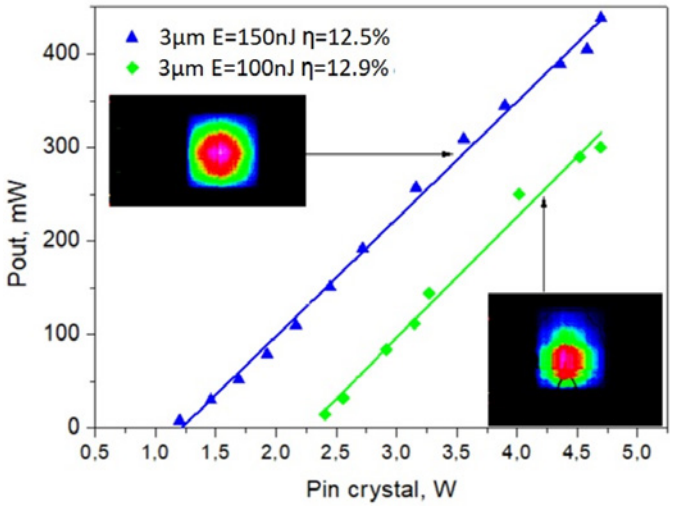


**Fig. 1.** Comparison of CW laser operation of 50 µm polycrystalline Cr:ZnS depressed cladding waveguide lasers written under different energies

[1] I.T. Sorokina and E. Sorokin, "Femtosecond $Cr^{2+}$-based lasers," IEEE J. Sel. Top. Quantum Electron. 21(1), 273–291 (2015)..
[2] S. B. Mirov, I. S. Moskalev, S. Vasilyev, et al., "Frontiers of mid-IR lasers based on transition metal doped chalcogenides," IEEE J. Sel. Top. Quantum Electron. 24(5), 1–29 (2018).
[3] A. G. Okhrimchuk, A. V. Shestakov, I. Khrushchev, et al., "Depressed cladding, buried waveguide laser formed in a YAG:$Nd^{3+}$ crystal by femtosecond laser writing," Opt. Lett. 30(17), 2248–2250 (2005).
[4] S. A. McDaniel, A. Lancaster, J. W. Evans, et al., "Power scaling of ultrafast laser inscribed waveguide lasers in chromium and iron doped zinc selenide," Opt. Express 24(4), 3502–3512 (2016).

# Enhancement of VUV radiation power in a continuous jet of noble gases with coherent control of multiphoton transitions

**K. Glushkov, I. Mukhin, M. Ryabikin, I. Khairulin, M. Emelin, V. Antonov, S. Perevalov**

*Federal Research Center A.V. Gaponov-Grekhov Institute of Applied Physics of the Russian Academy of Sciences (IAP RAS)*

*k.glushkov@ipfran.ru*

The main limitation of laser sources based on high-order harmonic generation is the low conversion efficiency. An extensive way to increase the HHG power is to raise the pulse repetition rate, which leads to an increase in the average power of the laser and to a more complex setup. Moreover, for certain applications (e.g., nonlinear attosecond physics), an increase in both the average and the peak power of the VUV radiation is required. This work presents a VUV radiation source based on a polychromatic (spectrally separated) laser pump and a continuous gas jet; according to calculations, this will significantly increase the VUV peak power in the moderate-order harmonic range.

Theoretical calculations performed by numerically solving the time-dependent Schrödinger equation predict a significant increase in HHG efficiency due to resonant and interference effects. In Ref. [1], it is shown that the maximum energy of moderate-order harmonics (3rd, 5th, 7th, and 9th) in helium is achieved under resonant multiphoton excitation with an optimal intensity in the range of ($2.5\times10^{14}$ – $1.2\times10^{15}$ W/cm$^2$); in the regime maximizing the 9th harmonic, an attosecond pulse train of ~130 as duration is formed. Interference effects are confirmed by Fano lineshape analysis [2]. For xenon, the generation of resonant radiation at 148 nm, which is important for the creation of nuclear clocks based on the thorium-229 isotope, has been studied: the transition from a single-color scheme (1030 nm) to a polychromatic scheme with the addition of the second harmonic increases the output by a factor of 6, while using the fourth harmonic yields a gain of almost 400 times under weak ionization conditions favorable for phase matching.

To validate the approaches for increasing the peak power of harmonics, an optical setup for high-order harmonic generation is being developed. To operate at a high pulse repetition rate, an integrated multi-chamber vacuum system has been created, consisting of an interaction chamber, a differential pumping stage, a VUV radiation filtering chamber, and a spectrometer. The interaction chamber is equipped with a 200 μm diameter nozzle made of a quartz capillary with an opening angle of 10º; the nozzle geometry (diameter, angle, capillary length) was experimentally optimized to minimize gas consumption while maintaining a stable gasdynamic regime. Continuous supply of Ar/Ne/Xe (up to 50 bar) forms a stable jet. Next, a differential pumping system is implemented for gas removal — a cascade of roughing pumps sequentially evacuates the escaping gas, reducing the residual pressure along the harmonic path to below $10^{-2}$ mbar. Interferometric measurements confirm that the gas density at the interaction point reaches $10^{20}$ cm$^{-3}$. The filtering chamber separates the harmonics from the residual pump radiation using a grazing-incidence scheme. For spectral analysis of the VUV radiation, a flat-field spectrometer based on a UV diffraction grating with a back-illuminated CCD camera is used. The pump is a femtosecond laser (1030 nm, ~200 fs, up to 2 mJ, 3 kHz). The radiation is converted into the second (515 nm) and fourth (257.5 nm) harmonics; in a separate channel, radiation at 2 μm (100 μJ, 25 fs) is generated. All spectral components are synchronized with sub-cycle accuracy and combined using dichroic mirrors. The first experiment in argon showed a spectrum up to the 11th order (~190 nm), confirming the operability of the setup. An important advantage of the developed setup is its operation in a continuous gas jet mode at a high pulse repetition rate, which allows us to speak of the development of the first HHG beamline in Russia suitable for practical applications.

Research on high-order harmonic generation and the development of the vacuum system was supported by the Russian Science Foundation No. 24-12-00461, https://rscf.ru/project/24-12-00461/. The development and modernization of the laser system was supported by the State Research Task for the Institute of Applied Physics, Russian Academy of Sciences (Project No. FFUF-2024-0043).

[1] V. A. Antonov et al., Optimal conditions for the generation of moderate-order harmonics of a short-wave field by helium atom, Phys. Rev. A 111, 053502 (2025).
[2] S. A. Bondarenko et al., Fano resonance in XUV generated by helium with few-cycle intense laser pulses and its classical analogy, Phys. Rev. A 111, 053104 (2025).

# Theoretical analysis of the time to reach the explosive boiling threshold during laser ablation

**A.A. Samokhin[1], A.V. Pento[1], V.I. Priklonsky[2], M.K. Gorshenina[1], N.S. Shubin[1]**

*1- Prokhorov General Physics Institute of the Russian Academy of Sciences, 38 Vavilova St., Moscow, 119991 Russia*
*2- Faculty of Physics, Lomonosov Moscow State University, 1 Leninskie Gory, Moscow 119991, Russia*

*asam40@mail.ru*

We investigate the ablation of an absorbing dielectric liquid (water) by submillisecond laser pulses within a surface vaporization model taking into account the experment [1,2]. We obtained the dependence of the time required to reach the threshold temperature for explosive boiling on the laser-pulse energy density. For an absorption depth on the order of a micron, this threshold is reached in a quasi-steady vaporization regime governed by the instantaneous irradiation intensity. In the free running mode with the laser wavelength of 2.94 um, the delay time as a function of pulse energy density shows step-like features that reflect the pulse's amplitude structure. The delay was defined as the moment when the maximum temperature in the volume of the liquid reaches the explosive boiling threshold value (Fig.1). We obtained the dependence of the delay for two values of the threshold temperature of 500K(black line on Fig.2) and 600K(red line on Fig.2). Non-steady effects appear only at the very beginning of irradiation at high intensities and at low intensities, where the temperature maximum is somewhat delayed with a laser pulse intensity. As the absorption depth increases (i.e., the absorption coefficient decreases), a steady evaporation regime becomes essentially unattainable on the submillisecond timescale.

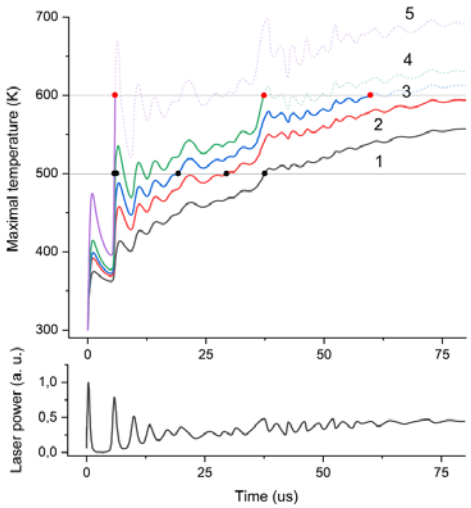


**Fig.1.** Maximal temperature in the volume of the liquid in dependence of time for various values of laser fluences: 1 - 5.39 J/cm$^2$; 2 - 7.06 J/cm$^2$; 3 - 8.09 J/cm$^2$; 4 - 9.24 J/cm$^2$; 5 - J/cm$^2$ (upper part). Laser pulse temporal shape (lower part)

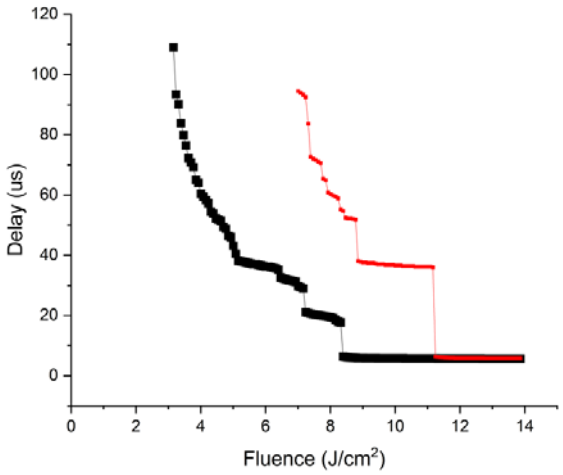


**Fig.2.** The dependence of the explosive boiling delay time on the laser fluence for two values of threshold temperature: 500K(black line), 600K(red line)

[1] A. Vogel, V. Venugopalan, Mechanisms of pulsed laser ablation of biological tissues, Chem. Rev. 103 (5), 577-644 (2003).
[2] A. Vogel, B. Kersten, I. Apitz, Material ejection in free-running Er:YAG laser ablation of water, liver and skin, Proc. SPIE 4961, (2003).

# Formation and morphology of microcracks in the laser-induced oxide layer on TiNi alloy surface

**M.Yu. Kandaurova, T.Yu. Sablina, I.A. Zyatikov, S.A. Yampolskaya, I.K. Lopatkin, Yu.N. Panchenko**

*Institute of High Current Electronics, Siberian Branch of the Russian Academy of Sciences, 2/3 Akademichesky Avenue, 634055 Tomsk, Russia*

*panchenko.marina4@gmail.com*

TiNi shape-memory alloys are widely used in biomedical devices, where surface integrity governs corrosion resistance, nickel release, and biological response [1]. A titanium-rich oxide barrier suppresses nickel leaching, and pulsed-laser oxidation is an attractive route to form it, offering localized, contactless, and tunable energy delivery [2]. Its principal drawback is microcracking of the brittle oxide, driven by thermal-expansion mismatch and the steep temperature gradients of pulsed irradiation; systematic data on crack initiation and network evolution remain scarce, however, particularly for TiNi processed with ultraviolet (UV) radiation, where the shorter wavelength concentrates energy in a thinner near-surface layer.

This work characterizes microcrack formation in oxide layers produced on TiNi by nanosecond UV laser exposure (266 nm) in air and establishes the role of laser fluence and scanning speed in crack initiation and network development. TiNi plates (50.0 at.% Ni, 10×10×1 mm$^3$) were ground, then polished with diamond paste to a mirror finish, and ultrasonically cleaned in ethanol. Treatment used a pulsed Nd:YAG laser (266 nm, 7 ns, 10 Hz, 3 mm spot) at fluences of 0.14–0.42 J/cm$^2$ and scanning speeds of 200–2000 μm/s). Two scanning strategies were compared: Type I, single non-overlapping tracks ($O_y$ = 0) with variable scanning speed and fluence, and Type II, overlapping tracks ($O_y$ = 0.67) at fixed speed with variable fluence; the in-track overlap $O_x$ was 0.93–0.99, giving 167–2020 pulses/cm² and a total accumulated fluence $E_{total}$ of 1.7–60 J/cm$^2$. The surface morphology, crack geometry, thickness and phase composition of the laser-induced oxide layer and were characterized by scanning electron microscopy (SEM), light microscopy, atomic force microscopy (AFM) and X-ray diffraction, and the thermal fields were modeled by finite elements (COMSOL). Oxygen enrichment was detected even on samples showing no visible morphological change, indicating that oxidation precedes cracking and proceeds while the stored stress stays below the oxide failure threshold. No cracking occurred at 0.14 J/cm$^2$ under any condition, even at a total accumulated fluence $E_{total}$ = 20 J/cm$^2$, whereas isolated cracks appeared at 0.28 J/cm$^2$ once $E_{total} \geq$ 13 J/cm² and developed into a polygonal "mudflat" network by 33 J/cm$^2$; crack initiation therefore correlates with single-pulse fluence. XRD confirmed a crystalline $TiO_2$ layer (rutile and anatase) and a contraction of the B2 lattice parameter from 3.0108 ± 0.0026 Å to 2.9993 ± 0.0016 Å with increasing fluence, consistent with near-surface Ti depletion. SEM analysis of the cross-section of the TiNi samples showed the oxide thickening with $E_{total}$, from 280 ± 76 nm (33 J/cm$^2$) to 645 ± 120 nm (60 J/cm$^2$), while AFM resolved a hierarchical pattern of primary cracks 0.4–1 μm wide and secondary cracks <0.2 μm, with depths up to ~200 nm and roughness $Ra$ = 17.9–30.9 nm. Average crack spacing decreased from ~25 to ~12 μm as $E_{total}$ rose from 20 to 60 J/cm$^2$, identifying $E_{total}$ as the governing variable for crack density. Thermal modeling gave peak surface temperatures of 640–1340 K for a 10 nm oxide and 560–1100 K for a 100 nm oxide across 0.14–0.42 J/cm$^2$. Applying an equilibrium crack-spacing model [3] to the measured distances between cracks yields a residual tensile stress of 0.4–1.3 GPa. Cracking is thus governed by two coupled conditions: a threshold single-pulse fluence that generates sufficient per-pulse stress, and a minimum $E_{total}$ that grows the oxide to the critical thickness at which fracture becomes energetically favorable.

This research was carried out with support from the Russian Science Foundation grant No. 25-79-31008 (https://rscf.ru/project/25-79-31008/).

[1] S.A. Shabalovskaya, Physicochemical and biological aspects of Nitinol as a biomaterial, Int. Mater. Rev. 46., pp. 233-250, (2001).
[2] L. Nanai, R. Vajtai, T.F. George, Laser-induced oxidation of metals: state of the art, Thin Solid Films 298., pp.160–164, (1997).
[3] S. Lawrence, D. Adams, D. Bahr, N. Moody, Deformation and fracture of a mudflat-cracked laser-fabricated oxide on Ti, J. Mater. Sci. 48., pp. 4050–4058 (2013).

# Microstructure and functional properties of surface layers of Ti-6Al-4V alloy after UV laser treatment

**T.Yu. Sablina, M.Yu. Kandaurova, I.A. Zyatikov, Yu.N. Panchenko**

*Institute of High Current Electronics, Siberian Branch of the Russian Academy of Sciences, 2/3 Akademichesky Avenue, 634055 Tomsk, Russia*

*panchenko.marina4@gmail.com*

The effect of pulsed ultraviolet laser radiation on the structure, phase composition, and functional properties of Ti-6Al-4V titanium alloy was investigated. Specimens of Ti-6Al-4V titanium alloy measuring 10×10×1 $mm^3$ were mechanically ground, polished with diamond paste to a mirror finish, and ultrasonically cleaned in ethanol. UV laser treatment was performed using a solid-state Nd:YAG laser (266 nm, 7 ns, 10 Hz, spot diameter 3 mm) at a fluence of 0.3 $J/cm^2$ and scanning speeds ranging from 500 to 5000 μm/s. The influence of the treatment parameters on surface topography, elemental composition, and the structural-phase state of the surface-modified layers was investigated using scanning electron microscopy (SEM), X-ray photoelectron spectroscopy (XPS), and X-ray diffraction (XRD). Changes in the structural-phase state of the Ti-6Al-4V alloy surface after exposure to pulsed nanosecond ultraviolet laser radiation at different line-by-line scanning speeds were studied by XRD in both Bragg–Brentano geometry and grazing incidence X-ray diffraction (GIXRD). In the Bragg–Brentano geometry, the thickness of the effectively reflecting layer varies from ~5 to ~10 μm. GIXRD allows the identification of specific features of the structural-phase state in the surface layer not exceeding 2 μm and reveals changes occurring in the thin surface layer when varying the scanning speed during UV laser treatment of the material.

It was found that UV laser treatment leads to surface oxidation with the formation of titanium oxides in the near-surface layers. On the X-ray diffraction patterns of specimens after UV laser treatment, reflections from titanium oxides (TiO and $TiO_2$) are detected in addition to the major phases of titanium (α and β phases). The volume fraction of titanium oxide on the Ti-6Al-4V alloy surface after UV laser treatment increases with decreasing scanning speed from 5000 to 100 μm/s, which results in a decrease in the lattice parameter of the α-Ti phase and the CDD size, accompanied by an increase in microstrains. Changes in functional and mechanical properties after UV laser treatment were experimentally demonstrated. The hardness of the Ti-6Al-4V specimens increased by 25–30%. After UV laser treatment, the specimens exhibited more hydrophilic behavior: the average contact angle decreased from 80° (initial state) to 9–13°. The observed changes in the contact angle are attributed to the enrichment of the surface layer with oxygen (with concentration increasing to 12–20%) and the formation of oxide phases, an increase in the free surface energy, and a change in the ratio of its components (a decrease in the dispersive component and a significant increase in the polar component, which directly affects wettability). Therefore, UV laser treatment of Ti-6Al-4V alloy provides an increase in surface hardness of 25–30% and a reduction in the contact angle from 80° to 9–13°. Consequently, laser treatment can serve as an effective method for the targeted modification of the functional properties of titanium alloys.

This research was carried out with support from the Russian Science Foundation grant No. 25-29-01116, https://rscf.ru/en/project/25-29-01116.

# Formation and morphology of microcracks in the laser-induced oxide layer on TiNi alloy surface

**M.Yu. Kandaurova, T.Yu. Sablina, I.A. Zyatikov, S.A. Yampolskaya, I.K. Lopatkin, Yu.N. Panchenko**

*Institute of High Current Electronics, Siberian Branch of the Russian Academy of Sciences, 2/3 Akademichesky Avenue, 634055 Tomsk, Russia*

*panchenko.marina4@gmail.com*

TiNi shape-memory alloys are widely used in biomedical devices, where surface integrity governs corrosion resistance, nickel release, and biological response [1]. A titanium-rich oxide barrier suppresses nickel leaching, and pulsed-laser oxidation is an attractive route to form it, offering localized, contactless, and tunable energy delivery [2]. Its principal drawback is microcracking of the brittle oxide, driven by thermal-expansion mismatch and the steep temperature gradients of pulsed irradiation; systematic data on crack initiation and network evolution remain scarce, however, particularly for TiNi processed with ultraviolet (UV) radiation, where the shorter wavelength concentrates energy in a thinner near-surface layer.

This work characterizes microcrack formation in oxide layers produced on TiNi by nanosecond UV laser exposure (266 nm) in air and establishes the role of laser fluence and scanning speed in crack initiation and network development. TiNi plates (50.0 at.% Ni, 10×10×1 mm$^3$) were ground, then polished with diamond paste to a mirror finish, and ultrasonically cleaned in ethanol. Treatment used a pulsed Nd:YAG laser (266 nm, 7 ns, 10 Hz, 3 mm spot) at fluences of 0.14–0.42 J/cm$^2$ and scanning speeds of 200–2000 μm/s). Two scanning strategies were compared: Type I, single non-overlapping tracks ($O_y$ = 0) with variable scanning speed and fluence, and Type II, overlapping tracks ($O_y$ = 0.67) at fixed speed with variable fluence; the in-track overlap $O_x$ was 0.93–0.99, giving 167–2020 pulses/cm² and a total accumulated fluence $E_{total}$ of 1.7–60 J/cm$^2$. The surface morphology, crack geometry, thickness and phase composition of the laser-induced oxide layer and were characterized by scanning electron microscopy (SEM), light microscopy, atomic force microscopy (AFM) and X-ray diffraction, and the thermal fields were modeled by finite elements (COMSOL). Oxygen enrichment was detected even on samples showing no visible morphological change, indicating that oxidation precedes cracking and proceeds while the stored stress stays below the oxide failure threshold. No cracking occurred at 0.14 J/cm$^2$ under any condition, even at a total accumulated fluence $E_{total}$ = 20 J/cm$^2$, whereas isolated cracks appeared at 0.28 J/cm$^2$ once $E_{total} \geq$ 13 J/cm² and developed into a polygonal "mudflat" network by 33 J/cm$^2$; crack initiation therefore correlates with single-pulse fluence. XRD confirmed a crystalline $TiO_2$ layer (rutile and anatase) and a contraction of the B2 lattice parameter from 3.0108 ± 0.0026 Å to 2.9993 ± 0.0016 Å with increasing fluence, consistent with near-surface Ti depletion. SEM analysis of the cross-section of the TiNi samples showed the oxide thickening with $E_{total}$, from 280 ± 76 nm (33 J/cm$^2$) to 645 ± 120 nm (60 J/cm$^2$), while AFM resolved a hierarchical pattern of primary cracks 0.4–1 μm wide and secondary cracks <0.2 μm, with depths up to ~200 nm and roughness $R$a = 17.9–30.9 nm. Average crack spacing decreased from ~25 to ~12 μm as $E_{total}$ rose from 20 to 60 J/cm$^2$, identifying $E_{total}$ as the governing variable for crack density. Thermal modeling gave peak surface temperatures of 640–1340 K for a 10 nm oxide and 560–1100 K for a 100 nm oxide across 0.14–0.42 J/cm$^2$. Applying an equilibrium crack-spacing model [3] to the measured distances between cracks yields a residual tensile stress of 0.4–1.3 GPa. Cracking is thus governed by two coupled conditions: a threshold single-pulse fluence that generates sufficient per-pulse stress, and a minimum $E_{total}$ that grows the oxide to the critical thickness at which fracture becomes energetically favorable.

This research was carried out with support from the Russian Science Foundation grant No. 25-79-31008 (https://rscf.ru/project/25-79-31008/).

[1] S.A. Shabalovskaya, Physicochemical and biological aspects of Nitinol as a biomaterial, Int. Mater. Rev. 46., pp. 233-250, (2001).
[2] L. Nanai, R. Vajtai, T.F. George, Laser-induced oxidation of metals: state of the art, Thin Solid Films 298., pp.160–164, (1997).
[3] S. Lawrence, D. Adams, D. Bahr, N. Moody, Deformation and fracture of a mudflat-cracked laser-fabricated oxide on Ti, J. Mater. Sci. 48., pp. 4050–4058 (2013).

# Electronic light scattering in crystalline and nanostructured semiconductors

**A. Minibaev, E. Battalova, S. Kharintsev**

*Department of Optics and Nanophotonics, Institute of Physics,*
*Kazan Federal University, Kremlevskaya str. 16a, Kazan, 420008, Russia*

*mai1417@yandex.ru*

Electronic light scattering (ELS) in semiconductors is observed as a broadband inelastic spectral component, which may overlap with heating, photoluminescence and conventional Raman scattering. Recent studies show that ELS can be driven by indirect optical transitions in media with broken spatial symmetry and spatially confined electromagnetic fields [1-3]. In such systems, structural heterogeneity and optical near fields can provide additional momentum to electrons, making transitions possible that are strongly suppressed in an ideal crystal.

In this work, ELS is considered in silicon-based crystalline and nanostructured semiconductors. Silicon is used as a model indirect-band-gap material with well-known electronic and vibrational properties. Several levels of structural order are analyzed: ideal crystalline Si, amorphous Si, defect-containing Si, and surface or nanostructured Si configurations. This set of systems makes it possible to trace how disorder, defects, surface electronic states and optical near-field effects modify the electronic structure and the ELS response.

The electronic structure is calculated within density functional theory using Quantum ESPRESSO [4]. For each model system, the density of states, band gap, midgap states and low-energy electronic transitions are analyzed. The vibrational Raman contribution near 520 $cm^{-1}$ is considered separately and related to structural order and phonon confinement effects [5], whereas the ELS contribution is interpreted through the density of available electronic transitions.

The calculations show that ideal crystalline Si gives a weak ELS response, while defective and surface-related models increase the density of states near the band gap and enhance electronic light scattering. Therefore, ELS can be used as a sensitive optical indicator of local disorder, defect states, surface electronic structure and near-field-induced indirect electronic transitions in silicon-based semiconductor systems.

This work is supported by the Russian Science Foundation (Grant No. 26-12-00321).

[1] S. S. Kharintsev, E. I. Battalova, A. I. Noskov, J. Merham, E. O. Potma, D. A. Fishman, Photon-Momentum-Enabled Electronic Raman Scattering in Silicon Glass, ACS Nano, 18, 9557-9565, (2024).
[2] E. I. Battalova, A. I. Minibaev, A. V. Petrov, S. S. Kharintsev, Off-Resonance Enhancement of the Refractive Index via Indirect Optical Transitions, Nano Letters, 25, 16855-16861, (2025).
[3] S. S. Kharintsev, E. I. Battalova, Heat Generation in Spatially Confined Solids Through Electronic Light Scattering, Nanophotonics, 14, 2411-2418, (2025).
[4] P. Giannozzi et al., QUANTUM ESPRESSO: a Modular and Open-Source Software Project for Quantum Simulations of Materials, Journal of Physics: Condensed Matter, 21, 395502, (2009).
[5] H. Richter, Z. P. Wang, L. Ley, The One Phonon Raman Spectrum in Microcrystalline Silicon, Solid State Communications, 39, 625-629, (1981).

# Mechanisms of synergism in the combined effect of intense electromagnetic radiation and other factors on complex objects of living and non-living Nature

**Ashurov M.Kh.[1], Oksengendler B.L.[2], Suleymanov S.Kh.[2], Turaeva N.N.[3], Iskandarova F.A.[4]**

*1-Institute of Nuclear Physics of the Academy of Sciences of the Republic of Uzbekistan, Tashkent. 100214.*
*2-Institute of Materials Science of the Academy of Sciences of the Republic of Uzbekistan, Tashkent. 100084, Uzbekistan*
*3-Department of Biological Sciences, Webster University, Saint Louis, MO 63119, USA*
*4-Nanotechnology Development Center at the National University of Uzbekistan named after M. Ulugbek, Tashkent, 100174, Uzbekistan*

*oksengendlerbl@yandex.ru*

Introduced in 1972, the new methodology "Complexity" (Ph.Anderson [1]), which was used to answer the question "how Nature works" (P.Buck [2]), was extended in the 21st century to the field of radiation-matter interaction; under the general name "RPCMCC" – radiation physics of condensed matter complex systems [3]. By now, it is successfully functioning as a combination of two complementary concepts: "synergetics" and "synergistics" (synergy). The RPCMCC has now a broad field of achievement in objects in both non-living and living Nature, both on Earth and in space (see [3-5]). These concepts have been implemented in five paradigms: self-organization, dynamic chaos, self-organized criticality, non-additivity, and network communication [3-6].

In this work, the methods of RPCMCC (more specifically, synergistics, which is applied to studying the effects of combined high-intensity radiation with other types of exposure) are used to construct the following models of the interaction of laser radiation with heat, ultrasound, X-rays, and the interaction of intense non-coherent light with heat, shock waves, and temperature gradients. The general 4-stage Platzman-Starodubtsev scheme [3,7] was used as a research method for constructing the model (combining successive physical, physico-chemical, chemical and biological stages of the radiation response of a complex environment as a whole. Hierarchical structures were chosen as the basic model of the environment, and new information was obtained on the implementation of a new type of elementary processes of atomic rearrangements, taking into account multi-electron effects in the presence of highly intense electromagnetic radiation. The Master equation approach was used to account for the kinetics of large fluctuations in the concentration of components. Two types of synergism were discovered: the multifactorial nature of primary radiation and the multifactorial nature of various combinations of radiation and other factors. New features of trophic chains of defective transformations and radiation shaking have been identified.

A number of conclusions have been drawn about the applicability of the proposed theoretical models in the radiation technology of objects of various medium dimensions, including fractal ones, where the ideas of the radiation response of living and non-living matter are combined [3-4, 8-9].

[1] P.W.Anderson, More Is Different *Science*, New Series, vol. 177, No. 4047, (1972).
[2] P. Buck, «How Nature Works. The Theory of Self-Organized Criticality», Moscow, Librokom, 194 p. 2015.
[3] B.L.Oksengendler, M. Ashurov, et. al., Synergism in radiation effects condensed matter: fundamental and application aspects, cond-mat.other 1-16 pp., (2026)
[4] B.L.Oksengendler A. Kh. Ashirmetov, et. al., «The features of Auger destruction in quasi-one-dimensional objects of inorganic and organic nature», Nucl. Instrum. Phys. Methods Res., Sec B 512, 66-75pp., (2022).
[5] B.L.Oksengendler, F.A.Iskandarova, et. al., «Interaction of Radiation with Hierarchical Structures», Journal of Surface Investigation X-ray, Synchrotron and Neutron Techniques. 17 (1), 31-42 pp., (2023).
[6] A.N. Zatsepin, B.L.Oksengendler et. al., «Radiation effects in complex objects and Complexity: genesis, structure, achievements and prospects», 9-17 pp., (2026).
[7] Yu.B. Kudryashov, «Radiation Biophysics, Ionizing Radiation», Moscow, Fizmatlit, 448p., (2004).
[8] B.L.Oksengendler, Fundamental and applied aspects of radiation degradation in solid state electronics materials in the light of modern radiation physics concepts, The 30th International Conference on Advanced Laser Technologies ALT'23, 47 p., (2023).
[9] S.Kh.Suleymanov B.L.Oksengendler,, et. al., Solar furnace and solar technologies in light of the concept of "Complexity"., Collection of scientific papers dedicated to the 30th anniversary of the Institute of Materials Science, 7-29 pp., (2023).

# Transadventitial Er:YAG laser treatment (RecoSMA) for mechanical arterial trauma

**N. Dobrovolski[1], I. Pikirenia[1], V. Yermachenka[2], K. Rubakhov[1]**

*1- Minsk Scientific and Practical Center of Surgery, Transplantology and Hematology, Belarus.*
*2- City Clinical Pathological Anatomy Bureau, Minsk, Belarus*

*777pik@gmail.com*

**Background.** Endothelial damage is a key mechanism of thrombosis, neointimal hyperplasia, and restenosis after vascular interventions. Spatially modulated ablation (SMA) with Er:YAG laser radiation is designed to stimulate reparative regeneration. This method is called RecoSMA. Its effect on the arterial wall has not been previously studied.

**Aim.** To evaluate the effect of transadventitial RecoSMA on reendothelialization and arterial wall remodeling after mechanical trauma.

**Materials and Methods.** The experiment involved 42 rabbits and 84 femoral artery segments divided into five groups: 1) compression injury with vascular clamp (n=12), 2) compression injury with RecoSMA exposure (n=20), 3) arteriotomy with interrupted sutures (n=20), 4) arteriotomy with suturing and RecoSMA (n=20), 5) RecoSMA on intact artery (n=12). Immediately after the injury, transadventitial exposure was performed with Er:YAG laser with SMA module: wavelength 2940 nm, energy density 2.1 J/cm², pulse duration 0.3 μs. Arteries were examined on days 3, 14, 30 and 60 (histological, immunohistochemical studies). The following endpoints were assessed: endothelial continuity, thrombus presence, intimal thickness, and expression of VEGF, MMP-3, and TIMP-3/-4 (median [IQR]). The Kruskal-Wallis test was used for intergroup comparisons.

**Results.** Morphological changes. In all mechanical injury groups, endothelial denudation, focal intimal and medial necrosis, and inflammatory infiltration were detected on day 3. After isolated laser irradiation of the intact artery, the endothelium and internal elastic lamina were completely preserved, and coagulative necrosis was absent. On day 14, restoration was predominant in the arteries treated with laser: in group 2, continuous endothelium was detected in 80% of segments (4 of 5), and in group 4, endothelium was restored in 100% of segments (5 of 5). In this case, thrombotic obliteration was not detected (0%). In the control groups without laser exposure, damage and obliteration persisted: in group 1, residual endothelial damage and inflammation were present in 100% of segments (3 of 3); in group 3, partial or complete lumen obliteration by organizing thrombi was detected in 60% of segments (3 of 5). On days 30 and 60 in groups 2, 4, and 5, continuous endothelium was preserved in 100% of cases, remodeling was limited to focal changes in the intima. In control groups 1 and 3, wall thickening was widespread with media involvement in all samples; after suturing without laser exposure, thrombus organization and recanalization were additionally detected.

Dynamics of molecular markers. On day 3, RecoSMA increased VEGF levels by 8% in group 4. In group 2, VEGF was 3-5% below control. MMP-3 increased briefly in group 2 (+5%) and decreased in group 4 (-2%). TIMP-3 and TIMP-4 levels remained unchanged. On day 14, VEGF fell below control in the laser-exposed groups (p=0.001), and TIMP-4 peaked, indicating early completion of angiogenesis. MMP-3 levels remained elevated in groups 2 and 4. On day 30, high TIMP-4 levels were retained only in the laser groups. VEGF and MMP-3 returned to normal levels during this period. On day 60, the differences in TIMP-4 levels disappeared. Accelerated arterial wall stabilization was confirmed: VEGF remained 25% lower than control in Group 2, and MMP-3 was 8-10% lower in Groups 2 and 4.

**Conclusion.** Transadventitial application of RecoSMA accelerates reendothelialization, reduces early thrombosis, and promotes physiological arterial remodeling without thermal damage to intact tissue. The data obtained substantiate the high translational potential of this method for vascular surgery.

# Finite Element Modeling of Scanning-Speed Effects on the Temperature Field in Femtosecond Laser-Induced Graphene on Polyimide

**J.O. Sadullayev, M.M. Akhmedov, M.E. Vapaev, I.Y. Davletov**

*Department of Technique, Urgench State University, Kh. Alimjan Str. 14, Urgench, 220100, Uzbekistan.*

*jurabek.s@urdu.uz*

Laser-induced graphene (LIG) has become a versatile and scalable method for directly writing conductive, graphene-like networks onto polymer substrates, owing to its straightforward implementation, mask-free patterning, and suitability for large-area processing. LIG is generally produced by moving a focused laser beam across a carbon-rich precursor such as polyimide, where localized photothermal conversion drives carbonization and graphitization and yields a porous, turbostratic graphene structure whose morphology and electrical conductivity can be tuned[1-2] Together with the freedom to define arbitrary planar geometries, these distinctive structural and electrical characteristics have opened up a wide range of uses in flexible and wearable electronics, including strain sensors, pressure sensors, and biointerfaces. In addition, the large specific surface area and strong electrical conductivity of LIG make it especially appealing for energy-harvesting and storage devices such as microsupercapacitors and electrochemical electrodes[3-5].

Laser-induced graphene (LIG) supports mask-free, direct writing of conductive carbon structures on polyimide substrates for flexible electronic and sensing applications. In femtosecond laser-induced graphene (FLIG), the scanning speed strongly influences the local temperature field and therefore governs the degree and quality of graphitization, yet this relationship remains insufficiently quantified. In this work, a time-dependent finite element model is developed in COMSOL Multiphysics to determine the temperature distribution produced by a femtosecond laser beam on a polyimide surface as a function of scanning speed. The laser is represented as a moving Gaussian surface heat source, and the transient heat conduction equation is solved to capture the ultrafast heating and cooling that occur throughout a pulse train. Simulations performed for scan speeds ranging from 0.05 to 0.20 m/s reveal that lowering the speed raises the peak temperature and broadens the heat-affected zone, while higher speeds diminish both. Comparing the computed peak temperatures with the graphitization thresholds reported in the literature for polyimide-derived graphene reveals an intermediate scanning-speed window in which the thermal budget is high enough to form graphene yet low enough to prevent excessive overheating and damage. This modeling approach offers a practical means of pre-selecting femtosecond laser parameters and of speeding up the optimization of FLIG processes for flexible graphene-based devices.

[1] S. P. Lee, H. Kim, and J. Park, A review on laser-induced graphene in flexible energy storage and conversion devices, Chem. Eng. J., art. 156110, (2024).
[2] J. Yang, J. Yu, K. Zhang, F. Qiao, and G. Yu, Laser-Induced Graphene Toward Flexible Energy Harvesting and Storage Electronics, Adv. Mater. Technol., (2024).
[3] H. Wang, Z. Zhao, P. Liu, and X. Guo, Laser-Induced Graphene Based Flexible Electronic Devices, Biosensors, vol. 12, p. 55, (2022).
[4] C. Francis, A. Rektor, T. Valayil-Varghese, N. McKibben, I. Estrada, J. Forbey, and D. Estrada, Laser-induced graphene gas sensors for environmental monitoring, Front. Chem., vol. 12, art. 1448205, (2024).
[5] T. Han, A. Nag, R. B. V. B. Simorangkir, N. Afsarimanesh, H. Liu, S. C. Mukhopadhyay, Y. Xu, M. Zhadobov, and R. Sauleau, Multifunctional Flexible Sensor Based on Laser-Induced Graphene, Sensors, vol. 19, p. 3477, (2019).

# Hydrodynamics and Heat Transfer during Femtosecond Laser-Induced Synthesis of Silver Microstructures from Aqueous Salt Solution

**F. Samokhvalov[1], N. Zorkina[1], M. Nichik[1], R. Bykovky[1,2], Yu. Shukhov[1], S. Starinsky[1]**

*1- Kutateladze Institute of Thermophysics SB RAS, 1 Academician Lavrentiev Avenue, Novosibirsk, 630090, Russia*
*2- Novosibirsk State University, 1 Pirogova Street, Novosibirsk, 630090, Russia*

*faddeysamokhvalov@gmail.com*

Laser–induced synthesis and patterning of metal microstructures from salt solutions is a promising additive technology for fabricating flexible electronics, microsensors, and microheat exchangers without vacuum equipment or lithography. The quality and morphology of deposited structures are strongly governed by thermophysical and hydrodynamic processes in the liquid: laser–induced convection controls precursor delivery to the substrate [1, 2], the Marangoni effect determines the surface morphology of deposited lines [3], and bubble dynamics critically affects mass transport in the reaction zone [4]. Lattice Boltzmann simulations confirm that laser–pulse–induced convection is the primary factor controlling film non–uniformity [5]. Despite this, direct experimental characterisation of convective flows and temperature fields during pulsed laser synthesis in bulk solution remains scarce, which motivates the present study.

Femtosecond laser deposition of silver from $AgNO_3$ solution was investigated in a ~5 ml volume. The optimal fluence range was determined, and continuous metallic lines were successfully fabricated. SEM and EDX analysis revealed that silver deposits as nanoparticles covering the substrate surface; metal content and surface coverage depend on the irradiation regime. Convective flows were characterised by PIV with polystyrene tracers in the solution volume. Stable laser–induced flows directed along the laser beam axis toward the substrate surface were identified. To separate laser–induced and gravity–driven effects, experiments were carried out in two irradiation geometries – horizontal and vertical. The temperature field in the synthesis zone was investigated by two–colour planar laser–induced fluorescence (2cPLIF); local solution temperature in the laser interaction zone was found to reach 50–60°C. Dimensionless analysis yielded Re≈300 (laminar regime), Pe≈2100 (convection dominates over conduction), and Nu≈22, confirming that directed convection – rather than molecular diffusion – is the governing mechanism of both heat and mass transport.

These results represent a first step toward a quantitative physical picture of the hydrodynamic and thermophysical processes underlying additive laser synthesis of silver microstructures from aqueous salt solution. Future work will extend the investigation to other precursors (copper formate, copper nitrate) with the aim of establishing universal relations between fluid dynamics, heat transfer, and deposit morphology across different reaction systems.

The work was supported by the Russian Science Foundation (Grant No. № 24-79-10070, https://rscf.ru/project/24-79-10070/);

[1] He Y., Liu S. Simulation of the nucleation and crystal growth process in the laser-induced deposition in solution by a lattice Boltzmann method, Nanomaterials, Vol. 12, No. 18, P. 3213, (2022).
[2] Gurevich E.L. The second laser revolution in chemistry: emerging laser technologies for precise fabrication of multifunctional nanomaterials and nanostructures, Advanced Functional Materials, Vol. 34, P. 2405457, (2024).
[3] Zhang M. et al. Opto-thermo-fluidic transport phenomena involving thermocapillary flow during laser microfabrication, International Journal of Heat and Mass Transfer, Vol. 163, P. 120491, (2020).
[4] Swami S., Chen Y.-B., Lee M.-T. Transport phenomena of bubble growth coupled with chemical reaction during laser-induced photothermal reduction and deposition processes, International Journal of Heat and Mass Transfer, Vol. 216, P. 124550, (2023).
[5] He Y., Liu S. Simulation of the nucleation and crystal growth process in the laser-induced deposition in solution by a lattice Boltzmann method, Nanomaterials, Vol. 12, No. 18, P. 3213, (2022).

# Evaluation of the spatiotemporal temperature distribution under single-pulse, pulsed-periodic, and continuous-wave laser irradiation

**A.V. Shepelev[1], E.V. Moiseenko[2], G.Kh. Kitaeva[3]**

*1- I.M. Gubkin Russian State University of Oil and Gas, Leninsky pr. 65, Moscow, Russia*
*2- Nuclear Safety Institute of Russian Academy of Sciences, B. Tulskaya str. 52, Moscow, Russia*
*3- Lomonosov Moscow State University, Moscow, Vorobyovy Gory, 1, Moscow, 119991 Russia*

*shepelev@rambler.ru*

In most cases of using laser radiation, the high power density is necessary. Even in the presence of weak absorption, various thermo-optical effects occur, which cause, firstly, thermal changes in the parameters of the substance up to its possible destruction, and secondly, thermo-optical distortions leading to a violation of the phase-matching conditions.

The methods we have developed allow: a) using simple algebraic relations, to estimate the order of magnitude of changes in the temperature of a substance and thermo-optical distortions when exposed to laser radiation; b) if necessary, to perform an accurate calculation of the spatiotemporal temperature distribution of the irradiated sample. These methods are applicable to any temporal structure of laser radiation – single-pulse, pulsed-periodic, or continuous-wave. A technique is presented that makes it possible, in the case of pulsed-periodic radiation, to easily reduce the solution of the problem of determining the space-time temperature field to known solutions available in the literature and in reference books.

In the case of short laser pulses, the standard equation of thermal conductivity is applicable for times $t > l / v$ where $l$ is the characteristic size, and $v$ is the speed of sound. If $t_r < t < l / v$, the space-time temperature distribution is described by a mixed parabolic-hyperbolic equation, i.e. the temperature waves should be taken into account. For times $t$ less than the maximum relaxation time of the photo-excited carriers and the phonon subsystem $t_r$ ($\sim 10^{-12}$ s), the concept of crystal temperature cannot be defined.

The report provides all the necessary mathematical relations and, as examples, the results of calculations of the temperature distribution and the magnitude of thermo-optical distortions for several specific optical schemes.

The work was financially supported by the Russian Science Foundation, Grant No. 22-12-00055-П, and in part by the state assignment of Lomonosov Moscow State University.

# Design and fabrication of tunable terahertz single-layer anti-reflection coatings on HRFZ-Si by direct nanosecond laser drilling

**D.A. Antipov [1], E.V. Barmina [2], E.D. Shevelkina [3], K.I. Zaytsev [4]**

*A.M. Prokhorov General Physics Institute of the Russian Academy of Sciences,*
*38, Vavilov street, 119991 Moscow Russian Federation*

*antipov.dima.99@mail.ru, e.shevelkina@yandex.ru*

High-resistivity float-zone silicon (HRFZ-Si) is a key material in terahertz (THz) optics; however, its high refractive index (nSi ≈ 3.41) causes ≈30% Fresnel losses per interface [1, 2], limiting its use in 6G systems, high-speed imaging and other THz applications [3]. Traditionally, dielectric films are employed to mitigate these losses; however, they often suffer from poor adhesion and thickness non-uniformity [4]. Other techniques are based on creating a surface layer with a modified refractive index through various structuring methods—such as photolithography, deep reactive ion etching (DRIE) and direct laser ablation. While photolithography and DRIE enable high-performance structures [5, 6], they are slow, multi-stage, and require costly vacuum equipment. Direct laser ablation offers a promising alternative, although it typically relies on expensive femtosecond laser systems [7].

In this work, we propose a cost-effective method for forming single-layer anti-reflection coatings on HRFZ-Si using direct nanosecond laser drilling in air. A nanosecond laser system (pulse duration of 50–200 ns, power of 7.1–8.6 W, repetition rate of 20 kHz) equipped with a galvanometer scanner was employed. The core concept involves the creation of hexagonal matrices of subwavelength micro-holes, which form a surface layer with an effective refractive index, $n_{eff}$. According to effective medium theory (EMT) [8], varying the matrix period allows for achieving the optimal value of $n_{eff} \approx \sqrt{n_{si}}$, satisfying the condition for ideal single-layer anti-reflection [9]. Specifically, the micro-hole diameters obtained under optimized ablation regimes for different pulse durations are precisely determined. The optimal ablation regime is defined as one that ensures a highly uniform and well-defined crater morphology. The optimal matrix-hole geometry was calculated using MATLAB. The expected spectral response was pre-verified via COMSOL Multiphysics simulations, accounting smoothed profile of the fabricated micro-holes. Adjusting the depth of the micro-holes allows for flexible tuning of the central anti-reflection frequency. Mandatory post-treatment includes HF and selective TMAH etching to remove the oxide and laser-induced amorphous/defective layers, which would otherwise degrade high-frequency transmittance.

To validate the method, coatings with anti-reflection peaks at wavelengths of 300 μm and 600 μm were fabricated. Silicon wafers with a single-layer coating on both sides exhibit total losses of less than 5% (reflection + absorption). The proposed approach is characterized by high performance predictability, the absence of adhesion issues, and low implementation costs, making it a competitive solution for the production of tunable THz optics.

[1] M. Born and E. Wolf, Principles of Optics (Cambridge University Press), (1999).
[2] A. J. Gatesman, J. Waldman, M. Ji, C. Musante, and S. Yngvesson, An Anti-Reflection Coating for Silicon Optics at Terahertz Frequencies, IEEE Microw. Guid. Wave Lett., vol. 10, pp. 264-266, (2000).
[3] A. V. Shevchik-Shekera, F. F. Sizov, O. G. Golenkov, I. O. Lysiuk, V. O. Petriakov, and M. Yu. Kovbasa, Silicon lenses with HDPE anti-reflection coatings for low THz frequency range, Semiconductor Physics, Quantum Electronics & Optoelectronics., vol. 26, pp. 059-067, (2023).
[4] W. Withayachumnankul, B. M. Fischer, S. P. Mickan, and D. Abbott, Retrofittable T-ray antireflection coatings, Proc. SPIE, vol. 6415, pp. 64150N, (2006).
[5] P. Han, Y. W. Chen, and X.-C. Zhang, Application of Silicon Micropyramid Structures for Antireflection of Terahertz Waves, IEEE J. Sel. Top. Quantum Electron., vol. 16, pp. 338-343, (2010).
[6] C. Brückner, T. Käsebier, B. Pradarutti, and A. Tünnermann, Broadband antireflective structures applied to high resistive float zone silicon in the THz spectral range, Opt. Express, vol. 17, pp. 3063-3077, (2009).
[7] H. Sakurai, N. Nemoto, K. Konishi, and M. Kuwata-Gonokami, Terahertz broadband anti-reflection moth-eye structures fabricated by femtosecond laser processing, OSA Continuum, vol. 2, pp. 2764-2772, (2019).
[8] Choy, T. C. Effective Medium Theory: Principles and Applications 2nd ed. (Oxford Science Publications), Chapter 1, (2016).
[9] E.S. Putilin, Optical Coatings (ITMO University), Chapter 2, (2010).

# Femtosecond NIR Laser Irradiation for Domain Switching in Single-domain and Polydomain SBN Single Crystals

**V.A. Shikhova[1], B.I. Lisjikh[1], A.R. Akhmatkhanov[1], M.D. Kholodenko[1], I.A. Kipenko[1], L.I. Ivleva[2], V.Ya. Shur[1]**

*1- School of Natural Sciences and Mathematics, Ural Federal University, 620002, Ekaterinburg, Russia*
*2- Prokhorov General Physics Institute, Russian Academy of Sciences, 119991, Moscow, Russia*

*vera@urfu.ru*

All-optical three-dimensional (3D) poling method based on tightly focused irradiation by femtosecond near-infrared (NIR) laser has been developed recently for creation of the ferroelectric domain structures with a given geometry in the bulk of various ferroelectric crystals [1-3].

In this work the domain structures were created by femtosecond NIR pulse laser irradiation in single crystals of relaxor ferroelectric strontium barium niobate ($Sr_{0.61}Ba_{0.39}Nb_2O_6$, SBN). The samples were cut perpendicular to the polar axis. The two different initial states of the domain structure were created in SBN single crystals before irradiation: polydomain and single-domain. The polydomain state was produced by zero-field cooling. The single-domain state was created by electron beam irradiation and by application of electric field.

Yb-solid state femtosecond laser TETA-10 (Avesta Project, Russia) with 1030 nm wavelength and 250 fs pulse duration was used for irradiation using 50x objective with NA = 0.65. The energy from 0.07 to 2.1 μJ was used. Irradiation was carried out in matrices (10*10) with 5 μm period. Cherenkov-type second harmonic generation microscopy was used for 3D domain imaging after femtosecond laser irradiation [4].

In polydomain SBN the spindle-like domains are formed in the vicinity of the focusing point of laser irradiation. The length of created domains was up to 70 μm, diameter – about 1.5 μm. The length of domains increases with pulse energy and pulse number.

In single-domain SBN the created domains consisted of two parts: the narrow spindle-like one and the lens-like one located closer to the irradiated Z- polar surface. The lens-like part expanded with increasing energy until domain merging. The domain length increased to 250 μm with an increase of the energy and the pulse number.

The unusual shape and length of domains produced in single-domain SBN crystals were attributed to the field produced by photoinduced space-charges. These charges appeared as a result of multiphoton absorption and localized at the boundaries of the lens-like area. We suppose that the value of the field is high enough for domain switching in SBN. The lens-like domain part is absent for irradiation of the polydomain SBN crystals as the appearance of this field requires existence of the polar axis whereas the polydomain state with zero value of averaged spontaneous polarization doesn't have a macroscopic polar axis. The inputs of domain growth under the actions of the photoinduced space-charge field and depolarization field were related as 3:1. The lens-like domain part is three times longer than the spindle-like one. The influence of space-charge field induced by multiphoton absorption should be taken into account for creating 2D and 3D nonlinear photonic crystals in ferroelectrics with low threshold values of the switching fields.

The work was supported by Russian Science Foundation (project 25-22-00231). The equipment of the Ural Center for Share Used «Modern Nanotechnologies» Ural Federal University (Reg. 2968) was used.

[1] X. Chen, P. Karpinski, V. Shvedov, K. Koynov, B. Wang, J. Trull, C. Cojocaru, W. Krolikowski, Y. Sheng, Ferroelectric domain engineering by focused infrared femtosecond pulses, Appl. Phys. Lett., vol. 107, pp. 141102 (2015).
[2] Y. Sheng, X. Chen, T. Xu, S. Liu, R. Zhao, W. Krolikowski, Research progress on femtosecond laser poling of ferroelectrics, Photonics, vol. 11 (5), pp. 447 (2024).
[3] B. Lisjikh, M. Kosobokov, A. Turygin, A. Efimov, V. Shur, Creation of a periodic domain structure in MgOLN by femtosecond laser irradiation, Photonics, vol.10, pp.1211 (2023).
[4] Y. Sheng, A. Best, H.-J. Butt, W. Krolikowski, A. Arie, K. Koynov, Three-dimensional ferroelectric domain visualization by Čerenkov-type second harmonic generation, Opt. Express, vol. 18, pp. 16539-16545 (2010).

# Applications of Ag Nanoparticles Deposited on Different Substrates by Femtosecond Pulsed Laser Deposition

**G.S. Boltaev,[1] R.A. Ganeev,[2] L. Normo'minova,[2] M. Vapaev,[3] N. Khalilova,[4] A.M. Tillaboev[5]**

*1- Material Research Center, American University of Sharjah, Sharjah, 26666, UAE*
*2- Institute for Advanced Studies, New Uzbekistan University, Tashkent 100007, Uzbekistan*
*3- Urgench State University, Urgench 220100, Uzbekistan*
*4- Tashkent University of Information Technologies, Tashkent 100200, Uzbekistan*
*5- Physics Department, Chirchik State Pedagogical University, Chirchik 111700, Uzbekistan*

*gboltaev@aus.edu*

Silver nanoparticles (Ag NPs) have attracted considerable attention in recent decades due to their unique physical, chemical, and optical properties. These properties primarily arise from their nanoscale dimensions, high surface-to-volume ratio, and strong interaction with electromagnetic radiation through localized surface plasmon resonance (LSPR) [1]. Owing to these features, Ag NPs have been widely explored for applications in catalysis, sensing, photonics, electronics, and biomedical technologies [2]. One of the key factors determining the functional performance of Ag NPs is their morphology, including particle size, shape, distribution, and surface structure. The morphology of nanoparticles significantly influences their optical absorption, catalytic activity, and electronic properties [3]. For instance, spherical, triangular, rod-shaped, or irregular nanoparticles exhibit different plasmonic responses and surface reactivity due to variations of their geometric structures [4].

Pulsed laser ablation of a silver target was performed in a vacuum chamber using the ultrafast laser pulses with a central wavelength of 1030 nm and a pulse duration of 250 fs. The experiments were conducted at a vacuum conditions of approximately $10^{-4}$ Torr to minimize collisions between the ablated species and background gas molecules and to allow the free expansion of plasma. The laser beam was introduced into the chamber through a quartz window and focused onto the Ag target using a plano–convex lens with a focal length of 250 mm, producing a laser spot of approximately 50 μm in diameter on the target surface. At an average laser power of 2.5 W and a repetition rate of 50 kHz, the fluence of the focused laser beam on the target surface reached approximately 5 J $cm^{-2}$. Under these conditions, the ultrashort laser pulses induced rapid excitation of the electron subsystem in the metal, followed by ultrafast energy transfer to the lattice, resulting in material removal and formation of a LIP composed of Ag atoms, ions, and nanoscale clusters.

The fabricated samples were further used to investigate the plasmonic-induced enhancement effects associated with Ag NPs. The deposited samples were characterized using several analytical techniques. SEM (TESCAN) equipped with energy-dispersive X-ray (EDX) analysis was employed to examine surface morphology, compositonal and nanostructure distribution. The resistance response of the sensor to the target VOC gases was monitored using a Keithley 2461 Source Meter Unit (SMU). Raman spectroscopy was used to analyze the vibrational and structural properties of the substrates and deposited layers. XUV spectroscopy was applied to investigate the nonlinear optical response of the LIP containing Ag NPs and the spectral distribution and harmonic outputs produced during HHG experiments.

In conclusion, understanding and controlling the deposition-induced morphology of Ag nanoparticles is essential for optimizing their performance across multiple applications. Tailoring substrate properties and deposition conditions enables precise control over nanoparticle size, distribution, and interparticle spacing, which are critical parameters governing both plasmonic and nonlinear optical responses.

Structural and optical characterization using SEM, EDX, and UV–Vis spectroscopy confirmed the formation of Ag NPs exhibiting strong LSPR. The plasmonic properties of Ag NPs were successfully utilized for SERS, where significant Raman signal enhancement of R6G was observed. FDTD simulations further revealed strong localization of electromagnetic fields at nanoparticle junctions (hotspots), where the enhancement factor scales as $[E/E_0]^4$, confirming that nanogaps and random nanoparticle distributions play a dominant role in signal amplification. The simulations also demonstrated that decreasing interparticle spacing leads to stronger field confinement and higher SERS activity due to plasmonic coupling effects.

In addition to sensing applications, laser-induced plasma containing Ag NPs was employed as a nonlinear medium for HHG. Plasma diagnostics based on optical emission spectroscopy allowed determining the LIP parameters, while XUV spectroscopy revealed harmonic generation in the 17–100 nm range, exhibiting characteristic plateau and cutoff regions. FDTD analysis of individual Ag NP under laser excitation demonstrated strong near-field enhancement, which can increase the effective electric field experienced by electrons. Such plasmonic field amplification contributes to enhanced electron acceleration and recombination probability, thereby improving HHG efficiency, as also predicted in plasmon-assisted HHG models.

These results demonstrate that Ag NPs-based nanostructures fabricated by ultrafast laser processing serve as multifunctional platforms integrating plasmon-enhanced sensing and nonlinear optical processes. The combination of experimental results and FDTD simulations highlights the critical role of nanoscale field enhancement in both SERS and HHG, paving the way for advanced applications in ultrasensitive detection and coherent XUV radiation generation.

[1] S. Iravani, Silver nanoparticles: synthesis, properties and applications, Int. J. Nanomed. 6 (2011) pp.123–142.
[2] C. Noguez, Surface plasmons on metal nanoparticles: the influence of shape and physical environment, J. Phys. Chem. C 111 (2007) pp.3806–3819.
[3] K.L. Kelly, E. Coronado, L.L. Zhao, G.C. Schatz, The optical properties of metal nanoparticles: the influence of size, shape, and dielectric environment, J. Phys. Chem. B 107 (2003) pp.668–677.
[4] M.A. El-Sayed, Some interesting properties of metals confined in time and nanometer space of different shapes, Acc. Chem. Res. 34 (2001) pp.257–264.

# Measurement of the dispersion of nonlinear crystals in the mid-infrared range by spontaneous parametric down-conversion

**E.S. Zatsepin[1], A.V. Veselovsky[2], A.S. Sabanin[1], D.V. Badikov[3], G.H. Kitaeva[2], S.P. Kulik[1,2], A.V. Paterova[1]**

*1- South Ural State University, Chelyabinsk, Russia*
*2- Moscow State University, Moscow, Russia*
*3- Kuban State University, Krasnodar, Russia*

*paterova@physics.msu.ru*

Traditional methods for measuring the dispersion characteristics of nonlinear crystals have a number of significant limitations related to the requirement for direct detection of infrared (IR) radiation and a relatively narrow operating spectral range. This imposes strict requirements on the efficiency of IR radiation detectors, as well as on the achievable signal-to-noise ratio during measurements. Direct detection in the mid- and far-IR range is often associated with the low quantum efficiency of available photodetectors and the need for cryogenic cooling, which complicates the experimental setup and limits the accuracy of the results obtained.

As an alternative, in our work we propose a method for studying the dispersion of nonlinear crystals based on the effect of spontaneous parametric down-conversion (SPDC) [1-2] generated in a non-degenerate regime. An important advantage of the approach is that the signal photons are in the visible and near-IR ranges, where highly efficient Si- and InGaAs- detectors with low noise levels are available. Using several spectra of SPDC photons detected at different phase-matching angles, it is possible to calculate the values of the ordinary and extraordinary refractive indices of the studied nonlinear material in the spectral region corresponding to idler SPDC photons, that are in the mid- and far-IR ranges. Thus, the proposed method allows to indirectly restore dispersion characteristics in the hard-to-reach IR region using measurements in a more favorable short-wavelength range.

This paper demonstrates the effectiveness of this method using the example of two nonlinear crystals: $AgGaS_2$ and $BaGa_2GeS_6$. The refractive indices of these materials, according to various sources [3,4], are known with sufficient accuracy only up to 10.6 μm. The proposed approach allows to expand this range up to 21 μm and obtain reliable dispersion dependences in the wavelength range, where direct detection is difficult, and the available reference data is often contradictory or missing.

[1] M. H. Rubin, D. N. Klyshko, Y. H. Shih, and A. V. Sergienko, "Theory of two photon entanglement in type-II optical parametric down-conversion," Physical Review A 50(6), pp. 5122-5131 (1994)
[2] L. J. Wang, X. Y. Zou, and L. Mandel, "Induced coherence without induced emission", Phys. Rev. A 44, 4614 (1991)
[3] K. Kato, T. Okamoto, S. Grechin, and N. Umemura, "New Sellmeier and Thermo-Optic Dispersion Formulas for AgGaS2", Crystals, 9(3), 129 (2019)
[4] V.V. Badikov, et al, "Crystal growth and characterization of new quaternary chalcogenide nonlinear crystals for the mid-IR: BaGa2GeS6 and BaGa2GeSe6", Opt. Mat. Exp. 6(9), 2933 (2016)

ALT INTERNATIONAL CONFERENCE
Advanced Laser Technologies

# NANOPHOTONICS

# Giant optical anisotropy in van der Waals materials: from magnetic excitons to hyperbolic materials

**G. Ermolaev, V. Volkov**

*Emerging Technologies Research Center, XPANCEO, Internet City, Emmay Tower, Dubai, United Arab Emirates*

*ermolaev-georgy@xpanceo.com*

The quest for the next-generation photonic architectures is fundamentally dependent on the discovery and control of materials exhibiting giant optical anisotropy [1]. Van der Waals (vdW) materials have emerged as a revolutionary platform for this endeavor, offering strong light-matter interactions [2]. However, an experimental challenge has existed in quantifying the full dielectric tensor for these low-symmetry crystals. This work presents a comprehensive determination of these fundamental properties, achieved by applying spectroscopic ellipsometry and Mueller matrix measurements. Our findings reveal new physical regimes, tracing a narrative from magnetically-induced resonances [3,4] to natural hyperbolicity [5].

This exploration begins with magnetic excitons, for which we demonstrate that the interplay of dimensionality, electronic correlations, and magnetism in vdW crystals is a powerful tool for engineering optical anisotropy. For example, we establish that short-range magnetic correlations can stabilize excitons even in bulk, non-magnetic phases of $CrCl_3$ [3] and CrSBr [4]. Moreover, we show that $CrCl_3$ has a record-breaking exciton binding energy of 1.64 eV, an order of magnitude larger than that of typical semiconductors, which we attribute to quasi-2D confinement and robust magnetic correlations that persist at room temperature [3]. In CrSBr, we observe a giant exciton oscillator strength that fundamentally defies established scaling dependencies, as predicted by the Arrhenius law [4]. This anomalous behavior, originating from the 1D electron-hole wavefunction overlap, generates a giant in-plane birefringence of $\Delta n \approx 1.5$ near the exciton resonance [4].

We then push this investigation to the most extreme form of anisotropy: natural hyperbolocity. This exotic state, in which the dielectric tensor components have opposite signs along orthogonal axes, is a primary goal of nanophotonics but has been largely restricted to the mid-IR. We report the first direct experimental determination of the full dielectric tensor of $MoOCl_2$, establishing it as a natural, broadband hyperbolic material for the technologically critical visible and near-infrared spectrum [5]. As a result, our work demonstrates a materials-centric approach using an advanced ellipsometry configuration as a powerful path to unlock novel regimes of light-matter interaction for next-generation nanophotonics.

[1] G. Ermolaev et al., Nature Communications, 12, 854 (2021)
[2] A. Slavich, G. Ermolaev et al., Light: Science & Applications, 13, 68 (2024)
[3] G. Ermolaev et al., arXiv:2505.00920 (2025).
[4] G. Ermolaev et al., arXiv:2509.18866 (2025).
[5] G. Ermolaev, Nano Letters, 26, 13, 4329-4338 (2026).

# Light emission from bulk $MoS_2$ nanostructures

**T.A. Kamenskaya, S.G. Martanov, E.V. Tarkaeva, A.Yu. Kuntsevich**

*P.N. Lebedev Physical Institute of the RAS, 119991, Leninsky prosp. 53, Moscow, Russia*

*alexkun@lebedev.ru*

Transition metal dichalcogenides (TMDCs) are semiconducting layered materials with fascinating properties in the 2D limit. The ideology of 2D materials and van der Waals heterostructures looks extremely attractive for nanoelectronics and nanophotonics because it allows to assemble extraordinary high quality structures mechanically[1] and avoid such expensive processes as molecular beam epitaxy.In the monolayer limit these TMDCs become direct band and acquire optical activity and strongest exciton effects[2]. Moreover, $MoS_2$ is the most stable among them and is the most promising 2D semiconductor for ultrasmall nanotransistors of the post-Moore era[3], flexible electronics[4] and sensing applications[5].

High refraction index ~4 makes $MoS_2$ also attractive for nanophotonics[6]. In the bulk crystalline form this material however has indirect bandgap and its luminescence is much weaker compared to the monolayer. Recent observation of the enhanced emission with modulated spectrum from the other TMDC circular microresonators[7], including lasing[8], motivated us to fabricate and study optical properties of the $MoS_2$ microdiscs. The fabrication was performed using nanolithography of the scotch-tape exfoliated flakes with subsequent dry etching in $SF_6$ plasma. The radii of the discs were in the range 1-10 μm ant the thicknesses varied from 17 to 100 nm. Similarly to Refs.[7,8] we observed enhanced emission close to indirect exciton (~900 nm) with a spectral modulation by some resonator modes. However phenomenology of the micro-photoluminescence does not allow us to attribute the modulation to the whispering gallery modes.

Bulk TMDC micro crystals are much easily available by mechanical exfoliation than the monolayers, though they are not scalable yet. We therefore performed DC-magnetron sputtering of $MoS_2$ films. Surprizingly to us, electronic and optical properties of the films differ dramatically from the bulk crystalline $MoS_2$., their structures was amorphous and did not demonstrate visible conductivity and optical resonances. The films were optically transparent with refraction index about 2. The stoichiometry was shifted towards molybdenum and the surface demonstrated slow oxidation (1 nm per week). More interestingly, these films demonstrated strong and broadband Raman scattering when they were sputtered onto silver. Our studies allow to identify this emission with plasmon-assited surface enhanced Raman scattering driven by chemically induced three-dimensional nanostructures formed in the silver film.

Sample fabrication was performed at the LPI Shared Facility Center. The work is supported by Russian Science Foundation grant № 25-42-01036.

[1] A. K. Geim and I. V. Grigoreva, Van der Waals Heterostructures, Nature, vol. 499, pp. 419-425, (2013).
[2] S. Manzeli,et al, 2D transition metal dichalcogenides, Nat. Rev. Mat. vol.2, p. 17033 (2017).
[3] F. Wu, H. Tian, Y.Shen, Z. Hou, J. Ren, G. Gou, Y. Sun, Y. Yang, T.-L. Ren, Vertical $MoS_2$ transistors with sub-1-nm gate lengths, Nature vol.603, p. 259 (2022).
[4] A.T. Hoang, et al, Low-temperature growth of $MoS_2$ on polymer and thin glass substrates for flexible electronics, Nature Nanotechnology, vol. 18, pp. 1439-1447, (2023).
[5] O Samy, S Zeng,M.D. Birowosuto, A E. Moutaouakil, A Review on $MoS_2$ Properties, Synthesis, Sensing Applications and Challenges, Crystals, vol. 11, p. 355, (2021).
[6] P. Zotev et al, Nanophotonics with multilayer van der Waals materials, Nat. Phot., vol. 19, p. 788, (2025).
[7] B.R. Borodin, et al,, Indirect bandgap MoSe2 resonators for light-emitting nanophotonics, Nanoscale Horiz. Vol. 8, pp. 396-403 (2023).
[8] J. Sung, et al, Room-temperature continuous-wave indirect-bandgap transition lasing in an ultra-thin WS2 disk, Nature Photonics, vol. 16, pp. 792-797, (2022).

# Anisotropic and nonlinear optical metasurfaces based on van der Waals materials

A.V. Prokhorov[1,2]

[1]Center for Photonics and 2D Materials, Moscow Institute of Physics and Technology, Institutskiy per. 9, Dolgoprudny 141701, Russia
[2]Department of Physics and Applied Mathematics, Vladimir State University named after A.G. and N.G. Stoletovs, Gorkogo str. 87, Vladimir 600000, Russia

alprokhorov33@gmail.com

In this paper, we discuss the fundamental principles of designing optical metasurfaces for control and nonlinear conversion of light. General approaches for numerical simulation, design and fabrication of optical metasurfaces intended for the observation of nonlinear and quantum optical phenomena on their basis, are considered. We propose two different types of metasurfaces based on highly nonlinear polytypes of van der Waals materials. The one type uses conventional concept with preliminary analysis of resonances of individual building blocks followed by their matching in order to excite the lattice eigenmodes. Another type corresponds to the so-called membrane metsurfaces, which are films of functional materials perforated throughout their thickness with arrays of holes. There are no common types of resonators in such structures, and the collective modes arising in them corresponds to non-radiating distributions of displacement currents causing the high concentration of near-field energy in the plane of metasurface. The common method of multipole analysis [1] is still applicable for tuning and studying of such states, but only to unit cells being allocated in the structure of membrane metasurfaces and comprising both hole and surrounding material. In this case, the excitation of collective modes can be caused by the fundamental effect of multipole coupling in the lattice [2]. Since the localization of the near field in membrane metasurfaces can occur inside the material, the proposed structures pave the way for a significant increase in the efficiency of nonlinear optical and quantum effects. Such an approach complements and strengthens the well-known Mie-void regimes [3], in which the localization of the near field mainly occurs inside holes. We consider the non-centrosymmetric 3R polytype of $MoS_2$ material as the basis for the fabrication of metasurfaces, which not only exhibits the strong second-order optical nonlinearity [4], but also allows for the tunable generation of biphotons at any orientation of pump polarization [5]. By developing these concepts, we present here various realizations of both conventional and membrane 3R $MoS_2$ metasurfaces for efficient second harmonic generation (SHG), see Fig. 1a-c, and the formation of non-classical biphoton states based on spontaneous parametric down-conversion (SPDC), see Fig. 1d-f.

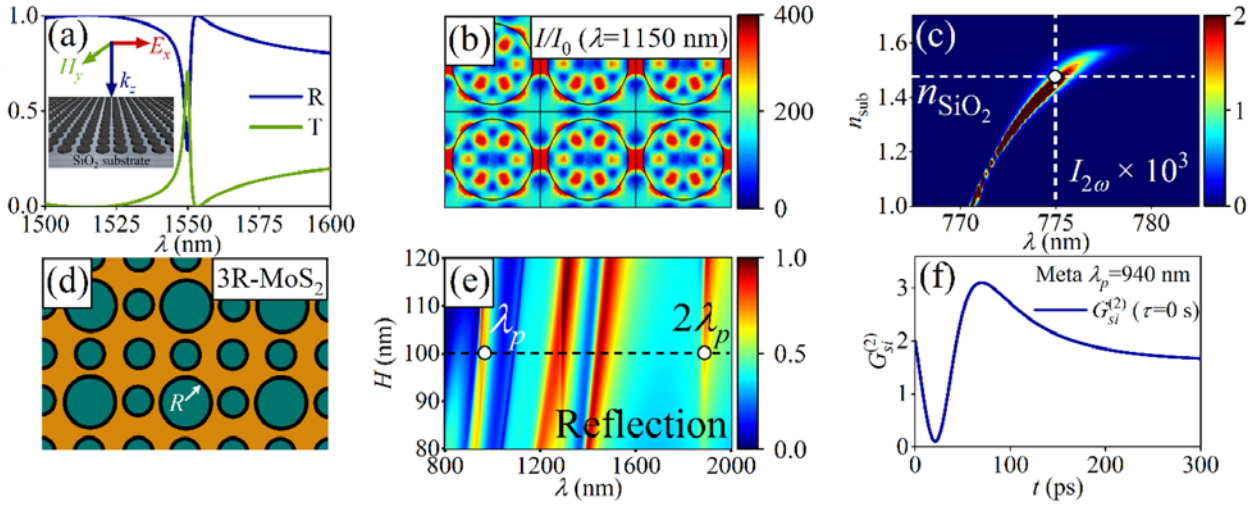


**Fig. 1.** Conventional and membrane 3R-$MoS_2$ metasurfaces for SHG and SPDC

This work was supported by the Russian Science Foundation (Grants No. 25-12-00154, 24-12-20015).

[1] A. Evlyukhin et al., Laser Photonics Rev., 15, 2100206 (2021).
[2] A. Prokhorov et al., ACS Photonics, 9, 3869–3875 (2022).
[3] Y. Kivshar et al., Light Sci. Appl. 12, 3 (2023).
[4] T. O. Shegai et al., Commun. Phys. 8, 271 (2025).
[5] I. Staude et al., Nat. Commun. 15, 7600 (2024).

# TMDC-Induced Ultrafast All-Optical Switching in Hybrid Metasurface

**A.M. Chernyak, A.I. Musorin, A.A. Fedyanin**

*Faculty of Physics, Lomonosov Moscow State University,*
*Leninskie gory 1-2, Moscow 119991, Russia*

Transition metal dichalcogenides (TMDCs) represent a prominent class of 2D materials with strong excitonic effects and a layer-tunable electronic structure [1-3]. Their optical absorption spectrum features pronounced excitonic resonances at room temperature with binding energy of ~100meV, making them attractive for nonlinear photonic applications.

Under intense laser excitation, TMDC exhibits several competing processes that modify its complex dielectric permittivity. Two-photon absorption (TPA) serves as the primary absorption channel, generating free carriers that introduce a Drude contribution to the permittivity and additional absorption, leading to reverse saturable absorption [4]. Bandgap renormalization is also observed, though it primarily shifts the indirect band edge rather than the sharp excitonic resonance [5]. Because of the small exciton binding energy, the high carrier densities generated by strong TPA pumping drive a Mott transition that dissociates residual excitons into an electron–hole plasma [6]. At high pump powers, this behavior is observed both near and far from the excitonic region. The subsequent relaxation follows the Drude free-carrier model combined with defect-mediated recombination, with characteristic timescales of ~10–100 ps.

Metasurfaces provide a powerful platform for controlling light properties at the nanoscale. Advances in active nanophotonics have driven the development of ultrafast all-optical metasurfaces [7]. Under intense optical excitation, the complex permittivity of the constituent material undergoes significant changes. In direct-gap semiconductor metasurfaces, all-optical picosecond modulation of the reflection coefficient and a resonance shift of 30 nm have been demonstrated at low pump fluences [8]. Complete temporal control over resonant effects—including resonance creation, annihilation, broadening, and sharpening—can be achieved using metasurfaces supporting high-quality-factor resonances such as bound states in the continuum (BIC) [9].

The integration of TMDCs with resonant photonic structures opens new avenues for ultrafast light-control devices. This potential has been demonstrated by nonlinear TMDC van der Waals metasuface, which enable ultrafast switching of second harmonic generation with nearly unity modulation depth [10]. The operation speeds are fundamentally limited only by the excitation pulse duration. These results establish hybrid TMDC-metasurface as a promising strategy for ultrafast all-optical control.

Here, we demonstrate ultrafast transmittance modulation in TMDC integrated with a dielectric metasurface supporting a high-Q quasi-BIC resonance. The dependence on the pump intensity reveals a continuous switching between positive and negative optical modulation passing through the saturable absorption regime with zero modulation. These results establish hybrid TMD–metasurface platforms as efficient ultrafast modulators for low-loss photonic circuits and highlight a pathway toward subpicosecond optical devices through Q-factor engineering.

[1] Y. Li, A. Chernikov, X. Zhang et.al., Measurement of the optical dielectric function of monolayer transition-metal dichalcogenides: $MoS_2$, $MoSe_2$, $WS_2$, and $WSe_2$, Phys. Rev. B, 90, pp. 205422, (2014).
[2] S. Tongay, J. Zhou, C. Ataca et.al., Thermally driven crossover from indirect toward direct bandgap in 2D semiconductors: MoSe2 versus MoS2, Nano Lett., 12, 11, pp. 5576–5580, (2012).
[3] G. Wang, A. Chernikov, M. M. Glazov et.al., Colloquium: Excitons in atomically thin transition metal dichalcogenides, Rev. Mod. Phys, 90, pp. 021001, (2018).
[4] H. Pan, H. Chu, Y. Li et al., Comprehensive study on the nonlinear optical properties of few-layered $MoSe_2$ nanosheets at 1 μm, Journal of Alloys and Compounds, 806, pp. 52–60, (2019).
[5] E.A. Pogna, M. Marsili, D. De Fazio et al., Photo-induced bandgap renormalization governs the ultrafast response of single-layer $MoS_2$, ACS Nano, 10, 1, pp. 1182–1188, (2016).
[6] X. Tian, R. Wei, Z. Ma, J. Qiu, Broadband Nonlinear Optical Absorption Induced by Bandgap Renormalization in CVD-Grown Monolayer $MoSe_2$, ACS Appl. Mater. Interfaces, 14, 6, pp. 8274–8281, (2022).
[7]M. Maiuri, A. Schirato, G. Cerullo, G. Della Valle, Ultrafast All-Optical Metasurfaces: Challenges and New Frontiers, ACS Photonics, 11, 8, pp. 2888–2905, (2024).
[8] M. R. Shcherbakov, S. Liu, V.V. Zubyuk et al., Ultrafast all-optical tuning of direct-gap semiconductor metasurfaces, Nat. Commun., 8, 17, (2017).
[9] A. Aigner, T. Possmayer, T. Weber et.al., Optical control of resonances in temporally symmetry-broken metasurfaces, Nature, 644, pp. 896–903, (2025).
[10] L. Seidt, T. Weber, A. A. Seredin et.al., Ultrafast all-optical switching in nonlinear 3R-$MoS_2$ van der Waals metasurfaces, npj Nanophotonics, 2, 37, (2025).

# Towards exciton-plasmon-polaritons observation in hybrid GaP nanowire/$WS_2$/Ag heterostructure

**A. Kuznetsov[1], A.V. Nikolaeva[1,2], M.V. Levichev[1,2], P.N. Kozhevin[3], T. Shugabaev[2], V.V. Neplokh[1,4], A.V. Nalitov[1], A.D. Bolshakov[1,2]**

*1- MIPT, Phystech, 9 Institutskiy per., Dolgoprudny, Moscow Region, 141700, Russia*
*2- Alferov University, Khlopina str. 8/3, Saint-Petersburg, 194021, Russia*
*3- Saint-Petersburg State University, Universitetskaya emb. 7/9, St. Petersburg, 199034, Russia*
*4- Russian Quantum Center, Novaya str. 100, Skolkovo Village, Moscow region, 143026, Russia*

*alkuznetsov1998@gmail.com*

The study of strong coupling effects and the formation of exciton-polaritons in hybrid nanostructures based on two-dimensional materials represents one of the most dynamically developing areas of modern nanophotonics and quantum optics [1]. The relevance of this field is driven by fundamental challenges in controlling light at subwavelength scales and developing a new generation of optical devices for information processing, sensing, and quantum technologies. Polaritonic states arising from the hybridization of photons with excitons or plasmons possess unique properties, such as low effective mass, strong nonlinearities, and the ability to condense at room temperature, opening prospects for energy-efficient and high-speed optoelectronic components [2]. A key step in this direction is the development of controllable platforms for achieving strong coupling, where dielectric or semiconductor nanoresonators effectively interact with two-dimensional materials or plasmonic systems.

This work is devoted to the investigation of coupling regimes between $WS_2$ excitons and hybrid plasmon-polaritons guided modes of a GaP nanowire (NW) on an Ag/Si substrate. Numerical simulation demonstrated the formation of a single hybrid plasmonic mode localized at the interface between the GaP NW and Ag in the range of NW diameters ~ 60-90 nm ($\lambda$ = 615 nm). Mode dispersion (d = 100 nm) demonstrates the anticrossing behavior with $\Omega_R$ = 81 meV.

Substrates fabricated by magnetron sputtering (Ag/Si) substrates demonstrated low surface roughness, not exceeding 1 nm (AFM, SEM), which is critically important for the efficient excitation of surface plasmons. GaP NWs of specified geometry, with a length of 3.8 ± 0.5 μm and a diameter of 104 ± 10 nm, were grown by molecular beam epitaxy. $WS_2$ monolayers were obtained by mechanical exfoliation and transferred onto the substrates using a dry transfer method, after which a single GaP NW was deposited on top via a “pick-and-place” technique.

The optical properties of the hybrid systems were investigated using photoluminescence (PL) microspectroscopy with 532 nm laser excitation. High spatial resolution mapping of PL signals allowed a detailed study of the influence of the excitation light polarization on the electromagnetic field distribution within the nanostructure. PL spatial distribution maps demonstrated that optical response polarized along the NW localized at its edges and is ~ 5-times higher in comparison with bare monolayer. PL at the edges is modified by the Fabry-Perot (F-P) cavity modes which vanish if the acquisition polarization is perpendicular to the NW. It means that PL is coupled to the fundamental hybrid plasmonic mode which travels at the NW/$WS_2$/Ag interface. PL measurements from different edges in transmission geometry (one edge is under excitation while PL is collected from the other) demonstrated F-P modes and exciton peak redshift of 6.5 nm in parallel acquisition polarization (in perpendicular redshift wasn’t observed) which corresponds to the coupling strength of 21.1 meV ($\Omega_R$ = 42.2 meV). Comparison with $\gamma_{SPP}$ = 47 meV and $\gamma_X$ = 30 meV demonstrates the strong-coupling regime between the exciton in $WS_2$ and the hybrid guided mode of the GaP NW.

The work is supported by the Russian Science Foundation (grant №25-12-00135).

[1] H. Kang, J. Ma, J. Li, X. Zhang, X. Liu, ACS nano. 17(24), 24449-24467 (2023).
[2] H. Deng, H. Haug, Y. Yamamoto, Reviews of modern physics. 82(2), 1489-1537 (2010).

# Multifunctional Titanium Metasurfaces with Plasmonic Generation for Sensing and Photocatalysis

**M. Kuritskij[1], A. Tsibulnikova[1], I. Lyatun[1], V. Slezhkin[1,2], I. Samusev[1]**

*1- Immanuel Kant Baltic Federal University, A. Nevsky St., 14, Kaliningrad, Russia, 236041*
*2- Kaliningrad State Technical University, 1 Sovetsky Prospekt, Kaliningrad, Russia, 236022*

*Mix-Mux@yandex.ru*

Today, various multifunctional nanometamaterials have become an integral part of modern electroanalytical chemistry. Sensors, biosensors, and electroanalytical devices based on nanostructured sensor surfaces demonstrate faster electron kinetics and enhanced analytical signal, as well as unique catalytic properties and adjustable selectivity [1]. One of the simplest and most effective methods for creating functional surface nano- and microstructures is pulsed laser structuring [2]. Moreover, the resulting metasurfaces exhibit a pronounced localized surface plasmon resonance effect, which enhances electromagnetic absorption and photocatalytic activity on such structures [3, 4]. This study aims to develop an optimal method for creating laser-induced titanium-based metasurfaces with plasmonic generation for use in biosensors and electroanalytical devices.

Structuring of anodized titanium plates was performed simultaneously by two harmonics of laser radiation 532 and 1064 nm with pulses of 10 ns duration with a frequency of 10 Hz. The beam trajectory was controlled to produce an ordered hexagonal grid with an element radius of 100 μm (Fig. 1, a – insert). SEM analysis of the obtained functional surfaces showed uniform cracking and pore formation throughout the irradiated area with the formation of nanotrenches with a width of 20-50 nm, as well as numerous islands of sponge-like porous titanium oxide with a period of laser-induced formations of the order of 40 nm (Fig. 1, a).

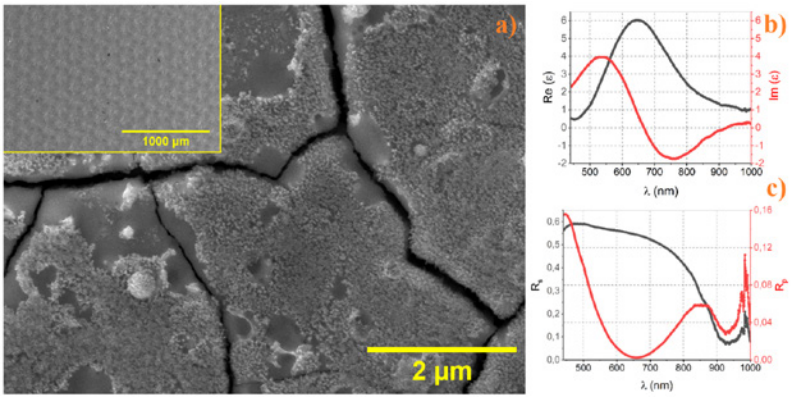


**Fig. 1.** Porous titanium metasurface: a – SEM images of the structured titanium surface;
b – spectral dependences of real and imaginary parts of dielectric permittivity;
c – spectra of reflection coefficient of p- and s-polarized radiation

Spectral ellipsometry of the samples demonstrates a negative imaginary part of the dielectric permittivity in the range of 670-920 nm, with a positive real component (Fig. 1, b). This is the region of plasmon generation, which is of the nature of free electrons [5]. Additionally, at 670 nm, there is a minimum reflection of p-polarized radiation, where it is almost completely absorbed (Fig. 1, c).

[1] F. Silveri, F. D. Pelle, D. Compagnone, Recent advances in sustainable strategies for the integration of nanostructured sensing surfaces in electroanalytical devices, Trends in Analytical Chemistry, vol. 185, 118175, (2025).
[2] H. Wang, D. Deng, Z. Zhai, Y. Yao, Laser-processed functional surface structures for multi-functional applications-a review, Journal of Manufacturing Processes, vol. 116, pp. 247–283, (2024).
[3] S. Zhu, G. Lu, X. Wang, T. Liu, Y. He, J. Sun, X. Xie, Surface plasmon resonance effect enhanced upconversion luminescence in Ag modified NaYF4: Yb/Er for photovoltaic efficiency improvement under solar irradiation, Renewable Energy, vol. 248, 123062, (2025).
[4] Z. Li, J. Zi, X. Luan, Y. Zhong, M. Qu, Y. Wang, Z. Lian, Localized Surface Plasmon Resonance Promotes Metal–Organic Framework-Based Photocatalytic Hydrogen Evolution, Advanced Functional Materials, vol. 33, 2303069, (2023).
[5] V. Klimov, Nanoplasmonics (Moscow: Physmathlit Publ.), (2009).

# Diamond as sensing platform

**A. Ermakova**[1,2]

*1- Institute for Materials Research, Hasselt University, Diepenbeek, Belgium*
*2- Space Physics Domain, Royal Belgian Institute for Space Aeronomy, Brussels, Belgium*

*anna.ermakova@uhasselt.be*

Over the last few years, the use of diamond color centers for sensing applications has become extremely popular. The key element in diamond-based quantum sensing is the nitrogen-vacancy (NV) center. NV centers can exist in two charge states: neutral ($NV^0$) and negative ($NV^-$), and only the $NV^-$ allows optical readout and spin manipulation, which are essential for sensing techniques [1]. NV centers in bulk crystals and nanodiamonds are suited to slightly different applications. However, the main detection schemes involve measuring magnetic field [2], electric field [3], or temperature [4]. Moreover, nanodiamonds with NV centers can be used for theranostics, combining their sensing capabilities are combined with drug delivery or photodynamic cancer therapy [5,6]. A significant advantage of fluorescent nanodiamonds over other optical markers is that they are inert and nontoxic. These diamond nanoparticles may contain unique crystal defects that enable imaging without photobleaching or photoblinking. Therefore, fluorescent nanodiamonds can be used for long-term monitoring.

Here, other sensing aspects of NV centers will be discussed in detail. In particular, it was shown that the magnetic field can be sensed by the NV center in a microwave-free regime [7] with a special case under near-zero-field conditions [8]. This detection scheme has advantages for studying biological systems, where the microwave field can induce heating, and for investigating systems where microwave delivery is complicated. Therefore, we are applying this microwave-free technique to measure micro- and nanoscale magnetic structures. The possibilities and limitations of this technique for nanodiamonds will be presented and discussed.

[1] M. W. Doherty, N. B. Manson, P. Delaney, F. Jelezko, J. Wrachtrup, and L. C. L. Hollenberg, The nitrogen-vacancy colour centre in diamond, Physics Reports, 528, 1-45 (2013)
[2] L. Rondin, J.-P. Tetienne, T. Hingant, J.-F. Roch, P. Maletinsky, and V. Jacques, Magnetometry with nitrogen-vacancy defects in diamond, Reports on Progress in Physics, 77, 056503 (2014)
[3] F. Dolde, H. Fedder, M. W. Doherty, T. Nöbauer, F. Rempp, G. Balasubramanian, T. Wolf, F. Reinhard, L. C. L. Hollenberg, F. Jelezko, and J. Wrachtrup, Electric-field sensing using single diamond spins, Nature Physics, 7, 459-463 (2011)
[4] G. Kucsko, P. C. Maurer, N. Y. Yao, M. Kubo, H. J. Noh, P. K. Lo, H. Park, and M. D. Lukin, Nanometre-scale thermometry in a living cell, Nature, 500, 54-58 (2013)
[5] Y. Wu, A. Ermakova, W. Liu, G. Pramanik, T. M. Vu, A. Kurz, L. McGuinness, B. Naydenov, S. Hafner, R. Reuter, J. Wrachtrup, J. Isoya, C. Förtsch, H. Barth, T. Simmet, F. Jelezko, and T. Weil, Programmable biopolymers for advancing biomedical applications of fluorescent nanodiamonds, Advanced Functional Materials, 25, 6576-6585 (2015)
[6] Y. Wu, M. N. A. Alam, P. Balasubramanian, P. Winterwerber, A. Ermakova, M. Müller, M. Wagner, F. Jelezko, M. Raabe, and T. Weil, Fluorescent nanodiamond-nanogels for nanoscale sensing and photodynamic applications, Advanced NanoBiomed Research, 1, 2000101 (2021)
[7] A. Wickenbrock, H. Zheng, L. Bougas, N. Leefer, S. Afach, A. Jarmola, V. M. Acosta, and D. Budker, Microwave-free magnetometry with nitrogen-vacancy centers in diamond, Applied Physics Letters, 109, 053505 (2016)
[8] S. Sengottuvel, O. Dhungel, M. Mrózek, A. Wickenbrock, D. Budker, W. Gawlik, and A. M. Wojciechowski, Microwave-free imaging magnetometry with nitrogen-vacancy centers in nanodiamonds at near-zero field, Physical Review Applied, 23, 034001 (2025)

# Clock transitions in Nitrogen-Vacancy color centers in diamond for Quantum Sensing

**G. Zanelli[1], E. Moreva[1], E. Bernardi[1], E. Losero[1], Z. Pastuovic[4], J. Forneris[2,3], P. Traina[1], I. P. Degiovanni[1], M. Genovese[1,3]**

*1- Istituto Nazionale di Ricerca Metrologica (INRiM), Turin, Italy*
*2- Physics Department, University of Torino, Turin, Italy*
*3- Istituto Nazionale di Fisica Nucleare (INFN), sezione di Torino, Turin, Italy*
*4- Centre for Accelerator Science, Australian Nuclear Science and Technology Organisation, New Illawarra rd., Lucas Heights, NSW 2234, Australia*

The Nitrogen-Vacancy (NV) center in diamond is a point defect occurring in the diamond crystalline matrix composed of a substitutional nitrogen atom coupled to a lattice vacancy in a adjacent site. This system presents a spin triplet manifold (S=1) with transition energies that are sensitive to external physical quantities and spin dependent fluorescence emission rates [1]. These couplings between the spin sublevels and external physical quantities enabled the use of NV as quantum sensors for numerous physical quantities such as temperature, electric fields, magnetic fields and pressure. However, decoupling the effect of different quantities on the NV sensor is challenging since the single contributions may be difficult to distinguish.

One possible solution is to use clock transitions, that are obtained when an external field shifts the energy levels creating avoided crossings. In correspondence of the avoided crossings, the eigenenergies are not shifted by small variations of the external field, leading to a decoupling from noise arising from a specific physical quantity.

In our recent work [3] we investigate the effect of a weak orthogonal bias magnetic field on the eigenstates of an ensemble of NV centers. The applied bias creates balanced superposition states (dressed states) that are decoupled from magnetic field at the first order, leading to a clock transition.

Also, unbalanced superposition states (partially-dressed states) are generated, which present a sub-linear coupling with magnetic fields. These new eigenstates present improved properties for temperature sensing with respect to the initial ones, mainly, a 3-fold improvement in coherence time due to the lower coupling with magnetic field noise sources. Furthermore, monitoring the transition energy of the dressed state clock transition while measuring magnetic fields with partially-dressed states enables temperature independent magnetic field sensing.

In our previous work [2], this clock transition is used for temperature sensing. We apply a transverse bias magnetic field to an ensemble of NV centers and investigate its effect on the temperature sensitivity. With simultaneous driving of dressed and partially-dressed states we observe a 3-fold temperature sensitivity improvement with respect to the $m_s = +1$ and $m_s = -1$ states and an overall reduction of the noise floor. Additionally, the effect of reduced magnetic coupling attenuates the signal of spurious noise harmonics and AC magnetic fields, proving the possibility of performing magnetic-field independent temperature sensing.

These results show how engineering quantum state superposition enables the creation of clock transitions, thus improving the performance of quantum sensors. In addition, these measurement schemes could be applied to shallow NV sensors or to NV in nanodiamonds to reduce the effects of surface noise and improve the sensitivity.

[1] M. W. Doherty et al., "The Nitrogen-Vacancy colour centre in diamond", Physics Report, vol. 528, 1, pp. 1-45, (2013).
[2] G. Zanelli et al., "Interplay between dressed and strong-axial-field states in nitrogen vacancy centers for quantum sensing and computation", Phys. Rev. B, 112, 235201 (2025).
[3] E. Moreva et al., "Practical Applications of Quantum Sensing: A Simple Method to Enhance the Sensitivity of Nitrogen-Vacancy-Based Temperature Sensors", Phys. Rev. App., vol.13, 054057, (2020).

# Luminescent diamonds for all-optical nanoscale thermometry and thermal control in biological systems

**A. Romshin[1], A. Kruglov[2], N. Aseyev[3], R. Bagramov[4], V. Filonenko[4], V. Sedov[1], I. Vlasov[4]**

*1- Prokhorov General Physics Institute of the Russian Academy of Sciences, Moscow, Russia*
*2- Institute of Theoretical and Experimental Biophysics of the Russian Academy of Sciences, Moscow, Russia*
*3- Institute of Higher Nervous Activity and Neurophysiology of the Russian Academy of Sciences, Moscow, Russia*
*4- Vereshchagin Institute of High-Pressure Physics of the Russian Academy of Sciences, Kaluzhskoe shoss 14, Troitsk, 108840 Russia*

*alex_31r@mail.ru*

Precise measurement and control of temperature at micro- and nanometer scales remain important challenges in biophysics, nanomedicine, and photonics. Local temperature variations accompany processes ranging from heat dissipation in nanostructures and photothermal conversion to intracellular signaling, mitochondrial activity, and thermal modulation of excitable cells. However, quantitative thermometry in such complex environments, especially under physiological conditions, remains difficult. Conventional luminescent thermometers based on fluorescent dyes, proteins, polymer nanoparticles, quantum dots, and rare-earth complexes are often limited by photobleaching, insufficient long-term stability, and sensitivity to pH, viscosity, ionic strength, membrane potential, and local chemical composition. Diamond particles containing optically active color centers offer an attractive alternative by combining photostability, biocompatibility, weak environmental sensitivity, and quantitative temperature readout in liquids, living cells, isolated organelles, and biological tissues.

In this talk, we will focus on diamond-based thermometry approaches developed by our group using silicon-vacancy (SiV) and H3 ($N_2V$) color centers [1-3]. Temperature sensing was implemented through two complementary optical mechanisms: the temperature-dependent spectral shift of the SiV zero-phonon line and the spectral redistribution of H3 luminescence intensity. These methods enabled quantitative temperature measurements in aqueous environments and biological systems of different complexity. A particular emphasis will be placed on multifunctional diamond heater-thermometers (DHT), in which a single diamond particle serves simultaneously as a local heat source and a temperature sensor. Such probes allow controlled thermal stimulation of individual cells with simultaneous temperature readout and subcellular localization. Local optical heating was shown to trigger calcium responses in HeLa cells and primary hippocampal neurons. Subsequent electrophysiological studies revealed a mechanism of membrane thermal capture, in which rapid local heating induces capacitive membrane currents and robust neuronal excitation without genetic modification. Action potentials were generated at repetition rates of up to 40 Hz, demonstrating an all-optical route toward thermal neuromodulation.

Beyond cellular stimulations, DHT enables quantitative studies of microscopic heat-transfer dynamics. Heating and cooling transients revealed thermal relaxation times from tens of nanoseconds to hundreds of microseconds, depending on particle size, with an approximately quadratic scaling consistent with thermal diffusion models, enabling estimate of local thermal diffusivity in biological liquids. More recently, chemically functionalized diamonds containing H3 centers were employed for ratiometric thermometry of isolated mitochondria. Covalent attachment of diamond particles to mitochondrial membranes significantly improved thermal coupling and enabled detection of local temperature changes of up to 10 °C associated with respiratory-chain modulation and oxidative phosphorylation uncoupling. Taken together, these results demonstrate the potential of SiV- and H3-based diamond probes for quantitative studies of nanoscale heat transfer in complex biological systems, opening new opportunities for investigating thermally driven biological processes.

[1] A. Romshin, et al. "Nanoscale thermal control of a single living cell enabled by diamond heater-thermometer", Scientific Reports, 13, 8546, (2023).
[2] A. Romshin, et al. "Rapid neurostimulation at the micron scale with an optically controlled thermal-capture technique", Biomaterials Science, 13(1), 250-260, (2025).
[3] A. Romshin, et al. "Chemically Anchored Diamond with H3 Centers for Ratiometric Measurement of Isolated Mitochondria Temperature", International Journal of Molecular Science, 26(23), 11395, (2025).

# Near-Surface Activation of SiV Fluorescence in a New Generation of HPHT Nanodiamonds

**D. Pasternak[1,2], A. Zhivopistsev[1], A. Romshin[1], O. Kudryavtsev[1], R. Bagramov[3], V. Filonenko[3], I.I. Vlasov[1]**

*Prokhorov General Physics Institute of the Russian Academy of Sciences, 38 Vavilov Str., Moscow 119991, Russia;*
*2- National Research Nuclear University MEPhI, 31 Kashirskoe sh., Moscow, 115409, Russia;*
*3- Vereshchagin Institute of High-Pressure Physics of the Russian Academy of Sciences, 14 Kaluzhskoe Shosse, Troitsk, Moscow 108840, Russia.*

*dg.pasternak@physics.msu.ru*

A new generation of fluorescent diamond nanoparticles synthesized from hydrocarbons at high pressure appears to be promising for the design of efficient single-photon diamond sources and nanometer-sized optical sensors [1,2]. A characteristic feature of such nanodiamonds (NDs) is the termination of their surface with hydrogen. This hydrogen induces the formation of free holes at the diamond surface, thereby affecting the charge state of nearby fluorescent centers. In this study, the effect of the H-terminated ND surface on negatively charged silicon-vacancy (SiV) fluorescence as a function of the ND size was investigated. Raman, photoluminescence and scanning electron microscopy techniques were used to characterize the NDs. Diamond nanoparticles of various sizes in the 50–300 nm range were analyzed before and after H desorption from their surface. It was shown that a significant increase in SiV fluorescence (>50%) upon hydrogen removal starts for particles smaller than 100 nm. The effective thickness of the diamond surface layer, within which charge neutralization of SiV centers occurs under the hydrogen influence, was determined to be 6 nm.

This study is supported by the Ministry of Science and Higher Education of the Russian Federation (agreement/grant 075-15-2025-609).

[1] O. S. Kudryavtsev, R. H. Bagramov, A. M. Satanin, A. A. Shiryaev, O. I. Lebedev, A. M. Romshin, D. G. Pasternak, A. V. Nikolaev, V. P. Filonenko and I. I. Vlasov, Fano-Type Effect in Hydrogen-Terminated Pure Nanodiamond, Nano Lett., vol. 22, pp. 2589–2594, (2022).
[2] D. G. Pasternak, A. A. Zhivopistsev, A. M. Romshin, O. S. Kudryavtsev, R. H. Bagramov, V. P. Filonenko, N. I. Kargin and I. I. Vlasov, Effect of H-Terminated Surfaces on "Silicon-Vacancy" Fluorescence in High-Pressure Nanodiamonds, Nanomaterials, vol. 15, pp. 1842, (2025).

# Two-photon direct laser writing of micro-optics: enabling quantum photonic devices and imprint-ready master structures

**A. Gritsienko[1,2], A. Zhivopistsev[3], G. Voskanyan[1], A. Vitukhnovsky[1,2]**

*1- Moscow Institute of Physics and Technology (National Research University), 9 Institutskii Per, Dolgoprudnyi, Moscow Region, Russia 141700*
*2- P. N. Lebedev Physical Institute of the Russian Academy of Sciences, 53 Leninskiy Pr, Moscow, Russia 119991*
*3- Prokhorov General Physics Institute of the Russian Academy of Sciences, 119991 Moscow, Russia*

*grits_alex@rambler.ru*

Two-photon polymerization (TPP) based direct laser writing (DLW) has become a versatile platform for additive manufacturing of three-dimensional micro-optical elements with sub-micrometer resolution [1–3]. By locally cross-linking photoresists, TPP-DLW can deliver free-form refractive and diffractive optics, customized photonic structures, and master templates for replication, bridging the gap between rapid prototyping and scalable production. Here we present a suite of TPP-fabricated micro-optics that advance quantum photonic device integration and imprint-ready master structures.

In the domain of quantum photonics, we developed DLW-TPP elliptical lenses and lenses with an integrated additional prism to collimate the emission from nanodiamonds containing NV and SiV color centers. Using both commercially available and newly developed low-fluorescence photocompositions, these lenses produce a collimated beam that can be efficiently coupled into an optical fiber. We further realized bull's-eye ring resonators with a ring period of ~700 nm for quantum emitters, fabricated by high-resolution DLW. Additionally, a self-written waveguide (SWW) technique in photopolymer was employed to integrate optical fibers with micro- and nanodiamonds; as a proof of concept, a fiber-based microthermometer utilizing the $N_2$V-center luminescence was demonstrated on a low-cost commercial multimode fiber.

Regarding imprint-ready master structures, test replicas of kinoform X-ray lenses were successfully produced from DLW-printed masters, validating the fabrication chain for synchrotron optics. We also explored the fabrication of functional imprint stamps directly on the tips of optical fibers. DLW-TPP was used to print working stamps for point-wise nanoimprinting of structures such as visible-range Fresnel lenses, as well as a microindenter tip for adhesion-force measurements. These results illustrate the potential of TPP-DLW not only to create high-performance micro-optics for quantum devices but also to provide scalable replication routes and multifunctional fiber-integrated tools.

The development of fiber-based microindenters was supported by the Russian Science Foundation (grant No. 25-29-01105), and the development of nanoimprint stamps — by grant No. 25-79-20031.

[1] M. Malinauskas, A. Žukauskas, S. Hasegawa, Y. Hayasaki, V. Mizeikis, R. Buividas, S. Juodkazis, Ultrafast laser processing of materials: from science to industry, Light: Science & Applications, vol. 5, pp. e16133, (2016).
[2] T. Gissibl, S. Thiele, A. Herkommer, H. Giessen, Two-photon direct laser writing of ultracompact multi-lens objectives, Nature Photonics, vol. 10, pp. 554-560, (2016).
[3] A.K. Petrov, V.O. Bessonov, K.A. Abrashitova, N.G. Kokareva, K.R. Safronov, A.A. Barannikov, P.A. Ershov, N.B. Klimova, I.I. Lyatun, V.A. Yunkin, M. Polikarpov, I. Snigireva, A.A. Fedyanin, A. Snigirev, Polymer X-ray refractive nano-lenses fabricated by additive technology, Optics Express, vol. 25, pp. 14173-14181, (2017).

# Coupling of SiV-fluorescent nanodiamonds with microresonators

**A.A. Zhivopistsev[1], A.M. Romshin[1], A.V. Gritsienko[2,3], R.H. Bagramov[4], V.P. Filonenko[4], I.I. Vlasov[1]**

*1- Prokhorov General Physics Institute of the Russian Academy of Sciences, Moscow, Russia*
*2- Moscow Institute of Physics and Technology (National Research University), Dolgoprudnyí, Moscow Region, Russia*
*3- P. N. Lebedev Physical Institute of the Russian Academy of Sciences, Moscow, Russia*
*4- Vereshchagin Institute of High-Pressure Physics of the Russian Academy of Sciences, Troitsk, Moscow, Russia*

*azh253@gmail.com*

Silicon-vacancy (SiV) centers in nanodiamonds are of significant interest as photonic emitters due to their exceptional optical properties, such as a narrow zero-phonon line (ZPL) at 738 nm and high photostability, even at room temperature [1]. These characteristics make them promising candidates for quantum photonic applications, including single-photon sources [2] and quantum sensing [3]. To further reduce the spectral width and enhance the intensity of single-photon source (SPS) emission, these sources are coupled with various types of microresonators [4].

This study examines the fluorescence properties of SiV centers in nanodiamonds integrated into microstructures, including a $Si_3N_4$ ring resonator, a cylindrical pit in a gold film, a bulls-eye plasmonic ring resonator from gold, and a Bragg resonator composed of $SiO_2$ and $Ta_2O_5$.

The spectral characteristics of SiV centers in nanodiamonds were initially examined prior to their transfer to microstructures. In particular, photoluminescence (PL) spectra, saturation curves, PL lifetimes, the second-order autocorrelation function $g^{(2)}$, and emission direction were measured. Subsequently, the "pick-and-place" method was employed to relocate the selected nanodiamonds to the microresonators, where similar measurements were conducted. Finally, a comparison of the optical properties before and after the relocation of the nanodiamonds is provided, highlighting enhanced fluorescence, increased radiation directivity, reduced lifetime, and narrowing of the SiV zero-phonon line. In particular, in the ring resonator composed of $Si_3N_4$, the SiV ZPL exhibited a full width at half maximum of approximately 0.3 nm when recorded from the waveguide under confocal laser excitation. The saturation intensity of individual SiV centers located in the cylindrical pits within a gold film increased by up to three times compared to similar centers on the gold surface. This was accompanied by a twofold reduction in saturation power and a 15% decrease in lifetime.

This work was supported by the Ministry of Science and Higher Education of the Russian Federation (Agreement/ Grant No. 075-15-2025-609).

[1] C. Bradac, W. Gao, J. Forneris, M. E. Trusheim, I. Aharonovich, Quantum nanophotonics with group IV defects in diamond, Nature communications, 10.1 (2019)
[2] S. A. Castelletto, R. E. Scholten, Heralded single photon sources: a route towards quantum communication technology and photon standard, The European Physical Journal-Applied Physics, 41.3 (2008).
[3] C. Chen, B. Jiang, X. Hu, Research progress on silicon vacancy color centers in diamond, Functional Diamond, 4.1, (2024)
[4] Radulaski M., Zhang J. L., Tzeng Y. K., Lagoudakis K. G., Ishiwata H., Dory C., Fischer K. A., Kelaita Y. A., Sun S., Maurer P. C., Alassaad K., Ferro G., Shen Z., Melosh N. A., Chu S., Vučković J., Nanodiamond integration with photonic devices. Laser & Photonics Reviews. 13.8 (2019)

# Natural diamonds emitting single photons

**D.G. Pasternak[1], A.M. Romshin[1], R.A. Khmelnitsky[2], G.Yu. Kriulina[3], I.I. Vlasov[1]**

*1- Prokhorov General Physics Institute of the Russian Academy of Sciences, Moscow, Russia*
*2- Lebedev Physical Institute of the Russian Academy of Sciences, Moscow, Russia*
*3- Department of Geology, Moscow State University, Moscow, Russia*

*vlasov@nsc.gpi.ru*

A single-photon sources (SPS) is a key component required for quantum communication devices. Here, we report the discovery of numerous SPS in the spectral range of 500- 800 nm on the rough surfaces of diamond crystals mined from the Yubileinaya kimberlite pipe (Yakutia, Russia). These diamonds are characterized by high concentrations of nitrogen and hydrogen, which suggests that similar SPS may be present in nitrogen- and hydrogen-rich diamonds from other deposits around the world. These SPS are believed to be donor-acceptor pairs (DAP) associated with nitrogen and hydrogen on the diamond surface. In their spectral characteristics, DAP-related SPS are superior to previously known SPS formed by various impurity defects in the diamond bulk. They exhibit the narrowest emission linewidth and some of the highest photon emission rates at room temperature among known SPS in diamond. Previously, SPS with similar characteristics were produced in nitrogen-rich and hydrogen-terminated synthetic NDs [1]. Thus, it turned out that nature was, probably, millions of years ahead of us in creating SPS based on diamonds with a high nitrogen and hydrogen content.

This work was supported by the Ministry of Science and Higher Education of the Russian Federation (Agreement/ Grant No. 075-15-2025-609).

[1] D.G. Pasternak, A.M. Romshin, R.H. Bagramov, A.I. Galimov, A.A. Toropov, D. A. Kalashnikov, V. Leong, A.M. Satanin, O.S. Kudryavtsev, A.V. Gritsienko, A. L. Chernev, V.P. Filonenko, I.I. Vlasov, Donor–acceptor recombination emission in hydrogen-terminated nanodiamond, Adv. Quantum Technol., 8, 2400263 (2025).

# Dielectric metasurfaces for analog optical image processing and neuromorphic photonic applications

**A.A. Fedyanin**

*Faculty of Physics, Lomonosov Moscow State University, Moscow 119991, Russia*

*fedyanin@nanolab.phys.msu.ru*

Image processing is used in a wide range of applications, such as objects detection and identification, evaluation of geometric transformations, noise filtering, image restoration, etc. These tasks are usually solved by rasterization of the image and its further digital processing. However, in the case of intensive workloads, this approach brings about significant power and time consumption overhead. The problem can be solved using analog image analysis. For this, before entering the camera, the input image passes through the optical system performing preliminary processing, which simplifies further image analysis. One of the most popular approaches for input image processing is Fourier filtering, but the use of conventional elements such as spatial light modulators for wavefront shaping is a serious drawback due to their weight and large size. Metasurfaces open new possibilities for creating compact and versatile optical components [1,2]. We perform numerical and experimental studies of the analog correlation analysis using an optical metasurface. For that, we design and fabricate a silicon-based device operating as a matched filter in the spatial Fourier filtering scheme. We have also developed an opto-electronic platform for neuromorphic photonic applications using light-stimulated artificial synapses based on nanocrystalline metal-oxide films. The basic properties of neuronal synapses including the ability to transfer spike signals, short-term memory, long-term memory, and paired-pulse facilitation are demonstrated as a synaptic-like response of photonic nanostructures to presynaptic light stimulation.

[1] V.V. Yushkov, A.S. Shorokhov, and A.A. Fedyanin, "Ultrafast optically tunable GaAs metasurfaces for analog image processing", ACS Omega 11, 3311 (2026).
[2] D.N. Gulkin, A.S. Shorokhov, V.S. Snigirev, S.A. Dagesyan, E.A. Kelm, V.O. Bessonov, and A.A. Fedyanin, "Ultrafast diffraction shaping by periodic arrays of GaAs nanoantennas", ACS Photonics 12, 6254 (2025).

# Halide perovskite components for integrated photonics

**S. Makarov**[1,2]

*1- ITMO University, Saint-Petersburg, Russia*
*2- Qingdao Innovation and Development Center, Harbin Engineering University, Qingdao 266000, Shandong, China*

*svmakarov@itmo.ru*

Halide perovskites have emerged as a remarkably versatile material platform for next-generation semiconductor optoelectronics, demonstrating exceptional performance in solar cells, light-emitting diodes, photodetectors, and lasers. Beyond these established applications, the unique chemical and electronic properties of halide perovskites—including high absorption coefficients, defect-tolerant band structures, and tunable bandgaps—have spurred intensive research into their nonlinear optical behavior, which holds immense promise for advancing integrated photonic circuits. Recent achievements with halide perovskite nanostructures that exhibit optical resonances in the visible and near-infrared ranges have revealed efficient multiphoton-induced photoluminescence, coherent harmonics generation, and ultrafast all-optical modulation, enabling dynamic control of light at sub-wavelength scales. Critically, for integrated photonics, light propagation must be guided and confined on-chip. Studies of nonlinear propagation through perovskite planar waveguides have demonstrated low-loss guiding and phase-matched frequency conversion, essential for parametric processes and signal processing. Furthermore, efficient coupling of emission from perovskite microlasers—both whispering-gallery-mode and Fabry–Pérot cavities—into various passive waveguiding systems, including metal-oxides, silicon, gallium phosphide, and polymer waveguides, has been successfully achieved, proving that perovskites can function as active on-chip light sources [1-7].

These demonstrations address one of the central challenges in integrated photonics: integrating high-gain, nonlinear emitters with low-loss passive routing components. The ability to solution-process perovskites at low temperatures further offers compatibility with hybrid integration schemes and flexible substrates, bypassing the epitaxial constraints of conventional III-V semiconductors. However, challenges remain regarding long-term stability, lithographic patterning fidelity, and mitigation of ion migration under electrical pumping. Nevertheless, the combination of strong nonlinearities, tunable resonances, and demonstrated waveguide coupling positions halide perovskites as a compelling material system for future integrated photonic platforms, enabling applications ranging from compact frequency combs and entangled photon sources to neuromorphic photonic circuits and on-chip optical interconnects.

[1] M.A. Masharin, T. Oskolkova, F. Isik, H. Volkan Demir, A.K. Samusev, and S.V. Makarov, Giant Ultrafast All-Optical Modulation Based on Exceptional Points in Exciton–Polariton Perovskite Metasurfaces. ACS nano, 18(4), pp.3447-3455 (2024).
[2] M.A. Sirotin, A.A. Popkova, V.O. Bessonov, I.V. Soboleva, E.V. Lyubin, , A.P. Pushkarev, S.V. Makarov, and A.A. Fedyanin,Direct ultrafast carrier imaging in a perovskite microlaser with optical coherence microscopy. Optica, 10(10), pp.1322-1330 (2023).
[3] M.A. Masharin, A.K. Samusev, A.A. Bogdanov, I.V. Iorsh, H.V. Demir, and S.V. Makarov, Room-Temperature Exceptional-Point-Driven Polariton Lasing from Perovskite Metasurface. Advanced Functional Materials, 33(22), p.2215007 (2023).
[4] M.A. Masharin, V.A. Shahnazaryan, I.V. Iorsh, S.V. Makarov, A.K. Samusev, and I.A. Shelykh, Room-temperature polaron-mediated polariton nonlinearity in MAPbBr3 perovskites. ACS Photonics, 10(3), pp.691-698 (2023).
[5] C. Soci, G. Adamo, D. Cortecchia, K. Wang, S. Xiao, Q. Song, A.L. Schall-Giesecke, P.J. Cegielski, M.C. Lemme, D. Gerace, and D. Sanvitto, Roadmap on perovskite nanophotonics. Optical Materials: X, 17, p.100214 (2023).
[6] M.A. Masharin, V.A. Shahnazaryan, F.A. Benimetskiy, D.N. Krizhanovskii, I.A. Shelykh, I.V. Iorsh, S.V. Makarov, and A.K. Samusev, Polaron-enhanced polariton nonlinearity in lead halide perovskites. Nano Letters, 22(22), pp.9092-9099 (2022).
[7] N.V. Glebov, M.A. Masharin, A. Yulin, A. Mikhin, M.R. Miah, H.V. Demir, D.N. Krizhanovskii, V. Kravtsov, A.K. Samusev, S.V. Makarov, Room-temperature exciton-polariton-driven self-phase modulation in planar perovskite waveguides. ACS Nano, 19(14), 14097-106 (2025).

# Whispering-Gallery Mode Microresonators: Biosensing and Cavity-Enhanced Phenomena

**N. Toropov**

*University of Southampton, Southampton, United Kingdom, SO17 1BJ*

*n.a.toropov@soton.ac.uk*

Whispering-gallery-mode (WGM) microresonators are promising tools for photonics due to their exceptionally high Q-factors. These properties enable a wide range of applications, including nonlinear optics, microlasers, frequency comb generation, and highly sensitive detection. Doping WGM resonators with gain media opens new directions in applied science, particularly for *in vivo* sensing and imaging, including labelling and barcoding in biological tissues [1,2].

In the first part of this contribution, we focus on WGM microresonators coupled with plasmonic nanoparticles. Such hybrid systems significantly leverage sensitivity and can outperform conventional WGM sensors. In particular, these sensors enable detection not only of single molecules but also of molecular dynamics associated with conformational changes. It has been shown that the near fields of plasmonic nanoparticles may affect molecular conformations, exerting mechanical forces down to the femtonewton scale [3].

These hybrid structures have also been used to demonstrate enzyme sensing via thermo-optoplasmonic detection of single enzymes [4]. In this mechanism, molecules whose absorption bands overlap WGM resonances generate localised heating. Consequently, conventional sensing produces red-shifted resonances, whereas localised thermal effects lead to blue-shifted resonances, enabling differentiation of molecules by their absorption.

The next part of the contribution reviews light–matter interactions in WGM resonators covered with carbon dots [5], doped with low-toxicity quantum dots [6], and made of defect-engineered polymers [7]. These materials demonstrate strong responses to biomolecules and have shown excellent biocompatibility. Furthermore, their incorporation into biological tissues revealed high survivability, highlighting their potential for biological sensing.

In the final part, we discuss the Purcell effect observed in WGM microresonators. This effect manifests as a significant shortening of luminescence lifetimes in quantum dots and rare-earth ions [8]. The Purcell enhancement was used to identify spectral manifolds of rare-earth elements in WGM resonators generating amplified spontaneous emission. The resulting spectra consisted of distinct peaks corresponding to different energy levels, confirmed by emission band narrowing and polarisation dependence.

[1] N. Toropov, F. Vollmer, Whispering-gallery microlasers for cell tagging and barcoding: the prospects for in vivo biosensing, *Light: Science & Applications*, **10**, 77, (2021).

[2] N. Toropov, G. Cabello, M. P. Serrano, et al., Review of biosensing with whispering-gallery mode lasers, *Light: Science & Applications*, **10**, 42, (2021).

[3] M. C. Houghton, N. A. Toropov, D. Yu, S. Bagby, F. Vollmer, Single Molecule Thermodynamic Penalties Applied to Enzymes by Whispering Gallery Mode Biosensors, *Advanced Science*, **11**, 2403195, (2024).

[4] N. A. Toropov, M. C. Houghton, D. Yu, F. Vollmer, Thermo-Optoplasmonic Single-Molecule Sensing on Optical Microcavities, *ACS Nano*, **18**, pp. 17534–17546, (2024).

[5] A. A. Starovoytov, E. O. Soloveva, K. Kurassova, K. V. Bogdanov, I. A. Arefina, N. N. Shevchenko, T. A. Vartanyan, D. R. Dadadzhanov, N. A. Toropov, Carbon Dot-Decorated Polystyrene Microspheres for Whispering-Gallery Mode Biosensing, *Photonics*, **11**, 480, (2024).

[6] K. Kurassova, N. Filatov, S. Karamysheva, A. Bukatin, A. Starovoytov, T. Vartanyan, F. Vollmer, N. A. Toropov, Microfluidics-Driven Dripping Technique for Fabricating Polymer Microspheres Doped with $AgInS_2$/ZnS Quantum Dots, *ACS Omega*, **9**, pp. 39287–39295, (2024).

[7] E. O. Soloveva, N. N. Shevchenko, N. S. Kirilkin, A. A. Rogachev, M. S. Kovova, A. S. Timin, V. A. Rusakova, S. A. Shipilovskikh, A. A. Starovoytov, D. R. Dadadzhanov, N. Toropov, Inherent luminescence in undoped polystyrene microbeads supporting whispering-gallery modes, *Optical Materials*, **165**, Art. 117058, (2025).

[8] N. A. Toropov, C. A. Codemard, N. Sessions, M. N. Zervas, Enhanced Ytterbium Emission – Manifold Resolution at Room Temperature Using the Purcell Effect in Doped Silica Microspheres, in Advanced Photonics Congress 2024, SoTh3D.5, (2024).

# Mechanically-induced crystallization of $CsPbBr_3$ nanocrystals on the surface of borogermanate glass for gas sensing applications

**E. Sgibnev[1], O. Lutikova[1], R. Kharisova[2], L. Mironov[2], A. Baryshev[1]**

*1- Dukhov Automatics Research Institute (VNIIA), st. Sushchevskaya 22, Moscow, Russia*
*2- ITMO University, av. Kronverkskiy 49, St. Petersburg, Russia*

*sgibnevem@yandex.ru*

Metal halide perovskite nanocrystals exhibit bright, narrow-band luminescence that can be tuned across the visible range by varying their composition. It makes them a promising material platform for photonics, optoelectronics, photovoltaics, and sensing [1]. It was previously discovered that $CsPbHal_3$ (Hal=Cl, Br, I) nanocrystals can be formed on the surface of a glass containing perovskite precursors by fracturing or mechanical treatment [2]. Only a few studies have been devoted to the mechanically-induced synthesis of perovskite nanocrystals on glass surface. Therefore, the formation mechanism and the range of conditions under which it occurs remain unclear. Several applications have been proposed for glass capable of perovskite crystallization on its surface, including lead-ion sensors [2] and temperature sensors [3]. In this work, we demonstrate the possibility of using perovskite crystals formed on a glass surface as multimodal $NO_2$ gas sensors.

Borogermanate glasses with the composition (mol.%) $41.29GeO_2$–$25.57B_2O_3$–$6.95Na_2O$–$5.87Cs_2O$–$5.45ZnO$–$x2.45PbO$–$x4.14K_2O$–$x8.28Br^-$, where $x$=0.5, 1, 2, were synthesized (Gx0.5, Gx1, and Gx2 glasses) in closed quartz crucibles under ambient atmosphere at 950 °C. A glass composition with x = 1.0 and additionally doped with 1.85 mol.% $TiO_2$ and 0.75 mol.% $P_2O_5$ was also synthesized (Gx1NA glass) to study the effect of nucleating agents on both bulk and surface crystallization of $CsPbBr_3$ nanocrystals. Two fabrication strategies were used: (i) bulk crystallization through a post-synthetic heat treatment at 550 °C for 1 h; and (ii) mechanically-induced surface crystallization involving initial fracture of glass monoliths in a hydraulic press followed by planetary ball milling for durations ranging from 1 to 40 min. The samples were analyzed by powder XRD, SEM/EDX, photoluminescence spectroscopy, absolute quantum yield measurements, and time-correlated single-photon counting. For gas-sensing experiments, glass powders were placed in a flow cell and exposed to $NO_2$ concentrations of 0–5 ppm in synthetic air under continuous excitation at 473 nm.

Bulk crystallization was observed in Gx1, Gx2 and Gx1NA glasses. Incorporation of nucleating agents enhanced the perovskite absorption peak intensity approximately fourteen-fold and raised photoluminescence quantum yield from 0.13 to 0.38. On the other hand, mechanically-induced surface crystallization occurred in all glasses. XRD patterns of the ground powders confirmed the formation of an orthorhombic perovskite phase in GxNA sample. Luminescence quantum yields reached maximum ~0.3–0.6 depending on perovskite precursor content after ~10 min of grinding, while prolonged milling continuously increased the total amount of surface perovskites. To examine the gas-sensing properties of the perovskite crystals on the glass surface, the influence of $NO_2$ on the spectral and luminescence characteristics of the perovskites was investigated. Upon exposure to $NO_2$, the surface perovskites exhibited strong and reversible photoluminescence quenching and shortening of average lifetime. Response and recovery times were found to be 20–45 s and 180–240 s, respectively, depending on the concentration, with a detection limit as low as 30 ppb. These results establish mechanically-induced surface crystallization as a facile and scalable method for producing glass particles with $CsPbBr_3$ nanocrystals for ultrasensitive optical $NO_2$ sensors operating at room temperature. Experiments with other gases are in progress.

The work was supported by the Ministry of Science and Higher Education of the Russian Federation (grant no. 075-11-2025-057).

[1] J. Shamsi, A.S. Urban, M. Imran, L. De Trizio, L. Manna, Metal halide perovskite nanocrystals: synthesis, post-synthesis modifications, and their optical properties, Chemical Reviews, vol. 119, pp. 3296-3348, (2019).
[2] X. Xiang, H. Lin, R. Li, Y. Cheng, Q. Huang, J. Xu, C. Wang, X. Chen, Y. Wang, Stress-induced $CsPbBr_3$ nanocrystallization on glass surface: Unexpected mechanoluminescence and application, Nano Research, vol. 12, pp. 1049-1054, (2019).
[3] C. Lu, Y. Duan, P. Li, Y. Lu, S. Xu, J. Zhang, Polychromatic tunable luminescence of $Eu^{3+}$ doped $CsPbBr_3$ quantum dot glass ceramic imduced by mechanical crystallization, Ceramics International, vol. 48, pp. 13826-13832, (2022).

# III-V hybrid nanostructures integrated with the silicon platform

**R. Reznik[1], I. Ilkiv[1-3], V. Gridchin[1-3], K. Kotlyar[1-3], A. Khrebtov[1-2], I. Soshnikov[2,3], I. Shtrom[1-3], E. Ubyivovk[1], P. Alekseev[4] D. Barettin[5], N. Kryzhanovskaya[6], G. Cirlin[1-3]**

*1- St. Petersburg State University, Universitetskaya Embankment 7-9, 199034 St. Petersburg, Russia*
*2- Alferov University, Khlopina street 8/3, St. Petersburg, 194021, Russia*
*3- IAI RAS, Ivana Chernykh street 31-33, St. Petersburg, 198095, Russia*
*4- Ioffe Institute, Polytechnicheskaya street 26, St. Petersburg, 194021*
*5- Abrikosov Center for Theoretical Physics, Moscow Institute of Physics and Technology, Dolgoprudnyi 141701, Russia*
*6- HSE University, Souyuza Pechatnikov 16, St. Petersburg 1940121, Russia*

*r.reznik@spbu.ru*

Nowadays, direct-bandgap III-V compounds are one of the key materials for developing applications in the fields of photonics, optoelectronics, power electronics, quantum technologies, and others [1,2]. To reduce device dimensions, increase performance, and create fundamentally new devices in these areas, nanoscale III-V nanostructures are attracting particular research attention due to its unique morphological, structural, optical and transport properties [3,4]. In particular, unlike two-dimensional thin films, (quasi)one- dimensional nanowires (NWs) can be formed directly on the silicon surface due to their unique morphology, which allows for a significant reduction of mechanical stresses due to lattice mismatch [5]. Moreover, quantum dots (QDs) based on a narrower bandgap material can be formed in the body of NWs [6-8].

In this work we present results of experimental and theoretical studies on the molecular-beam epitaxy growth and physical property characterization of functional III-V NWs, NWs with QDs on a silicon surface, as well as self-organized quantum dots in a silicon matrix. In particular, III-V nanowires on silicon have been shown to hold great promise for applications in nanopiezoelectric and nanotriboelectric generators, as well as in pressure, light, and gas sensors, solar cells, and light-emitting diodes. Furthermore, quantum dots embedded in nanowires exhibit single-photon emission over a broad wavelength range. These QD in NW structures can be lifted off from an cheap silicon wafer and transferred onto any other platform, such as a solid-state waveguide for use in photonic integrated circuits. In addition, we have established the size dependence of In(Ga)As quantum dots in a silicon matrix on the amount of deposited material, investigated their optical properties, and successfully grown laser nanostructures based on these quantum dots. It is worth noting that nanowire synthesis allows forming previously unstudied III-V materials, for example, wurtzite AlGaAs. In this work, we have for the first time established the dependence of the bandgap of wurtzite AlGaAs on the aluminum content and evaluated the potential of this material for future device applications.

The authors acknowledge Saint-Petersburg State University for a research project 122040800254-4.

[1] A. Dasgupta, S. Sen, P. Singh and A. A. Raman, Comprehensive Overview of the Foundations of Semiconductor Materials, Semiconductor Nanoscale Devices: Materials and Design Challenges, pp. 80-109, (2025).
[2] T. F. Kuech, III-V compound semiconductors: Growth and structures, Progress in crystal growth and characterization of materials. vol. 62, pp. 352-370, (2016).
[3] A. Agarwal, G. Misra and K. Agarwal, Semiconductor III–V nanowires: synthesis, fabrication and characterization of nanodevices, Journal of The Institution of Engineers (India): Series B, vol. 103, pp. 699-709, (2022).
[4] E. Barrigón, M. Heurlin, Z. Bi, B. Monemar and L. Samuelson, Synthesis and applications of III–V nanowires, Chemical reviews, vol. 119, pp. 9170-9220, (2019).
[5] G. Boras, X. Yu and H. Liu, III–V ternary nanowires on Si substrates: growth, characterization and device applications, Journal of Semiconductors, vol. 40, pp. 101301, (2019).
[6] L. Leandro, C. P. Gunnarsson, R. Reznik, K. D. Jöns, I. Shtrom, A. Khrebtov, T. Kasama, V. Zwiller, G. Cirlin and N. Akopian, Nanowire quantum dots tuned to atomic resonances, Nano letters, vol. 18, 7217-7221, (2018).
[7] R. R. Reznik, I. V. Ilkiv, K. P. Kotlyar, V. O. Gridchin, D. N. Bondarenko, V. V. Lendyashova, E. V. Ubyivovk, A. S. Dragunova, N. V. Kryzhanovskaya and G. E. Cirlin, Molecular-Beam Epitaxy Growth and Properties of AlGaAs Nanowires with InGaAs Nanostructures, physica status solidi (RRL)–Rapid Research Letters, vol. 16, pp. 2200056, (2022).
[8] M. K. Alqedra, C. T. Huang, W. H. Chang, S. Haffouz, P. J. Poole, D. Dalacu, A. W. Elshaari and V. Zwiller, Indistinguishable single photons from nanowire quantum dots in the telecom O-band, Applied Physics Letters, vol. 127, pp. 164001, (2025).

# Resonant subspace approximation for optical modes in photonic crystal slabs: fast parametric mapping and applications

**I. Fradkin, N. Salakhova, S. Dyakov, N. Gippius**

*Skolkovo Institute of Science and Technology, Bolshoy Boulevard 30, bld. 1, Moscow 121205, Russia*

*I.Fradkin@skoltech.ru*

Optical resonances in photonic crystal slabs are central to phenomena from bound states in the continuum to enhanced light–matter interaction, and underpin applications in sensing, lasing, and nonlinear optics. Efficient description of mode dispersion, quality factors, and hybridization across wide ranges of structural and illumination parameters remains computationally challenging.

We present a resonant subspace approximation that replaces full-wave simulations with a compact phase-matrix model. From a few rigorous calculations one extracts a restricted round-trip matrix and extrapolates it smoothly, enabling rapid reconstruction of high-resolution spectral maps and mode evolution while naturally capturing multi-mode hybridization. Beyond numerical speed, the method provides a simple and intuitive framework to understand resonance interactions over broad parameter spaces - revealing how coupling changes with geometry or material composition - without the need for large-scale sweeps.

The approach is general and can be adapted to various periodic layered systems, including structures with anisotropic constituents, van der Waals materials, or hexagonal lattice symmetry. Adaptive point grids further allow faithful spectral reconstruction across very wide parameter ranges. The technique may be applied to accelerate the design and optimization of photonic devices, and to analyse quantities such as Purcell enhancement, Casimir forces, and near-field heat transfer.

# Optical nonlinearities in copper-doped cadmium selenide nanotetrapods

**I.D. Laktaev[1], S.G. Dorofeev[2], A.M. Smirnov[1,3]**

*1 - Faculty of Physics, Lomonosov Moscow State University, Leninskie Gory 1-2, Moscow 119991, Russia*
*2 - Faculty of Chemistry, Lomonosov Moscow State University, Leninskie Gory 1-3, Moscow 119991 Russia*
*3 - Kotelnikov Institute of Radioengineering and Electronics of RAS, Mokhovaya 11-7, Moscow 125009, Russia*

*alsmir1988@mail.ru*

Copper-doped CdSe colloidal nanocrystals attract considerable attention due to their tunable photoluminescence, broad impurity-related emission bands, weak self-absorption and strong nonlinear optical response, making them promising for photonics, optical sensing, bioimaging and spectral conversion applications. Here we summarize a series of our studies devoted to the optical and nonlinear optical properties of Cu-doped CdSe quantum dots and nanotetrapods under nanosecond and femtosecond laser excitation.

Using pump-probe spectroscopy and nonlinear transmission measurements, we experimentally demonstrated strong differences between the nonlinear dynamics of the fundamental exciton transition and Cu-associated photoluminescence. In particular, saturation of Cu-related photoluminescence was shown to occur significantly faster than saturation of the excitonic transition, indicating the important role of localized impurity states and exciton-phonon interaction processes [1]. A strong dependence of nonlinear absorption and induced absorption formation on Cu concentration was experimentally revealed for heavily doped CdSe quantum dots [2].

Special attention is devoted to anisotropic Cu-doped CdSe nanotetrapods, whose morphology provides enhanced nonlinear optical response and modified carrier relaxation dynamics. The synthesized nanostructures demonstrated broad impurity-related absorption bands associated with Cu-induced intragap states and efficient nonlinear excitation of the fundamental exciton transition under femtosecond pumping at 1026 nm. Simultaneous two-photon absorption and optical self-defocusing were experimentally observed in colloidal Cu-doped CdSe nanotetrapods under femtosecond excitation [3]. The measured nonlinear optical response exhibited pronounced asymmetry in open-aperture Z-scan profiles caused by the combined contribution of two-photon absorption and nonlinear refraction. The two-photon absorption coefficient was determined to be $\beta = 0.14–0.20$ cm/GW, while the nonlinear refractive index reached $n_2 = –4.9 \times 10^{-16}$ to $–5.3 \times 10^{-15}$ cm²/W depending on excitation conditions and nanocrystal concentration.

Additionally, spatial self-phase modulation accompanied by the formation of concentric diffraction rings was observed at high excitation intensities, indicating strong photoinduced refractive nonlinearities in Cu-doped nanotetrapods. The obtained results demonstrate that copper-doped CdSe nanostructures represent a promising platform for nonlinear nanophotonics, ultrafast optical modulation, biosensing, and multiphoton imaging applications.

The research was funded by the Russian Science Foundation grant № 23-72-10008-П.

[1] Smirnov A. M., Golinskaya A. D., Kotin P. A., Dorofeev S. G., Palyulin V. V., Mantsevich V. N., Dneprovskii V. S. Photoluminescence and nonlinear transmission of Cu-doped CdSe quantum dots, Journal of Luminescence 213, 29–35 (2019).
[2] Smirnov A. M., Golinskaya A. D., Kotin P. A., Dorofeev S. G., Zharkova E. V., Palyulin V. V., Mantsevich V. N., Dneprovskii V. S. Damping of Cu-Associated Photoluminescence and Formation of Induced Absorption in Heavily Cu-Doped CdSe Quantum Dots, Journal of Physical Chemistry C 123, 27986–27992 (2019).
[3] Laktaev I. D., Dorofeev S. G., Smirnov A. M. Simultaneous two-photon absorption and self-defocusing in colloidal Cu-doped CdSe nanotetrapods, Physica B: Condensed Matter 727, 418324 (2026).

# Studying fluorescent properties of olive carbon dots using time-resolved fluorescence measurements

**U. Saidvaliev[1], D. Fixler[1], N. Dudchenko[2]**

*1- School of Biomedical Engineering, Faculty of Engineering, Jan Koum Center for Nanoscience and Nanotechnology, Tel-Aviv University, Ramat Aviv 6997801, Israel*
*2- Bar Ilan Institute of Nanotechnology & Advanced Materials, Bar Ilan University, Ramat Gan, 529002, Israel*

*usaidvaliev@gmail.com*

In the modern world, carbon derived nanoparticles (especially carbon dots - CDs) are revolutionizing nano-sensing and nanophotonic applications [1,2] due to their unique properties (large surface area, tunable fluorescence, excellent biocompatibility, etc.). CDs were synthesized from bio-renewable sources (olive tree leaves) via a hydrothermal route and studied in our experiments using time-resolved frequency domain fluorescence lifetime imaging microscopy techniques [3,4]. These nanoparticles demonstrate relatively modest changes in fluorescence lifetime (FLT) values of 5.0 ± 0.2 ns in water and glycerol solutions of different concentrations (0%, 30%, 60% and 80% glycerol) with fluorescence emission intensity increasing with the solution viscosity, i.e. glycerol concentration. Fluorescence anisotropy decay measurements showed increasing steady state anisotropy $r_{ss}$ values from 0.058 ± 0.03 to 0.3 ± 0.03, while $r_0$ remaining the same around 0.38 ± 0.02 and rotational correlation time θ growing significantly from 1.01 ± 0.02 ns to 16 ± 0.1 ns across all glycerol solutions with the increasing viscosity correspondingly. The study indicates that CDs retain relatively stable FLT in glycerol solutions, while θ shows evident changes in viscosity and is most beneficial for reflecting variations in local spatial properties.

**Keywords**: carbon dots; olive leaves; nano photonics; fluorescence anisotropy; fluorescence lifetime imaging microscopy; frequency domain; rotational correlation time.

[1] H. Tumallah, S. Sreenivasan. Next-Generation Green Carbon Dots: Toward Standardized Synthesis and Purification for Translational Nanomedicine — A Comprehensive Review, J.Inorg.Organomet. Polym, 2026. https://doi.org/10.1007/s10904-026-04279-9
[2] Sh. Pawar, D.Fixler, et al. "Carbon Dots-Based Logic Gates", Nanomaterials, 2021, 11(1), 232. https://doi.org/10.3390/nano11010232
[3] S. Sahu, M. Mishra, M. Green Synthesis of Carbon Nanodots, 2026, J. (eds) Carbon Nanodots, Singapore, pp 63-77. https://doi.org/10.1007/978-981-95-4705-0_3
[4] G. Yahav, D.Fixler, et al. "Imaging the rotational mobility of carbon dot-gold nanoparticle conjugates using frequency domain wide-field time-resolved fluorescence anisotropy", JBO, 2023, 28(5), 056001. https://doi.org/10.1117/1.JBO.28.5.056001
[5] G. Yahav, Sh. Pawar, D. Fixler et al. Probing Polarity and pH Sensitivity of Carbon Dots in Escherichia coli through Time-Resolved Fluorescence Analyses. Nanomaterials, 2023, 13, 2068. https://doi.org/10.3390/nano13142068

# Nonlinear response of a semiconductor microcavity with excitonic layers

**O.A. Dmitrieva[1,2,3], S.G. Tikhodeev[1,2,3]**

*1- Lomonosov Moscow State University, GSP-1, Leninskie Gory, Moscow, 119991, Russia*
*2- Skolkovo Institute of Science and Technology, Bolshoy Boulevard, 30, bld. 1, Moscow 121205, Russia*
*3- Prokhorov General Physics Institute of the RAS, GSP-1, Vavilova str., 38, Moscow 119991, Russia*

*dmitrieva.oa16@physics.msu.ru*

The nonlinear properties of systems in which a resonant optical mode interacts with excitons in the active region of a semiconductor microcavity are currently being actively studied [1–4] due to their potential applications in microelectronics and computer science. This work presents a self-consistent theoretical description of bi- and multistability phenomena in a semiconductor microcavity with quantum wells under strong resonant optical excitation, taking into account the inhomogeneity of the spatial distribution of the electromagnetic field in regions where nonlinear excitons are localized.

It has previously been shown [1–3] that in a Bragg microcavity with quantum wells in the active region, the appearance of bi- and multistability of response can be observed as the optical pumping increases, due to a blue shift in the exciton frequency that arises at high exciton densities as a result of their interaction (repulsion). In the case of chiral systems, the lifting of degeneracy between states of light with right- and left-handed circular polarization leads to the emergence of sharp jumps in the intensity and degree of circular polarization of the response as the intensity of the external pumping is increased at a frequency close to the system's resonance frequency in the linear case [5].

In this work, a self-consistent calculation was performed, taking into account the inhomogeneity of the electric field distribution and the exciton density in the system [6]. To calculate the linear response of the system, Fourier-modal decomposition and the optical scattering matrix method were used [7,8]. In this case, the nonlinearity associated with exciton-exciton interaction was accounted for in the variation of the dielectric permittivity values as a function of the exciton density. For a given pump intensity, an initial distribution of the dielectric permittivity in the exciton region was selected, and for this distribution, the electric field and exciton density distributions were calculated using the scattering matrix method, and based on these, the new dielectric permittivity was calculated, taking into account the blue shift of the exciton resonance frequency. The difference between the initial and new dielectric permittivities was minimized using the Newton method.

The calculations yielded distributions of the exciton density and the electric field in the system as a function of the injection field.

[1] N. A. Gippius, S. G. Tikhodeev, V. D. Kulakovskii et al., Nonlinear dynamics of polariton scattering in semiconductor microcavity: Bistability vs. stimulated scattering, Europhys.Lett., **67**, p. 997 (2004).
[2] N.A. Gippius, I. A. Shelykh, D. D. Solnyshkov et al., Polarization Multistability of Cavity Polaritons, Phys. Rev. Lett., **98**, p. 236401 (2007).
[3] S.S. Gavrilov, Nonequilibrium transitions, chaos, and chimera states in exciton—polariton systems, Phys. Usp., **63**, pp. 123–144 (2020).
[4] V. Kravtsov et al., Nonlinear polaritons in a monolayer semiconductor coupled to optical bound states in the continuum, Light: Science & Applications, **9** 56 (2020).
[5] O. A. Dmitrieva, N. A. Gippius, and S. G. Tikhodeev, Multistability in a chiral semiconductor microcavity, Doklady Rossijskoj akademii nauk. Fizika, tehnicheskie nauki, 510, 10-15 (2023)
[6] O. A. Dmitrieva, N. A. Gippius, and S. G. Tikhodeev, Multistability of a chiral semiconductor microcavity: a self-consistent approach, JETP, **169**, 181-188 (2026).
[7] Whittaker D.M., Culshaw I.S., Scattering-matrix treatment of patterned multilayer photonic structures, Phys. Rev. B, **60** (15), 2610– 2618 (1999).
[8] Tikhodeev S.G., Yablonskii A.L., Muljarov E.A., Gippius N.A., Ishihara T., Quasiguided modes and optical properties of photonic crystal slabs, Phys. Rev. B, **66** (4), 045102 (2002).

# Photoluminescence Enhancement of Single-Walled Carbon Nanotubes on a Metasurface

**F.M. Maksimov[1,2], A.R. Vildanova[3], M.I. Petrov[4], A.I. Chernov[1,2]**

*1- Moscow Institute of Physics and Technology, Moscow, Russia*
*2- Russian Quantum Center, Moscow, Russia*
*3- Skolkovo Institute of Science and Technology, Moscow, Russia*
*4- ITMO University, Saint-Petersburg, Russia*

*maksimov.fm@phystech.edu*

Single-walled carbon nanotubes (SWCNTs) are promising near-infrared emitters and single-photon sources, yet their practical use demands improved pump efficiency and emission collection [1]. Dielectric metasurfaces offer low-loss local field enhancement and directional emission control; bound states in the continuum (BIC) provide high-Q resonances that can significantly boost optical signals [2]. Here we report a silicon dielectric metasurface designed to enhance the photoluminescence (PL) of functionalized SWCNTs and experimentally characterize its resonant behavior.

A periodic array of cylindrical holes was fabricated in a silicon substrate by electron-beam lithography. Semiconducting (6,5)-chirality SWCNTs functionalized with diazonium salts to introduce $sp^3$ defects were deposited onto the metasurface. Reflection spectra of the bare metasurface were measured in the visible range and compared with simulated resonance modes; near-infrared PL of the SWCNT-covered metasurface was recorded at varying numerical apertures (NA).

Reflection spectra of the bare metasurface for TE and TM polarizations show narrow resonance features in good agreement with simulations, along with enhanced-reflection branches near normal incidence—a hallmark of BIC modes. In the PL spectra of the SWCNT-coated surface, narrow peaks emerge on the broad emission background; reducing the collection NA reveals a sharp line coinciding spectrally with the BIC resonance, while the overall signal is enhanced relative to a bare silicon substrate. The aperture dependence of PL, together with reflection data, confirms local field enhancement near BIC resonances, demonstrating the potential of such metasurfaces for improving pump and collection efficiency in SWCNT-based single-photon sources.

This work was supported by the Russian Science Foundation (project No. 25-43-02217).

[1] Chang Y. R. et al., Quantum defects in carbon nanotubes as single-photon sources, Communications Materials, vol. 7, no. 1, p. 55, (2026).
[2] Koshelev K., Kivshar Y., Bogdanov A., Engineering with bound states in the continuum, Optics and Photonics News, vol. 31, no. 1, pp. 38–45, (2020).

# MBE Growth of GaN Nanowires on GaN/AlN/Si Templates: Toward UV Nanolasers

**V.O. Gridchin[1-3], T.Shugabaev[1-3], A.M. Dautov[1-3], A.A. Kalinichev[1-3], R.R. Reznik[1-3], K.P. Kotlyar[1-3], V. A. Sharov[1], V.V. Lendyashova[1-2], G.E. Cirlin[1-3]**

*1- Alferov University, Saint Petersburg, Russia*
*2- Saint Petersburg State University, Saint Petersburg, Russia*
*3- Institute for Analytical Instrumentation, Saint Petersburg, Russia*

*gridchin@spbau.ru*

III-nitride semiconductor nanowires (GaN, AlN, InN) are promising structures for advanced optoelectronics. Interest in these structures stems from the possibility of realizing room-temperature single-photon sources, polariton and plasmon–polariton nanolasers, and flexible nano- and micro-LEDs. The fabrication of such devices requires nanowires of excellent crystalline quality and highly uniform longitudinal and transverse dimensions to ensure high optical gain coefficients. The growth of such structures is feasible using lattice-matched systems, e.g., GaN nanowires on GaN layers. This approach, for instance in micro-LED fabrication, demonstrates promising emission efficiencies (~25% for green and 8% for red spectral ranges) with record-small individual emitter sizes (nanowire diameter ~250 nm) [1]. However, the propagation of threading dislocations from the underlying layer into the nanowires imposes strict requirements on the quality of the initial buffer layer, and the need to form a patterned mask with openings significantly complicates the technology. Importantly, in this case, the mask is used not only to obtain uniform nanowires but also for nanowire nucleation itself, since without lattice mismatch, the formation of III-N nanowires is extremely difficult.

In this work, we present results on the direct growth of GaN nanowires on GaN/AlN/Si(111) layers in a single growth process without using a patterned mask. To initiate nanowire nucleation on the GaN surface, a multistep technique was developed, involving the formation of regions with different polarities in the GaN layer and deposition of a thin SiN layer above. The obtained results show that this approach ensures efficient nanowire nucleation. It is established that the nanowires grow coherently with the (111) substrate plane, maintaining a constant lateral faceting along their entire length. Atomic force microscopy revealed that nanowire nucleation occurs only on nitrogen-polar domains of the GaN layer. Transmission electron microscopy studies showed no dislocations in the measured nanowires, which is probably due to the use of the SiN layer. It is shown that the nanowire diameter is determined by the diameter of the nitrogen-polarity domains in the initial GaN layer. Specifically, nanowires with a diameter of ~800 nm were obtained. Furthermore, coherent emission with a maximum near 363 nm at room temperature under pulsed laser excitation was observed from the single nanowires. The linewidth of the coherent emission in such structures was as low as ~0.8–1 Å.

Thus, a method for the homoepitaxial growth of GaN nanowires on GaN layers has been developed, providing high crystalline quality and uniform geometric dimensions of the nanowires. The possibility of achieving coherent emission is demonstrated. The obtained results open up the prospect of fabricating nanolasers for the ultraviolet range and applying this approach to other III-nitride semiconductor nanostructures to extend the emission wavelength range.

The authors acknowledge Saint-Petersburg State University for a research project 122040800254-4.

[1] A. Pandey, M. Reddeppa, Z. Mi Recent progress on micro-LEDs, Light: Advanced Manufacturing, vol. 4, pp. 519, (2024).

# Luminescent Vancomycin-Stabilized Copper Nanoclusters as Optical Sensors and Chiral Selectors

**E. Kolobova, A. Demenshin, Y. Zimarina, E. Solovyeva**

*Saint Petersburg State University, Universitetskaya Emb. 7/9, 199034 St Petersburg, Russia*

*ekatderyabina@mail.ru*

Nanoclusters of elements of 11th group (Cu, Ag, Au) represent an emerging class of photonic nanomaterials. Their unique properties originate from semi-molecular electronic structure that determines their key optical feature – intrinsic fluorescence [1]. Owning to this advantage, metal nanoclusters are widely explored in fluorometric sensing. The optical behavior of a nanocluster is strongly governed by the nature of stabilizing molecules used during a synthesis. Changing a stabilizer, it is possible to tune pH-dependent emission or acquire sensitivity to specific molecules, including drugs [2].

Copper was chosen as a metal core for its low cost, availability and strong fluorescence in the visible range. Antibiotic vancomycin is chiral and able to react with various compounds due to its functional groups, contributing to selectivity towards bioactive compounds. The proposed design of vancomycinstabilized copper nanoclusters (CuNC-Vanc) provides high biocompatibility and enables fluorometric sensing of pH in the physiologically relevant range of 5–9, making these nanoclusters attractive for biological studies. Moreover, in our study we suggest a principally new application of metal nanoclusters in capillary electrophoresis (CE) for chiral recognition of drug molecules.

CuNC-Vanc exhibit strong pH-dependent blue emission with the sigmoidal response and linear region between pH 6 and 9 (**Figure 1**). Their low cytotoxicity was confirmed *in vitro* using HeLa cell line. For the first time, these nanoclusters were applied in CE for chiral separation of ketoprofen and amlodipine enantiomers. Notably, in the case of amlodipine, enantioselectivity was observed only when using CuNC-Vanc, whereas vancomycin alone did not provide a chiral resolution. This demonstrates that the nanocluster core introduces a synergetic effect, enhancing enantioselectivity of chiral stabilizer.

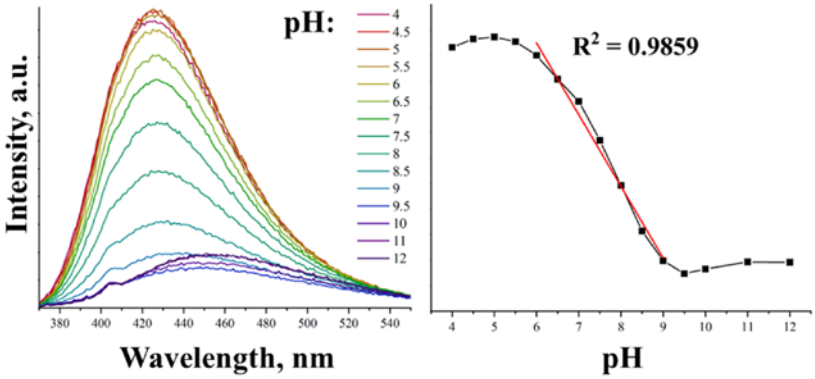


**Fig. 1.** Dependence of CuNC-Vanc fluorescence on pH.

The work was supported by Saint-Petersburg State University, project № 122040800256-8. The authors thank the resource centers of SPbU Research Park: "Chemical Analysis and Material Research", "Optical and Laser Materials Research".

[1] Alexandru-Milentie Hada et al, Recent Advances in Metal Nanoclusters: From Novel Synthesis to Emerging Applications, Molecules, 30(19), 3848, (2025).
[2] A.I. Demenshin et al, *L*-Proline-Stabilized Copper Nanoclusters: Synthesis, Optical Properties, and Testing in Bioanalysis by Fluorimetry and Capillary Electrophoresis, Nanobiotechnology Reports, 20(6), 802-808, (2025).

# Autonomous sources of optical radiation based on wide-bandgap materials

**M. Zamoryanskay, B. Burakov, E. Dementeva, K. Orekhova, G. Gusev, V. Kravets, A. Trofimov**

*Ioffe Institute, St. Petersburg, Russia*

*zam@mail.ioffe.ru:*

The development of optical radiation sources using radionuclides has long been considered attractive due to the potential for long-time using. Such research primarily considers mixing a scintillator with a material containing a radionuclide. This line of work has several significant drawbacks, including the need for expensive disposal of such sources and the rapid formation of radiation defects in the phosphor due to the high radionuclide content. The most promising approach is the introduction of radionuclides as structural impurities into chemically, mechanically, and radiation-resistant crystalline matrices with good scintillation properties. If the crystalline matrices have high scintillation properties, the energy of radioactive decay will stimulate the scintillator's optical emission, causing it to become self-glowing throughout the spontaneous decay of the radionuclide. Such an optical radiation source requires no special disposal and will retain the radionuclide for millions of years. Moreover, such materials will be sources of optical radiation for two to two and a half half-lives of the actinide (for Pu-238, this is a couple of hundred years, and for Am-241, a thousand years. For C-14, it's 10,000 years). This line of research appears promising for practical applications. The optical radiation of a self-glowing matrix can be converted into electric current using a photoconverter. In this case, the optical radiation sources could form the basis of a nuclear battery—a low-power current source.

The most attractive radionuclides for the development of self-glowing materials are alpha and beta emitters. This is due to the fact that alpha and beta particles have short ranges in solids, and upon deceleration, almost all of the particle energy (the energy associated with radio decay) remains in the solid and can be converted into the optical radiation. Therefore, radionuclides from the heavy fraction of radioactive waste, such as Pu-238 and Am-241, which are alpha emitters, are promising elements for the development of self-glowing materials. The energy of alpha particles formed as a result of the radioactive decay of these elements is 5.6–6 MeV. The range of such particles in solids does not exceed 15–30 μm. The decay of the C-14 radionuclide produces beta particles with an energy of 156 keV. Their range in solids does not exceed 50–80 μm. The next important issue is the selection of a matrix in which the radio decay energy is converted into optical radiation. These matrices must have the following properties: high chemical, mechanical, and radiation resistance; efficient conversion of radio decay energy into optical radiation (good scintillation properties); and high solubility of radionuclides in the matrix, resulting in the formation of solid solutions. In this regard, for the creation of self-glowing materials activated by Pu-238 and Am-241, the most optimal are complex oxides such as $ZrO_2$, $ZrSiO_4$, $YPO_4$, etc. For the radioisotope C-14, such a material is artificial diamond.

Methods for synthesizing such crystals were developed, and a series of crystals emitting in various optical ranges were obtained. Oxide crystals were grown in the laboratory using the flux method (a solution-in-melt method). Synthetic diamond enriched in C-14 was produced using the HPHT method. The self-glowing spectra of these materials were studied. The optimal content of luminescence centers and radionuclides was determined. It was shown that with a radionuclide content of less than 0.1%, the emission power of such crystals allows a response of up to 0.2 μWatt to be achieved on standard photoconverter.

The study was funded by a grant from the Russian Science Foundation, grant No. 26-19-00562, https://rscf.ru/project/26-19-00562/

# Nanoscale dielectric properties of disordered media

**Y.M. Beltukov**

*Ioffe Institute, Politechnicheskaya st. 26, 194021 St. Petersburg, Russia*

*yaroslav.beltukov@mail.ioffe.ru*

Dielectric properties at the nanoscale differ from macroscopic ones, and continuous medium theories cannot be directly applied. This is especially relevant for disordered media such as glassy polymers, which are inherently inhomogeneous at the nanometer scale. Experimental studies of polymer nanocomposites have conclusively demonstrated that each nanoparticle is surrounded by an interphase region with modified dielectric properties, where the interphase thickness correlates directly with the heterogeneity length scale of the glass-forming matrix [1]. Optical high-frequency dielectric properties of polymer films of nanometer-scale thickness also deviate substantially from bulk behavior [2, 3]. Therefore, understanding the microscopic mechanisms of polarization is crucial for nanophotonics, while other properties, such as electron transport in semiconductor nanostructures, are also influenced by dielectric contrast at the nanoscale [4].

A theoretical description of the nanoscale dielectric response of strongly disordered solids is quite challenging, as it must sustain strong local fluctuations while remaining causal and dissipative under any external influence. We employ the random matrix theory recently developed for mechanical response, which shares the same fundamental properties [5, 6]. We find that for a strongly disordered dielectric medium, the local disorder-averaged permittivity $\varepsilon(\mathbf{r})$ can be decomposed as $\varepsilon(\mathbf{r}) = \varepsilon_b + \varepsilon_d(\mathbf{r})$, where $\varepsilon_b$ is the bulk value and the disorder-induced contribution $\varepsilon_d(\mathbf{r})$ obeys the differential equation $\varepsilon_d(\mathbf{r}) = \xi^2\nabla^2\varepsilon_d(\mathbf{r})$, with boundary conditions at interfaces determined by the dielectric contrast and the disorder length scale $\xi$. This equation predicts that interfaces generate a boundary layer of thickness $\sim\xi$ over which the effective permittivity varies exponentially from its interfacial value to the bulk.

The obtained results explain, for the first time, the observed interphase thickness and its connection to the boson peak length scale [1]. They complement studies of nonlocal nanoscale dielectric properties [7] by emphasizing that the properties at a point r depend on the material structure within a radius ξ, which may exceed the spatial dispersion scale under strong disorder. These insights are particularly relevant to nanophotonics, as surface resonances exhibit pronounced sensitivity to the local dielectric environment. Recent experiments on polymer-filled nanogaps between self-assembled gold nanoparticles are also significant in this context [8]. Finally, our framework can be extended to describe the influence of dielectric contrast on electronic properties of colloidal quantum dots embedded in glasses or polymers.

This work was supported by the Russian Science Foundation under Grant No. 23-12-00300-П.

[1] S. Cheng et al., Interfacial properties of polymer nanocomposites: role of chain rigidity and dynamic heterogeneity length scale, Macromolecules, vol. 50, p. 2397, (2017).
[2] E. T. Hoppe, I. Hopp, M. Port, B. Menges, C. M. Papadakis, Optical properties of polybutadiene in the bulk and near a gold interface, Colloid. Polym. Sci., vol. 290, p. 1731, (2012).
[3] Y. Han, C. B. Roth, Gradient in refractive index reveals denser near free surface region in thin polymer films, J. Chem. Phys., vol. 155, p. 144901, (2021).
[4] Y. M. Beltukov, A. V. Rodina, A. Alekseev, Al. L. Efros, Non-perturbative macroscopic theory of interfaces with discontinuous dielectric constant, Appl. Phys. Rev., vol. 12, p. 41415, (2025).
[5] D. A. Conyuh, A. A. Semenov, Y. M. Beltukov, Effective elastic moduli of composites with a strongly disordered host material, Phys. Rev. E, vol. 108, p. 045004, (2023).
[6] D. A. Conyuh, D. V. Babin, I. O. Raikov, Y. M. Beltukov, Large-scale exponential correlations of nonaffine elastic response of strongly disordered materials, Phys. Rev. B, vol. 113, p. 174207, (2026).
[7] S. S. Kharintsev, E. I. Battalova, V. Mkhitaryan, V. M. Shalaev, How near-field photon momentum drives unusual optical phenomena: opinion, Opt. Mater. Express, vol. 14, p. 2017, (2024).
[8] N. Kim, J. Huh, Y. Cho, S. H. Park, H. H. Kim, K. H. Rho, J. Lee, S. Lee, Achieving optical refractive index of 10-plus by colloidal self-assembly, Small, vol. 20, p. 2404223, (2024).

# Non-Hermitian Singularities in Mie Resonators and Metasurfaces

**A. Bogdanov**[1,2,]

*1- Qingdao Innovation and Development Center, Harbin Engineering University, Qingdao 266000, Shandong, China*
*2- School of Physics and Engineering, ITMO University, Saint Petersburg 197101, Russia*

*a.bogdanov@hrbeu.edu.cn*

Subwavelength high-index dielectric resonators provide a compact platform for non-Hermitian photonics because radiative coupling makes their eigenfrequencies intrinsically complex. In this contribution, we discuss how exceptional points (EPs) emerge in individual Mie resonators through the interference of multipolar modes coupled to a common radiation channel. By tuning the resonator geometry, the EPs can be connected by a bulk Fermi arc on a two-sheeted Riemann surface, establishing single-particle scattering as a minimal setting for non-Hermitian topology [1,2].

Building on this picture, we show how the same physical mechanism appears in periodic and stacked dielectric metasurfaces. Collective-mode hybridization allows bound states in the continuum (BICs) to merge into exceptional bound states in the continuum (EP-BICs) [3]. These singular states combine the suppressed radiation of BICs with the square-root dispersion and enhanced parametric response of EPs, providing a route to non-Hermitian behavior without strong radiative losses.

Finally, we discuss how EP and EP-BIC platforms can enhance nonlinear optical response in compact structures [4]. Near-exceptional coupling reshapes the field distribution and dissipation landscape, enabling low-threshold thermo-optical bistability and multistability. The resulting framework connects Mie resonances, topology, metasurface design, and optical nonlinearity, with opportunities for reconfigurable photonic devices, ultrasensitive sensing, and neuromorphic photonic functions.

[1] F. Zhang, N. S. Solodovchenko, H. Fan, et al., "Non-Hermitian singularities in scattering spectra of Mie resonators," Sci. Adv. 11, eadr9183 (2025).
[2] N. Solodovchenko, F. Zhang, M. Bochkarev, et al., "Experimental observation of bulk Fermi arc in a single dielectric resonator," arXiv:2502.12711 (2026).
[3] A. Canós Valero, Z. Sztranyovszky, E. A. Muljarov, A. Bogdanov, and T. Weiss, "Exceptional bound states in the continuum," Phys. Rev. Lett. 134, 103802 (2025).
[4] Z. Liu, X. Yin, A. Bogdanov, et al., "Optical multistability in a compact microcavity enabled by near-exceptional coupling," Nat. Nanotechnology (2026).

# Ultrafast optical nonlinearities and harmonic generation in resonant metasurfaces and metastructures

**M. Petrov**

*Department of Physics and Engineering, ITMO University, ITMO University, 197101 St. Petersburg, Russia*

*m.petrov@metalab.ifmo.ru*

Optical nonlinearities are a fundamental ingredient of optical computing, enabling switching, thresholding, memory, signal regeneration, and nonlinear activation functions. While linear photonic systems excel at information transport and parallel data processing, scalable optical computing architectures require efficient nonlinear interactions operating at low energies and ultrafast timescales. Resonant metastructures and metasurfaces provide a powerful route toward this goal by strongly enhancing light–matter interactions through high-quality-factor resonances and bound states in the continuum (BICs).

In this talk, I will present recent advances in nonlinear and dynamically tunable metasurfaces based on resonant dielectric nanophotonics. I will first discuss nonlinear wavefront engineering enabled by flat optics, including nonlinear total angular momentum addition and structured-light generation for optical information encoding and processing [1].

The central part of the talk will focus on ultrafast nonlinear phenomena in high-Q metasurfaces. Ultrafast all-optical switching in 3R-$MoS_2$ van der Waals metasurfaces demonstrates resonantly enhanced nonlinear interactions and efficient modulation on femtosecond timescales [2]. Complementary to this approach, transient optical symmetry breaking in dielectric metasurfaces provides a fundamentally new mechanism for activating quasi-bound states in the continuum on sub-picosecond timescales, enabling ultrafast switching of high-Q resonances beyond the limits imposed by carrier relaxation dynamics [3].

I will further discuss optical and thermo-optical bistability in resonant silicon nanostructures, which provide key ingredients for optical memory and logic operations. In particular, BIC-based silicon metasurfaces exhibit pronounced thermo-optical bistability and nonlinear feedback [4], while optical bistability has been demonstrated even in nanosilicon resonators with record-low quality factors [5], highlighting the robustness of nonlinear state formation in dielectric nanophotonics.

Finally, I will present actively tunable ultra-high-Q silicon membrane metasurfaces operating in the mid-infrared spectral range [6]. These structures combine experimentally measured quality factors approaching 3000 with both electro-thermal and ultrafast all-optical tuning, enabling dynamic modulation from kilohertz frequencies to projected sub-gigahertz rates and establishing a versatile platform for programmable photonic functionalities.

Together, these results demonstrate how resonantly enhanced optical nonlinearities can implement the key building blocks required for future photonic computing architectures, including ultrafast switches, optical memory elements, reconfigurable modulators, and high-dimensional information-processing units. The combination of strong field confinement, ultrafast response, multifunctionality, and CMOS-compatible fabrication positions resonant metasurfaces as a promising foundation for next-generation optical and neuromorphic computing systems operating beyond the speed and energy-efficiency limits of conventional electronic hardware.

This work was supported by the Ministry of Science and Higher Education (project No. FSER-2025-0012).

[1] E. Menshikov et al., *Light structuring via nonlinear total angular momentum addition with flat optics*, Light: Science & Applications **14**, 381 (2025).
[2] L. Seidt et al., *Ultrafast all-optical switching in nonlinear 3R-$MoS_2$ van der Waals metasurfaces*, npj Nanophotonics **2**, 37 (2025).
[3] G. Crotti et al., *Ultrafast switching of a metasurface quasi-bound state in the continuum via transient optical symmetry breaking*, Light: Science & Applications **14**, 240 (2025).
[4] A. Barulin et al., *Thermo-Optical Bistability Enabled by Bound States in the Continuum in Silicon Metasurfaces*, Laser & Photonics Reviews (2024).
[5] K. Nishida et al., *Optical Bistability in Nanosilicon with Record Low Q-Factor*, Nano Letters **23**, 11727–11733 (2023).
[6] F. U. Brikh et al., *Mid-IR Light Modulators Enabled by Dynamically Tunable Ultra High-Q Silicon Membrane Metasurfaces*, arXiv:2509.23167 (2025).

# Interpreting the Lipkin tensor: anisotropic structure of electromagnetic chirality

**I. Smagin, S. Dyakov**

*Department of Physics, Skolkovo Institute of Science and Technology, Moscow, Russia*

*Ilia.Smagin@skoltech.ru*

Optical chirality density is widely used to describe chiral electromagnetic fields, but it represents only the scalar component of a richer tensorial structure. In this contribution, we discuss the physical meaning of the Lipkin zilch tensor components and show how its spatial density block provides anisotropic descriptors of electromagnetic chirality[1]. We demonstrate that these tensorial components naturally appear in the electric-dipole-magnetic-dipole interaction with anisotropic chiral matter. In this picture, the field is characterized by Lipkin tensor channels, while the material response is determined by the symmetry-dependent components of the optical activity tensor. This provides a transparent way to understand how structured light and anisotropic media can selectively probe different chiral channels beyond conventional optical chirality density.

[1] I. Smagin and S. Dyakov, Beyond optical chirality density: tensor-based description of electromagnetic chirality, 10.48550/arXiv.2603.14071, (2026).

# Casimir Effect and Casimir Torque in Chiral Photonic Gratings

**N.S. Salakhova[1], S.A. Dyakov[1], I.M. Fradkin[1,2], N.A. Gippius[1]**

*1- Skolkovo Institute of Science and Technology, Moscow 121205, Russia*
*2- Moscow Institute of Physics and Technology, Moscow Region 141701, Russia*

*natalia.salakhova@skoltech.ru*

The Casimir interaction originates from quantum electromagnetic fluctuations and is shaped by the symmetry and optical response of the interacting bodies [1,2]. Beyond parallel plates, material anisotropy and periodic patterning can generate rotational torques [3-5]. Chiral photonic gratings made of anisotropic media provide a flexible setting because their geometrical and optical axes are not equivalent. Therefore, the equilibrium orientation can be governed by the coupling between structural twist and material anisotropy rather than by grating alignment alone.

We analyze the Casimir energy, normal force, and torque in twisted anisotropic gratings using the reflection-matrix Casimir-Lifshitz formalism with Fourier-modal calculations. The angular dependence of the energy is described by a shifted cosine law

$$\varepsilon(\alpha,\theta) = -a(\theta)\, cos(2\alpha+\phi(\theta))+c(\theta),$$

where $\alpha$ is the twist angle, $\theta$ is the anisotropy-axis orientation, and the torque $\eta = d\varepsilon/d\alpha$ vanishes at angles determined by the phase shift $\phi$. Thus, the zero-torque state is shifted away from symmetric orientations and becomes sensitive to the anisotropic optical contrast.

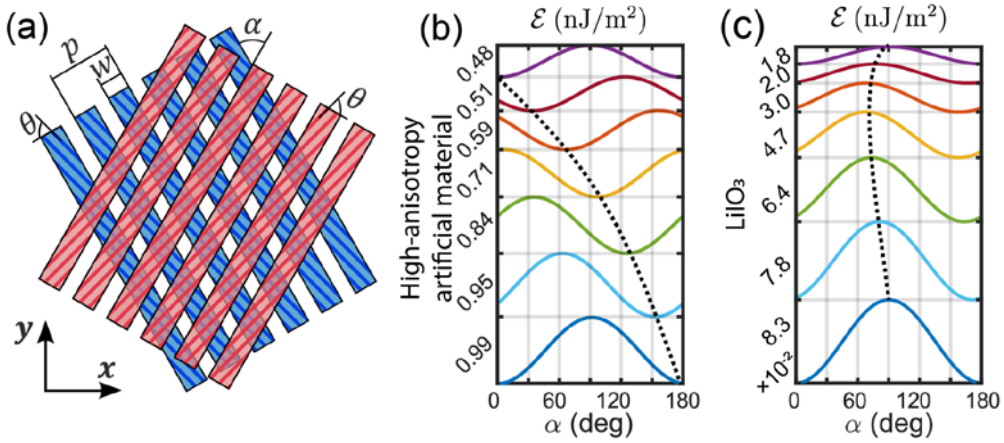


**Fig. 1.** Casimir energy in twisted photonic gratings. (a) Geometry with twist angle $a$ and anisotropy-axis orientation $\theta$. (b,c) Energy versus $a$ for a high-anisotropy model material and $LiIO_3$; dashed lines mark shifted energy minima (maxima) corresponding to zero Casimir torque.

The zero-torque angle is not a fixed geometrical property of the grating stack. For a high-anisotropy model material, the equilibrium shifts over a wide angular range and occurs when the anisotropy axes nearly align while the grating patterns remain twisted. For lithium iodate, the same mechanism persists but the shift is smaller because the broadband anisotropy is weaker. These results identify anisotropic contrast as a control parameter for passive self-alignment, Casimir-driven nanoactuation, and reconfigurable chiral photonic systems related to twisted architectures supporting chiral optical modes [6].

This work was supported by the Russian Science Foundation Grant No. 25-12-00454.

[1] H. B. G. Casimir, On the attraction between two perfectly conducting plates, Proc. K. Ned. Akad. Wet., vol. 51, pp. 793-795, (1948).
[2] E. M. Lifshitz, The theory of molecular attractive forces between solids, Sov. Phys. JETP, vol. 2, pp. 73-83, (1956).
[3] J. N. Munday, D. Iannuzzi, Y. Barash, and F. Capasso, Torque on birefringent plates induced by quantum fluctuations, Phys. Rev. A, vol. 71, 042102, (2005).
[4] A. Lambrecht and V. N. Marachevsky, Casimir interaction of dielectric gratings, Phys. Rev. Lett., vol. 101, 160403, (2008).
[5] M. Antezza, H. B. Chan, B. Guizal, V. N. Marachevsky, R. Messina, and M. Wang, Giant Casimir torque between rotated gratings and the θ = 0 anomaly, Phys. Rev. Lett., vol. 124, 013903, (2020).
[6] S. A. Dyakov, N. S. Salakhova, A. V. Ignatov, I. M. Fradkin, V. P. Panov, J.-K. Song, and N. A. Gippius, Chiral light in twisted Fabry-Perot cavities, Adv. Opt. Mater., vol. 12, 2302502, (2024).

# Asymmetric Optical Harmonic Generation in Silicon Metasurfaces

**A. Musorin[1,2], A. Nazarenko[2,1], A. Popkova[1,2], A. Shorokhov[1], D. Smirnova[3], A. Fedyanin[1]**

*1- Lomonosov Moscow State University, Leninskie gory 1-2, Moscow 119991, Russia*
*2- Shenzhen MSU-BIT University, No. 1 International University Park Road, Shenzhen 517182, China*
*3- Research School of Physics, Australian National University, 60 Mills Rd, Canberra 2601, Australia*

*musorin@nanolab.phys.msu.ru*

Dielectric metasurfaces, composed of subwavelength arrays of high-index resonant nanoantennas, have emerged as a revolutionary platform for nonlinear nanophotonics. Unlike plasmonic counterparts, all-dielectric structures avoid Ohmic losses. They support strong Mie-type electric and magnetic resonances, leading to light field localization at extremely small volumes, thereby enhancing nonlinear effects. Over the past decade, this field has witnessed remarkable progress. For instance, frequency mixing was demonstrated in an all-dielectric metasurface acting as a broadband optical frequency mixer [1]. High-harmonic generation up to the fifth order was reported in gallium phosphide metasurfaces, while tunable non-integer high-harmonic generation was recently shown in topological insulators [2]. Furthermore, externally driven time-variant metasurfaces have enabled non-integer harmonic generation via dynamic refractive index modulation [3]. Despite these achievements, the vast majority of nonlinear metasurface studies have focused on symmetric meta-atoms. In such symmetric systems, the forward and backward nonlinear emission intensities are nearly equal due to reciprocity and mirror symmetry along the propagation direction. This limits practical applications that require directional control of nonlinear signals, such as on-chip optical isolation, or background-free harmonic imaging. Only a few recent works have addressed asymmetric nonlinear signal generation. Asymmetric parametric image generation was experimentally demonstrated in two-material ($Si/Si_3N_4$) metasurfaces [4]. AlGaAs nano-chairs metasurface was used to numerically demonstrate asymmetric second harmonic generation [5].

In our study we use a single-material metasurface and experimentally show that reversing the fundamental beam direction results in a 24-fold switching of third harmonic signal. The metasurface is composed of silicon nanodiscs with coaxial half-height etched holes. This structural asymmetry breaks the vertical mirror symmetry of the Mie-type resonances, leading to a pronounced imbalance in the third harmonic forward/backward emission ratio.

Our results introduce a compact device for directional nonlinear conversion. The proposed geometry is CMOS-compatible and can be extended to higher harmonics. Asymmetric third harmonic generation in silicon metasurfaces opens new paths for on-chip nonlinear optical diodes.

[1] S. Liu et al, An all-dielectric metasurface as a broadband optical frequency mixer, Nat. Commun. 9, 2507 (2018).
[2] C.P. Schmid et al., Tunable non-integer high-harmonic generation in a topological insulator, Nature 593, pages 385–390 (2021)
[3] V. V. Zubyuk et al., Externally Driven Nonlinear Time-Variant Metasurfaces, ACS Photonics 9, 493−502 (2022)
[4] S. S. Kruk, et al., "Asymmetric parametric generation of images with nonlinear dielectric metasurfaces," Nat. Photonics 16, 561–565 (2022).
[5] D. Rocco, et al., "Nonlinear asymmetric imaging with AlGaAs metasurface," Opt. Express 32, 11673–11680 (2024).

# Virtual absorption beyond the linear regime: Influence of nonlinearity on energy accumulation

**V. A. Maslova[1,2,3], D.G. Baranov[1,2]**

*1- Moscow Center for Advanced Studies, Moscow 123592, Russia*
*2- Emerging Technologies Research Center, XPANCEO, Internet City, Emmay Tower, Dubai, United Arab Emirates*
*3- C.H.O.S.E. (Center for Hybrid and Organic Solar Energy), Electronic Engineering Department, University of Rome Tor Vergata, 00118, Rome, Italy*

*lera.maslova00@gmail.com*

The concept of virtual absorption illustrates how light-matter interaction in a resonant system can be controlled by tailoring the amplitude of the incident field [1-3]. Numerical simulations show that when a linear system is driven by a field with a specially chosen frequency and an exponentially growing amplitude, the scattered field vanishes and the system stores energy, which is then released once the exponential pumping stops.

However, taking nonlinearity into account changes the resonant properties of the system. Using a simple model, we demonstrated that under nonlinear conditions the resonance undergoes a redshift, which violates the condition for destructive interference between the incident field and the field emitted by the resonator mode, and the emergence of nonzero scattering.

We derived an analytical expression for the incident field that restores zero scattering in the presence of nonlinearity. By modulating not only the amplitude but also the instantaneous frequency of the incident wave, the destructive interference condition can be preserved, enabling energy accumulation within the resonator even in the nonlinear regime.

Next, we examined how nonlinearity and the resonance Q-factor influence the amount of energy dissipated when the system is pumped by an incident field with a constant frequency equal to the cold-system resonance. Numerical simulations showed that increasing either the nonlinearity strength or the resonance Q-factor leads to a larger fraction of scattered energy and in turn lower fraction of stored energy. This behavior highlights the amplified impact of nonlinearity in high-Q resonant systems.

In the final part of this work, we examine the full system of thermo-optical equations and numerically determine the incident field at which zero scattering occurs, in the general case of time-dependent nonlinearity. Furthermore, we systematically demonstrate the limits of applicability of the instantaneous Kerr-type nonlinearity model discussed previously.

Thus, in the presence of nonlinearity, virtual absorption acquires fundamentally new features. The results obtained open up additional opportunities for controlling light and expand the potential functionality of compact optical devices based on emerging materials with nonlinear response.

The work was supported by BASIS Foundation (grant No. 24-1-5-136-1).

[1] G. Baranov, A. Krasnok, and A. Alù, Coherent virtual absorption based on complex zero excitation for ideal light capturing, Optica, vol. 4, pp. 1457–1463, (2017).
[2] J. Hinney, S. Kim, G. J. Flatt, I. Datta, A. Alù, and M. Lipson, Efficient excitation and control of integrated photonic circuits with virtual critical coupling, Nature Communications, vol. 15, article 2741, (2024).
[3] Q. Zhong, L. Simonson, T. Kottos, and R. El-Ganainy, Coherent virtual absorption of light in microring resonators, Physical Review Research, vol. 2, article 013362, (2020).

# Numerical Analysis of Second-Harmonic Generation Efficiency and Pulse Dynamics in Periodically Poled GaN under Femtosecond Excitation

**O.I. Sobirov[1], B.G. Urinov[1], U.K. Sapaev[2]**

*1- Urgench State University, Kh. Alimjan Str. 14, Urgench, 220100, Khorezm Region, Uzbekistan*
*2- Branch of Gubkin Russian State University of Oil and Gas, Durmon Yuli Str. 34, Tashkent, 100125, Uzbekistan*

*obid7432505@gmail.com*

This work presents a numerical analysis of femtosecond second-harmonic generation (SHG) in periodically poled gallium nitride (PP-GaN) crystals. The coupled-wave equations governing the nonlinear interaction are solved numerically, accounting for group-velocity dispersion, linear absorption, and quasi-phase matching (QPM) conditions defined by the periodic domain structure. The influence of pulse duration on conversion efficiency and temporal pulse evolution is systematically examined. It is shown that linear absorption in GaN constitutes a significant limiting factor, reducing the effective interaction length and suppressing conversion efficiency. In the femtosecond regime, group-velocity dispersion induces pronounced temporal distortions, including pulse splitting, accompanied by a steep decline in SHG efficiency as pulse duration decreases. Furthermore, the sensitivity of the QPM scheme to periodic domain length errors is quantitatively assessed; it is demonstrated that even small deviations from the ideal domain period lead to a substantial degradation of phase matching conditions and a corresponding reduction in output efficiency. The results provide quantitative guidelines for the design and fabrication of high-efficiency PP-GaN femtosecond nonlinear frequency converters.

## 1. Introduction

Despite these advantages, efficient SHG in bulk GaN is hindered by pronounced material dispersion, which generally prevents the realization of conventional birefringent phase matching over broad spectral bandwidths. This limitation can be overcome using the quasi-phase-matching (QPM) technique, which relies on the periodic inversion of the sign of the nonlinear susceptibility $\chi^{(2)}$ along the propagation direction [1,2]. Such periodic modulation introduces an additional reciprocal lattice vector that compensates for the intrinsic wave vector mismatch $\Delta k=k_{2\omega}-2k_{\omega}$, enabling coherent growth of the second-harmonic field over propagation lengths far exceeding the coherence length.

The implementation of QPM in the femtosecond regime, however, introduces a number of additional challenges associated with the ultrabroad spectral bandwidth of short pulses. While QPM can be optimized for the central frequency of the pulse, spectral components away from the center experience residual phase mismatch. Moreover, different frequency components propagate with different group velocities, giving rise to group-velocity mismatch (GVM) between the fundamental and second-harmonic waves and to dispersive temporal broadening of the pulses. These effects reduce the effective interaction length and degrade the temporal overlap between the interacting fields. As a result, for pulse durations shorter than approximately 100 fs, dispersive effects become a dominant limiting factor for SHG efficiency, even in structures that satisfy the quasi-phase-matching condition [3,5]. The present work aims to provide a systematic numerical analysis of these limiting mechanisms in periodically poled GaN photonic crystals and to quantify their impact on conversion efficiency and temporal pulse characteristics.

## 2. Theoretical Model and Numerical Methods

### 2.1. Coupled-wave equations with group-velocity dispersion

The spatiotemporal dynamics of SHG in the femtosecond regime is described using a system of coupled-wave equations for the slowly varying envelopes of the fundamental and second-harmonic fields. In contrast to continuous-wave or picosecond regimes, femtosecond pulse propagation requires explicit inclusion of dispersive effects (Sabirov et al. 2023).

The evolution equations for the complex field envelopes $A_1(z,t)$ and $A_2(z,t)$ are given by

$$\begin{aligned}\frac{\partial A_1}{\partial z}+\frac{1}{v_{g1}}\frac{\partial A_1}{\partial t}-\frac{ik_1''}{2}\frac{\partial^2 A_1}{\partial t^2}+\frac{\alpha_1}{2}A_1&=-i\frac{\omega_1}{2n_1c}\chi^{(2)}A_1^*A_2e^{i\Delta kz},\\ \frac{\partial A_2}{\partial z}+\frac{1}{v_{g2}}\frac{\partial A_2}{\partial t}-\frac{ik_2''}{2}\frac{\partial^2 A_2}{\partial t^2}+\frac{\alpha_2}{2}A_2&=-i\frac{\omega_2}{2n_2c}\chi^{(2)}A_1^2e^{-i\Delta kz},\end{aligned}\quad(1)$$

where $v_{g1}$ and $v_{g2}$ are the group velocities of the fundamental and second-harmonic waves, $k_1''$ and $k_2''$ are the corresponding group-velocity dispersion (GVD) coefficients, $\alpha_1$ and $\alpha_2$ denote the linear absorption coefficients, $n_1$ and $n_2$ are the refractive indices, and $c$ is the speed of light in vacuum.

The second-order temporal derivatives explicitly account for pulse broadening and temporal distortion induced by GVD, while the first-order temporal derivatives describe group-velocity mismatch (GVM) between the interacting waves. This model therefore captures both temporal walk-off and dispersive pulse deformation, which are critical in the femtosecond regime.

Initial conditions and numerical implementation

The incident fundamental pulse is assumed to have a Gaussian temporal profile,

$$A_1(z=0,t) = A_0 \exp\left(-2ln2\frac{t^2}{\tau^2}\right), \quad (2)$$
$$A_2(z=0,t) = \eta_{\text{seed}} A_0,$$

where $A_0$ is the peak amplitude, $\tau$ is the pulse duration (50, 130, or 200 fs), and $\eta_{\text{seed}}$ = 0.00001 is a small seed amplitude introduced to mimic spontaneous second-harmonic generation and to ensure numerical stability.

The coupled equations were solved numerically using a split-step Fourier method combined with a fourth-order Runge–Kutta algorithm. This approach allows accurate treatment of both dispersive and nonlinear effects and provides stable solutions for femtosecond pulse propagation over the considered crystal lengths.

## 3. Results and Discussion

Figure 1 illustrates the influence of dispersive effects on the second-harmonic generation efficiency for a femtosecond pulse with duration $\tau$ = 50 *f*s. In the idealized case where dispersive effects are neglected (dashed curve), the conversion efficiency increases rapidly with propagation distance and approaches its maximum value determined by the chosen input intensity and phase-matching conditions. This regime represents the theoretical upper bound for the given excitation parameters.

When realistic dispersive properties of GaN are taken into account (solid curve), the growth of the second-harmonic field is strongly suppressed and saturates at a significantly lower efficiency. This behavior is primarily attributed to the combined action of group-velocity mismatch and group-velocity dispersion, which substantially reduce the effective nonlinear interaction length.

Group-velocity mismatch leads to a progressive temporal walk-off between the fundamental and second-harmonic pulses. As a result, only a limited number of periodically poled domains contribute efficiently to the nonlinear interaction, even though the total number of domains in the structure may be considerably larger. Beyond this effective interaction region, the temporal overlap between the pulses becomes insufficient for further energy transfer.

### 3.1. Detrimental Role of Group-Velocity Mismatch and Dispersion

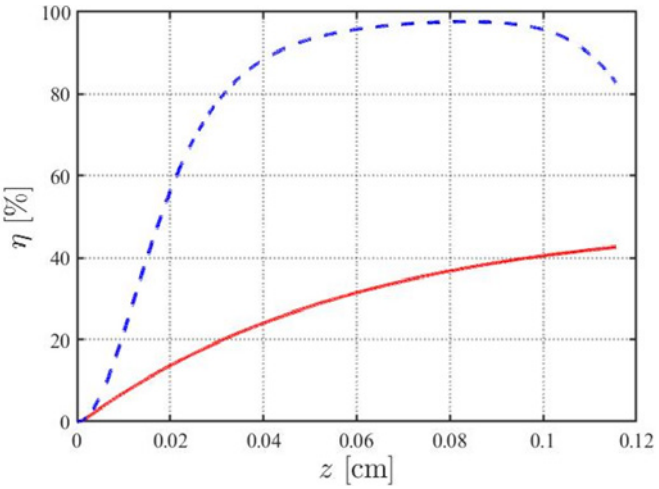


**Fig.1.** Influence of dispersive effects on SHG efficiency for a $\tau$ = 50 *f*s pulse.
Dashed line: idealized case neglecting group-velocity mismatch and group-velocity dispersion.
Solid line: realistic case including dispersive effects intrinsic to GaN.

3.2. Sensitivity to Domain Length Deviation

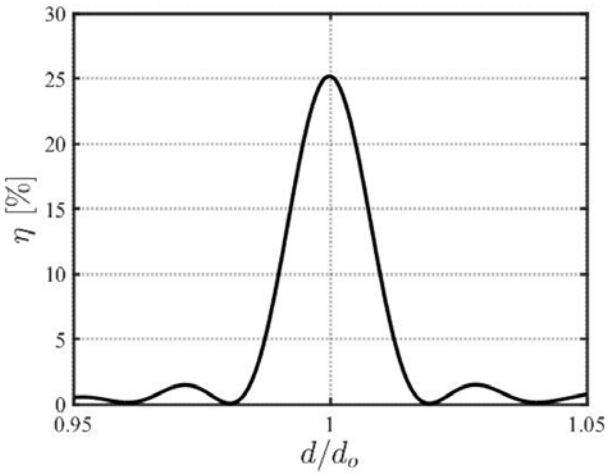


**Fig.2.** Dependence of SHG efficiency $\eta$ on the relative domain length $d/d_0$, where $d_0$ corresponds to the optimal domain length required for first-order quasi-phase matching. Results are shown for a $\tau$ = 50 *f*s pulse.

Figure 2 illustrates the dependence of the second-harmonic generation efficiency on deviations of the domain length from the value corresponding to the quasi-phase-matching condition. The efficiency exhibits a well-defined maximum at $d/d_0 = 1$, where the domain length exactly compensates the accumulated phase mismatch between the fundamental and second-harmonic waves. This condition ensures constructive interference of the nonlinear polarization over successive domains and maximizes the coherent buildup of the harmonic field.

Any deviation of the domain length from the optimal value leads to a monotonic reduction of the conversion efficiency. This behavior reflects the cumulative nature of phase errors in quasi-phase-matched structures. When the domain length differs from , the phase compensation at each domain boundary becomes imperfect, resulting in a residual phase mismatch that accumulates with the number of domains.

In the femtosecond regime, this effect is further amplified by temporal walk-off between the interacting pulses. Due to group-velocity mismatch and dispersion, only a finite number of domains contribute effectively to the nonlinear interaction, even when the total number of domains in the structure is large. Within this effective interaction region, deviations of the domain length lead to rapid degradation of the phase coherence and a corresponding reduction of the local conversion efficiency.

4. Conclusion

The analysis of domain length deviations revealed a strong sensitivity of the SHG process to the accuracy of the periodic poling. Any departure from the optimal domain length results in the accumulation of phase errors across successive domains and leads to a monotonic degradation of the conversion efficiency within the effective interaction region. This effect is particularly pronounced in the femtosecond regime, where the number of actively contributing domains is already limited by temporal walk-off.

Taken together, these findings indicate that efficient femtosecond second-harmonic generation in GaN-based nonlinear photonic crystals requires a careful balance between quasi-phase matching, dispersion control, and loss reduction. High conversion efficiency can be achieved only when the domain geometry is precisely matched to the quasi-phase-matching condition and when dispersive effects are mitigated to preserve temporal overlap and peak intensity.

The results of this study provide clear guidelines for the design of compact GaN-based frequency conversion devices operating in the femtosecond regime. Future work should focus on dispersion-engineered waveguide geometries, aperiodic or chirped quasi-phase-matching structures, and further reduction of linear losses through advanced material growth and fabrication techniques.

[1] Sapaev, U., and G. Assanto. 2024a. "On the Generation of Optical Third Harmonic Through Quasi-Phase Matching in Quadratic Nonlinear Crystals." *Wave Motion* 130: 103372.
[2] Sabirov, O. I., Rajabov, A. E., Matnazarov, A. R., Eshchanov, B. K., Otajanov, S., & Sapaev, U. K. (2025). Study of femtosecond laser amplification in MgO: LiTaO3 crystals with periodic nonlinear properties. Наносистемы: физика, химия, математика, 16(3), 291-297.
[3] Sapaev, U., and G. Assanto. 2024b. "Quadratic Cascading in Quasi-Phase-Matching: An Alternative Route to Efficient Third-Harmonic Generation." *Electronics* 13 (22): 4348.
[4] Sabirov, O. I., Assanto, G., & Sapaev, U. K. (2023). Efficient Third-Harmonic Generation by Inhomogeneous Quasi-Phase-Matching in Quadratic Crystals. Photonics 2023, 10, 76.
[5] Shen, Yuen-Ron. 1984. *The Principles of Nonlinear Optics*. Wiley-Interscience.

# Enhanced Goos-Hänchen Effect in ENZ Metamaterials

V.B. Novikov[1], S.V. Sotnichuk[2], N.K. Davidenko[3], K.S. Napolskii[2,3], T.V. Murzina[1]

*1- Department of Physics, M.V. Lomonosov Moscow State University, Leninskie Gory, Moscow 119991, Russia*
*2- Department of Chemistry, M.V. Lomonosov Moscow State University, Leninskie Gory, Moscow 119991, Russia*
*3- Department of Materials Science, M.V. Lomonosov Moscow State University, Leninskie Gory, Moscow 119991, Russia*

*vb.novikov@physics.msu.ru*

The Goos-Hänchen (GH) effect is a longitudinal shift ($\Delta x$) of the light beam at total internal reflection [1]. This deviation from geometrical optics is usually smaller than the light wavelength and is specified by the expression $\Delta x = -\partial \arg(r)/\partial k_x$, where r is the electric field reflection coefficient, $k_x$ is the tangential component of the incident wave vector. As a result, optical structures with a pronounced angular dependence of the complex phase of r, e.g. plasmonic crystals, have attracted much attention to harness the GH effect perspective, e.g., for sensorics [2]. Similar beam shifts occur in the light transmission through 1D photonic crystals supporting waveguide modes or bound states in the continuum [3]. The effect of zero transmission, accompanied by phase singularities, offers a way to enhance the GH shift. Such phase singularities of the complex transmission coefficient were observed recently in metamaterials based on arrays of metal nanorods in a dielectric matrix [4]. These structures can be treated as an uniaxial effective optical medium with ordinary ($\varepsilon_o$) and extraordinary ($\varepsilon_e$) permittivities, with the epsilon-near-zero (ENZ) spectral region at which $\varepsilon_e \approx 0$. Optical nonlocality of the metamaterial's response plays an impressive role in the ENZ regime, giving birth to zero transmission points in the metamaterial's transmission spectrum. In this work, we study the GH effect experimentally and theoretically in ENZ metamaterials possessing the optical nonlocality.

The experimental structure consisted of an array of 1000 nm-long gold nanorods with the diameter of 27 nm in anodic aluminum oxide (AAO); center-to-center nanorod distance was 100 nm. The thickness of the unfilled by gold AAO template was 29 μm. The metamaterial exhibited the ENZ-regime at the wavelength of $\lambda_{ENZ} = 720$ nm, near which the zero-transmission points at the incident angle of $\theta_0 = 16°, 35°$ were found. In the experiment, focused femtosecond radiation of the parametric oscillator with 200 fs pulse duration was focused to a line with a width of 2.5 μm oriented in y-direction (Fig. 1(a)).

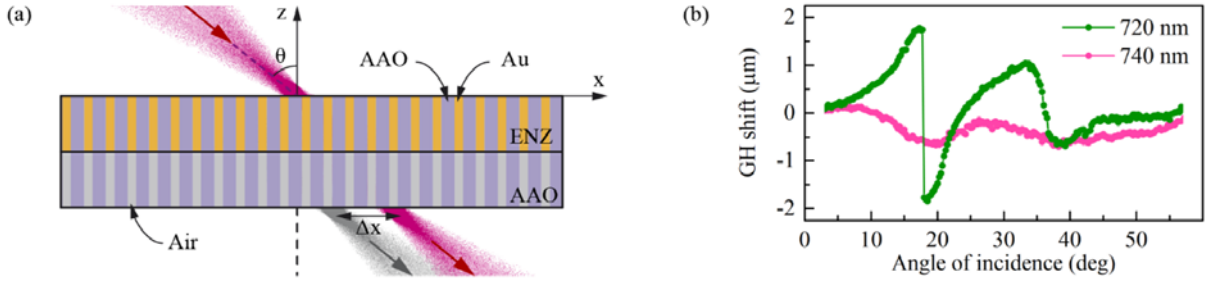


**Fig. 1.** (a) Scheme of the light incidence on the ENZ structure; gray is the beam transmitted through the reference AAO film, red is the beam transmitted ENZ metamaterial and AAO template. (b) The angular dependence of the GH shift for light wavelengths of 720 nm and 740 nm.

The image of the waist of the transmitted beam was obtained by an objective on CMOS matrix. The GH shift in the metamaterial was measured as a difference of the waist x-positions for the case of the metamaterial and of the reference empty AAO template (Fig. 1(a)). Near $\lambda_{ENZ}$, we observed a peculiar sign change of $\Delta x$ reaching 2 μm, which demonstrates the GH effect enhancement in the vicinity of $\theta_0$ (Fig. 1(b)). Numerical simulations confirm the observed effect and the role of nonlocality of the ENZ metamaterial response in its appearance. We believe these findings can be applied for optical sensing.

This work was supported by Russian Science Foundation Grant No. 26-72-10022.

[1] K.Y. Bliokh and A. Aiello, Goos–Hänchen and Imbert–Fedorov beam shifts: an overview, J. Opt., vol. 15, p. 014001, (2013).
[2] S. Zhu, R. Jaffiol, A. Crunteanu, C Vézy, S. Chan, W. Yuan, H. Ho, S. Zeng, Label-free biosensing with singular-phase-enhanced lateral position shift based on atomically thin plasmonic nanomaterials, Light Sci. Appl., vol. 13, p. 2, (2024).
[3] Z. Wu, W. Zhen, Z. C. Ren, X. L. Wang, H. T. Wang, J. Ding, Controlling enhancement of transmitted Goos-Hänchen shifts: From Symmetric to Unidirectional, Laser Photonics Rev., vol. 20, p. e01398, (2026).
[4] V. B. Novikov and T. V. Murzina, Nonlocality-mediated spatiotemporal optical vortex generation in nanorod-based epsilon-near-zero metamaterials, Opt.Lett., vol. 48, pp. 2134-2137, (2023).

# Investigation of up-converting fluoride nanocrystals using ultrahigh resolution UV microscopy technique

**I. Goriachuk, V. Glebov, A. Maliutin, S. Molchanova, V. Sokolov**

*NRC «Kurchatov Institute», Academician Kurchatov square 1, Moscow, Russia*

*io.gorjachuk@physics.msu.ru*

Doped with Yb, Tm, Er, Ce fluoride $NaYF_4$ nanocrystals find applications in technology, medicine and science. There are up-converting fluoride nanoparticles luminescing in visible and UV region of wavelengths λ under the IR laser excitation with λ = 980 nm [1]. Ultrahigh resolution optical UV microscopy represents promising technique for the investigation of these nanoobjects [2]. In consistence with Rayleigh criterion spatial resolution of the UV microscope, which has the objective with *NA* numerical aperture, can be estimated by $R = 0.61\ \lambda/NA$. Equipped by "dry" objectives with *NA* = 0.90 modern microscopes with the illumination in 248 ± 8 nm band provide *R* = 168 nm [3].

In the present study the up-converting β-$NaYF_4$ nanocrystals obtained by the thermal decomposition in oxygen-free medium of Na and rare earth threefluoroacetates are investigated. Their microphotographs made at scanning electron microscope (SEM) are demonstrated in Fig. 1 a, b, c. The microscope equipped by the digital UV camera has been employed for obtaining optical photographs of the crystals. The deuterium lamp, the elaborate narrow-band interference filter and the monochromator have constituted the illumination system. The photographs made in the transmitted light of λ = 225 ± 1 nm spectral range are shown in Fig. 1 d, e, f. *R* = 125 nm is achieved by using ONZ-125 immersion objective with *NA* = 1.10. Individual β-$NaYF_4$ particles and their agglomerates are resolved in the images. The hexagonal shape of the crystals with the average size of 451 nm (Fig. 1 e) and 683 nm (Fig. 1 f) is observed.

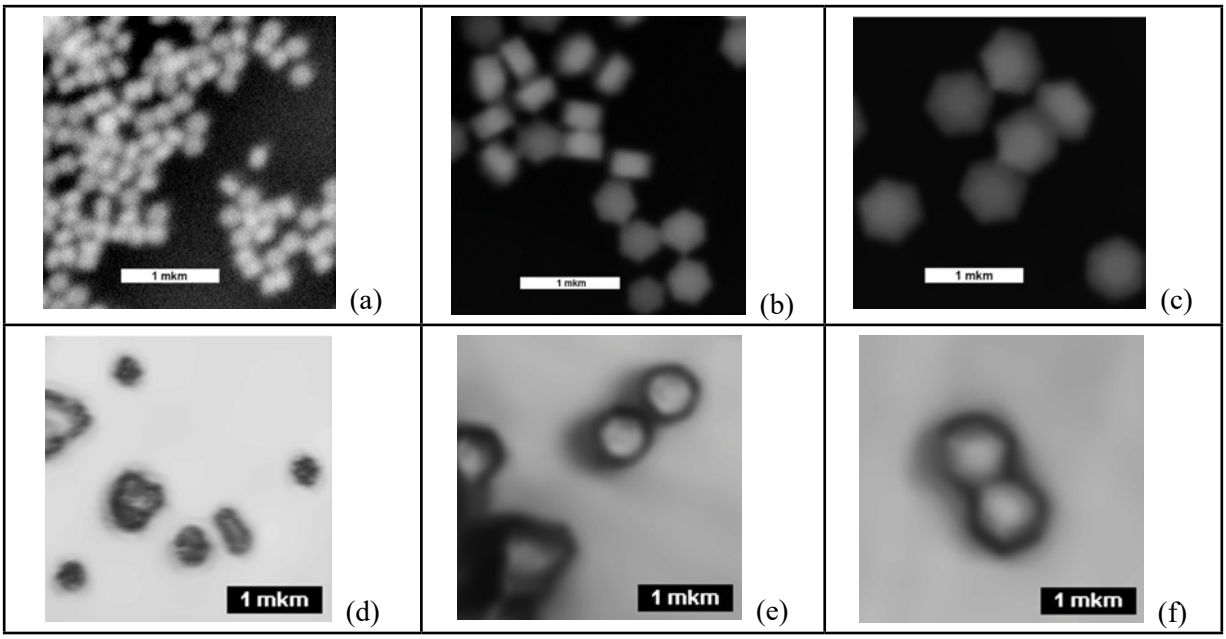


**Fig.1.** SEM images of β-$NaYF_4$ particles (a,b,c) and their optical photographs (d,e,f) in the transmitted light with λ = 225 ± 1 nm. The sizes of individual nanocrystals are 220 ± 12 (a), 451 ± 15 (b) and 683 ± 13 nm (c).

The work was carried out within the state assignment of NRC "Kurchatov Institute".

[1] D.N. Karimov, P.A. Demina, A.V. Koshelev, V.V. Rocheva, A.V. Sokovikov, A.N. Generalova,V.P. Zubov, E.V. Khaydukov, M.V. Koval'chuk, V. Ya. Panchenko, Upconversion nanoparticles: synthesis, photoluminescence properties, and applications, Nanotechnologies in Russia, vol. 15, pp. 655-678, (2020).
[2] V.I. Sokolov, V.N. Glebov, I.O. Goriachuk, A.M. Malyutin and S.I. Molchanova, Deep ultraviolet optical microscopy in the study of upconverting fluoride nanocrystals (in Russian), Izvestiya Vuzov. Radiofizika, vol. 69, pp. 321-329, (2026).
[3] W. Vollrath, Ultra-high-resolution DUV microscope optics for semiconductor applications, Proc. SPIE, vol. 5865, pp. 1-9, (2005).

# Numerical model of reflective phase–amplitude spatial light modulator based on GSST phase-change material

**A. Kokhanovskiy**

*School of Physics and Engineering, ITMO University, 197101 Saint Petersburg, Russia*

*alexey.kokhanovskiy@ru*

Reconfigurable spatial light modulators (SLMs) operating at telecom wavelengths are key building blocks for free-space beam shaping, holography and optical computing. Chalcogenide phase-change materials (PCMs) such as $Ge_2Sb_2Se_4Te_1$ (GSST) provide a non-volatile, reversible refractive-index contrast between amorphous and crystalline states while remaining low-loss in the near-infrared, which makes them attractive for compact, energy-efficient modulation. We propose a reflective multilayer $Si_3N_4$/GSST structure deposited on a gold mirror and optimized for operation at 1550 nm. Phase patterns are imprinted and rewritten all-optically by femtosecond-laser irradiation that locally switches the crystallization state of the GSST layers, so that the device requires no electrodes and can be reconfigured pixel-by-pixel (*Fig. 1a*).

The effective permittivity of intermediate phases is described by a Lorentz–Lorenz mixing rule with crystallization fraction m ϵ [0, 1], so that both the amplitude and the phase of the reflected light depend on m, i.e. the device exhibits intrinsic phase–amplitude coupling. Two GSST films separated by $Si_3N_4$ spacers are used, and the layer thicknesses set the trade-off between the achievable phase-shift range and the reflectivity: thicker stacks favour a larger phase shift at the cost of amplitude, and vice versa. Phase masks are computed with a modified Gerchberg–Saxton algorithm that explicitly accounts for this coupling, while thermal modelling is used to ensure equal peak temperatures in both PCM layers — a requirement for reliable re-amorphization.

Optimization of the thickness landscape ($t_{GSST}$, $t_{SiN}$) yields a reflective phase shift of up to ≈320° at 1550 nm while maintaining high reflectivity (*Fig. 1b*). The diffraction efficiency of the resulting phase gratings is analysed for sinusoidal (33.8% max), blazed (40.5% max) and multilevel rectangular profiles (approaching 100% for a large number of discretization levels), and the influence of inter-pixel crosstalk (fringing fields) on the modulation is evaluated. The results demonstrate an all-optically rewritable reflective phase–amplitude SLM platform suitable for beam shaping and optical computing at telecom wavelengths.

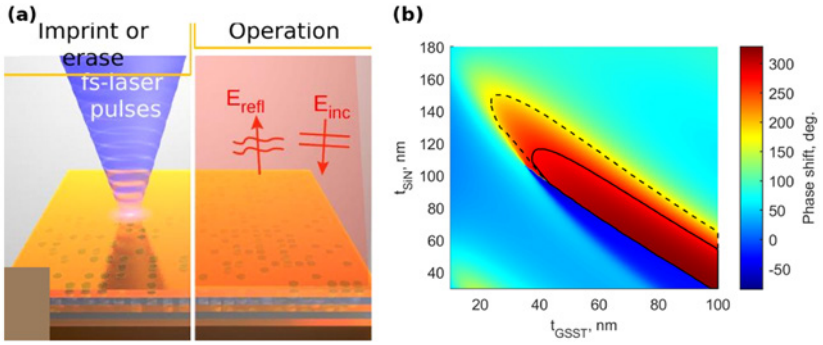


**Fig. 1.** (a) Concept of the reflective $Si_3N_4$/GSST SLM: phase patterns are imprinted/erased by fs-laser pulses and read out in reflection at 1550 nm. (b) Computed phase-shift map versus GSST and $Si_3N_4$ layer thicknesses, reaching up to ≈320°.

[1] Y. Zhang et al., Nat. Commun. 10 (2019) 4279.
[2] M. Wuttig, H. Bhaskaran, T. Taubner, Nat. Photonics 11 (2017) 465–476.
[3] E. Menshikov et al., ACS Appl. Mater. Interfaces 16(29) (2024) 38345–38354.

# Enhancement of the Faraday Effect in the Inverted Au-Co/Pt Magnetoplasmonic Metasurface

**M.O. Sivkov[1], D.A. Safiullin[1], M.A. Kiryanov[1], M.E. Letushev[2], M.A. Bazrov[2], T.V. Dolgova[1], A.S. Samardak[2], A.A. Fedyanin[1]**

*1- Faculty of Physics, Lomonosov Moscow State University, 1 Leninskie Gory, Moscow 119991, Russia*
*2- Laboratory of Spin-Orbitronics, Institute of High Technologies and Advanced Materials, Far Eastern Federal University, Ajax 10, Russky Island, Vladivostok, Primorsky Krai 690922, Russia*

*sivkovmo@my.msu.ru*

The demand for high-speed magnetic memory motivates the search for new approaches to magnetization control. Femtomagnetism, which explores the manipulation of magnetization in materials using femtosecond laser pulses, represents a promising direction in this field. Of particular interest for ultrafast optical memory applications are multilayer structures based on alternating thin Co and Pt layers exhibiting pronounced perpendicular magnetic anisotropy. An integration of plasmonic elements into such magneto-optical media not only enables nanoscale localization of the electromagnetic field, but also significantly enhances magneto-optical effects such as the Faraday and inverse Faraday effects, thereby enhancing an interaction of femtosecond laser pulses with the electronic subsystem of a magnetic material [1,2]. In this work, we experimentally and numerically studied the optical and magneto-optical properties of an inverted plasmonic metasurface composed of alternating ultrathin cobalt and platinum layers covered with a perforated gold film.

The structure consisted of a Co/Pt multilayer was prepared on a quartz substrate by magnetron sputtering and covered with a nanostructured gold film using thermal evaporation in vacuum. The magnetic multilayer contained the following layer sequence: Pt(20 Å)/Co(6 Å)/Pt(8 Å)/Co(6 Å)/Pt(8 Å)/Co(6 Å)/Pt(60 Å), while the top Au layer had a thickness of 100 nm. The gold film with a periodic square lattice of circular nanoholes with a hole radius of $r_{Au}$ = 240 nm and a lattice period of d = 775 nm was fabricated by electron-beam lithography. Such nanopatterning of the metal layer enables resonant plasmon excitation in the structure. As a result, the transmission spectra exhibited distinct resonant signatures in the 780-800 nm spectral range, which can be attributed to plasmonic lattice modes supported at the Au/air interface.

At normal incidence, the magneto-optical measurements revealed a pronounced enhancement of the Faraday rotation angle in the vicinity of the plasmonic resonances compared to non-resonant spectral regions. The enhancement is attributed to efficient coupling of dipolar modes localized within the nanoholes, i.e., to increased energy transfer into orthogonally polarized modes, leading to emission with the rotated polarization [3]. These results suggest that the observed enhancement of the Faraday effect may also be accompanied by an enhancement of the inverse Faraday effect [4], capable of generating strong effective magnetic fields and enabling ultrafast magnetization reversal in magnetic domains.

This work was supported by the Russian Science Foundation (project No. 24-12-00210).

[1] F. Cheng, Z. Du, B. Yao, L. Pan, X. Guo, J. Tang, H. Zhang, Q. Xu, X. Zhou, and Y. Liu, All-Optical Helicity-Dependent Switching in Hybrid Metal-Ferromagnet Thin Films, Advanced Optical Materials, 8, 2000379, (2020).
[2] Z. Du, B. Yao, and L. Pan, Numerical Study of All-Optical Switching of Ferromagnetic Thin Film Using Temporally Controlled Optothermal and Optomagnetic Pulses, Optics and Lasers in Engineering, 150, 106860, (2022).
[3] N. Maccaferri, A. Berger, S. Bonetti, V. Bonanni, M. Kataja, Q. H. Qin, S. van Dijken, Z. Pirzadeh, A. Dmitriev, J. Nogués, J. Åkerman, and P. Vavassori, Tuning the Magneto-Optical Response of Nanosize Ferromagnetic Ni Disks Using the Phase of Localized Plasmons, Physical Review Letters, 111, 167401, (2013).
[4] M. Battiato, G. Barbalinardo, and P. M. Oppeneer, Quantum Theory of the Inverse Faraday Effect, Physical Review B, 89, 014413, (2014).

# Use of molybdenum Oxide (VI) as matrix for thin film organic-inorganic luminescent hybrid materials

**D.Volkov, V. Kirilina, R. Avetisov**

*Mendeleev University of Chemical Technology of Russia,*
*125480, Moscow, 20 Geroyev Panfilovtsev Street, Building 1*

*daniilvolkov121810@gmail.com*

OLED devises have a number of disadvantages: low thermal and chemical stability, high cost of synthesizing organic semiconductors, forming the light-emitting diode itself and low stability of organic films. The use of inorganic matrix would solve the problem of low stability of OLED devices. The idea of combining inorganic and organic compounds in a finished product, which can compensate for each other's shortcomings in a symbiotic way, gave rise to hybrid materials (HM) - nanocomposite materials whose components are usually less than 1 micron apart. [1].

One of the promising materials for the formation of hybrid organo-inorganic materials by thermal evaporation in a vacuum is molybdenum (VI) oxide. This compound has high thermal stability, no polymorphic transitions, and a high vapor pressure. The highest molybdenum oxide, $MoO_3$, is a wide-band n-type semiconductor compound (Eg = 3.0-3.2 eV). [2, 3].

Hybrid organo-inorganic structures with different thicknesses of the organic and inorganic components were obtained based on molybdenum (VI) oxide and aluminum 8-hydroxyquinolate. The photoluminescence spectra of these hybrid materials were studied at an excitation wavelength of 310 nm.

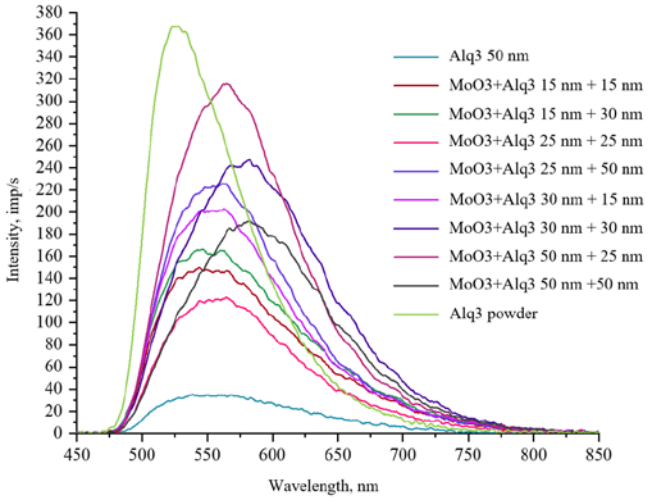


**Fig. 1.** PL spectra of fabricated HM based on molybdenum oxide (VI) and aluminum 8-hydroxiquinolinate.

[1] Runina, K. I. Chemical Foundations of Hybrid Organic-Inorganic Luminescent Materials Technology: Speciality 2.6.7 "Technology of Inorganic Substances": Dissertation for the Degree of Candidate of Chemical Sciences / Runina Kristina Igorevna. — Moscow, 2021. — 157 p.
[2] Zarifov Sh. S. STUDY OF MOLYBDENUM NANOSTRUCTURES AND THEIR OXIDES //Economics and Society. – 2026. – No. 3-1 (142). – Pp. 642-645.
[3] Al-Hailani, H. I. D. The Influence of Formation Conditions on the Atomic Structure and Optical Properties of Wide-Band Semiconductor Micro- and Nanostructures of $MoO_3$ and $MoS_2$. Dissertation for the Degree of Candidate of Physical and Mathematical Sciences. Voronezh, 2019. 111 p.

# From Ag Nanopillar–Nanoflower Arrays to Endotaxial Ag Nanoparticles in Si: Periodic Ordering via Lithographically Controlled Galvanic Displacement

**Yu.A. Zharova[1], E.S. Fedorova[1,2], D.P. Markov[1], A.A. Ermina[1], N.S. Solodovchenko[1,3], V.O. Bolshakov[1], K.V. Prigoda[1], A.O. Larin[3]**

*1- Ioffe Institute, Polytechnicheskaya street 26, 194021, St. Petersburg, Russia*
*2- Peter the Great Saint-Petersburg Polytechnic University, Polytechnicheskaya street 29, 195221, St. Petersburg, Russia*
*3- ITMO University, Kronverksky Prospect 49, building A, 197101, St. Petersburg, Russia*

*piliouguina@mail.ioffe.ru*

Excitation of localized plasmon resonance (LPR) in metallic nanostructures is accompanied by strong localization of the electromagnetic field near the surface of nanoparticles, as well as a pronounced enhancement of the absorption and scattering of light at the resonant frequency [1]. These effects lead to a unique optical response of plasmonic nanostructures and underlie a wide range of applications, including sensorics [2], energy [3], nonlinear optics [4], surface-enhanced Raman scattering (SERS), and biosensors [5–6]. The spectral position and intensity of LPR significantly depend on the material, size, shape of nanoparticles (NPs), and the surrounding medium. Therefore, controlling the morphology and spatial arrangement of metallic nanoparticles is one of the key approaches to tuning their optical response. Unlike disordered arrays, where the «hot spots» distribution and spectral response are poorly reproducible, ordered arrays provide more controllable optical properties and can support high-Q collective lattice resonances [7].

To create such structures, we proposed for the first time a lithographically controlled galvanic displacement (LCGD) method, which enables the reproducible formation of ordered Ag nanostructures on a Si(100) substrate with controlled morphology. The developed approach combines (i) electron beam lithography, which defines the structure's topology, and (ii) a galvanic displacement reaction from an $AgNO_3$/HF solution, which ensures the growth of the metallic nanostructure. In this study, three types of ordered Ag nanostructures were created on Si: «nanoflowers,» «nanopillars,» and endotaxial pyramidal AgNPs. A mask made of electron-beam resist or a thermally grown $SiO_2$ layer served as a physical template guiding the growth of Ag. Ordered arrays of nanostructures were thus obtained, ranging from «nanoflowers» (with diameters (d) ranging from 50 to 300 nm) to vertical nanopillars (with d ~ 50 nm and a height of ~ 200 nm). Subsequent high-temperature annealing of the Ag «nanoflowers» in a humid atmosphere (at 1000 °C) allowed the creation of ordered endotaxial AgNPs in the shape of tetrahedral «pyramids». The morphology of the resulting structures was studied using scanning electron microscopy. Their optical properties were investigated using spectroscopic ellipsometry and elastic scattering spectroscopy in dark-field geometry. The potential application of the created structures as SERS substrates for detecting low concentrations of triphenylmethane brilliant green dye was also explored. The developed LCGD method is characterized by its technological simplicity and reproducibility. It is of interest for scaling to smaller periods and sizes of nanoparticles, and also opens up new possibilities for forming nanostructures with a given topology and shape. However, potential limitations on minimum characteristic dimensions will most likely be determined by the maximum resolution of electron-beam lithography.This work was supported by the Ministry of Science and Higher Education of the Russian Federation under a state assignment (project no. FFUG-2024-0017).

[1] U. Kreibig, M. Vollmer. Optical properties of metal clusters (Berlin, Springer, 2013).
[2] M. Pan, J. Yang, K. Liu, Z. Yin, T. Ma, S. Liu, L. Xu, S. Wang, Noble Metal Nanostructured Materials for Chemical and Biosensing Systems, Nanomaterials, 10(2), 209 (2020).
[3] H. A. Atwater, A. Polman, Plasmonics for improved photovoltaic devices, Nat. Mater., 9, 205-213 (2010).
[4] Z.-W. Yang, L. Meng, J.-S. Lin, W.-M. Yang, 3D Hotspots Platform for Plasmon Enhanced Raman and Second Harmonic Generation Spectroscopies and Quantitative Analysis, Adv. Opt. Mater., 7(23), 1901010 (2019).
[5] J. Aizpurua, R. Hillenbrand. Localized surface plasmons: basics and applications in field-enhanced spectroscopy (Berlin, Springer, 2012).
[6] A.A. Ermina, N.S. Solodovchenko, K.V. Prigoda, V.S. Levitskii, V.O. Bolshakov, M. Yu. Maximov, Y.M. Koshtyal, S.I. Pavlov, V.A. Tolmachev, Y.A. Zharova, Silver particles embedded in silicon: The fabrication process and their application in surface enhanced Raman scattering (SERS), Appl. Surf. Sci, 608, 161771 (2023).
[7] Wurtz G.A., Dickson W., O'Connor D., Atkinson R., Hendren W., Evans P., Pollard R., Zayats A.V. Guided plasmonic modes in nanorod assemblies: strong electromagnetic coupling regime // Opt. Express. 2008. V. 16. № 10. P. 7460–7470.

ALT INTERNATIONAL CONFERENCE
Advanced Laser Technologies

# NONLINEAR AND TERAHERTZ PHOTONICS

# Study of polyps of different life support systems organs by high-resolution THz spectroscopy

**V.L. Vaks[1,2], E.G. Domracheva[1,2], M.B. Chernyaeva[1,2], V.A. Anfertev[1], K.A. Glushkova[3], A.S. Cherniaeva [1], V.A. Atduev[1,4,5], K.A. Atduev[1,4]**

*[1]Institute for Physics of Microstructures RAS 603950, Nizhny Novgorod, GSP-105*
*[2]Lobachevsky University 603022, Nizhny Novgorod, Gagarina av., 23*
*[3] Children Clinical Hospital No.1, 603081, Nizhny Novgorod, Gagarina av., 76*
*[4]Privolzhsky District Medical Center of the Federal Medical and Biological Agency of Russia, 2 Nizhnevolzhskaya embankment, Nizhny Novgorod*
*[5]Privolzhsky Research Medical University 10/1 Minin and Pozharsky sq., Nizhny Novgorod*

*elena@ipm.sci-nnov.ru*

Metabolic approaches to diagnosing various diseases and pathologies are currently being actively developed worldwide. In clinical settings, study and analysis of biological tissue is performed solely through histological or chemical analysis. Among physical methods, gas and liquid chromatography, often combined with mass spectrometry, are most commonly used to identify pathological metabolite markers in biological samples. Furthermore, spectroscopic methods, including those in the THz frequency range, can be used in such studies. Terahertz spectroscopy, based on transient effects and possessing both high resolution and sensitivity [1], enables the identification of the composition of thermolysis products of polyp tissues from various organs and life-support systems. Differences in the chemical composition of thermal decomposition products between healthy and pathologically altered tissues provide information on the potential sets of marker molecules for a specific pathology. This work is devoted to the study of the chemical composition of secondary metabolites formed during thermal decomposition of polyps of various organs of the body's life support systems, using high-resolution THz spectroscopy.

Spectroscopic measurements were conducted using a high-resolution THz spectrometer (with an operating range of 118-175 GHz) with phase-switched gas-induced radiation developed by the authors [1]. The tissue samples were heated, and a mixture of vapor and gaseous thermal decomposition products was introduced into a pre-evacuated measuring cell. Using online spectroscopic data catalogs, substances whose composition differed between healthy and pathologically altered tissues were identified based on the identified spectral lines. The markers were compared with markers identified in previous studies of ENT polyps [2]. The list of substances in the thermal decomposition products of polyp tissue includes a number of organic acids, aldehydes, nitriles and some organic compounds. Identifying the precursors in polyp tissues of the same type in organs of various life-support systems and identifying differences between polyps and healthy tissues may be the first step toward determining the metabolic profile of tissues during polyps growth.

This research was funded by the Russian Science Foundation, grant No. 24-19-00623, https://rscf.ru/en/project/24-19-00623/.

[1] Vaks V.L., Anfertev V.A., Balakirev V.Yu., Basov S.A., Domracheva E.G., Illyuk A.V., Kupriyanov P.V., Pripolzin S.I., Chernyaeva M.B. High resolution terahertz spectroscopy for analytical applications // Phys. Usp., **63**, 708–720 (2020), DOI 10.3367/UFNe.2019.07.038613.
[2] Vaks, V.; Anfertev, V.; Ayzenshtadt, A.; Chernyaeva, M.; Domracheva, E.; Glushkova, K.; Larin, R.; Shakhova, M. Novel Approaches in the Diagnostics of Ear-Nose-Throat Diseases Using High-Resolution THz Spectroscopy. Appl. Sci. **2023**, 13, 1573. https://doi.org/10.3390/app13031573

# Correlation of optical and terahertz photons generated in a non-collinear scheme of parametric down-conversion

**G. Kitaeva, T. Novikova, A. Osipenkov, P. Prudkovskii**

*Lomonosov Moscow State University, Leninskie Gory 1-2, Moscow 119991 Russia*

*gkitaeva@physics.msu.ru*

We study correlation of optical and terahertz-frequency (THz) photons generated in a non-collinear scheme of strongly non-degenerate parametric down-conversion (PDC) in non-linear Mg:$LiNbO_3$ crystal, *type-0* geometry, under pumping by 20 ns pulses of the 2nd harmonic of $Nd^{3+}$:YLF laser at 532 nm wavelength [1]. THz photons at idler frequencies $\omega_i=\omega_{THz}$ leave the crystal through its side surface equipped with a special silicon adapter, pass through spectral-selective filters and are detected by a hot electron bolometer HEB. To exclude any contribution from the external thermal radiation at THz frequencies, the crystal is placed in the same cryostat as the bolometer's sensing element and is maintained at a temperature ~4.5K; the input and output cryostat windows are equipped with ITO filters, that are opaque at THz frequencies. The optical photons at conjugated signal frequencies $\omega_s = \omega_p - \omega_{THz}$ pass the windows, propagate through the system of spectral and angular selection, and are detected by a photo-multiple tube (PMT) receiver. The biphoton correlation function $g^{(2)}$ is determined based on the statistical distributions of the simultaneous detected readings from PMT ($i_{opt}$) and HEB ($i_{HEB}$), The quantum excess of the correlation function $g^{(2)}$*-1* measured in this way turns out to be approximately two orders of magnitude higher than the expected value calculated simply as $1/N_{THz}$, where $N_{THz}$ is a number of detected THz photons [2].

To understand this discrepancy, we revised the standard PDC theory by taking into account the case of the geometry that is highly noncollinear with respect to the idler (in our case, THz) waves. In the considered configuration, the idler photons are produced at a large angle $\theta_i$ to the pump and leave the nonlinear interaction region through the lateral surface of the crystal, while the signal photons propagate at negligeabe angle $\theta_s \approx \sin \theta_i k_i / k_s$ (here, $k_i$, $k_s$ are the wavevectors) and interact with the pump radiation along the whole crystal length. Using a simple example of two-dimentional single-mode interaction under phase-matched conditions, it will be shown that in this case the PDC parameters, such as the biphoton correlation function and the numbers of idler and signal photons per mode, depend on the parametric gain differently than in the usual case of collinear PDC. The higher the ratio $K \approx tg\theta_i / tg\theta_s$, the greater is the difference compared to generally accepted dependencies.

The obtained results reveal specific features of the quantum characteristics of PDC in non-collinear geometry. Taking into account the potential negative or, conversely, positive influence of these features is necessary in further developing schemes for generating single-photon states, quantum ghost imaging, absolute calibration of single-photon detectors, and other PDC-based applications.

The work was done under financial support of the Russian Science Foundation, grant No. 22-12-00055-П.

[1] T.I. Novikova, K.A. Kuznetsov, I.V. Korolev, I.V. Pentin, P.A. Prudkovskii, G.Kh. Kitaeva, Statistical features of the response of a superconducting hot-electron bolometer to extremely weak terahertz pulses of picosecond and nanosecond duration, Applied Physics Letters, vol. 125, p. 124004 (2024).
[2] T.I. Novikova, A.A. Leontyev, G.Kh. Kitaeva, Measurement of the quantum efficiency of analog detectors in the field of parametric down-conversion, JETP Letters, vol. 116, pp. 353–359 (2022).

# Nitrogen-doped diamond as a new material for high-power photoconductive terahertz antenna

**M. Komlenok, V. Kononenko, T. Kononenko, T. Dolmatov, A. Bolshakov**

*Prokhorov General Physics Institute of the Russian Academy of Sciences, Vavilova 38, Moscow, Russia*

*komlenok@nsc.gpi.ru*

Diamond doping has enabled the use of commercially available femtosecond (fs) infrared lasers for optical pumping of photoconductive antennas (PCAs) [1] instead of complex UV fs lasers for generating photocarriers in pure diamond [2]. However, the demonstrated power of the generated terahertz radiation is still far from the maximum achievable level. The main limiting factor is that the electrodes generating the electric field in the diamond substrate are located on the diamond surface, and the bias voltage level is limited by electrical breakdown across the diamond surface (20 kV/cm). Such antennas do not utilize the potential of the diamond substrate to achieve peak power. Their parameters do not exceed those of antennas made of narrow-gap semiconductors. Increasing the peak power requires the implementation of multipole antennas, i.e., antennas containing multiple emitters over a large area. A multiple increase in the THz radiation intensity is achieved by reducing the distance between the electrodes in each dipole and, correspondingly, increasing the intensity of the static electric field. To utilize the full potential of diamond, it is necessary to create conductive structures inside the diamond bulk. This work demonstrates the possibility of embedding conductive structures into the diamond bulk to significantly increase the electric field in the antenna.

This research was funded by the Russian Science Foundation, grant number 25-19-00796, https://rscf.ru/en/project/25-19-00796/.

[1] H. Yoneda, K. Tokuyama, K. Ueda, H. Yamamoto, K. Baba, High-power terahertz radiation emitter with a diamond photoconductive switch array, Applied Optics, vol. 40, pp. 6733–6736, (2001).
[2] P.A. Chizhov, M.S. Komlenok, V.V. Kononenko, V.V. Bukin, A.A. Ushakov, V.V. Bulgakova, A.A. Khomich, A.P. Bolshakov, V.I. Konov, S.V. Garnov, Photoconductive terahertz generation in nitrogen-doped single-crystal diamond, Optics Letters, vol. 47(1), pp. 86-89, (2022).

# Probing Structural Symmetry Breaking in TMDC Alloy via Terahertz Emission

**E. Chiglintsev, F. Shuklin, K. Shevyakova, A.V. Syuy, D.I. Yakubovskiy, A. Chernov**

*Center for Photonics and 2D Materials, Moscow Institute of Physics and Technology, Institutskiy per., 9, Dolgoprudny, 141700, Moscow Region, Russia*

*chiglintsev.eo@phystech.edu*

Terahertz (THz) emission spectroscopy has emerged as an exceptionally powerful and versatile technique for comprehensively investigating structural symmetry and internal built-in electric fields within various layered materials [1]. In the case of pristine transition metal dichalcogenides (TMDs), the generation of THz radiation is primarily driven by well-established mechanisms such as second-order optical rectification or ultrafast transient photocurrents [2]. However, due to the strict constraints imposed by the inherent crystal symmetry of these pristine materials, the efficient generation and emission of THz radiation propagating directly along the sample normal remains heavily restricted or completely forbidden.

In this work, we systematically investigate the generation of THz emission in bulk single crystals of the ternary $Mo_{0.5}W_{0.5}Se_2$ alloy, a system that presents a natural and elegant pathway for tailoring intrinsic material properties through controlled compositional modulation. Within these specific alloys, the material undergoes a phase arrangement that forms quasi-ordered, stripe-like domains [3]. These localized domains are alternatingly rich in molybdenum (Mo) and tungsten (W), thereby acting as a dense, interconnected network of lateral heterojunctions that harbor strong local built-in electric fields.

A detailed comparative analysis of the resulting THz emission was conducted under optical excitation using femtosecond laser pulses at two distinct wavelengths: 515 nm (corresponding to above-bandgap excitation) and 1030 nm (corresponding to below-bandgap excitation). This investigation unveiled fundamental, qualitative differences in their underlying physical generation mechanisms. Under the above-bandgap excitation regime (515 nm), the peak amplitude of the generated THz signal exceeds the sub-bandgap photoresponse by more than an order of magnitude. Furthermore, systematic measurements of the THz electric field as a function of the pump laser fluence, excitation polarization angle, and sample azimuthal angle conclusively confirm that the dominant generation mechanism in this scenario is driven by an ultrafast, in-plane transient photocurrent.

The key and most prominent finding of this study is the observation of intense THz emission that propagates directly along the normal to the sample surface, even under a strictly normal incidence configuration of the optical pump beam. This intriguing phenomenon strongly indicates the emergence of a macroscopic, uncompensated net photocurrent. This directional current arises precisely because the unique, quasi-ordered morphology of the alloy's phase-separated stripe domains effectively breaks the macroscopic lateral symmetry of the crystal plane.

In conclusion, THz emission spectroscopy is successfully demonstrated to be a highly reliable, non-contact, and non-invasive diagnostic method for probing structural anisotropy and internal built-in fields in complex van der Waals materials. Furthermore, the discovered phenomenon of robust surface-normal THz emission renders these engineered TMD alloys highly promising candidates for integration into next-generation optoelectronic technologies, specifically for developing ultracompact, vertical, on-chip THz emitters.

This research was supported by the Russian Science Foundation under grant № 25-12-00154.

[1] Y. Wu et al., "Emerging probing perspective of two-dimensional materials physics: terahertz emission spectroscopy," Light Sci. Appl. 13, 146 (2024).
[2] Y. Huang et al., "Surface optical rectification from layered mos2 crystal by thz time-domain surface emission spectroscopy," ACS Appl. Mater. Interfaces 9, 4956–4965 (2017).
[3] A. Azizi et al., "Spontaneous formation of atomically thin stripes in transition metal dichalcogenide monolayers," Nano Lett. 16, 6982–6987 (2016).

# Optically pumped THz modulation in 2D transition metal dichalcogenide/ silicon heterostructures

**K. Brekhov, E. Bulavintseva, M. Lapteva, S. Lavrov, E. Mishina**

*MIREA - Russian Technological University, Vernadsky Avenue 78, Moscow, 119454, Russia*

*brekhov_ka@mail.ru*

With the rapid development of terahertz (THz) technologies, the THz radiation in the 0.1–10 THz frequency range, is increasingly finding applications in both scientific research and advanced technological applications. To date, THz waves have been employed in a wide range of fields, including next-generation telecommunications, security screening, non-destructive quality control, medical diagnostics and pharmaceutical analysis due to their high spectral resolution, broad bandwidth, better penetration depth, low photo energy, and high transparency.

However, the further progress of THz technology is limited by the lack of highly efficient active electro-optical devices for THz-wave control, primarily modulators. These devices are essential for tuning the amplitude, phase, or polarization of THz waves in information transmission systems. Although electrical and magnetic approaches to THz modulation have been proposed, they still suffer from several drawbacks, including low modulation depth, the need for electrode fabrication and slow modulation speed.

In contrast, all-optical modulation offers enhanced flexibility and simpler control of THz waves through optical illumination of active devices. All-optically controlled THz modulators provide several key advantages, including higher modulation depth, faster response, broader bandwidth, and improved sensitivity. In these devices, THz-wave modulation depends on the changes in the absorption coefficient induced by optical excitation [1].

Semiconductors, including 2D transition metal dichalcogenides (TMDs) and TMD/silicon heterostructures, are among the most promising materials for all-optical THz modulators. The unique characteristics of 2D TMDs, such as atomic thickness, fast charge carrier recombination, moderate band gap, and high lateral carrier mobility, enable efficient control of their electronic and optical characteristics by irradiating them with optical pump, which generates charge carriers and excites excitons in these materials. An important practical advantage of these materials is their compatibility with silicon technology, enabling cost-effective and scalable integration into semiconductor devices. Therefore, a comprehensive investigation of relationship between photogenerated carriers and the corresponding changes in optical properties of 2D TMD/silicon heterostructures in THz range as well as optically induced THz modulation in these structures, is both an important and relevant tasks.

Here, we present the results of the THz modulation amplitude study in the range up to 2.5 THz in TMD/silicon heterostructures fabricated by liquid-phase exfoliation [2] and high-resistivity silicon substrate. We compare the results obtained using both CW and pulsed visible/IR lasers as optical pumps. We also present calculations of the optically induced photoconductivity change in the studied structures, which explain the experimentally observed dependences.

This work was supported by the Russian Science Foundation, grant № 25-19-00575.

[1] S. Ghosh, K. Bhattacharya et. al, Optically pumped ultrafast and broadband terahertz modulation with scalable molecular beam epitaxy grown MoTe2/Si heterostructures, Adv. Mater. Technol., 10, 2402036, (2025).

[2] Е. Булавинцева, Д. Абдуллаев, Е. Лебедева и др., Свойства пленок дихалькогенидов переходных металлов, полученных методом жидкофазной эксфолиации, для терагерцовой спектроскопии, Физика твердого тела, том 68, вып. 4, сс. 649-659, (2026).

# Broadband spectroscopy of astrophysical ice analogues: recent results, possibilities and perspectives

**A.A. Gavdush[1], M.K. Matveishina[1], B.M. Giuliano[2], K.I. Zaytsev[1], A.V. Ivlev[2], P. Caselli[2]**

*1- Prokhorov General Physics Institute of the Russian Academy of Sciences, Russia, 119991 Moscow, Russia*
*2- Max-Planck-Institut für Extraterrestrische Physik, Gießenbachstraße 1, Garching 85748, Germany*

*arsenii.a.gavdush@gmail.com*

Ices of different molecular compositions, phases, and morphologies in gas-dust clouds and protoplanetary disks serve as a reservoir of key volatile elements, impact the properties of emerging planetary systems, growth, migration, coagulation, and evaporation cooling of the fundamental building blocks of planets – the dust grains, thermodynamics, chemistry, and mass transfer in a disk, efficiency of planetesimal formation, and other phenomena. All mentioned problems [1] requires understanding the physical and chemical properties of interstellar and circumstellar ices and their structure. For instance, optical properties of astrophysical ices of different molecular composition, phases, porosities, are required to model both the continuum emission by the dust grains covered with thick icy mantles and the radiative transfer in the dense cold regions of the interstellar medium [2-4]. Moreover, the structural features of ices, such as their porosity, significantly affect the evolution of the chemical composition of ices, whereas, according to laboratory astrophysics, such features depend on a variety of factors and are a subject of distinct research [5-8].

Our ongoing research series [8-12] is focused on the broadband optical properties of various laboratory ice analogues including CO, $CO_2$, $N_2$ and $H_2O$ ices. In these works, we discuss the preparation of ice analogues in the laboratory, the methodology of their spectroscopy, processing and analysis of the experimental data. Among the obtained results, the most important include the broadband dielectric and optical properties of ices, analysis of the structural ice features and the scattering of electromagnetic radiation in ices. Approaches developed in our research are relevant for modern laboratory astrophysics and has broad prospects in systematic studies of laboratory analogues of interstellar and circumstellar ices.

This work was supported by the Russian Science Foundation (RSF), Project 25-72-00139.

[1] A.C.A. Boogert, P.A. Gerakines, D.C.B. Whittet, Observations of the Icy Universe, Annual Review of Astronomy and Astrophysics, vol. 53(1), pp. 541–581 (2015).
[2] S.L. Widicus Weaver, Millimeterwave and Submillimeterwave Laboratory Spectroscopy in Support of Observational Astronomy, Annual Review of Astronomy and Astrophysics, vol. 57(1), pp. 79–112 (2019).
[3] D.V. Mifsud et al., The Role of Terahertz and Far-IR Spectroscopy in Understanding the Formation and Evolution of Interstellar Prebiotic Molecules, Frontiers in Astronomy and Space Sciences, vol. 8 (2021).
[4] D.V. Mifsud et al., Sulfur Ice Astrochemistry: A Review of Laboratory Studies, Space Science Reviews, vol. 217(1), pp. 14 (2021).
[5] J.H.E. Cartwright, B. Escribano, C.I. Sainz-Diaz, The Mesoscale Morphologies of Ice Films: Porous and Biomorphic Forms of Ice under Astrophysical Conditions, The Astrophysical Journal, vol. 687(2), pp. 1406-1414 (2008)
[6] M.J. Loeffler, M.H. Moore, P.A. Gerakines, The effects of experimental conditions on the refractive index and density of low-temperature ices: solid carbon dioxide, The Astrophysical Journal, vol. 827(2), pp. 98 (2016)
[7] C. Millán, C. Santonja, M. Domingo, R. Luna, M. Á. Satorre, An experimental test for effective medium approximations (EMAs): Porosity determination for ices of astrophysical interest, Astronomy & Astrophysics, vol. 628, pp. A63 (2019)
[8] A.A. Gavdush et al., Broadband spectroscopy of astrophysical ice analogues: III. Scattering properties and porosity of CO and CO2 ices, Astronomy & Astrophysics, vol. 701, pp. A287 (2025).
[9] B.M. Giuliano et al., Broadband spectroscopy of astrophysical ice analogues: I. Direct measurement of the complex refractive index of CO ice using terahertz time-domain spectroscopy, Astronomy & Astrophysics, vol. 629, pp. A112 (2019).
[10] A.A. Gavdush et al., Broadband spectroscopy of astrophysical ice analogues: II. Optical constants of CO and CO2 ices in the terahertz and infrared ranges, Astronomy & Astrophysics, vol. 667, pp. A49 (2022).
[11] F. Kruczkiewicz et al., Broadband spectroscopy of astrophysical ice analogues: IV. Optical constants of $N_2$ ice in the terahertz and mid-infrared ranges, DOI: 10.1051/0004-6361/202556818 (2026).
[12] A.A. Gavdush et al., Broadband spectroscopy of astrophysical ice analogues. V. Optical constants of Ih, Ic, and amorphous $H_2O$ ices in the terahertz-infrared range / Astronomy & Astrophysics, vol. 710, pp. A89 (2026).

# Hybridization of Kerr Solitons in Coupled Microresonators

**A.Yu. Kolesnikova, I.A. Pshenichnyuk, A.A. Gelash**

*Skolkovo Institute of Science and Technology, Moscow, 121205, Russia*

*a.kolesnikova@skoltech.ru*

Hybridization of physical systems is a fundamental phenomenon responsible for the formation of complex structures in nature, as illustrated by the well-known omnipresent linear mixing of atomic orbitals [1]. Nonlinear interactions result in fundamentally different hybridized states emerging beyond the conventional superposition of the system components. In optics, the coupling of nonlinear soliton coherent states of light has recently been experimentally demonstrated, promising various applications in the development of photonic devices [2–5].

We report theoretical prediction of a novel phenomenon in nonlinear photonics: the formation of hybridized dissipative Kerr solitons (DKS) in coupled microresonator systems [6]. This research reveals a fundamentally new type of coherent light states that cannot be generated in single-component setups.

The system under investigation consists of two coupled optical microresonators with opposite dispersion properties (normal and anomalous) and equal free spectral range. The key feature of this configuration is the ability to create hybridized dispersion landscapes through inter-resonator coupling.

The main findings demonstrate the observation of fully coherent soliton states in both resonators, formed via an unconventional four-wave mixing process. These hybridized solitons generate unique optical frequency combs characterized by flat-topped spectra near the pump frequency and high-power spectral lines (see Fig.1).

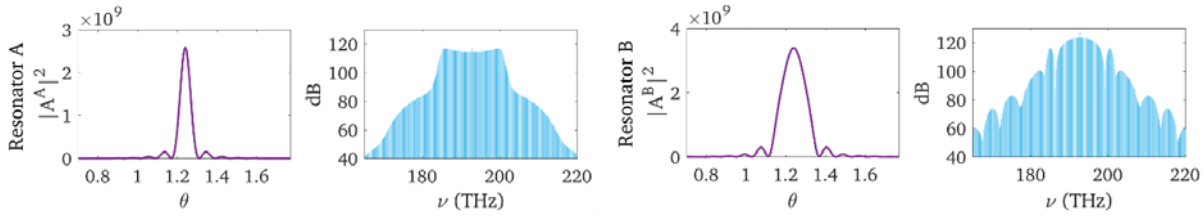


**Fig. 1.** Numerical modeling of fully coherent hybridized DKS and its flat-topped optical frequency comb in each $Si_3N_4$ microresonator.

The physical mechanism behind this phenomenon is based on the nonlinear hybridization of coherent optical pulses in the supermode basis of the coupled system. The resulting soliton states cannot be described by a single Lugiato-Lefever equation, demonstrating a truly multicomponent nature.

Experimental realization is proposed on a silicon nitride ($Si_3N_4$) platform, where precise control over system parameters (pump power, coupling strength, and dispersion) is achievable. The platform allows for tuning of hybridized dispersion and control via heating mechanisms.

The practical significance of this discovery lies in potential applications for advanced telecommunications systems, high-precision frequency metrology, and integrated photonic devices. Future research directions include investigating the effect of Vernier detuning and exploring lattice configurations of microresonators.

This work opens new perspectives in the field of integrated photonics, providing a platform for generating and controlling complex coherent light states with tailored spectral properties. The observed hybridized solitons represent a new class of nonlinear coherent states with promising applications in modern photonics.

This work was supported by Russian Science Foundation project № 25-72-31023.

[1] K. Ruedenberg, The phusical nature of the chemical bound, Reviews of Modern Physics 34, 326 (1962).
[2] A. Tikan, J. Riemensberger, K. Komagata, S. H¨onl, M. Churaev, C. Skehan, H. Guo, R. N. Wang, J. Liu,P. Seidler, and T. J. Kippenberg, Emergent nonlinear phenomena in a driven dissipative photonic dimer, Nature Physics 17, 604 (2021).
[3] Z. Yuan, M. Gao, Y. Yu, H. Wang, W. Jin, Q.-X. Ji, A. Feshali, M. Paniccia, J. Bowers, and K. Vahala, Soliton pulse pairs at multiple colours in normal dispersion microresonators, Nature Photonics 17, 977 (2023).
[4] Q.-X. Ji, P. Liu, W. Jin, J. Guo, L. Wu, Z. Yuan, J. Peters, A. Feshali, M. Paniccia, J. E. Bowers, et al., Multimodality integrated microresonators using the Moire speedup effect, Science 383, 1080 (2024).
[5] T. P. Letsou, D. Kazakov, P. Ratra, L. L. Columbo, M. Brambilla, F. Prati, C. Rimoldi, S. Dal Cin, N. Opa˘cak, H. O. Everitt, et al., Spectral Dynamics in Broadband Frequency Combs with Overlapping Harmonics, Physical Review Letters 134, 023802 (2025).
[6] A. Kolesnikova, I. Pshenichnyuk, & A. Gelash, Hybridization of Kerr Solitons in Coupled Microresonators. arXiv preprint arXiv:2604.21609 (2026).

# Even harmonic generation from the air-based femtosecond plasma for remote sensing applications

**O.G. Kosareva[1,2], I.A. Nikolaeva[1,2], D.E. Shipilo[1,2], N.A. Panov[1,2], G.E. Rizaev[1,2], A.V. Koribut[1,2], D.V. Pushkarev[1], Ya.V. Grudtsyn[1,2], A.B. Savel'ev[1,2], L.V. Seleznev[1,2], A.A. Ionin[2], A.P. Shkurinov[1]**

*1 -Faculty of Physics, Lomonosov Moscow State University, Moscow, Russia*
*2 - Lebedev Physical Institute RAS, Moscow, Russia*

*kosareva@physics.msu.ru*

Experimental [1,2] and theoretical [3–5] study of terahertz (THz) and the second harmonic radiation from a single-color plasma channel is important for remote spectroscopy applications, especially when the even harmonics' yield is enhanced using multiple filaments from terawatt peak power femtosecond laser [2].

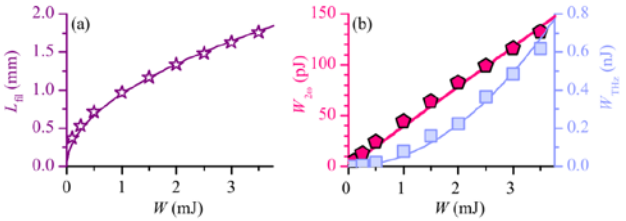


**Fig. 1.** Dependence of (a) the filament length $L_{fil}$, (b) the second-harmonic $W_{2\omega}$ (pink pentagons) and the terahertz $W_{THz}$ (lilac squares) energy on the laser pulse energy $W$.

We measured spectral and 2D spatial distribution in the far-field of the second harmonic and terahertz generated in a single-color 940 nm, 90-fs, 3.5-mJ filament in air in loose and tight focusing geometry. We developed a numerical approach to simulate this radiation using the Stratton-Chu vectorial diffraction integral [6], in which the second-order nonlinear current was obtained at each propagation step from the solution of Unidirectional Pulse Propagation Equation and integrated over distance to get the far field spectral and spatial distribution of the 2nd harmonic and the THz. The energy yield of these even harmonics was obtained through integration over the transverse spatial domain and spectrum at the end of the plasma channel. Such integration procedure was performed for each initial laser pulse energy and focusing geometry.

In agreement with the experiment, the second harmonic energy varies directly proportional to the initial laser pulse energy and, respectively, directly proportional to the squared filament length in the range 0.1 – 3.5 mJ (Fig.1). In the same conditions the terahertz energy varies as the square of the initial pulse energy (Fig.1b). The difference in the THz and second harmonic scaling with the initial pulse energy is associated with different sources arising from the ponderomotive and the light pressure force contributions to the second-order photocurrent. The major source of the second harmonic is the ponderomotive force, while the light pressure almost vanishes at the doubled carrier frequency [7]. Instead, the main contribution to the THz yield comes from the light pressure force, while the ponderomotive force adds up at the selected frequencies only.

[1] C. D'Amico, A. Houard, M. Franco, B. Prade, A. Mysyrowicz, A. Couairon, and V. T. Tikhonchuk, Conical forward THz emission from femtosecond-laser-beam filamentation in air, Phys. Rev. Lett. 98, 235002 (2007).
[2] E. Mitina, D. Uryupina, I. Nikolaeva, D. Shipilo, N. Panov, A. Ushakov, R. Volkov, O. Kosareva, A. Savel'ev Enhanced forward THz yield from the long DC-biased femtosecond filament, Optics and Laser Technology 159, 108949 (2023).
[3] P. Sprangle, J.R. Penano, B. Hafizi, and C.A. Kapetanakos, Ultrashort laser pulses and electromagnetic pulse generation in air and on dielectric surfaces, Phys. Rev. E 69, 066415 (2004).
[4] I. Thiele, R. Nuter, B. Bousquet, V. Tikhonchuk, S. Skupin, X. Davoine, L. Gremillet, and L. Berg´e, Theory of terahertz emission from femtosecond-laser-induced microplasmas, Phys. Rev. E 94, 063202 (2016).
[5] R.M. Arkhipov, A.V. Pakhomov, M.V. Arkhipov, I. Babushkin, Yu. A. Tolmachev, and N. N. Rosanov, Generation of Unipolar Pulses in Nonlinear Media, JETP Letters, 105, 408 (2017).
[6] J. A. Stratton and L. Chu, Diffraction theory of electromagnetic waves, Phys. Rev. 56, 99 (1939).
[7] I. A. Nikolaeva et al, Second harmonic generation in the air-based femtosecond plasma, Phys. Rev. E 113, 025206 (2026).

# Control of the polarization of coherent radiation from a chiral semiconductor microcavity using resonant optical pumping

**O.A. Dmitrieva[1-3], N.A. Gippius[3], S.G. Tikhodeev[1-3]**

*1- Lomonosov Moscow State University, 119991 Moscow, Russia*
*2- Prokhorov General Physics Institute of the Russian Academy of Sciences, 119991 Moscow, Russia*
*3- Skolkovo Institute of Science and Technology, 121205 Moscow, Russia*

*tikh@gpi.ru*

A theoretical study has been conducted into the possibility of switching the polarization state of coherent radiation from a semiconductor Bragg microcavity featuring exciton-polaritons in the quantum wells of the active layer and a chirally modulated upper mirror. Circularly polarized lasers based on such chiral micro-resonators have been demonstrated under optical [1] and electrical [2] pumping. Furthermore, semiconductor microcavities containing exciton-polaritons exhibit strong bistability and multistability effects—due to the nonlinearity of the latter's optical response—which manifest as abrupt changes in the intensity and polarization of coherent radiation during resonant optical pumping [3-6]. Interest in such devices stems from their potential applications in spectroscopy, sensor technology and information technology. In this work, the characteristics of multistabilities in chiral semiconductor microcavities are investigated. Even if the system is not optimized for obtaining photoluminescence with a high degree of circular polarization in the spontaneous mode, it is shown that linear-polarized pumping can cause [7] nonlinear switching to states with a degree of circular polarization of polaritons up to 90%. Calculations were performed in both the mean-field and self-consistent approximations, accounting for the difference in exciton density among the microcavity's quantum wells.

This research was supported by a grant from the Russian Science Foundation (№22-12-00351-П).

[1] A. A. Demenev, V. D. Kulakovskii, C. Schneider, S. Brodbeck, M. Kamp, S. Нцfling, S. V. Lobanov, T. Weiss, N. A. Gippius, S. G. Tikhodeev, Circularly polarized lasing in chiral modulated semiconductor microcavity with GaAs quantum wells, Appl. Phys. Lett., vol. 109, 171106, (2016).
[2] A. A. Maksimov, E. V. Filatov, I. I.Tartakovskii, V. D. Kulakovskii, S. G. Tikhodeev, C. Schneider, S. Нцfling, Circularly Polarized Laser Emission from an Electrically Pumped Chiral Microcavity, Phys. Rev. Applied, vol. 17, L021001, (2022).
[3] A. Baas, J. Ph. Karr, H. Eleuch, and E. Giacobino, Optical bistability in semiconductor microcavities, Phys. Rev. A, vol. 69, 023809, (2004).
[4] N. A. Gippius, S. G. Tikhodeev, V. D. Kulakovskii, D. N. Krizhanovskii, and A. I. Tartakovskii, Europhys. Nonlinear dynamics of polariton scattering in semiconductor microcavity: Bistability vs. stimulated scattering, Lett., vol. 67, 997, (2004).
[5] N. A. Gippius, I. A. Shelykh, D. D. Solnyshkov, S. S. Gavrilov, Y. G. Rubo, A. V. Kavokin, S. G. Tikhodeev, and G. Malpuech, Polarization Multistability of Cavity Polaritons, Phys. Rev. Lett., vol. 98, 236401, (2007).
[6] S. S. Gavrilov, Nonequilibrium transitions, chaos, and chimera states in exciton-polariton systems, Physics-Uspekhi , vol. 63, pp. 123-144, (2020).
[6] O. A. Dmitrieva, N. A. Gippius, and S. G. Tikhodeev, Multistability of a chiral semiconductor microcavity: a self-consistent approach, Zh. Exp. Teor. Fiz. vol. 169, pp. 181-188, (2026) (in Russian; English translation: arXiv:2604.05945v1 [physics.optics]).

# Towards THz HgCdTe-based quantum cascade laser

**A.A. Dubinov[1], A.A. Afonenko[2], D.V. Ushakov[2]**

*1- Institute for Physics of Microstructures RAS, GSP-105, 603950, Nizhny Novgorod, Russia*
*2- Belarusian State University, 4 Nezavisimosti Av., 220030, Minsk, Belarus*

*sanya@ipmras.ru*

Over the two decades of their existence, quantum cascade lasers in the terahertz frequency range (THz QCLs) have come a long way from cryogenic devices with relatively low output powers to powerful THz sources with thermoelectric cooling based on Peltier elements [1]. However, there is a frequency range of the "terahertz gap" (6–10.5 THz), where QCLs do not work due to strong phonon absorption in the arsenide-based heterostructures (AlInGaAs) from which they are made.

Heterostructures with HgCdTe-based quantum wells (QWs) are a promising active medium for solving the problem of creating QCLs with an operating "terahertz gap" frequency range, due to their lower optical phonon energies compared to arsenides.

The low-energy gap semiconductor HgCdTe theoretically allows the number of cascades needed for operation of a QCL with a double metal waveguide (active region is between two metal layers) to be considerably decreased [2] because of an appreciably larger material gain factor [3]. At the same time, development of a HgCdTe-based QCL faces a problem related to the production process of this type of waveguide that requires heating of the structure to above 250°C [4]. Note that qualitative growth of HgCdTe structures with quantum wells occurs at much lower temperatures of 180–190°C [5], and heating to above these temperatures will lead to their degradation.

In this work, it is proposed to construct an 8.3-THz QCL based on the HgCdTe structure with quantum wells using a surface plasmon waveguide widely employed in arsenide-based QCLs [2]. Manufacture of this type of waveguide and contacts does not require considerable heating of the structure. Parameters of a surface plasmon waveguide in an 8.3-THz quantum cascade laser based on $Hg_{0.8}Cd_{0.2}Te/Hg_{0.6}Cd_{0.4}Te$ quantum wells are optimized. With this waveguide, a QCL with an active medium made of cascades of quantum wells and barriers considered in [6] will be able to lase in the frequency region inaccessible to current QCLs (~8.3 THz) up to a temperature of 125 K [7].

The study was supported by the Ministry of Science and Higher Education of the Russian Federation (theme No. 124050300055-9/FFUF-2024-0045).

[1] A. Khalatpour, A. K. Paulsen, C. Deimert, Z. R. Wasilewski, Q. Hu, High-power portable terahertz laser systems, Nat. Photonics, **15**, 16-20 (2021).
[2] B. Wen, D. Ban, High-temperature terahertz quantum cascade lasers, Prog. Quant. Electron. **80**, 100363 (2021).
[3] A. A. Dubinov, D. V. Ushakov, A. A. Afonenko, R. A. Khabibullin, M. A. Fadeev, S. V. Morozov, Thin active region HgCdTe-based quantum cascade laser with quasi-relativistic dispersion law, Opt. Lett. **47**, 5048–5051 (2022).
[4] B. S. Williams, Terahertz quantum cascade lasers, PhD Thesis (MIT, 2003).
[5] S. Dvoretsky, N. Mikhailov, Yu. Sidorov, V. Shvets, S. Danilov, B. Wittman, S. Ganichev, Growth of HgTe quantum wells for IR to THz detectors, J. Electron. Mater. **39**, 918–923 (2010).
[6] D. Ushakov, A. Afonenko, R. Khabibullin, D. Ponomarev, V. Aleshkin, S. Morozov, A. Dubinov, HgCdTe-based quantum cascade lasers operating in the GaAs phonon Reststrahlen band predicted by the balance equation method, Opt. Exp. **28**, 25371–25382 (2020).
[7] A. A. Dubinov, A. A. Afonenko, D. V. Ushakov, Optimization of surface plasmon waveguide in 8.3-THz HgCdTe-based quantum cascade laser, Phys. Wave Phenomen. (accepted).

# Long-Term Variability of Precipitable Water Vapor Above Maidanak Observatory

**Y. Tillayev[1,2], Sh. Ehgamberdiev[1,2], I. Xurramov[1], A. Azimov[1], E. Habibullayev[2]**

*1- Ulugh Beg Astronomical Institute, Uzbekistan Academy of Sciences, Astronomy St. 33, Tashkent, Uzbekistan*
*2- National University of Uzbekistan, University. 4, Tashkent, Uzbekistan*

*yusuf@astrin.uz*

Atmospheric water vapor is one of the key factors limiting the performance of astronomical observations in both optical and radio wavelength regimes. The amount of precipitable water vapor (PWV) directly affects atmospheric transparency, signal attenuation, and the achievable sensitivity of astronomical instruments. Consequently, the long-term characterization of PWV is essential for evaluating the suitability of an observatory site for optical, infrared, and radio astronomical applications.

In this study, we investigate the long-term variability of PWV above the Maidanak Observatory (Uzbekistan), one of the premier astronomical sites in Central Asia. The analysis is based on GNSS-derived measurements of tropospheric water vapor obtained between 2013 and 2025, complemented by ERA5 reanalysis data covering the period 2010–2025, where atmospheric moisture content is represented by the Total Column Water Vapour (TCWV) parameter. Seasonal and interannual variations of PWV were analyzed to assess the stability of atmospheric conditions and their impact on observational quality.

The results indicate that the annual mean PWV has remained remarkably stable over the past 15 years, typically ranging between 6 and 7 mm. A weak negative trend suggests a slight long-term decrease in atmospheric moisture content. Seasonal analysis reveals a pronounced annual cycle, with minimum PWV values occurring during winter (3.5–4.0 mm in January–February) and maximum values during summer (8–9 mm in July). The exceptionally low water vapor content during winter provides particularly favorable conditions for infrared, millimeter, and submillimeter observations.

Although ERA5 products tend to slightly overestimate PWV over complex mountainous terrain, the observed long-term stability confirms the excellent atmospheric characteristics of the Maidanak site. A comparison between ERA5-derived and GNSS-derived PWV measurements is currently being performed to quantify systematic biases and improve the accuracy of atmospheric characterization. The combined analysis provides a robust assessment of atmospheric transparency and further strengthens the case for Maidanak Observatory as a promising site for future optical and radio astronomical facilities.

# Oxidation state engineering in cobalt ferrite for terahertz telecommunications

**L. Alyabyeva[1], E.A. Gorbachev[2], E.S. Kozlyakova[1], L.A. Trusov[2]**

*1- Moscow Institute of Physics and Technology, 141700, Institutskii lane 9, Dolgoprudny, Russia*
*2- Faculty of Materials Science, MSU-BIT University, Shenzhen, 517182, China*

*aliabeva.ln@mipt.ru*

Telecommunication technologies for the last few decades have been keeping a trend toward increasing working frequencies. From the 4G standard, a step has been made towards 5G, which operates in the tens of gigahertz. Modern high-tech areas such as telecommunications, terahertz photonics, spintronics, etc., have ever-increasing demands for such functional parameters as working speeds and transmitted information densities — demands that could be satisfied by increasing operational frequency ranges. Thus, a never-ending search for materials suitable for use in the delicate frequency range of 100 GHz to 1 THz is ongoing.

With the above in mind, we performed thorough research on a promising insulating oxide with superior magnetic characteristics: cobalt ferrite $CoFe_2O_4$. An important key feature of the investigated material is its pronounced ferromagnetic resonance peaking in the sub-terahertz to terahertz region. We managed to develop a synthesis methodology that allows effective control of the desired functional characteristics of these materials, including fine-tuning of the resonance frequency of the line (and its quality factor) over a broad frequency range from below 100 to 488 GHz in a zero bias field (natural FMR or NFMR). The latter is the largest value of NFMR frequency reported to date.

The core point for enhancing magnetic characteristics is the balance of oxidation states of ions in the lattice of cobalt ferrite. Previously, introduction of $Co^{3+}$ and/or $Fe^{2+}$ into the structure of partially inverse spinel $Co^{2+}Fe^{3+}{}_2O_4$ was treated as an unintentional impurity depending on synthesis conditions and was not properly acknowledged. However, it is the targeted control of the concentration of $Co^{3+}$ and $Fe^{2+}$ that allows pushing NFMR to world-record high values (or, vice versa, tuning it to lower frequencies if required by a particular application).

We synthesized a series of single-phase substituted cobalt ferrites $Co^{2+}Fe^{3+}{}_{2-x}Co^{3+}{}_xO_4$ and $Co^{2+}{}_{1-y}Fe^{2+}{}_yFe^{3+}{}_2O_4$ with x = 0.0–1.5 and y = 0.0–0.5, characterized them using X-ray phase analysis, magnetic thermogravimetry, and X-ray absorption, and studied their functional characteristics using SQUID magnetometry and TDSTHz spectroscopy.

Among the strong points of our research, we note the direct observation of NFMR as the frequency dispersion of the complex transmission coefficient and complex refractive index in the 0.1–2 THz frequency region (Fig. 1), obtained by means of time-domain terahertz spectroscopy with temperature variation from room temperature down to helium temperature.

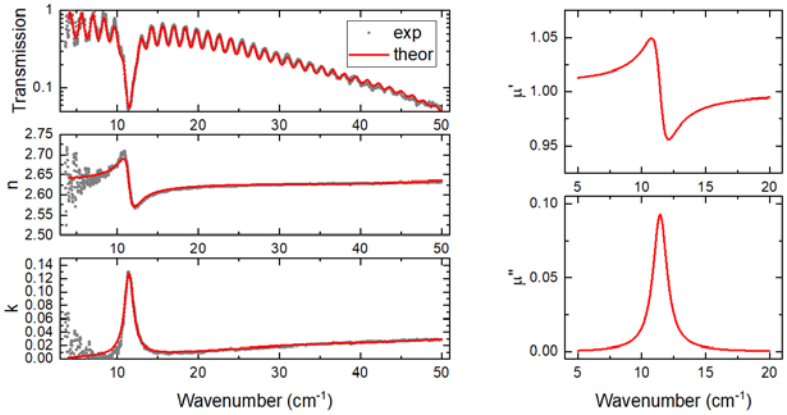


**Fig. 1.** Spectra of $Co^{2+}Fe_{2-x}Co^{3+}{}_xO_4$, x=0.5 at T=5 K. Left panel: transmission amplitude, real and imaginary parts of complex refractive index, grey dots are experimental data, red lines are approximation with . Right panel: spectra of complex magnetic susceptibility, calculated from the fit.

This work was supported by RSF (24-79-10053).

# High-order harmonics and terahertz radiation ellipticity: influence of atomics state symmetry

**S. Stremoukhov**[1,2]

*1- Faculty of Physics, Lomonosov Moscow State University, Moscow, Russia;*
*2- P.N. Lebedev Physical Institute of the Russian Academy of Sciences, Moscow, Russia;*

*stremoukhovsy@my.msu.ru*

Generation of elliptically polarized coherent radiation continues to be a focal point of research [1-3], motivated by the quest for optimal interaction parameters to achieve intense radiation with prescribed polarization characteristics due to it crucial role in advanced applications such as chiral spectroscopy, spintronics, and polarization-sensitive imaging and communication. Despite these efforts, the role played by the symmetry of the ground as well as excited states in the generation of elliptically polarized radiation, generated due to non-linear interaction of atomic systems with intense laser field, has yet to be comprehensively addressed. Here we present the results of a study of the ground state overall symmetry on the value of ellipticity of long- and short-wavelength radiation generated by two-color laser radiation with single atoms.

The study utilizes a unique non-perturbative theory for investigating the response of a single atom to intense, multicomponent, and arbitrarily polarized radiation [4]. The theory has been successfully validated in the calculation of generated radiation parameters [5-7]. The investigations were conducted for a two-color laser field, formed by the linearly polarized fundamental and the second harmonics of a Ti:Sa laser, with the non-zero angle between the polarization directions of the field components. Calculations have been carried out for silver, argon and thorium atoms.

[1]. B.Ghomashi, S.Walker, A.Becker, Generation of elliptically polarized high-order harmonics in cross-polarized bichromatic laser pulses: mechanism and control. Journal of Physics B: Atomic, Molecular and Optical Physics. 58, 235601 (2025).
[2]. O.Neufeld, M.Tzur, G.Lerner, O. Kfir, A. Fleischer, and O. Cohen, Light symmetry, chirality, and their role in nonlinear optics and ultrafast phenomena. Adv. in Opt. and Phot., 560140 (2026).
[3]. L. Gan, J. Liu, L. He, X. Zhu, P. Lan, and P. Lu, Generation of elliptically polarized terahertz radiation from a water column, Optics Letters Vol. 51, Is. 4, pp. 1056-1059 (2026)
[4]. A.V. Andreev, S.Yu. Stremoukhov, O.A. Shoutova, Light-induced anisotropy of atomic response: prospects for emission spectrum control. European Physical Journal D, V. 66:16 (2012).
[5]. S. Stremoukhov, A. Andreev, B. Vodungbo, P. Salières, B. Mahieu, G. Lambert, Origin of ellipticity of high-order harmonics generated by a two-color laser field in the cross-polarized configuration, Physical Review A, V. 94, p. 013855 (2016).
[6]. B. Mahieu, S. Stremoukhov, D. Gauthier, C. Spezzani, C. Alves, B. Vodungbo, P. Zeitoun, V. Malka, G. De Ninno, and G. Lambert, Control of ellipticity in high-order harmonic generation driven by two linearly polarized fields, Phys. Rev. A, 97, 043857 (2018).
[7]. S. Yu.Stremoukhov, A.A.Yakovlev, A.V.Andreev, High harmonic generation in two-color elliptical laser fields of different helicity. Laser Phys. Lett., 17, 085405 (2020).

# Powerful sub-THz gyrotrons with instantaneous switch-on

**M.Yu. Glyavin[1], E.P. Taradaev[2], G.G. Sominskii[2], S.P. Taradaev[2], A.P. Fokin[1], A.G. Luchinin[1], A.S. Sedov[1], A.S. Zuev[1], A.A. Ananichev[1], G.A. Shneerson[2], K.V. Voloshin[2]**

*1- Institute of Applied Physics RAS,46 Ul'yanov str., Nizhny Novgorod, Russia*
*2- Peter the Great St.Petersburg Polytechnic University (SPbPU), St.Petersburg, Russia*

In traditional gyrotrons, which use a cathode operating in temperature-limited emission current mode and magnetic systems based on cryomagnets or electromagnets, preparing the gyrotron for operation requires time to warm up the cathode (this time can range from several minutes to several minutes) and time to inject the solenoid current (or energy expenditure to maintain the operating current of the magnetic system). The series of pulsed magnetic field gyrotrons with traditional high-temperature emitter demonstrate record frequency and power at the band 0.6-1.3 THz [1,2]. However, for some applications quick switch-on scenario looks preferable [3]. Same, for quite a long time, work has been carried out on the creation of field emitters capable of providing a relatively high emission current in a technical vacuum in both pulsed and CW regimes [4]. It should be noted that, in parallel, quite successful work is being carried out to create force-free magnetic systems capable of generating pulsed fields of tens of Tesla at room temperatures [5]. This paper describes the concept of a low-power gyrotron using a field cathode and a pulsed magnetic system, which will enable instantaneous startup of the gyrotron upon power supply activation. T

This paper presents an experimental study of a 140 GHz gyrotron equipped with a multi-tip cold field emitter [6]. The conditions for radiation generation were determined, and the feasibility of achieving an output power of approximately 13 W was demonstrated. The gyrotron electron gun provided a stable electron beam with currents of up to ~ 100 mA and operated reliably at typical technical vacuum pressures of $10^{-7}$–$10^{-8}$ Torr. The developed multi-tip cathodes with fullerene protective coatings exhibit exceptional atmospheric resistance, maintaining functionality after air exposure without regeneration procedures and preserving operational readiness during unlimited storage time under ambient conditions.

Near-future experiments will focus on testing the gyrotron with optimized electron-optical gun geometry. This new design features a significantly larger cathode diameter of 18 mm and is expected to eliminate the need for cathode solenoids, thereby simplifying the system. In the longer term, we plan to increase the radiation frequency by exploring operation at higher cyclotron harmonics or by attempting a transition to large-orbit gyrotron configurations. These results establish promising prospects for developing compact microwave devices capable of instant operation while requiring no special storage or handling conditions - features particularly valuable for mobile and field-deployable applications.

Gyrotron development was supported, in part, by the IAP RAS projects FFUF-2022-0007.

[1] M. Yu. Glyavin, A.G. Luchinin, and G. Yu. Golubiatnikov. Generation of 1.5-kW 1-THz coherent radiation from a gyrotron with a pulsed magnetic field, *Phys. Rev.Lett*, **100**, 1, 015101, (2008) doi:10.1103/PhysRevLett.100.015101

[2] M.Yu.Glyavin, A.G.Luchinin, G.S.Nusinovich, et al. A 670 GHz gyrotron with record power and efficiency, *Applied Physics Letters*, **101**, 153503, (2012), doi: 10.1063/1.4757290

[3] M. Yu. Glyavin, A. G. Luchinin, V. N. Manuilov, et al. Development of a high-power pulsed subterahertz gyrotron for remote detection of sources of ionizing radiation. *Radiophysics and Quantum Electronics* **54**, 8, 600-608 (2012), doi: 10.1007/s11141-012-9319-7

[4] M.Yu.Glyavin, V.N.Manuilov, G.G.Sominski, et al. The concept of an electron-optical system with field emitter for a spectroscopic gyrotron. *Infrared Physics & Technology*, **78**, 185-189 (2016) doi:10.1016/j.infrared.2016.08.006

[5] O.A.Emelyanov, M.Y.Glyavin, S.V.Golubev, et al. Quasi-force-free magnets of small volume for generators of short-wave microwave radiation. *IEEE Transactions on Applied Superconductivity*, **34**, 5, 1-4 (2024) doi: 10.1109/TASC.2023.3342763

[6] G.G.Sominskii, E.P.Taradaev, S.P.Taradaev, et al. Experimental Study of a Gyrotron with a Multi-Tip Cold Field Emitter. *IEEE Transactions on Electron Devices*, **73**, 1, 613-618 (2026) doi: 10.1109/TED.2025.3631457

# Nonlinear Absorption of Ultrashort Laser Pulses in a Barium Tungstate Crystal

**V. I. Kovalev**

*Lebedev Physical Institute of RAS, Russia, 119991 Moscow, Leninskii av. 53*

*kovalevvi@lebedev.ru*

The work analyzes and demonstrates why the experimentally observed nonlinear four-photon absorption of 300 fs laser pulses in a barium tungstate (BWO) crystal "saturates" when the incident radiation energy exceeds a certain level.

A light pulse with $\lambda$ = 515 nm, duration $t_p$ = 300 fs and energy $E_p$ up to 3 μJ was focused by a lens with $F$ = 4 cm into a BWO crystal of length $L$ = 0.8 cm. The waist radius and length were ~10 μm and ~0.25 cm, respectively. Figure 1 shows transmittance of the sample $T$ defined as the pulse energy at the output of the sample divided by the multiply of the pulse energy incident on the sample, $E_p$, and the sample's linear transmittance $T_0 = (1 - R)^2\exp(-\alpha L) = 0.69\pm0.02$. Since the Fresnel reflection by the BWO surface is $R$ = 0.089, the sample's linear absorption coefficient $\alpha = 0.23\pm0.03$ cm$^{-1}$ determined.

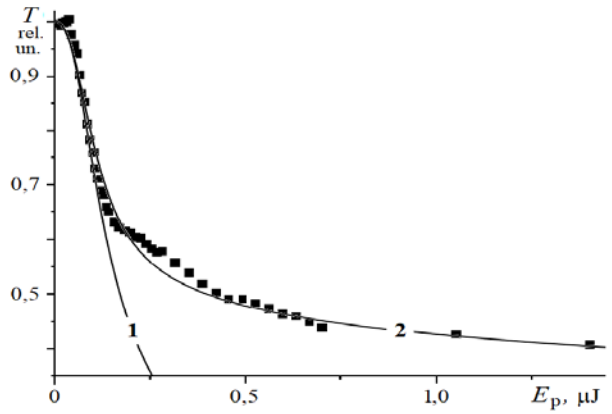


**Fig. 1.** Dependence of transmission $T$ on the energy of the incident pulse $E_p$, squares are experimental data, curves 1 and 2 are calculations using formulas (1) and (2).

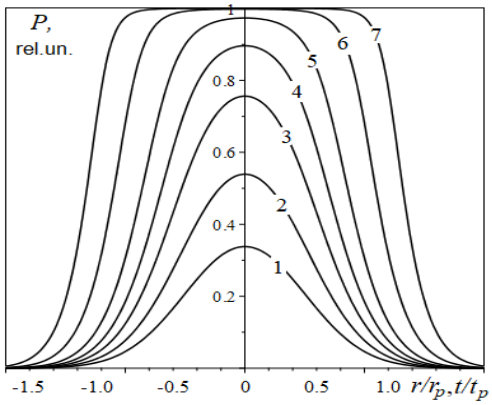


**Fig. 2.** Amplitude and shape of the transmitted pulse at $E_p$ = 0.03(1), 0.05(2), 0.08(3), 0.12(4), 0.2(5), 0.5(6) and 1.0(7) μJ.

Considering that the ratio of the BWO band gap $Eg$ (5.28 eV) to the radiation quantum $\hbar\omega$ (2.4 eV) is 2.2, the observed $T(E_p)$ should be associated with three-photon interbond (3PA) transition, which, in transmission measurements, results in four-photon absorption (4PA) due to single-photon absorption by the three-photon generated electrons and ions [1], and for which [2],

$$T(E_p) = \left(\sqrt[3]{1+\eta_{ef} L_{ef} E_p^3 t_p^{-3} S_p^{-3}}\right)^{-1} = \left(\sqrt[3]{1+1500E_p^3}\right)^{-1}, \qquad (1)$$

where $\eta_{ef}$ is the effective 4PA coefficient, $S_p = \pi r_p^2$ is the beam cross section and $L_{ef}$ is the effective interaction length. Curve 1 in Fig. 1 presents $T(E_p)$ when all other parameters in Eq. (1) are constant. Inconsistency between the experiment and calculation becomes significant at $E_p > 0.1$ μJ.

A search for the reason of this have led us to the concieve that it may be a consequence of change due to 4PA of the magnitude and shape of a beam cross section [3] and of a pulse. Fig. 2 shows 4PA transformation of an entered gaussian pulse to hypergauss shape and increased radius and duration of the transmitted pulse on increase $E_p$. To account for this effect, the equation (1) was modified to,

$$T(E_p) = \left(\sqrt[3]{1+1500E_p^3/(1+CE_p^n)}\right)^{-1}, \qquad (2)$$

where $C$ and $n$ are some constants. The best fit of Eq. (2) to the experiment, curve 2 in Fig. 1, obtained with $C$ = 120 μJ$^{-2,5}$ and $n$ = 2,5.

[1]. A. Penzkofer, W. Falkenstein, Opt. Commun., vol. 16, pp. 247-250 (1976).
[2]. V. I. Kovalev, M. A. Musaev, F. S. Faizullov, Quantum Electron., vol. 14, pp. 668-675 (1984)].
[3]. V. I. Kovalev, Quantum Electron., vol. 17, pp. 1180-1182 (1987).

# Sustaining Hot Electrons in Graphene via Terahertz Pulse Waveform Shaping

**E.A. Migal[1], D. Z. Suleimanova[1], A.V. Boniuk[1], D.P. Borisenko[2], F.V. Potemkin[1]**

*1- Faculty of Physics, M.V. Lomonosov Moscow State University, Moscow, Russia*
*2- National Research Nuclear University, Moscow, Russia*

*ea.migalj@physics.msu.ru*

The development of high-intensity, ultrafast near-IR, mid-IR, and THz laser sources [1] has established a robust framework for strong-field physics experiments and multi-parameter optical diagnostics. Recent studies utilizing these systems have successfully elucidated the wavelength dependence of plasma formation threshold in bulk dielectrics [2] and resolved the long-wavelength response in low-dimensional materials [3]. Extending these concepts to the THz domain, in this work we investigate how the pulse duration, temporal profile, and bandwidth affect the non-linear transmittance of monolayer graphene, where the precise roles of these parameters remain unclear.

In particular, we experimentally study the non-linear THz transmission of CVD monolayer graphene on a flexible PET substrate under intense excitation (up to 2.5 MV/cm) generated via optical rectification in DAST and OH1 crystals. We contrast three driving configurations: broadband DAST (2 THz, 0.67 ps), broadband OH1 (1 THz, 1.2 ps), and narrowband filtered OH1 (1 THz, 4 ps) pulses. At an identical peak field of 0.6 MV/cm, we observe a dramatic enhancement in the integrated energy transmittance for the narrowband 4-ps excitation, reaching 81%, compared to 68% for broadband OH1 and 59% for DAST (Fig. 1). High-field scaling reveals distinct saturation plateaus for the broadband regimes: 62% for DAST and 72% for OH1 near 2.5 MV/cm. Due to filter insertion losses, the narrowband transmission was evaluated only up to 0.6 MV/cm; yet, it vastly outperforms the saturated states of the shorter pulses.

This substantial difference is governed by the interplay between pulse duration and the picosecond-scale carrier cooling time in graphene. The 4-ps drive interacts with the hot electron gas more efficiently, continuously pumping energy into the system. Furthermore, at a fixed peak field, the longer pulse carries higher total energy, leading to more efficient electronic heating and sustaining an elevated electronic temperature. The enhanced transmittance at 1 THz compared to 2 THz can probably be attributed to lower substrate absorption at lower frequencies.

Our findings prove that spectral filtering and carrier frequency optimization are key strategies to maximize THz modulation efficiency and nonlinear response.

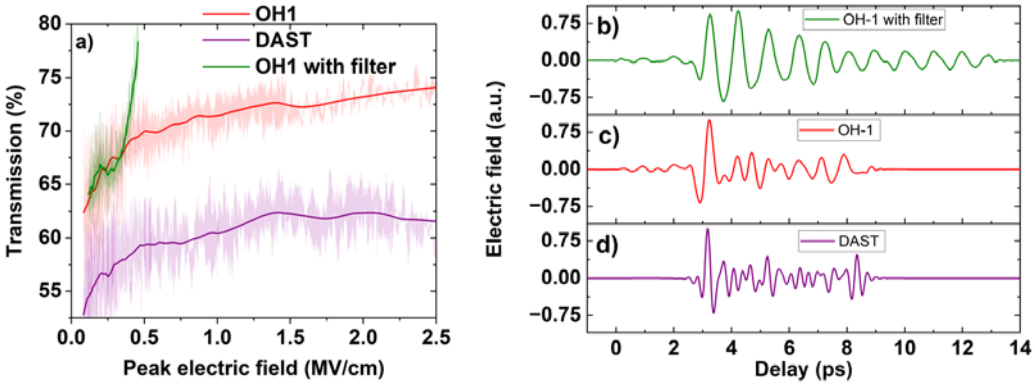


**Fig. 1** a) Nonlinear transmission of the single-layer graphene on PET substrate subjected to a different waveforms generated in DAST (purple, d) and OH1 (red, c) organic crystals and additionally filtered by a band-pass filter (green, b).

This work has been supported by Russian Science Foundation Project No. 25-22-00084.

[1] A. Pushkin, E. Migal, D. Suleimanova, E. Mareev, F. Potemkin, High-Power Solid-State Near- and Mid-IR Ultrafast Laser Sources for Strong-Field Science. *Photonics*, *9*, 90 (2022).
[2] E. Migal, E. Mareev, E. Smetanina et al., Role of wavelength in photocarrier absorption and plasma formation threshold under excitation of dielectrics by high-intensity laser field tunable from visible to mid-IR. *Sci Rep* 10, 14007 (2020).
[3] A.Pushkin, F. Potemkin, Refining the Performance of mid-IR CPA Laser Systems Based on Fe-Doped Chalcogenides for Nonlinear Photonics. *Photonics* , *10*, 1375 (2023).

# Terahertz-wave scattering in tissues: the applicability limits of effective medium theory

**A.S. Kucheryavenko[1,2], I.N. Dolganova[2], N.V. Chernomyrdin[1], K.I. Zaytsev[1]**

*1- Prokhorov General Physics Institute of the Russian Academy of Sciences, Russia*
*2- Institute of Solid State Physics of the Russian Academy of Sciences, Russia*

*ans.kucher@mail.ru*

## I. INTRODUCTION

Terahertz (THz) band of electromagnetic waves is used for research in various fields of biophotonics and medicine [1-3], most of which are based on the use of tissue water as the primary endogenous marker of pathological processes [4]. Like liquid water and aqueous solutions, the complex dielectric permittivity of tissues in the THz range is typically described using different relaxation models [4] within the framework of effective medium theory (EMT).

This description of the THz response of biological tissues relies on the assumption of optical isotropy and homogeneity of tissues at the THz wavelength scale. Meanwhile, recent developments in high-resolution THz technology have made it possible to visualize the inhomogeneity of various biological tissues at the wavelength scale [3 – 6], which can lead to Mie scattering and fall outside the EMT formalism. A recent study demonstrated birefringence in various rat tissues [7], which also cannot be accounted for within the EMT framework. These advances have stimulated further research into THz wave propagation in soft tissues.

## II. RESULTS

The first stage of our study involved the creation of a phantom with spherical scatterers. We chose connective tissue with localized inclusions of adipose tissue cells to model. An analytical calculation based on Lorenz-Mie theory predicts non-Rayleigh scattering, which casts doubt on the applicability of EMT to such tissues. However, we theoretically discovered and experimentally confirmed that the effective optical properties of the proposed phantom are still described by EMT over a wide range of scatterer diameters ($d \leq 0.47\lambda$) and volume fractions ($f_v \leq 0.2$) [8]. This effect is explained by strong losses of THz waves in the carrier medium and, therefore, should be characteristic of various soft tissues in the THz range.

The second stage involved creating a phantom with an ordered system of cylindrical scatterers. Examples of simulated tissue in this case include muscles, tendons, and nerve fibers in a more humid environment. Approaches based on Lorenz-Mie scattering theory also predict non-Rayleigh scattering and no dependence on the polarization direction of the radiation. However, experimental data demonstrated the influence of the anisotropy of the medium on the transmission spectra. The Bruggeman EMT model allows for a fairly accurate description of the interaction of TM-polarized radiation with this phantom over a wide range of scatterer diameters ($d \leq 0.7\lambda$) and volume fractions ($f_v \leq 0.2$), but is unsuitable for describing TE-polarized radiation. This necessitates the development of a polarization-dependent model to describe radiative transfer in such systems.

Thus, our results extend the applicability of effective medium theory to describe the interaction of THz radiation with soft turbid tissue.

[1] X. Yang et al. Biomedical Applications of Terahertz Spectroscopy and Imaging, *Trends in Biotechnology*, **34** (10), pp. 810-824, (2016).
[2] G. M. Katyba et al. Terahertz endoscopy of hard-to-access objects in the context of neoplasms diagnosis–A review, *Light: Advanced Manufacturing*, **6**(3), pp. 504-521 (2025).
[3] K. I. Zaytsev et al. The progress and perspectives of terahertz technology for diagnosis of neoplasms: a review, *Journal of Optics*, **22**(1), pp. 013001 (2020).
[4] O. A. Smolyanskaya et al. Terahertz biophotonics as a tool for studies of dielectric and spectral properties of biological tissues and liquids. *Progress in Quantum Electronics,* **62**(1), pp. 1–77 (2018).
[5] N. V. Chernomyrdin et al., Reflection-mode continuous-wave 0.15 λ -resolution terahertz solid immersion microscopy of soft biological tissues, *Applied Physics Letters*, **113**(11), pp. 1471 (2018).
[6] A. S. Kucheryavenko et al. Terahertz dielectric spectroscopy and solid immersion microscopy of ex vivo glioma model 101.8: brain tissue heterogeneity, *Biomedical Optics Express*, **12**(8), pp. 5272–528 (2021).
[7] D.S. Il'enkova et al. Heterogeneity and birefringence of soft tissues probed by the polarization-sensitive terahertz solid immersion microscopy, *Journal of Biophotonics*, **19**(1), pp. e70232 (2026).
[8] A. S. Kucheryavenko et al. Terahertz-wave scattering in tissues: Examining the limits of the effective medium theory applicability. *Physical Review Applied*, **20**(5), pp. 054050 (2023).

# Nonlinear conversion to lower frequencies under femtosecond filamentation in air

**D. Pushkarev[1], D. Uryupina[1], E. Mitina[1], M. Ustyuzhanin[1], N. Zdidovtsev[1], N. Panov[1,2], A. Bulygin[3], N. Vrublevskaya[1], P. Chizhov[4], T. Dolmatov[4], V.V. Bulgakova[4], K. Galuyk[4], A. Ushakov[4], O. Kosareva[1,2], Yu. Geints[3], S. Garnov[4], A. Savel'ev[1,2]**

*[1]Faculty of Physics, Lomonosov Moscow State University, Moscow, Russia*
*[2] Lebedev Physical Institute of the Russian Academy of Sciences, Moscow, Russia*
*[3]Zuev Institute of Atmospheric Optics of the Russian Academy of Sciences, Tomsk, Russia*
*[4]Prokhorov General Physics Institute of the Russian Academy of Sciences, Moscow, Russia*

*savelevab@my.msu.ru*

Non-linear conversion of laser power to other spectral ranges occurs during filamentation of a high-power femtosecond laser pulse in gases. This report presents our recent experimental and numerical restudies of conversion to IR, THz and microwaves. First, Raman spectral component can be formed in molecular gases. This component is localized along the optical axis of the initial radiation, as well as spectrally and temporally. This effect is of significant interest because it involves a noticeable and controllable transfer of laser energy to the infrared region. The central wavelength of this component shifts toward longer wavelengths with distance and propagates in the near-axis region, thus forming a "light bullet" that behaves like a soliton. Question of how such a bullet is formed without anomalous dispersion is crucial. We present series of experimental studies, including the measurement of single-pulse frequency-angular spectra, of the filamentation of a femtosecond laser pulse with terawatt peak power in air under various focusing conditions, chirping, and other parameters and compare it with the case of filamentation in noble gases. We revealed optimal conditions for the light bullet formation. Further we consider THz production from a single and multiple filaments with orthogonal DC biasing. We showed that with long electrodes THz signal are added constructively while the angular distribution is getting narrower. The optimum length equals roughly to the filament length deduced from acoustic measurements. We also achieved pronounced enhancement in the THz yield with laser pulse energies (peak powers) corresponding to the multifilamentation regime. We studied angular distribution for the case regular filament bundle formed by the Damman phase mask. Finally, we report observation of microwave radiation from the femtosecond filament in air biased by 10-kV/cm static transverse field with an amplitude ~2 orders of magnitude higher than in the unbiased or weakly biased cases. Such powerful microwaves with the broadband spectrum at least from 2 to 13 GHz propagate at relatively small angles with respect to the laser beam axis.

# Long-term research cycles of the microwave astroclimate at Suffa and other promising sites for subterahertz astronomy

**D. Danilevskiy[1], M. Efimova[2], A. Marukhno[2,3], N. Marukhno[2,3], G. Shanin[1], B. Sultanov[1], V. Vdovin[2]**

*1- RT-70 Observatory, Tashkent 100000, Uzbekistan*
*2- Institute of Applied Physics of the Russian Academy of Sciences, 603950 Nizhny Novgorod, Russia*
*3- Special Astrophysical Observatory of the Russian Academy of Sciences, 369167 Karachai-Cherkessian, Russia*

*vdovin@ipfran.ru*

Interest in the development of a network of subterahertz observatories, especially stimulated in the last decade by the program for the development of the Event horizon telescope [1], has generated extensive interest in the study of the microwave astroclimate [2]. However, as a rule, these are either short cycles or maximum studies within a year. At the same time, the construction of the telescope is a long-term matter and the characteristic of long-term trends within at least during a half of century are quite interesting.

The protracted construction of the Suffa Observatory made it possible to collect almost half a century (45 years since the beginning at 1981-st) [3] of data on the astroclimate on Suffa. No such data has been collected at Russian sites, but at the same time, it is possible to make an estimate on approximately the same time scale back at the site of the BTA SAO RAS optical telescope in the Caucasus [4] and make a forecast for the next half century based on the available data for both sites. The paper presents some results of such estimations and demonstrate prospects of those locations for installations of subterahertz observatories and possibilities and limitations of radioastronomical observations at wavelength of particular interest for radioastronomy: atmospheric windows at 3, 2, 1.3 and 0.8 mm. The last two of them are most interesting for the Event horizon telescope. The forecast presented here for the time horizon of half a century tacking into account the global warming trends is of considerable interest in assessing the prospects of proposed here telescopes for observations in the sub-terahertz range.

The work is supported by the Russian Science Foundation grant No. 23-79-00006, and research equipment for measuring atmospheric propagation have being developed on the capabilities and technologies of the Unique scientific installation Center for Microwave and Terahertz Research of Materials and Substances.

[1] Raymond, A.W.; Palumbo, D.; Paine, S.N.; Blackburn, L.; Rosado, R.C.; Doeleman, S.S.; Farah, J.R.; Johnson, M.D.; Roelofs, F.; Tilanus, R.P.J.; et al. Evaluation of New Submillimeter VLBI Sites for the Event Horizon Telescope. Astrophys. J. Suppl. Ser. 2021, 253, 5.
[2] Balega Y, Bubnov G, Glyavin M, Gunbina A, Danilevsky D, Denisov G, Khudchenko A, Lesnov I, Marukhno A, Mineev K, et al. Atmospheric Propagation Studies and Development of New Instrumentation for Astronomy, Radar, and Telecommunication Applications in the Subterahertz Frequency Range. Applied Sciences. 2022; 12(11):5670. https://doi.org/10.3390/app12115670.
[3] Artemenko, Y.N.; Balega, Y.Y.; Baryshev, A.M.; Zinchenko, I.I.; Vdovin, V.F. New stage of the Suffa submm observatory in Uzbekistan project. In Proceedings of the ISSTT 2019—30th International Symposium on Space Terahertz Technology, Proceedings Book, Gothenburg, Sweden, 15–17 April 2019; pp. 196–201. Available online: https://www.nrao.edu/meetings/isstt/papers/2019/2019196201.pdf
[4] Balega, Y.Y.; Bataev, D.K.-S.; Bubnov, G.M.; Vdovin, V.F.; Zemlyanukha, P.M.; Lolaev, A.B.; Lesnov, I.V.; Marukhno, A.S.; Marukhno, N.A.; Murtazaev, A.K.; et al. Direct Measurements of Atmospheric Absorption of Subterahertz Waves in the Northern Caucasus. Dokl. Phys. 2022, 67, 1–4.

# Electron dynamics in metal nanostructures and petahertz effects

**V.E. Gruzdev, S.A. Kozlov, A.O. Ismagilov, E.N. Oparin, A.N. Tcypkin**

*Research and Educational Center of Photonics and Optical IT, ITMO University, St. Petersburg, Russia*

*vegruzdev@itmo.edu*

Two fundamental issues block developments in modern electronics and digital circuits: (a) the ultimate clocking frequencies in the range of few GHz that cannot be exceeded since early 2000s; and (b) a need for new approaches in heat management to support the growing density of electronic elements per microchips [1]. Those issues arise from the fundamental limitations on electron transport in semiconductors and cannot be properly addressed by available methods or approaches. The growing interest to interactions of high-intensity few-cycle femtosecond (fs) laser pulses with metal and metal-semiconductor-metal nanostructures [2] is backed up by the promise to deliver a new paradigm of electronics capable of operating at sub-petz-hertz (PHz) frequencies, i. e., 5 to 6 orders of magnitude faster than the available digital electronic circuits. In parallel, this approach suggests reduction of heat losses by at least one order of magnitude because of use of ballistic (i. e., non-collision) regime of electron transfer through nanostructures [1]. The interactions aim to convert electric field of few-cycle laser pulses carrying from 1 to 3 cycles of electric field into electric-current pulse or short sequence of pulses with individual duration below one fs [1,2]. Building a solid and reliable theoretical description of the interactions is of high importance for success of the entire field. However, there are some basic issues and gaps in this area that prevent progress of this highly important research.

Since 2020, use of bow-tie metal structures deposited on dielectric substrates dominates in this field because of a common belief regarding their better ability to generate sub-fs electric-current pulses with reduced background and noise [2]. For those nano-devices, the light-to-current conversion is done by strong-field emission from metal parts of the structure followed by transport of emitted electrons in inter-electrode gaps over a distance varying from 8 to 50 nm [2]. Theoretical description of those processes frequently employs the Keldysh photo-ionization and Fowler-Nordheim emission model for the emission, and classical description of electron motion through nanogaps (Simple Man's Model – SMM) [2,3]. The essence of SMM is the use of zero initial speed of emitted electrons [2,3]. However, the zero-initial-speed assumption is incorrect and contradicts both experimental data on cold-field emission from metals and basics of emission models [4]. To address this issue, we recently proposed a version of SMM with non-zero initial speed [4] and employed it to simulate ballistic electron transport through nanogaps. This minor correction delivers several qualitative changes to the standard paradigm [2,3]. First, it suggests the electron transport can happen in either quantum or classical regime. For the latter one, electrons come out of the potential barrier between the metal parts and enter a segment of the gap where classical motion is allowed. This regime surprisingly correlates with large amounts of electric charge transferred via a nanostructure per single laser pulse [4]. The quantum regime considers electron motion without entering classically allowed space and correlates with transfer of per-pulse charges well below one electron charge [4]. We also proposed an analytical criterion to distinguish between classical and quantum regimes of electron transport. Finally, our results suggest a modification of the Keldysh parameter frequently used for qualitative analysis of the light-to-current conversion processes in metal nanostructures [2]. Keeping the fundamental definition of the parameter the same as in the original Keldysh paper, we replaced the classical speed of electron motion with Fermi speed [4].

The modified SMM fixes some basic issues of the traditional models. It also has exceptional predictive capabilities and is highly instrumental for optimization of laser-pulse and nanostructure parameters to enhance light conversion to fs pulses of current. Predicted regime of quantum electron transfer and the analytical criterion for it support designing experiments to study quantum regimes of electron transport.

[1] F. Krausz, M. Stockman, Attosecond metrology: from electron capture to future signal processing, *Nature Photon,* v. 8, pp. 205–213 (2014).
[2] C. Heide, P. D. Keathley, M. F. Kling, Petahertz electronics, *Nature Reviews Physics,* v. 6, pp. 648-662 (2024).
[3] M. Kruger, Ch. Lemell, G. Wachter, J. Burgdorfer, P. Hommelhoff, Attosecond physics phenomena at nanometric tips, *J. Phys. B: At. Mol. Opt. Phys.,* v. 51, p. 172001 (2018).
[4] V.E. Gruzdev, S.A. Kozlov, A. O. Ismagilov, E. N. Oparin, A. N. Tcypkin, Quantum and classical regimes of charge transfer through nanoscale gaps driven by few-cycle laser pulses, *Phys. Rev. Lett.*, submitted, (2026).

# Incoherent superconducting receivers for ground-based radio astronomy

**M. Tarasov[1], A. Gunbina[1,2], M. Strelkov[1], R. Kozulin[1], V. Vdovin[2], V. Edelman[3]**

*1- V. Kotelnikov Institute of Radio Engineering and Electronics, 125009 Moscow, Mokhovaya 11, bld 7*
*2- A. Gaponov-Grekhov Institute of Applied Physics, 603950 Nizhni Novgorod, Ulyanova 46*
*3- P. Kapitza Institute for Physical Problems, 119334 Moscow, Kosygina 2*

*tarasov@hitech.cplire.ru*

Superconducting incoherent receivers are detectors that respond to changes in the power (energy) of incident radiation, rather than to the phase or frequency of the electromagnetic field. Unlike coherent (heterodyne) systems, they have a wide bandwidth and extreme sensitivity, making them indispensable in submillimeter astronomy and particle physics. Incoherent detectors are mainly limited by quantum background fluctuations and phonon noise, while coherent detectors are limited by the quantum noise of the mixer. Incoherent arrays are easier to scale because they do not require a local oscillator (heterodyne oscillator) for each channel. Incoherent superconducting millimeter-wave receivers can have fluctuation sensitivities at the level of a few microkelvins, while heterodyne superconducting receivers in this wave range have a noise temperature of 2-3 quantum limits hf/k, i.e., in the region of 20-40 K. Incoherent receivers can be used at domestic telescopes SAO-BTA, Bauman MSTU, IPA, with main reflector diameter of 6 m, 7.8 m, 13 m, whose surface accuracy is 1 μm, 100 μm, 60 μm, which is sufficient for observations at frequencies 95, 150, 220, 350 GHz (transparency ranges 3 mm, 2 mm, 1.5 mm, 0.85 mm).

A bolometer with an absorber made of normal metal, in which the sub-gap current of tunnel junctions connected to the absorber is measured, was first presented in [1]. One of the best experimental results for equivalent noise temperature or fluctuation sensitivity for a SINIS bolometer in [2] 0.6 μK/Hz$^{1/2}$ was obtained at a temperature of 270 mK at a frequency of 0.5 GHz. This type of bolometer was later transformed into a SINIS detector. It is based on the effective measurement of excitations in the electronic subsystem of the absorber due to the tunneling of hot electrons through the SIN structure (superconductor — insulator — normal metal). The advantages of such detectors are: high counting speed, immunity to cosmic background radiation, and the ability to operate at temperatures of 100 mK and below.

We developed and manufactured several versions of SINIS detectors and tested such a receiver at the BTA telescope in June 2025 [3].

[1] Nahum, M. and Martinis, J. M. Ultrasensitive-hot-electron microbolometer. Applied Physics Letters, 63:3075, 1993..
[2] D.R. Schmidt, K.W. Lehnert, A.M. Clark, W.W. Duncan, K.D. Irwin, N. Miller, J.N. Ullom, Superconductor-insulator-normal metal bolometer with microwave readout suitable for large-format arrays, Appl.Phys.Lett. 86, 053505 (2005).
[3] M.A. *Tarasov*, A.A. *Gunbina*, A.M. *Chekushkin*, M.A. *Markina*, R.A. *Yusupov*, M.Yu. *Fominskii*, L.V. *Filippenko*, V.S. *Edelman*, V.F. *Vdovin*, V.S. *Stolyarov*, I.I. *Zinchenko*, A.M. *Krasilnikov*, A.S. *Marukhno*, M.A. *Mansfeld*, D.E. *Kukushkin*, D.A. *Sazonenko*, O.S. *Bolshakov*, A.B. *Ermakov*, I.V. *Lesnov*, A.F. *Valeev*, SINIS Detectors in the Subterahertz Range as a Basis for a Receiver for Radio Astronomical Research on the BTA Optical Telescope (SAO RAS), Astrophysical Bulletin, 2025, Vol 80, No 3, pp 502-518).

# Ultra-fast response times in sub-THz graphene photodetectors

**E. Titova[1,3], A. Titchenko[2], K. Shein[2], M. Titova[1], A. Kuksov[1], A. Sobolev[3], G. Goltsman[2], A. Svintsov[3], I. Gayduchenko[2]**

*1- Programmable Functional Materials Lab, CNNT, Moscow, Russia*
*2 - HSE University, Pokrovsky Boulevard 11, Moscow 109028, Russia*
*3 - Center for Advanced Studies, Kulakova str, Moscow*

*titova.elenet@gmail.com*

Terahertz (THz) radiation plays a key role in a wide range of modern applications, from wireless communications to medical diagnostics. However, in this frequency range, the sensitivity of conventional photodetectors is significantly lower than in the optical and radio-frequency domains. Graphene, owing to its low electronic heat capacity, high phonon energy, and ultrafast carrier dynamics, enables rapid heating of photoexcited electrons and relatively slow cooling, resulting in a strong and fast photo-thermoelectric response [1].

We previously demonstrated that bilayer graphene detectors incorporating split gates to form electrically induced p–n junctions, combined with bow-tie THz antennas, can achieve record-low noise and high responsivity at cryogenic temperatures [2,3]. To enable efficient operation at room temperature, we adopt an alternative design strategy.

Instead of relying on split gates, we introduce a geometrically induced asymmetry via a tooth-like contact, which enhances the photothermoelectric response without requiring electrostatically defined junctions. In addition, we redesign the THz antenna concept. Rather than employing conventional metallic antennas that concentrate incident radiation, we implement a slot antenna, where the electromagnetic field is expelled from the metal and strongly localized within the slot region, leading to enhanced field confinement.

This approach enables record-fast response times for graphene-based detectors. It should be noted that the presented detector operates at room temperature and zero bias. For a device with a carrier frequency of approximately 130 GHz, the bandwidth exceeds 43 GHz, corresponding to a response time on the order of 4 ps (see Fig. 1) [4]. The achieved high-frequency performance is attributed to careful impedance matching between the antenna and the graphene channel, combined with the optimized asymmetric contact geometry.

These results highlight the strong potential of the proposed device architecture for high-speed terahertz communication systems, including emerging sixth-generation (6G) technologies.

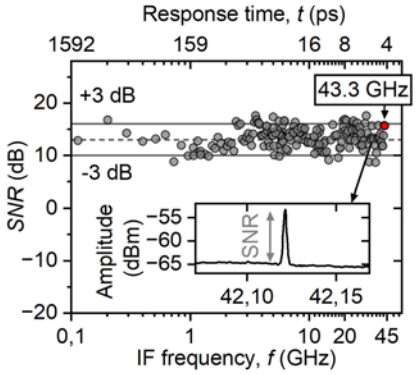


**Fig.1.** Signal-to-noise ratio of the graphene detector measured as a function of intermediate frequency in a heterodyne setup with a carrier frequency of 130 GHz. The inset shows the measured signal as recorded by an electrical spectrum analyzer.

[1] Sebastián Castilla et al., Nano Lett. 2019, 19, 2765−2773.
[2] E. Titova, et al., ACS Nano, 17, 9, 8223–8232 (2023).
[3] E. Titova, et al., Adv. Optical Mater., 2500167 (2025).
[4] E. Titova et al., arXive https://doi.org/10.48550/ARXIV.2603.03554 (2026)

# Terahertz and Ultrasound Multimodal Diagnostics of Bioresorbable Ceramics TPMS Scaffolds

**I. Shishkovsky**

*Lebedev Physical Institute of the RAS, 443011 Samara, Russia*

*shiv@fian.smr.ru*

Triply Periodic Minimal Surface (TPMS) scaffolds fabricated from bioresorbable materials such as hydroxyapatite (HA), β-tricalcium phosphate (β-TCP), and piezoelectric barium titanate represent a promising class of metamaterials for tissue engineering [1]. However, non-invasive 'in situ' monitoring of scaffold resorption remains a significant challenge. Terahertz (THz) and ultrasound (US) diagnostic modalities offer complementary sensitivity to surface and bulk structural changes, respectively.

Early we developed and validated a numerical framework based on the Finite-Difference Frequency-Domain (FDFD) method for simulating THz wave propagation (0.65–3 THz) and ultrasound (US) propagation (3–9 MHz) through TPMS scaffolds undergoing PLA bioresorption in soft biological tissue [2-3]. Here, the electromagnetic problem was solved using a verified FDFD solver with periodic boundary conditions in (x,y) and SCPML absorbing layers in (z) HA gyroid structure. Complex dielectric properties of soft tissue ($\varepsilon' = 40$, $\tan\delta = 0.6$) and biomaterials (HA: $\varepsilon' = 6.2$, $\tan\delta = 0.18$; Mg-alloys: Drude model) were incorporated from literature. Effective medium approximations (Hashin-Shtrikman, Gibson-Ashby) were employed to model the composite "material + tissue + pores" system as a function of porosity φ. A logarithmic resorption kinetics model $\varphi(t) = \varphi_0 + k\cdot\log(1 + t/\tau)$ linked porosity to 'in vitro' degradation time. Ultrasound propagation was FEMed using acoustic impedance matching and Helmholtz equation.

At porosity $\varphi \approx 0.52$, a sharp increase in THz transmission (TRN: $<10^{-15} \rightarrow 0.18$ at 1 THz) and maximum field amplitude ($\mathrm{Max}|E_x|$: $0 \rightarrow 4.0$ V/m) was observed, indicating the onset of electromagnetic connectivity through the scaffold. Reflectance (REF) increased from 0.05 at 1 THz to 0.66 at 3 THz for $\varphi = 0.52$, demonstrating strong frequency-dependent interaction with TPMS geometry. At 0.65 THz (local minimum of water absorption), complete field suppression occurred for all φ, confirming the method's applicability to near-surface diagnostics (< 0.3 mm tissue depth). Ultrasound reflectance ($R_{US}$) varied from 0.04 to 0.19 across $\varphi = 0.80$–$0.52$, providing bulk-sensitive contrast where THz signals are attenuated. A weighted multimodal index ($w_{THz} = 0.4$, $w_{US} = 0.6$) enabled staging of resorption: initial (<20%), early (20–50%), active (50–80%), late (>80%).

However, REF values exceeding unity at low porosity indicate numerical artifacts in power normalization for highly absorbing media; future work will implement impedance-corrected normalization. Scalar Helmholtz approximation assumes moderate refractive index contrast; vectoral formulation may be required for high-contrast ceramics/tissue interfaces. At current state, model does not yet account for dynamic hydration, vascularization, or cellular infiltration 'in vivo'.

Thus, the developed FDFD-based framework demonstrates high sensitivity to TPMS scaffold porosity and frequency, substantiating THz probing as a trigger for detecting the onset of biodegradation in minimally invasive, near-surface applications. Integration with ultrasound diagnostics extends monitoring depth to 5–10 mm, enabling comprehensive multimodal assessment of scaffold degradation. The numerical results provide a foundation for experimental THz-TDS and US validation and support the design of adaptive implant systems with real-time feedback.

[1] T. Arshad, O. Dubinin., I. Shishkovsky, 3D printing of topological composites by photopolymerization from submicron piezoceramics. Technical Physics Letters, Vol. 50(9), pp. 92-95 (2024)

[2] I. Shishkovsky, Terahertz detection of the percolation threshold in bioresorbable gyroid TPMS scaffolds. Radiophysics and Quantum Electronics, Vol. 69(1-2), pp. 133-145 (2026)

[3] I. Shishkovsky, 3D-printed hierarchical lattice metamaterials: Integrating mechanical strength and ultrasonic sensitivity for biomedical applications. Bulletin of the Lebedev Physics Institute, Vol. 52 (6), pp. S679-S687 (2025)

# Terahertz-induced electron emission from single-layer graphene

**S. Bodrov, A. Korytin, A. Murzanev, A. Romashkin, A. Stepanov**

*Institute of Applied Physics, Russian Academy of Sciences, Nizhny Novgorod, 603950 Russia*

*step1an@ipfran.ru*

Graphene, an allotropic form of carbon discovered about twenty years ago, continues to attract the interest of researchers due to its unusual mechanical and electrical properties. Many of these properties are highly nonlinear.

In this work, we present the results of a study of electron emission from single-layer graphene induced by a strong terahertz field. THz radiation generated by the tilted-pulse-front technique in a $LiNbO_3$ crystal provided a field value of up to 250 kV/cm when focused in the sample area. Time of flight diagnostic (Microchannel Plate) was used to measure electron emission. The dependence of electron emission from graphene as a function of the THz field strength is shown in Fig. 1 (a). The dependence is highly nonlinear, increasing sharply with increasing field strength. The role of various electron emission mechanisms (field-induced or thermal) in the observed results is discussed.

Figure 1(b) shows the electron energy distribution function extracted from the emission time signal. The main contributions to the distribution function's shape are the bias voltage on the sample (U = -30 V) and the acceleration of the emitted electrons in the terahertz field.

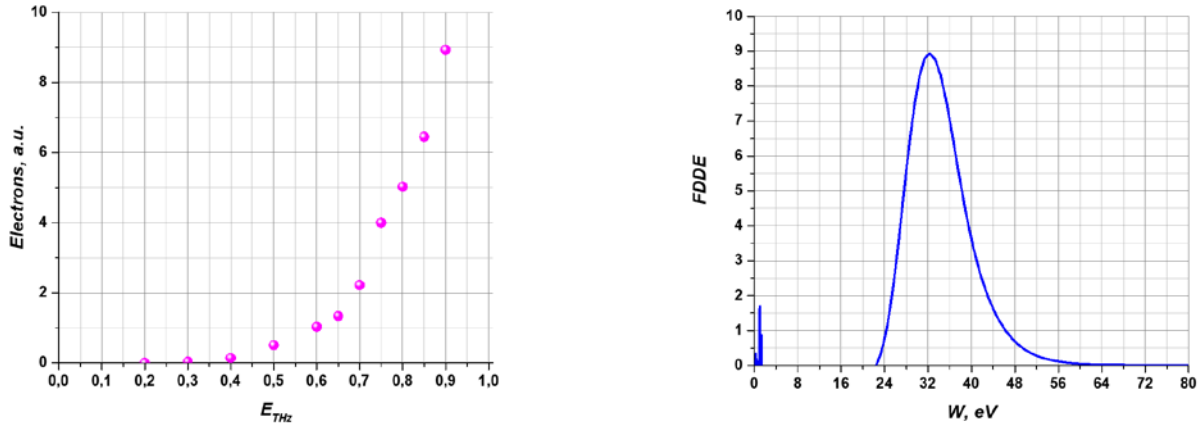


(a) (b)

**Fig. 1.** Dependence of the electron emission signal from graphene on the magnitude of the terahertz field, maximum THz field – 250 kV/cm (a), the electron energy distribution function at the maximum THz field (b)

The work was supported by the Russian Science Foundation the project No. 24-62-00032.

# Microwave radiation generation from DC-biased femtosecond laser air filament

**A. Ushakov[1], N. Vrublevskaya[2,3], E. Mitina[2], D. Uryupina[2], P. Chizhov[1,4], T. Dolmatov[1], V. Bulgakova[1], K. Galuyk[1], S. Garnov[1], N. Panov[2,3], A. Savel'ev[2,3]**

*1- Prokhorov General Physics Institute of the Russian Academy of Sciences, Moscow, Russia*
*2- Faculty of Physics, M.V. Lomonosov Moscow State University, Moscow, Russia*
*3- P.N. Lebedev Physical Institute of the Russian Academy of Sciences, Moscow, Russia*
*4- Moscow Institute of Physics and Technology, Dolgoprudny, Russia*

*ushakov.aleksandr@physics.msu.ru*

Femtosecond laser filamentation [1] in gases generates secondary radiation across a broad range of frequencies, from optical to microwave [2-5]. Microwave (MW) radiation is of particular interest because it can propagate freely through the atmosphere, opening prospects for data transmission and remote sensing. However, without an external field, the generation of MW is previously reported in [6]. In this work, we demonstrate a significant enhancement of microwave emission by applying a transverse DC electric field to an air filament.

The laser pulse (805 nm, 55 fs, 15 mJ) is focused into a 2-cm gap between electrodes creating a ~60-cm long plasma channel. A bias field of 10 kV/cm is applied perpendicular to the laser propagation axis. The MW emission is detected by a horn antenna (2–32 GHz) at a distance of 1 m from the filament.

It is found that the transverse DC field increases the MW amplitude up to ~500 mV/cm, which is approximately two orders of magnitude higher than in the unbiased or weakly biased cases. The MW signal exhibits a broadband spectrum spanning at least from 2 to 13 GHz. The angular distribution of the radiation is bell-shaped with a maximum on the laser beam axis (FWHM ~85°), in contrast to the ring-like pattern observed for unbiased filaments. Low-frequency components (2–4 GHz) diverge over ~90°, while higher frequencies (10 GHz) are confined within ~30°.

The proposed physical mechanism attributes the MW emission to a transverse plasma current induced by the external field. This current decays over 100–500 ps due to electron-ion recombination, consistent with the measured single-cycle pulse duration. A simple dipole model based on the interference of radiation from moving ionization front reproduces the experimental directional diagrams with high correlation (PCC 0.7–0.9) at frequencies above 6 GHz.

These results demonstrate that transversely biased femtosecond filaments can serve as efficient and directional sources of broadband microwave radiation for applications in data transmission and atmospheric remote sensing.

[1] A. Couairon and A. Mysyrowicz, «Femtosecond filamentation in transparent media,» Phys. Rep. 441, 47-189 (2007).
[2] P. Corkum and C. Rolland, «Femtosecond continua produced in gases,» IEEE J. Quant. Electronics 25, 2634-2639 (1989).
[3] A. B. Fedotov, N. I. Koroteev, M. Loy, X. Xiao, and A. M. Zheltikov, «Saturation of third-harmonic generation in a plasma of self-induced optical breakdown due to the self-action of 80-fs light pulses,» Opt. Commun. 133, 587-595 (1997).
[4] H. Hamster, A. Sullivan, S. Gordon, W. White, and R. Falcone, «Subpicosecond electromagnetic pulses from intense laser-plasma interaction,» Phys. Rev. Lett. 71, 2725 (1993).
[5] C. d'Amico, A. Houard, M. Pellet, C. Pichot, and A. Mysyrowicz, «Dipolar-like antenna emission in the radiofrequency range by laser-produced plasma channels in air,» Journal of Physics D: Applied Physics 41, 245206 (2008).
[6] A. Englesbe, J. Elle, R. Reid, A. Lucero, H. Pohle, M. Domonkos, S. Kalmykov, K. Krushelnick, and A. Schmitt-Sody, «Gas pressure dependence of microwave pulses generated by laser-produced filament plasmas,» Optics Letters 43, 4953-4956 (2018).

# Achievements and prospects of ground-based millimeter astronomy

**I. Zinchenko**

*Federal Research Center A.V. Gaponov-Grekhov Institute of Applied Physics of the Russian Academy of Sciences*

*zin@ipfran.ru*

Millimeter and submillimeter astronomy are essential tools for studying various astrophysical objects and phenomena. First, they explore the “cold” Universe. It primarily comprises dense interstellar gas and dust clouds, both within our Galaxy and beyond. These clouds are the site of star formation, many aspects of which are still not fully understood. Their emission peak lies in the submillimeter range. This category also includes studies of the microwave background (CMB), whose temperature is approximately 2.73 K. Another class of problems where millimeter and submillimeter astronomy plays a key role is the study of distant astronomical objects with very high angular resolution using very-long-baseline radio interferometry. Importantly, scattering in the interstellar medium in this range decreases with shorter wavelengths. This has allowed imaging of supermassive black holes in the galaxy M87 and at the center of our Galaxy.

Several projects to create new ground-based instruments for this range are currently being implemented and discussed worldwide. Various options for constructing such antennas are also being considered in Russia. Highly sensitive receiving equipment is being developed. Work is actively underway to select potential sites for millimeter telescopes. This report will provide an overview of the relevant work.

# Terahertz characterization of Advanced Superconducting and Ferroelectric Heterostructures: Bridging Fundamental Electrodynamics to NextGeneration Device Performance

**E.S. Zhukova[1], M.V. Talanov[1], A. Terentiev[1], V.S. Stolyarov[1], V.P. Koshelets[2], A.E. Parafin[3], N.S. Sokolov[4], F.V. Khan[2], D.V. Masterov[3], B.P. Gorshunov[1]**

*1- Moscow Institute of Physics and Technology, 141700 Dolgoprudny, Russia*
*2- Kotelnikov Institute of Radio Engineering and Electronics of RAS, Moscow, 125009, Russia*
*3- Institute for Physics of Microstructures of RAS, Nizhny Novgorod, 603950, Russia*
*4- Ioffe Physical-Technical Institute, 26 Politekhnicheskaya Street, St. Petersburg 194021, Russia*

*zhukova.es@mipt.ru*

Superconducting and ferroelectric heterostructures are critically important for next-generation electronic devices targeting the terahertz band. A key bottleneck is establishing a quantitative link between the fundamental electrodynamic properties of such heterostructures (and their constituent materials) and the functional performance of practical devices (see, e.g., [1]). The challenge arises from the inherently multiscale, multi-level nature of interactions: interface effects, dimensional quantization, and interlayer coupling can dramatically alter the electrodynamical response compared to that of individual bulk materials. In this context, experimental methods that not only characterize thin films and heterostructures but also reveal how technological processes (e.g., deposition/synthesis conditions) impact final films, structures and device parameters become indispensable.

Among the most powerful tools in this regard are optical spectroscopies, which combine non-contact operation, high sensitivity, and direct insight into parameters of electronic and magnetic subsystems (complex dynamical conductivity, permittivity, magnetic permeability, etc.) as well as to macroscopic electrodynamic characteristics (transmissivity, reflectivity, absorptivity). Terahertz (THz) and infrared (IR) spectroscopies are particularly valuable, as they provide direct access to the corresponding frequencies that are promising for advanced telecommunication systems (see, e.g., [2]).

Here we employ two complementary approaches for quantitative THz analysis of advanced thin films and heterostructures: THz pulsed time-domain spectroscopy (TDS) and monochromatic coherent-source BWO-spectroscopy (BWO-backward-wave oscillator, source of coherent THz radiation). Both enable direct extraction of complex conductivity and permittivity of materials. Crucially, the BWO-based approach provides record-high frequency resolution ($\sim 10^{-6}$), unattainable by TDS, which is essential for resolving narrow resonances.

We present our latest results from systematic and detailed THz–IR spectroscopic studies (frequencies 3 to 700 $cm^{-1}$, temperatures 3 to 300 K) of thin films and heterostructures of ferroelectrics and superconductors (both conventional and high) – materials that rank among the most promising for nextgeneration THz devices. We will demonstrate examples where spectroscopic data on films and heterostructures are used to directly improve the performance of THzrange devices – from filters and modulators to resonators and switches. Thus, we show a direct pathway bridging fundamental electrodynamics to the engineered performance of nextgeneration devices.

This work was supported by the Ministry of Science and Higher Education under grant № 075-15-2025-010 (preparation of films and structures), by the Russian Science Foundation under grant №23-79-00019 (THz experiments) and № 26-12-00493 (data analysis).

[1] Hyuk-Jun Kwon, Electronics 11, 931 (2022).
[2] Jia Du1, Xiang Gao, Ting Zhang and He Zhu . J. Phys. D: Appl. Phys. V. 58, 313001 (2025).

# Anisotropy of photoelasticity in doped lead molybdate crystals

**Akhmedzhanov F.R., Mirzaev S.Z., Nuzhdov G.S.**

*Institute of Ion-Plasma and Laser Technologies, Tashkent, Uzbekistan*

*akhmedzhanov.f@gmail.com*

Lead molybdate ($PbMoO_4$) crystals are among the most popular working media used in acousto-optic devices [1]. Modeling and optimization of the parameters of such systems require a detailed analysis of the anisotropy of the photoelastic effect. The aim of this work is to investigate the effect of low concentrations of sodium (Na) and neodymium (Nd) impurities on the effective photoelastic constant in $PbMoO_4$ crystals. The studies were performed on single-crystal samples of $PbMoO_4$, $PbMoO_4$:0.3Na, and $PbMoO_4$:0.2Nd oriented along the [100] and [001] axes. Longitudinal acoustic waves with frequencies of 0.8–1.2 GHz were excited by X-cut quartz piezoelectric transducers.

The effective photoelastic constants were determined using Bragg diffraction of light using a modified Dixon-Cohen method with laser radiation ($\lambda_0$ = 632.8 nm) [2]. A fused quartz sample was used as a standard. The accuracy of peff determination was ~10%. Based on the obtained values of the effective photoelastic constants, all independent components of the photoelasticity tensor were determined.

Figure 1 shows the dependence of the effective photoelastic constant on the polarization direction of light incident on the crystal along the [010] axis and diffracted by a longitudinal acoustic wave along the [100] axis. In general, this dependence is described by the expression:

$$p_{eff}=p_{ijkl}\,a_i\,\beta_j\,\gamma_k\,k_l, \qquad (1)$$

where $a_i$ and $\beta_j$ are the components of the unit polarization vector of the incident and diffracted light; $\gamma_k$ and $k_l$ are the components of the polarization and wave vector of the acoustic wave.

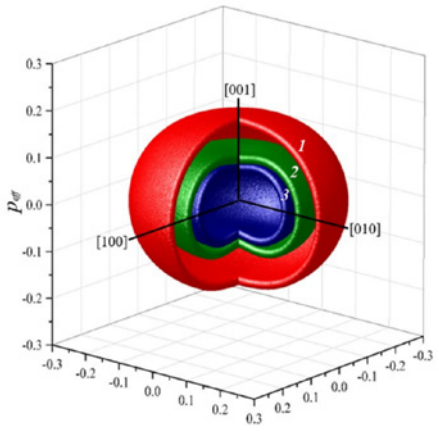


**Fig. 1.** Dependence of the effective photoelastic constant on the polarization direction of light incident along the <010> axis in $PbMoO_4$ (1), $PbMoO_4$:0.2Nd (2), and $PbMoO_4$:0.3Na (3) crystals

It is evident that the introduction of impurities leads to a noticeable change in the magnitude and degree of anisotropy of the effective photoelastic constant. The influence of sodium and neodymium dopants on the effective photoelastic constant in $PbMoO_4$ crystals may be due to the high mobility of $Na^+$ and $Nd^{3+}$ ions. The displacement of the ionic subsystem induced by a high-frequency acoustic field leads to strong electrostatic shielding of changes in the crystal's permittivity and a corresponding decrease in peff. The observed effect of reduced photoelasticity in doped lead molybdate crystals must be taken into account when developing working elements of acousto-optic deflectors and light modulators.

[1] F.R. Akhmedzhanov, M.I. Elboeva, S.Z. Mirzaev. Exploring of Anisotropy of Acousto-Optic Interaction in Lead Molybdate Crystals. Ultrasonics, Vol. 137 107203 (2024) https://doi.org/10.1016/j.ultras.2023.107203

[2] F.R. Akhmedzhanov, J.O. Kurbanov, A.F. Boltabaev. Attenuation of Acoustic Waves in Single-domain and Polydomain LiTaO3 Crystals. Sensors & Transducers. **246**, p. 43-47 (2020).

# Frequency and spatial dispersion of attenuation of acoustic waves in lanthanum gallosilicate crystals

**Akhmedzhanov F.R., Tursunov I.O.**

*Institute of Ion-Plasma and Laser Technologies, Tashkent, Uzbekistan*

*akhmedzhanov.f@gmail.com*

The main material for piezoelectric transducers and frequency stabilizers are thermally stable quartz crystals. They can be competed with by lanthanum gallosilicate crystals ($La_3G_5SiO_{14}$), which have an electromechanical coupling coefficient 3-4 times higher and exhibit higher temperature stability of piezoelectric characteristics [1]. One of the parameters limiting the use of these crystals is the acoustic attenuation. This coefficient, under the condition $\omega\tau<<1$ ($\omega$ is the circular frequency of the acoustic wave, $\tau$ is the relaxation time of thermal phonons), is determined mainly by the Akhiezer mechanism [2]. In this case, the acoustic attenuation coefficient can be calculated using the complex elasticity tensor, the imaginary part of which describes the energy loss of the acoustic wave [2].

$La_3G_5SiO_{14}$ samples were shaped as rectangular prisms, oriented along the [100] and [001] axes with an error of no more than $1^0$. Acoustic waves were excited by X-cut lithium niobate transducers. The attenuation of acoustic waves was determined by the Bragg diffraction method [2]. A helium-neon laser ($\lambda_0$ = 632.8 nm) was used as a light source. The accuracy of determining the attenuation coefficient was ~ 5%. The dependences of the acoustic attenuation coefficient on frequency are shown in Figure 1. It is evident that these dependences well follow the quadratic law, according to the Akhiezer mechanism.

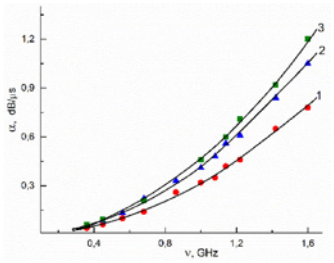


**Fig. 1.** Dependence of the acoustic attenuation coefficient on frequency for longitudinal waves along the directions [001] (1) and [100] (2) and transverse waves along [100] (3). Solid lines are drawn under the assumption of a quadratic dependence.

The obtained values of acoustic wave velocity and attenuation allow us to determine the effective real and imaginary elastic constants, and, based on these, the velocity V and the acoustic wave attenuation coefficient $\alpha$ for an arbitrary wave vector direction. The spatial dispersion of attenuation for acoustic waves propagating in the (100) plane is shown in Figure 2.

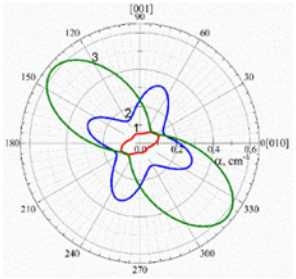


**Fig. 2.** Cross-section of the attenuation surface of longitudinal (1) and fast (2) and slow (3) transverse acoustic waves by plane (100) in $La_3Ga_5SiO_{14}$ crystals

It is evident that the strongest spatial dispersion of attenuation is observed for transverse acoustic waves. The identified features of the frequency and spatial dispersion of acoustic wave attenuation will be useful in the development of acoustic and acoustoelectronic devices, including sensors, piezoelectric resonators, and delay lines based on lanthanum gallosilicate crystals.

[1] Jingxiang Si, Changhong Yang, Rui Guo, Yifan Wu, Xiujuan Lin and Shifeng Huang. Preparation and acoustic properties of high-temperature acoustic emission sensor based on $La_3Ga_5SiO_{14}$ crystal. J. Adv. Dielect. **13**, 342001-8 (2023).

[2] F.R. Akhmedzhanov, J.O. Kurbanov, A.F. Boltabaev. Attenuation of Acoustic Waves in Single-domain and Polydomain $LiTaO_3$ Crystals. Sensors & Transducers. **246**, p. 43-47 (2020).

# Liquid-Phase Exfoliation of $WS_2$: A Scalable Approach for Terahertz Modulators

**M.S. Lapteva[1], K.G. Kuznetsov[1], E.A. Bulavintseva[1], K.A. Brekhov[1], D.A. Abdullaev[1,2], S.D. Lavrov[1], E.D. Mishina[1].**

*1- MIREA – Russian Technological University (78, Vernadskogo pr., Moscow 119454, Russia)*
*2- Institute of Nanotechnology of Microelectronics RAS (32A, Leninsky pr., Moscow 119991, Russia)*

*bulavinceva@mirea.ru*

Terahertz range (500 GHz – 30 THz) has long remained largely inaccessible due to the lack of reliable radiation sources, yet it holds enormous potential for applications in telecommunications (including 6G), security systems, imaging, and spectroscopy of materials, including biomedical ones. For the full realization of THz technologies, in addition to sources and detectors, the development of additional devices, such as optical modulators that alter the parameters of the THz signal, is necessary.

Of particular interest are optically controlled THz modulators based on films of transition metal dichalcogenides (TMDs) [1], where the modulation depth can reach 90% or more [2]; however, the reproducibility of film properties is critically important for mass applications [3]. The thickness and coating density of the film play a crucial role.

Various approaches exist for fabricating TMD films. Chemical vapor deposition (CVD) enables monolayer films with full coverage and precise thickness control, but suffers from low reproducibility, high defect density [4-5], expensive equipment, and long processing times. Mechanical exfoliation, the laboratory gold standard, lacks controlled surface coverage and thickness. In contrast, liquid-phase exfoliation (LPE) stands out for mass production due to its high scalability and low cost [6]. LPE produces a suspension of nanolayers (few to tens of monolayers) for drop-casting. For applications not requiring a direct bandgap monolayer, this method is optimal.

For THz modulators, liquid-phase $WS_2$ films were chosen because liquid-phase exfoliation (LPE) provides control over coating thickness while maintaining process simplicity [7]. In the future, the developed methods and approaches based on LPE structures can be used for rapid prototyping of THz-range devices based on TMDs.

This work presents the results of a study of $WS_2$/Si structures obtained by liquid-phase exfoliation. A detailed characterization of the structures was carried out using optical methods, atomic force microscopy, and energy-dispersive analysis. The structural and chemical integrity of the films after the technological process operations was confirmed. The transmission of terahertz radiation in the range of 0.5–2.5 THz by such structures was studied both without illumination and under illumination. Continuous radiation with a wavelength of 532 nm was used as the pump. The dependence of the modulation depth on the film parameters is also presented. A more continuous film provides a larger TMD/Si contact area and more efficiently generates photocarriers under optical illumination. Under periodic 532 nm illumination, electron-hole pairs are generated in the TMD and silicon, which separate at the TMD/Si interface due to the difference in work functions, thereby increasing the carrier lifetime in the substrate and enhancing the photoconductivity of the entire structure.

This work was supported by the Russian Science Foundation, grant № 25-19-00575.

[1] Peter Weis, Juan L. Garcia-Pomar, Michael Höh, et al.. Spectrally Wide-Band Terahertz Wave Modulator Based on Optically Tuned Graphene. ACS Nano. 6. 10. 9118-9124. 2012-10-23.
[2] Seung Hoon Lee, Muhan Choi, Teun-Teun Kim, et al.. Switching terahertz waves with gate-controlled active graphene metamaterials. Nature Mater. 11. 11. 936-941. 2012-11.
[3] Yuan Meng, Hongkun Zhong, Zhihao Xu, et al.. Functionalizing nanophotonic structures with 2D van der Waals materials. Nanoscale Horiz.. 8. 10. 1345-1365. 2023.
[4] Ana Senkić, Antonio Supina, Mert Akturk, et al.. Microscopic investigation of intrinsic defects in CVD grown MoS2 monolayers. Nanotechnology. 34. 47. 475705. 2023-11-19.
[5] Jin Liu, Tsz Wing Lo, Jianhui Sun, et al.. A comprehensive comparison study on the vibrational and optical properties of CVD-grown and mechanically exfoliated few-layered WS2. J. Mater. Chem. C. 5. 43. 11239-11245. 2017.
[6] Chen-Xia Hu, Yuyoung Shin, Oliver Read, et al.. Dispersant-assisted liquid-phase exfoliation of 2D materials beyond graphene. Nanoscale. 13. 2. 460-484. 2021.
[7] Priyanka Yadav, Anirban Das, Manoj Kumar Sharma, et al.. A biodegradable polymer-assisted efficient and universal exfoliation route to a stable few layer dispersion of transition metal dichalcogenides. Materials Chemistry and Physics. 276. 125347. 2022-1.

# The influence of ultrashort pulse propagation on the optical properties of gases

**K. Galyuk, P. Chizhov, A. Ushakov**

*Prokhorov General Physics Institute of the Russian Academy of Sciences, Moscow, Russia*

*karina272001@yandex.ru*

Propagation of ultrashort laser radiation in a gas leads to the formation of nonlinear effects: Kerr self-focusing and plasma defocusing. The dynamic balance of these phenomena results in the formation of a filament. Thus, an ultrafast change in the optical properties of the gaseous medium is induced: the appearance of anisotropy of the refractive index, absorption, scattering, etc. The study of this allows for non-invasive determination of the laser radiation and filament parameters. Furthermore, optimization of the laser radiation and the medium parameters is relevant for improving the efficiency of secondary radiation generation from laser plasma.

In this work, we investigate the propagation of laser radiation (duration 40 fs, central wavelength 800 nm, pulse energy 2.7 mJ) under various conditions. Different gaseous media (air, argon, nitrogen, and carbon dioxide) at pressures of 1–5.5 atm are considered. The study of the optical properties of the gas in the pre-focal region of the laser radiation is carried out using the transverse pump-probe method [1]. The pump radiation is focused into a gas cell and leads to the formation of a plasma channel. The probe radiation is needed to study the optical properties of the medium in the region of laser radiation propagation. The probe pulse crosses the investigated region of the pump beam. The propagation axes of the pump and probe radiations are mutually orthogonal. Using an analyzer and a camera, the spatial distribution of the intensity of the depolarized probe radiation is recorded [2]. Several spatial regions of pump radiation propagation in the pre-focal region are investigated, which allows us to study the temporal dynamics of changes in the optical properties of the medium.

It was found that the change in polarization is both a phase and an amplitude phenomenon. An increase in gas pressure leads to an increase in the intensity of the depolarized radiation. Also, under tight focusing with a parabolic mirror, the depolarization of radiation is non-uniform across the spectrum.

[1] V. Loriot, E. Hertz, B. Lavorel, O. Faucher, High rate concentration measurement of molecular gas mixtures using a spatial detection technique, J. Chem. Phys., vol. 132, pp. 184303, (2010).
[2] A. Ushakov, P. Chizhov, V. Bukin, T. Dolmatov, and S. Garnov, Narrow intensity range optical anisotropy in air induced by a femtosecond laser breakdown, Appl. Opt., vol. 62, pp. 8000–8006, (2023).

# Superconducting Terahertz Fabry–Pérot Resonators: Electrodynamic Characterization and Quality Factor Analysis Using Coupled-Mode Theory

**A.V. Melentev[1,2], D.G. Baranov[1], A. Terentiev[1], B.P. Gorshunov[1], E.S. Zhukova[1]**

*1- Moscow Institute of Physics and Technology, Dolgoprudny, Russia*
*2- HSE University, Moscow, Russia*

*aleksandr.melentyev@phystech.edu*

Terahertz (THz) resonators with low dissipative losses are of considerable interest for spectroscopy, sensing, and emerging quantum technologies [1-3]. In this work, we present an experimental investigation of THz Fabry–Pérot resonators employing superconducting thin films as reflectors. The use of superconducting films enables a substantial reduction of internal losses and enhanced reflectivity compared to conventional metallic structures, providing access to regimes of enhanced electromagnetic energy storage and high quality factors [4].

We performed transmission measurements on Fabry–Pérot resonators formed by superconducting $Mo_{0.6}Re_{0.4}$ films deposited on both sides of a plane-parallel highly-insulating silicon substrate in the frequency range of 2–50 $cm^{-1}$. The experiments combined a commercial terahertz time-domain spectroscopy (THz-TDS) system with a continuous-wave spectrometer based on backward-wave oscillators, providing broadband high-frequency resolution characterization of the resonator performance. Resonance frequencies, linewidths, and peak transmission were extracted from the measured spectra and used to determine the frequency- and temperature-dependent complex conductivity of the $Mo_{0.6}Re_{0.4}$ films. Upon cooling below the superconducting transition temperature, a substantial increase in the resonator quality factor and enhanced FWHM was observed, consistent with the suppression of dissipative losses and high reflectivity in the superconducting mirrors.

To analyze the loss mechanisms governing the resonator performance, the experimental results were interpreted within the framework of temporal coupled-mode theory. The total decay rate was decomposed into radiative and ohmic contributions, enabling quantitative evaluation of the coupling regime and the relative importance of dissipative losses. The extracted parameters demonstrate that superconducting mirrors significantly suppress ohmic loss channels and allow the resonator characteristics to approach the regime where radiative losses dominate. The developed approach provides a unified framework linking the intrinsic electrodynamic properties of superconducting films, measured by THz-TDS, with the macroscopic resonator response.

These results establish superconducting Fabry–Pérot resonators as a promising platform for low-loss THz photonics and provide a foundation for future studies of critical coupling and extreme electromagnetic energy confinement in open resonant systems.

This work was supported by the Ministry of Science and Higher Education of the Russian Federation grants FSMG-2024-0014 (data analysis), No. 075-15-2025-010 (terahertz measurements) and 26-12-00493 (preparation of the resonator).

[1] P. U. Jepsen, D. G. Cooke, and M. Koch, Terahertz spectroscopy and imaging – Modern techniques and applications, Laser & Photonics Reviews, vol. 5, pp. 124–166, (2011).
[2] S. Hazra, A. Sharma, S. Chakrabarti, and S. Ghosh, Enhanced Transmission at the Zeroth-Order Mode of a Terahertz Fabry–Pérot Cavity, ACS Omega, vol. 9, pp. 11858–11865, (2024).
[3] J. E. Lee, J. Kim, and coauthors, Gapless superconductivity in Nb thin films probed by terahertz spectroscopy, Nature Communications, vol. 14, article 3303, (2023).
[4] A. Terentiev, A. Melentev, A. G. Shishkin, M. S. Sidelnikov, and A. M. Chekushkin, Thin Superconducting Films as Reflectors for High-Q Terahertz Fabry–Pérot Resonators, IEEE Transactions on Terahertz Science and Technology, Early Access, pp. 1–13, (2026)

# Optical properties of β-$BaB_2O_4$ crystals grown in the $BaB_2O_4$-$NaBaBO_3$-$BaMoO_4$ system

**E. Simonova[1], D. Ezhov[2], A. Goreyavcheva[1], A. Kokh[1], V. Svetlichnyi[2]**

*1- Sobolev Institute of Geology and Mineralogy SB RAS, Novosibirsk 630090, Russia*
*2- Tomsk State University, Tomsk 634050, Russia*

*simonovaea@igm.nsc.ru*

In the modern era of photonics and laser technology, NLO crystals play a pivotal role in expanding the spectral range of coherent light sources through frequency conversion. Among these materials, borate family of NLO crystals are particularly promising [1] due to their high laser damage threshold [2], moderate to high nonlinear susceptibility coefficients [3], and wide transparency window extending into the deep ultraviolet.

A bulk β-$BaB_2O_4$ crystal was grown from a novel $BaB_2O_4$-$NaBaBO_3$-$BaMoO_4$ ternary solvent system with an optimal solvent composition using top-seeded solution growth (TSSG) and its optical properties were compared to those of a reference crystal grown from the conventional binary $BaB_2O_4$-$NaBaBO_3$ system. The linear absorption spectrum was measured for both polarizations over an exceptionally broad range from ultraviolet (UV) to terahertz (THz) range (0.2–1500 μm), revealing high transparency and low absorption coefficients, indicative of excellent material uniformity and purity. Nonlinear optical (NLO) performance was evaluated via secondharmonic generation (SHG) at 266 nm, showing comparable efficiency to the reference sample. These results demonstrate that the ternary system enables scalable crystal growth with preserved high optical quality, making it a promising candidate for industrial production of nonlinear optical elements.

In this study, a novel ternary $BaB_2O_4$-$NaBaBO_3$-$BaMoO_4$ solvent system was developed and optimized for the scalable growth of highquality β-$BaB_2O_4$ nonlinear optical crystals. Comprehensive phase equilibria studies identified the optimal solvent composition (0.70•$BaB_2O_4$-0.25•$NaBaBO_3$-0.05•$BaMoO_4$ mol%) and allowed for the refinement of the primary crystallization fields of five compounds: $BaB_2O_4$, $BaMoO_4$, $NaBaBO_3$, $Ba_5B_4O_{11}$, and $NaBa_4(BO_3)_3$, which are separated by joint crystallization curves. A large β- $BaB_2O_4$ crystal, 75 mm in diameter and 30 mm in height, was successfully grown using the TSSG method. This demonstrates the enhanced crystallization stability for greater crystal height and extended crystallization temperature range (>100 ◦C) offered by the ternary composition compared to the reference binary solvent system. Optical elements fabricated from the grown crystal exhibited excellent quality, as confirmed by low absorption coefficients (≤0.003 cm− 1 on average for both polarizations in the 300–700 nm range) and high second-harmonic generation efficiency at 266 nm. Notably, the linear and nonlinear optical properties of these elements are indistinguishable from those of reference samples grown from the binary $BaB_2O_4$-$NaBaBO_3$ system. These results demonstrate that the $BaB_2O_4$-$NaBaBO_3$-$BaMoO_4$ system enables the production of large, high-performance β-BBO crystals without compromising optical quality, making the proposed solvent system a strong candidate for industrial-scale manufacturing of nonlinear optical elements for advanced laser and photonic technologies.

This work was supported by the RSF project (№ 25-23-20004).

[1] C. Chen, T. Sasaki, R. Li, Y. Wu, Z. Lin, Y. Mori, Z. Hu, J. Wang, S. Uda, M. Yoshimura, Y. Kaneda, Nonlinear Optical Borate Crystals, Wiley, Weinheim, Germany, 2012, https://doi.org/10.1002/9783527646388.
[2] D.N. Nikogosyan, Nonlinear Optical Crystals: a Complete Survey, Springer-Verlag, New York, 2005, https://doi.org/10.1007/b138685.
[3] Chen, C., Sasaki, T., Li, R., Wu, Z., Lin, Z., Mori, Y., Hu, Z., Wang, J., Uda, S., Yoshimura, M. and Kaneda, Y., [Nonlinear Optical Borate Crystals: Principals and Applications], Weinheim Wiley-VCH (2012).

# Advancing High-Q Superconducting THz Fabry–Perot Resonators: From BCS to high-Tc Reflectors

**E.S. Zhukova[1], A. Terentiev[1], A.E. Parafin[2], D.V. Masterov[2], S.A. Pavlov[2], A. Melentev[1], B.P. Gorshunov[1]**

*1- Moscow Institute of Physics and Technology, 141700 Dolgoprudny, Russia*
*2- Institute for Physics of Microstructures of RAS, Nizhny Novgorod, 603950, Russia*

*zhukova.es@mipt.ru*

Recently [1], we designed, fabricated, and thoroughly characterized high-Q terahertz (THz) Fabry–Perot (FP) resonators based on thin BCS-type superconducting (SC) $Mo_{0.6}Re_{0.4}$ films. Due to a monolithic design with two films deposited on both sides of a high-resistivity plane-parallel dielectric (silicon) slab, the resonators are super-compact (0.5×8×8 mm³), require no mirror alignment, simple in design and analysis, and easy and cheap to manufacture. At T = 2.5 K, we demonstrated record parameters: quality factors Q up to 830, finesse F up to 580, peak transmission $Tr_{max}$ up to 60%, and FWHM of 150 MHz.It is clear that such resonators are inherently limited in their operational temperature interval (up to $T_c \approx$ 8 K in $Mo_{0.6}Re_{0.4}$) and frequency range (up to the BCS gap frequency $2\Delta/h \leq 1$ THz in $Mo_{0.6}Re_{0.4}$; here Δ is SC energy gap and h is Planck's constant). To overcome these limitations and extend both the temperature and frequency windows, we have now fabricated and investigated FP resonators employing high-temperature superconductor (HTSC) $YBa_2Cu_3O_{7-\delta}$ (YBCO) films as reflectors, keeping the same monolithic design with sapphire plane-parallel substrate. The YBCO-based resonators enable stable operation up to $2\Delta/h$ ~3 THz and at much higher temperatures, up to $T_c \approx$90 K. Using magnetron sputtering, the 30 nm thick YBCO films were deposited on both planes of sapphire plane-parallel substrate (r-plane sapphire, thickness 0.45 mm). The cerium oxide buffer sublayer (50nm) was deposited using laser sputtering (KrF 248 nm excimer laser). With THz time-domain and coherent-source BWO spectroscopic techniques (BWO-backward-wave oscillator, source of coherent THz radiation), we systematically investigate the frequency ($\nu$=5 – 55 $cm^{-1}$ or 0.15 – 1.5 THz) and temperature (T=5–300 K) dependences of the resonator transmission spectra of the YBCO-based resonator, extract key parameters of the resonances (quality factor, finesse, FWHM, peak transmittance), and benchmark them against previously reported low-temperature superconducting MoRe systems. We show that while the YBCO resonators offer broader temperature/frequency coverages, they exhibit somewhat reduced peak transmittance due to subgap absorption inherent to the d-wave symmetry of the HTSC order parameter. We quantitatively compare the figure-of-merit of BCS-based*vs.* HTSC-based resonators, discuss the trade-offs between gap frequency, operating temperature, losses, and practical cooling requirements, and propose routes to mitigate d-wave absorption in HTSC mirrors. Our progress demonstrates that BCS-based THz FP resonators remain optimal for high-Q, ultralow-loss, narrow-band applications below 1 THz at cryogenic temperatures, whereas HTSC-based resonators open the door to higher-frequency, higher-temperature THz interferometry, relevant for compact sensing, communication, and quantum technologies.

This work was supported by the Ministry ofScience and Higher Education grant № FSMG-2025-0005(THz experiments) and by the Russian Science Foundation under grant№ 26-12-00493(data analysis).

[1] A. Terentiev, A. Melentev, A. G. Shishkin, M. S. Sidelnikov, Z. V. Gagkaeva, V. S. Stolyarov, B. P. Gorshunov, and E. S. Zhukova. Thin Superconducting Films as Reflectors for High-Q Terahertz Fabry-Perot Resonators. IEEE Transactions on Terahertz Science and Technology. 16, No. 4, 393-405 (2026).

# Simulations of Enhancing Output Characteristics of Megawatt-Class Gyrotrons via Frequency-Locking Techniques

**G. Denisov, I. Zotova, I. Zheleznov, A. Sergeev, A. Ananichev, A. Kirsanov, M. Glyavin**

*A.V. Gaponov-Grekhov Institute of Applied Physics of the Russian Academy of Sciences, Russia*

*zotova@ipfran.ru*

As is well known, gyrotrons are the most powerful sources of continuous-wave (CW) millimeter-wave radiation, providing radiation power up to 1 MW at frequencies of 110–170 GHz [1]. The primary application of these gyrotrons is electron cyclotron resonance (ECR) plasma heating in thermonuclear fusion facilities. Currently, the role of ECR heating is expanding compared to other plasma heating methods, which drives the need to increase both the output power (e.g., up to 1.2 MW for the ITER project) and the efficiency of gyrotrons. A second trend involves increasing the generation frequency of megawatt-class gyrotrons up to 230–250 GHz, which is required for next-generation fusion facilities such as TRT and DEMO.

It is well known that increasing the frequency and output power of gyrotrons can only be achieved by utilizing strongly oversized resonators in which high-order transverse modes are excited. At the same time, increasing the cavity dimensions is limited both by the internal bores of modern magnetic systems and by the mode competition problem, which inevitably intensifies due to the increasing density of the mode spectrum. As one of the approaches to solving these problems, the gyrotron can be locked by a weak external signal which provides priming for the operating mode, suppressing spurious oscillations [2]. In particular, a significant increase in output power (by more than 10%) was demonstrated in experiments with a 170-GHz gyrotron for ITER [3] and a prototype 230-GHz gyrotron [4] developed for the TRT tokamak.

This paper presents the simulation results for the aforementioned experiments based on an advanced non-stationary multi-mode model of electron-wave interaction, and discusses further prospects related to frequency locking. In particular, we demonstrate the feasibility of a megawatt-class gyrotron operating at the second cyclotron harmonic and show the potential for increasing the power up to 2.5–3 MW at the fundamental resonance.

This work was supported by the Institute of Applied Physics of the Russian Academy of Sciences (IAP RAS) under Project No. FFUF–2022–0007.

[1] A.G. Litvak, G.G. Denisov, M.Y. Glyavin, “Russian Gyrotrons: Achievements and Trends,” IEEE J. Microwaves, vol.1, art.no.260 (2021).
[2] V. S. Ergakov, M. A. Moiseev, and V. I. Khizhnyak, “On the theory of Cyclotron-Resonance-Maser (CRM) synchronization,” (in Russian), Radiotekh. Elektron., vol. 23, no. 12, pp. 2591–2599 (1978).
[3] A.N. Kuftin, G.G. Denisov, A.V. Chirkov, M.Yu. Shmelev, V.I. Belousov, A.A. Ananichev, B.Z. Movshevich, I.V. Zotova, M.Yu. Glyavin. “First Demonstration of Frequency-Locked Operation of a 170 GHz/ 1 MW Gyrotron,” IEEE Electron Dev. Lett., vol.44, no.9, pp.1563-1566 (2023)
[4] A.A. Ananichev, A.P. Fokin, A.N. Kuftin, V.N. Manuilov, L.G. Popov, A.V. Chirkov, E.M. Tai, M.V. Morozkin, M.Yu. Glyavin, G.G. Denisov, “Experimental Study of a Short-Pulse Prototype Megawatt-Power 230-GHz Gyrotron for the TRT Tokamak,”IEEE Electron Dev. Lett., vol.46, no.11, p.2142-2144 (2025).

ALT INTERNATIONAL CONFERENCE
Advanced Laser Technologies

# PHOTONICS IN QUANTUM TECHNOLOGIES

# Waveguide-Integrated Superconducting Nanowire Single-Photon Detectors: From Technology to Hybrid Platforms

**V. Kovalyuk[1,2], I. Venediktov[3,1], V. Korovin[1,2], A. Nevzorov[1], K. Sedykh[3,1], D. Kobtsev[3,1], A. Golikov[1,2], A. Prokhodtsov[1], A. Kuzin[1], I. Florya[1,2], R. Kasimov[1], A. Semenov[1], E. Lebedeva[1,2], A. Semenov[1], G. Goltsman[2,4]**

*1-University of Science and Technology MISIS, 119049 Moscow, Russia*
*2-Moscow State Pedagogical University, 119991 Moscow, Russia*
*3-National Research University Higher School of Economics, 109028 Moscow, Russia*
*4- Russian Quantum Center, 121205 Moscow, Russia*

*kovaliuk.vv@misis.ru*

This work presents a comprehensive overview of the development, scalability, and application of superconducting nanowire single-photon detectors (SNSPDs), tracing their evolution from pioneering 2001 [1] standalone devices to state-of-the-art waveguide-integrated components for Quantum Photonic Integrated Circuits (QPICs).

While early SNSPDs yielded limited quantum efficiency, modern variants exceed 95% efficiency across a broad electromagnetic spectrum (visible to near-IR). These high-performance metrics empower critical fields such as optical quantum computing, cryptography, metrology, and deep-space communications. The device physics rests on ultra-thin (~4 nm thick, 100 nm wide) superconducting nanostrips (typically NbN) operating near critical current at cryogenic temperatures (~2 K). Light absorption causes local superconductivity suppression via hot-spot and vortex generation and electrical pulse generation. To overcome the scaling limits of free-space optics, the research shifts toward chip-scale QPICs composed of single-photon sources, integrated photonics, and embedded detectors [2]. While silicon nitride is predominantly used due to its low optical losses, thin-film lithium niobate on an insulator (LNOI) is actively introduced to achieve high-speed cryogenic electro-optic modulation (GHz range) compared to standard thermal microheaters (kHz range) [3]. Cryogenic characterization of these chips is performed in a custom-built, closed-cycle cryostat setup featuring automated multi-channel fiber arrays and RF electrical probes. A key innovation involves moving from vertical fiber-coupled architectures to horizontal waveguide-integrated schemes where absorption occurs through evanescent mode coupling. Precise absorption engineering determines that optical coupling depends highly on the waveguide dimensions, nanowire geometry, and etching depth. The advanced functional designs include integrating detectors with waveguide resonators to drop the decay time to 500 ps, creating integrated spectrometers, and implementing high-speed (6 Mbps) quantum key distribution (QKD) nodes. Fabricated detectors demonstrate robust material performance, maintaining a high critical temperature (~8 K) and high critical current density (~ 5 MA/cm$^2$) under protective hydrogen silsesquioxane (HSQ) encapsulation. Experimental testing exhibits a timing jitter of 40–50 ps and high sensitivity optimized for GaAs quantum dots (925 nm). Finally, the work outlines a visionary roadmap toward a fully hybrid quantum photonic platform. This architecture combines Si3N4 waveguides, LNOI modulators, and high-purity single-photon sources (InGaAs quantum dots in micropillars showcasing 91% indistinguishability), interconnected via advanced 3D photon bonding. Extrapolations of this hardware are demonstrated in ion-trap computing scalability (integrating 2D Paul traps with SNSPDs under indium tin oxide (ITO) radio-frequency shielding) [4] and a plug-and-play cryogenic system combining fiber-pigtail quantum-dot sources and detectors in a single compact cryostat, ready for commercial deployment in optical quantum computing networks.

[1] Gol'tsman, G. N., Okunev, O., Chulkova, G., Lipatov, A., Semenov, A., Smirnov, K., ... & Sobolewski, R. (2001). Picosecond superconducting single-photon optical detector. Applied physics letters, 79(6), 705-707.
[2] Pernice, W. H., Schuck, C., Minaeva, O., Li, M., Goltsman, G. N., Sergienko, A. V., & Tang, H. X. (2012). High-speed and high-efficiency travelling wave single-photon detectors embedded in nanophotonic circuits. Nature communications, 3(1), 1325.
[3] Kobtsev, D. M., Venediktov, I. O., Svyatodukh, M. I., Golikov, A. D., Nevzorov, A. A., Lazarenko, P. I., ... & Goltsman, G. N. (2025). A study of the response time of an electro-optical modulator based on a ring microresonator made of thin-film lithium niobate on an insulator. Nanoindustry, 18(12s), 82-89.
[4] Sedykh, K. O., Suleimen, E., Svyatodukh, M. I., Podlesnyy, A., Kovalyuk, V. V., An, P. P., ... & Goltsman, G. N. (2023). Effect of an external alternating electric field on the efficiency of a superconducting single-photon detector. Technical Physics, 68(7), 907-914.

# Resonant subspace method for composite photonic crystal systems

**I.M. Fradkin, N.S. Salakhova, S.A. Dyakov, N.A. Gippius**

*Skoltech, Bolshoy Boulevard, 30, bld. 1, Moscow 121205, Russia*

*N.Gippius@skoltech.ru*

Nanostructures occupy a central place in modern photonics. To correctly describe their optical properties, it is often necessary to consider the redistribution of the electromagnetic field near the structures and the possibility of its resonant amplification for a photon frequency close to the resonance of the photonic system. This paper discusses a method for constructing a resonant approximation for the scattering matrix describing the redistribution of the light field in the vicinity of a photonic nanostructure.

Using structures that can be partitioned into two nonresonant subsystems, the possibility of con-structing a regular approximation of the resonance positions of a composite system is demonstrated. All elements of the resonant representation are determined by direct calculation at a limited number of points in the parameter space and subsequently allow a fairly accurate approximation over a wider range of structure parameters. The proposed method allows for the identification of the resonant part of the scattering matrix and the construction of regular approximation schemes for calculating the optical properties of resonant photonic structures without requiring numerous and resource-intensive computations.

The photonic systems under consideration are layered structures with periodic modulation of the permittivity in the plane of the layers and can be fabricated using well-developed semiconductor micro and nanotechnologies. The ability to control the dispersion properties of optical resonances in semiconductor structures by modifying the architecture of the photonic crystal cell opens up wide possibilities for using these systems as basic photonic elements.

The Fourier modal method (FMM) (or scattering matrix method) is a very effective tool for studying the optical properties of multilayer structures consisting of two-dimensionally periodic layers that are invariant in the vertical direction [1-6]. However, for problems requiring integration over wave vectors in the plane of the structure, the need for numerous similar calculations reduces the effectiveness of this method. The approach discussed in this paper significantly expands the capabilities of FMM.

[1] S.G. Tikhodeev et al., Phys. Rev. B 66(4), 045102 (2002).
[2] N.A. Gippius et al., Phys. Rev. B 72(4), 045138 (2005).
[3] N.A. Gippius et al., Optics Express 18(7), 7569 (2010).
[4] I.M. Fradkin et al., Phys. Rev. B 99(7), 075310 (2019).
[5] S.A. Dyakov et al., Laser Photonics Rev. 15, 2000242 (2021).
[6] S.A. Dyakov et al., JETP Letters, 122(10), 619 (2025).

# Template Optical Magnus Effect and Spin-Orbit Interaction of Light – 35 Years from the First Publication

**E.A. Bibikova[1,2], N.D. Kundikova[1,2]**

*1- The Institute of Electrophysics of the Ural Branch of the Russian Academy of Sciences, 106,Amundsen st., Ekaterinburg, Russia, 620016*
*2- South Ural State University (national research university), 76, Lenin pr., Chelyabinsk, Russia, 454080*

*kundikovand@susu.ru*

From a historical perspective, we review early optical phenomena that preceded to the experimental discovery of the Optical Magnus Effect and to the subsequent formulation of the concept of the spin–orbit interaction of light. These phenomena include well-known effects such as the Imbert–Fedorov shift and the Goose-Hanken shift, and the linear light polarisation rotation, which hinted at a subtle coupling between the spin and orbital degrees of freedom of photons long before the underlying theory was fully developed. Furthermore, we survey the key optical effects discovered over the entire period from 1991—the year of the first publication explicitly addressing these ideas—to the present. This period has witnessed remarkable progress, including the observation of the spin-Hall effect of light, optical vortex phenomena, and other manifestations of spin–orbit coupling in structured light fields, which have profoundly influenced modern photonics and quantum optics.

# Ion trap based coupled quantum memristors for creating neural networks and reservoir computing

**S. Stremoukhov[1,2], A. Frolova[1,2], I. Kovalishin[1], P. Forsh[1,2], K. Khabarova[2], N. Kolachevsky[2,3]**

*[1]Faculty of Physics, Lomonosov Moscow State University, Moscow, Russia;*
*[2]P.N. Lebedev Physical Institute of the Russian Academy of Sciences, Moscow, Russia;*
*[3]Russian Quantum Center, Skolkovo, Russia*

*stremoukhovsy@my.msu.ru*

Quantum memristors combine the history-dependent nonlinear response of classical memristors with the richness of quantum state space. They have recently been demonstrated in photonic [1] and superconducting circuit [2] platforms. In our previous works, we proposed a realization of a quantum memristor in a three-level system of a trapped ion and showed how two or three such quantum memristors can be coupled on a single trapped $^{171}Yb^{+}$ion [3,4]. Here, we demonstrate their applicability for neuromorphic computing

First, we test the construction of fully connected neural networks using the Adam optimization algorithm on the MNIST dataset, which consists of 60,000 labeled images of handwritten digits. The achieved recognition accuracy lies in the 91–92% range, indicating that quantum memristor-based models perform on par with an "ideal memristor" having arbitrary weight values [5].

Second, we show that a quantum memristor can serve as a powerful nonlinear reservoir for reservoir computing – a framework well suited for temporal tasks. We benchmark the reservoir on several standard tasks: reconstruction of nonlinear functions ($y = x^n$) (with (n) up to 6), NARMA (nonlinear autoregressive moving average), the Mackey–Glass chaotic time series, and the Santa Fe laser intensity dataset. In all cases, the reservoir with active feedback significantly outperforms the same system without feedback. The results exceed those recently reported for a photonic quantum memristor reservoir [6].

The study was supported by Russian Science Foundation Grant No. 24-12-00415.

[1] M. Sanz, L. Lamata, and E. Solano, Invited article: Quantum memristors in quantum photonics, APL Photon. 3, 080801 (2018).
[2] P. Pfeiffer, I. L. Egusquiza, M. D. Ventra, M. Sanz, and E. Solano, Quantum memristors, Sci. Rep. 6, 29507 (2016).
[3] S. Stremoukhov, P. Forsh, K. Khabarova, N. Kolachevsky, "Proposal for Trapped-Ion Quantum Memristor", Entropy, 25, 1134 (2023).
[4] S.Yu. Stremoukhov, P.A. Forsh, K.Yu. Khabarova, N.N. Kolachevsky, "Model of Coupled Quantum Memristors Based on a Single Trapped 171Yb+ Ion", JETP Letters, Vol. 119, No. 5, pp. 352-356 (2024).
[5] S. Stremoukhov, P. Forsh, A. Frolova, I. Kovalishin, D. Rusakov, M. Shakirov, K. Khabarova, N. Kolachevsky, "Quantum memristors: Towards scalable quantum neuromorphic architectures with coupling", Physical Review A, 113, 032619 (2026).
[6] M. Selimović, I. Agresti, M. Siemaszko, J. Morris, B. Dakić, R. Albiero, A. Crespi, F. Ceccarelli, R. Osellame, M. Stobińska, P. Walther, Experimental neuromorphic computing based on quantum memristor, arXiv:2504.18694 (2025).

# Novel nonlinear crystals for mid-infrared quantum metrology

**E.S. Zatsepin[1], A.S. Sabanin[1], D.V. Badikov[2], S.P. Kulik[1,3], A.V. Paterova[1]**

*1- Laboratory of Quantum Engineering of Light, South Ural State University, Chelyabinsk, Russia*
*2- High Technologies Laboratory, Kuban State University, Krasnodar, Russia*
*3- Quantum Technology Centre, Lomonosov Moscow State University, Moscow, Russia*

*paterovaav@susu.ru*

Nonlinear optical crystals with broad mid-infrared transparency are essential for the development of quantum spectroscopy, imaging, and sensing technologies based on spontaneous parametric down-conversion (SPDC). In particular, strongly non-degenerate SPDC enables the generation of correlated photon pairs in which visible or near-infrared photons are detected, while their conjugated photons probe the mid-infrared spectral region. The performance of such systems critically depends on the optical properties of the nonlinear material, including its transparency range, dispersion characteristics, and nonlinear conversion efficiency.

In this work, we investigate two nonlinear crystals for mid-infrared quantum metrology, silver thiogallate ($AgGaS_2$, AGS) and barium gallium germanium sulfide ($BaGa_2GeS_6$, BGGS). Using a continuous-wave near-infrared pump laser, we record wavelength-angular spectra of highly non-degenerate spontaneous parametric down-conversion (SPDC) generated in both materials. The signal photons are detected in the 815-900 nm spectral range, while the corresponding idler photons extended up to 21-24 μm [1].

For AGS crystals, SPDC spectroscopy is employed to determine ordinary and extraordinary refractive indices beyond the previously available experimental range. New Sellmeier equations are derived, providing accurate description of crystal dispersion up to 21 μm. The measurements revealed characteristic spectral features associated with lattice absorption and confirmed the existence of a narrow transparency window around 15.7-17.5 μm [2].

For BGGS crystals, highly non-degenerate SPDC is demonstrated for the first time. Direct comparison with AGS under identical experimental conditions show that BGGS exhibits approximately two times higher nonlinear conversion efficiency and a narrower external SPDC emission cone. These properties improve photon collection efficiency and make BGGS attractive for nonlinear interferometry schemes [1].

The obtained results demonstrate that SPDC can serve both as a source of correlated photon pairs and as a powerful tool for characterization of nonlinear materials in spectral regions inaccessible to conventional infrared techniques. The investigated crystals represent promising platforms for future quantum-enhanced mid-infrared spectroscopy, imaging, gas sensing, and optical metrology [3].

[1] E.S. Zatsepin et al., Dispersion analysis of silver thiogallate in a broad mid-infrared range, Adv. Photonics Res. 7, e202500267 (2026).
[2] E.S. Zatsepin et al., Generation of spontaneous parametric down conversion from $BaGa_2GeS_6$ crystal, Laser Phys. Lett. 23, 015201 (2026).
[3] A.V. Paterova et al., Broadband quantum spectroscopy at the fingerprint mid-infrared region, ACS Photonics 9, 2151-2159 (2022).

# Synchrotron Radiation in Photonic Materials Research: Electronic Excitations, Defects, and Ultrafast Processes

**V. Pankratov**

*Institute of Solid State Physics, University of Latvia, 8 Kengaraga, LV-1063 Riga, Latvia*

*vladimirs.pankratovs@cfi.lu.lv*

Understanding how electronic excitations are converted into light is one of the central challenges in modern photonics. Synchrotron radiation provides a unique experimental platform for investigating these processes over exceptionally broad energy and time scales, enabling direct studies of electronic excitations, energy relaxation pathways, defect formation, and luminescence phenomena in advanced photonic materials.

This invited talk will present recent advances in synchrotron-radiation-based luminescence spectroscopy and its application to the study of wide-bandgap optical and photonic materials. Particular attention will be devoted to identifying the fundamental mechanisms governing light generation and energy conversion following high-energy excitation, including excitonic processes, defect-assisted recombination, and intrinsic radiative relaxation channels. Special emphasis will be placed on the role of intrinsic and radiation-induced defects in energy relaxation and light-emission processes. These studies contribute to establishing design principles for next-generation photonic materials with tailored optical and timing characteristics.

Examples from investigations performed at the SUPERLUMI station at DESY [1] and the FINESTLUMI endstation at MAX IV [2, 3] will be discussed, covering fluoride crystals, oxide scintillators, garnets, and other functional materials [4, 5]. The presentation will demonstrate how selective VUV and X-ray excitation spectroscopy reveals the interplay between electronic structure, defects, and luminescence kinetics, providing information inaccessible by conventional optical methods.

Particular emphasis will be placed on intrinsic fast-emission mechanisms, including cross-luminescence and the recently identified core-to-core luminescence in complex fluoride systems [6]. These processes represent distinct radiative relaxation pathways in wide-bandgap materials. They provide new insights into the fundamental limits of light-generation speed and open promising opportunities for the development of advanced photonic materials and radiation detectors with timing performance towards the picosecond regime.

The presented results illustrate how modern synchrotron-radiation spectroscopy is evolving from a characterization tool into a powerful approach for discovering, understanding, and engineering photonic materials with tailored optical properties and ever-faster response characteristics.

[1] Y. Smortsova, O. Chukova, M. Kirm, et al., Time-resolved photoluminescence spectroscopy at PETRA III storage ring of DESY, Journal of Synchrotron Radiation, 32, 1539-1548, (2025).
[2] K. Chernenko, A. Kivimäki, R. Pärna, et al., Performance and characterization of the FinEstBeAMS beamline at the MAX IV Laboratory, Journal of Synchrotron Radiation, 28, 1620–1630, (2021)
[3] V. Pankratov, R. Pärna, M. Kirm, et al., Progress in development of a new luminescence setup at the FinEstBeAMS beamline of the MAX IV laboratory, Radiation Measurements, 121, 91-98, (2019).
[4] V. Khanin, I. Venevtsev, K. Chernenko, V. Pankratov, et al., Exciton interaction with $Ce^{3+}$ and $Ce^{4+}$ ions in $(LuGd)_3(Ga,Al)_5O_{12}$ ceramics, Journal of Luminescence, 237, 118150, (2021).
[5] E.A. Radzhabov, R.Yu. Shendrik, V. Pankratov, K. Chernenko, Fine structure of 4f-5d absorption spectra of $MeF_2$-$Yb^{3+}$ in the vacuum ultraviolet region under synchrotron excitation, Optical Materials, 135, 113235, (2023).
[6] R. Shendrik, E. Radzhabov, A. Myasnikova, et al., Ultrafast core-to-core luminescence in $BaF_2$-$LaF_3$ single crystals, Scientific Reports 15, 26558, (2025).

# Ultimate photon entanglement in biexciton cascade

**V.N. Mantsevich[1], E.L. Ivchenko[2], D.S. Smirnov[2]**

*1- Lomonosov Moscow State University, Moscow, Russia*
*2- Ioffe Institute, Saint-Petersburg, Russia*

*vmantsev@gmail.com*

Entanglement is the core concept in the quantum science. Immense efforts are focused nowadays on the development and optimization of the entanglement generation in various physical systems. Particularly important direction is the generation of entangled photons, which are necessary for quantum key distribution, one way quantum computing, quantum teleportation etc. [1]. Apart from the probabilistic entangled photon generation by spontaneous parametric down-conversion, semiconductor quantum dots stand out as a fast and deterministic source of single and entangled photons [2].

Recently, the fidelity of the entangled state was pushed up already to 98%, but a number of factors limit the photon entanglement in practice [3]. Historically, the first important factor was the splitting of the intermediate exciton state due to the long-range electron hole interaction in anisotropic quantum dots [4]. A few strategies for suppression of the anisotropic exchange splitting since have been developed, including electric and magnetic fields and strain. One more important factor is hyperfine interaction with the spins of the host lattice nuclei [5]. This interaction results in the random effective magnetic field acting on the exciton state and leading to its detrimental splitting. To date there was apparently no way of suppressing this interaction even in the perspective. We suggest a long awaited solution for this fundamental and important problem [6].

We develop a theory of entangled photon pair generation by symmetric colloidal quantum dots mediated by triplet exciton.We obtain general analytical expressions for the concurrence as a function of the hyperfine interaction strength and show that it is higher than in the conventional case of doublet excitons in self-assembled quantum dots. The entanglement sensitively depends on the shape anisotropy and strain applied to the nanocrystal. In particular, we uncover a possibility to completely suppress the hyperfine interaction for electrons due to the interplay between nanocrystal anisotropy and electron-hole exchange interaction. We argue that this represents an ultimate limit for the generation of entangled photon pairs by semiconductor quantum dots.

[1] N. Gisin and R. Thew, Quantum communication, Nat. Photon. 1, 165 (2007).
[2] D. Cogan, Z.-E. Su, O. Kenneth, and D. Gershoni, Deterministic generation of indistinguishable photons in a cluster state, Nat. Photon. 17, 324 (2023).
[3] A. Orieux, M. A. M. Versteegh, K. D. J¨ons, and S. Ducci, Semiconductor devices for entangled photon pair generation: A review, Rep. Prog. Phys. 80, 076001 (2017).
[4] S. V. Goupalov and E. L. Ivchenko, Electron-hole longrange exchange interaction in semiconductor quantum dots, J. Cryst. Growth 184–185, 393 (1998).
[5] C. Schimpf, F. B. Basset, M. Aigner, et. al., Hyperfine interaction limits polarization entanglement of photons from semiconductor quantum dots, Phys. Rev. B 108, L081405 (2023).
[6] V.N. Mantsevich, D.S. Smirnov, E.L. Ivchenko, Ultimate photon entanglement in biexciton cascade, arXiv:2511.05065.

# Structural, electronic and optical properties of rare-earth-doped $LiYF_4$

**N. Tuvjargal[1,2], D. Lili[1], N. Tsogbadrakh[1], J. Davaasambuu[2,3]**

*1- Department of Physics, National University of Mongolia*
*2- Laser Research Center, National University of Mongolia*
*3- Institute of Physics and Technology, Mongolian Academy of Sciences*

*davaasambuu@mas.ac.mn*

In recent years, rare-earth elements have attracted increasing interest owing to their growing demand and wide range of applications. The demand for rare-earth elements has increased significantly because of their essential role in high-tech applications. Due to their unique and often irreplaceable properties, rare-earth metals are widely used in various fields, including advanced materials and other cutting-edge technologies such as magnets, catalysts, lasers, and light phosphors.

Laser technology and photonics research have advanced rapidly in recent years, with extensive studies focusing on laser generators for diverse applications. Trivalent rare-earth ions exhibit multiple emission levels arising from 4f–4f transitions in the visible and near-infrared regions. Owing to their ability to form long-lived, high-energy excited states, ions are highly suitable for up-conversion and multi-wavelength emission systems.

The Lithium yttrium fluoride (LiYF4) compound doped and co-doped with rare-earth (Pr, Nd) ions was synthesized using a solid-state reaction method. The successful formation of the doped and co-doped powder samples were confirmed through X-ray diffraction measurements. The optical properties of the (Nd:Pr)$LiYF_4$ compound were systematically investigated by combining experimental characterization with computational analysis. The results of both ab-initio and experimental studies provide insights into the electronic structure and optical behavior of the doped and co-doped (Nd:Pr)$LiYF_4$ compound. Our results indicated that a synergistic enhancement of the whole visible-light optical absorption and emission intensities was observed in the (Nd:Pr)$LiYF_4$ compound.

# Intracellular Nanothermometry: Quantum Sensors, Physical Limits and Microscopic Heat-Transport Models

**T. Plakhotnik**

*School of Mathematics and Physics, The University of Queensland, Brisbane, QLD 4072, Australia*

*taras@physics.uq.edu.au*

Over the past decade, considerable experimental effort has been devoted to measuring temperature inside living cells. Fluorescent molecules, polymers, nanoparticles and quantum sensors have been used to map intracellular temperature, with an increasing number of studies reporting variations of several kelvin across individual cells and organelles. Such measurements could provide valuable insight into metabolism, mitochondrial activity and cellular function. However, their physical interpretation remains controversial because the reported temperature differences are difficult to reconcile with elementary estimates of cellular heat generation and heat transport.

This talk will overview the major experimental developments in intracellular nanothermometry over the last decade and discuss the fundamental physical concepts required for their interpretation. Particular attention will be given to the meaning of temperature at microscopic length scales, energy conservation, thermal diffusion, entropy production and the limits imposed by realistic cellular power generation. Nanoscale thermometers do not respond to temperature alone: their signals may also depend on refractive index, viscosity, pH, electric fields, molecular binding, optical excitation and local nonequilibrium conditions. Nanodiamonds containing optically active colour centres represent one of the most advanced approaches to intracellular thermometry because of their exceptional photostability and chemical stability, biocompatibility, optical excitation and readout, microwave control, and sensitivity to temperature. The presence of multiple colour centres and transitions within the same nanocrystal also provides opportunities for internal consistency checks and identification of artefacts. Nevertheless, intracellular temperature variations reported using even these advanced quantum sensors remain orders of magnitude larger than estimates based on elementary heat-generation and heat-transport arguments.

Back-of-the-envelope estimates provide powerful constraints on the interpretation of intracellular temperature measurements, but they necessarily simplify microscopic mechanisms of heat generation and transport. Molecular-dynamics simulations may therefore provide an important link between experiment and fundamental physical interpretation by testing whether microscopic interactions, fluctuations or nonequilibrium effects can invalidate conclusions based on continuum models and order-of-magnitude estimates.

Realistic molecular-dynamics modelling of heat transport at cellular length and time scales is, however, extremely challenging. Such simulations require very large systems, and their conclusions may depend on numerous poorly constrained interaction parameters. We therefore developed a deliberately simple model as a playground for testing physical ideas that might demonstrate the feasibility of the large intracellular temperature variations reported experimentally. In the model, two fluids initially at different temperatures exchange energy only through collisions with a flexible atomic string.

Despite its simplicity, the model displays unexpectedly rich behaviour, including a strong separation between equilibration of the fluids and thermalisation of the string, mode-dependent and non-exponential relaxation, finite-conductivity effects within dense fluids, and nontrivial dependence on string stiffness and numerical timestep. These results illustrate that microscopic heat transport cannot always be represented by a single thermal conductivity or relaxation time. Nevertheless, the simulations have so far revealed no mechanism capable of overcoming the stringent limits suggested by simple energy-balance and diffusion arguments.

The combined experimental overview, physical analysis and microscopic modelling reinforce the need to validate intracellular temperature measurements using independent controls, quantitative modelling and elementary order-of-magnitude estimates. Such validation is essential if intracellular quantum thermometry is to become a reliable tool for biology and medicine.

[1] T. Plakhotnik, Nanothermometry in Living Cells: Physical Limits, Conceptual and Material Challenges, Advanced Functional Materials, 36, e28655 (2026). https://doi.org/10.1002/adfm.202528655

# Laser formation of high-speed integrated optical devices using fluorinated polymer and nano-materials

**V.I. Sokolov**

*NRC «Kurchatov Institute», Academician Kurchatov square 1, Moscow, Russia*

*visokol@rambler.ru*

Laser techniques for fabricating waveguide integrated optical devices, operating in the telecommunication C – band 1530 – 1565 nm, using fluorinated polymer materials with embedded fluorinated nanocrystals doped with rare-earth elements and fluoropolymers containing electro-optical chromophores are presented. The devices include high-speed optical bus for optical data transfer on the printed circuit board for microprocessor computing systems on the base of multimode polymer waveguide arrays, compact waveguide amplifiers of optical signals, single-frequency distributed feedback waveguide lasers, ultra-high-speed (> 100 GHz) optical waveguide modulators and routers.

We review the high-pressure technique (1.5 – 1.6 GPa) for synthesizing new amorphous perfluorinated polymers, technique for fabricating nanocrystals β-$NaYF_4$:$Yb^{3+}$,$Er^{3+}$,$Ce^{3+}$ with diameter of 20 – 600 nm, electro-optical chromophores, as well as methods for incorporating chromophores into polymer matrix.

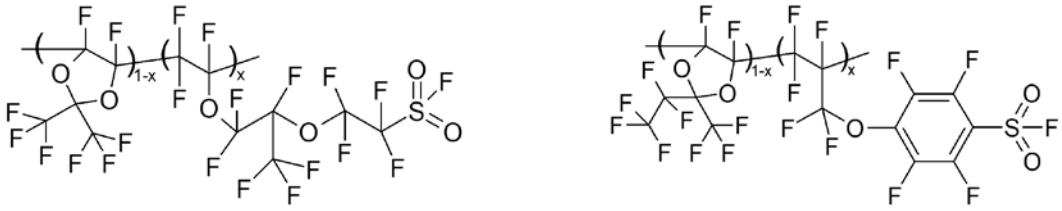

**Fig. 1.** Amorphous perfluorinated polymers, synthesized using high-pressure technique.

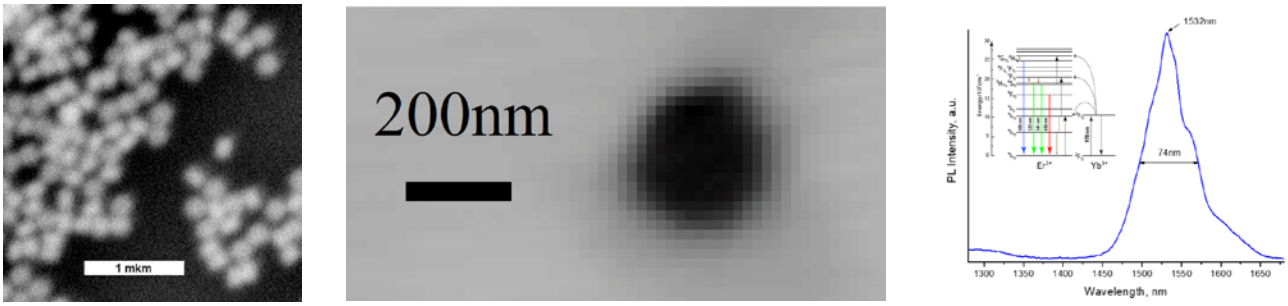


a) b) c)

**Fig. 2.** (a) SEM photo of nanocrystals β-$NaYF_4$:$Yb^{3+}$,$Er^{3+}$,$Ce^{3+}$ of $D \approx 200$ nm diameter.
(b) Photo of sigle nonocrystal, taken using deep UV optical microscopy technique ($\lambda = 225$ nm).
(c) Photoluminescence down-conversion spectrum of nanocrystals pumped with 980 nm laser light.

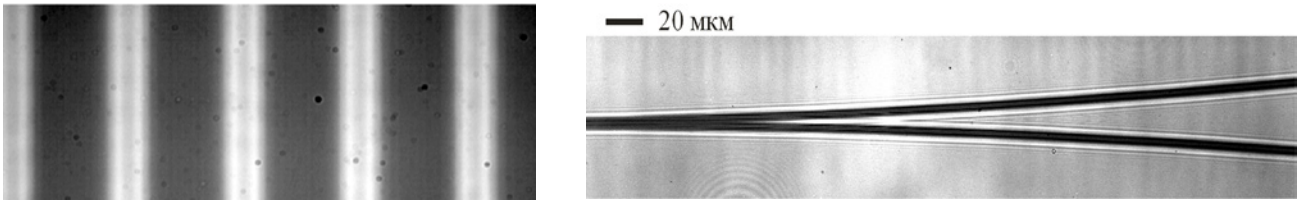


**Fig. 3.** Photo of polymer waveguides with embedded electro-optical chromophores, fabricated using direct laser writing technique.

The work was carried out within the state assignment of NRC "Kurchatov Institute".

# Spectral matching the modes of the multimode squeezed light with the broadened by microstructured fiber local oscillator.

**D. Kalalshnikov[1,3], A. Chudakov[1,2], V. Severin[1], A. Poshevkina[1,2], A. Finochenko[2], K. Kuznetsov[1,3], A. Levchenko[4], E. Serebryannikov[1,3], A. Fedotov[1,3], P. Sharapova[1,3]**

*1- Russian Quantum Center, 121205, Moscow, Skolkovo Innovation Center, Bolshoi Boulevard, 30, 1*
*2- Moscow Institute of Physics and Technology, 141701, Moscow Oblast, Dolgoprudny, Institutskiy Pereulok, 9*
*3- M. V. Lomonosov Moscow State University, 119991, Moscow, GSP-1, Leninskiye Gory, 1, 2*
*4- Dianov Fiber Optics Research Center, Prokhorov General Physics Institute of RAS, 119991, Moscow, GSP-1, Vavilova str., 38*

*d.kalashnikov@rqc.ru*

In recent years, multimode squeezed states of light, i.e. the ones with multiple time-frequency and spatial modes, have attracted a considerable attention. They constitute the basis for the measurement-based quantum computations (MBQC), which is one of the prominent ways of realizing fault-tolerant quantum computations in continuous variables with largely expanded Hilbert space [1,2]. Under this approach, the information is encoded via squeezed states of light referred to as qumodes [3], and the algorithm efficiency grows up with the number of the qumodes. The multimode squeezed light is usually produced via parametric downconversion (PDC) in nonlinear media using ultrafast pump. The typical scheme of the measurement is based on homodyne detection, where the light to measure is superimposed with a strong phase-coherent reference beam, the so-called local oscillator (LO), at a beam splitter followed by balanced detection [4]. In the case of multimode light, for a correct measurement of squeezing of a qumode, the LO should precisely match the selected qumode in both the spectral and phase domain. A difference in the LO and qumode shapes leads to the improper measurement results. However, the LO is usually taken from the same laser source as the pump used to generate squeezed light, therefore the LO shape is significantly narrower than the bandwidth of squeezed light. This makes the proper measurement of qumodes problematic. In this work, we suggest and verify this experimentally to expand the spectral bandwidth of the LO by passing it through the microstructured fiber, where the propagating light experiences broadening due to self-phase modulation. For the case of type-II PDC, we achieved that the broadened LO spectrally matches the estimated qumodes of the generated squeezed light (Fig. 1a). We also demonstrate that the broadened LO provides the level of squeezing comparable to that before the procedure, but benefits in the expanded bandwidth (Fig. 1b). Our results might be useful and provides greater flexibility in the experimental realizations of MBQC schemes based on single-pass PDC.

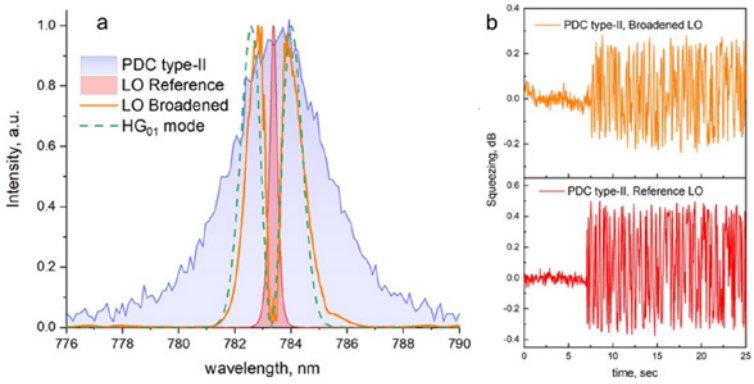


**Fig. 1:** a) spectral distributions for the measured PDC type-II (blue shaded area), measured refence LO (red shaded area), theoretically calculated mode $HG_{01}$ (dashed green line), measured broadened LO (orange solid line); b) squeezing measurements for the type-II PDC with the reference LO (red solid line) and broadened LO (orange solid line).

[1] M.V. Larsen, et al., "Deterministic generation of a two-dimensional cluster state," Science 366, 369-372 (2019).
[2] W. Asavanant, et al., "Generation of time-domain-multiplexed two-dimensional cluster state," Science 366, 373-376 (2019).
[3] Y.-S. Ra, et al., "Non-gaussian quantum states of a multimode light field," Nat. Phys. 16, 144-147 (2020).
[4] A.I. Lvovsky and M.G. Raymer, "Continuous-variable optical quantum-state tomography," Rev. Mod. Phys. 81, 299-332 (2009).

# Efficient phase encoding of arbitrary interactions in a spatial photonic Ising machine

M.A. Kunets[1,2], A.A. Ashurkova[1,2], D. Korbashov[1], A.E. Shitikov[1], D.A. Chermoshentsev[1,2]

*1- Russian Quantum Center, 143026 Skolkovo, Russia*
*2- Moscow Institute of Physics and Technology, 141701, Dolgoprudny, Russia*

*maxkunets1.0@gmail.com*

Spatial photonic Ising machines (SPIM) are a promising analog computing platform for solving binary combinatorial optimization problems by mapping them to an Ising model [1].

In this work, we assembled and tested a SPIM prototype, shown in Fig. 1a, using a new method for jointly encoding the interaction matrix and spin states in a single device – a phase-only spatial light modulator (SLM). This method, based on the spin gauge transformation [2] and SPE [3], enables processing arbitrary interaction matrices without multiplexing and reduces the size requirements for the SLM matrix.

We demonstrated the prototype's performance in optimal state search problems for systems with dimensions up to 50 spins and a random interaction matrix. Fig. 1b) presents the results of a series of 50 runs of the simulated annealing algorithm for a 20-spin system. The optimal state was achieved in 66% and 67% of the experimental and numerical simulation cases, respectively. In addition to 2-local systems, 3-local systems were also considered. Thus, Fig. 1c) demonstrates the energy dynamics of a 50-spin system with interaction order 3 within the framework of a single run of the optimization algorithm.

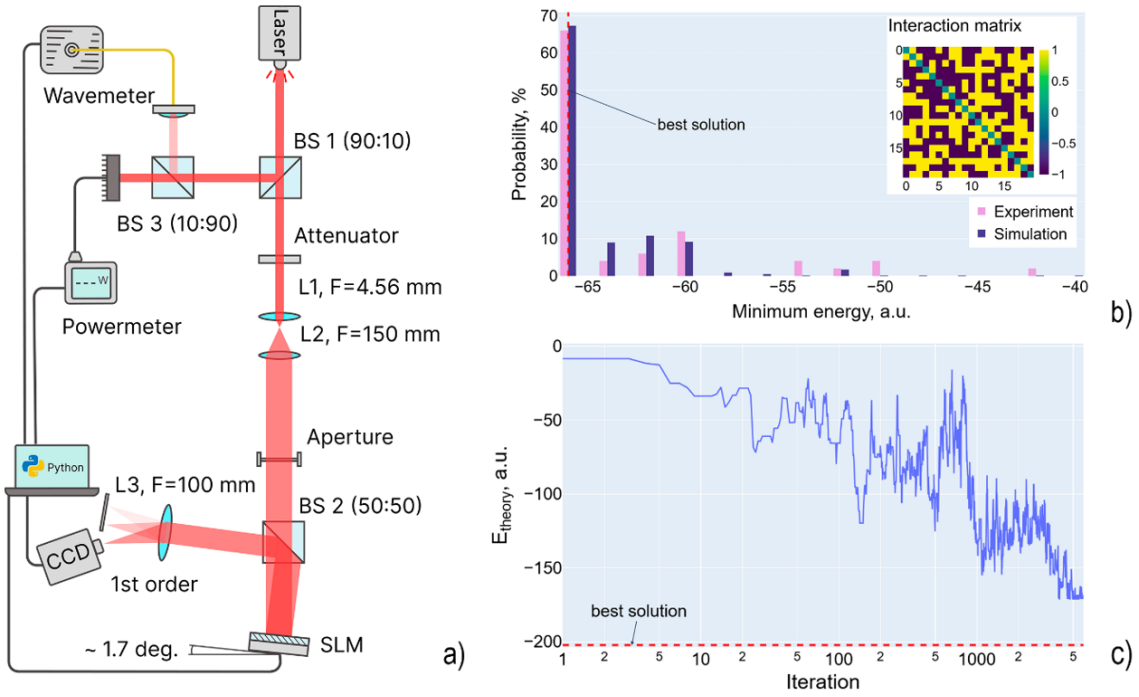


**Fig. 1.** a) Schematic diagram of the experimental setup; b) statistics of the solutions obtained over 50 runs for a 20-spin system with the interaction matrix shown in the inset in the upper right corner, for the experiment (pink) and the simulation (dark purple); c) energy dynamics for a 3-local Hamiltonian of a 50-spin system.

The work of M.A. Kunets, A.A. Ashurkova, D. Korbashov, A.E. Shitikov, D.A. Chermoshentsev was supported by Rosatom in the framework of the Roadmap for Quantum computing (Contract № 868/1759-D dated 3 October 2025).

[1] N. Mohseni, P. L. McMahon, and T. Byrnes, "Ising machines as hardware solvers of combinatorial optimization problems," Nature Reviews Physics 4, 363–379 (2022).
[2] Y. Fang, J. Huang, and Z. Ruan, "Experimental observation of phase transitions in spatial photonic ising machine," Phys. Rev. Lett. 127, 043902 (2021).
[3] J. Sakellariou, A. Askitopoulos, G. Pastras, and S. I. Tsintzos, "Encoding arbitrary ising hamiltonians on spatial photonic ising machines," Phys. Rev. Lett. 134, 203801 (2025).

# Increasing the modulation instability threshold in a direct-diode-pumped Kerr-lens mode-locked Ti:Sa oscillator

**K. Reznikov[1,2], A. Mavritskiy[1], M. Esaulkov[1], A. Naumov[2,3]**

*1- AVESTA Ltd., 108840 Troitsk, Moscow, Russia*
*2- P.N. Lebedev Physical Institute of the Russian Academy of Sciences, Troitsk Branch, 108840 Moscow, Russia*
*3- Institute of Spectroscopy of the Russian Academy of Sciences (ISAN), 108840 Troitsk, Moscow, Russia*

*k.reznikov@avesta.ru*

High-power, few-cycle femtosecond (fs) pulses are essential for numerous scientific applications [1]. While Ti:sapphire (Ti:Sa) oscillators are ideal sources due to their broad gain bandwidth, conventional systems using Diode-Pumped Solid-State (DPSS) pumps remain highly expensive. Direct diode pumping offers a cost-effective alternative, but its average output power is fundamentally limited by the onset of modulation instability (MI), which causes pulse splitting, bifurcations, and loss of mode-locking. For highly divergent diode beams, pump focusing strongly influences the Kerr soft aperture and, consequently, the MI threshold.

In this work, we theoretically and experimentally demonstrate that optimizing the pump focal length (***F***) suppresses MI and boosts the average power of direct-diode-pumped Ti:Sa lasers. Using the wave equation, we modeled how pump focusing affects active-medium gain, Kerr-lens aperture diffraction losses, and self-amplitude/phase modulation. Numerical simulations reveal that reducing ***F*** shifts the MI onset toward higher pump powers, expanding the stable single-pulse operating regime.

To validate this, a Ti:Sa laser was pumped by two combined GaN diodes (455 and 465 nm, up to 11 W total). Beam shaping was optimized via cylindrical telescopes, and a spherical lens focused the pump into the crystal. Experimentally, using an ***F = 80*** mm lens limited the stable average power to 300 mW (at 8 W pump) due to MI. Decreasing the focal length to ***F = 50*** mm successfully shifted the MI threshold, enabling stable generation of 10-fs pulses with a 127-nm FWHM spectrum and an increased average output power of 500 mW at 11 W pump. Thus, controlling the pump geometry provides a robust approach to scaling the power of diode-pumped KLM Ti:Sa oscillators.

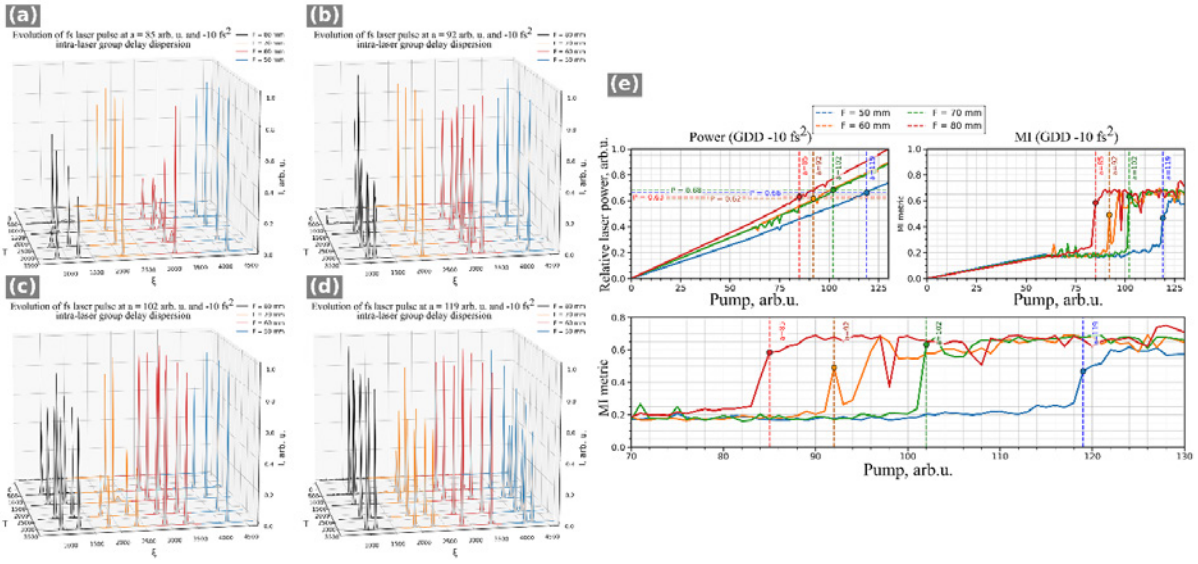


**Fig. 1**: Calculated evolution of the fs pulse for GDD = −3 fs². Panels (a)–(d) show the evolution of intensity of the fs pulse at pump values a = 9, 18, 19, and 25 for different focal lengths. Panel (e) shows the relative output power of Ti:Sa laser and the MI metric. If 0 < MI < 0.1, the pulse remains single and MI is absent. For 0.1 < MI < 0.3, weak asymmetry and small side structures appear. For 0.3 < MI < 0.6, the side sub-pulses become pronounced. For MI > 0.6, the main pulse evolves into a multi-pulse regime.

[1] U. Morgner, F.X. Kärtner, S.H. Cho, Y. Chen, H. A. Haus, J.G. Fujimoto, T. Ippen, V. Scheuer, G. Angelow, and T. Tschudi, "Sub-two-cycle pulses from a Kerr-lens mode-locked Ti:sapphire laser", Opt. Lett. 24(6), 411-413 (1999).

# Dynamics Analysis of Quantum Dot Light-Emitting Devices Based on Time-Resolved Optoelectronic Technologies

**Sh. Chang[1], Y. Liu[1], R.B. Vasiliev[2]**

*1- Faculty of Materials Science, Shenzhen MSU-BIT University, Shenzhen, China*
*2- Faculty of Materials Science, Lomonosov Moscow State University, Moscow*

*schang@smbu.edu.cn*

Quantum dot electroluminescence, as a next-generation self-emissive display technology, boasts advantages such as high brightness, high efficiency, wide color gamut, and low-cost solution preparation. However, its operating mechanism and failure mechanism still require further investigation. Traditional steady-state testing methods often involve irreversible aging damage, limiting non-destructive analysis and dynamic process research of devices. Time-resolved electroluminescence (TREL) technology, as an in-situ, non-destructive testing method, is particularly suitable for analyzing the dynamic processes in complex multilayer structure devices.

By combining time-resolved current (TRC) testing, we extracted key parameters such as series resistance, parallel resistance, and capacitance from the equivalent circuit of quantum dot light-emitting diodes (QLEDs) [1]. This allowed us to simulate the delay, rise, and decay stages in the TREL spectrum, enabling quantitative analysis of charge accumulation and recombination processes during QLED operation (Fig. 1). Based on the electrically pumped transient absorption technology (E-TA), the electron dynamics (time resolution ~ 1 ns) were realized and accumulated electron concentration was calculated during the operation of QLED [2]. These finding provide key parameters and theoretical basis for the operating mechanism of this type of device.

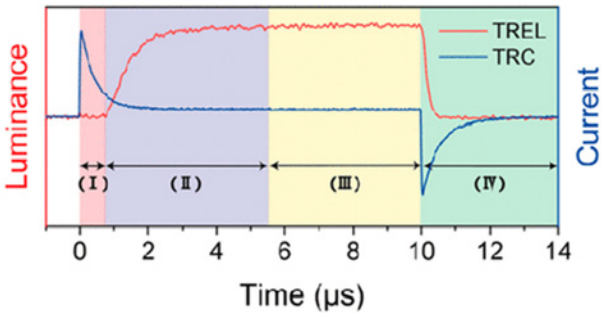


**Fig. 1.** Typical results of TREL and TRC measurements and their stage division

We further developed a frequency-modulated color-tunable quantum dot AC electroluminescence device [3]. By combining transient electroluminescence and impedance analysis, the physical mechanism of frequency-selective luminescence was revealed, and a wavelength prediction model was established. Building on our study of the emission and color-tuning mechanisms, we demonstrate a full-color pixel using two coplanar subpixels, achieving continuous RGB tuning with a color gamut approaching DCI-P3 through frequency modulation (Fig. 2), providing a feasible technical path for novel display technologies with high resolution and low driving complexity.

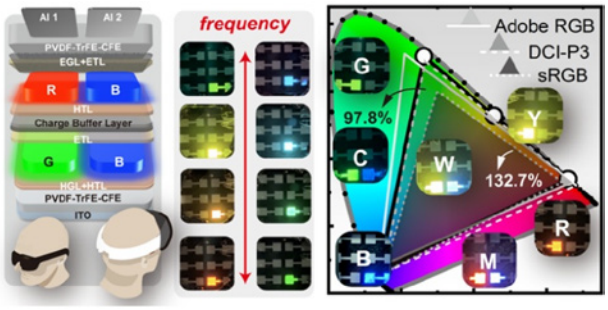


**Fig. 2.** Design of a coplanar full-color pixel unit and its CIE 1931 color gamut coverage

[1] H. Bao, S. Chang*, H. Zhong* et al., J. Phys. Chem. Lett. **14**, 1777-1783 (2025).
[2] X. Yan, S. Chang*; S. Jin* et al., Nano Lett. **24**, 13374-13380 (2024).
[3] Y. Liu, R. B. Vasiliev, S. Chang* et al., Adv. Opt. Mater. e02689 (2025).

# Atomic Magnetometry Using an Elliptically Polarized Light For Applications in Geology, Archeology and Medicine

**D.V. Brazhnikov[1*], A.O. Makarov[1], K.S. Kozlova[1], M.A. Rusina[1], R.A. Tkachenko[1], A.M. Mikhailov[1], V.A. Vasiliev[1], E.V. Tanakov[1], A.N. Goncharov[1], M.A. Bobrov[2], Ya.N. Kovach[2], A.A. Blokhin[2], N.A. Maleev[2], S.A. Blokhin[2]**

*1- Institute of Laser Physics SB RAS, 15B Lavrentyev Ave, Novosibirsk, Russia*
*2- Ioffe Physical Technical Institute RAS, 26 Politekhnicheskaya Str., Saint Petersburg, Russia*

*x-kvant@mail.ru*

Optically pumped magnetometers (OPMs) based on laser spectroscopy of alkali-metal atoms are among the most sensitive magnetic sensors. They have a vast range of applications. For example, OPMs are being actively implemented in the field of noninvasive medical diagnostics. The use of compact and energy-efficient OPMs enables compelling opportunities for mineral exploration and archeology. For medical diagnostics, OPMs are based on the ground-state Hanle effect (GSHE) and operate in the spin-exchange relaxation-free (SERF) regime. The OPM systems offer a high spatial resolution (~ 1 mm) and are well suited for diagnosing deep brain structures. These sensors are capable of detecting many brain disorders at the earliest stages. However, SERF magnetometer requires an extremely high degree of magnetic shielding against the Earth's field and its housing heats up noticeably (≈ 50°C).

At the Institute of Laser Physics, a few novel atomic magnetometry techniques have been developed for operation under both magnetically shielded environments and in the geomagnetic field. The proposed techniques do not require the SERF regime. The first approach enables vector measurements of the magnetic field and is based on the GSHE. The second approach provides scalar measurements and relies on the Bell-Bloom technique. Both approaches depart from their classical implementations through a set of modifications. In particular, instead of employing linear or circular light polarization as in conventional schemes, elliptical polarization is utilized in conjunction with detection of magnetic resonance via polarimetric technique. In the Hanle sensor, cw emission from an external-cavity diode laser is employed, whereas in the Bell-Bloom sensor, frequency-modulated emission from a vertical-cavity surface-emitting laser (VCSEL) is used. The sensitivity of the modified Hanle technique is 180 fT/√Hz, with a bandwidth of 190 Hz. This sensor is suitable for magnetocardiography and magnetomyography. The scalar sensor exhibits a sensitivity of 70 fT/√Hz with a bandwidth of 1 kHz. It can operate either in a quasi-vector single-axis mode for medical applications or in a fully scalar mode for operation in the Earth's magnetic field. The latter mode is of particular interest for applications in geology and archeology.

The work was supported by the Russian Science Foundation (Project Grant nos. 26-12-00132 and 23-12-00195). The development of a VCSEL was supported by the Ministry of Science and Higher Education of the Russian Federation under the state-funded research assignment of Ioffe Institute RAS (Project Code : FFUG-2025-0006).

# High-power GaAs/AlGaAs-based semiconductor lasers and high-frequency pulsed lasers

**A.A. Pulatov, I. Zakhidov**

*Namangan State University, Namangan, Uzbekistan*

Abstract — GaAs/AlGaAs heterostructures remain a key platform for high-power and high-frequency pulsed semiconductor lasers. This review summarizes their physical advantages, principal device configurations, current power- and pulse-scaling approaches, functional materials, and major applications. Particular attention is given to the balance among output power, beam quality, electro-optical efficiency, thermal management, repetition rate, and reliability.

*Keywords— GaAs/AlGaAs; high-power semiconductor laser; quantum well; mode locking; high repetition rate; distributed Bragg reflector; thermal management; photonic integration*

The practical development of semiconductor lasers accelerated with the GaAs-AlGaAs double heterostructure. The wide-bandgap AlGaAs layers confine electrons and holes in the GaAs active region while the refractive-index difference provides optical waveguiding. This combination reduced threshold current and enabled continuous-wave operation at room temperature [1]. Mature heterostructure technology now supports efficient near-infrared sources, particularly in the approximately 900-1000 nm spectral range.

High-power designs include broad-area edge-emitting lasers, tapered lasers, laser arrays, vertical-cavity devices, and structures with improved transverse mode control. Power scaling requires coordinated optimization of epitaxial layers, the waveguide, emitting aperture, mirrors, heat sink, and current distribution [2,3]. The central engineering trade-off is to raise power and brightness without degrading beam quality through higher-order modes, filamentation, thermal lensing, parasitic lasing, or spectral instability. Multijunction structures illustrate the efficiency potential of advanced architectures [5].

High-frequency pulsed operation is obtained with gain switching, passive or active mode locking, external cavities, quantum-well lasers, VCSELs, and VECSELs. Compact semiconductor resonators allow picosecond and femtosecond pulses at repetition rates from the gigahertz to the tens-of-gigahertz range. Recent GaAs-on-SiN mode-locked operation at 23.3 GHz demonstrates a promising route toward integrated laser-photonic systems [4]. Such integration can improve compactness, stability, modulation speed, and compatibility with photonic circuits.

Materials engineering is equally important. InGaAs/GaAs quantum wells tailor gain and emission wavelength, whereas AlAs/GaAs distributed Bragg reflectors provide high refractive-index contrast and close lattice matching for vertical-cavity and disk-laser designs. High-reflectivity coatings, high-thermal-conductivity heat spreaders, damage-resistant optical materials, and low-loss waveguides further determine attainable power and lifetime. These lasers are relevant to LiDAR and ranging, optical communications, spectroscopy, biophotonics, micromachining, metrology, 3D scanning, and the pumping of fiber and solid-state lasers. Future progress will depend on simultaneous improvements in power, efficiency, beam quality, pulse stability, thermal resistance, and reliability.

[1] Zh.I. Alferov, Injection heterojunctions, in Semiconductor Devices and Their Applications, vol. 25, pp. 204-225 (Sovetskoe Radio, Moscow, 1971).
[2] X. Zhang, H. Dong, Z. Jia et al., Progress of GaAs-based high-power semiconductor lasers, Materials Reports 36(12) (2022).
[3] P. Crump, A. Boni, M. Elattar et al., Power and efficiency scaling of GaAs-based edge-emitting high-power diode lasers, IEEE J. Sel. Top. Quantum Electron. (2025).
[4] D. Wang, T. Reep, T.N.L. Tran et al., High-repetition-rate GaAs-on-SiN mode-locked laser using a Fabry-Perot cavity, Opt. Lett. 51(15), 4184-4187 (2026).
[5] Y. Xiao, J. Wang, H. Liu et al., Multi-junction cascaded vertical-cavity surface-emitting laser with a high power conversion efficiency of 74%, Light Sci. Appl. 13, 60 (2024).

# Photodegradation mechanism in all-inorganic metal halide perovskite nanocrystals

A. Tarasevich[1], A.G. Son[2], S. Kozyukhin[2], A. Naumov[1], I. Eremchev[3]

*1- P.N. Lebedev Physical Institute RAS, Leninskiy Prospekt 53, Moscow, 119991, Russia*
*2 – Kurnakov Institute of General and Inorganic Chemistry, Leninskiy Prospekt 31, Moskow, 119071, Russia*
*3 - Institute of Spectroscopy RAS, Fizicheskaya 5, Troitsk, Moscow 108840, Russia*

*ao.tarasevich@gmail.com*

Metal halide perovskites have emerged as one of the most intensively studied classes of semiconductor materials owing to their outstanding optical and electronic properties [1]. In particular, $CsPbX_3$ (X = Cl, Br, I) perovskite nanocrystals exhibit high photoluminescence quantum yields (PLQY) and tunable emission spectra, making them promising candidates for light-emitting diodes, lasers, photodetectors, and single-photon sources [2]. However, their practical application remains limited by insufficient photostability. Under illumination, photo-induced chemical and structural transformations can alter the optical properties of perovskite nanocrystals and lead to luminescence degradation [3]. Despite extensive research efforts, the microscopic mechanisms responsible for photodegradation remain poorly understood.

Most previous studies have focused on ensembles of nanocrystals, where the measured response is averaged over a large number of particles. Such averaging obscures individual degradation pathways and complicates the identification of underlying mechanisms. In contrast, investigations at the single-particle level enable direct monitoring of the temporal evolution of the optical properties of individual nanocrystals.

In this work, we investigated the photoluminescence (PL) of individual $CsPbBr_3$ nanocrystals with sizes ranging from 10 to 30 nm. Under continuous laser excitation, the nanocrystals exhibited a gradual blue shift of the PL spectrum (from 520 nm to less than 480 nm) accompanied by a decrease in PL intensity (by orders of magnitude) and changes in photon statistics (Fig. 1). Significant particle-to-particle variability in photodegradation behavior was observed. Furthermore, no direct correlation was found between the PL peak wavelength and the $g^2(0)$ value. Based on these observations, we propose that photodegradation is governed by a gradual reduction of the emitting core of the nanocrystal, potentially driven by ion migration and material loss from the particle surface. These findings provide new insight into the microscopic mechanisms of photodegradation and may contribute to the development of strategies for improving the photostability of perovskite nanocrystals.

This project was supported by a grant from the Russian Science Foundation (№ 26-72-00108).

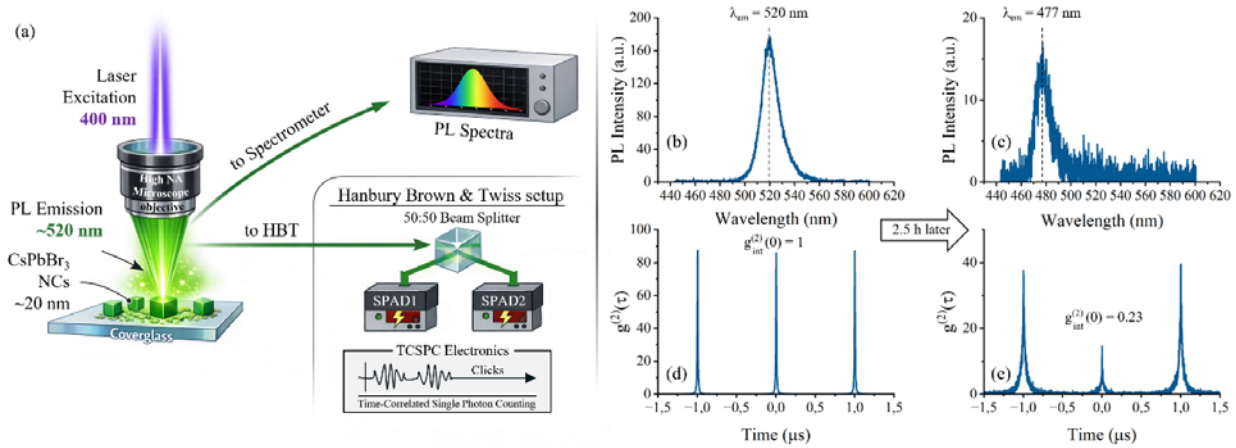


**Fig. 1.** (a) – Schematic diagram of the experiment. (b) PL spectrum and (d) cross-correlation function of a single $CsPbBr_3$ nanocrystal. (c) PL spectrum and (e) cross-correlation function of the same nanocrystal after 2.5 hours of laser irradiation.

[1] S. D. Stranks and H. J. Snaith, Metal-halide perovskites for photovoltaic and light-emitting devices, Nat. Nanotechnol., 10, 391 (2015).
[2] L. Zhang et al., Advances in the Application of Perovskite Materials, Nano-Micro Lett., 15, 177 (2023).
[3] Z. Wang, Z. Zhang, L. Xie, S. Wang, C. Yang, C. Fang, and F. Hao, Recent Advances and Perspectives of Photostability for Halide Perovskite Solar Cells, Advanced Optical Materials, 10, 2101822 (2022).

# Firn-Line Altitude Changes as Indicators of Climate Variability and Atmospheric Moisture Conditions in the Mountain Regions of Uzbekistan Using Radar and Optical Remote Sensing Data

**E. Semakova, D. Semakov**

*Ulugh Beg Astronomical Institute of the Uzbekistan Academy of Sciences, Tashkent 100052, Uzbekistan*

*ella9sem@gmail.com*

Climate change alters both temperature and atmospheric moisture regimes, affecting environmental processes as well as the propagation of electromagnetic signals used in remote sensing and radio astronomical observations. Assessing long-term changes in atmospheric conditions is particularly challenging in high-mountain regions, where meteorological observations remain sparse and unevenly distributed. In such environments, glaciers serve as sensitive natural indicators of climatic variability because their state reflects the combined influence of temperature and precipitation over extended periods.

This study investigates changes in firn-line altitude across the glacierized regions of Uzbekistan, including the Western Tien-Shan and Hissar-Alay mountain systems. Firn-line altitude is considered an integral indicator of glacier health and long-term climatic conditions, reflecting the balance between snow accumulation and ice ablation [1].

The analysis combines historical glacier inventory data from the Catalogue of Glaciers of the 1970s–1980s with modern remote sensing observations [2]. Optical satellite data from the Landsat series were used for glacier mapping and inventory updates, while ALOS PALSAR radar imagery acquired around 2010 enabled firn-line identification independently of cloud cover and illumination conditions [3]. To improve the accuracy of elevation estimates, digital elevation models from different sources were co-registered and refined using satellite laser altimetry data.

The results reveal a systematic upward shift of firn-line altitude relative to historical observations, indicating continuing glacier degradation throughout the mountain regions of Uzbekistan. The observed rise of the firn-line altitude is consistent with regional warming and changes in moisture availability reported for Central Asian mountain regions. The spatial distribution of firn-line elevations also demonstrates a relationship with the upper limit of mountain juniper (Juniperus seravschanica) vegetation, suggesting a common response of both glacial and ecological systems to changing climatic conditions.

The study demonstrates the value of integrating optical, radar, and laser-altimetry datasets for monitoring environmental change in data-scarce mountain regions. Firn-line altitude can serve as an effective proxy for assessing long-term climate variability, atmospheric moisture conditions, and their impacts on glacier systems, particularly in the poorly monitored highlands of the Hissar-Alay.

[1] A.Schetinnikov, L. Podkopaeva. Catalog lednikov SSSR [Catalogue of glaciers of USSR]. Leningrad: Gidrometeoizdatm vol. 14, parts 1, 3, (1968-1969), in Russian.
[2] G. Glazirin, M. Glazirina. Catalogue of Pamir and Hissaro-Alay glaciation for 1980 (database of A.S. Schetinnikov). Almaty: ExLibris LLP, (2012).
[3] JAXA ALOS Data Portal – https://www.eorc.jaxa.jp/ALOS

# Collimated microlenses at the end of multimode optical fibers

**A. Pankov, L. Zhukov, R. Ponomarev**

*Perm State National Research University, 15, Bukireva, Perm, 614068, Russia*

*lab.photon.psu@gmail.com*

Collimating microlenses based on multimode optical fibers are indispensable components for working with laser optical radiation. They are used for short-distance data transmission in data centers and for coupling with photonic integrated circuits and vertical radiation lasers [1]. They are widely used in sensor applications for detecting chemical molecules [2] and temperature [3]. These microlenses can be the basis for a class of sensors operating on the principles of RAMAN scattering [4].

This work is an attempt to form collimating fiber microlenses using a standard coupling machine. An electric arc makes it possible to form a variety of structures at the end of the fiber with different geometric parameters. In this case, the optimal mode was chosen for the formation of a hemisphere capable of collimating the optical beam coming out of the fiber structure. The parameters of the outgoing beam were estimated using a Spiricon IR-camera and a system based on a Fabry-Perot interferometer.

The IR-camera used in the experiment allows us to obtain intensity distributions. For this purpose, the program code was implemented on Phyton. The light profile was recorded at a distance of 0 to 5 mm in steps of 500 microns, where the focal point of the IR-camera lens was taken as the zero coordinate. In the experiment, 10 two-dimensional radiation profile images were obtained, which made it possible to estimate the profile of the output radiation (Fig.1).

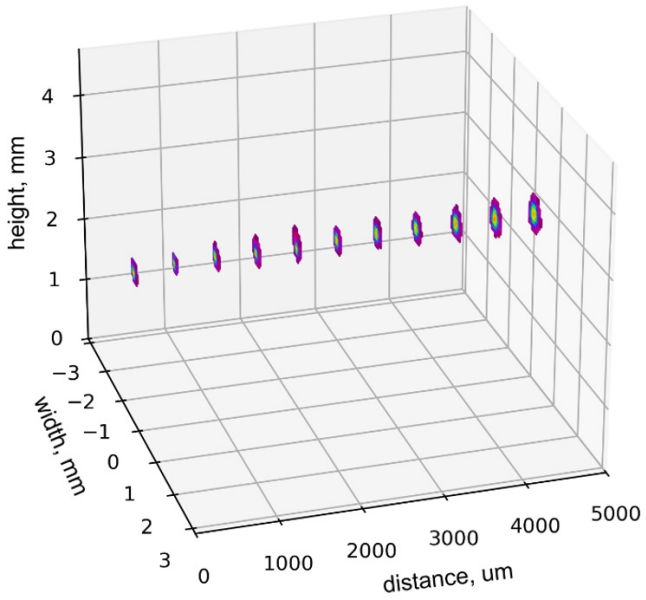


**Fig. 1.** Distribution of the intensity of the light beam at different points.

The Fabry-Perot interferometer method is based on the detection of reflected optical radiation coming out of the studied structure. The main elements of the optical circuit are the end face of the structure under study and the mirror. They form the cavity of the interferometer, in which optical radiation propagates. On the graph (Fig.2) shows the power distribution of the reflected signal from the length of the interferometer cavity.

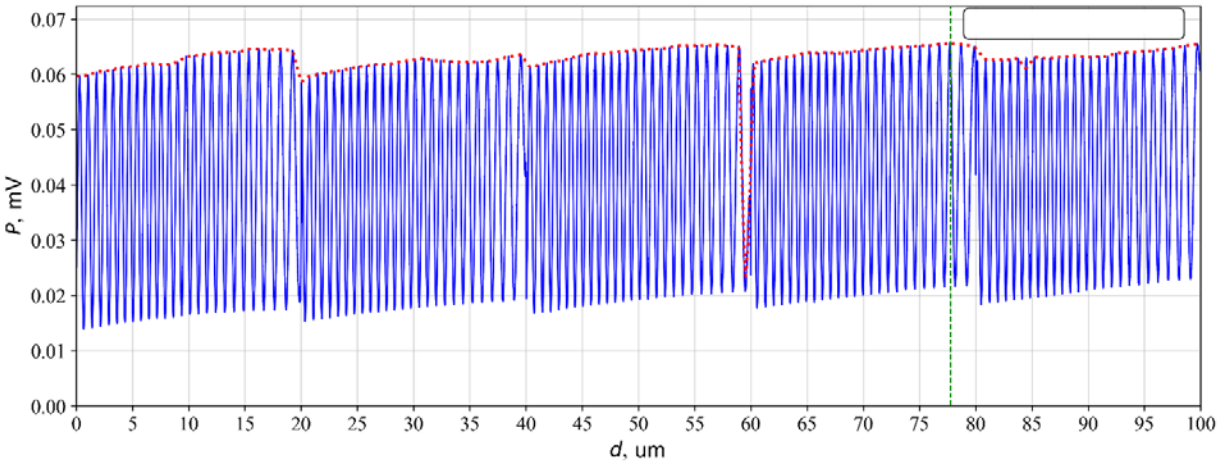


**Fig. 2.** Distribution of the microlensed collimated signal.

Based on the results obtained, it is possible to hypothesize that the structures under study on multimode optical fibers have the ability to collimate optical radiation. This hypothesis will be tested in the course of further research. The research was funded under the state assignment, № FSNF-2024-0001.

[1] K. Gradkowski, Mixed-mode fiber array alignment and coupling to photonic integrated circuits, IEEE Transactions on Components, Packaging and Manufacturing Technology, vol.15(6), pp. 1156-1160 (2025).
[2] H. Niu, et al, Mach-Zehnder interferometer based integrated-photonic acetone sensor approaching the sub-ppm level detection limit, Optics Express, vol.30(16), pp. 29665-29679 (2022).
[3] G. Li, T. Li, Y. Liu and Y. Zheng, A new Mach–Zehnder interference temperature measuring sensor based on silica-based chip, Scientific Reports, vol.14(1), pp. 8657 (2024).
[4] D. Kita, J. Michon and J. Hu, A packaged, fiber-coupled waveguide-enhanced Raman spectroscopic sensor, Optics Express, vol.28(10), pp. 14963-14972 (2020).

# Study of the photophysical properties of semiconductor colloid quantum dots: fundamental and applied aspects

**K. Karimullin[1,2], A. Arzhanov[1,2], K. Magaryan[2], A. Savostianov[1], A. Naumov[1,2,3]**

*1- Lebedev Physical Institute, Russian Academy of Sciences, Branch in Troitsk, 108840, Moscow, Russia*
*2- Moscow State Pedagogical University, 119435 Moscow, Russia*
*3- Institute of Spectroscopy, Russian Academy of Sciences, 108840 Moscow, Russia*

*kamil_karimullin@mail.ru*

We discuss the results of the research devoted to methods of synthesis and the study of the spectral and photophysical properties of semiconductor nanocrystals – quantum dots (QDs). Fundamental regularities linking QD morphology with their optical and spectral properties are considered, as well as the mechanisms of the quantum-size effect, electron-phonon interaction, local field effects, photoluminescence blinking of single QDs, and other phenomena. The results of experimental and theoretical studies of the temperature dependences of the spectra of colloidal QDs with an emitting CdSe core [1] are analyzed: the electron-phonon interaction in solid-state nanocomposites with CdSe/CdS/ZnS quantum dots [2]. Promising applications of QDs in various fields of modern photonics are considered: optoelectronics, biophysics, quantum optics, sensorics, photovoltaics [3].

The theoretical studies were carried out with financial support from the Russian Ministry of Education and Science on the topic of the state assignment of the Lebedev Physical Institute of the Russian Academy of Sciences (FFMR-2024-0017). Experimental part of the study was carried out within the framework of the state assignment of the Ministry of Education of the Russian Federation "Physics of nanostructured materials and highly sensitive sensors: synthesis, fundamental research and applications in photonics, life sciences, quantum and nanotechnologies" (reg. number 124031100005-5).

[1] Arzhanov A.I., Savostyanov A.O., Magaryan K.A., Karimullin K.R., Naumov A.V., Photonics of semiconductor quantum dots: basic aspects, Photonics Russia, vol. 15(8), pp. 622-641, (2021).
[2] Karimullin K.R., Arzhanov A.I., Surovtsev N.V., Naumov A.V., Electron–phonon interaction in composites with colloidal quantum dots: a study by luminescence spectroscopy and Raman scattering, Optics and Spectroscopy, vol. 131(10), pp. 995-999, (2023).
[3] Arzhanov A.I., Savostyanov A.O., Magaryan K.A., Karimullin K.R., Naumov A.V., Photonics of semiconductor quantum dots: applied aspects, Photonics Russia, vol. 16(2), pp. 96-113, (2022).

# Laser Fluorescence Ratiometric Thermometry: Elimination of Key Methodological Artifacts and the Thermo-Memory Effect in Porphyrin Molecules

**Yu.A. Batishcheva[1,2], Yu.G. Gorbunova[2], K.A. Magaryan[1,2], A.V. Naumov[1,3,4]**

*1- Moscow Pedagogical State University (MPGU), Moscow, Russia*
*2- M.V. Lomonosov Moscow State University, Russia*
*3- P.N. Lebedev Physical Institute of the Russian Academy of Sciences, Troitsk Branch, Moscow, Russia*
*4- Institute of Spectroscopy RAS, Moscow, Troitsk, Russia*

*a_v_naumov@mail.ru; www.single-molecule.ru*

The technique of photoluminescence ratiometric thermometry has been investigated in detail for applications in the physiologically relevant temperature range (25–75 °C) using tetraphenylporphyrin (TPP) as a model system. Since ratiometric thermometry involves measuring absolute luminescence intensities over a broad wavelength range to determine the luminescence intensity ratio (LIR) of individual spectral peaks, particular attention was paid to spectrometer calibration for spectral sensitivity using the blackbody radiation curve. It is shown that neglecting the spectral sensitivity of the detection system can introduce systematic errors comparable in magnitude to the temperature-induced changes in LIR. The dependences of LIR on various experimental parameters are also discussed, including the photobleaching efficiency of the dye, the excitation laser power density, and the concentration of TPP in benzene solution. In heating–cooling cycles, a "thermomemory" effect was observed, manifesting as hysteresis in the temperature dependence of LIR, LIR(T). This indicates the presence of long-lived thermally stimulated excited states of TPP molecules, which must also be taken into account in the practical application of fluorescence ratiometric thermometry.

This work was completed as part of a state assignment from the Ministry of Education of the Russian Federation (Topic No. 126030618412-6 "Photonic Technologies in Science and Education: Materials, Methods, and Tools for Ultra-High-Sensitivity Optical Sensors and Microscopy").

# DNA-Origami Nanomaterials for Photonics, Quantum- and Nanotechnologies: Synthesis and Characterization

**A.I. Arzhanov[1,2], T.V. Egorova[1], E.V. Khaidukov[2], U.A. Khokhryakova[1], K.A. Magaryan[1], M.E. Stepanov[1], A.V. Naumov[1-3]**

*1- Moscow Pedagogical State University (MPGU), Moscow, Russia*
*2- P.N. Lebedev Physical Institute of the Russian Academy of Sciences, Troitsk Branch, Moscow, Russia*
*3- Institute of Spectroscopy RAS, Moscow, Troitsk, Russia*

*a_v_naumov@mail.ru; www.single-molecule.ru*

Modern photonics and quantum technologies impose stringent requirements on the precision of nanostructure fabrication, since key optical processes occur at subdiffraction scales and demand nanometer-level positional control of individual building blocks [1–3]. Alongside conventional techniques such as colloidal synthesis, CVD, laser writing, and nanolithography, the DNA-origami approach is rapidly emerging as a cost-effective route to structures with predefined morphology [1–3].

The fundamental principle of this method relies on a long single-stranded DNA scaffold and a set of short staple strands. Through biomimetic complementary nucleobase pairing (adenine–thymine double bonds and cytosine–guanine triple bonds), the staples fold the scaffold into user-defined two- or three-dimensional shapes. The unique advantage of DNA origami lies in its capacity for site-specific placement of nanoobjects, including quantum dots (QDs) and macromolecules at arbitrary positions along the assembly, rendering it an ideal platform for constructing photonic building blocks [2, 3].

A particularly active area of research involves the synthesis and subsequent hybridization of DNA-origami nanostructures with active elements, namely quantum emitters. In a recent study [4], rectangular nanoplatelets of DNA origami were synthesized in the form of parallelepipeds (61 × 52 × 6 nm) featuring a rectangular aperture (15 × 9 nm), and the spontaneous attachment of colloidal QDs to these nanoplatelets was investigated. The resulting hybrids were characterized by atomic force microscopy (AFM) followed by advanced two-dimensional deconvolution processing, which enabled correction of imaging artifacts and reliable determination of the geometry of individual hybrid structures. It was found that the probability of QD attachment to the designated positions on the nanoplatelets was approximately 25% [4]. This finding confirms the feasibility of fabricating DNA-origami/QD hybrid structures for photonic applications, while also highlighting the need for further optimization of self-assembly conditions to enhance the yield.

We have also examined the application of DNA origami in nanoscopy and proposes a model nanostructure with positions for anchoring fluorescent emitters. It is shown that the structure can be used as a calibration nanoruler for STORM, PALM, cryogenic ZPL nanoscopy, and luminescent QD-based imaging, as well as a platform for DNA-PAINT [5].

In conclusion: DNA origami provides a platform for assembling complex optical systems with unprecedented spatial precision. It represents a promising route to the controlled synthesis of nanomaterials, opening new avenues for manipulating light at the *nm*-scale and enabling the development of components for photonics, quantum technologies, biomedicine, and other related fields.

This work was completed as part of a state assignment from the Ministry of Education of the Russian Federation (Topic No. 126030618412-6 “Photonic Technologies in Science and Education: Materials, Methods, and Tools for Ultra-High-Sensitivity Optical Sensors and Microscopy”).

[1] M. E. Stepanov et al, Photonics Russia, 2024, Vol. 18, No. 1, pp. 72–80. DOI: 10.22184/1993-7296.FRos.2024.18.1.72.80
[2] M. E. Stepanov et al, Photonics Russia, 2024, Vol. 18, No. 2, pp. 166–174. DOI: 10.22184/1993-7296.FRos.2024.18.2.166.174
[3] M. E. Stepanov et al, Photonics Russia, 2024, Vol. 18, No. 5, pp. 398–405. DOI: 10.22184/1993-7296.FROS.2024.18.5.398.405
[4] A.I. Arzhanov et al, Colloid Journal, 2025, Vol. 87, Iss. 6, pp. 790–803. DOI: 10.1134/S1061933X25601398.
[5] U.A. Khokhryakova et al, Bulletin of the Russian Academy of Sciences: Physics, 2026. DOI: 10.1134/S1062873826701376

# Luminescent and Scintillation Hybrid Materials in the LiF-Liq System and Film Based on Them

**Petrova O.B., Chernova E.A., Strekalov P.V., Runina K.I., Serkina K.S.**

*D. Mendeleev University of Chemical Technology, Miusskaya Sq. 9, 125047 Moscow, Russia*

*petrova.o.b@muctr.ru*

Hybrid materials (HM's) combine organic and inorganic components and can exhibit unique functional properties based on the synergy of their component properties. Luminescent organo-inorganic HMs in glass, polycrystalline, and film oxide and fluoride matrices have demonstrated high efficiency and stability [1-2]. As shown in [3], the organic coordination phosphor lithium 8-hydroxyquinoline (Liq) is capable of exhibiting not only photo-, electroluminescence, and electron transport properties, but also pronounced scintillation properties. Synthesizing HM's in the LiF-Liq system appears promising for neutron detection.

HM's were obtained by co-precipitation from aqueous-alcohol solutions and solid-phase synthesis using both Liq and 8-hydroxyquinoline (Hq) as starting reagents, which allowed us to obtain HM's with a reproducible luminescence spectrum (Fig. 1a). Films were obtained based on HM and polyvinyl alcohol (PVA) that showed intense X-ray luminescence (Fig. 1b).

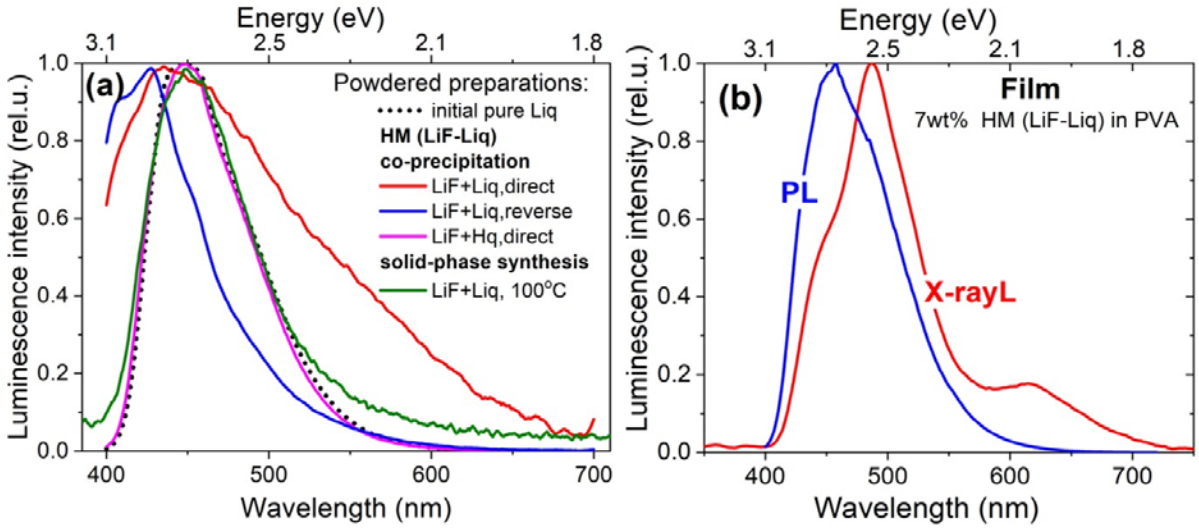


**Fig. 1.** Photoluminescence spectra of powdered Liq and HM LiF-Liq preparations obtained by different methods (a) and photo- and X-ray luminescence films based on them (b).

HM's LiF-Liq research is promising for producing phosphor for markings and scintillation films.

This research was financially support by the Ministry of Science and Higher Education of Russia through the project FSSM-2025-0006.

The authors are grateful to the National Analytic Certification Laboratory of D. Mendeleev University of Chemical Technology of Russia for ICP-MS, XRD, FTIR, and luminescence measurements.

[1] O.B. Petrova, K.I. Runina, M.N. Mayakova, I.V. Taydakov, A.V. Khomyakov, R.I. Avetisov, I.C. Avetissov, Luminescent hybrid materials based on metal-organic phosphors in $PbF_2$ powder and $PbF_2$-containing glass matrix, Optical Materials, vol. 88, pp. 378–384 (2019).
[2] M. Zykova, K. Runina, L. Popkova, O. Petrova, A. Barkanov, D.T. Do, T. T. Ta, V. L. Nguyen, A. Khomyakov, I. Avetissov, R. Avetisov, Luminescent properties of organic–inorganic hybrid films fabricated by capillary coating technique, Applied Physics A: Materials Science and Processing, vol. 128, no. 3, p. 240 (2022).
[3] K.I. Runina, S.S. Zykova, P.V. Strekalov, L.V. Popkova, O.B. Petrova, A S. Chepurnov, D.C. Do, T.C. Ta, Obtaining a new film scintillator based on (8-oxyquinolate) lithium: An overview, Glass and Ceramics, vol. 79, no. 11-12, pp. 522–525 (2023).

# Fundamentals of Direct Multi-Wavelength Diode Pumping of Ti:Sapphire Lasers for Enhanced Optical-to-Optical Conversion Efficiency Across a Broad Spectral Range

**K. Reznikov[1,2], A. Mavritskiy[1], M. Esaulkov[1], A. Naumov[2,3]**

*1- AVESTA Ltd., 108840 Troitsk, Moscow, Russia*
*2- P.N. Lebedev Physical Institute of the Russian Academy of Sciences, Troitsk Branch, 108840 Moscow, Russia*
*3- Institute of Spectroscopy of the Russian Academy of Sciences (ISAN), 108840 Troitsk, Moscow, Russia*

*k.reznikov@avesta.ru*

Direct diode pumping of Ti:Sapphire lasers offers a compact, cost-effective alternative to traditional DPSS systems. However, achieving high output power and slope efficiency in femtosecond (fs) operation remains a challenge due to beam poor quality, limited commercial diode availability in the 470–510 nm range, and mode-matching issues [1].

In this study, we demonstrate a high-performance Ti:Sapphire laser utilizing a novel spectral and spatial combination of four available diode sources: 455 nm, 465 nm, and two 525 nm. Each diode beam is individually shaped using cylindrical telescopes and combined via dichroic and D-shaped mirrors into a Z-fold cavity. To maximize the optical efficiency, the pump beam profile was tailored to optimize the spatial overlap with the intracavity mode. This was achieved by offsetting the green pump beams from the geometric center of the focusing spherical lens, supported by numerical modeling using Fresnel diffraction integrals and a four-level laser gain model.

The developed system delivers an outstanding optical output of 2.5 W in CW mode at 770 nm under 15 W of pump power, corresponding to a 16.6% optical-to-optical efficiency, with a tuning range of 705–1020 nm. In the Kerr-lens mode-locking (KLM) regime, the laser generates stable 75-fs pulses at 798 nm with a record output power of 1.84 W at 14.5 W pump. The fs emission wavelength is continuously tunable from 730 to 860 nm. These parameters represent the state-of-the-art for directly diode-pumped Ti:Sapphire oscillators, providing a scalable and modular platform for multiphoton microscopy and ultrafast spectroscopy.

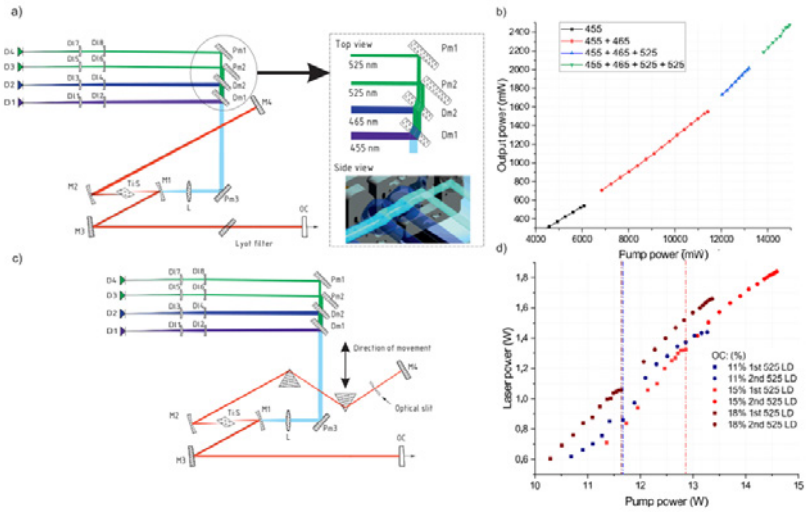


**Fig. 1.** (a) The optical scheme of the laser cavity for CW operation. The pump part consists of four laser diodes D1-D4, cylindrical lenses DL1-DL8 with focal lengths $F_{convex}$ = 80 mm and $F_{concave}$ = −25 mm, pump mirrors Pm1-Pm3, dichroic mirrors DM1-DM2, spherical lens (F = 80 mm). The laser cavity includes high-reflectance mirrors M# (two of them are spherical concave mirrors with a curvative radius R = 100 mm), Lyot filter and an output coupler. (b) Output power of the laser in CW mode versus pump power. Laser wavelength is 770 nm. The slope efficiencies of the D1-D4 LDs are 13.8%, 18.3%, 24.9% and 26.6% respectively. (c) Laser cavity for FS operation (P1, P2 prisms made from the dense flint). The P2 prism is located on the a movable mechanical table with electromagnetic starter. An optical slit is attached to the table with P2 prism. (d) The FS mode laser output power as a function of pump power is shown for various OCs. Blue LDs pump power was fixed at 10 W, while green LD pump power was increased. Vertical lines denote the points where the first 525 nm LD pump power was stopped and the second 525 nm LD was activated. Slope efficiencies for the first and second 525 nm LDs were 34.4% and 31.7% (18% OC), 27.4% and 31.4% (11% OC), and 43.6% and 26.9% (15% OC). The optimal OC is 15%.

[1] P. W. Roth, A.J. Maclean, D. Burns, A.J. Kemp, Opt. Lett. 34, 3334-3336 (2009).

# Application of nonlinear interferometry for gas sensing

**A. Sabanin[1], L. Krivitsky[2], A. Paterova[1,2]**

*1- South Ural State University (SUSU), Laboratory of Quantum Engineering of Light, 76, Lenin prospekt, Chelyabinsk, Russia.*
*2- Institute of Materials Research and Engineering (IMRE),*
*Agency for Science Technology and Research (A*STAR), Singapore, Singapore*

*artem.sabanin@mail.ru*

The mid-infrared (IR) range of wavelengths is of particular interest due to the concentration of spectral absorption lines of various gases [3]. However, classical metrological approaches in this area face technical difficulties: high noise levels, low photodetectors efficiency, and a narrow instrument tuning range. Nonlinear interferometry offers an effective alternative, translating the study of IR properties of objects into the recording of visible radiation [2].

The method is based on interferometry of spontaneous parametric down conversion (SPDC) generated in a nonlinear medium [1]. In the case of a highly non-degenerate regime, the signal SPDC photons are generated in the visible range, and the idler photons in the mid-IR range. Nonlinear interferometry exploits the correlations of photon pairs (signal and idler), when the interference pattern at the wavelength of signal photons depends on the amplitude-phase characteristics of the idler photons.

In the present work we demonstrate gas sensing in a common path nonlinear interferometer design. A laser with 532 nm wavelength is used as pump source for lithium niobate crystal, thereby providing generation of non-degenerate pairs of SPDC photons. In this case, the signal mode is recorded in the spectral range of 580-615 nm, and the idler mode - at 4-6 μm. A gas mixture of $N_2O$ and $CO_2$ affects the visibility of the interference pattern at 603 and 608 nm, respectively, corresponding to their absorption lines at 4.5 μm and 4.27 μm, see figure 1. As a result, detection of the frequency-angular spectra of signal photons in a visible range allows sensing greenhouse gases without using IR detection.

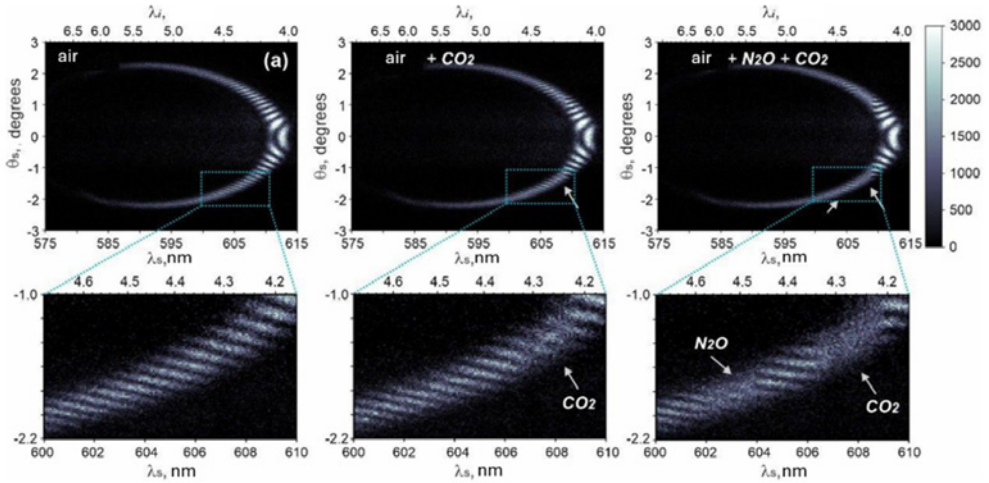


**Fig.1** Frequency-angular spectrum of signal photons:
a) with air (reference data); b) air and $CO_2$; c) air, $CO_2$ and $N_2O$

[1] D. N. Klyshko, A. N. Penin, and B. F. Polkovnikov, Parametric luminescence and light scattering by polaritons, JETP Lett., vol. 11, pp. 11-14, (1970).
[2] A. V. Paterova, H. Yang, C. An, D. A. Kalashnikov, and L. A. Krivitsky, Tunable optical coherence tomography in the infrared range using visible photons, Quantum Sci. Technol., vol. 3, pp. 025008, (2018).
[3] B. H. Stuart, Infrared Spectroscopy: Fundamentals and Applications (Wiley & Sons, Ltd.), Chapter 4, (2004)